

# UNCLASSIFIED

AD NUMBER
AD858513
NEW LIMITATION CHANGE
TO Approved for public release, distribution unlimited
FROM Distribution authorized to U.S. Gov't. agencies and their contractors; Administrative/Operational Use; Nov 1968. Other requests shall be referred to Air Force Materials Lab., Wright-Patterson AFB, OH 45433.
AUTHORITY
USAFSC ltr, 26 May 1972

THIS PAGE IS UNCLASSIFIED

AD 858513

# FINAL REPORT ON HIGH VELOCITY FORGING TECHNOLOGY

D. W. Truelock  
J. R. Russell  
C. M. Phelan  
et al

**VOUGHT AERONAUTICS DIVISION**  
LTV AEROSPACE CORPORATION  
P.O. BOX 5907 DALLAS TEXAS 75222

This document is subject to special export controls and each transmittal to foreign governments or foreign nationals may be made only with prior approval of the Manufacturing Technology Division, Air Force Materials Laboratory, Wright-Patterson Air Force Base, Ohio 45433.

*attn: MATY*

## FOREWORD

This final Technical Report covers the work performed under Contract F33615-67-C-1179 from 1 December 1966 through 30 November 1968. The report was released by the authors on 15 December 1968 for publication.

This contract with the Vought Aeronautics Division of LTV Aerospace Corporation, P.O. Box 5907, Dallas, Texas, 75222, was initiated under Manufacturing Methods Project 9-133, "High Velocity Forging". It was accomplished under the technical direction of Mr. William T. O'Hara, MATP, of the Manufacturing Technology Division, Air Force Materials Laboratory, Wright-Patterson Air Force Base, Ohio.

The contract was conducted under the direction of Messrs. W. W. Wood, Chief of Manufacturing Research, and D. W. Truelock, Manufacturing Research Project Engineer for the Vought Aeronautics Division. Those who actively participated in the research and preparation of this report were: Messrs. J. R. Russell, and J. A. Fouse, Manufacturing Research Engineer Specialists; G. R. DiGiacomo, and C. M. Phelan, Manufacturing Research Engineers; F. R. Sivley, Manufacturing Engineering Aide; and R. E. Duval, Materials Engineer.

This project has been accomplished as part of the Air Force Manufacturing Methods Program, the primary objective of which is to implement, on a timely basis, manufacturing processes and techniques for use in economical production of USAF materials and components. The program encompasses the following technical areas:

Metallurgy - Rolling, Forging, Extruding, Drawing, Casting, Powder Metallurgy, Composites

Chemical - Propellants, Plastics, Textile Fibers, Graphite, Fluids & Lubricants, Elastomers, Ceramics

Electronic - Solid State, Materials & Special Techniques, Thermionics

Fabrication- Forming, Material Removal, Joining, Components

Suggestions concerning additional Manufacturing Methods projects required on this or other subjects will be appreciated.

This technical report has been reviewed and is approved.

*George M. Glenn*  
for H. A. JOHNSON  
Chief, Materials Processing Branch  
Manufacturing Technology Division

### ABSTRACT

This is a manufacturing methods program to investigate the dynamic response of selected aerospace alloys deformed by upset forging from room temperature to 1950°F at impact strain rates from quasi-static (100 in/in/sec.) to 8000 in/in/sec. This was accomplished in two phases. Phase I included the selection and the ambient temperature forging of ten representative aerospace materials to evaluate the effects of strain rate on material forgeability and to select four of the most responsive materials for extensive testing at elevated temperatures. In Phase II, the four selected materials were forged at varying combinations of strain rate and temperature to determine the conditions for optimum forgeability and mechanical properties including tensile yield, tensile ultimate, elongation, hardness and fatigue. This report covers a period of eighteen months and is divided into five sections: Introduction, Technical Background, Test Materials, Phase I Room Temperature Screening, and Phase II Elevated Temperature Testing.

This document is subject to special export controls and each transmittal to foreign nationals may be made only with prior approval of the Advanced Fabrication Techniques Branch, Manufacturing Technology Division, Air Force Materials Laboratory, Wright-Patterson Air Force Base, Ohio.



## TABLE OF CONTENTS

	<u>Page No.</u>
SECTION I - INTRODUCTION -----	1
SECTION II - TECHNICAL BACKGROUND -----	3
Static Forging -----	3
High Energy Impact Forging -----	8
The Influence of Temperature and Strain Rate on the Coefficient of Friction ( $\mu$ ) -----	17
SECTION III - TEST MATERIALS -----	21
SECTION IV - AMBIENT TEMPERATURE MATERIAL SCREENING -----	23
Introduction -----	23
Forgeability Evaluation -----	23
Mechanical Properties Evaluation of Material Upset Forged at Room Temperature -----	29
Metallurgical Data -----	32
Discussion of Results -----	44
SECTION V - PHASE II COMBINED EFFECT OF TEMPERATURE AND HIGH STRAIN RATE IN UPS <sup>ET</sup> FORGING -----	47
Introduction -----	47
Forgeability Evaluation -----	47
Energy Requirements -----	59
Instantaneous Process Variables -----	60
Mechanical Properties Evaluation -----	67
Discussion of Results -----	81
APPENDIX I - PROPERTIES AND IDENTIFICATION OF PROGRAM TEST MATERIALS -----	89
APPENDIX II - FORGEABILITY TESTS -----	101
APPENDIX III - DATA TABLES -----	217

TABLE OF CONTENTS (CONTINUED)

	<u>Page No.</u>
APPENDIX IV - DEVELOPMENT OF STRESS EQUATIONS -----	287
APPENDIX V - PHOTOMICROGRAPHS OF STATIC AND DYNAMIC FORGED SPECI- MENS -----	293
APPENDIX VI - DETAIL DESCRIPTION OF EQUIPMENT -----	315
APPENDIX VII - MEASUREMENT AND CALIBRATION OF THE COMPRESSED GAS GUN -----	331
REFERENCES -----	337
DISTRIBUTION LIST -----	339

# LIST OF ILLUSTRATIONS

<u>Figure No.</u>		<u>Page No.</u>
1	Typical Pressure Distribution on a Cylindrical Billet for $\sigma_0=10,000$ psi, $\mu=0.2$ Assuming Zero Strain Hardening -----	3
2	Typical Pressure Distribution On a Cylindrical Billet for Various Values of $\mu$ ( $\sigma_0=10,000$ psi) ---	4
3	Surface Appearance After Forging -----	5
4	Anvil Deflection in Upset Forging -----	6
5	Die Deflection on (D) VS. Coefficient of Friction ( $\mu$ ) For Various Strength Materials -----	7
6	Comparison of Static and Dynamic Equilibrium Stress Distribution -----	9
7	Variation of Maximum Pressure With Projectile Velocity -----	10
8	Impact Pressure VS. Impact Velocity -----	11
9	Typical Velocity Profiles With Resultant Strain Rate Profiles -----	14
10	Ductility VS. Temperature Under Low Strain Rate Conditions -----	16
11	<del>Effect of Strain and Strain Rate On The Frictional Coefficient (<math>\mu</math>) -----</del>	<del>18</del>
12	Effect of Friction On Grain Flow At Low Strain Rates -----	19
13	Effect Of Temperature On Graphite Lubricant -----	19
14	Temperature Effect On Friction For Unlubricated Material -----	20
15	Typical Upset Test Series -----	24
16	Typical Phase I Upset Test -----	24
17	Projectile Configurations Used -----	25
18	Classification Of Phase I Materials Based On Dynamic Response -----	27
19	Experimental Test Conditions -----	29

# LIST OF ILLUSTRATIONS (CONTINUED)

<u>Figure No.</u>		<u>Page No.</u>
20	Billet Location In Bar Stock -----	30
21	Fabrication of Static Tensile Test Coupon -----	31
22	Fixed Anvil Shown With Specimens In Forging Position	31
23	Photomicrograph View Directions -----	34
24	Electron Photomicrographs of L-605 -----	35
25	Material Properties Data For Specimens in X-Ray Diffraction Tests -----	36
26	Target Area For X-Ray Diffraction -----	36
27	X-Ray Spectra For A-286 Using $Fe_{K\alpha}$ Radiation -----	38
28	$Cr_{K\alpha}$ Peak For Specimen F1-016 -----	39
29	$Cr_{K\alpha}$ Peak For Specimen F1-003 -----	40
30	$Cr_{K\alpha}$ Peak For Specimen F1-011 -----	41
31	Grain Flow Patterns For Vascomax 300 (18% Ni Maraging Steel) Upset At Room Temperature -----	42
32	Grain Flow At High Strain Rate For A Cylindrical Billet (Room Temperature) -----	43
33	Grain Flow At Static Strain Rate (Room Temp.) -----	43
34	Strain Distribution For Various Process Condition -	45
35	Test Temperatures For Phase II Forgeability Evalua- tion -----	48
36	Forging Temperatures For Mechanical Properties Evaluation -----	50
37	The Effect Of Temperature On Forgeability Limit At Various Strain Rates For 2024-C Al -----	51
38	The Effect of Strain Rate On Forgeability Limit At R.T. To 750°F For 2024-C Al -----	52
39	The Effect Of Temperature On Forgeability Limit At Various Strain Rates For Ti-5Al-2.5Sn -----	53

# LIST OF ILLUSTRATIONS (CONTINUED)

<u>Figure No.</u>		<u>Page No.</u>
40	The Effect Of Strain Rate On Forgeability Limit At R.T. To 1950°F For Ti-5Al-2.5Sn -----	54
41	The Effect Of Temperature On Forgeability Limit At Various Strain Rates For 17-4 PH -----	55
42	The Effect Of Strain Rate On Forgeability Limit At R.T. To 1950°F For 17-4 PH -----	56
43	The Effect Of Temperature On Forgeability Limit At Various Strain Rates For A-286 -----	57
44	The Effect Of Strain Rate On Forgeability Limit At R.T. To 1950°F For A-286 -----	58
45	Method For Plotting Forging Energy -----	59
46	Work VS. Strain Rate (Room Temperature) -----	61
47	Work VS. Strain Rate (400°F) -----	62
48	Work VS. Strain Rate (600°F) -----	63
49	Photograph of Optical Extensometer -----	64
50	Optical Extensometer Schematic -----	65
51	Error In Billet Height Measurements Resulting From Anvil Deflection -----	66
52	Instantaneous Velocity, Strain Rate And Die Force For A7-926 -----	68
53	Instantaneous Velocity, Strain Rate And Die Force For A7-927 -----	69
54	Instantaneous Velocity, Strain Rate And Die Force For A7-928 -----	70
55	Instantaneous Velocity, Strain Rate And Die Force For F7-929 -----	71
56	Instantaneous Velocity, Strain Rate And Die Force For F7-931 -----	72
57	Mechanical Properties Tested -----	73

# LIST OF ILLUSTRATIONS (CONTINUED)

<u>Figure No.</u>		<u>Page No.</u>
58	Fabrication Of Tensile And Fatigue Specimens -----	74
59	Selection Of Strain And Forging Temperature -----	74
60	Experimental Test Schedule -----	75
61	Furnace And Loading Method For Bar Specimens -----	77
62	Bar Specimen Loading Tool -----	78
63	Fatigue And Tensile Specimens -----	79
64	Fatigue Test Conditions -----	80
65	Combined Effects of Temperature And Strain Rate On Forgeability Of Phase II Materials -----	81
66	Combined Effect Of Temperature And Strain Rate On The Mechanical Properties Of Titanium And Aluminum -	83
67	Combined Effect Of Temperature And Strain Rate On The Mechanical Properties Of 17-4 PH -----	84
68	Combined Effect Of Temperature And Strain Rate On The Mechanical Properties Of A-286 -----	85
69	Fatigue Life Of 2024 Aluminum -----	86
70	Fatigue Life Of A-286 -----	87
71	Fatigue Life Of 17-4 PH -----	87
72	2024-O Al Forgeability Specimens At Room Temperature (Utilizing Energy Absorbing Rings) -----	104
73	7075-O Al Forgeability Specimens At Room Temperature (Utilizing Energy Absorbing Rings) -----	106
74	Ti-5Al-2.5Sn Forgeability Specimens At Room Tempera- ture (Utilizing Energy Absorbing Rings) -----	108
75	Ti-6Al-4V Forgeability Specimens At Room Temperature (Utilizing Energy Absorbing Rings) -----	110
76	17-4 PH Forgeability Specimens At Room Temperature (Utilizing Energy Absorbing Rings) -----	112

# LIST OF ILLUSTRATIONS (CONTINUED)

<u>Figure No.</u>		<u>Page No.</u>
77	A-286 Forgeability Specimens At Room Temperature (Utilizing Energy Absorbing Rings) -----	114
78	Vascomax 300 Forgeability Specimens At Room Temperature (Utilizing Energy Absorbing Rings) -----	116
79	TZM Forgeability Specimens At Room Temperature (Utilizing Energy Absorbing Rings) -----	118
80	Rene' 41 Forgeability Specimens At Room Temperature (Utilizing Energy Absorbing Rings) -----	120
81	L-605 Forgeability Specimens At Room Temperature (Utilizing Energy Absorbing Rings) -----	122
82	2024-O Al Forgeability Limit Specimens At Room Temperature -----	124
83	2024-O Al Forgeability Limit Specimens At 550°F ----	126
84	2024-O Al Forgeability Limit Specimens At 750°F ----	128
85	Ti-5Al-2.5Sn Forgeability Limit Specimens At Room Temperature -----	130
86	Ti-5Al-2.5Sn Forgeability Limit Specimens At 750°F	132
87	Ti-5Al-2.5Sn Forgeability Limit Specimens At 1050°F -----	134
88	Ti-5Al-2.5Sn Forgeability Limit Specimens At 1350°F -----	136
89	Ti-5Al-2.5Sn Forgeability Limit Specimens At 1550°F -----	138
90	Ti-5Al-2.5Sn Forgeability Limit Specimens At 1750°F -----	140
91	Ti-5Al-2.5Sn Forgeability Limit Specimens At 1950°F -----	142
92	17-4 PH Forgeability Limit Specimens At 550°F -----	144
93	17-4 PH Forgeability Limit Specimens At 950°F -----	146

# LIST OF ILLUSTRATIONS (CONTINUED)

<u>Figure No.</u>		<u>Page No.</u>
94	17-4 PH Forgeability Limit Specimens At 1350° F ---	148
95	17-4 PH Forgeability Limit Specimens At 1550° F ---	150
96	17-4 PH Forgeability Limit Specimens At 1750° F ---	152
97	17-4 PH Forgeability Limit Specimens At 1950° F ---	154
98	A-286 Forgeability Limit Specimens At Room Tempera- ture -----	156
99	A-286 Forgeability Limit Specimens At 550° F -----	158
100	A-286 Forgeability Limit Specimens At 750° F -----	160
101	A-286 Forgeability Limit Specimens At 950° F -----	162
102	A-286 Forgeability Limit Specimens At 1050° F -----	164
103	A-286 Forgeability Limit Specimens At 1350° F -----	166
104	A-286 Forgeability Limit Specimens At 1550° F -----	168
105	A-286 Forgeability Limit Specimens At 1750° F -----	170
106	A-286 Forgeability Limit Specimens At 1950° F -----	172
107	As Forged Microstructure Of 2024-0 Aluminum At Three (3) Different Strain Rates (Normal View) ---	295
108	As Forged Microstructure Of 2024-0 Aluminum At Three (3) Different Strain Rates (Transverse View)	296
109	As Forged Microstructure Of 2024-0 Aluminum At Three (3) Different Strain Rates ( Longitudinal View) -----	297
110	As Forged Microstructure Of 7075-0 Aluminum At Three (3) Different Strain Rates (Normal View) ----	298
111	As Forged Microstructure Of 7075-0 Aluminum At Two (2) Different Strain Rates (Normal View) -----	299
112	As Forged Microstructure Of 17-4 PH Stainless At Two (2) Different Strain Rates (Normal View) -----	300
113	As Forged Microstructure Of 17-4 PH Stainless At Two (2) Different Strain Rates (Transverse View) --	301



# LIST OF ILLUSTRATIONS (CONTINUED)

<u>Figure No.</u>		<u>Page No.</u>
114	As Forged Microstructure Of 17-4 PH Stainless At Two (2) Different Strain Rates (Longitudinal View) -	302
115	As Forged Microstructure Of A-286 Steel At Three (3) Different Strain Rates (Normal View) -----	303
116	As Forged Microstructure Of A-286 Steel At Three (3) Strain Rates (Transverse View) -----	304
117	As Forged Microstructure Of A-286 Steel At Three (3) Different Strain Rates (Longitudinal View) -----	305
118	As Forged Microstructure Of 18% Ni Maraging Steel At Three (3) Different Strain Rates (Normal View) --	306
119	As Forged Microstructure Of 18% Ni Maraging Steel At Three (3) Different Strain Rates (Transverse View)	307
120	As Forged Microstructure Of 18% Ni Maraging Steel At Three (3) Different Strain Rates (Longitudinal View) -----	308
121	As Forged Microstructure Of Rene' 41 At Three (3) Different Strain Rates (Normal View) -----	309
122	As Forged Microstructure Of Rene' 41 At Three (3) Different Strain Rates (Transverse View) -----	310
123	As Forged Microstructure Of Rene' 41 At Three (3) Different Strain Rates (Longitudinal View) -----	311
124	As Forged Microstructure Of L-605 At Three (3) Different Strain Rates (Normal View) -----	312
125	As Forged Microstructure Of L-605 At Three (3) Different Strain Rates (Transverse View) -----	313
126	As Forged Microstructure Of L-605 At Three (3) Different Strain Rates (Longitudinal View) -----	314
127	2500 Ton Lake Erie Hydraulic Press -----	320
128	Static Upset Tooling -----	321
129	Typical Hardened Steel Die Inserts For Static Upset Tests -----	321

# LIST OF ILLUSTRATIONS (CONTINUED)

<u>Figure No.</u>		<u>Page No.</u>
130	Special Deflection Gage For Static Upset Tests -----	322
131	Low Velocity, Elevated Temperature Upset Test Equipment -----	322
132	Velocity Measurement For Drop Hammer Forgeability Test -----	323
133	Pressure Chamber Valving Diagram -----	324
134	High Pressure Valving And Vacuum System -----	325
135	Schematic Of Automatic Billet Loading Mechanism For Furnace Heated Specimens -----	326
136	Specimen Holding Fixture For Elevated Temperature Testing -----	327
137	Automatic Loading Mechanism For Elevated Temperature Testing -----	327
138	Schematic Of Billet Heating System -----	328
139	Billet In Heating Position -----	329
140	Bar Upset Loading Mechanism -----	329
141	Rear View Of Control System -----	330
142	Front Panel View Of Control System -----	330
143	Instrumentation For Projectile Velocity Measurement-	333
144	Typical Oscilloscope Curve For Measuring Projectile Velocities -----	334
145	Experimental Verification Of Analytically Predicted Projectile Velocities -----	334
146	Muzzle Velocity And Energy VS Chamber Pressure And Projectile Mass -----	335

# LIST OF TABLES

<u>Table No.</u>		<u>Page No.</u>
I	Adiabatic Temperature Increase For Phase I Materials -----	15
II	Strain Rate Effects on the As-Forged Mechanical Properties at Room Temperature -----	33
III	Chemical Composition of Test Materials -----	91
IV	Mechanical Properties of Test Materials -----	95
V	Billet Identification and Application -----	98
VI	As Received Hardness Measurements -----	100
VII	High Strain Rate Ductility Results for Phase I Specimens -----	220
VIII	Phase I Tensile Properties of Forged Specimens -----	227
IX	Static Forgeability Data (Performed on Hydraulic Press -----	232
X	Static Ductility Results -----	237
XI	High Strain Rate Ductility Results for Phase II Specimens -----	246
XII	Phase II Tensile Properties of Forged Specimens -----	273
XIII	Fatigue Data for Static and Dynamic Forged Test Specimens -----	278

# LIST OF GRAPHS

<u>Graph No.</u>		<u>Page No.</u>
1	Forgeability Limit Curves For 2024-0 At Room Temperature (Utilizing Energy Absorbing Rings) -----	105
2	Forgeability Limit Curves For 7075-0 At Room Temperature (Utilizing Energy Absorbing Rings) -----	107
3	Forgeability Limit Curves For Ti-5Al-2.5Sn At Room Temperature (Utilizing Energy Absorbing Rings) -	109
4	Forgeability Limit Curves For Ti-6Al-4V At Room Temperature (Utilizing Energy Absorbing Rings) -	111
5	Forgeability Limit Curves For 17-4 PH At Room Temperature (Utilizing Energy Absorbing Rings) -----	113
6	Forgeability Limit Curves For A-286 At Room Temperature (Utilizing Energy Absorbing Rings) -----	115
7	Forgeability Limit Curves For Vascomax 300 At Room Temperature (Utilizing Energy Absorbing Rings) -----	117
8	Forgeability Limit Curves For TZM At Room Temperature (Utilizing Energy Absorbing Rings) -----	119
9	Forgeability Limit Curves For Rene' 41 At Room Temperature (Utilizing Energy Absorbing Rings) -----	121
10	Forgeability Limit Curves For L-605 At Room Temperature (Utilizing Energy Absorbing Rings) -----	123
11	Forgeability Limit Curves For 2024-0 Al At Room Temperature -----	125
12	Forgeability Limit Curves For 2024-0 Al At 550°F ----	127
13	Forgeability Limit Curves For 2024-0 Al At 750°F ----	129
14	Forgeability Limit Curves For Ti-5Al-2.5Sn At Room Temperature -----	131
15	Forgeability Limit Curves For Ti-5Al-2.5Sn At 750°F -----	133
16	Forgeability Limit Curves For Ti-5Al-2.5Sn At 1050°F -----	135
17	Forgeability Limit Curves For Ti-5Al-2.5Sn At 1350°F -----	137

# LIST OF GRAPHS (CONTINUED)

<u>Graph No.</u>		<u>Page No.</u>
18	Forgeability Limit Curves For Ti-5Al-2.5Sn At 1550°F -----	139
19	Forgeability Limit Curves For Ti-5Al-2.5Sn At 1750°F -----	141
20	Forgeability Limit Curves For Ti-5Al-2.5Sn At 1950°F -----	143
21	Forgeability Limit Curves For 17-4 PH At 550°F -----	145
22	Forgeability Limit Curves For 17-4 PH At 950°F -----	147
23	Forgeability Limit Curves For 17-4 PH At 1350°F -----	149
24	Forgeability Limit Curves For 17-4 PH At 1550°F -----	151
25	Forgeability Limit Curves For 17-4 PH At 1750°F -----	153
26	Forgeability Limit Curves For 17-4 PH At 1950°F -----	155
27	Forgeability Limit Curves For A-286 At Room Temperature -----	157
28	Forgeability Limit Curves For A-286 At 550°F -----	159
29	Forgeability Limit Curves For A-286 At 750°F -----	161
30	Forgeability Limit Curves For A-286 At 950°F -----	163
31	Forgeability Limit Curves For A-286 At 1050°F -----	165
32	Forgeability Limit Curves For A-286 At 1350°F -----	167
33	Forgeability Limit Curves For A-286 At 1550°F -----	169
34	Forgeability Limit Curves For A-286 At 1750°F -----	171
35	Forgeability Limit Curves For A-286 At 1950°F -----	173
36	Position - Time Curve For Specimen Number A7-943 ---	174
37	Position - Time Curve For Specimen Number A7-940 ---	175
38	Position - Time Curve For Specimen Number A7-927 ---	176
39	Position - Time Curve For Specimen Number A7-925 ---	177

# LIST OF GRAPHS (CONTINUED)

<u>Graph No.</u>		<u>Page No.</u>
40	Position - Time Curve For Specimen Number F7-944 ---	178
41	Position - Time Curve For Specimen Number F7-929 ---	179
42	Position - Time Curve For Specimen Number F7-930 ---	180
43	Position - Time Curve For Specimen Number F7-931 ---	181
44	Material Strength And Elongation As A Function Of Strain Rate (Phase I) -----	183
45	Material Strength And Elongation As A Function Of Strain Rate (Phase II) -----	195
46	Effects Of Strain Rate On Fatigue For 2024-0 At Room Temperature -----	206
47	Effects Of Strain Rate On Fatigue For 2024-0 At 550°F -----	207
48	Effects Of Strain Rate On Fatigue For 2024-0 At 750°F -----	208
49	Effects Of Strain Rate On Fatigue For Ti-5Al-2.5Sn At 1550°F -----	209
50	Effects Of Strain Rate On Fatigue For Ti-5Al-2.5Sn At 1950°F -----	210
51	Effects Of Strain Rate On Fatigue For 17-4 PH Stainless At 1550°F -----	211
52	Effects Of Strain Rate On Fatigue For 17-4 PH Stainless At 1950°F -----	212
53	Effects Of Strain Rate On Fatigue For Heat Treated 17-4 PH Stainless Steel At 1950°F -----	213
54	Effects Of Strain Rate On Fatigue For A-286 At 1050°F	214
55	Effects Of Strain Rate On Fatigue For A-286 At 1950°F	215
56	Effects Of Strain Rate On Fatigue For Heat Treated A-286 At 1950°F -----	216

## LIST OF SYMBOLS

$P$	forging pressure
$\sigma_0$	yield stress in simple tension
$\bar{\sigma}$	average flow stress
$E$	elastic modulus
$\gamma$	Poisson's ratio
$n$	strain hardening coefficient
$f$	frictional force
$\mu$	coefficient of friction
$K$	experimental constant
$H_0$	initial billet height (before deformation)
$H_f$	final billet height
$h$	instaneous billet height
$R_0$	initial billet radius
$R_f$	final billet radius
$r$	radial distance from center line of billet
$v$	instantaneous projectile and velocity
$V_0$	projectile velocity at impact
$\epsilon$	engineering strain
$\dot{\epsilon}_t$	average instantaneous strain rate $V_0/H_0$
$W$	projectile weight
$t$	time

## SECTION I

### INTRODUCTION

The dynamic response of metal alloys deformed under very high loading rates has attracted special interest. In some instances, improvements in the workability as well as the mechanical properties of the finished part can only be attributed to the fact that during deformation the material is subjected to high sustained strain rate

In the high energy impact forging process, velocity is substituted for mass to rapidly impart high levels of energy to the workpiece both in terms of shock loading and rapid deformation.

The specific objective of this program was to determine the effect of forging velocity (strain rate) on the ductility and toughness for a representative group of alloys in a temperature range from ambient to 1950°F.

The test program was accomplished in two phases. In Phase I, ten selected alloys were investigated over the zero to 8000 in/in/sec strain rate range for a determination of the overall dynamic effects on representative alloy systems.

In Phase II, four of the ten alloys were tested in greater detail by increasing the number of impact velocities as well as varying the amount of deformation at each velocity and forging temperature. The effect of temperature in the forging process and material response to post forming heat treatment was investigated.



## SECTION II

### TECHNICAL BACKGROUND

#### Static Forging

##### Forging Pressure

A cylindrical billet upset between two parallel plates develops a non-uniform pressure distribution across its surfaces. The pressure distribution at any time during the upset will depend on the following:

- (1) The original height and diameter of the billet
- (2) The instantaneous height at the time under consideration
- (3) The original flow stress of the material and its strain hardening characteristics
- (4) The frictional forces generated at the interfaces during deformation

Neglecting barreling, and making the usual assumptions of the theory of plasticity, a useful though non-rigorous equation is shown in equation 1, Appendix IV. This equation was used to estimate the peak die loads expected in static forging and to provide a basis for understanding the mechanical factors involved. Illustrations of typical static pressure distribution are shown in Figures 1 and 2.

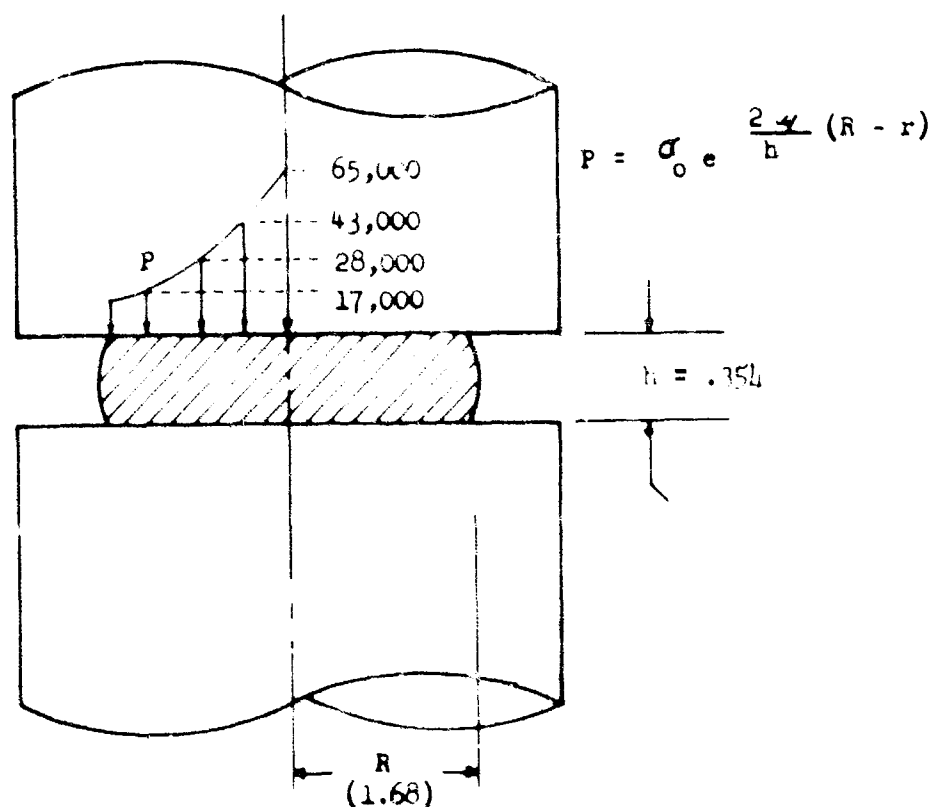


FIGURE 1. TYPICAL PRESSURE DISTRIBUTION ON A CYLINDRICAL BILLET  
FOR  $\sigma_0 = 10,000$  PSI,  $\mu = .12$  ASSUMING ZERO STRAIN HARDENING

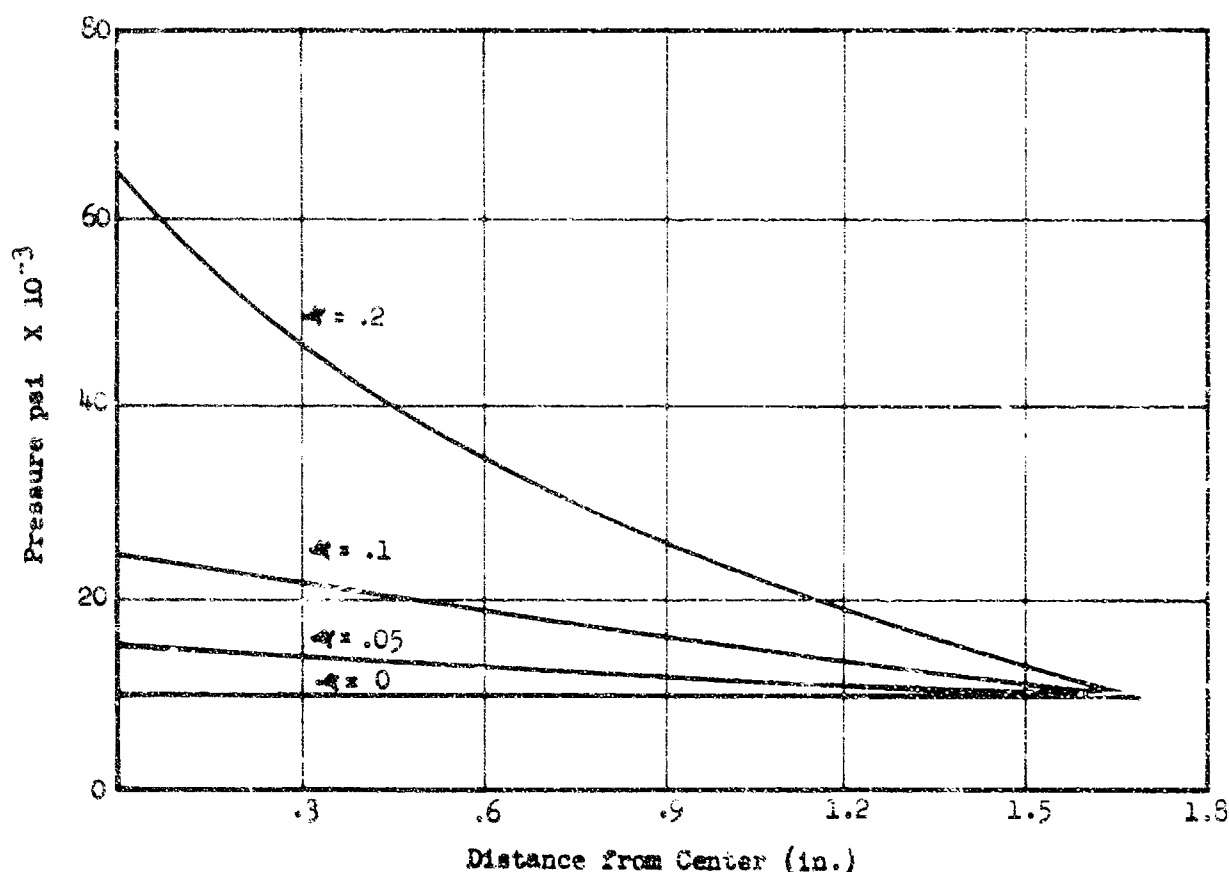


FIGURE 2. TYPICAL PRESSURE DISTRIBUTION ON A CYLINDRICAL BILLET FOR VARIOUS VALUES OF  $\mu$  ( $\sigma_0 = 10,000$  PSI)

The peak pressure occurs at the center of the billet where  $r = 0$

$$P_{(\max)} = \sigma_0 \left( 1 + \mu \frac{R}{h} \right)$$

The minimum die pressure occurs at the edge where ( $r = R$ ) and  $P_{(\min)} = \sigma_0$ .

#### Friction

It is evident that the primary result of interface friction is the generation of a pressure gradient through the specimen. The choice of  $\mu = .2$  in Figures 1 and 2 was completely arbitrary. In actual room temperature upsetting using a good lubricant, values of  $\mu$  are probably less than .05 based on the appearance of the billet surface after deformation. Good lubrication is evidenced by a smooth appearance of the billet surface. Sticking (a term used to signify an absence of sliding) of the inner area of the face due to poor lubrication is illustrated in Figure 3.

It has been shown (1) that at some critical value of  $\mu$ , relative sliding will not occur and upset takes place by the process of shear deformation

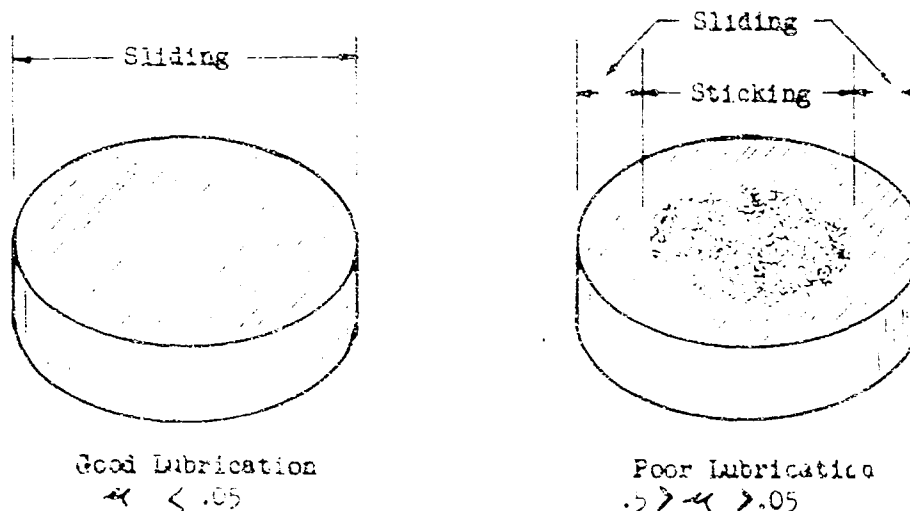


FIGURE 3. SURFACE APPEARANCE AFTER FORGING

within the billet. In general, sticking can occur when the frictional force is high enough to cause shear flow. Under these conditions the relation  $d\sigma_r/dr = dP/dr$  (equation 2, Appendix IV) is no longer valid. It can be corrected by re-evaluating the distortion-energy equation for a hydrostatic pressure equal to the normal pressure  $P$  and a superimposed shear stress  $f = \mu P$ . Under these conditions yielding will occur when

$$f = .577 \sigma_0 \quad (\mu = .577)$$

and the equation for pressure distribution becomes a linear function

$$P = K \sigma_0 \left( \frac{R - r}{h} \right)$$

The conditions resulting in combined sticking and sliding (illustrated in Figure 3) are especially useful in evaluating lubricants. The lubricant selected for this program provides a low frictional coefficient for all program materials with no visual evidence of sticking.

#### Die Deflection

As a result of the pressure rise in the center of the billet, a significant deformation of the anvils can occur as shown in Figure 4.

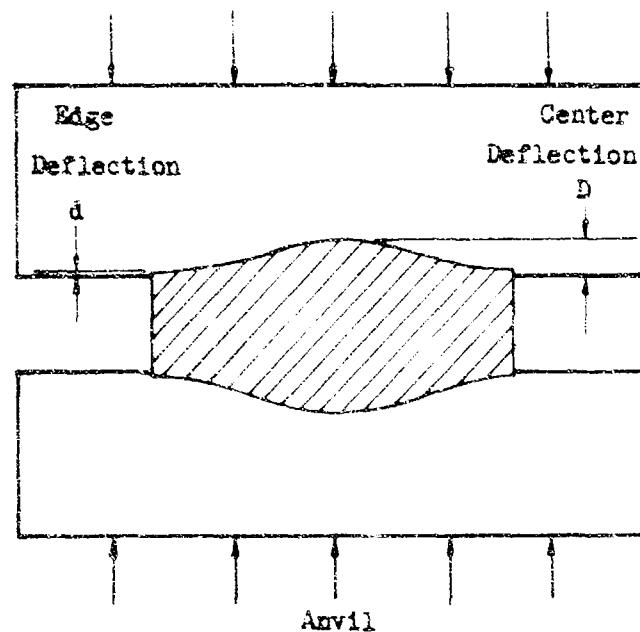


FIGURE 4. ANVIL DEFLECTION IN UPSET FORGING

The center and edge deflections can be derived in terms of the forging variables. The maximum deflection at the center of the billet is:

$$D = \frac{(1 - \nu^2) R}{2 E} \sigma_0 \left[ \frac{\exp\left(\frac{\mu R}{2h}\right) - 1}{\frac{\mu R}{2h}} \right]$$

where:  $\nu$  = Poisson's ratio  
 $E$  = Elastic Modulus  
 $\sigma_0$  = Yield Strength of Billet

The effect of die deflection is difficult to assess in terms of pressure distribution (note: rigid tooling was a necessary simplifying assumption in developing the pressure distribution equations). From sample calculations using the equation for die deflection, values of  $D$  on the order of .003 inches are reasonable for the high strength materials as shown in Figure 5.

In practice, this information is most useful in predicting the part tolerances and in the design of tooling relative to the selection of the die materials and heat treat requirements.

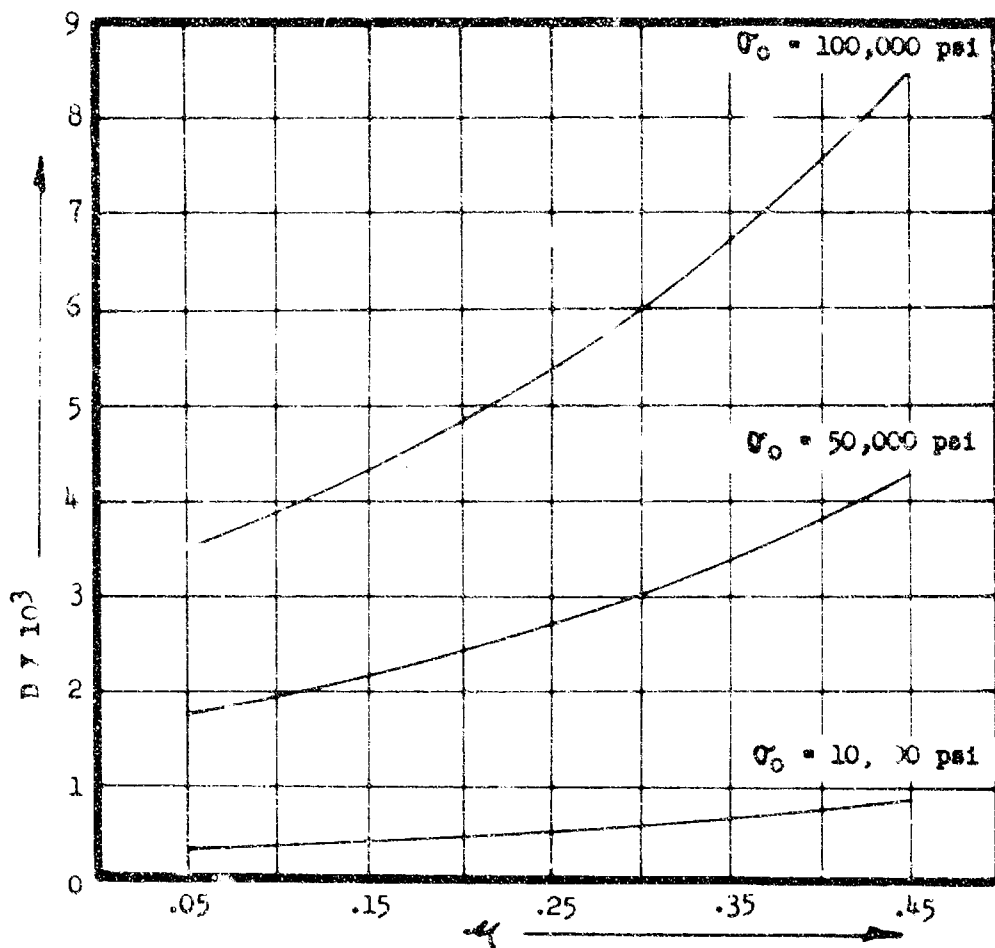


FIGURE 5 DIE DEFLECTION (D) VS COEFFICIENT OF FRICTION ( $\mu$ ) FOR VARIOUS STRENGTH MATERIALS

The most probable result of die deflection with regards to material ductility is a reduction in forgeability limits since the frictional forces leading to shear deformation or "sticking" of the surface layers of the billet are increased. This condition is illustrated in Figure 3.

### Strain Hardening

The equations for pressure distribution (equation 4, Appendix IV) and forging force (equation 5 Appendix IV) show the yield stress,  $\sigma_0$ , as a constant. Although this is a reasonable assumption for elevated temperature forging, serious deviations will occur at room temperature upsets above 20 to 30%. The flow curve can be approximated by the expression,

$$\sigma_0 = K e^n$$

where  $n$  is the strain hardening coefficient. An increase in the value of this material constant ( $n$ ) will have a similar effect on the forging force and pressure distribution, as an increase in the coefficient of friction and/or the  $R/h$  ratio. This becomes evident substituting  $K e^n$  in the equation for forging pressure shown in Figure 1.

$$P = K e^n \cdot e^{\frac{2\mu}{h} (R - r)}$$

### Temperature Rise

As a material undergoes plastic deformation, heat is generated internally. Approximately 90% of the work expended is converted into heat. Because of the variation in the quantity of heat required to produce a unit change in temperature (thermal capacity) for different metals, there is a considerable difference in the temperature rise exhibited by different alloys deformed equal amounts. Calculations for the adiabatic temperature rise for the program materials are shown in Table 1.

Isothermal conditions obtained only at very low strain rates and under favorable heat transfer conditions are usually not obtained in "static" tensile or compressive testing. Under normal press forging conditions at room temperature, the temperature rise from plastic work is sufficient to offset the increase in flow stress due to strain hardening. This type of strain rate effect is obviously less significant at elevated temperature.

### High Energy Impact Forging

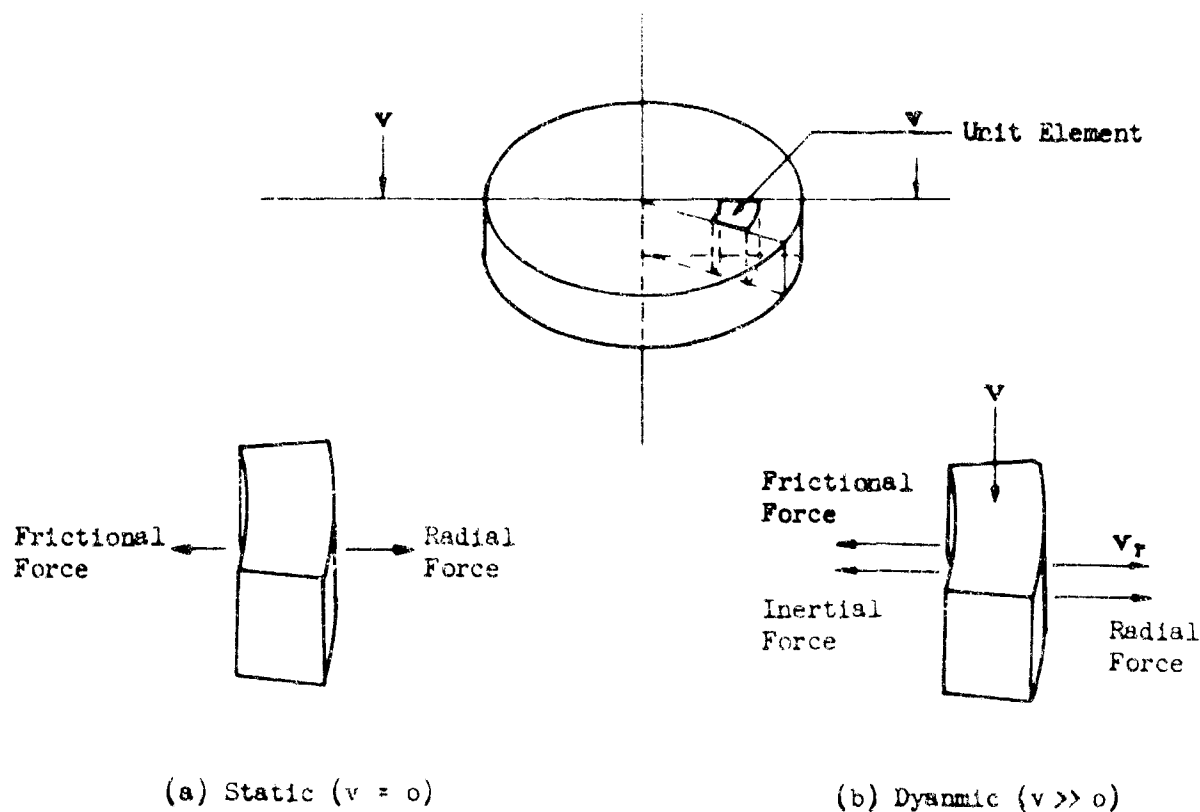
#### Forging Force

A cylindrical billet in high speed compressive deformation is subjected to dynamic forces due to the inertia of the deforming material. These forces act over a long time span as compared to time required for the plastic shock waves to dissipate. During the initial portion of deformation, the inertial forces are directed toward the center of the billet and give rise to a compressive radial stress.

The magnitude of the inertial forces at any time will depend on the following:

- (1) The projectile velocity
- (2) The deceleration of the projectile
- (3) The density of the test material
- (4) The instantaneous billet geometry
- (5) The particular location in the billet under consideration

The radial forces acting on a unit element, assuming a constant projectile velocity, are shown in Figure 6.



$$\frac{d\sigma_r}{dr} = -\frac{2f}{h}$$

$$\frac{d\sigma_r}{dr} = -\frac{2f}{h} - \rho \left( v_r \frac{\partial v_r}{\partial r} + \frac{\partial v_r}{\partial t} \right)$$

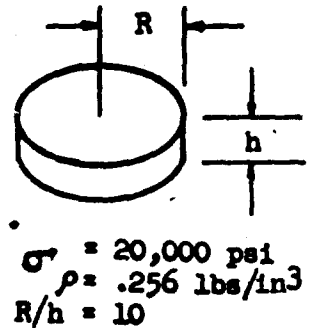
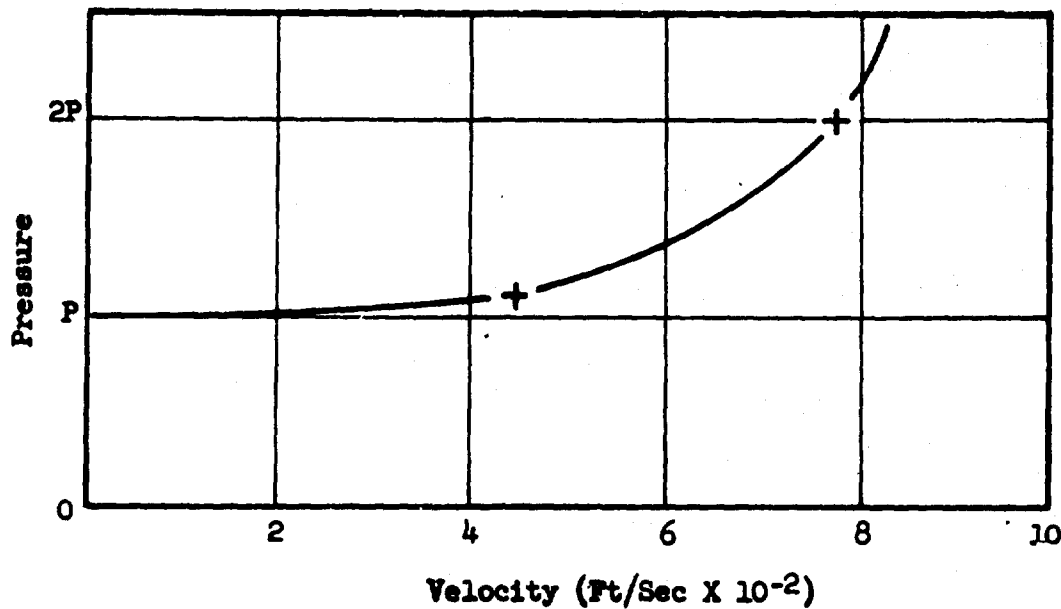
FIGURE 6. COMPARISON OF STATIC AND DYNAMIC EQUILIBRIUM STRESS DISTRIBUTION

The magnitude (2) of the dynamic pressure effect at the center of a cylindrical billet is illustrated in Figure 7.

This estimate shows the center pressure to be twice the static value at a velocity of 775 ft/sec.

The numerical value of the pressure ( $P$ ) at zero velocity, assuming a coefficient of friction ( $\mu = .05$ ), is given by:

$$P_{max} = \sigma_c e^{2\mu R/h} = 54,000 \text{ psi}$$



$$\begin{aligned}\sigma &= 20,000 \text{ psi} \\ \rho &= .256 \text{ lbs/in}^3 \\ R/h &= 10\end{aligned}$$

FIGURE 7. VARIATION OF MAXIMUM PRESSURE WITH PROJECTILE VELOCITY

In this example the value  $\sigma_0$  (yield strength in simple tension) is assumed constant. The value of  $\sigma_0$  is known (3) to be dependent on strain rate. Since the flow stress increases significantly with increasing strain rate for most materials and the effect of strain hardening has not been considered, a value of  $P$  on the order of 2 to 3 hundred thousand psi could reasonably be expected at 775 ft/sec for the material and billet geometry shown in Figure 7.

From a material forgeability standpoint, the inertial forces are of greater significance near the end of the forming sequence. As the projectile velocity approaches zero the test material is flowing outward at a high radial velocity. At some point in the process, the inertial force initially directed toward the center of the billet must reverse and appear as an outwardly directed tensile stress. This important aspect of impact forming is discussed in detail under "Strain Rate Effects".

#### Shock Wave Effects

Many instances of metallurgical changes occurring as a direct result of the passage of a high energy shock wave have been reported. For most of the experimental work in this area, high explosives have been used to generate the high impact pressures obtained. Although the mechanisms involved are presently the subject of much research effort, several types of changes have been considered:

- (a) Phase transformation of some component of the alloy system as, for example, the alpha-gamma transformation in carbon steel.



- (b) Ordinary deformation mechanisms that can occur in a very short time interval such as the formation of mechanical twins and slip bands.
- (c) Miscellaneous effects such as grain distortion and precipitation.

The importance of shock wave effects under the conditions that exist in this program will depend on two factors: (1) the pressure magnitude developed in the shock and (2) its time duration. The magnitude for peak pressure in an iron to iron impact at 2000 ft/ sec is roughly  $1.16 \times 10^6$  psi (80 kilobars). This is at the low end of the velocity spectrum usually studied using explosives and the upper limit for the present program. Although the observable changes in the metal structure diminish at lower shock wave pressures, some experimenters in this field place considerable significance on the effect of the initial shock impulse on subsequent deformation even in the lower velocity regime.

Figure 8 shows the relationship between impact velocity and the initial pressure in the shock wave (4).

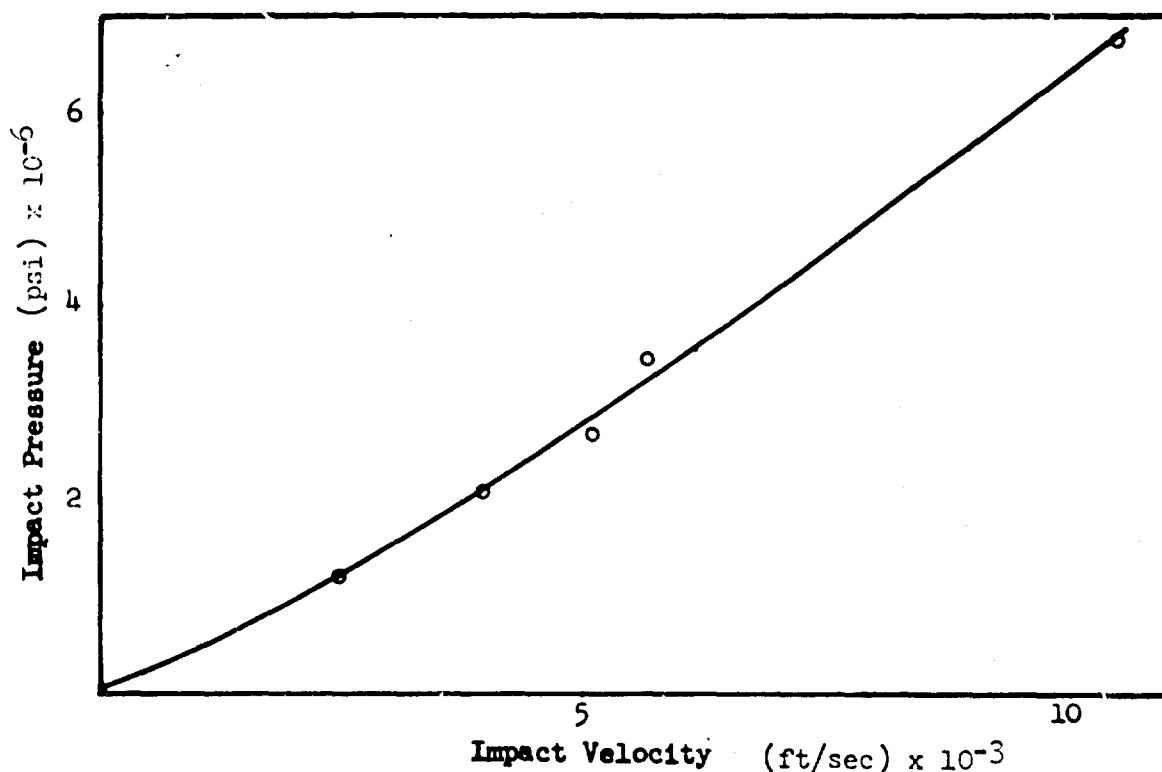


FIGURE 8. IMPACT PRESSURE VS IMPACT VELOCITY FOR AN IRON TO IRON IMPACT

## Strain Rate Effects

In order to arrive at a meaningful comparison between various high velocity impact forging processes, it is necessary to use parameters which have a common effect on each process. The present industrial practice of rating these processes by ram velocity alone leaves much to be desired for several reasons. Impact velocity influences deformation directly with respect to shock effects and the subsequent influence on the forming process, but it must be considered with respect to both gage length and geometry of the forging billet. At a point within the billet, local effects will be determined by the strain rate at that point. In addition, the billet geometry will determine the dynamic forces throughout the billet and alter the flow and stress fields.

As a result of these considerations, it may be seen that impact velocity must be considered in combination with other factors to arrive at a satisfactory solution to the comparison of results.

Strain rate, which is a point function within the field of the billet, may be used as a measure of local deformation and may be related satisfactorily to other variables with respect to material properties. Unfortunately, the general field mechanic equations, which describe material flow, have not as yet yielded a general solution that can be used with strain rate to develop a rigorous evaluation of the dynamic billet mechanics. Thus, it is necessary to formulate a scheme whereby these processes may be compared. Since flow fields should be similar for billets of the same geometry, it is reasonable to assume a one-to-one linear relationship between corresponding points so that the processes could be compared by means of external or surface boundary parameters. However, it should be remembered that variations in such parameters as friction and strain hardening will invalidate this correspondence to some degree. Under these assumptions it becomes feasible to evaluate and compare forging processes based on average strain rate which is generally defined as the product of the relative velocity of the ram or die faces and the reciprocal of their distance at any time during the deformation. If two billets are then deformed by equal amounts with similar velocity profiles (velocity vs. distance), meaningful comparisons of different materials will be possible. Neglecting differences in the dynamic forces, this comparison may be extended to billets of various sizes provided it is made on the basis of initial average strain rate, equal percentages of deformation and similar velocity profiles.

Average strain rate during forming is affected by both the velocity profile and the deformation as shown by the relationship of variables in the following equation.

$$\dot{\epsilon}_i = \frac{v(h)}{h} = \frac{v(h)}{(1-\epsilon)H_0}$$

where  $\dot{\epsilon}_i$  = average strain rate (instantaneous)  
 $v(h)$  = velocity profile  
 $h$  = instantaneous billet height  
 $H_0$  = initial billet height  
 $\epsilon$  = engineering strain (instantaneous)

It is apparent that the average strain rate will remain constant only for a velocity distribution which is a linear function of the instantaneous billet height. This would require either 100% deformation of the billet or a discontinuous velocity profile (one which instantaneously drops to zero). Obviously neither of these conditions can be attained in a normal forging operation. In addition, the forging force normally increases with deformation due to such factors as friction, work hardening, and surface area growth thus increasing the ram deceleration. Consequently, unless the initial velocity profile has a negative slope greater than  $V_0/H_0$ , the average strain rate will exceed the initial strain rate. This effect is illustrated in Figure 9 which shows the resultant strain rate profiles for typical velocity profiles. This effect is especially important for extreme deformations since most of the ram deceleration occurs in the latter portion of the deformation due to increased billet area and effects of friction as well as increases in flow stress due to higher strain rates.

Another important factor to be considered is the effect of billet size on forging forces and on the stresses produced by the dynamics of the forming process. As the billet geometry changes, the relative velocities of the boundaries also change. Assuming the billet volume remains constant, the boundary velocities are defined by a relationship such that the sum of the products of the velocity of each face and its respective area remains constant. This relationship also holds for the accelerations. At high deformations this means that the free portions of the billet may have a velocity much higher than the ram velocity. Since maximum deceleration of the ram occurs in the latter portion of forming, fracture will be initiated in some cases due to the dynamic stresses within the material. This must be considered when comparing billets of similar geometry and different sizes. If the initial strain rates are equal and equal deformations occur, higher ram velocities must be used on the larger billet. This results in higher acceleration of corresponding points in the larger billet, which also has a greater mass, and produces greater dynamic stresses. Consequently, similar results cannot be expected if large scale changes occur, and, in some instances, the applicability of high strain rate forming may be limited by the size of the billet.

In order to accomplish an effective study of high velocity impact forging on various materials, it is necessary to hold the variations in process parameters to a minimum. Thus, it becomes necessary to hold strain rate profiles uniform within a reasonable allowable deviation. Since differences in flow stress, friction effects, and strain rate effects eliminate this possibility with direct ram forging, it is desirable to control ram velocity by a method which is independent of the material being deformed. For this program, this is accomplished by deforming a secondary material simultaneously with the billet under study. The majority of the ram energy will be consumed by the secondary material, allowing a large degree of independence from the billet under study. In production applications, some form of damping could be used, especially in the reduction of peak strain rates.

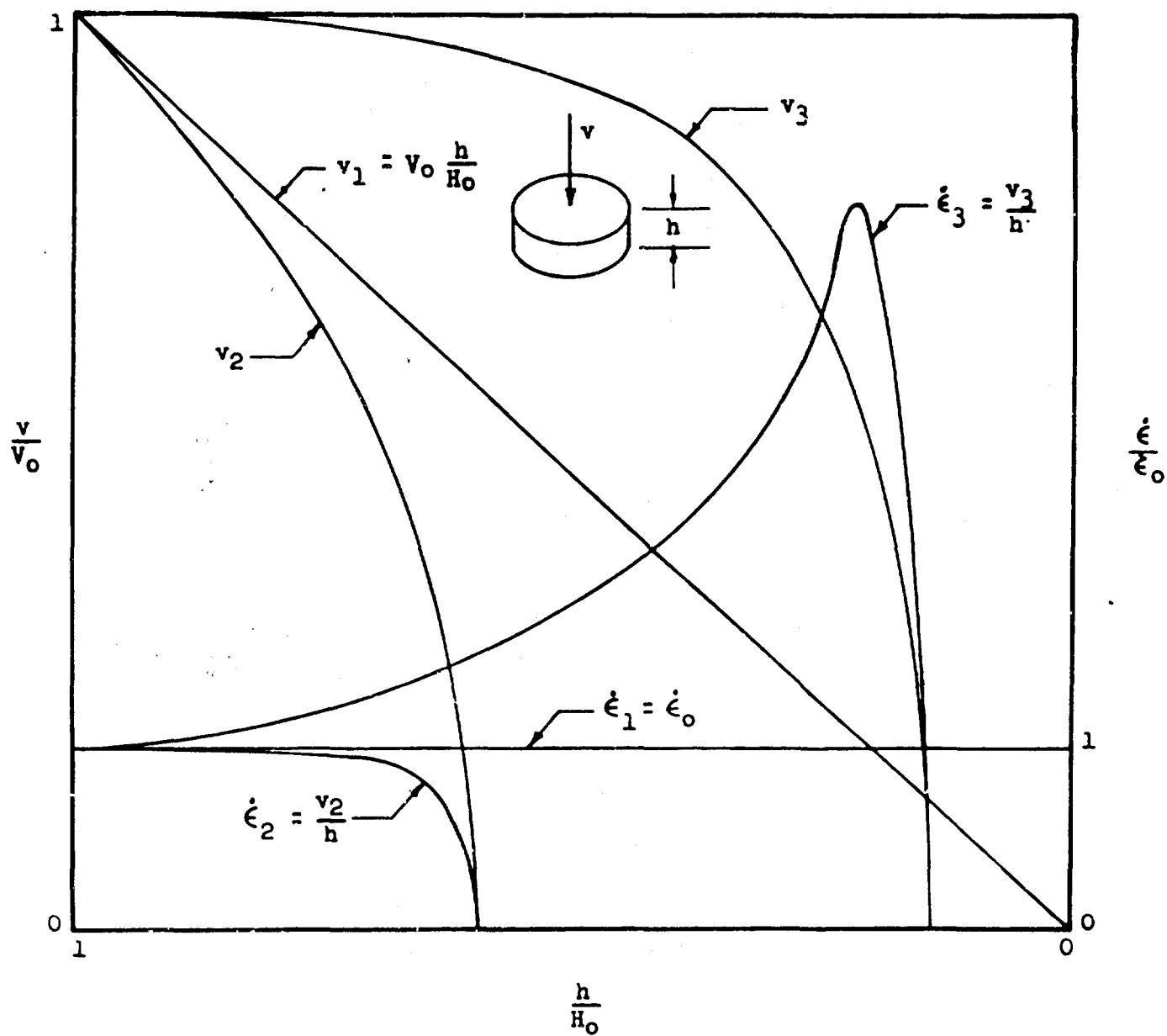


FIGURE 9. TYPICAL VELOCITY PROFILES WITH RESULTANT STRAIN RATE PROFILES

### Adiabatic Heating

The heat generated by high speed deformation produces effects not encountered in the low strain rate regimes associated with press forging and static tensile testing. The amount of heat generated is proportional to the mechanical work expended during deformation. The work per unit volume is given by the product of the average stress applied and the maximum principal strain. Neglecting variations in average stress due to strain rate effects, the amount of heat generated for a given amount of deformation is constant.

The temperature rise is given by the equation:

$$\Delta T = \frac{\bar{\sigma} e}{778.2 \rho S_H}$$

where:  $\Delta T$  = Temperature increase  
 $\bar{\sigma}$  = Average flow stress  
 $e$  = Maximum principal strain  
 $\rho$  = Material density  
 $S_H$  = Specific heat

Values for the adiabatic temperature increase for the Phase I materials upset to 50% strain are listed in Table 1.

TABLE 1. ADIABATIC TEMPERATURE INCREASE FOR PHASE I MATERIALS

Material	$\Delta T @ \epsilon = 0.5$ (°F)	Material	$\Delta T @ \epsilon = 0.5$ (°F)
Al 2024-0	44.3	A-286	122
Al 7075-0	55.5	18% Ni	123
Ti-5Al-2.5 Sn	300	TZM Moly	254
Ti-6Al-4V	310	Rene' 41	226
PH 15-7 Mo	222	L-605	190

The effects that adiabatic heating will have on material behavior under high energy impact conditions depend to a large extent on the deformation mechanics of a particular material. Materials with a large number of active slip systems would be expected to show a comparatively uniform temperature distribution throughout the specimen. Although a detail summary of the extensive research effort in the area of metallurgy dealing with adiabatic heating and associated strain rate effect is beyond the scope of this program, examples may be cited to illustrate the variety of material behavior that can occur. For example, it has been shown that most materials have a temperature range of reduced ductility, as shown in Figure 10. This is attributed to intergranular rupture arising from excessive grain boundary shearing.

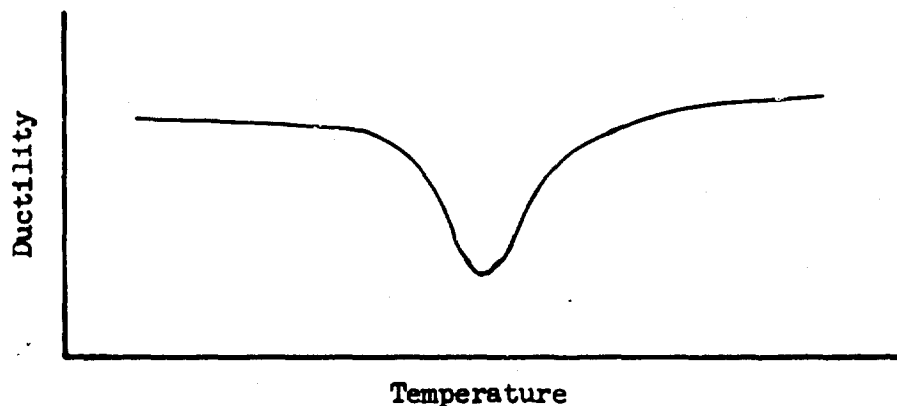


FIGURE 10. DUCTILITY VS TEMPERATURE UNDER LOW STRAIN RATE CONDITIONS

If this decrease in ductility is the result of grain boundary precipitation of a brittle phase, then increasing the strain rate in that temperature range would improve the ductility, since deformation would occur prior to the precipitation reaction. Adverse effects due to localized adiabatic heating can also occur when a low melting point second phase is present in the alloy structure.

## The Influence of Temperature and Strain Rate on the Coefficient of Friction ( $\mu$ )

### Introduction

Literature research in this area is difficult for several reasons not the least being that friction is usually regarded as a contributing factor in the various metalworking processes and, as such, may not be mentioned in report abstracts. In addition,  $\mu$  is usually calculated by different indirect methods, depending on the process, such that the numerical values obtained cannot be correlated with respect to temperature and strain rate effect without correction factors related to the individual process condition. Experimental work where  $\mu$  is investigated without regard to process applications is usually done under stringent laboratory conditions that cannot be obtained in production situations. With these qualifications, an order-of-magnitude quantitative evaluation may be obtained that is sufficient for the purposes of this program.

### Hydrodynamic Lubrication

In all processes involving large plastic deformation the machine designer concentrates on maintaining a continuous lubricant layer between the tools and the workpiece. The physical properties of the lubricant other than its shear strength are of prime importance in this respect. For upset forging the lubricant may fail after a certain amount of deformation, as shown in Figure 11, due to the fact that at this deformation the thickness of the lubricant film is not sufficient to separate the sliding metal surfaces.

### The Effect of Friction on Grain Flow

The analysis of friction based on the methods of Schreder and Webster (1) shows that sliding will occur up to a value of  $\mu = .577$ . If this critical value exists over the surface of the billet, deformation will be concentrated in the material near the surfaces, and will radically alter the grain flow pattern, as shown in Figure 12.

### Effect of Temperature on the Lubricant

There is experimental data (5) showing that lamellar solids such as graphite fail to provide lubrication when applied to heated billets or dies above 550°F. If this lubricant is applied to cold dies, good lubrication is obtained for titanium billets up to 1400°F range under low strain rate forging. This is illustrated in Figure 13.

$\epsilon$	D	$\mu$
65	87	.35
60	56	.23
50	33	.18
40	15	.13

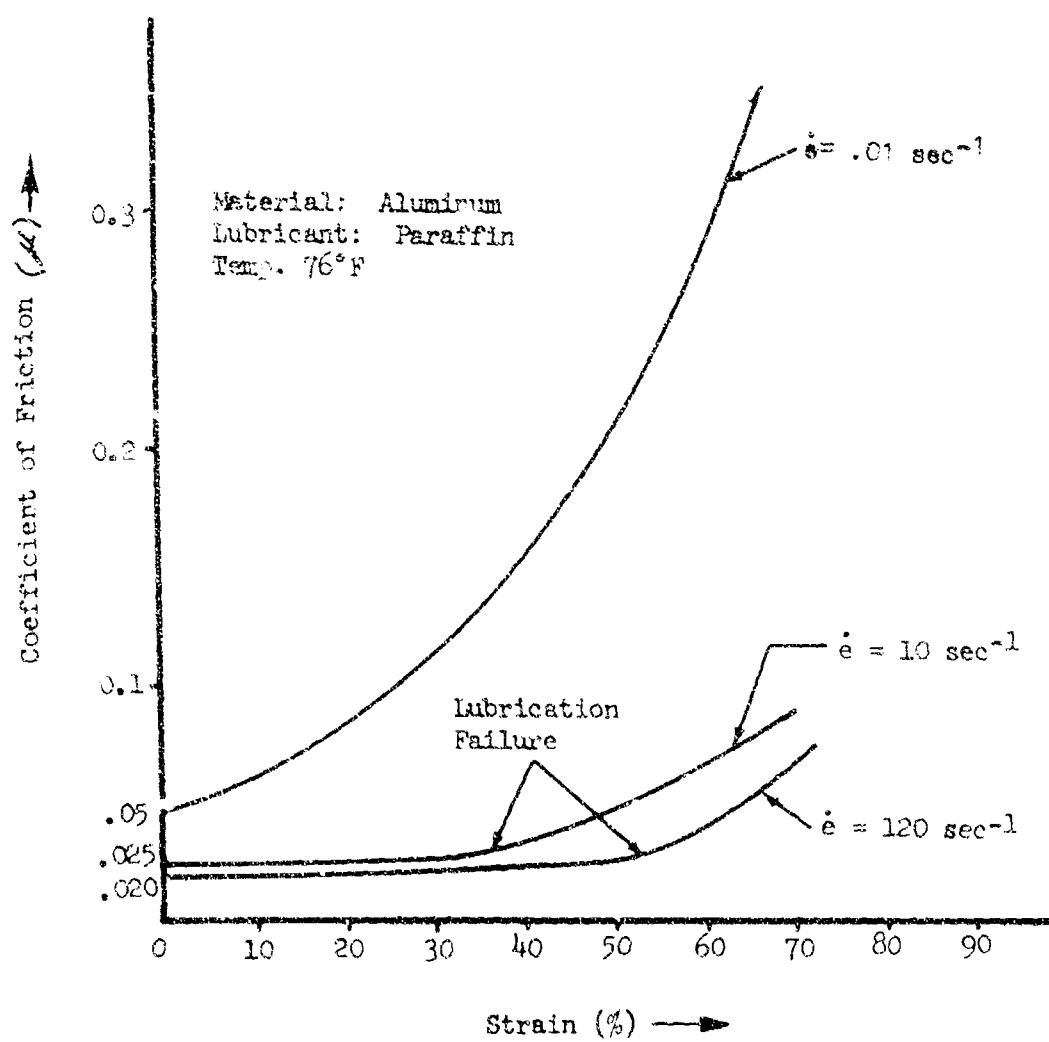
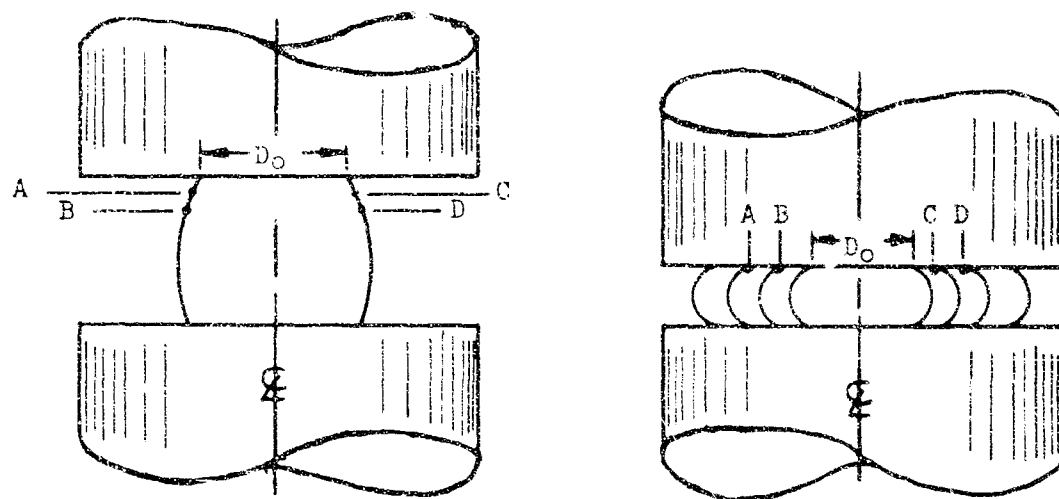
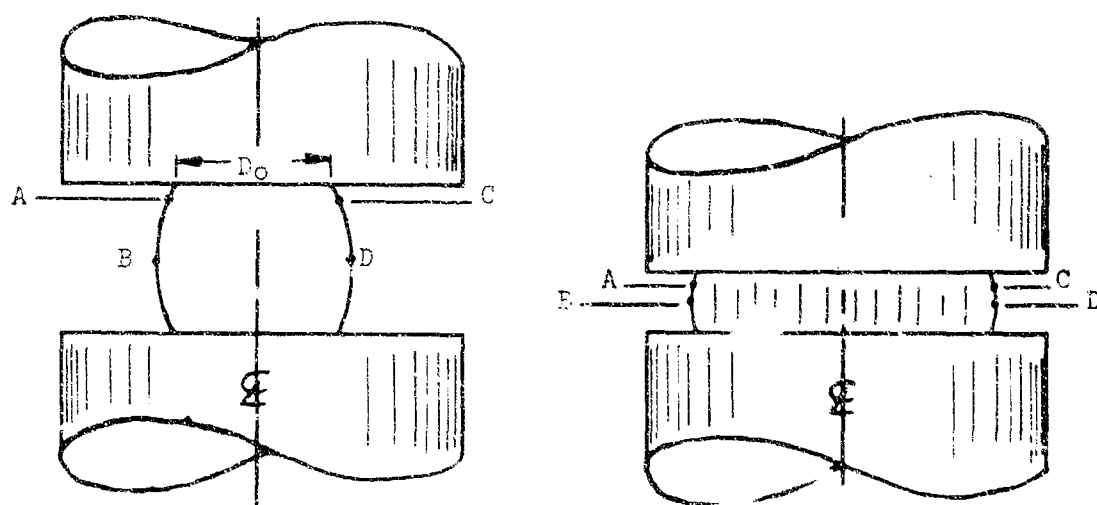


FIGURE 1.1. EFFECT OF STRAIN AND STRAIN RATE ON THE FRICTIONAL COEFFICIENT ( $\mu$ )





(a)  $\mu \geq .577$  (sticking)



(b)  $\mu \ll .577$  (sliding)

FIGURE 10. EFFECT OF FRICTION ON GRAIN FLOW AT LOW STRAIN RATES

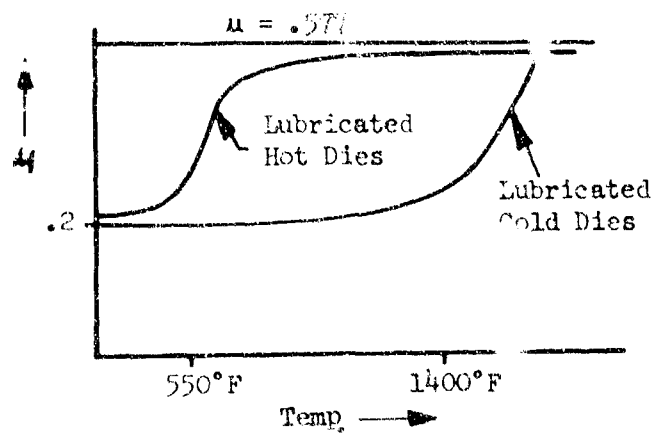


FIGURE 11. EFFECT OF TEMPERATURE ON GRAPHITE LUBRICANT

### Effect of Temperature on Friction ( $\mu$ )

Studies in a number of different hot metalworking processes (5) involving bulk plastic deformation show a general qualitative agreement for the effect of temperature on the frictional coefficient although the calculated values differ somewhat. Figure 14 shows the temperature effect for mild steel and aluminum.

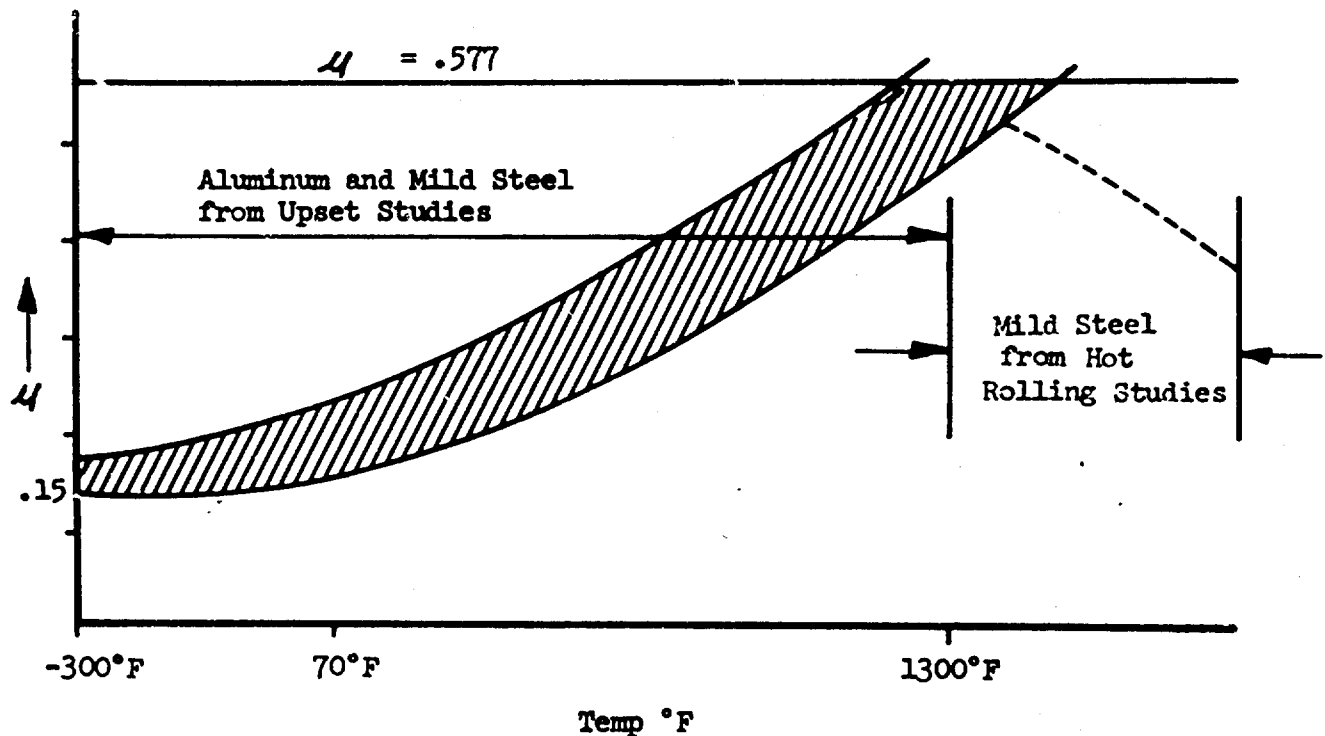


FIGURE 14. TEMPERATURE EFFECT ON FRICTION FOR UNLUBRICATED MATERIAL

### Effect of Strain Rate on Friction

The frictional coefficient is dependent on the strain and strain rate as shown in Figure 15. The two highest strain rates show that  $\mu$  is independent of the amount of strain up to the 30-40% range where the lubricant film is no longer thick enough to separate the metal surfaces. Since the forging force required to produce a given amount of deformation is constant, and from the fact that lubricant failure occurred at a larger deformation for the higher strain rate, it is reasonable to assume that less lubricant was "squeezed out" at the higher strain rate.

## SECTION III

### TEST MATERIALS

#### Vendor Data

All of the test materials were purchased through normal procedures and are representative of currently available stock. The materials were ordered to the appropriate specification for upset forging. For all alloys other than aluminum, specifications requiring vacuum induction melting and/or vacuum consumable electrode arc melting in the primary processing were used. The molybdenum alloy (T7M), was ordered arc-cast, extruded and recrystallized. The chemical compositions compiled from vendor supplied certified test reports are presented in Appendix I, Table III. Certified test data for mechanical properties, material specifications, and miscellaneous heat treat information are given in Appendix I, Table IV.

#### Material Processing

##### Billet Identification

In order to maintain "Traceability," individual billets were given identification numbers composed of a letter designating the alloy and a number to distinguish the different billets received for each material. Table V, Appendix I, lists the billet identification, materials and type of tests performed.

##### Billet Inspection

Upon receipt, the measured dimensions of each billet were verified against the purchase order and the vendors test report. Ultrasonic inspection was used to inspect each material for internal defects.

##### Control Specimen

A one half inch length of material was removed from the end of each billet at the time of the initial identification. This control specimen was steel stamped with the letter "C" in addition to the billet identification and placed in storage.

## SECTION IV

### PHASE I AMBIENT TEMPERATURE MATERIAL SCREENING

#### Introduction

In Phase I, ten selected alloys were investigated over the strain rate range from static to 8000 in/in/sec at room temperature. The material behavior in large plastic deformation was tested as a function of upsetting speed. The two main areas of material behavior considered were; (1) forgeability and (2) as-forged mechanical properties. The ten materials selected for investigations in this phase of the program were:

- 2024-aluminum
- 7075-aluminum
- Ti-5Al-2.5Sn
- Ti-6Al-4V
- 17-4 PH steel
- A-286 steel
- 18% Ni maraging steel (Vascomax 300)
- TZM molybdenum alloy
- Rene' 41 super alloy
- L-605 super alloy

#### Forgeability Evaluation

##### Introduction:

Forgeability was tested by the standard upset method wherein a cylindrical billet is upset between parallel plane surfaces until failure by metal separation occurs in the billet.

For this program the diameter and height (one inch each) of all billets were made equal with the exception of a small number of aluminum specimens as noted in the test data.

Experimental Plan - The plan for investigating the effect of forming speed on forgeability was to upset a series of billets for a particular material to increasing amounts of deformation, using a given projectile, until a failure limit was reached. This test was then repeated for a number of different ram projectiles such that the net effect of deformation rate on ductility was obtained. All other factors that influence the failure limit, such as lubricant and surface finish, were held constant. Figure 15 shows a typical test series for varying degrees of deformation.

The ram velocity change between points c and d is small in relation to the slope of the limit line, therefore strain rate effects over this interval can be neglected.

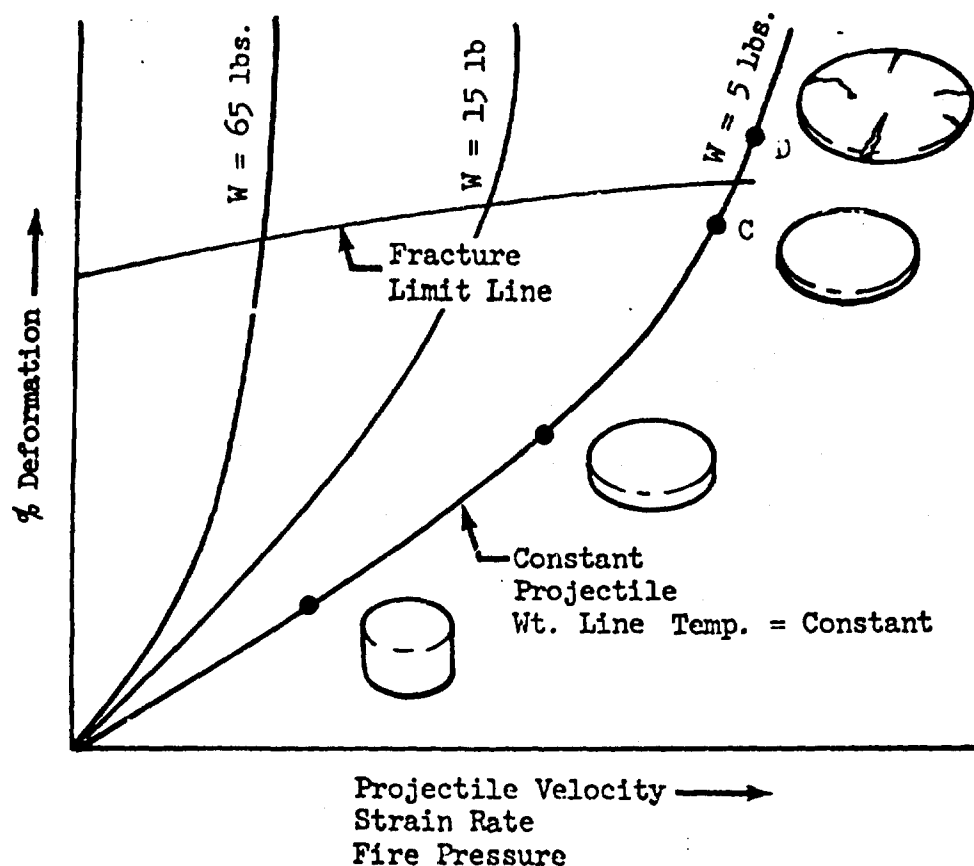


FIGURE 15. TYPICAL UPSET TEST SERIES

Energy absorbing rings were used as part of the test machine to provide a nearly constant projectile deceleration for the various materials tested. A second consideration was that without the use of bumper rings the testing of brittle materials, capable of absorbing only small amounts of energy, would be limited to very low velocities even with the lightest practical projectile design. Other alternative experimental plans were prohibitive from a program scope standpoint. The mild steel bumper rings were machined to the same height as the billet with the inside and outside diameters varied to adjust for the amount of excess energy in a given test condition. In all tests the inside diameters of the rings were sufficiently large to prevent contact with the billet during upset as shown in Figure 16.

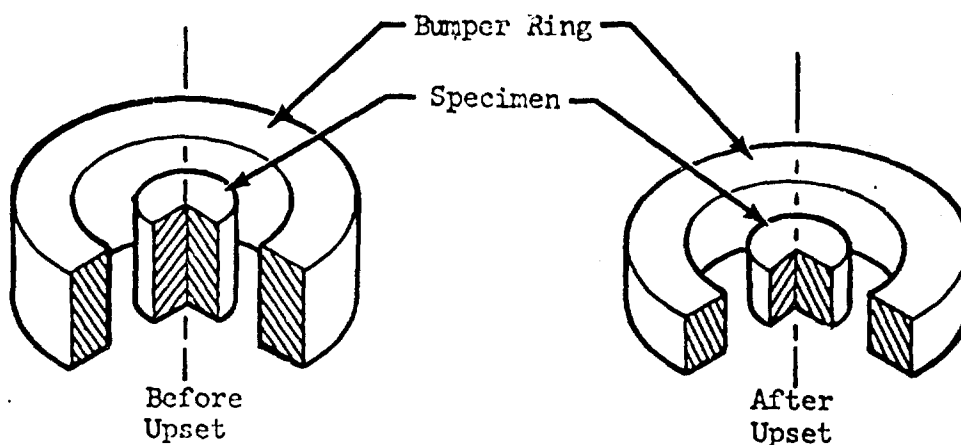


FIGURE 16. TYPICAL PHASE I UPSET TEST

Bumper rings were not used on the 1.5 inch diameter specimens for both of the aluminum alloys. As is evident from Figure 16, most of the projectile energy goes into plastically deforming the ring because of its larger volume. Using this technique, the instantaneous values of ram velocity during upset are practically independent of the material being tested.

#### Equipment Used

The static upset testing was accomplished using a production hydraulic press fitted with a special tool designed to transfer the load to the work piece through replaceable, hardened die inserts. The ram speed was controlled manually with the aid of an extensometer. A nominal ram speed of four inches per minute was used. The detailed description of this equipment is given in Appendix VI.

Dynamic upset tests were performed using a compressed gas high velocity projectile mechanism also discussed in Appendix VI. The projectile (moving ram) and the anvils for this program were fabricated of 4340 tool steel hardened to Rockwell C-50. The projectile and anvil faces were ground to a finish on the order of 20 RMS. Three basic projectile designs were used as shown in Figure 17. For low velocity shots requiring high energy, sectional projectiles

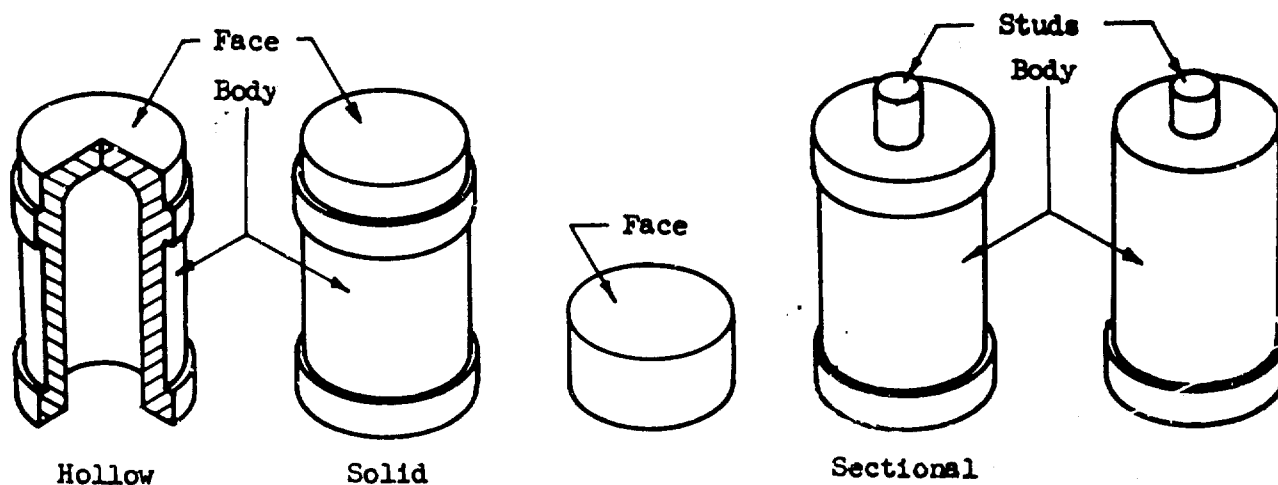


FIGURE 17. PROJECTILE CONFIGURATIONS USED

weighing up to 120 lbs were used. High velocity tests required the use of hollowed projectiles in order to obtain the necessary velocity and energy combination.

#### Data Acquisition

The raw data generated by these tests is as follows:

- (1) Specimen Number - Each specimen is identified by a five digit number as, for example, B3-004. The first two characters identify the type of material and the particular bar from which the specimen was

cut. The example given identifies the fourth specimen (-004) cut from 7075 aluminum (B) bar (3).

- (2) Projectile weight - (W) pounds
- (3) Gas Gun Fire Pressure ( $P_o$ ) psi
- (4) Projectile Impact Velocity - ( $V_o$ ) - This is the measured velocity of the projectile in ft/sec. at a point on the barrel approximately six inches from the point of impact.
- (5) Initial Billet Height - ( $H_o$ ) inches
- (6) Final Billet Height - ( $H_f$ ) inches
- (7) Temperature - All of the Phase I tests were performed at ambient temperature.
- (8) Failure Observation - after upset, each specimen was cleaned and visually inspected for surface cracks. The specimens were classified as good, incipient, or fractured. The term incipient is used in two senses; (1) in the usual sense to denote a small crack or cracks and (2) to indicate that a very slight reduction in deformation would have produced a good part regardless of the severity of the fracture.
- (9) Photographs - Photographs of representative specimens are presented with each forgeability limit plot in order to show the various types of fracture obtained.

## Results

The raw and processed data for Phase I forgeability testing are presented in Appendix II, Graphs 1 through 10 and Appendix III, Table VII.

In the forgeability graphs, ductility is plotted in terms of engineering strain vs. the strain rate at impact. Strain and initial strain rate are calculated as follows:

$$e = \frac{H_o - H_f}{H_o} \times 100 \text{ and } \frac{de}{dt} = \dot{e} = \frac{V_o}{H_o}$$

These values are listed in the tables as well as the kinetic energy of the projectile at impact. The energy is calculated from the weight and velocity of the projectile as shown by the following equation.

$$K.E. = \frac{W V_o^2}{64.4}$$

All Phase I materials with the exception of the molybdenum alloy (TZM) were found to exhibit significant ductility at room temperature over the program strain rate range from 0 to 8000 in/in/sec. Analysis of the processed data suggests an empirical classification based on the strain rate response of the test materials as shown in Figure 18.

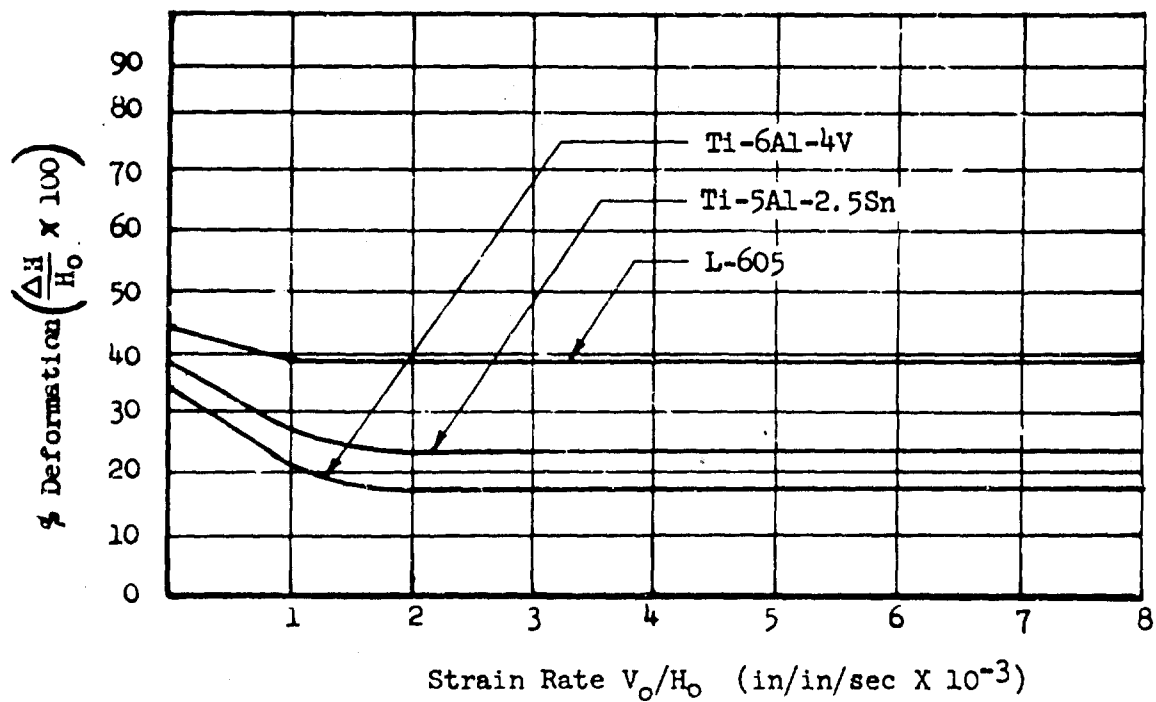
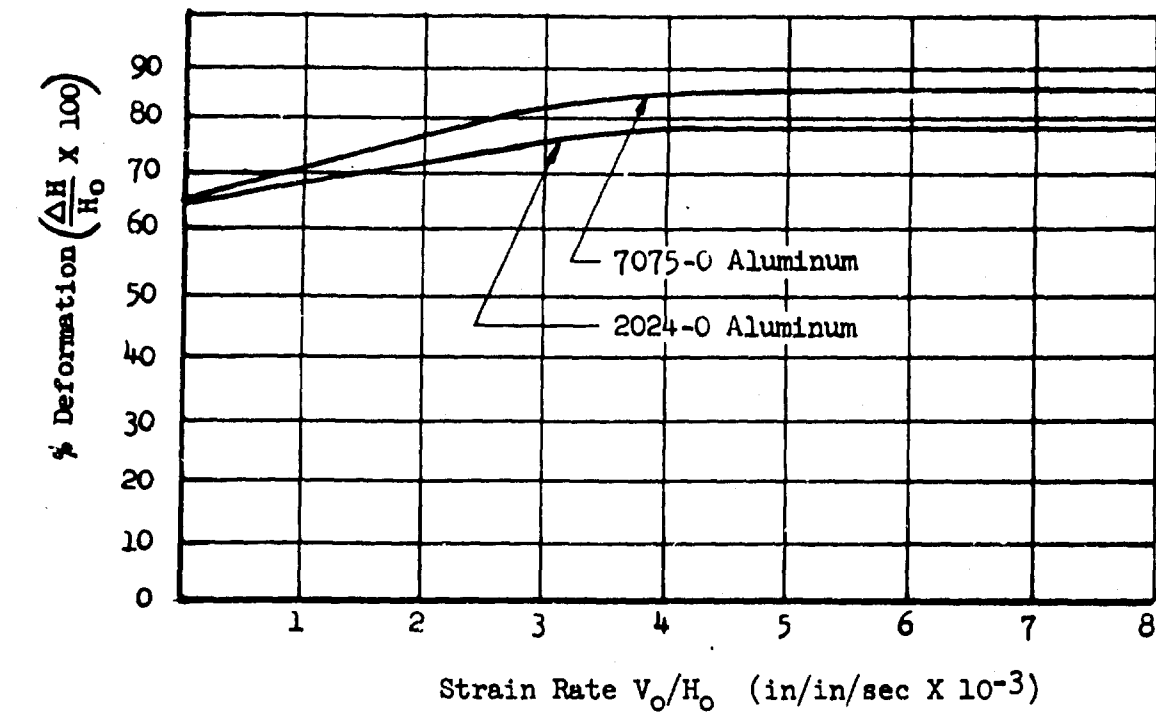


FIGURE 18. CLASSIFICATION OF PHASE I MATERIALS BASED ON DYNAMIC RESPONSE.



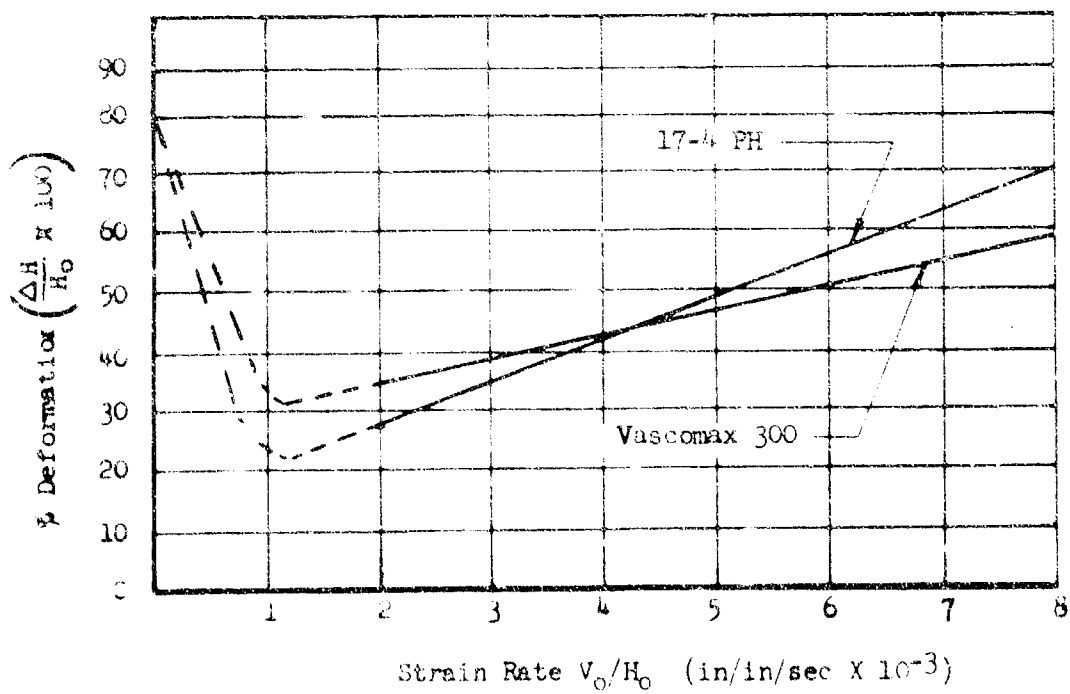
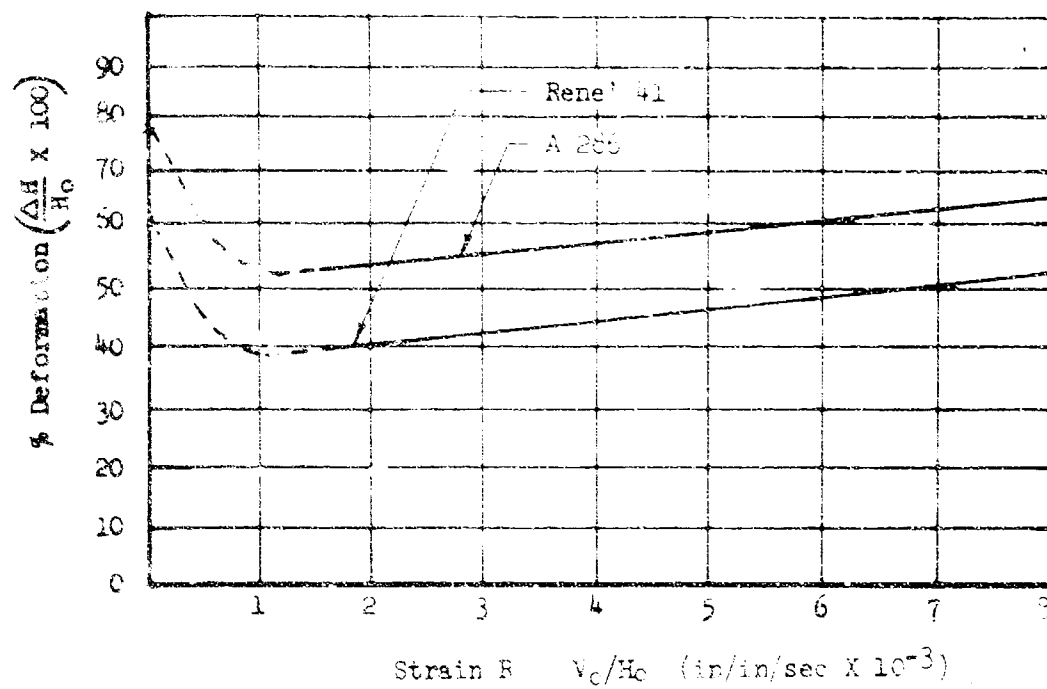


FIGURE 18. CLASSIFICATION OF PHASE I MATERIALS BASED ON DYNAMIC RESPONSE. ( CONTINUED )

The predominant feature of the deformation vs. strain rate limit curves is the pronounced change in behavior that occurs for all materials with the possible exception of L-605, at strain rates in excess of 1000 in/in/sec. The ductility limit of L-605 is for all practical purposes independent of strain rate. The recovery of ductility exhibited by Rene' 41, A-286, 17-4 PH, and Vascomax 300 at the high strain rates is significant from the standpoint of developing processes for small parts.

Mechanical Properties Evaluation  
of  
Material Upset Forged at Room Temperature

Introduction

The purpose of this segment of the program was to investigate, under controlled conditions, the effect of forging rate on the final mechanical properties of a broad cross-section of metal alloys.

The mechanical properties being considered were hardness, yield strength, ultimate strength, modulus, and one inch elongation. These mechanical properties were measured at room temperature using as-forged specimens.

Experimental Plan

Based on the room temperature forgeability test results, eight of the ten Phase I materials were selected for mechanical properties evaluation as shown in Figure 19.

Material	CALCULATED TEST CONDITIONS				
	% Upset Required	Intermediate $\epsilon = (4000)$		High $\epsilon = (8000)$	
		Proj. Wt.	Chmbr. Pres.	Proj. Wt.	Chmbr. Pres.
2024-0 Al	35	23.8	150	7.48	225
	65	23.8	230	12	465
7075-0 Al	35	23.8	175	7.48	235
	65	23.8	260	12	480
Titanium	15	67.3	170	18.9	175
17-4 PH	20	67.3	155		
A-286	35	57.5	320	23.8	300
	50	57.5	320	15	420
Vascomax 300	20	18.9	175	9.7	225
Rene' 41	25	67.3	245	9.2	370
L-605	20	67.3	165	9.7	235
	35	67.3	325	18.9	390

FIGURE 19. EXPERIMENTAL TEST PLAN

The two materials not listed (Titanium 6Al-4V and TZM) were not sufficiently ductile at room temperature under high velocity conditions to permit enough upset for a meaningful evaluation.

In order to evaluate the effect of deformation rate on as-forged mechanical properties, bar shaped test specimens ( $\frac{1}{2}$ " x  $\frac{1}{2}$ " x  $4\frac{1}{2}$ " ) were cut from round stock as shown in Figure 20.

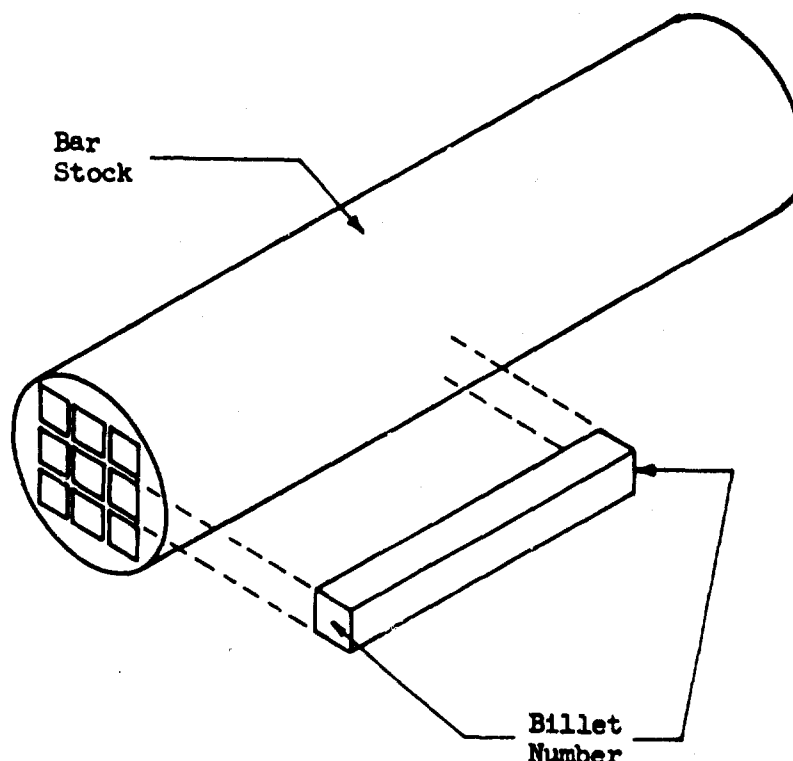


FIGURE 20. BILLET LOCATION IN BAR STOCK

The individual bar specimens were assigned numbers and identified by steel stamping prior to being removed from the round stock. In addition, their location in the stock material was recorded. Hardness tests were performed on billet specimens taken from both the center and edge areas of the bar stock. Representative photomicrographs were made for each material in the as-received state.

The next step in the experimental test plan was to upset the specimens according to the predetermined conditions listed in Figure 19. The test sequence is illustrated in Figure 21.

Preliminary testing showed that two mild steel bumper bars of the same dimensions as the test billet were required to absorb the excess projectile energy for tests in the 3000 in/in/sec strain rate range. The specimen was taped tightly between the bumper bars. Although the projectile face was flat, the fixed anvil was ground with a transverse slot .012" x 1.55" to insure that the specimen and bars remained in contact during passage of the initial elastic shock wave. The placement of the test piece on the fixed anvil is shown in Figure 22.

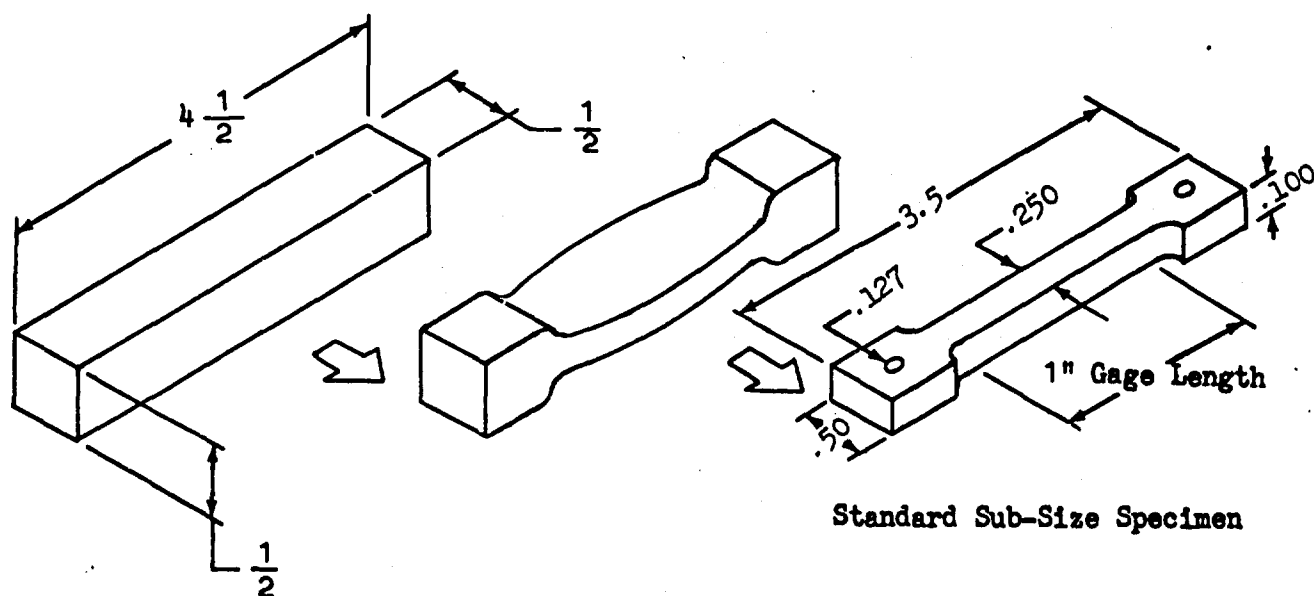


FIGURE 21 . FABRICATION OF STATIC TENSILE TEST COUPON

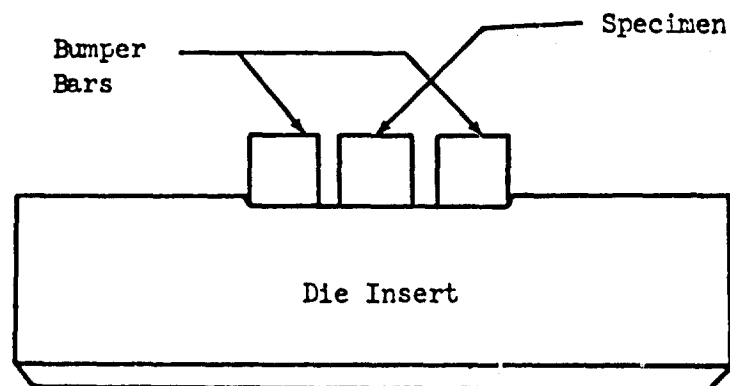


FIGURE 22 . FIXED ANVIL SHOWN WITH SPECIMEN IN FORGING POSITION

Projectile weight and fire pressure, as listed in Figure 19 , were determined from preliminary bumper bar tests and by making use of the gas gun performance curves shown in Figure 146 , Appendix VII.

ASTM Standard sub-size tensile specimens were cut from the center portion of the upset billets to the dimensions shown in Figure 21.

The last step in the experimental plan was the tensile and hardness testing by standard test methods. Modulus was calculated from load deflection curves recorded over the initial portion of the tensile test.

#### Equipment Used

The equipment used for bar upsetting at low and high velocities was the same as that used for upsetting cylindrical billets. This equipment is discussed in detail in Appendix VI.

#### Data Acquisition

The primary data for mechanical properties evaluation is presented in two different tables. In Table VII, Appendix III, entitled High Strain Rate Ductility Results for Phase I Specimens, raw data including specimen number, projectile weight, gas chamber pressure, initial specimen height, final specimen height and temperature and calculated data including impact velocity, strain rate, kinetic energy and percent reduction is recorded. The recorded data in Table VIII, Appendix III, entitled Phase I Tensile Properties of Forged Specimens, includes tensile yield, tensile ultimate, percent elongation, hardness and modulus.

The strain rate at impact ( $\dot{\epsilon}_0$ ) was calculated from the projectile velocity ( $V_0$ ) and the specimen height ( $H_0$ ), as given in Table VII. Values from the tensile test data are plotted against initial strain rate.

#### Results

The effect of strain rate on tensile ultimate, tensile yield and elongation are demonstrated by the curves in Graph 44, Appendix II. The results of the mechanical properties tests for all Phase I materials are summarized in Table II. In general the program materials show increased strength and ductility as the strain rate is increased. For 2024-O aluminum, A-286 and L-605 there is a appreciable increase in yield and ultimate strength with no loss in ductility. For four materials 7075-O Al, Ti 5Al-2.5Sn, Vascomax 300 and 17-4 PH the final mechanical properties are seen to be independent of the strain rate within experimental limits. Rene' 41, while showing a 10,000 psi and a 5,000 psi increase respectively in yield and ultimate strength, suffers a ductility decrease of approximately 2.5 percent.

#### Metallurgical Data

##### Introduction

The primary objective of the tests conducted in this part of the program was to provide additional information that might aid in explaining the dynamic behavior experimentally established previously in the forgeability and the as-forged mechanical properties investigation.

TABLE II. STRAIN RATE EFFECTS ON THE AS-FORGED  
MECHANICAL PROPERTIES AT ROOM TEMPERATURE

Material	Property				
	% Def.	Hardness	Yield Strength	Ultimate Strength	1 Inch Elongation
2024-0 Aluminum	35	I	I	I	NC
	65	I	NC	D(S)	NC
7075-0 Aluminum	35	I	NC	NC	NC
	65	I	NC	NC	NC
Ti-5Al-2.5Sn	15	NC	NC	NC	NC
A-286	35	I	I	I	D(S)
	50	---	I	I	D(S)
17-4 PH	20	NC	NC	NC	I
Vascomax 300	20	NC	NC	NC	NC
Rene' 41	25	I	I	I	D(L)
L-605	20	NC	I	I	NC
	35	---	---	---	NC

D(L)-Large Decrease  
D -Decrease  
D(S)-Slight Decrease

I -Increase  
NC-No Change

Four methods of obtaining information on the metallurgical level were used:

- (1) Standard Photomicrographs
- (2) Electron Photomicrographs
- (3) X-Ray Diffraction
- (4) Photomacrographs

The first two methods are useful in showing basic changes in the deformation mechanisms by which plastic flow occurs. The third, x-ray diffraction, is an accurate method of finding minute differences in the atomic spacing below the level of direct observation and was used in this investigation to examine the atomic lattice for residual elastic strain. The fourth, photomacrographs, are required to examine the grain flow aspects of the problem.

### Photomicrographs

Specimens selected for examination were taken from the Phase I test program therefore are for conditions of room temperature upset with no subsequent heat treatment. As can be seen from the data given with each photomicrograph, strain (the amount of upset deformation) is constant for a given material with strain rate variable.

Photomicrographs were made at three different sectional views for each specimen. For a given material, strain rates corresponding to static, intermediate (approximately 5000 per sec) and high (approximately 8000 per sec) were examined. These data are presented in Figures 107 thru 126, Appendix V.

The view direction in relation to the billet geometry and the impact direction is given in Figure 23 below.

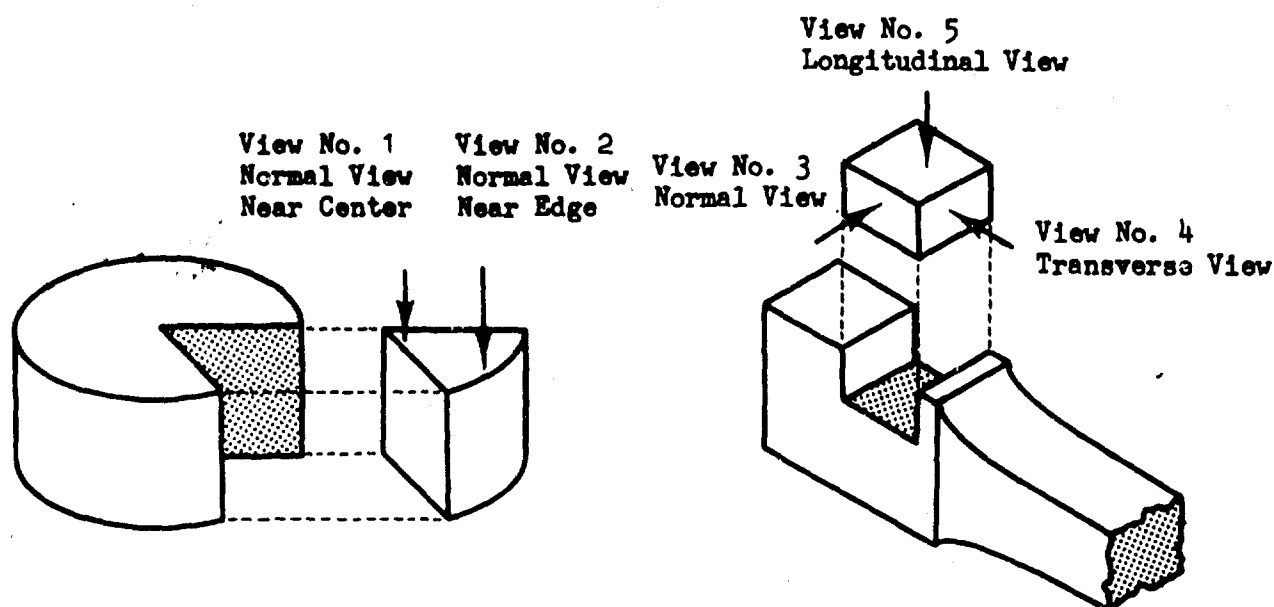
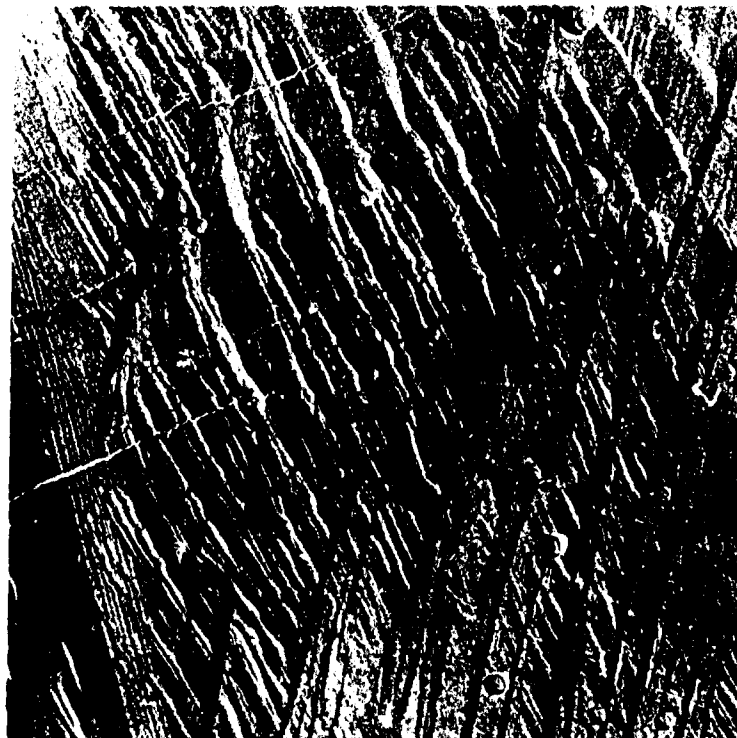


FIGURE 23. PHOTOMICROGRAPH VIEW DIRECTIONS

### Electron Photomicrographs

The electron photomicrographs of Figure 24, show a typical area within a grain boundary of specimen no. J1-009. The approximate location is noted on the photomicrograph in Figure 125, Appendix V and shows slip bands present in the L-605.

Specimen no.: J1-009  
Direction: View no. 4  
Magnification: 6000X  
Strain: 35.0%  
Strain rate: 7010 (1/sec.)



Specimen no.: J1-009  
Direction: View no. 4  
Magnification: 20,000X  
Strain: 35.0%  
Strain rate: 7010 (1/sec.)

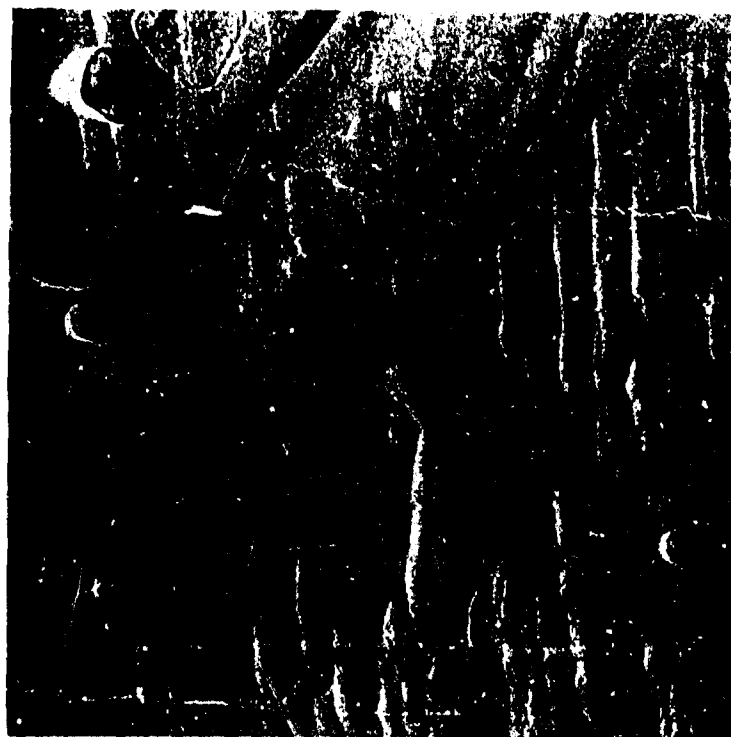


FIGURE 24. ELECTRON PHOTOMICROGRAPHS OF L-605



### X-Ray Diffraction

The data presented in this section were obtained for three specimens of A-286 stainless deformed to a constant 35% deformation by upset forging as shown in Figure 25.

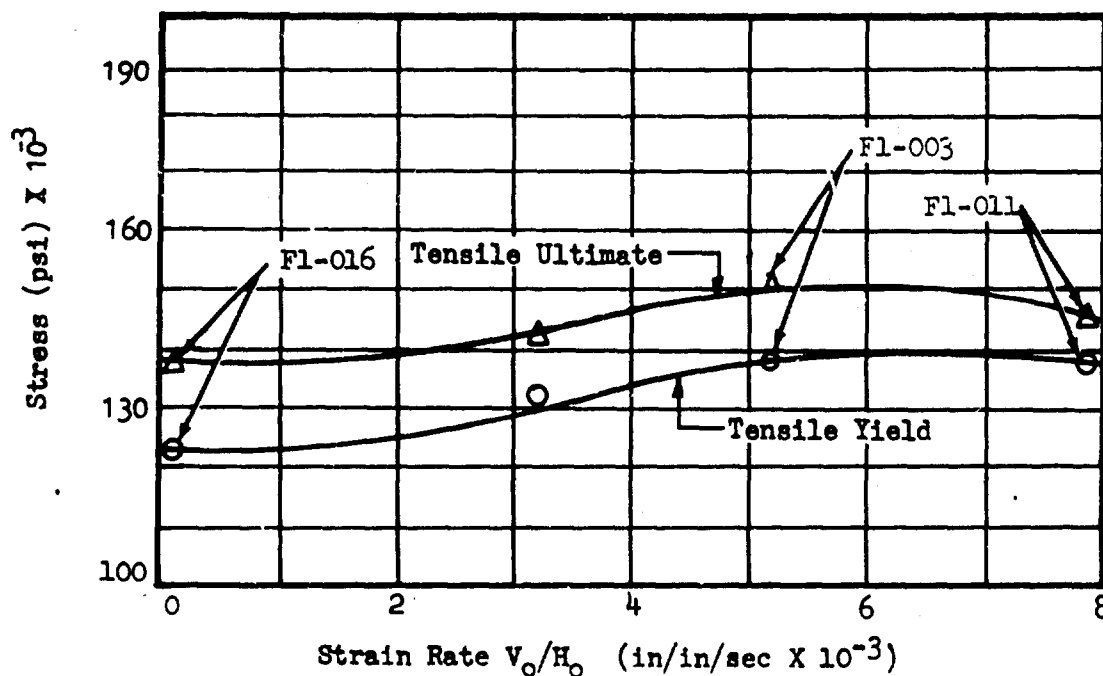


FIGURE 25. MATERIAL PROPERTIES DATA FOR SPECIMENS USED IN X-RAY DIFFRACTION TESTS

The X-ray target area used was located outside of the gage length as indicated in Figure 26.

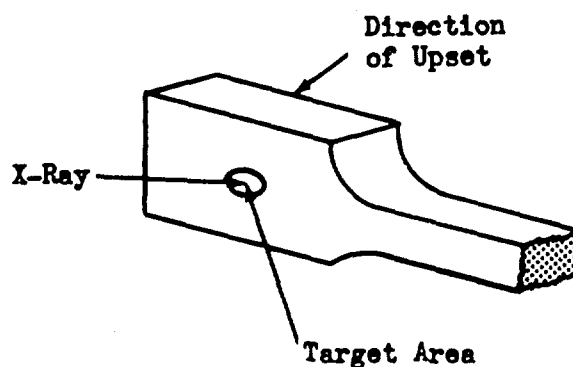


FIGURE 26. TARGET AREA FOR X-RAY DIFFRACTION

Preliminary tests were made using different spectrometer target materials. A portion of the spectra using iron ( $K_{\alpha}$  wave length of  $1.937\text{\AA}$ ) for two specimens of A-286 are shown in Figure 27.

The corresponding peaks from three x-ray spectra are shown in Figures 28, 29, and 30. In each case chromium radiation was used to investigate the effect of strain rate on the crystal plane spacing of one material (A-286) which had previously been deformed by a constant amount (approximately 35%) at three strain rates.

#### Photomacrographs

Photographs were taken showing the grain flow pattern for 18% Ni maraging steel and for 7075-aluminum. Static and high strain rate upsets show a marked difference in flow as is evident in Figures 31, 32, and 33. The marked difference in edge geometry in relation to the grain flow pattern for the two strain rate regimes may also be noted.

#### Results

The as-forged grain structure of specimens deformed under static conditions was compared to that of specimens upset at strain rates in the 5000 and 8000 per second ranges. The overall results based on the seven materials investigated were negative. No indication was found of any visual differences between the worked grains relative to the strain rate. In addition the electron photomicrographs of one material, L-605, showed usual slip banding at magnifications of 6,000x and 20,000x. On the basis of these results it is concluded that the final microstructure is independent of strain rate. This does not include effects that may occur in post forming heat treatment.

X-ray diffraction patterns of specimens of A-286 stainless steel using  $FeK_{\alpha}$  radiation as well as  $CrK_{\alpha}$  radiation are presented in Figures 27 through 30. In the case of  $FeK_{\alpha}$  radiation patterns made from specimens F1-016 and F1-011 corresponding to strain rates of zero and 8000 in/in/sec. respectively are shown.  $CrK_{\alpha}$  patterns made from F1-016, F1-003 and F1-011 corresponding to zero, 5000 in/in/sec., and 8000 in/in/sec. respectively are shown.

Since a stress free specimen of the material was not available the actual amount of stress in each case could not be determined. However it can be seen that (1) the  $K_{\alpha}$  doublet is resolved in the pattern corresponding to zero strain rate, (2) the  $K_{\alpha}$  doublet is not resolved for either 5000 in/in/sec. or for 8000 in/in/sec., and (3) the peak width is broader for 8000 in/in/sec. than for 5000 in/in/sec. strain rate. In order to analyze the resolved doublet in (1) above an idealized unresolved peak is constructed assuming a pure gaussian distribution. Comparison of peak width for the three specimens then indicates that as strain rate increased the residual stress also increased.

The grain flow patterns shown in Figures 31 and 32 illustrate the most significant strain rate effect observed during this investigation. In

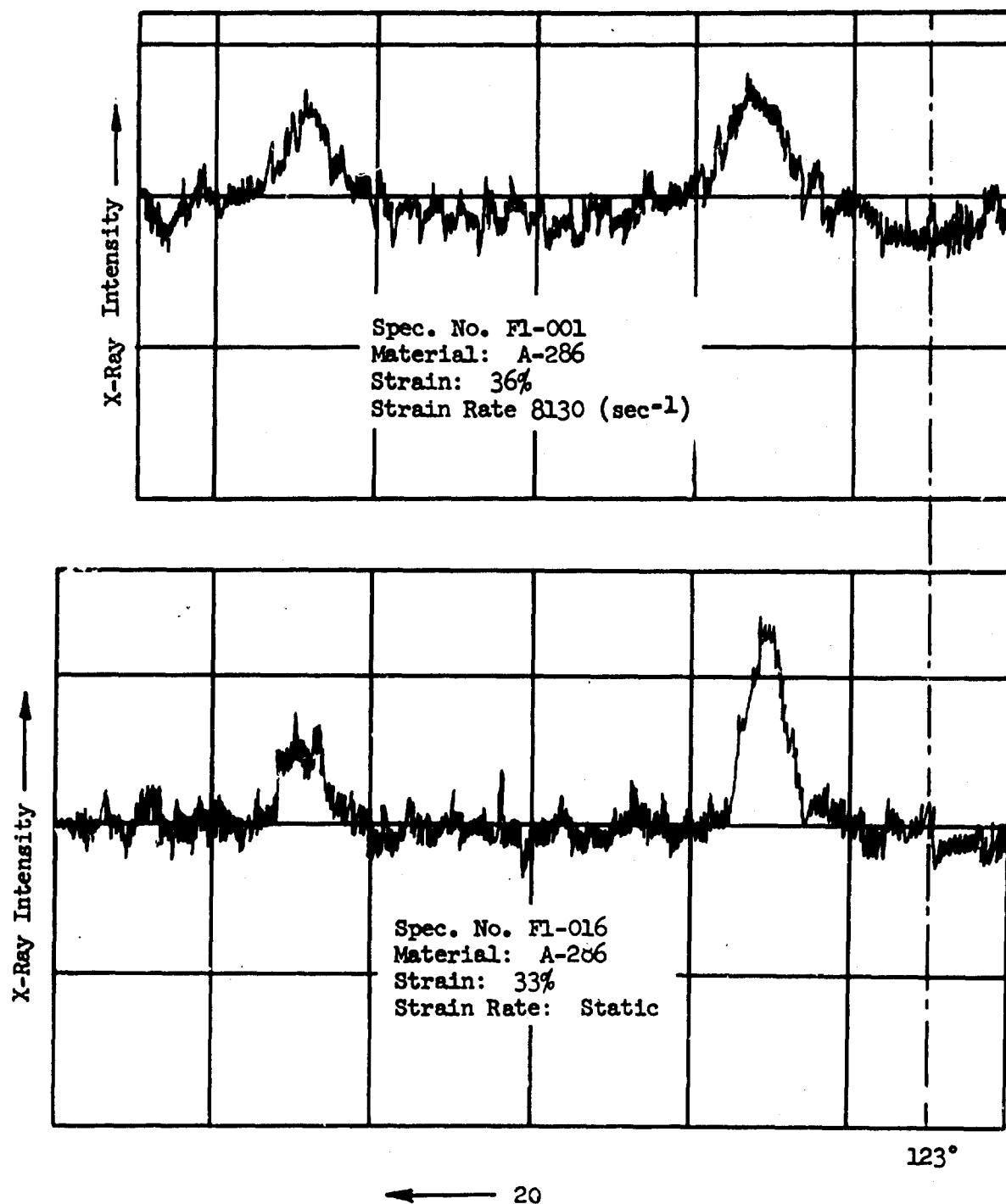


FIGURE 27. X-RAY SPECTRA FOR A-286 USING  $\text{FeK}_{\alpha}$  RADIATION

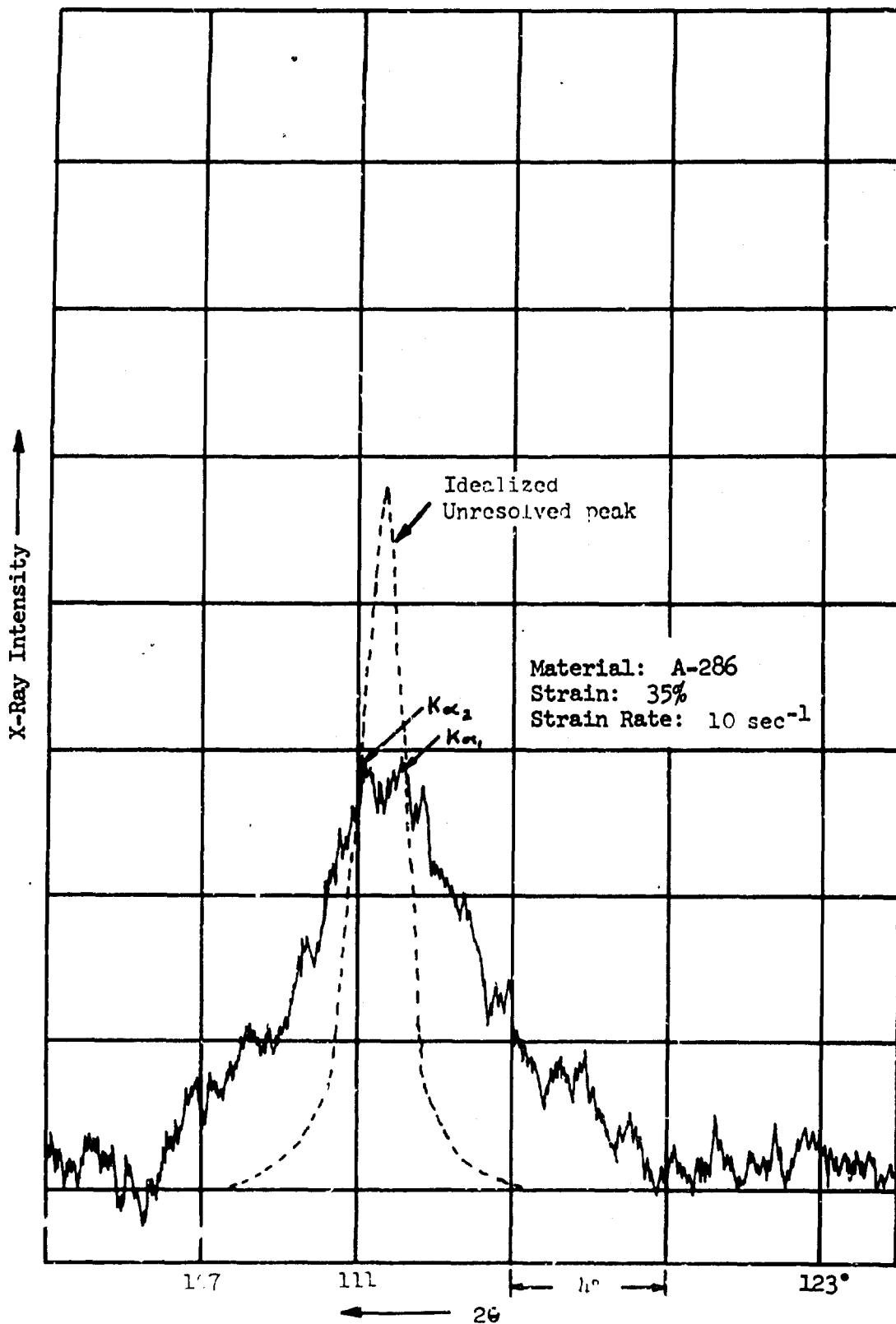


FIGURE 28.  $Cr_{K\alpha}$  PEAK FOR SPECIMEN F1-016

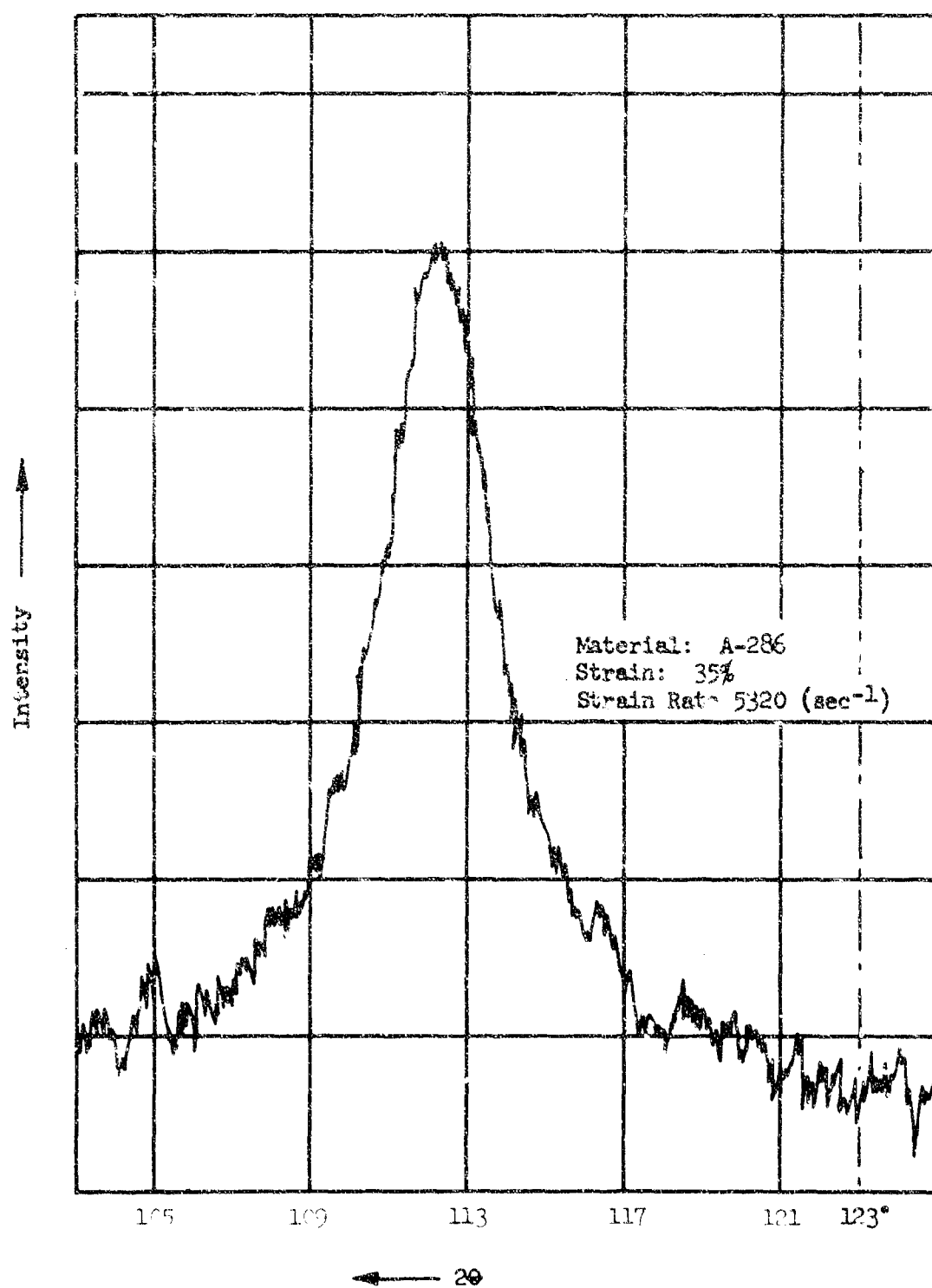


FIGURE 29.  $\text{Cr}_{\text{max}}$  PEAK FOR SPECIMEN F1-003

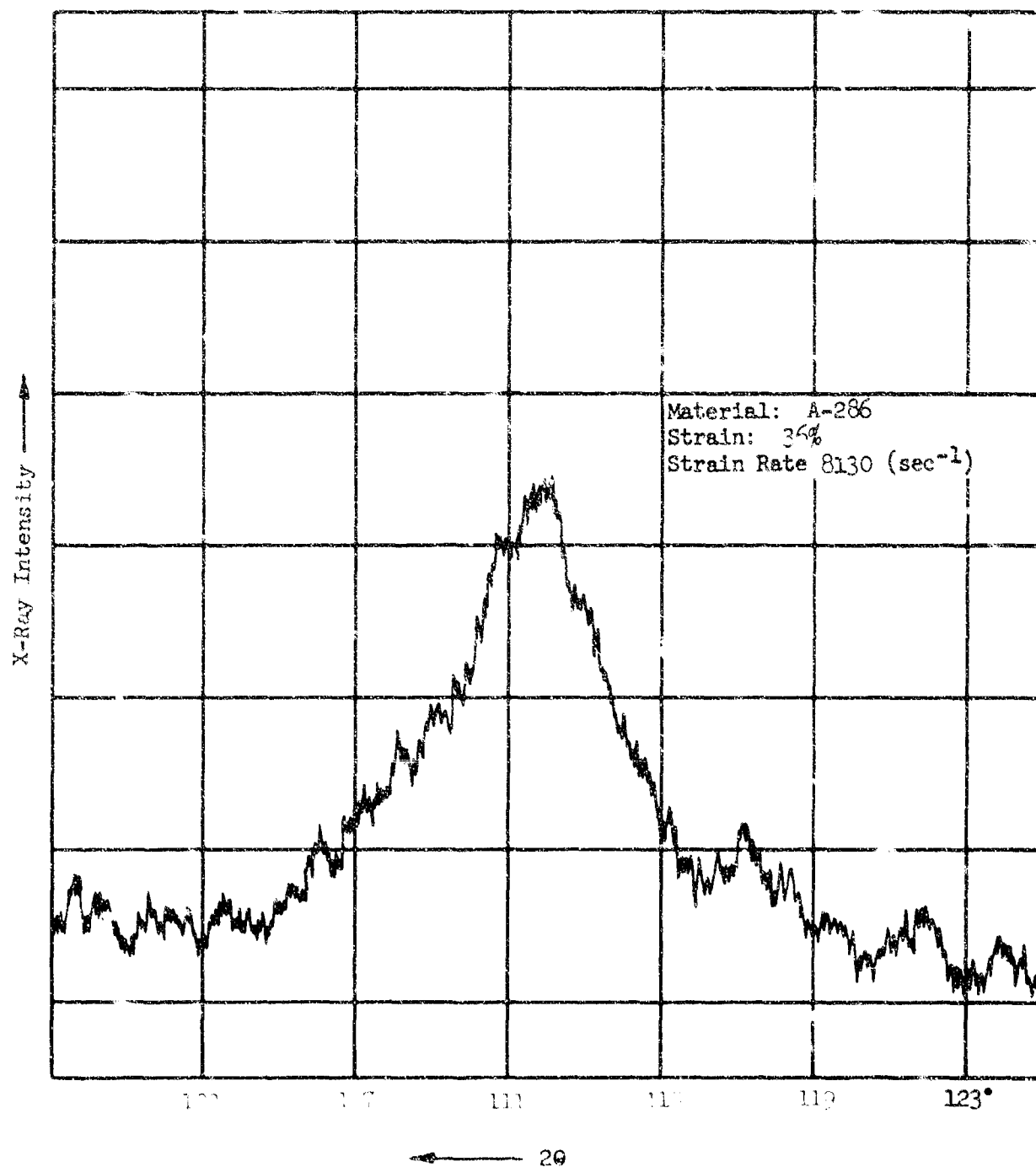
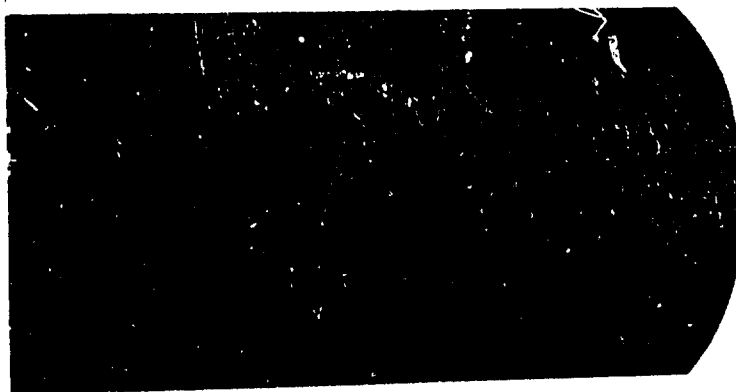


FIGURE 30.  $\text{Cr}_{\text{max}}$  PEAK FOR SPECIMEN FI-011

Spec. No. G3-005  
Mag. 2X  
Strain 0.4 %  
Strain Rate Static



C<sub>1</sub> Billet

Spec. No. G3-009  
Mag. 2X  
Strain 52.2 %  
Strain Rate 6270 Sec<sup>-1</sup>

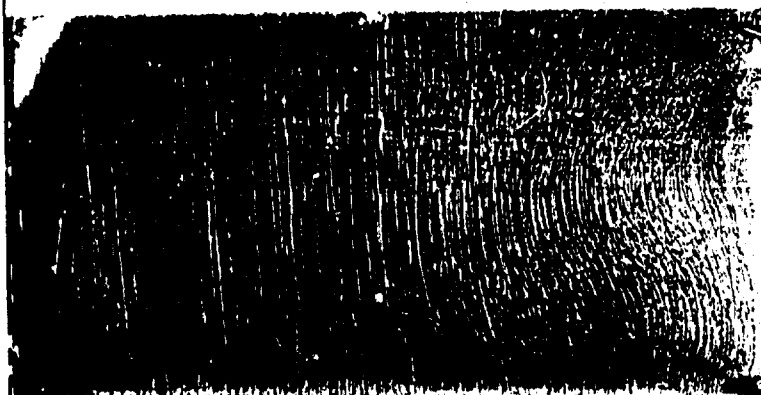


FIGURE 31. GRAIN FLOW PATTERNS FOR VASCOMAX 300 (18% NI MARAGING STEEL)  
UPSET AT ROOM TEMPERATURE

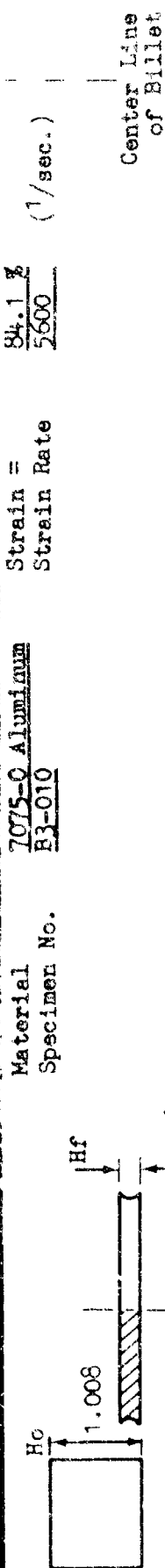


FIGURE 32 GRAIN FLOW AT HIGH STRAIN RATE FOR A CYLINDRICAL BILLET. (Room Temperature)

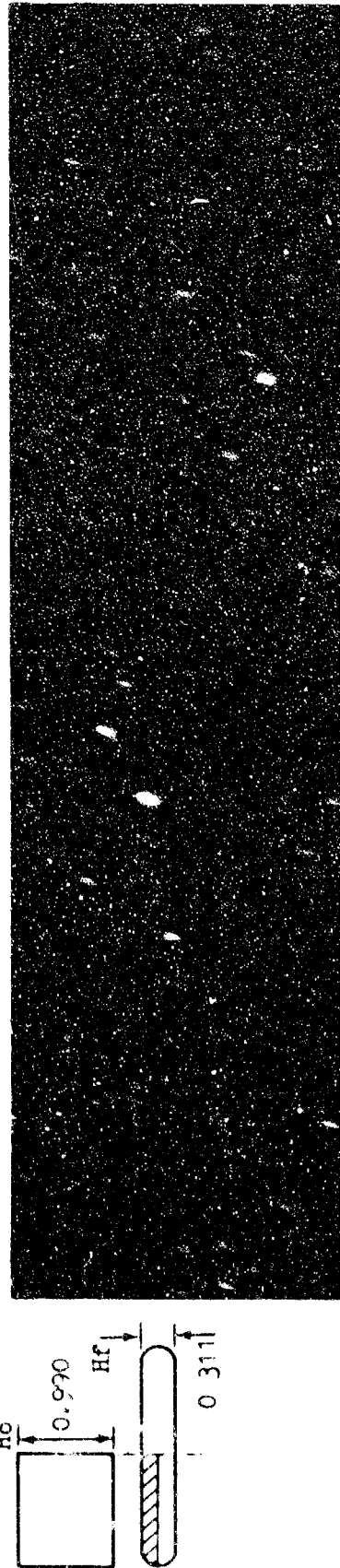


FIGURE 33. GRAIN FLOW NEAR ZERO STRAIN RATE (Room Temperature)



tained at low strain rates only under very special conditions. In conventional forging a concave edge geometry is obtained with good lubrication and by operating the dies at a higher temperature than the part. In this case the effect is easily explained by the lower yield strength of the heated material in contact with the die faces. In high velocity upsetting the flow field is influenced by factors such as adiabatic heating, velocity effect on friction, strain rate effects on the material yield strength, and inertial forces in the specimen. As yet there is not sufficient data to support a theory explaining this phenomenon. Strain distributions for the various test conditions are shown in Figure 34.

### Discussion of Results

The test results of the Phase I investigation show that the forging process is not limited in strain rate because of adverse material response for many high-use alloys. The behavior of aluminum, specifically, suggests an improvement in forgeability for alloys in which alloying elements are soluble or exist as a highly dispersed, coherent second phase at the forging temperature.

The highly desirable changes in grain flow that can be attributed to improvement in lubricating action with increasing strain rate as shown in Figures 31, 32 and 33 result in a more homogeneous distribution of residual strain energy which is of vital importance in post-forming heat treatments involving recovery and recrystallization. X-ray diffraction results for A-286, show that for specimens deformed a constant amount at static, 5000 and 8000 in./in./sec strain rates exhibit increasing residual strain as the strain rate is increased.

The as-forged tensile test results shown in Table II, together with x-ray and photomicrographic examination strongly support the conclusion that there is significant structural improvement to be gained by the use of high strain rates in upset forging.

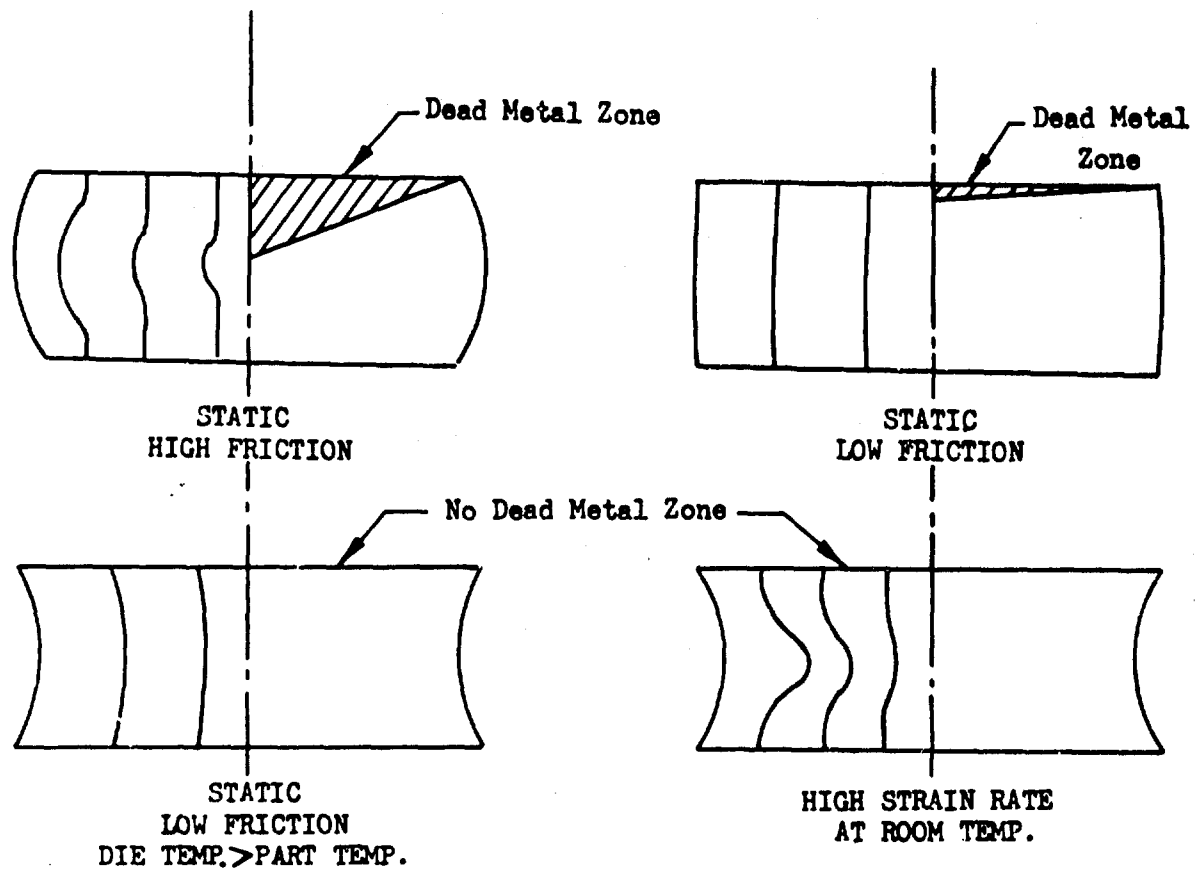


FIGURE 34. STRAIN DISTRIBUTION FOR VARIOUS PROCESS CONDITIONS

## SECTION V

### PHASE II COMBINED EFFECT OF TEMPERATURE AND HIGH STRAIN RATE IN UPSET FORGING

#### Introduction

In this phase, four materials were selected from the ten alloys of Phase I for detailed investigation. The alloys selected were:

2024 aluminum  
Ti-5Al-2.5Sn  
17-4 PH  
A-286

The material behavior in large plastic deformation was tested as a function of strain and strain rate over the temperature and strain rate ranges from room temperature to 1950°F and static to 8000 in/in/sec respectively. The two principal areas considered were: (1) forgeability and (2) as-forged mechanical properties.

In addition to the establishing of forgeability limits over the defined temperature range, a small number of tests were performed using a high strain rate optical extensometer recently developed by the Ling-Temco-Vought Corp. Instantaneous values of velocity, strain rate and forging force were obtained during the deformation event using this system.

The as-forged mechanical properties portion of the program was expanded to include the effect of temperature and strain rate on the tensile and fatigue properties in both as-forged and post heat treated conditions. Supplementary information was provided by metallographic data from selected specimens.

#### Forgeability Evaluation

##### Introduction

Forgeability was evaluated by the method of cylindrical billet upset between parallel plane surfaces with one surface moving at a controlled velocity. The forgeability limit was measured by the percent reduction that could be obtained under the various test conditions prior to failure by metal separation at the surface of the specimen.

The two objectives of the forgeability tests were (1) to determine the net combined effect of high impact velocities and forging temperature on the ductility or forgeability limit and (2) to establish a basis for selecting test temperatures at which meaningful as-forged mechanical properties data could be obtained.

### Experimental Plan

The basic experimental plan for evaluating the combined effect of strain rate and temperature on forgeability follows that used in Phase I for investigating the strain rate-ductility relation at room temperature (see Figure 19). In this Phase, a series of cylindrical billets for each projectile weight and forging temperature were deformed to establish the ductility limit. The billets were upset to successive amounts of deformation using one impact on each billet until a fracture occurred.

In the Phase II testing, all of the projectile energy was absorbed by the test billet. This test condition differs from Phase I in that the energy absorbing rings shown in Figure 16 were not used.

A series of forging temperatures were selected based on the known low speed ductility of the four materials as shown in Figure 35 .

Material	Forging Temperature °F	Material	Forging Temperature °F
2024-0	R.T., 350 550, 750	17-4 PH Austinized	550, 950 1350, 1550 1750, 1950
Ti 5Al-2.5Sn	R.T., 750, 1050, 1350, 1550, 1750 1950	A-286	R.T., 550, 750, 950 1350, 1950

FIGURE 35 . TEST TEMPERATURES FOR PHASE II FORGEABILITY EVALUATION

The strain rate or ram velocity range for this phase was originally set to extend from static, using the hydraulic press to an upper limit of 4000 sec<sup>-1</sup>. Because of severe die quenching in the initial press forging tests, this static series was replaced by drop hammer upsetting. The revised strain rate range

thus extended from 50-5000 in/in/sec which in the case of a one inch high billet requires ram velocities from approximately 4-400 ft/sec. Within this range three different projectiles weighing 64, 15, and 5 pounds were selected as the best compromise with respect to velocity and energy for the four program materials. Thus for each forging temperature the test schedule called for establishing the limit at four different strain rates with an anticipated total of 100 to 150 individual test specimens per material.

#### Equipment

A detailed discussion of the test equipment is presented in Appendix VI. Special tooling used with the hydraulic press and the drop hammer are shown in Figures 128, 129, 130 & 131. The method of measuring the drop hammer ram velocity is shown in Figure 132. All high velocity tests utilized the LTV high energy impact machine as shown in Figures 133 and 134, with the automatic billet heating and loading mechanism illustrated in Figures 135 through 138.

#### Procedures

The thermal history of the forgeability specimens prior to upset followed usual forging practice. Aluminum 2024, Ti-5Al-2.5Sn, and A-286 were heated directly to the forging temperature and allowed to soak for approximately 10 minutes. The PH stainless steel alloy 17-4 PH was heated to 1800°F to obtain the single phase structure. This was accomplished using a pre-heat furnace from which the specimen was transferred to the mechanized billet furnace and allowed to cool to desired forging temperature before upset.

#### Data Acquisition

The raw data generated in the forgeability tests are listed as follows:

- A. Drop Hammer Upset Tests
  - (1) Specimen dimensions - original height ( $H_o$ ), final height ( $H_f$ ).
  - (2) Time for the moving ram to travel 1" at impact ( $\Delta t$ ).
  - (3) Forging temperature of the billet as measured in the furnace (°F).
- B. High Velocity Impact Tests
  - (1) Specimen dimensions ( $H_o$ ,  $H_f$ ).
  - (2) Cannon fire pressure and projectile weight.
  - (3) Forging temperature (furnace temp. °F).
- C. Visual Inspection Data
  - (1) Surface condition and edge shape of the forged billet.
  - (2) Type and severity of failure. The specimens were evaluated as either good, incipient fracture, or fractured. As in the Phase I evaluation, the term incipient fracture is used to denote the presence of a small crack or in the brittle failure conditions, to indicate that a slight reduction in deformation did produce a good specimen.

#### D. Photographs

Representative photographs, Figures 73 through 106, Appendix II, were made of selected specimens upset to reductions below and above the forgeability limits for the various test conditions of temperature and strain rate and shown with the corresponding limit curves.

#### Results

The forgeability limits are plotted from the data listed in Table XI, Appendix III. Percent of upset  $(H_o - H_f)/H_o \times 100$  is plotted against the initial impact strain rate.

$$de/dt = \dot{\epsilon} = V_o/H_o$$

$V_o$  - Impact projectile velocity

$H_o$  - Initial billet height

Composites of the forgeability limit curves at the various test temperatures for the four Phase II materials are shown in Figures 38, 40, 42 and 44.

Test temperatures for evaluating the combined effect of temperature and strain rate on the final mechanical properties were selected from the forgeability limit vs. temperature curves shown in Figures 37, 39, 41 and 43. The two temperatures selected as most useful in production forging are: (1) the hot forging temperature with an optimum combination of reduced material resistance to plastic flow and maximum ductility and (2) the highest warm forging temperature at which the billet may be held for prolonged times without atmosphere protection and at which the material has reasonably good plasticity.

Under these conditions, forging temperatures for bar specimen upset preparatory to subsequent tensile and fatigue properties evaluation were selected as shown in Figure 36.

Material	Forging Temperature		Maximum Deformation Allowed (%)
	Warm	Hot	
Aluminum 2024	550	750	50
Titanium 5Al-2.5Sn	1550	1950	25
17-4 PH	1550	1950	40
A-286	1050	1950	50

FIGURE 36. FORGING TEMPERATURES FOR MECHANICAL PROPERTIES EVALUATION

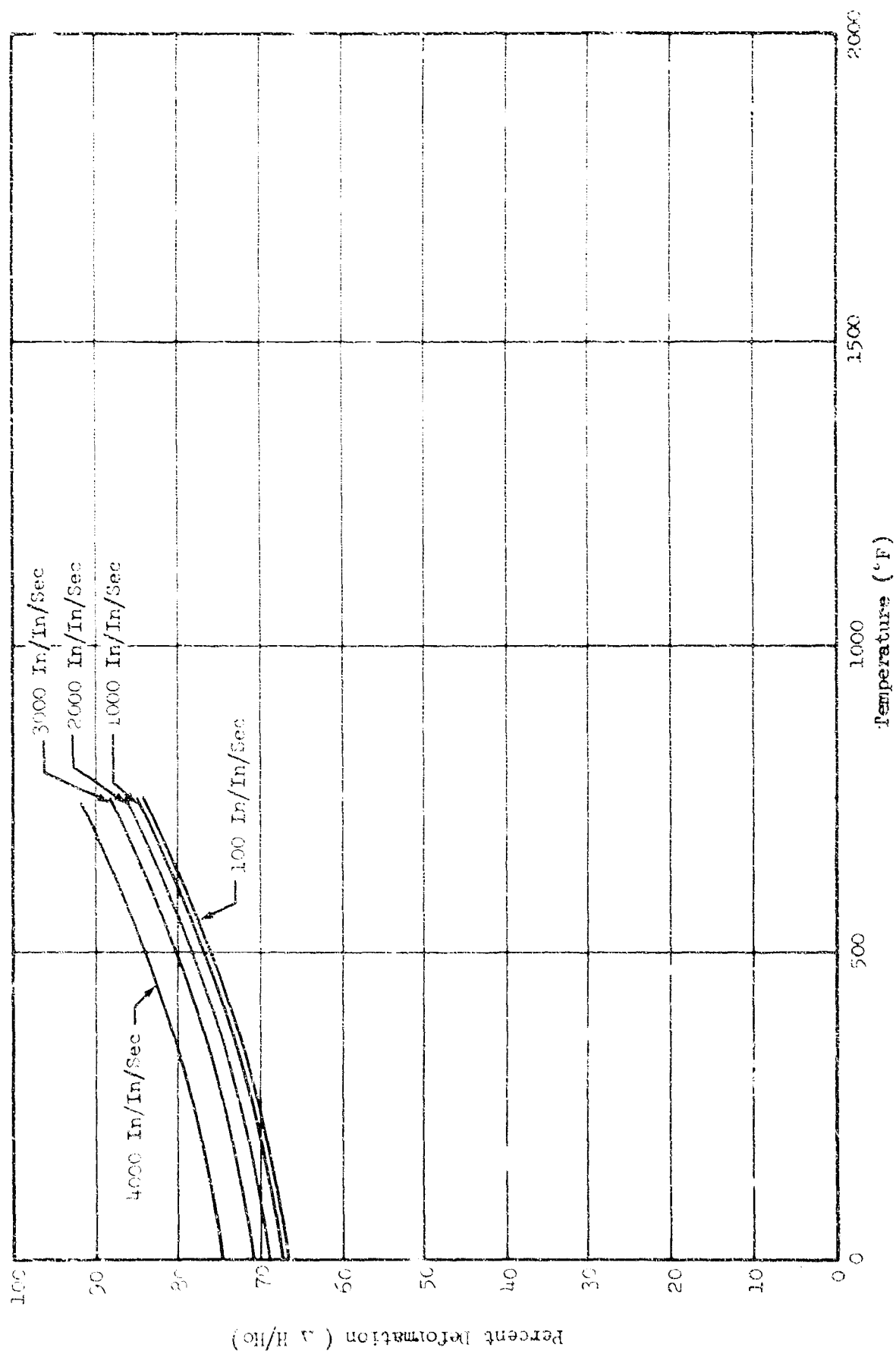


FIGURE 37. THE EFFECT OF TEMPERATURE ON FORGEABILITY LIMIT AT VARIOUS STRAIN RATES FOR 2024-T3 AL.

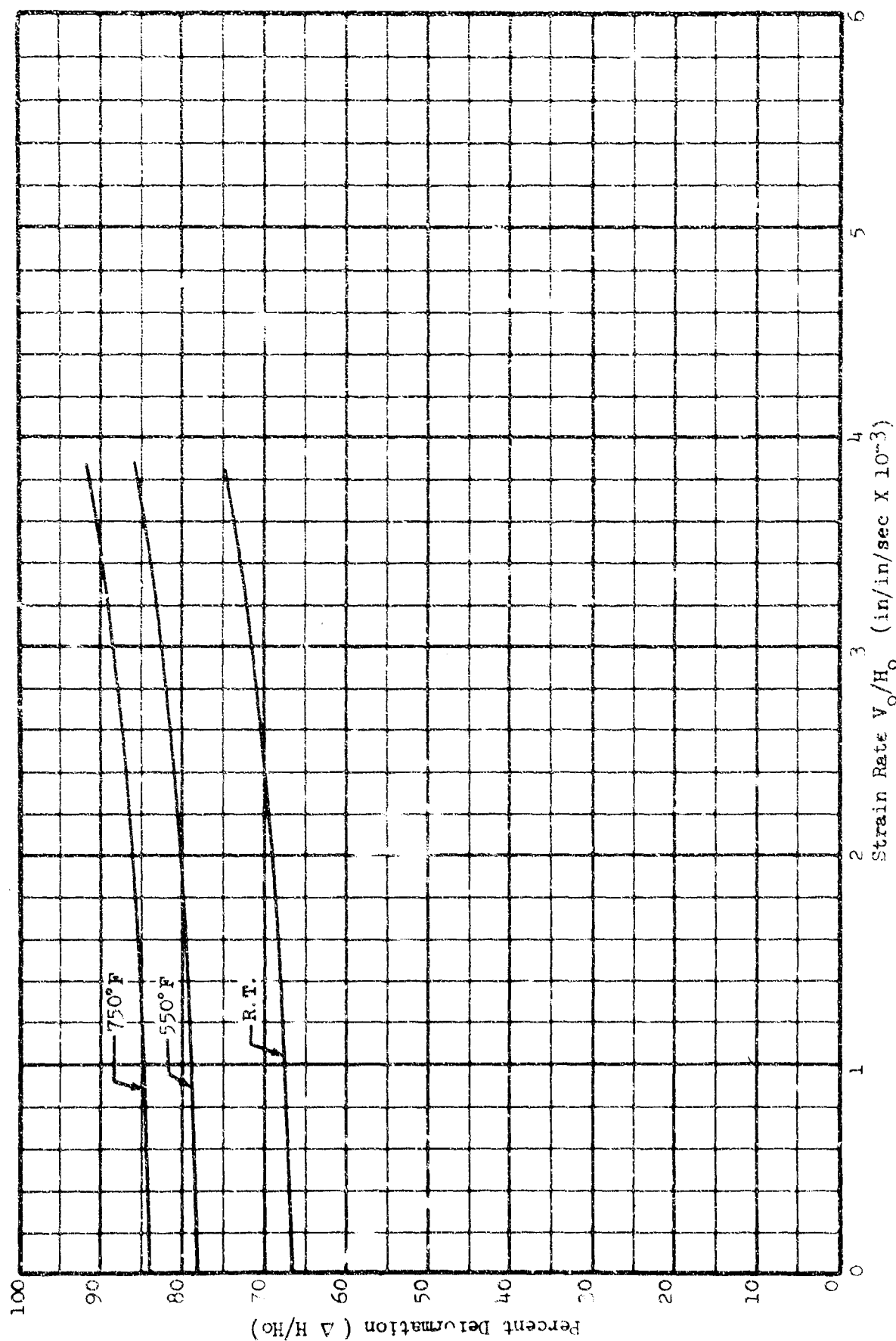


FIGURE 38. THE EFFECT OF STRAIN RATE ON PORTEABILITY  
LIMIT AT R.T. TO 750°F FOR 2024-T3 AL.



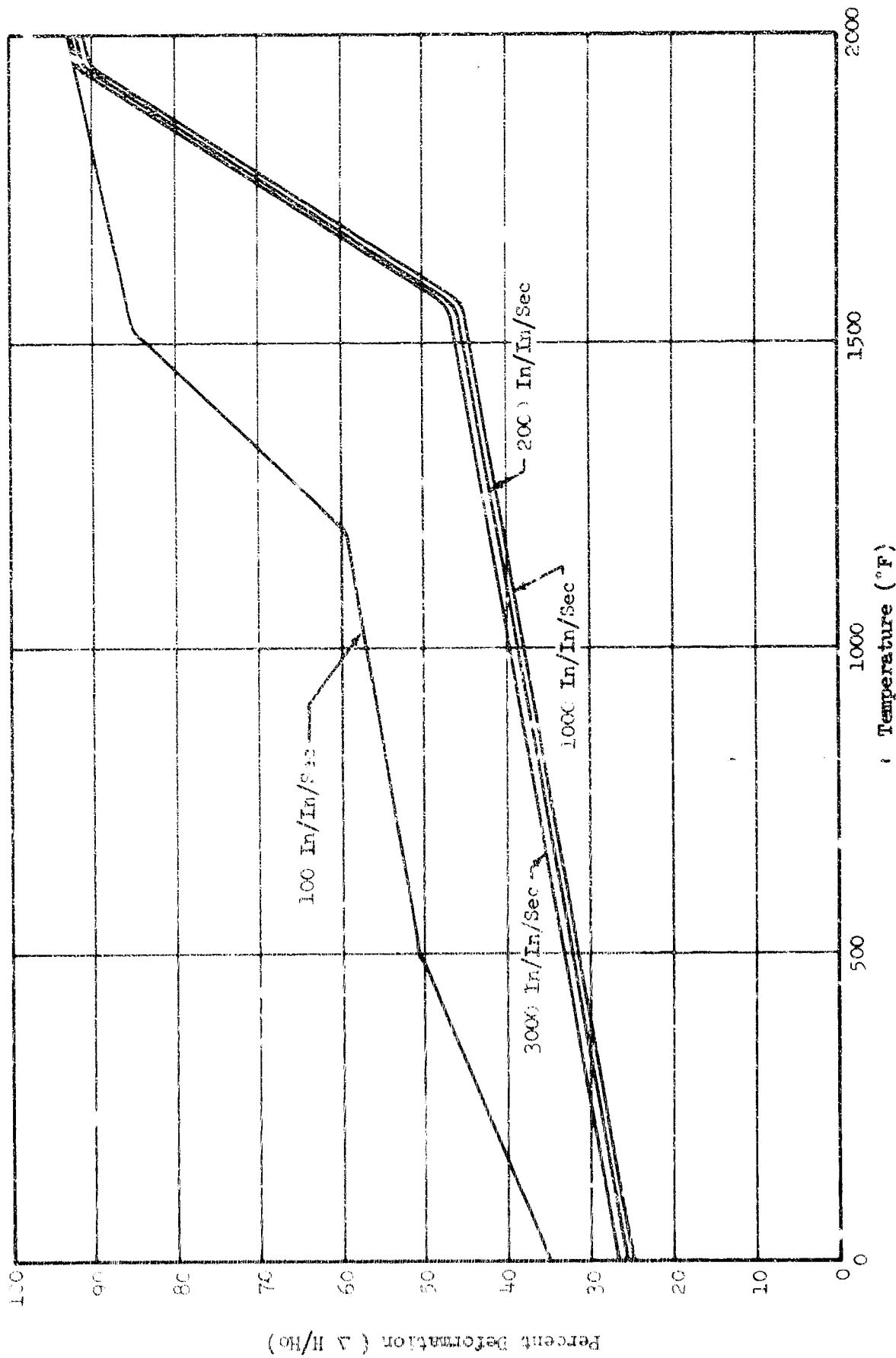


FIGURE 39. THE EFFECT OF TEMPERATURE ON FORGEABILITY LIMIT AT VARIOUS STRAIN RATES FOR Ti-5.2Al-2.5Sn

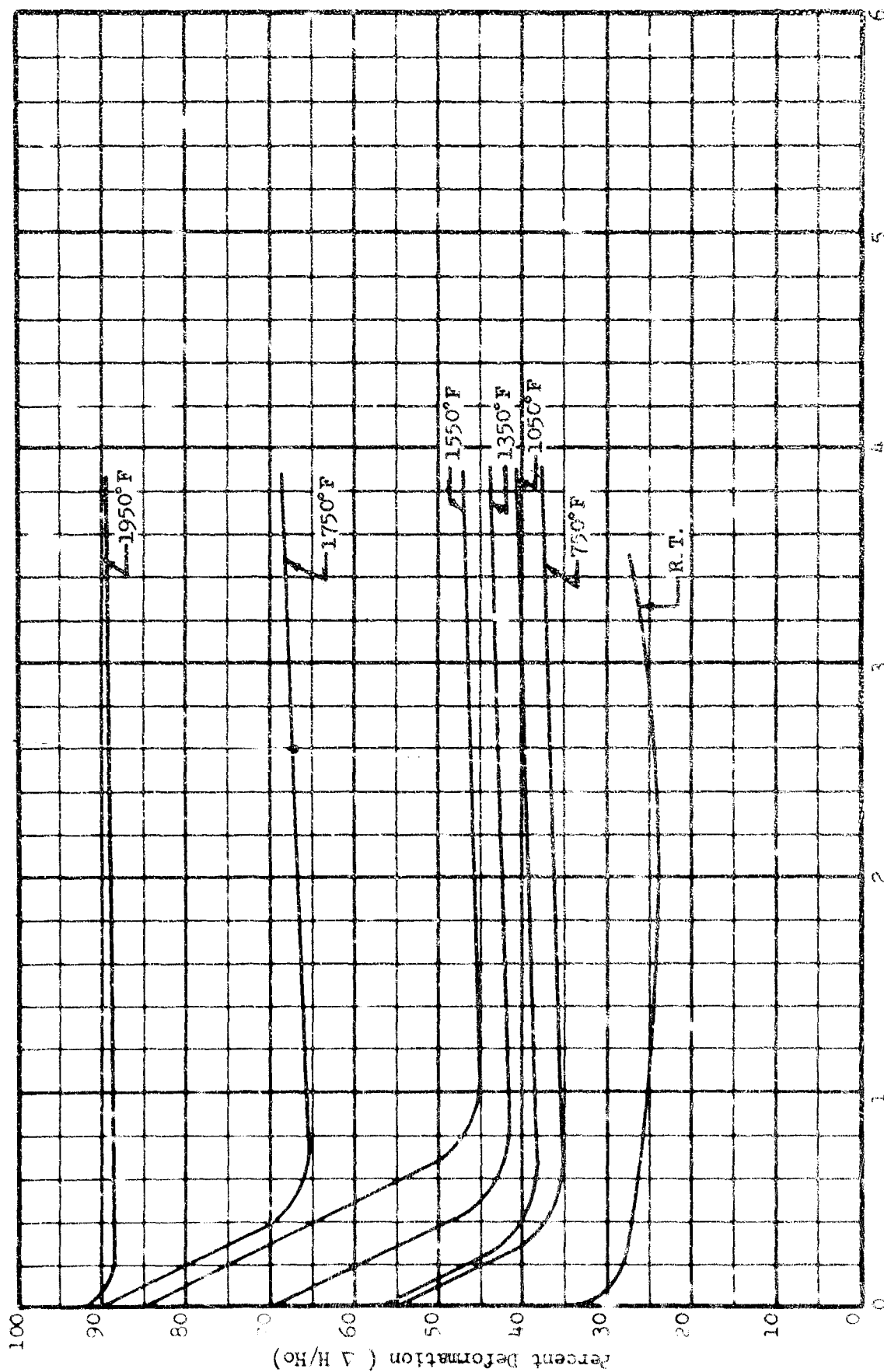


FIGURE 4C. THE EFFECT OF STRAIN RATE ON FORGEABILITY  
LIMIT AT R. T. TO 1950°F FOR Ti-5Al-2Zr-2.5Sn

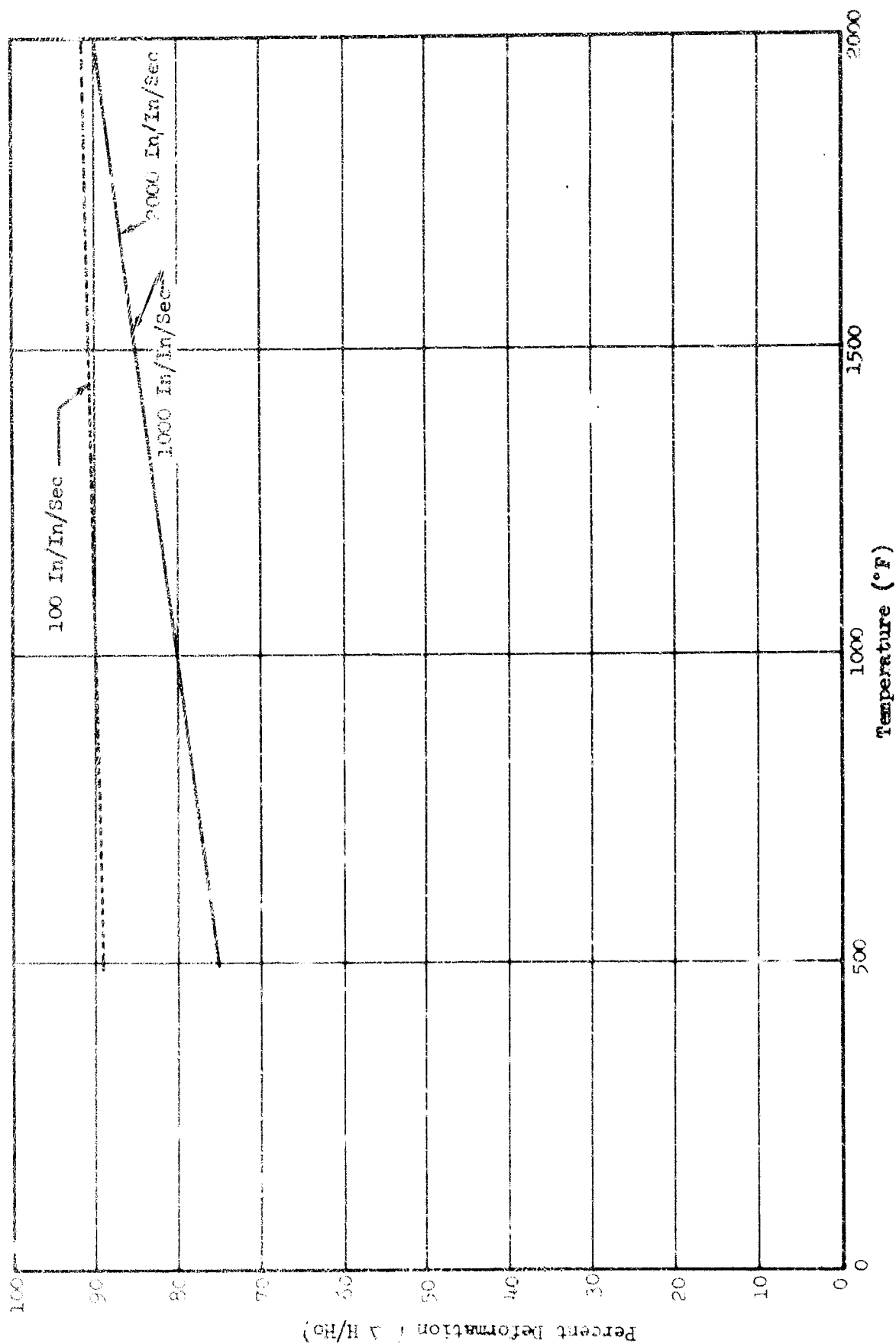


FIGURE 41. THE EFFECT OF TEMPERATURE ON FORCEABILITY LIMIT AT VARIOUS STRAIN RATES FOR 17-4 PH

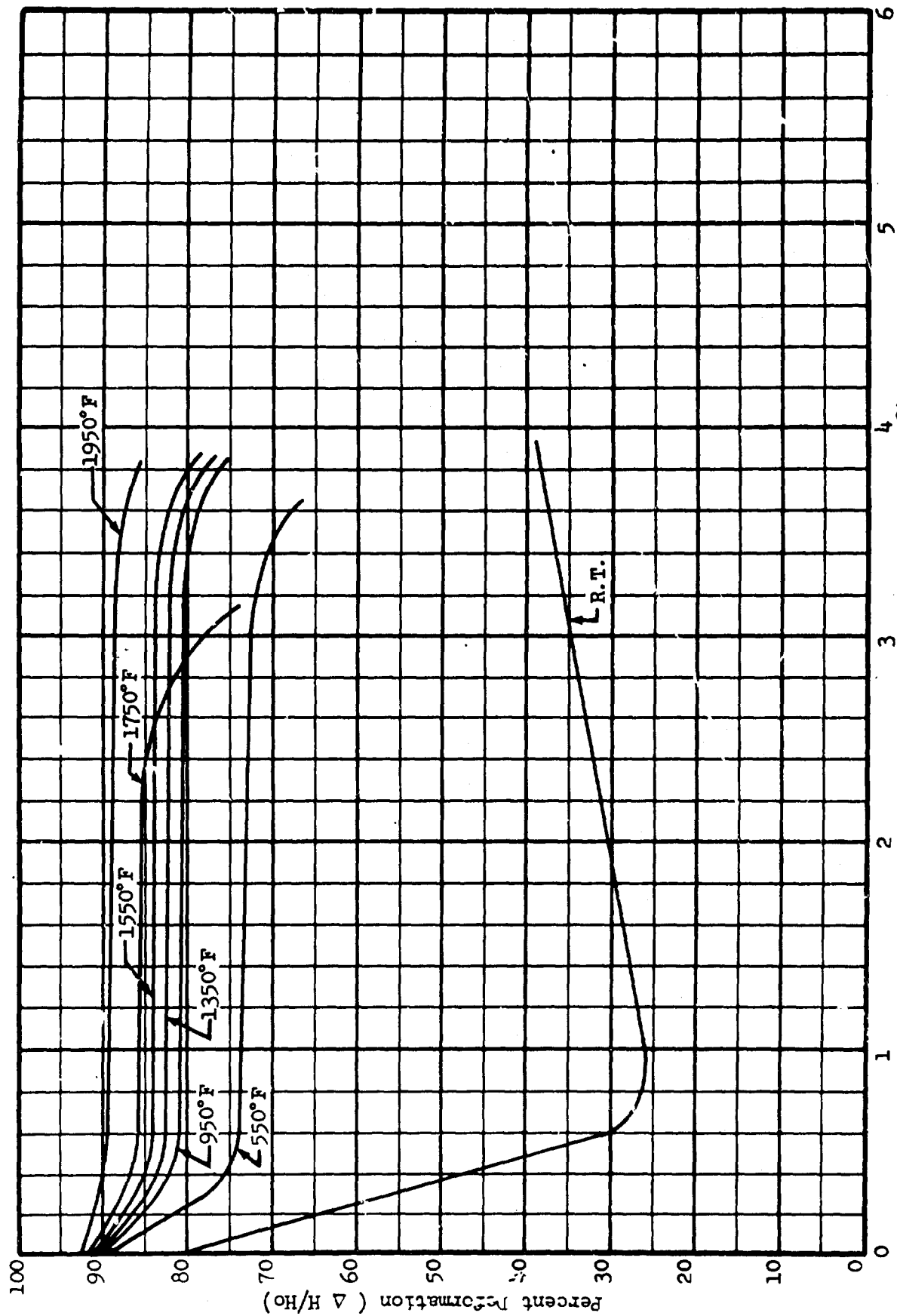


FIGURE 42. THE EFFECT OF STRAIN RATE ON FORGEABILITY  
LIMIT AT R.T. TO 1950°F FOR 17-4 PH

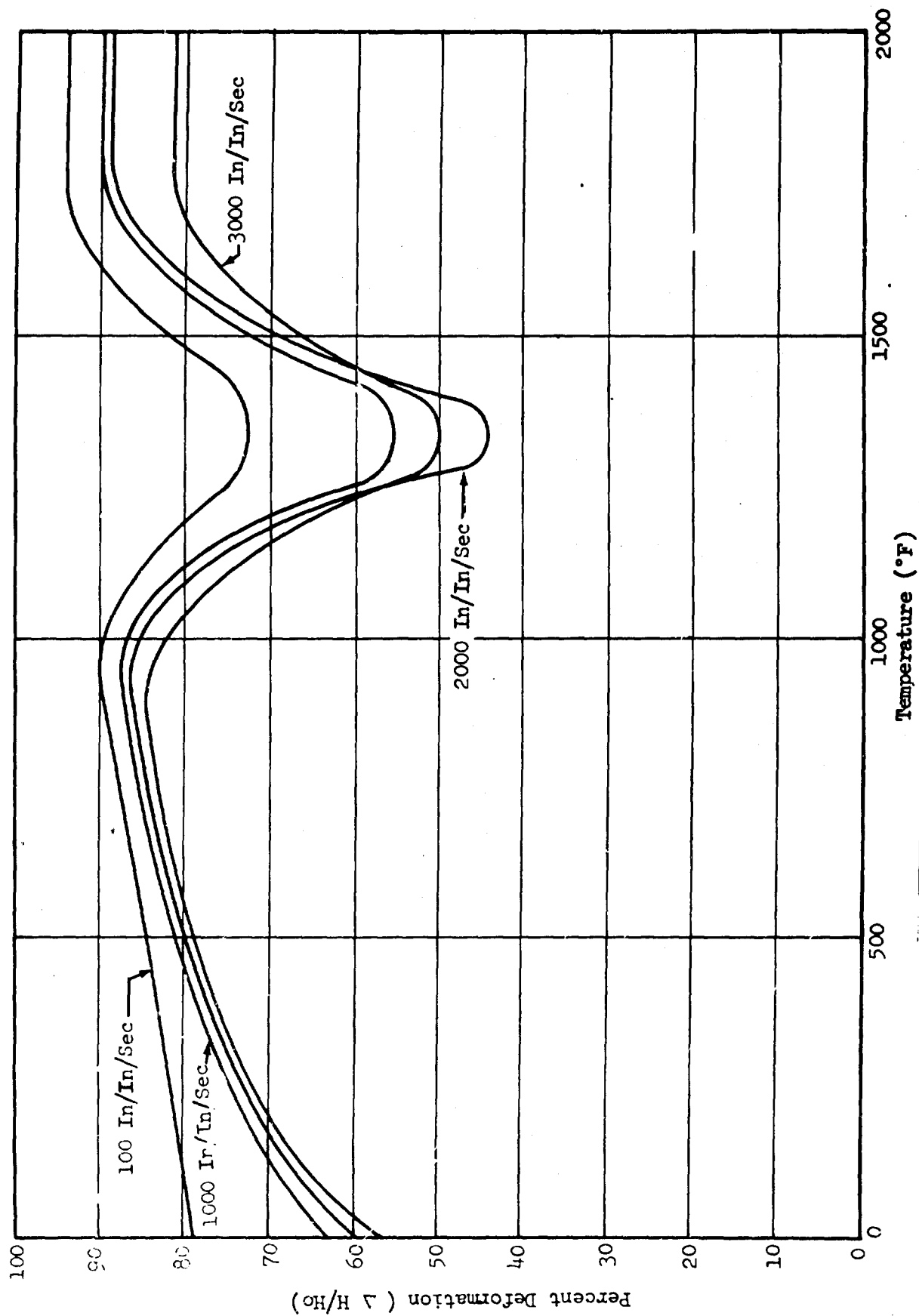


FIGURE 43. THE EFFECT OF TEMPERATURE ON FORGEABILITY LIMIT AT VARIOUS STRAIN RATES FOR A-286

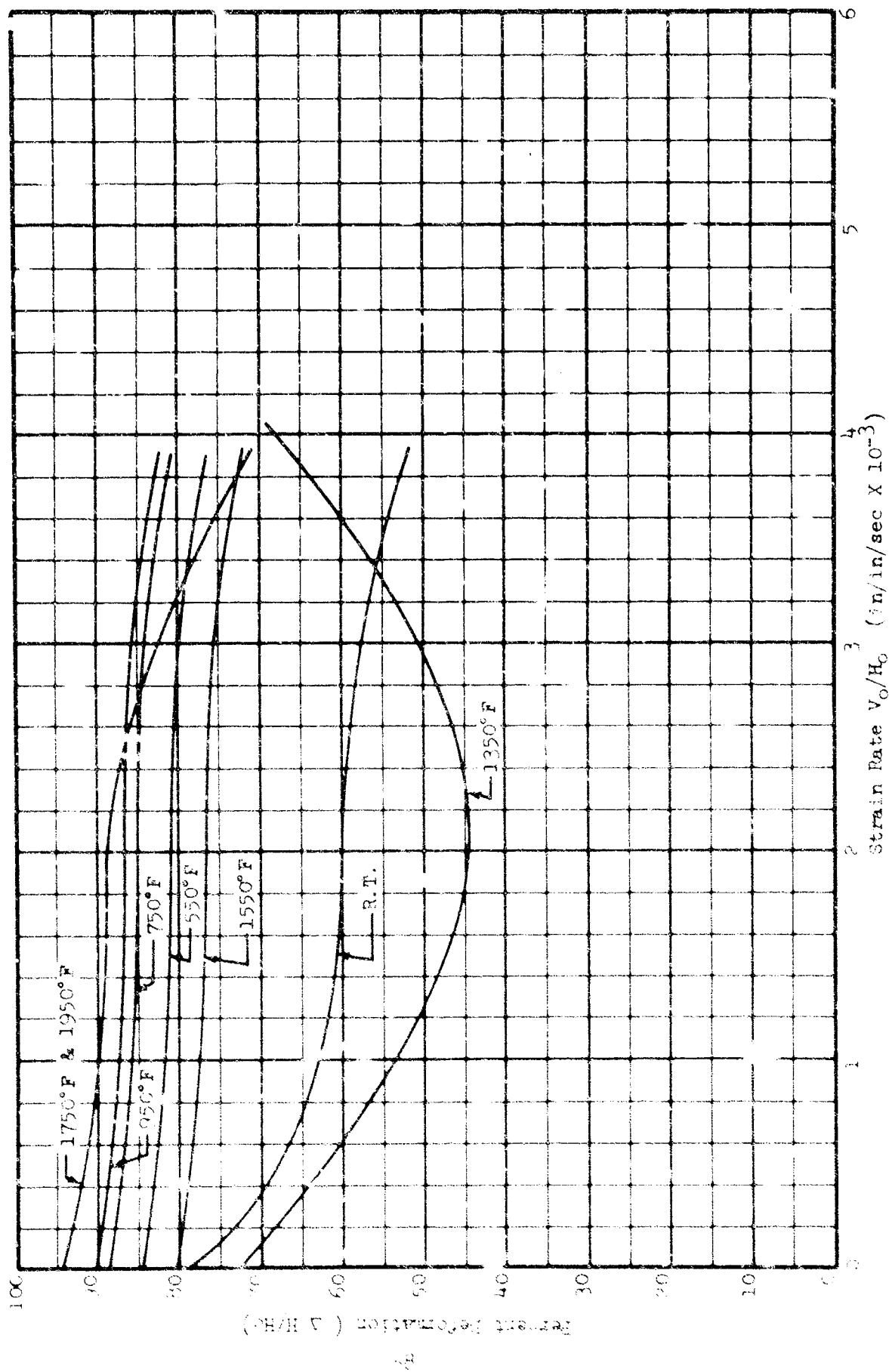


FIGURE 44. THE EFFECT OF STRAIN RATE ON FORGEABILITY LIMIT AT R.T. TO 1950°F FOR A-286

## Energy Requirements

### Introduction

A first approximation for the forging energy as a function of strain rate can be obtained by comparing the projectile energies required to cause a given amount of deformation at several different strain rates. Because of the fact that the required forging energy increases rapidly with the amount of strain, and since the projectile velocity (initial strain rate) must be increased to produce larger amounts of energy, it would require a large number of projectiles of different weights to maintain a constant amount of strain while varying the strain rate. Using three different projectile weights and performing a sufficient number of tests to establish the energy vs deformation curve for each projectile, test material, and test temperature, the desired relation between forging energy and strain rate at a constant strain may be obtained by interpolation.

It is noted that not all of the kinetic energy is expended in plastic deformation of the specimen. A portion of the initial energy is dissipated in the machine structure and its surroundings. The unused remainder appears in the rebounding projectile. In comparing the energy requirements for impact machines, it is the usual practice to assume ideal conditions and to ignore the rebound velocity of the ram.

### Data Acquisition

The forgeability data for 2024 aluminum was used to investigate the strain rate effect on the required impact energy, specifically the kinetic energy of the moving projectile,

$$K.E. = W V_o^2/64.4$$

where W and V are the weight and projectile impact velocity. The procedure for obtaining projectile energy as a function of strain rate for a constant deformation is shown in Figure 45.

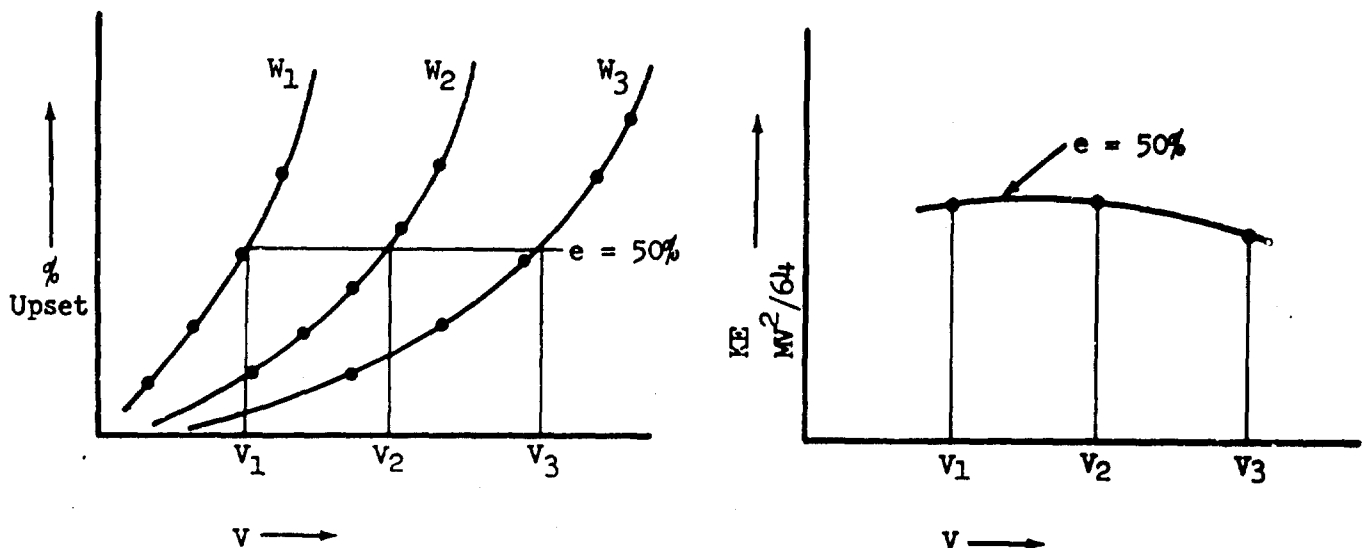


FIGURE 45 . METHOD FOR PLOTTING FORGING ENERGY.

## Results

Using the data in Table XI, Appendix III for 2024-O aluminum at three temperatures, projectile energy vs strain rate values were plotted at strains of 20% up to the forging limit as shown in Figures 46, 47, and 48.

## Instantaneous Process Variables

### Introduction

Measurements of instantaneous process variables were performed in an attempt to correlate variations with other program data. Such parameters as die force, surface velocities, and strain rate are of great interest in applying the data generated in this program to the development of reliable manufacturing procedures and methods.

Measurements were made of the projectile position as a function of time for a number of representative forging conditions. These measurements were made using the optical extensometer, which records discrete positions of the ram during deformation. These measurements confirmed previous predictions that the average instantaneous strain rate reaches a peak near the latter portion of the forging cycle, with attendant reduced die face loads.

### Experimental Plan

The LTV optical extensometer was used to measure the projectile position during forming. This device is shown in Figure 49 and schematically illustrated in Figure 50. An optical window was placed in the barrel near the exit end, allowing the projectile image to be monitored during forming. The barrel was vented near the extensometer to reduce lubricant spray and other extraneous matter which could interfere with proper projectile imaging. A light source capable of being focused to very high intensities was directed at the projectile from the side as illustrated in Figure 49. The high intensity light source was necessary to prevent room lighting from interfering with the optical instrumentation.

All tests were performed at room temperature, since the dynamics of the forging process are sufficiently similar to permit extrapolation of results to higher temperatures. Similarly, tests were performed on only two materials, 2024 aluminum and A-286 austenitic stainless steel. Lubrication was considered a variable but only in the case of A-286. The billets were held on the anvil with tape since the high temperature loading equipment was not necessary for the tests performed and would have introduced more error in the centering of the billets on the anvil. The billets were forged to two values of strain for each of the test conditions.

The output of the optical extensometer is in the form of electrical pulses, corresponding to small increments of the projectile position. These were amplified a short distance from the instrument and recorded with a Tektronix 535 A oscilloscope with a Polaroid camera attachment. Time intervals chosen were such that the entire forging process was recorded including rebound, which allows the calculation of strain energy contained in the anvil and



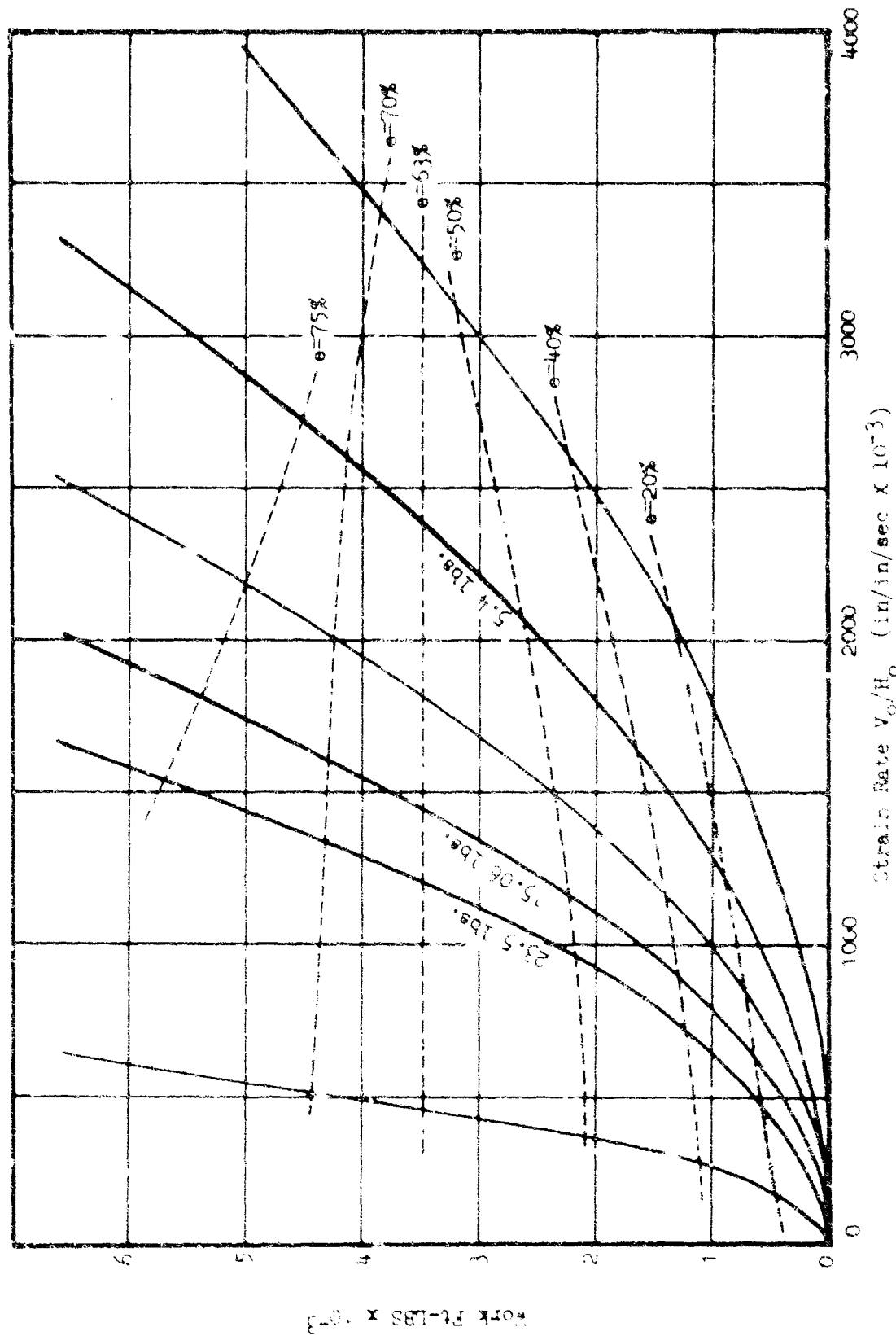


FIGURE 46. WORK VS. STRAIN RATE ( ROOM TEMPERATURE )

2024 Aluminum

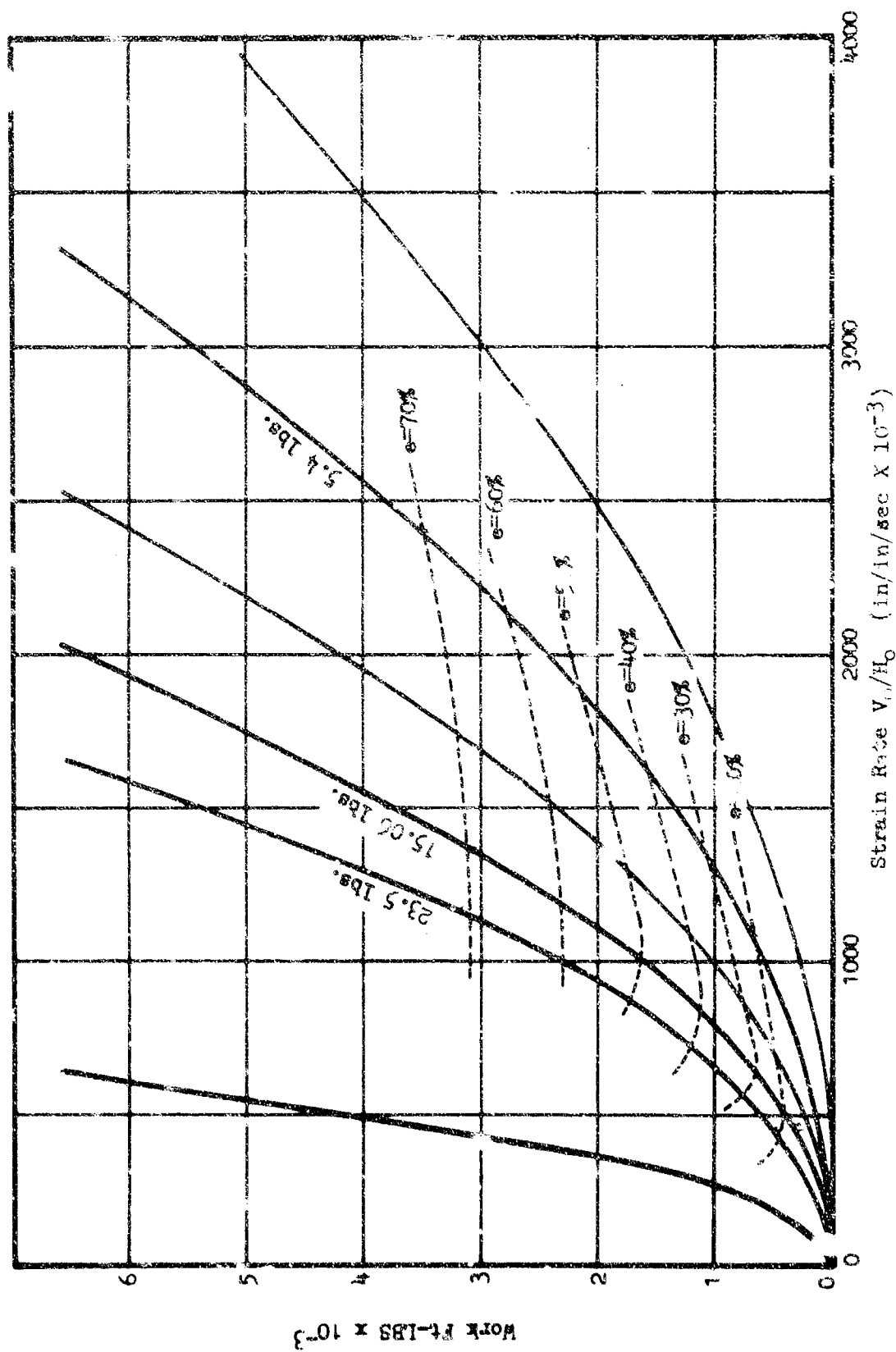
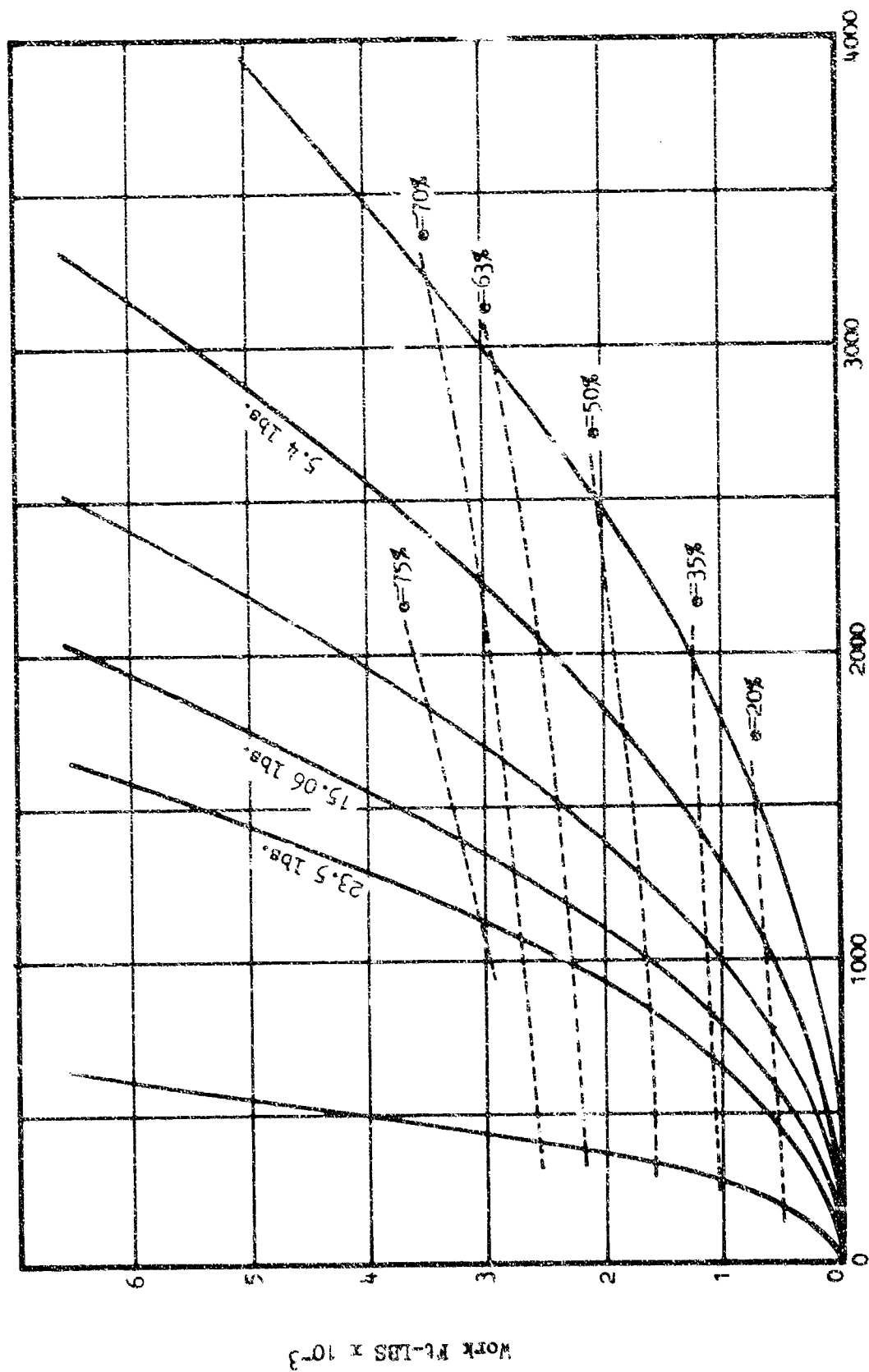


FIGURE 47. WORK VS. STRAIN RATE (400 F)  
2024 ALUMINUM



Strain Rate  $V_o/H_o$  (in/in/sec  $\times 10^{-3}$ )

FIGURE 48. WORK VS. STRAIN RATE (600°F)

2024 Aluminum

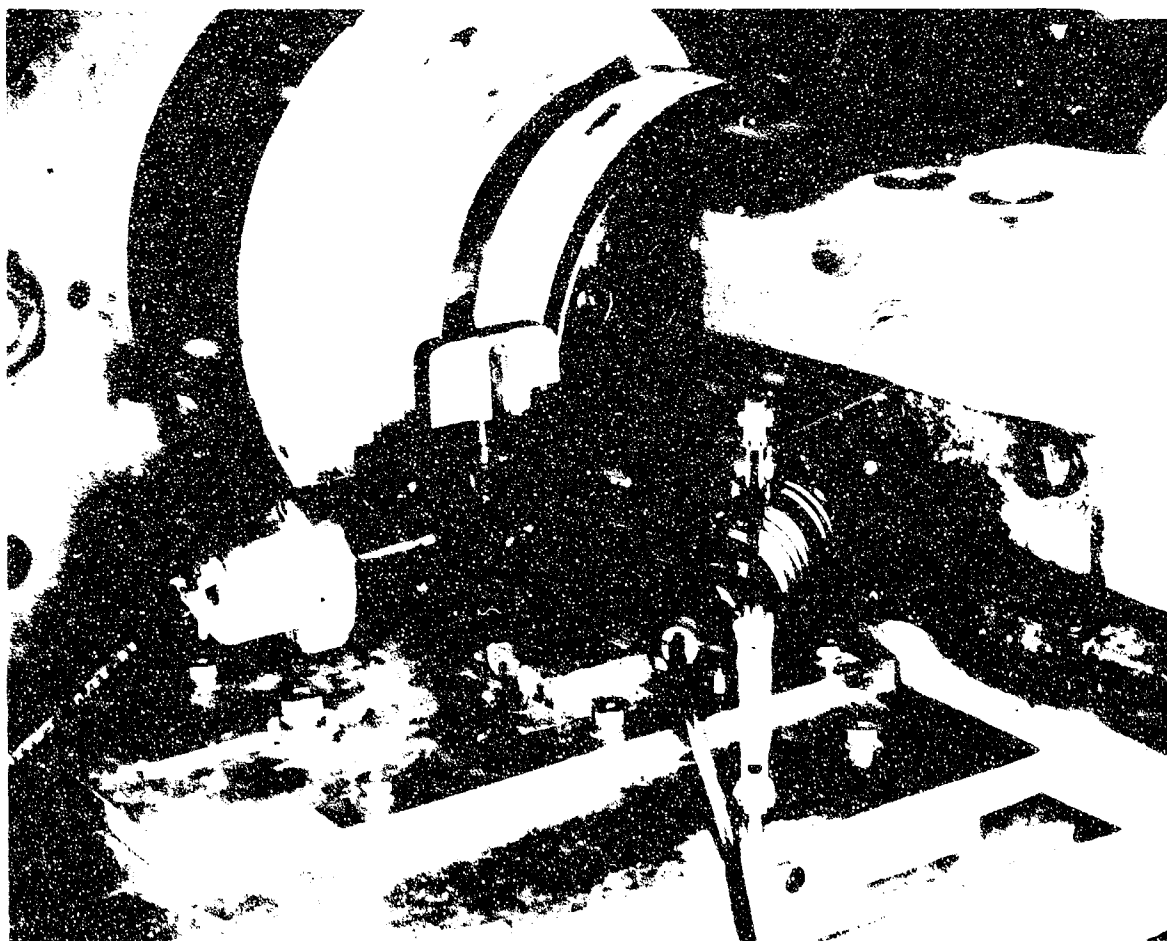


FIGURE 49. PHOTOGRAPH OF OPTICAL EXTENSOMETER

projectile at the time of direction reversal. Some error was introduced into these measurements due to deflection of the anvil under load as shown in Figure 51. The distance  $d_1$ , is that measured by the optical extensometer, while the distance  $d_2$  is the anvil deflection. The true billet deflection would be the difference of these two values. The projectile and anvil forces are only a function of the first, however, and may be calculated with excellent accuracy. Since the anvil deflection is a function of billet force, correlations may be made to give very reasonable accuracy for instantaneous billet height. The forming energy may also be found from the difference in the projectile and rebound energies.

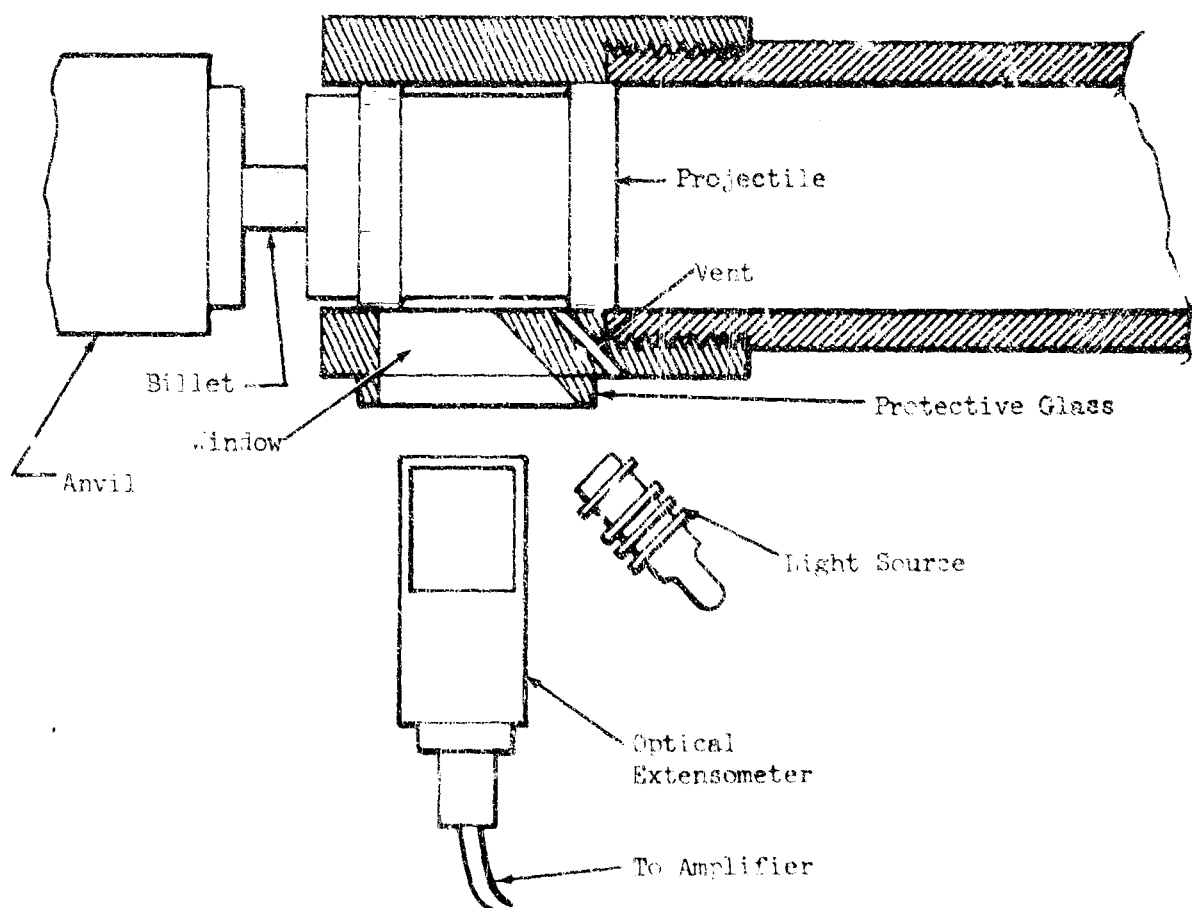


FIGURE 50 SCHEMATIC ILLUSTRATION OF OPTICAL EXTENSOMETER EXPERIMENTAL SETUP.

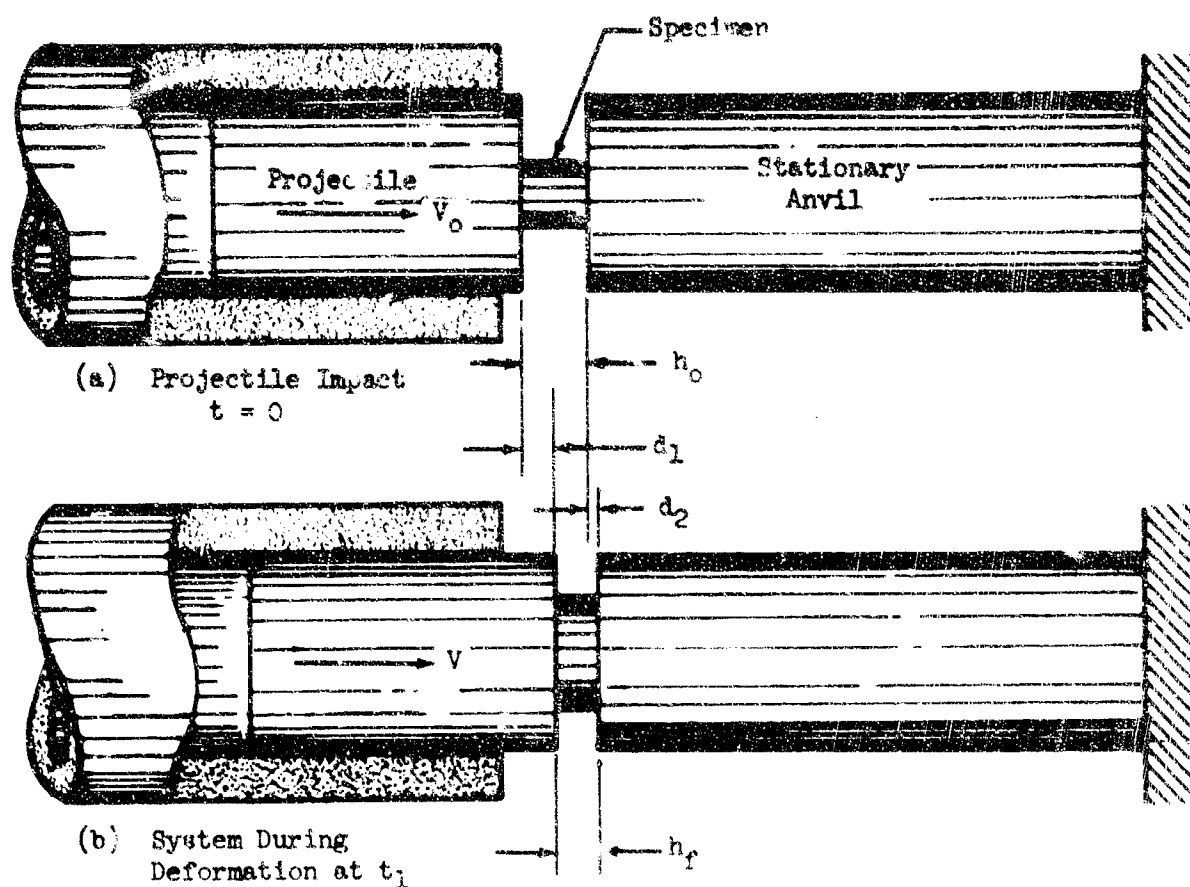


FIGURE 51. ERROR IN BILLED HEIGHT MEASUREMENTS  
RESULTING FROM ANVIL DEFLECTION

#### Data Processing

Since the distance increments used in recording the projectile position were on the order of ten mils, a rather large quantity of data was generated with each test. To insure accurate results, the locations of the time points on the oscilloscope trace were measured using an optical comparator. Further, to reduce the effects of nonlinearities in the oscilloscope and camera, accurate time marker signals were superimposed on each tract at the time of recording. The markers were produced with a crystal controlled oscillator at a frequency which would produce a minimum of 10 marks on a given scope trace. The positions of the time marks were measured in the same set up as the projectile position data.

The data from the comparator were then reduced with a digital computer. Since the interval between the marker points was known and remained constant, the time coordinates of the data were found using a linear interpolation scheme.

The point of reversal of the projectile could be located quite accurately from the oscilloscope traces and was arbitrarily assigned a time coordinate of zero. Since the billet deformation and anvil deflection were known, the impact point could be accurately located. The use of a time marker at the impact point would prove desirable if future work of this nature is performed.

The reduced data were then used to obtain plots of distance vs time for the projectile. The curves were faired and graphically differentiated to obtain plots of velocity and acceleration. The strain rate and anvil force profiles were then calculated on the basis of these curves. Corrections for anvil deflection were made from the anvil force profile.

### Results

The results are presented in graphical form in Figures 52 through 56. Velocity, strain rate, and die force are plotted as a function of deformation. The plots of velocity and strain rate are nondimensionalized in the manner by the theoretical curve in Figure 9.

For convenience, velocity profiles for different values of strain rate are superimposed on the velocity curve. These have great merit, as the strain rate may be read directly from a nondimensionalized curve.

The degree of accuracy of the curves was sufficient for the evaluation demands of this program. The method of data reduction employed should be born in mind, however, before attempts at rigorous comparisons are made. The data could be reduced to much higher accuracy through the use of digital curve fitting and differentiating technique, since a resolution of greater than  $\pm 10^{-3}$  inches is obtainable with the present model of the optical extensometer, for readings taken at 0.01 inch intervals. With some development these could be reduced by a factor of 10, the theoretical resolution being limited only by the numerical aperture of the lens and the frequency response of the electronics.

The curves provide excellent agreement with theoretical performance calculations. The magnitude of the strain rate peaks increases with increasing deformation, which supports the idea of reduced die loads at reversal. Accurate analysis methods would yield data which could possibly be applied to a fundamental analysis of the deformation mechanism.

## Mechanical Properties Evaluation

### Introduction

The primary objective of this segment of the program was to determine the combined effect of temperature and high strain rate on the final mechanical properties for four Phase II alloys. In contrast to the forgeability investigation, where the problem of process was considered, this segment dealt with the equally important question of the structural quality of the processed material.

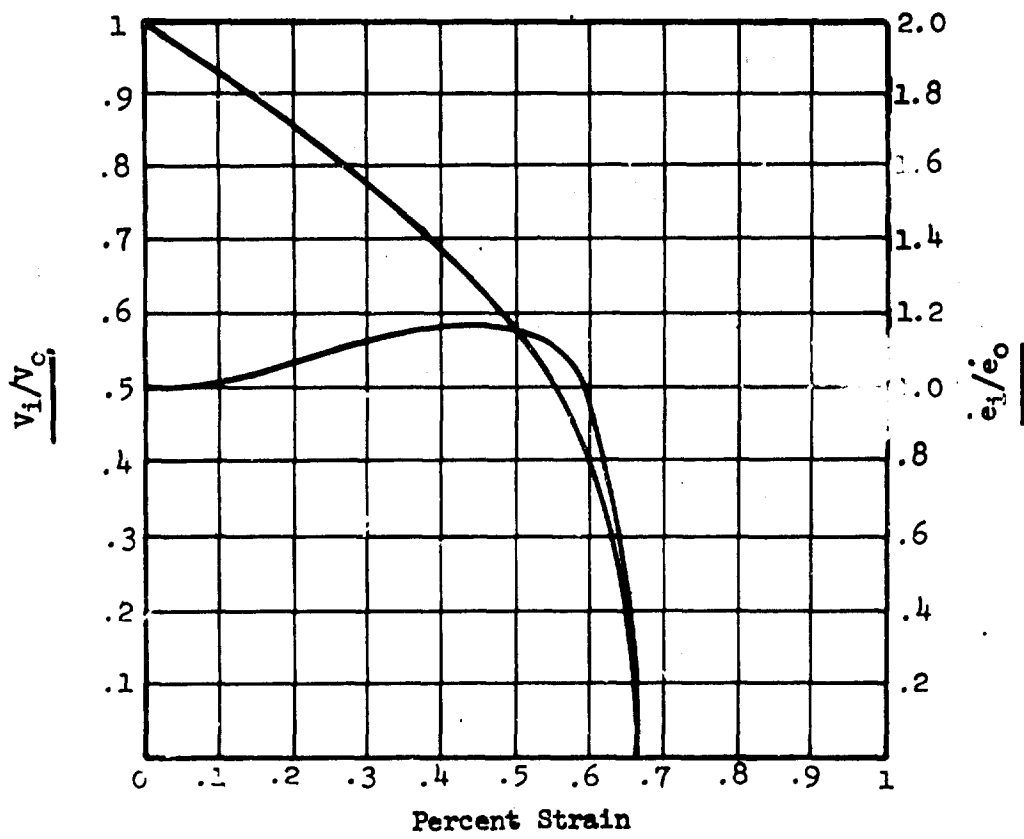
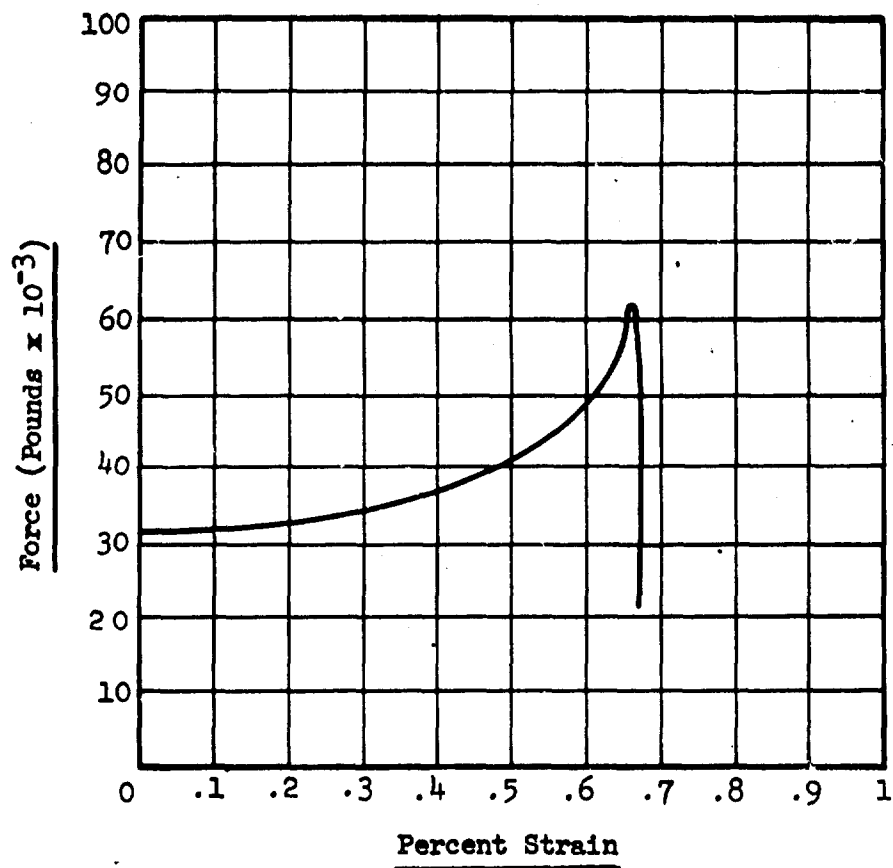


FIGURE 52. INSTANTANEOUS VELOCITY, STRAIN RATE AND DIE FORCE FOR A7-925



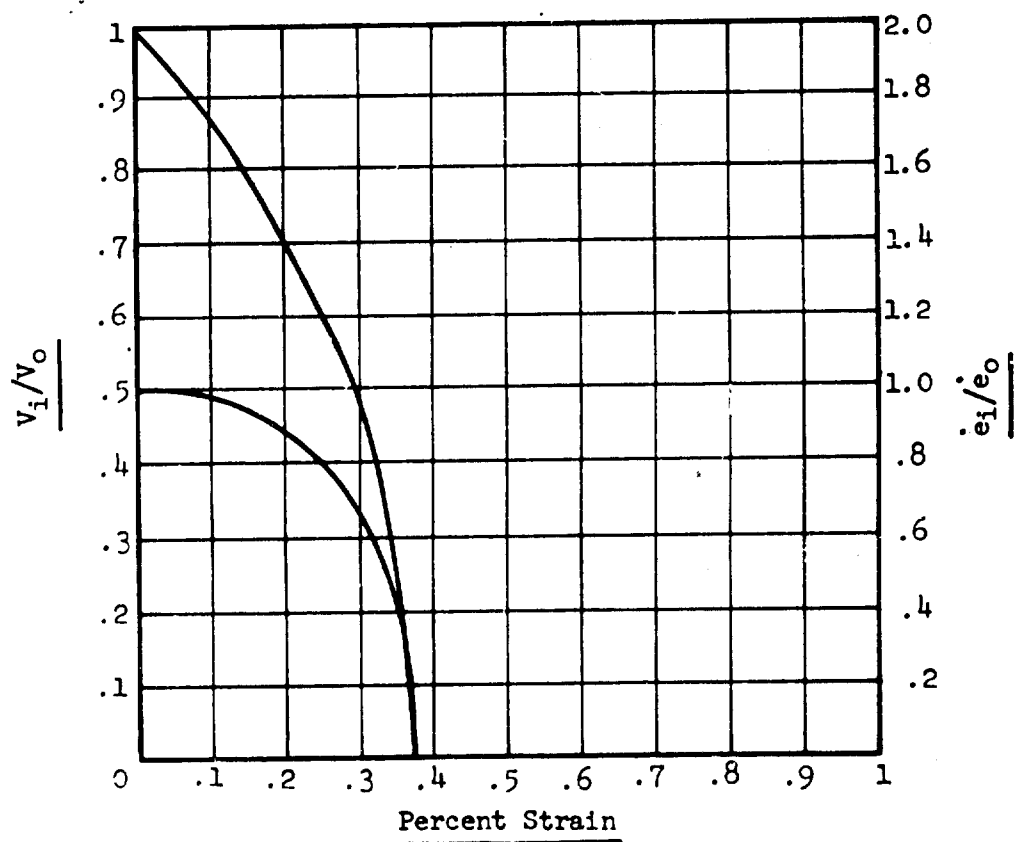
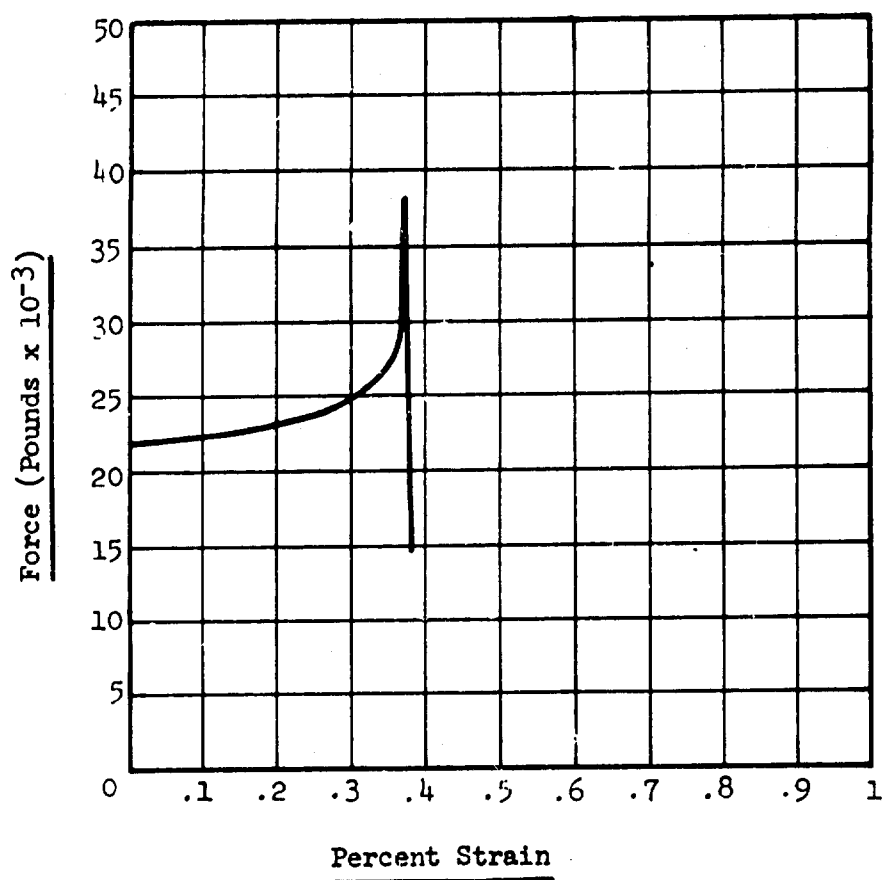


FIGURE 53. INSTANTANEOUS VELOCITY, STRAIN RATE AND DIE FORCE FOR A7-927

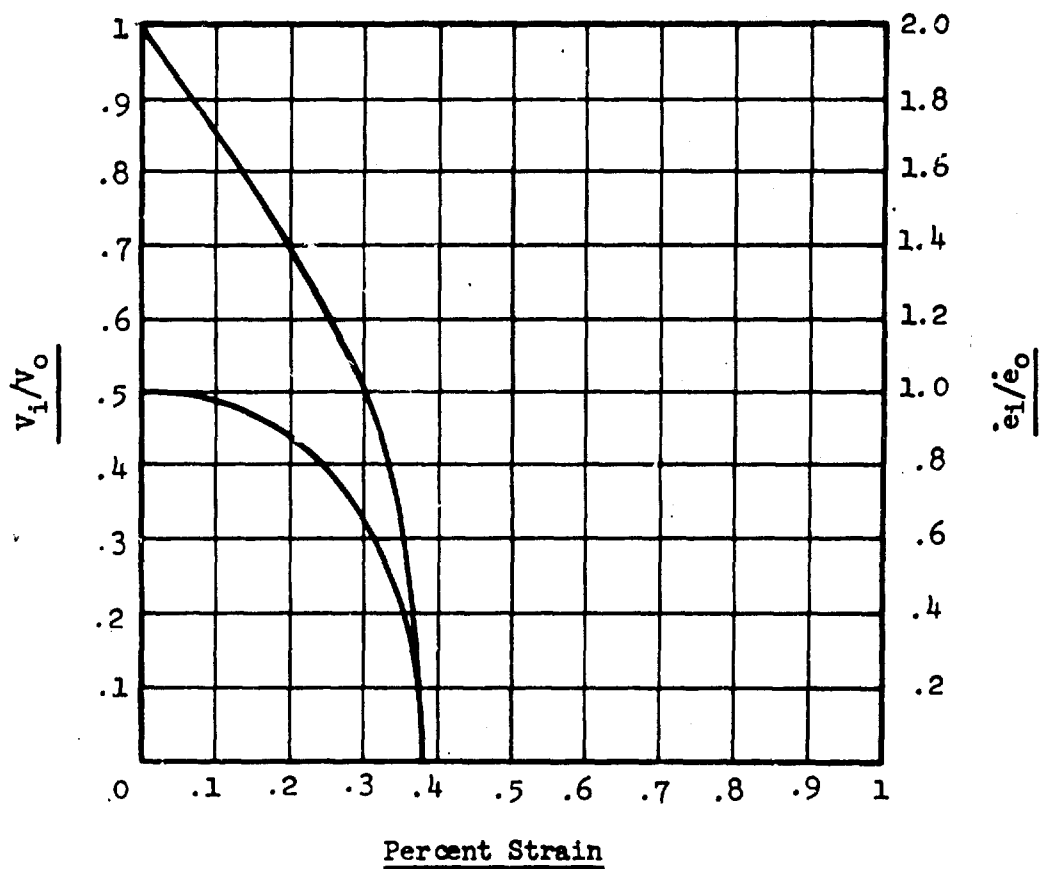
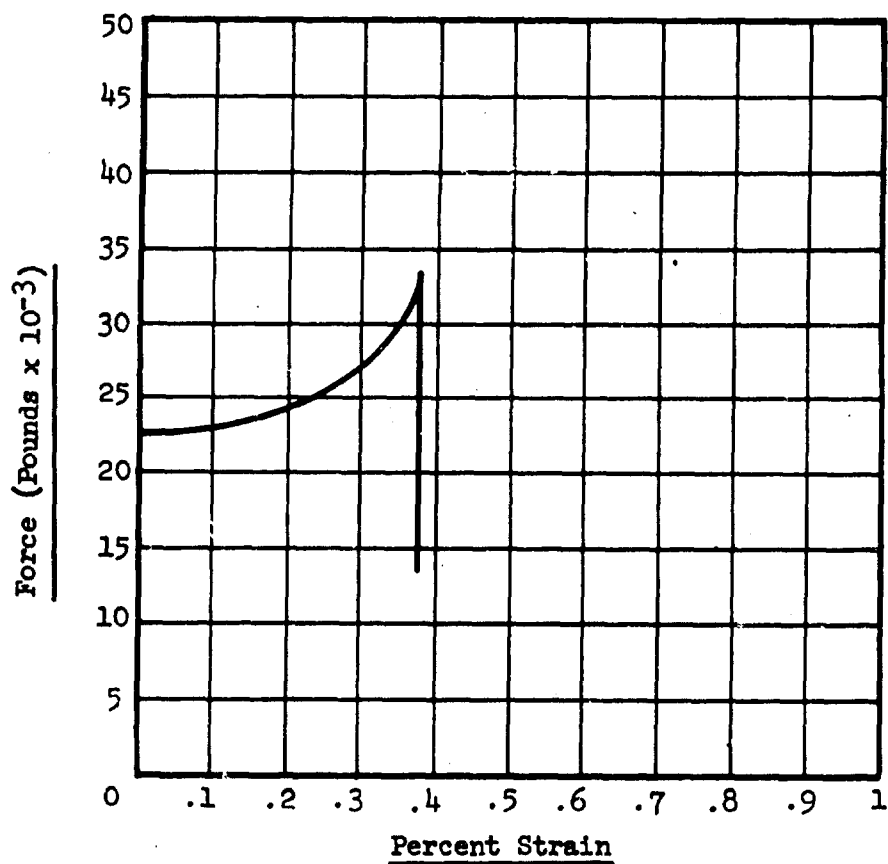


FIGURE 54. INSTANTANEOUS VELOCITY, STRAIN RATE AND DIE FORCE FOR A7-928

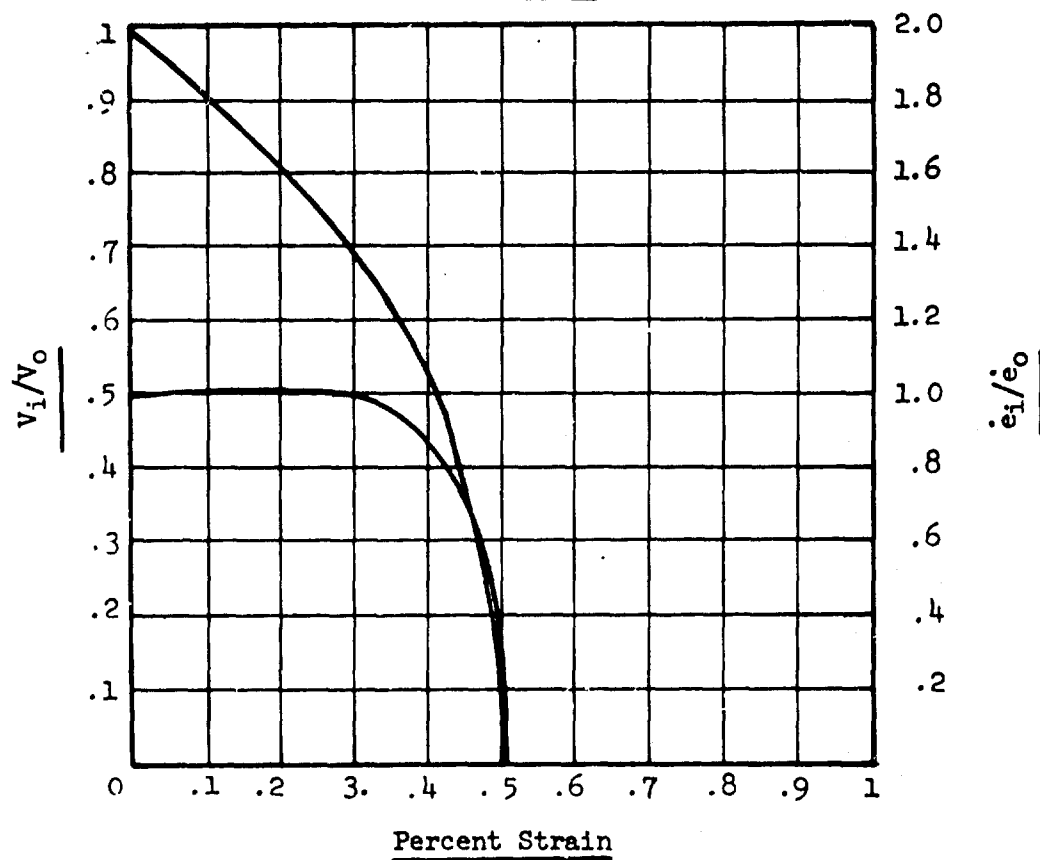
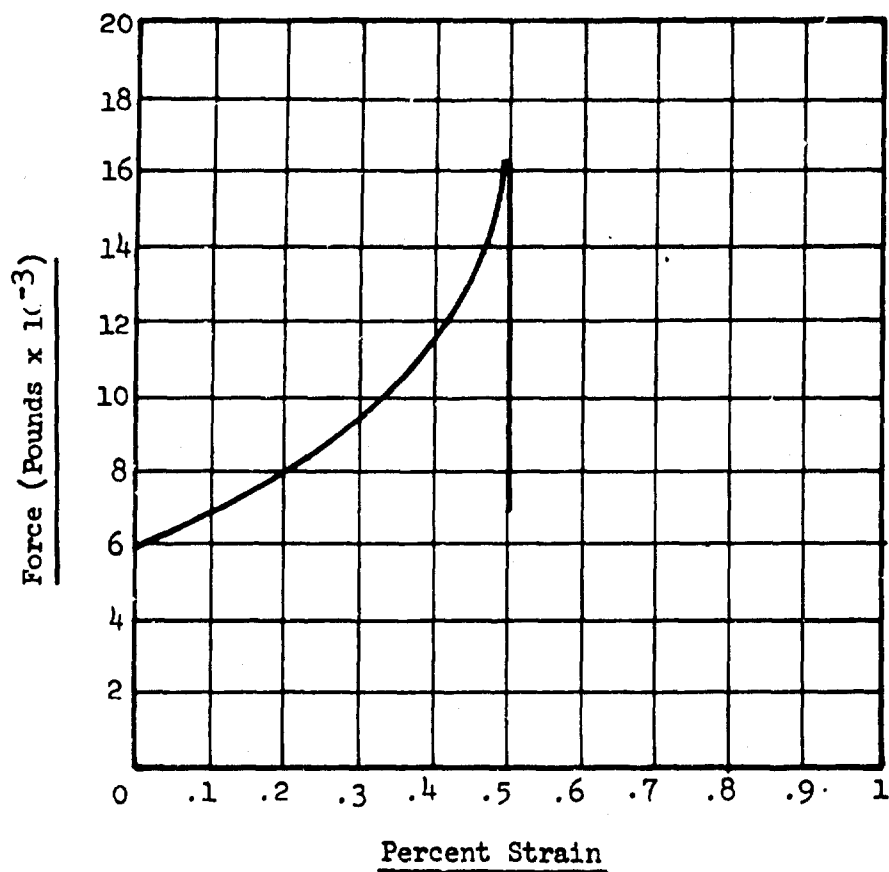


FIGURE 55. INSTANTANEOUS VELOCITY, STRAIN RATE AND DIE FORCE FOR F7-929

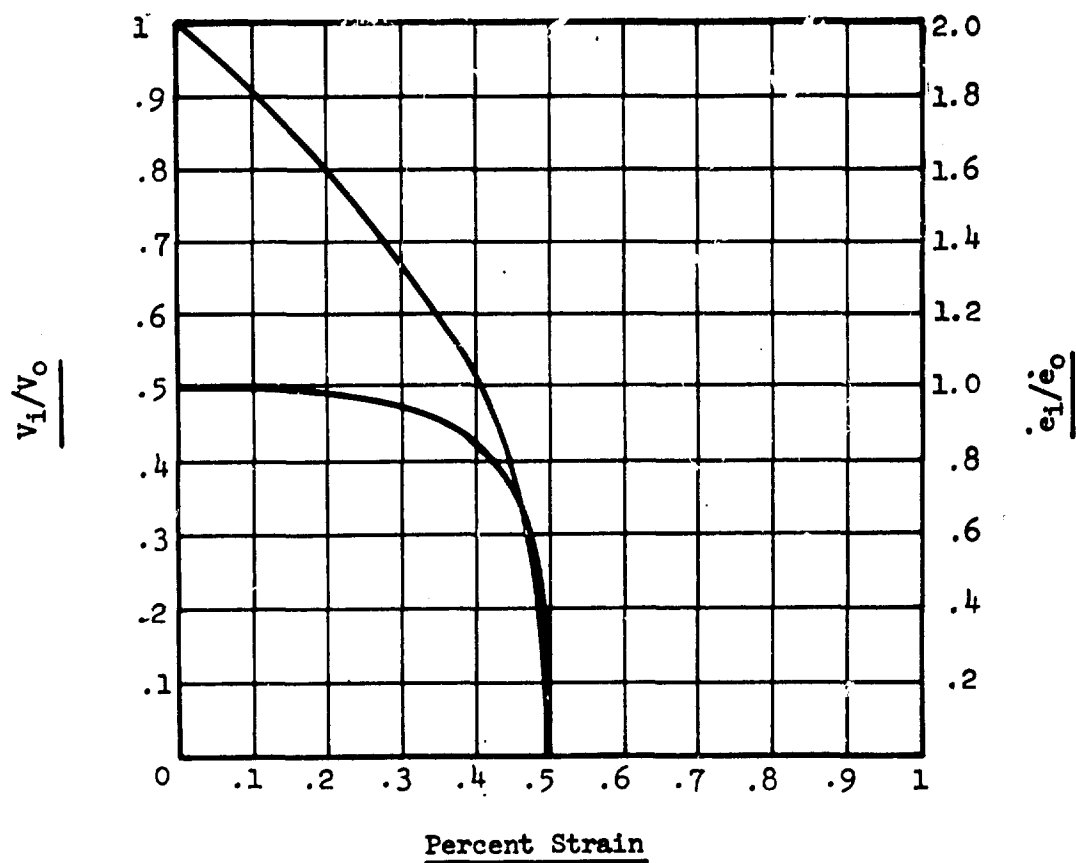
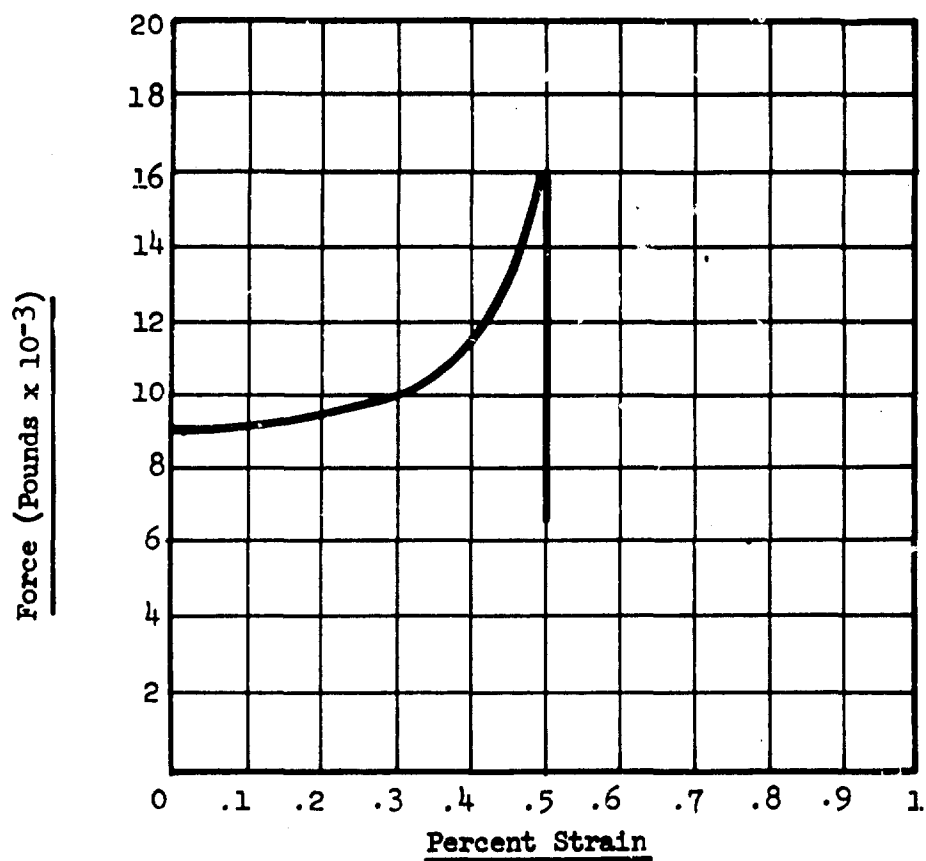


FIGURE 56. INSTANTANEOUS VELOCITY, STRAIN RATE AND DIE FORCE FOR F7-931

The types of material evaluation tests employed are given in Figure 57 .

TYPE OF TEST	DATA
Macro Hardness	Rockwell Hardness
R.T. Static Tensile Test	Sty, Sth, Elongation
R.T. Fatigue Test	Comparative fatigue life (no. of cycles to failure at constant stress level)

FIGURE 57 . MECHANICAL PROPERTIES TESTED

For both tensile and fatigue evaluation, test coupons were taken from forged bars upset a constant amount under different combinations of temperature and strain rate. For two alloys, 17-4 PH and A-286, the mechanical properties were tested after a standard post forging heat-treatment as well as in the as forged conditions. From this data conclusions may be drawn as to the nature and extent of changes that can be expected in material properties subjected to very high deformation rate processes.

#### Experimental Plan

The experimental plan may be divided into two parts; (1) the preparation of test coupons and (2) mechanical properties testing. The preparation of test coupons is shown in Figure 20 . Bar shape forging billets,  $\frac{1}{2} \times \frac{1}{2} \times 4$  inches, were cut from stock and upset forged under the program test conditions. The bars were forged to a nearly constant percent upset for a given material at a minimum of three strain rates. The lower strain rate was obtained using a drop hammer while the remaining points were established using the high energy impact machine.

The forging temperature and the amount of upset were chosen based on the forgeability test results as shown schematically in Figure 59 . It is noted the strain value was chosen low enough to keep this factor constant at both temperature levels. The hot forging temperature was chosen for an optimum combination of reduced flow stress and high ductility. The warm forging temperature was selected in a range of acceptable ductility at a temperature low enough to allow prolonged heating in air without significant surface oxidation. The general plan for testing the tensile and fatigue properties is outlined in Figure 60 which gives the test conditions for both initial upsetting and properties testing.

For tensile testing a minimum of two duplicate specimens were provided for each test condition. The tensile properties at room temperatures were obtained by standard static tensile testing procedures.

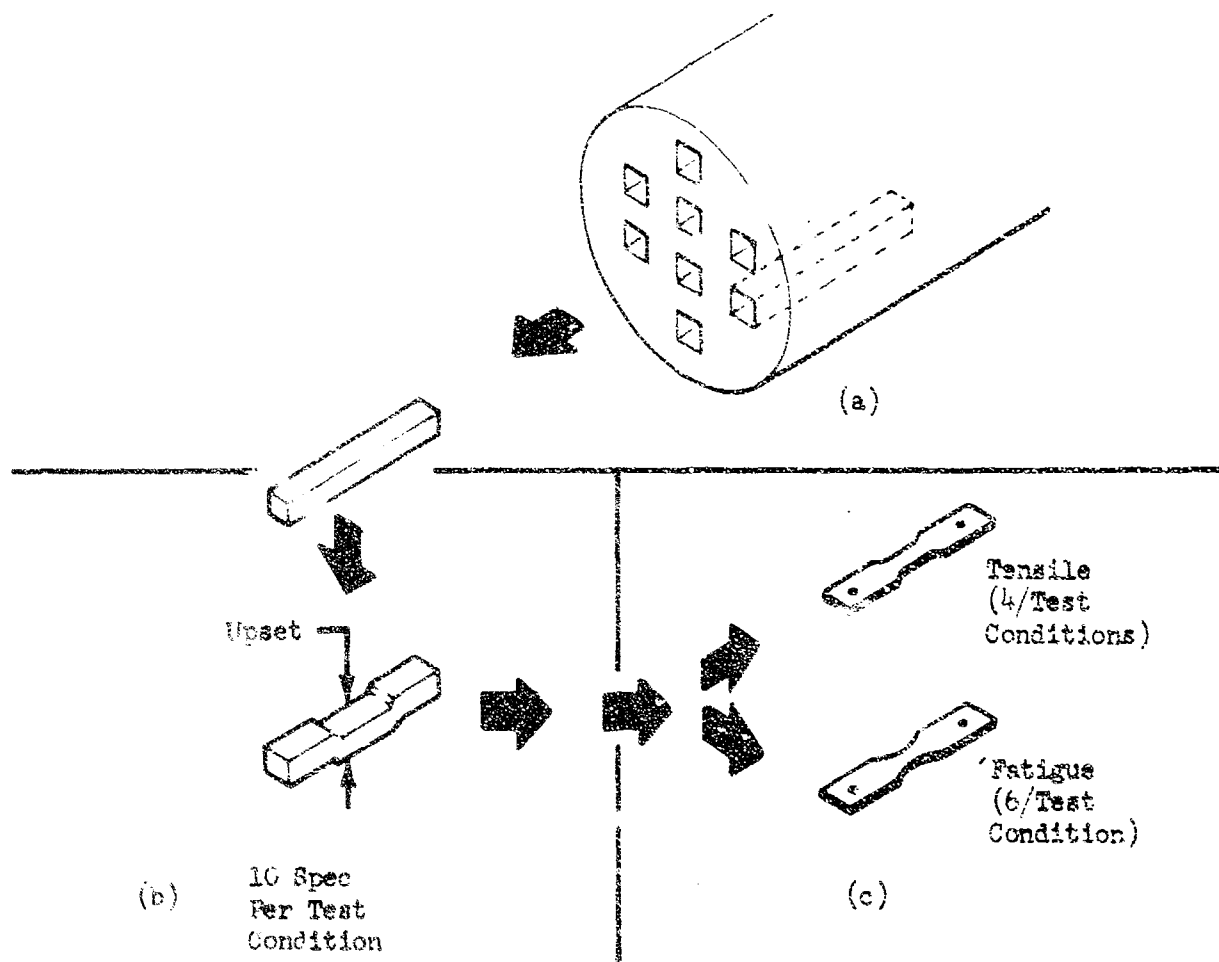


FIGURE 58. FABRICATION OF TENSILE AND FATIGUE SPECIMENS

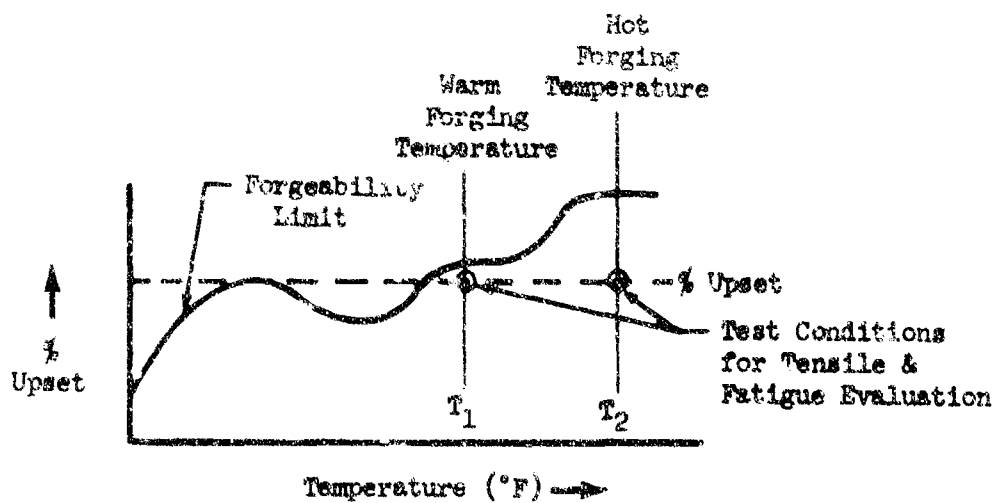


FIGURE 59. SELECTION OF STRAIN AND FORGING TEMPERATURE

Material	Test Conditions			Minimum Number of Tests per Condition			
	Percent Unset	Forging Temperature °F	Number of Forging Strain Rates	As Forged		Forged and Heat Treated	
				Tens.	Fat.	Tens.	Fat.
2024-C Aluminum	50	Room	3	2	3	0	0
		550	3	2	3	0	0
		750	3	2	3	0	0
5Al-2.5Sn Titanium	25	1550	3	2	3	0	0
		1950	3	2	3	0	0
17-4 PH Stainless Steel	40	1550	3	2	3	2	3
		1950	3	2	3	2	3
A-286	50	1050	3	2	3	2	3
		1950	3	2	3	2	3

FIGURE 60 EXPERIMENTAL TEST SCHEDULE

The fatigue specimens were tested to failure in tension - tension fatigue at room temperature. A minimum of three duplicate tests were conducted for each test condition, that is, for each combination of temperature and strain rate. Because of the program limitations it was necessary to formulate an experimental plan to provide a qualitative evaluation of the temperature-strain rate effect with regards to fatigue. Since only one stress level was feasible, it cannot be specified exactly at what point on the S-N curve the fatigue life comparison is to be made. The stress level was chosen, based on preliminary tests, to allow specimen failure in the 100 to 200 thousand cycle range. Further, it was decided to hold the stress level constant for the three forging strain rates at each forging temperature in a given material. This compromise plan was judged optimum to give a sufficient number of cycles for minimal scatter and still keep the testing time down to approximately 1.5 hrs. per test. This test plan had the advantage, therefore of permitting the investigation of a maximum number of test conditions on a qualitative basis within the allotted time span.

#### Equipment and Procedures

The bar upset operation was accomplished with the same basic equipment used for forgeability testing. The low strain rate drop hammer forging set-up is shown in Figures 131 and 132. High velocity forging utilized the high energy impact equipment shown in Figures 133 and 134. Billet heating was accomplished in a special furnace located above the anvil as shown in Figures 61 and 140. Because of the excess kinetic energy in the light weight projectiles at high velocities energy absorbing bars were mandatory. This problem was solved by dropping the heated forging billet into an expendable container as shown in Figure 61. In addition to allowing high impact velocities by absorbing the excess energy, this technique was found to produce a more nearly plain-strain condition in the forged piece as compared to bars upset without restraint.

Specimens were brought to the final forging temperature as measured by a thermocouple resting on the upper end of the specimen. The heating of specimens upset at low strain rate in the drop hammer was accomplished in a standard muffle furnace using the special tool shown in Figure 62. This tool was designed to aid in transferring the billet with a minimum temperature loss. In both the high and low velocity processes, the temperature recorded was the soak temperature and the billet was transferred and forged within a time span of 3 to 5 seconds.

Aluminum 2024, Ti-5Al-2.5 Sn, and A-286 were heated directly to forging temperature, allowed to soak for 10 minutes, and forged. The alloy 17-4 PH was austenitized at 1950°F for 15 minutes in a preheat furnace, placed in the forging furnace and allowed to cool to the desired temperature. After the upset operation, the billets were allowed to cool in their containers.

Tensile and fatigue specimens were machined from the forged bars by removing material from both faces such that coupon blanks, approximately 3.75 x 0.5 x 0.1 inches, were obtained from the center of the bar. Tooling holes were drilled in the coupon blank to establish the specimen center line and the specimen profile was machined. Cutter marks were removed by hand sanding followed by hand polishing to remove transverse scratches. Inspection on a specially designed check fixture showed the profile to be symmetrical about the center line within a tolerance of 0.002 inches for all specimens.



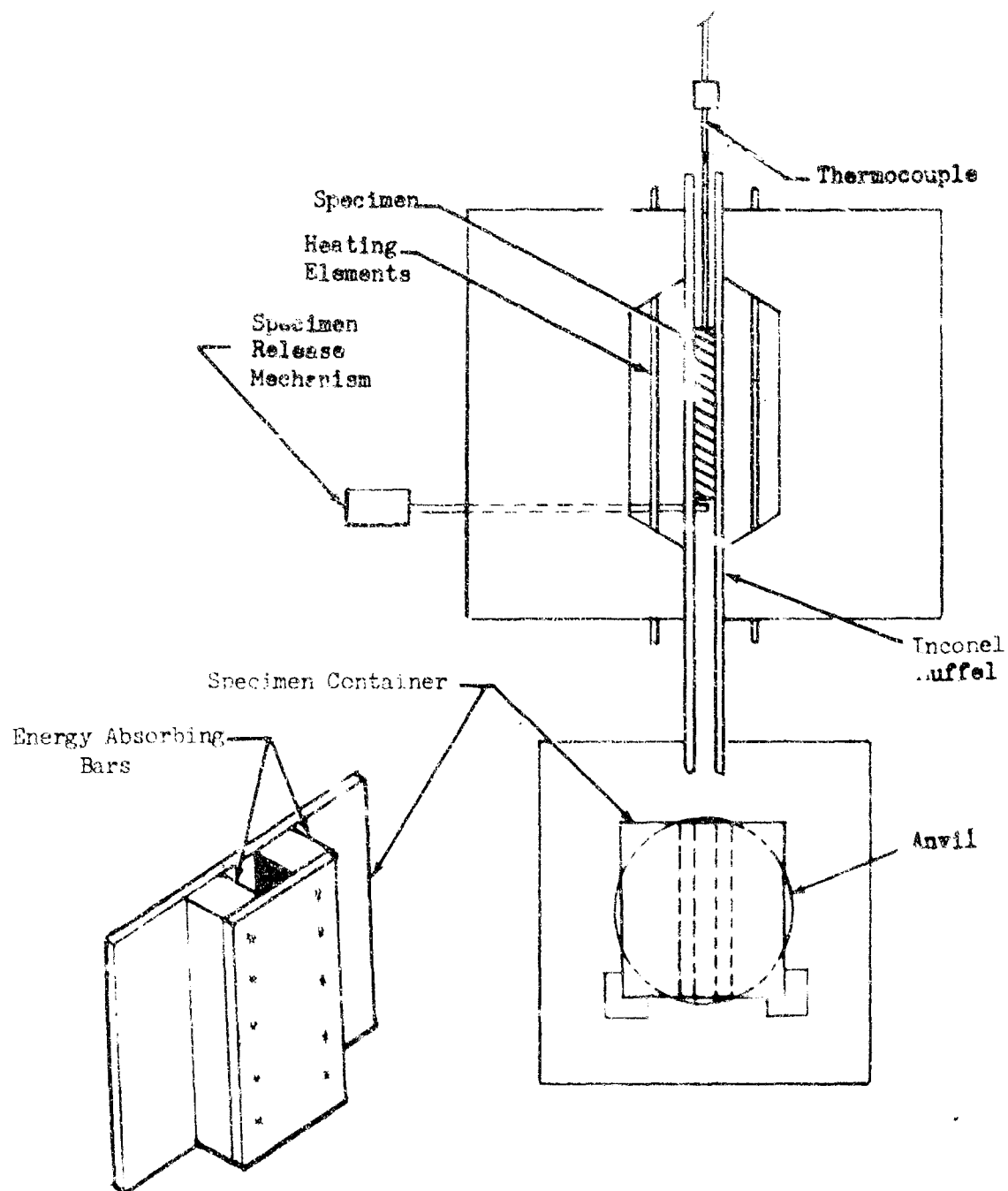


FIGURE 61. FURNACE AND LOADING METHOD FOR BAR SPECIMENS

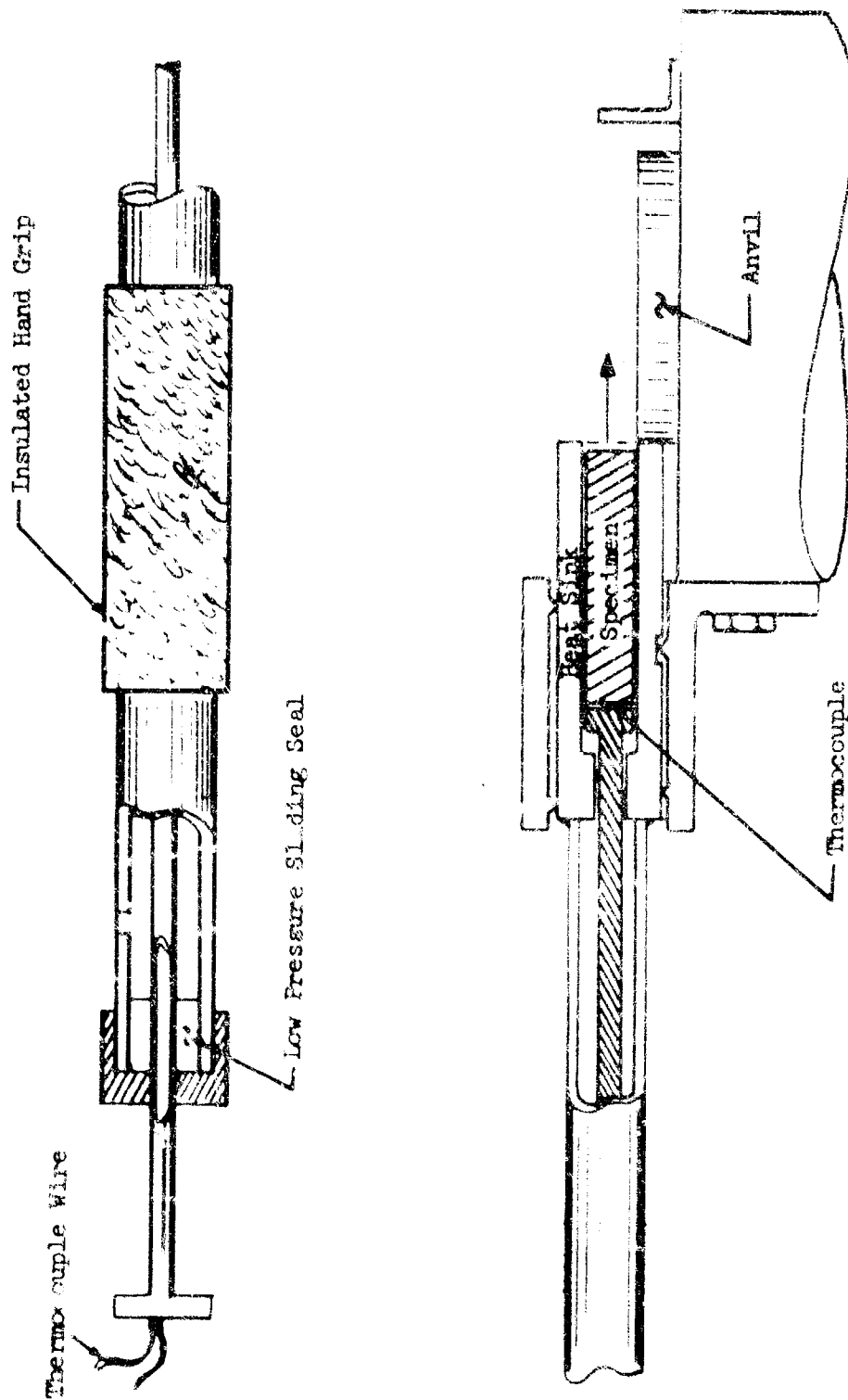


FIGURE 69. BAR SPECIMEN LOADING TOOL.

The dimension of the fatigue and tensile specimens were based on ASTM standards, as shown in Figure 63.

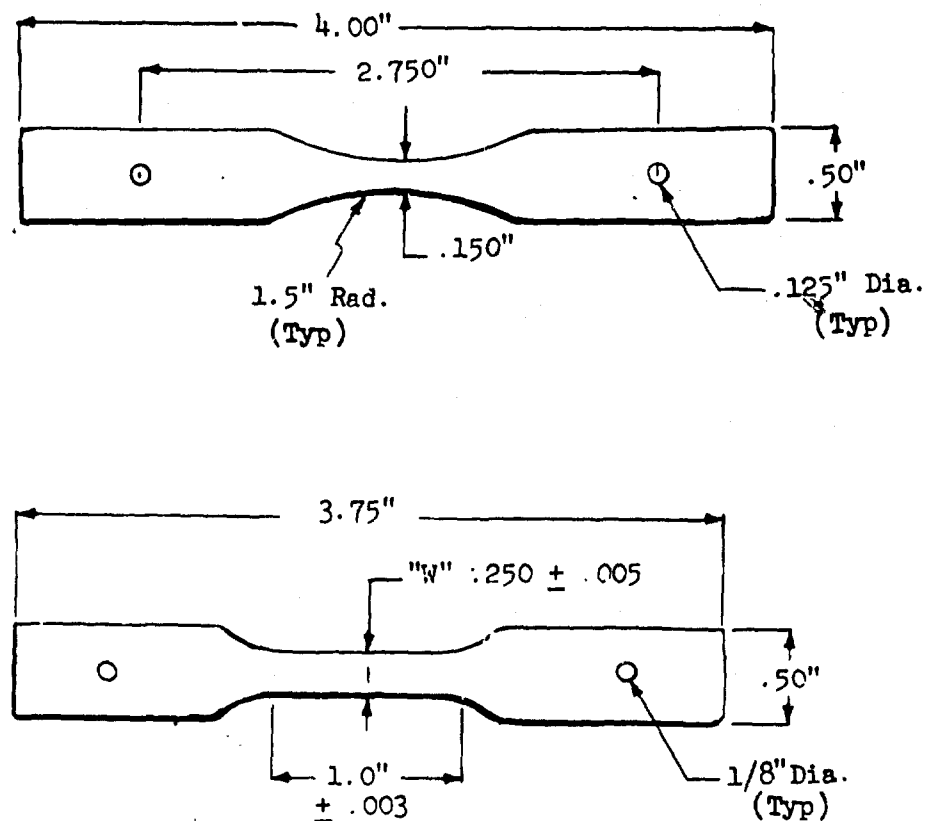


FIGURE 63. FATIGUE AND TENSILE SPECIMEN DIMENSIONS

At this point specimens were selected at random for post forging heat treatment in accordance with the test plan. All such specimens, both tensile and fatigue, of the same material were heat treated in one batch. The heat treatment used for 17-4 PH and A-286 was as follows:

- A-286 (1) Solution HT-1800°F  $\pm$  25°F for 1 hr., oil quench
- (2) Precipitation HT- 1325°F  $\pm$  15°F for 16 hrs., air cool
- 17-4 PH (1) Solution HT - 1900°F  $\pm$  25°F, for 1 hr., air cool
- (2) Sub cool at -50°F for 1 hr.
- (3) Precipitation HT - 925°F  $\pm$  10°F 1 hr., air cool

### Data Acquisition

The tensile properties of forged specimens at the specified test conditions of strain rate and forging temperature are given in Table XII, Appendix III. The temperature listed is the furnace temperature of the billet. The percent reduction given to the specimen during upset was calculated from the original and final thickness of the billet in the forging direction as follows:

$$\% \text{ Red.} = (H_0 - H_f)/H_0 \times 100$$

The initial strain rate ( $\dot{\epsilon}_0$ ) listed in the right hand column was calculated from the projectile velocity ( $V_0$ ) at impact and the initial billet thickness ( $H_0$ ) by the relation:

$$\dot{\epsilon}_0 = V_0/H_0$$

For the fatigue data given in Table XIII, Appendix III the test conditions are also listed in terms of temperature strain and strain rate. In this table the average ultimate stress (ave.  $S_{tu}$ ) was obtained from the tensile data. The stress level percentage was determined experimentally to give an expected fatigue life on the order of 150 thousand cycles. For all tests the oscillating load was set for a range ratio of 0.1 as shown schematically in Figure 64. All fatigue testing was done using a Sonntag inertia-type constant force test machine.

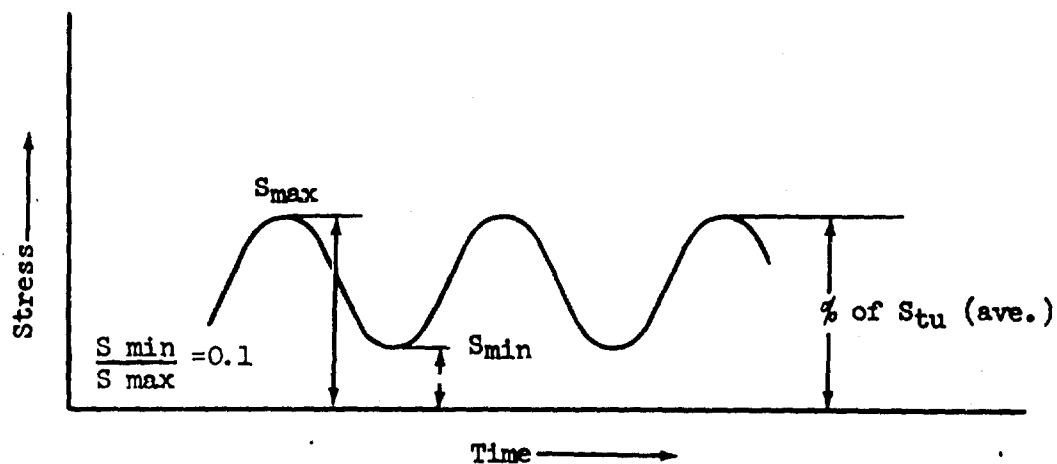


FIGURE 64. FATIGUE TEST CONDITIONS

### Results

The mechanical properties data is presented in graph form in Appendix II, Graph 44.

## Discussion of Results

### Forgeability

The combined effect of temperature and strain rate over the range from 100 to 4000 in/in/sec for the four Phase II alloys is shown in Figure 65.

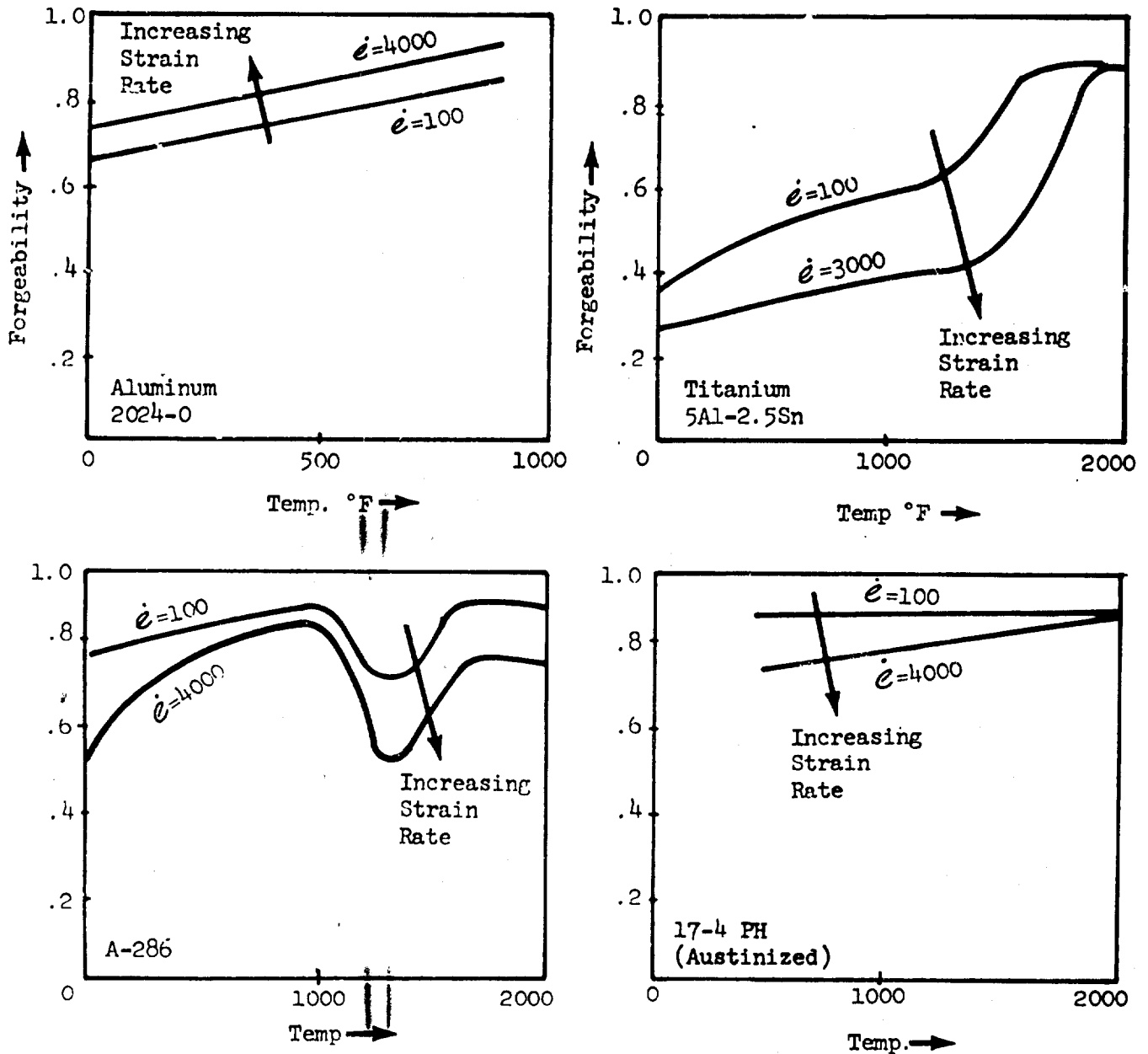


FIGURE 65. COMBINED EFFECTS OF TEMPERATURE AND STRAIN RATE ON FORGEABILITY OF PHASE II MATERIALS

It is noted that for three of the alloys (Ti 5Al-2.5Sn, 17-4 PH & A-286) there is a general decrease in forgeability over the temperature range with increasing strain rate while for 2024 aluminum the forgeability increases with both temperature and strain rate. It is also noted that for each of the four alloys with the exception of 2024 aluminum there is at least one temperature range where forgeability is not affected by changes in strain rate. This occurs in the 1800 to 2000°F range for titanium and 17-4 PH and in the 900 to 1000°F range for A-286.

### Forging Energy

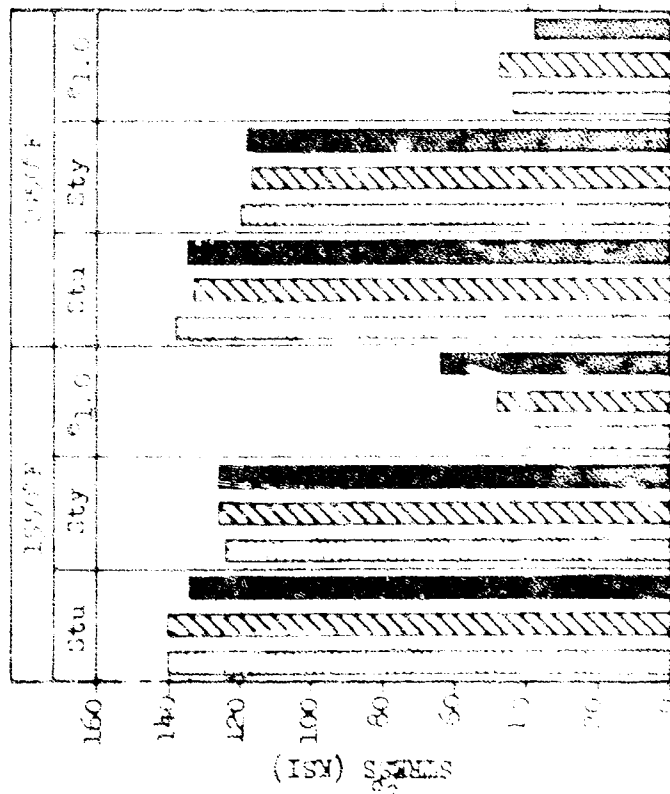
Most metals when worked in a soft condition show a pronounced increase in flow stress under high strain rate tensile deformation. Further, the die force in uniaxial compression has been shown (6) to increase with increasing strain rate. The iron base superalloy A-286, for example, upset 50% at 2000°F requires a specific energy increase of 5 to 30 thousand inch lbs per cubic inch over the strain rate range from 0.1 to 100 in/in/sec. Based on these data it would be reasonable to expect even higher forging energy levels through the 100 to 8000 range investigated in the present program. The results of this program however, show no such increase based on two independent methods of analysis. First, the forging energy as measured by the mass and velocity of the projectile at impact was found to either increase or decrease with increasing strain rate depending on the percent upset as shown in Figures 46, 47, and 48 for 2024 aluminum. In the second method instantaneous forging force was calculated from accurate measurements of the projectile deceleration during the upset event. This method, described under "Instantaneous Process Parameters" also showed that forging energy is essentially constant with respect to strain rate above 200 in/in/sec for 2024 aluminum and A-286.

### Mechanical Properties

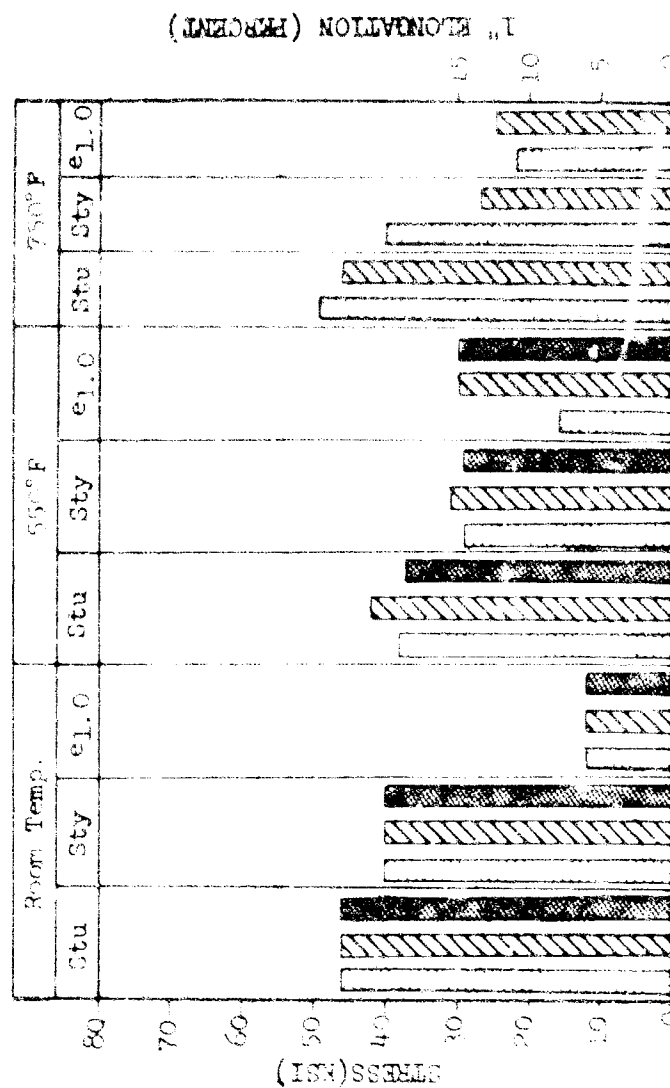
The effect of strain rate and temperature on the final tensile properties for the four phase II alloys is summarized in Figures 66 through 68.

The strain rate values are, for simplicity, order-of-magnitude values. Exact strain rates are listed in Table XII, Appendix III. The data of Figures 67 and 68 for 17-4 PH and A-286 are most significant since they show both the properties as forged and after heat treatment. In both materials it can be noted that the highest strain rates resulted in a better heat treat response. This is particularly significant since no preliminary testing was done to find the optimum heat treatment. The room-temperature and warm forged specimens tested in the as forged condition show no deleterious effect as a result of increasing strain rate.

The results of fatigue testing are difficult to evaluate because of the excessive scatter. For 2024-O aluminum, the fatigue life increases with increasing strain rate. Metallurgical examination of these specimens showed incipient grain boundary melting at the high strain rate sample forged at 750°F and for all strain rates at 850°F. This result is illustrated in Figure 69.



(a) Ti-6Al-2V



(b) 2024-T3 Aluminum

1000 in/in/sec  
100 in/in/sec  
10 in/in/sec

FIGURE 66. COMBINED EFFECT OF TEMPERATURE AND STRAIN RATE ON THE MECHANICAL PROPERTIES OF TITANIUM AND ALUMINUM

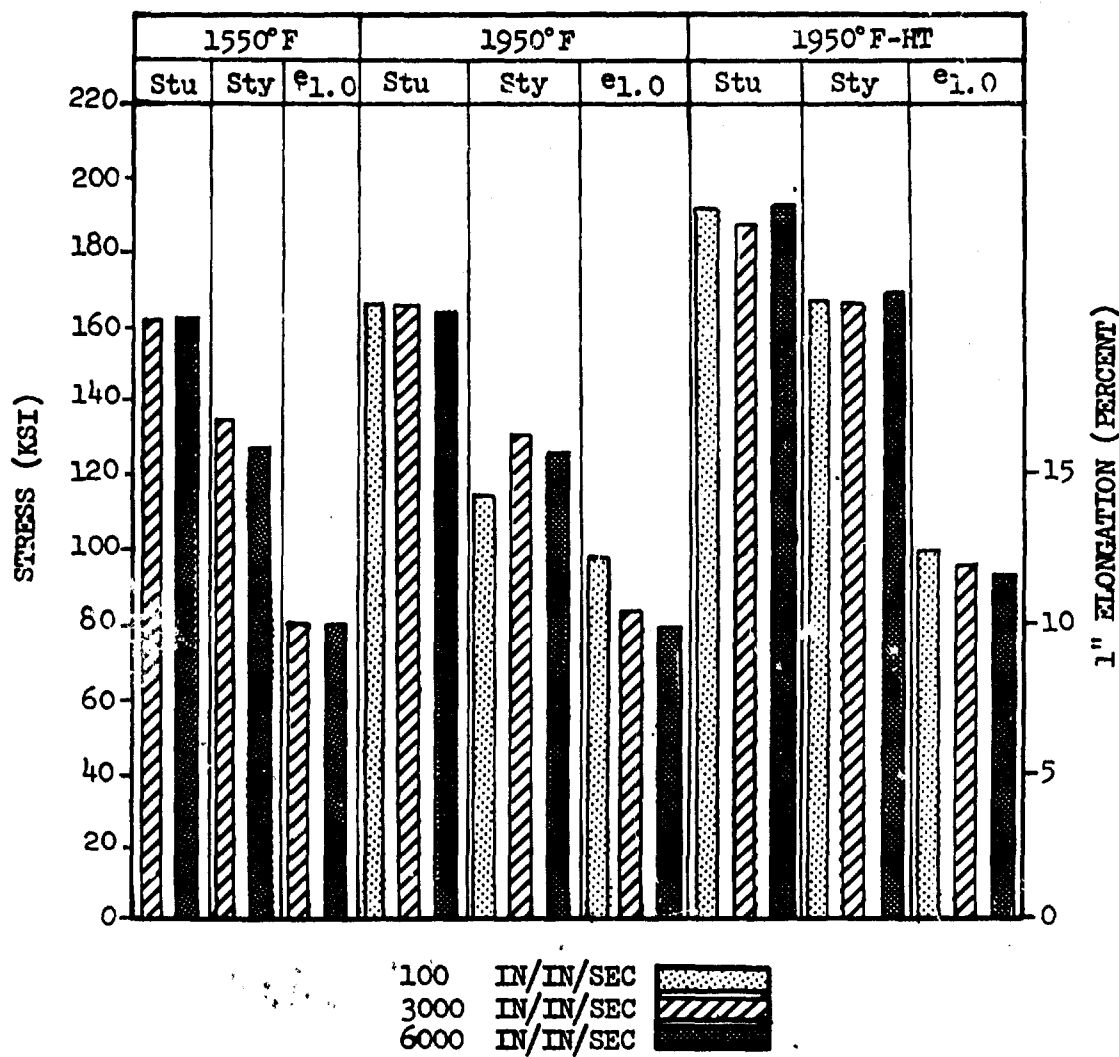


FIGURE 67. COMBINED EFFECT OF TEMPERATURE AND STRAIN RATE ON THE MECHANICAL PROPERTIES OF 17-4 PH.



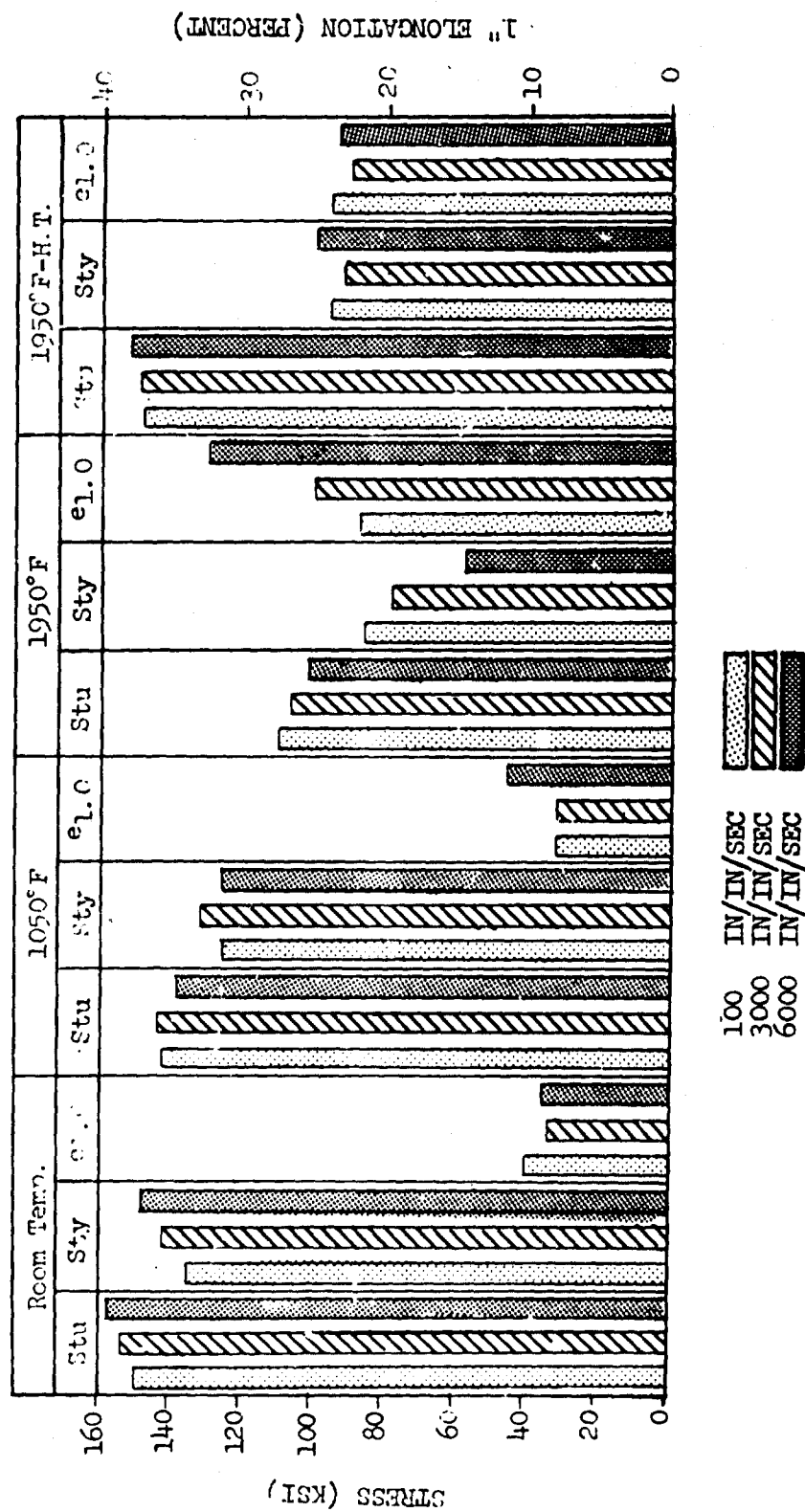


FIGURE 68. COMBINED EFFECT OF TEMPERATURE AND STRAIN RATE ON THE MECHANICAL PROPERTIES OF A-286.

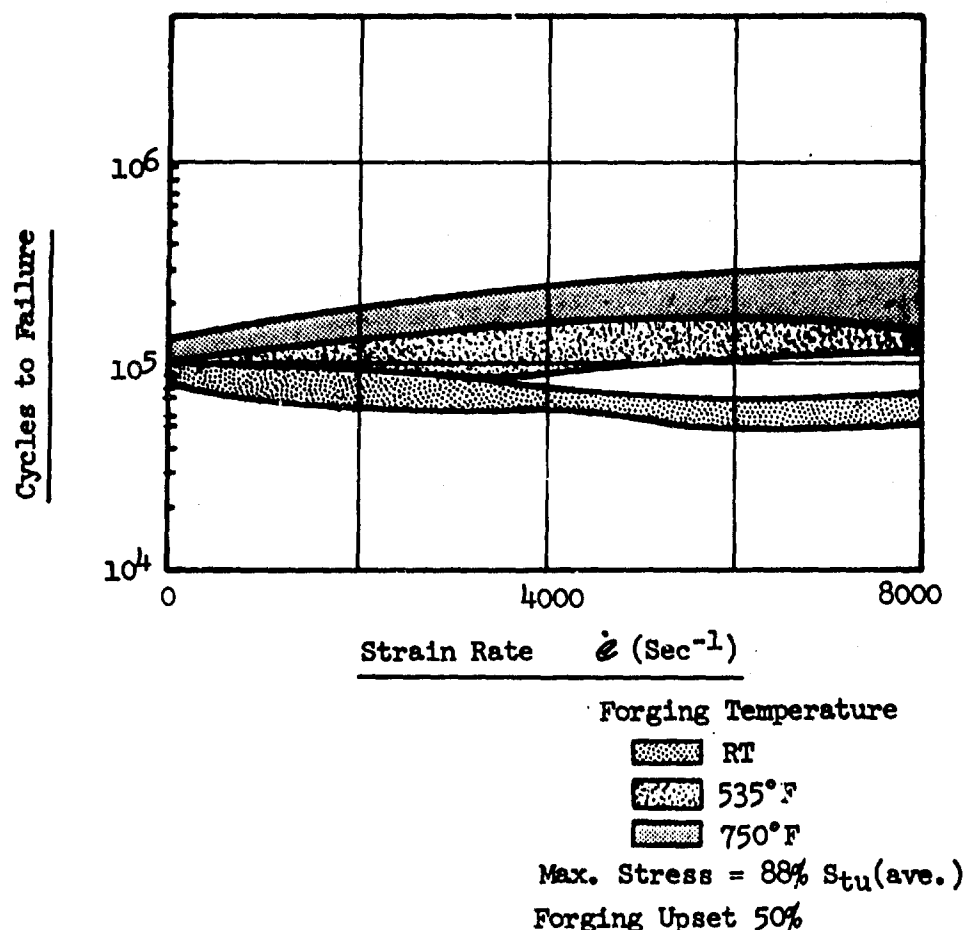


FIGURE 69. FATIGUE LIFE OF 2024 ALUMINUM

The erratic results obtained for titanium, and 17-4 PH fatigue specimens tested in the as forged condition can be attributed to residual stress although the degree of scatter is considerably greater than expected. Discounting two test points in Graph 55, all of the A-286 fatigue data can be evaluated as shown in Figure 70. The most significant data are for the heat treated specimens.

The as-forged and post heat treat fatigue results for 17-4 PH upset at 1950°F is shown in Figure 71. As with the A-286 there is clear evidence of residual compressive stresses in the material prior to heat treatment. In both materials the fatigue life is relatively constant over the 100-7000 strain rate range with a slight improvement indicated at the high strain rate for 17-4 PH.

#### Metallographic Data

Metallographic examination of 15 selected fatigue and tensile specimens did not reveal any definite change in the micro-structure that could be associated with strain rate other than the grain boundary melting in 2024-O aluminum at the high strain rates at hot forging temperatures. Further, this cursory examination failed to reveal a cause for the large scatter encountered in fatigue tests on the as-forged titanium and 17-4 PH alloys.

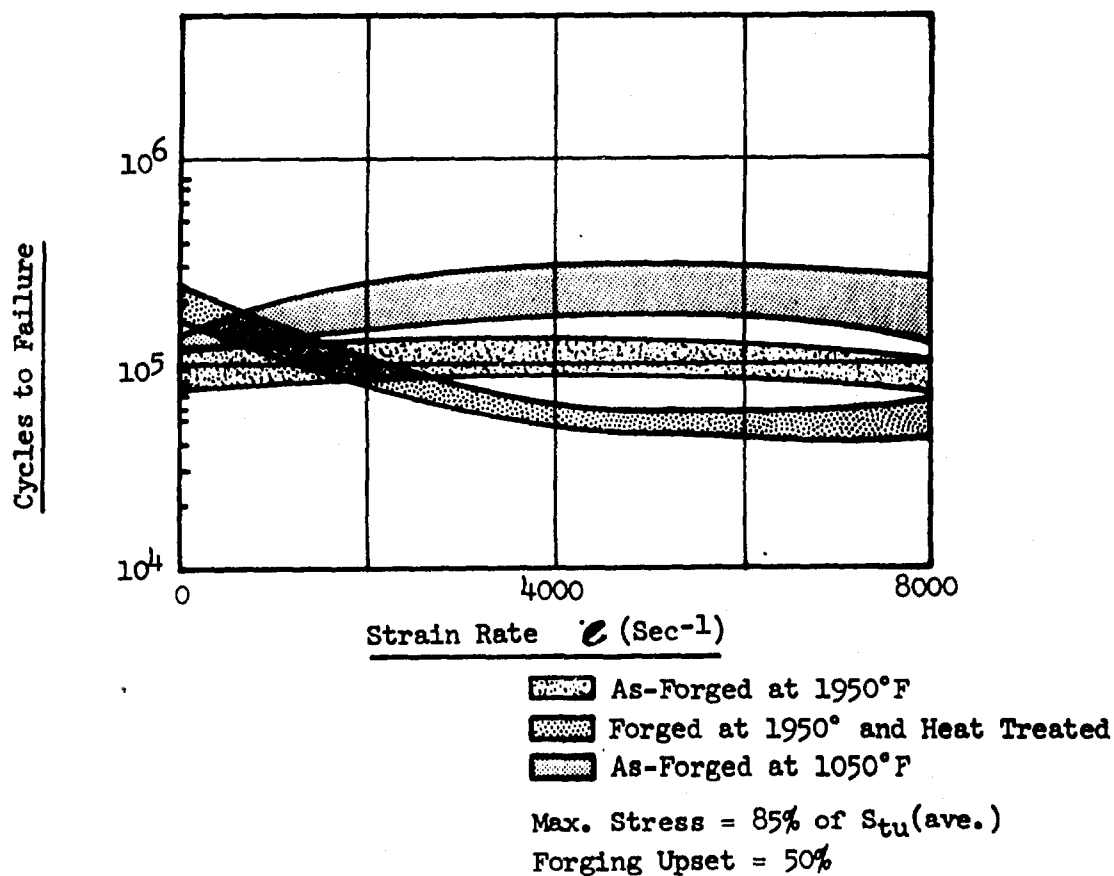


FIGURE 70. FATIGUE LIFE OF A-286

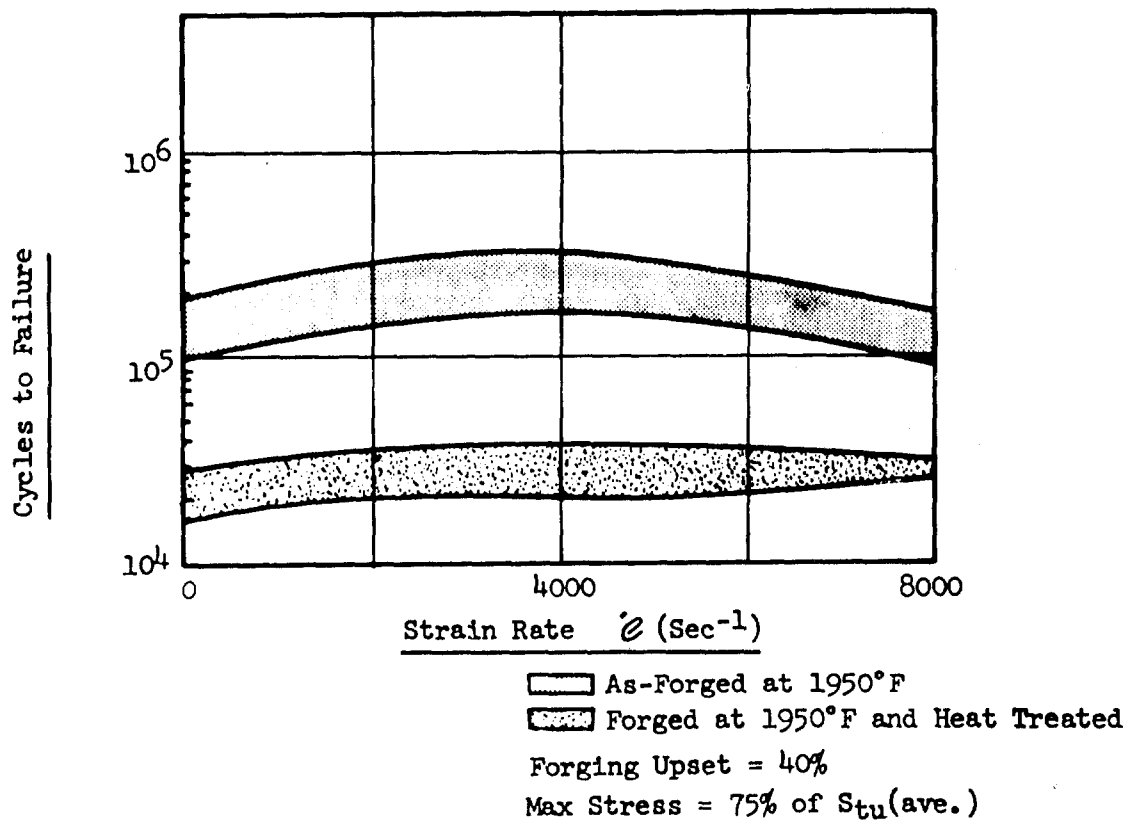


FIGURE 71. FATIGUE LIFE OF 17-4 PH

### Summary

The Phase II results show conclusively that the forging processes within the program test range present no problems with regard to forgeability, tooling, or structural integrity of the finished product. An improvement of the final tensile properties are indicated as a result of improved heat treat response. This effect, firmly established in present high energy rate systems as typified by the Fairchild CEFF and the Dynapak processes appear to extend into the higher strain rate range investigated in this program as evidenced by the heat treat response of 17-4 PH and A-286.

APPENDIX I  
PROPERTIES AND IDENTIFICATION  
OF PROGRAM TEST MATERIALS

TABLE IV. MECHANICAL PROPERTIES OF TEST MATERIALS

MATERIAL	BILLET IDENT	YIELD	TENSILE	% ELONG.	% RED.	HARDNESS	STDS.	CONDITION
2024-0 Aluminum	A-1	15,750	34,900	11.0			QQ-A 225/6	
	A-2	18,400	34,500	11.0			"	
	A-3			Not Available			"	
	A-4						"	
	A-5	17,000	33,750	14.0			"	
	A-6			Not Available			"	
2024T351	A-7	45,000	62,000	10.0			"	Annealed to "0" condition. 750°F for 2 hours and cooled 50° per hour to 450°F.
7075 Aluminum	B-1	23,400	39,900	9.0			QQ-A 225/9	
	B-2	23,700	39,000	9.0			"	
	B-3			Not Available				
5Al-2.5Sn Titanium	C-1	124,300	134,800	13.0	31.9	27.5R <sub>C</sub>	AMS 4629B	Production annealed 1500°F for one hour and air cooled.
	C-2	126,900	137,400	16.0	31.3	33.1R <sub>C</sub>	"	Production annealed 1500°F for one hour and air cooled.
	C-3	134,000	143,400	15.0	33.0	32.5R <sub>C</sub>	"	Production annealed 1500°F for one hour and air cooled.
	C-4	129,800	141,750	15.0	33.6	31.5	"	Production annealed 1500°F for one hour and air cooled.
	C-5	125,600	133,300	17.5	36.7	30.5R <sub>C</sub>	"	Production annealed 1500°F for one hour and air cooled.

TABLE III. CHEMICAL COMPOSITION OF TEST MATERIAL (CONT'D)

MATERIAL	BILLET IDENT.	Mn	Si	Zr	Ca	Mo	S	P	Ti	C	Ni	B	Al	Co
18% Maraging (Vascomax-300)	G-2	.08	.01	.010	.05	4.80	.005	.003	.68	.007	18.70	.002	.13	9.10
	G-3	.04	.07	.010	.05	4.82	.009	.006	.59	.013	18.90	.003	.10	8.67
Rene' 41		Mn	Si	Cr	Fe	Mo	S		Ti	C	Ni	B	Al	Co
	I-1	.04	.22	19.01	1.61	9.9	.010		3.10	.07	BAL	.0053	1.44	11.23
	I-2	.01	.06	18.6	1.10	9.65	.009		3.16	.11	BAL	.0057	1.44	11.12
L-605		C	Mn	Si	S	P	Cr	Fe	Hi	W	Co			
	J-1	.089	1.46	.34	.006	.005	19.5	.61	9.77	14.77	BAL			
	J-2	.086	1.40	.48	.006	.011	19.58	2.45	10.06	14.37	BAL			
TZM Moly		C	Si	Hi	Mo	Ti	Zr	O	N	H	Fe			
	H-1	.022	.0035	.0048	99.25	.45	.076	.0012	.0002	.0001	.0015			
	H-2	.021	.0035	.001	99.25	.40	.083	.0025	.0007	.0003	.004			
	H-3	.021	.0024	.0001	BAL	.46	.1	.0029	.0004	.0001	.0039			

TABLE III. CHEMICAL COMPOSITION OF TEST MATERIAL (CONT'D)

MATERIAL	BILLET IDENT.	Mn	Si	Cr	V	Cu	S	P	Ta	C	Ni	Co	Ti	Mo
17-4 PH Stainless	E-7	.30	.66	15.86		3.34	.016	.015	.01	.033	4.34	.26		
A-286		Mn	Si	Cr	V	Mo	S	P	Ti	C	Ni	B	Al	
	F-1	1.26	.48	14.05	.24	1.19	.016	.021	2.24	.053	24.26	.0048	.18	
	F-2	1.40	.68	14.95	.28	1.32	.012	.016	2.10	.045	26.04	.005	.15	
A-286		Mn	Si	Cr	V	Mo	S	P	Ti	C	Ni	B	Al	Co
	F-3	1.27	.50	14.32	.25	1.28	.005	.014	2.12	.040	25.68	.003	.26	
	F-4													
	F-5	1.63	.77	14.87	.35	1.25	.008	.017	2.21	.049	25.34	.003	.13	
	F-6	1.61	.86	15.3	.26	1.23	.008	.019	2.09	.059	25.62	.0049	.15	
	F-7	1.51	.51	14.64	.31	1.25	.013	.017	2.22	.050	25.29	.0031	.11	
18% Maraging (Vas. 300)		Mn	Si	Zr	Ca	Mo	S	P	Ti	C	Ni	B	Al	Co
	G-1	.05	.07	.013	.05	4.89	.006	.010	.51	.02	18.54	.003	.14	9.0



TABLE III. CHEMICAL COMPOSITION OF TEST MATERIAL (CONT'D)

MATERIAL	BILLET IDENT.	Mn	Si	Cr	Fe	Cu	Mg	Zn	Ti	C	N	Al	Sn	V
5Al-2.5Sn Titanium	C-6	.001			.34					.020	.010	5.2	2.6	
	C-7	.001			.30					.020	.012	5.1	2.5	
6Al-4V Titanium		Mn	Si	Cr	Fe	Cu	S	P	Ta	C	N	Al	Sn	V
	D-1				.14					.02	.009	6.5		4.2
	D-2				.08					.03	.010	6.5		4.2
	D-3				.17					.03	.010	6.2		4.30
17-4 PH Stainless		Mn	Si	Cr	V	Cu	S	P	Ta	C	Ni	Cb	Ti	Mo
	E-1	.23	.86	15.97		3.31	.013	.018	.01	.031	4.33	.28		
	E-2	.23	.59	15.93		3.21	.019	.019	.01	.032	4.36	.23		
	E-3	.26	.90	15.98		3.32	.013	.019	.01	.031	4.37	.26		
	E-4													
	E-5	.30	.66	15.86		3.34	.016	.015	.01	.033	4.34	.26		
	E-6	.20	.53	15.81		3.40	.017	.021	.01	.039	4.34	.28		

TABLE III. CHEMICAL COMPOSITION OF TEST MATERIALS

MATERIAL	BILLET IDENT.	Mn	Si	Cr	Fe	Cu	Mg	Zn	Ti	C	N	Al	Sn	V
2024-0 Aluminum	A-1	.60	.50	.10	.50	4.20	1.60	.25						
	A-2	.60	.50	.10	.50	4.20	1.60	.25						
	A-3	.60	.50	.10	.50	4.20	1.60	.25						
	A-4	.60	.50	.10	.50	4.20	1.60	.25						
	A-5	.60	.50	.10	.50	4.35	1.60	.25						
	A-6	.60	.50	.10	.50	4.35	1.60	.25						
	A-7	.60	.50	.10	.50	4.35	1.60	.25						
7075-0 Aluminum	B-1	.30	.50	.30	.50	1.60	2.50	5.60	.20					
	B-2	.30	.50	.30	.50	1.60	2.50	5.60	.20					
	B-3	.30	.50	.30	.50	1.60	2.50	5.60	.20					
5Al-2.5Sn Titanium	C-1	.01			.35					.020	.008	5.2	2.6	
	C-2	.02			.41					.023	.007	5.7	2.6	
	C-3	.01			.39					.022	.010	5.1	2.5	
	C-4	.01			.43					.020	.005	5.6	2.5	
	C-5	.001			.43					.020	.005	5.6	2.7	

TABLE IV. MECHANICAL PROPERTIES OF TEST MATERIALS (CONT'D)

MATERIAL	BILLET IDENT	YIELD	TENSILE	% ELONG.	% RED.	HARDNESS	STDS.	CONDITION
5Al-2.5Sn Titanium	C-6	129,000	140,750	15.0	32.4		AMS 4629B	Production annealed 1500°F for one hour and air cooled.
	C-7	127,000	138,000	18.0	40		"	Production annealed 1500°F for one hour and air cooled.
6Al-4V Titanium	D-1	120,300	134,100	16.0	36.0	25.0R <sub>c</sub>	AMS 4928-C	
	D-2	130,500	144,500	13.0	34.3	33.1R <sub>c</sub>	"	
	D-3	143,400	154,700	13.0	43.2	31.4R <sub>c</sub>	"	
	E-1	185,000	198,000	12.0	45.6	BHN415	AMS 5643H	
17-4 PH Stainless	E-2	198,000	200,010	12.0	49.0	BHN415	"	
	E-3	192,000	197,000	14.0	56.3	BHN415	"	
	E-4							
	E-5	198,000	200,000	15.0	55.6	BHN415	AMS 5643H	
	E-6	178,000	198,000	11.5	45.0	BHN415	"	
	E-7	198,000	200,000	15.0	55.6	BHN415	"	
	F-1	103,000	153,000	25.0	47.0	BHN159	AMS 5736-C	Solution treated and centerless ground
A-286	F-2	95,600	139,200	18.0	26.0	BHN190	AMS 5736-C	Solution treated and centerless ground
	F-3	110,200	153,500	26.0	40.7	BHN163	AMS 5736-B	Solution treated and centerless ground

TABLE IV. MECHANICAL PROPERTIES OF TEST MATERIALS (CONT'D)

MATERIAL	BILLET IDENT	YIELD	TENSILE	% ELONG.	% RED.	HARDNESS	STDS.	CONDITION
A-286	F-4							
	F-5	100,000	160,000	28.0	44.0	BHN156	AMS 5734	Solution Treated
	F-6	134,000	164,300	22.0	46.5	BHN166	"	Solution Treated
	F-7	103,500	155,900	26.0	42.6	BHN163	"	Solution Treated
Vascomax 300	G-1	270,700	274,500	10.0	52.0		MB 300	
	G-2	281,600	285,200	11.0	58.6		"	
	G-3	290,500	294,500	10.0	50.2		"	
	H-1							
TZM Hbly	H-2	88,000	100,000	13.4		V 247	AMS 7819	2100°F for 30 minutes - Rapid cool
	H-3	116,600	135,300	15.0	21.5	V 310	"	2100°F for 30 minutes - Rapid cool
	I-1	135,000	186,000	11.0	11.0		AMS 5712	
Rene' 41	I-2	146,000	194,000	23.0	29.7	BHN279	"	
	X							
	J-1	69,500	133,000	65.7	47.0	BHN212	AMS 5759/C	1500°F for 24 hours
L-605	J-2	64,000	129,000	64.4	49.4	BHN183	"	1500°F for 24 hours

TABLE V. BILLET IDENTIFICATION AND APPLICATION

Material	Billet Iden.	Type of Program Testing	
		Ductility	Mechanical Properties
2024-0 Al	A-2		X
	A-3	X	
	A-4	X	
	A-5		X
	A-6	X	
	A-7		X
7075 Al	B-2		X
	B-3	X	
5Al-2.5Sn Titanium	C-1		X
	C-2		X
	C-3	X	
	C-4	X	
	C-5	X	
	C-6		X
	C-7	X	
6Al-4V Titanium	D-2		X
	D-3	X	
17-4 PH Stainless Steel	E-2		X
	E-3	X	
	E-4	X	
	E-5	X	

TABLE V. (CONT'D)

Material	Billet Iden.	Type of Program Testing	
		Ductility	Mechanical Properties
17-4 PH (Cont'd)	E-6		X
	E-7	X	
A-286	F-1		X
	F-2	X	
	F-3	X	
	F-4	X	
	F-5		X
	F-6	X	
	F-7		X
Vascomax 300	G-2		X
	G-3	X	
TZM Moly	H-1		X
	H-2		X
	H-3	X	
Rene' 41	I-1		X
	I-2	X	
L-605	J-1		X
	J-2	X	

TABLE VI. AS RECEIVED HARDNESS MEASUREMENTS

Material	Bar #	Center Hardness	Edge Hardness	Type Spec.*
2024-O Al	A-2	19.5 R/B	21.5 R/B	1
	A-3	18.5 R/B	18.5 R/B	2
7075 Al	B-2	20.0 R/B	21.5 R/B	1
	B-3	11.0 R/B	11.0 R/B	2
5Al-2.5Sn Titanium	C-1	36.0 R/C	37.5 R/C	1
	C-3	36.0 R/C	36.0 R/C	2
6Al-4V Titanium	D-2	35.0 R/C	36.0 R/C	1
	D-3	38.0 R/C	36.0 R/C	2
17-4 PH Stainless	E-2	34.0 R/C	35.0 R/C	1
	E-3	34.5 R/C	35.5 R/C	2
A-286	F-1	80.5 R/B	84.0 R/B	1
	F-2	81.0 R/B	82.5 R/B	2
Vascomax 300	G-2	31.5 R/C	31.5 R/C	1
	G-3	32.5 R/C	32.0 R/C	2
T.M Moly	H-2	24.0 R/C	22.5 R/C	1
	H-3	26.5 R/C	26.5 R/C	2
Rene' 41	I-1	46.0 R/C	41.0 R/C	1
	I-2	30.0 R/C	30.0 R/C	2
J.-605	J-1	19.5 R/C	22.0 R/C	1
	J-2	29.5 R/C	34.0 R/C	2

- \*(1)  $\frac{1}{2}$ " x  $\frac{1}{2}$ " x  $4\frac{1}{2}$ " Bar (Used for Mechanical Properties Evaluation)  
 (2) 1" x 1" Cylinder (Used for Forgeability Tests)

APPENDIX II  
FORGEABILITY TESTS



## APPENDIX II

### FORGEABILITY TESTS

#### Forgeability Limits

Graphs 1 thru 43 represent the experimental results obtained for 2024-O Al, 7075-O Al, Ti-5Al-2.5Sn, Ti-6Al-4V, 17-4 PH Stainless Steel, A-286, Vascomax 300, Rene' 41, L-605 and TZM forged at room temperature and for 2024-O Al, Ti-5Al-2.5Sn, A-286 and 17-4 PH Stainless Steel forged at temperature up to 1950°F.

The numbered forgeability limit specimens shown in the photographs in Figures 72 thru 106 represent points on corresponding limit curves shown on the opposite pages.

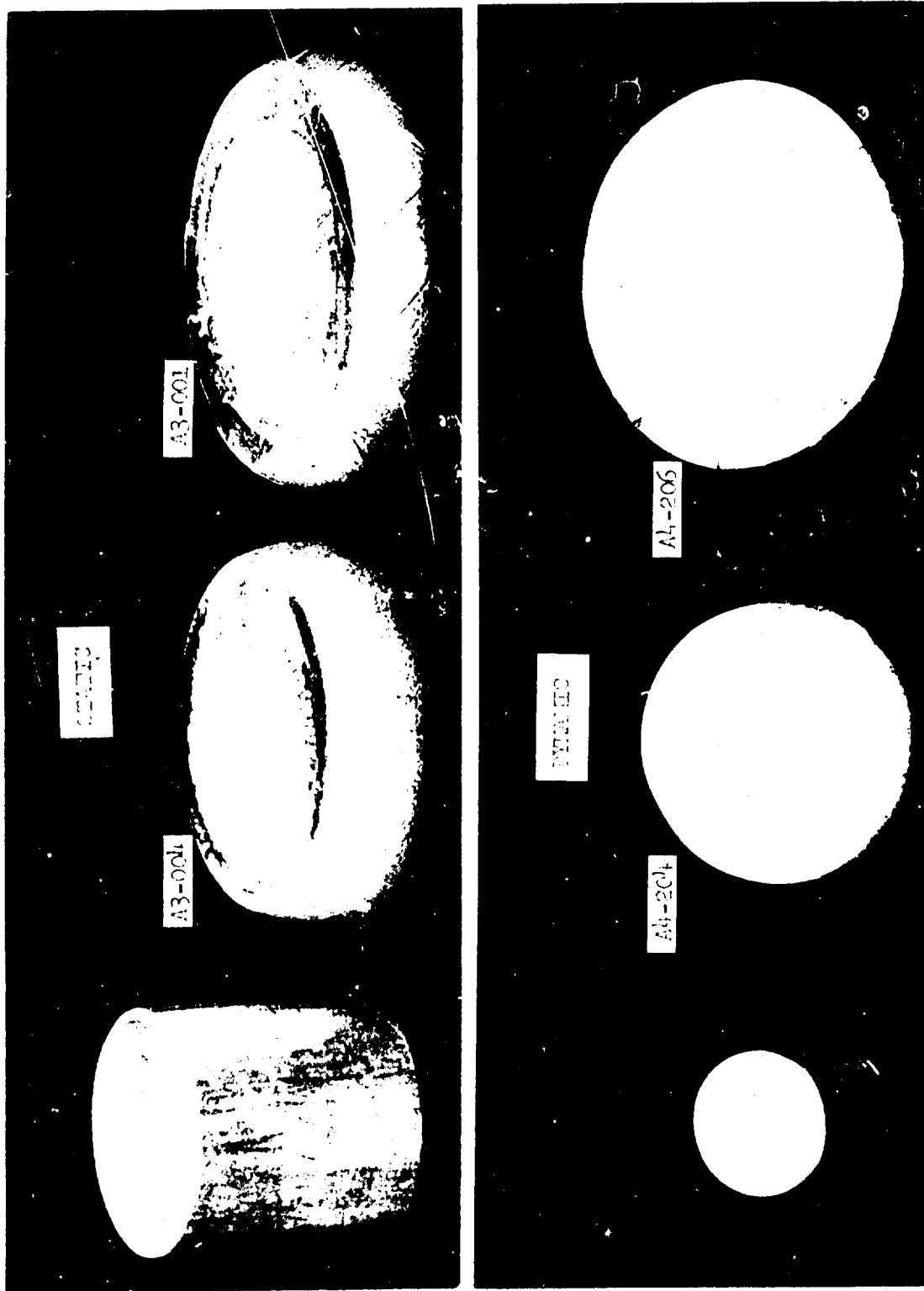
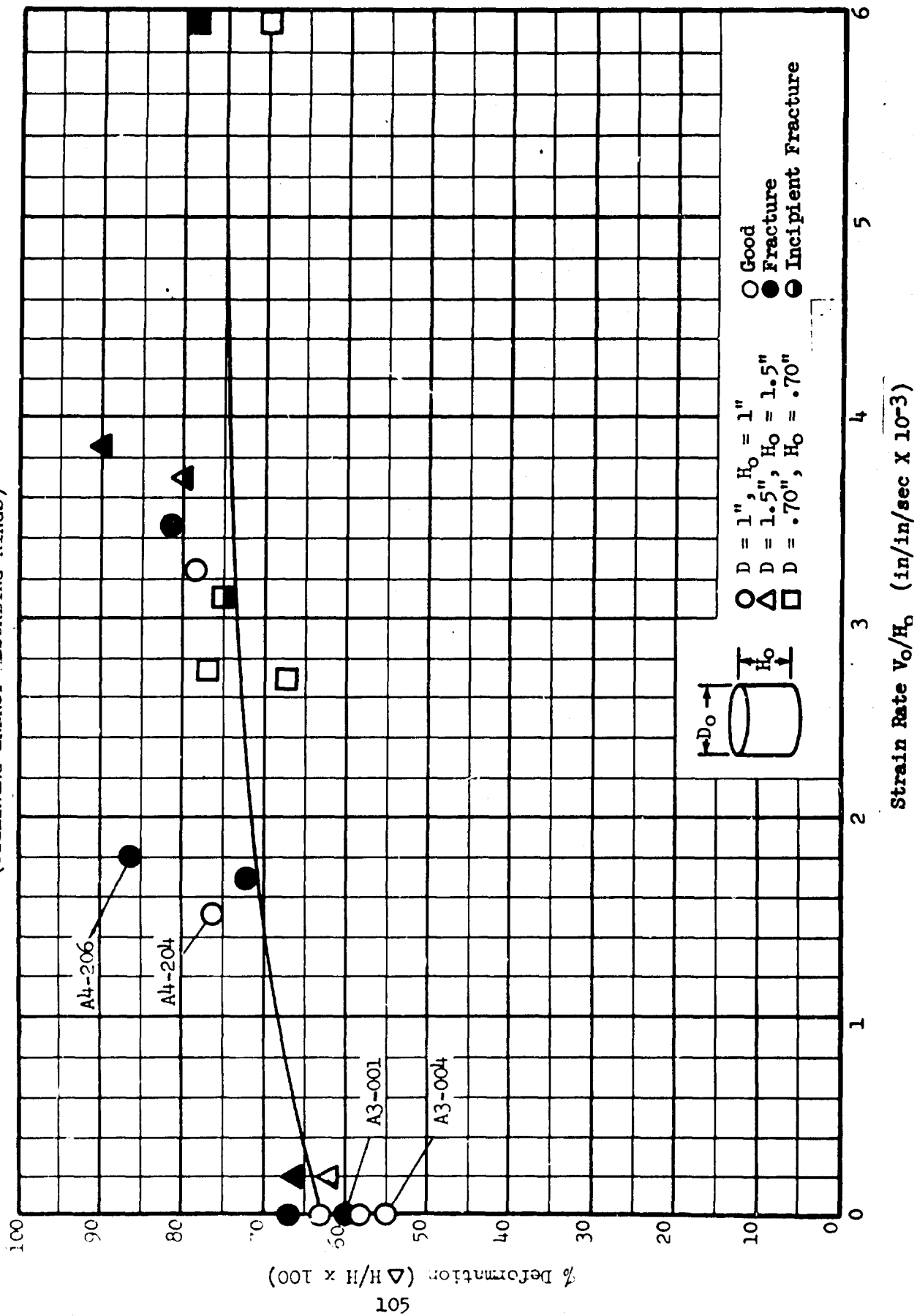


FIGURE 72. 2024-O Al FORGEABILITY SPECIMENS AT ROOM TEMPERATURE  
(UTILIZING ENERGY ABSORBING RINGS)

GRAPH 1. FORGEABILITY LIMIT CURVES FOR 2024-0 AL AT ROOM TEMPERATURE  
(UTILIZING ENERGY ABSORBING RINGS)



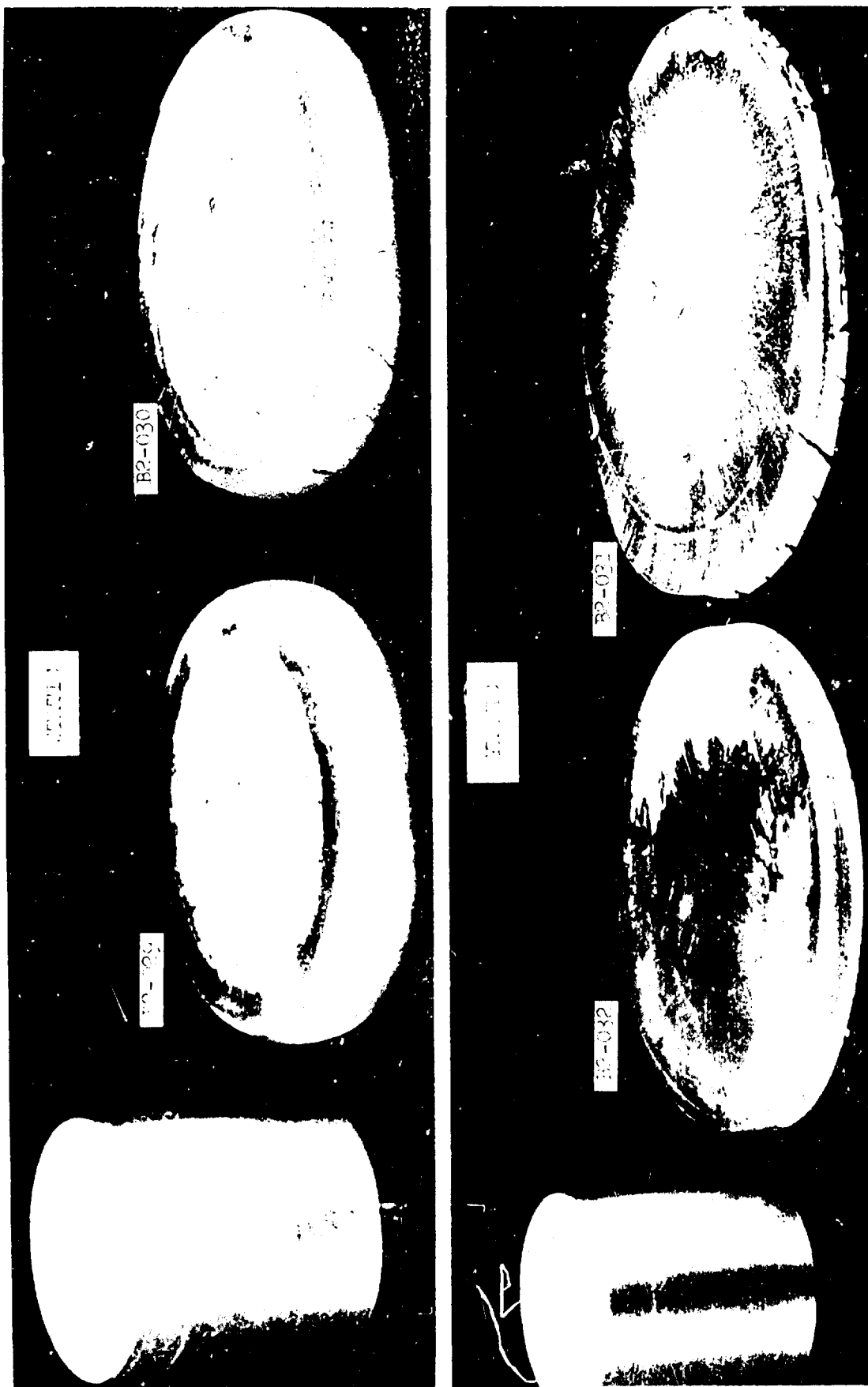
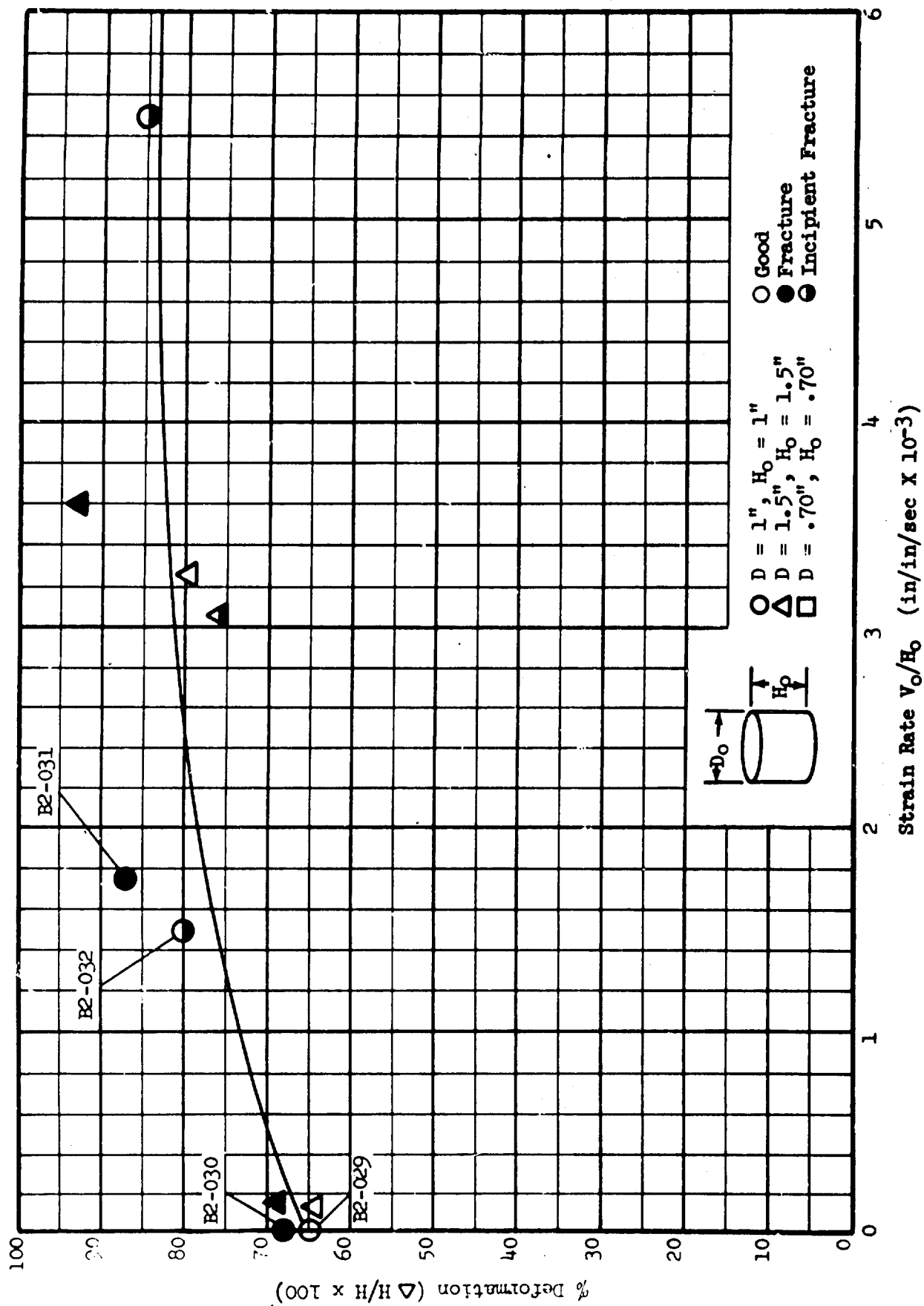


FIGURE 73. 7075-O AL FCGEABILITY SPECIMENS AT ROOM TEMPERATURE  
(UTILIZING ENERGY ABSORBING RINGS)

GRAPH 2. FORGEABILITY LIMIT CURVES FOR 7075-0 AL AT ROOM TEMPERATURE  
(UTILIZING ENERGY ABSORBING RINGS)



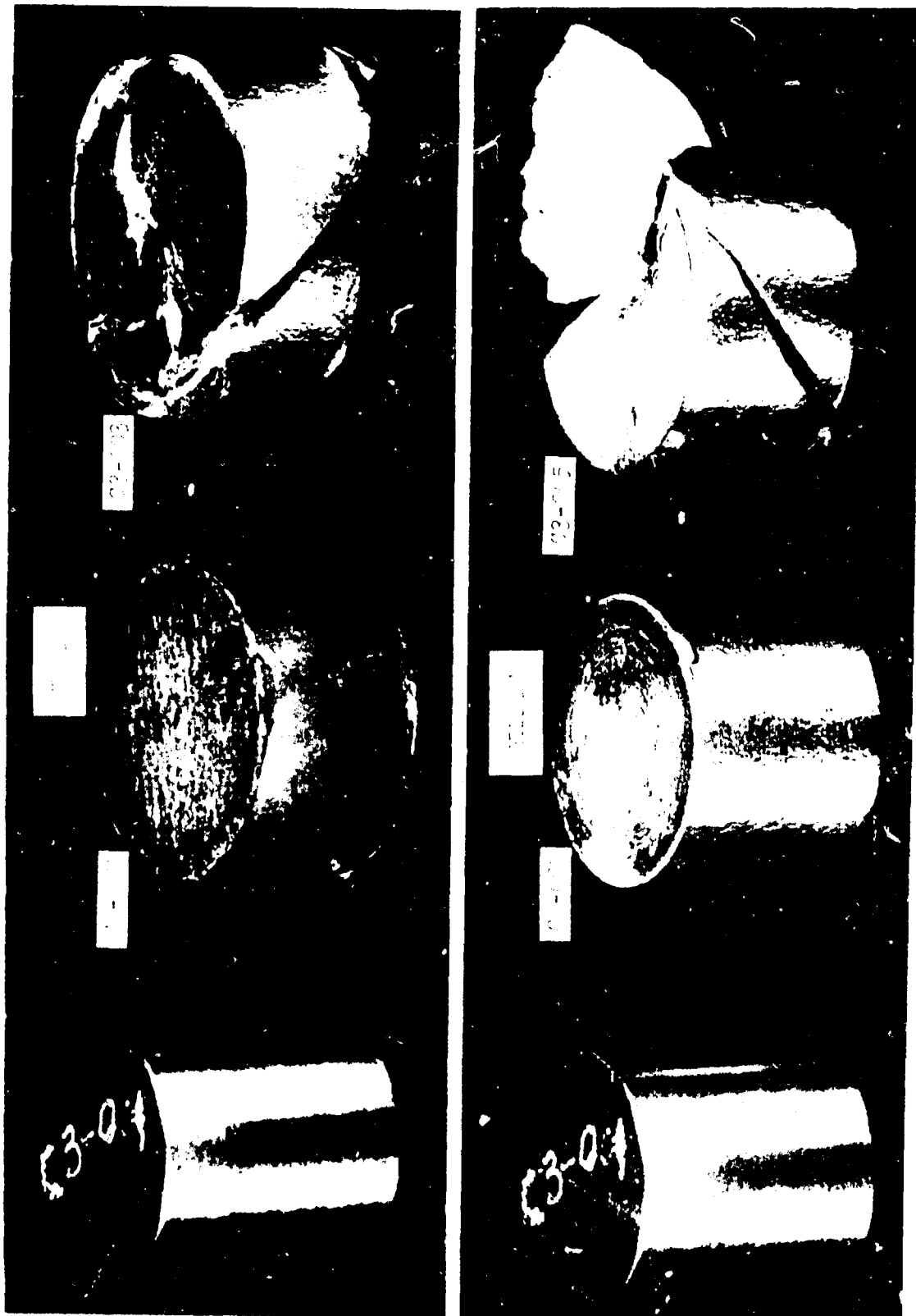
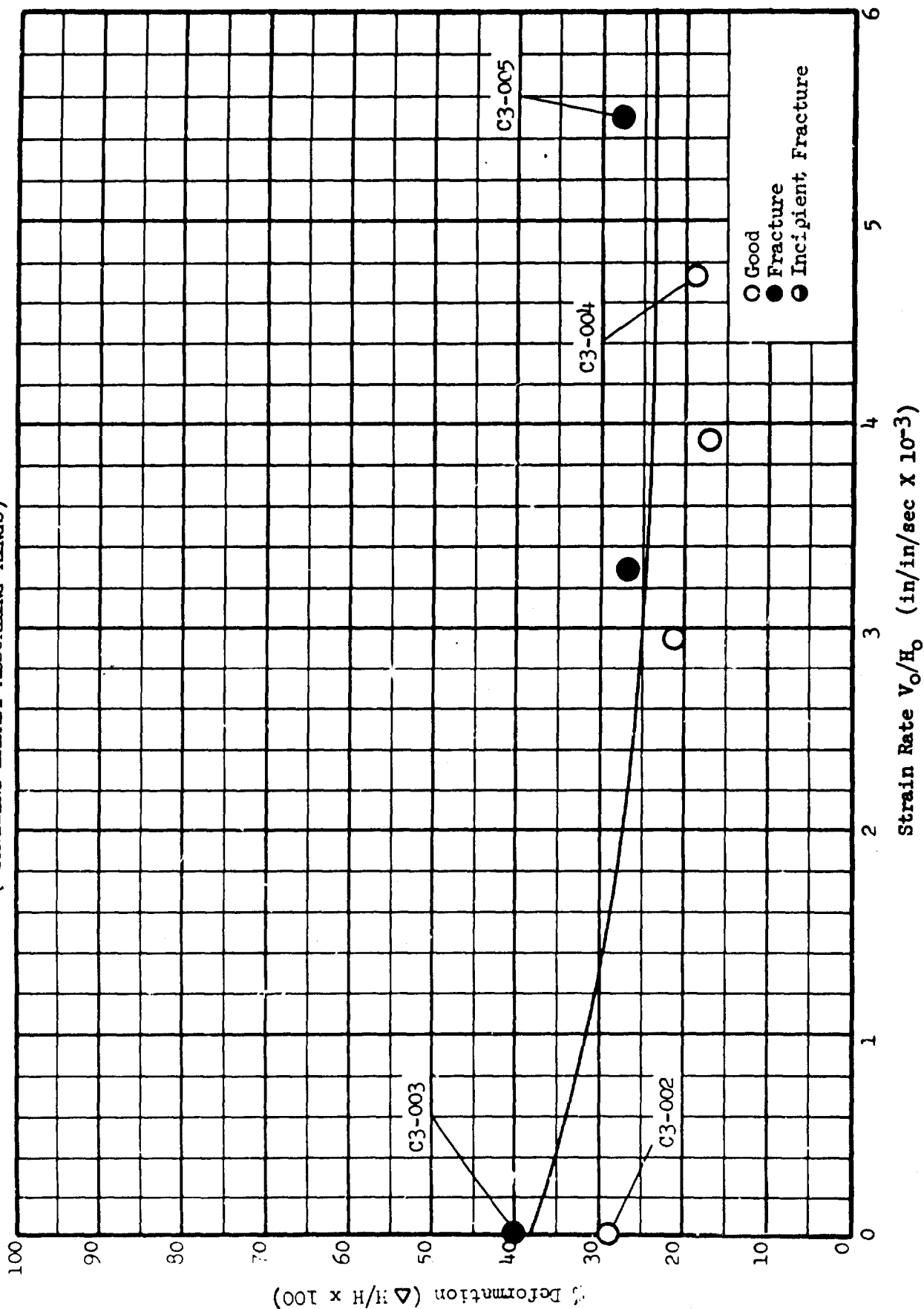


FIGURE 74. Ti-5Al-2.5Sn FORGABILITY SPECIMENS AT ROOM TEMPERATURE  
(UTILIZING ENERGY ABSORBING RINGS)

GRAPH 3. FORCEABILITY LIMIT CURVES FOR Ti-5Al-2.5Sn AT ROOM TEMPERATURE  
(UTILIZING ENERGY ABSORBING RINGS)



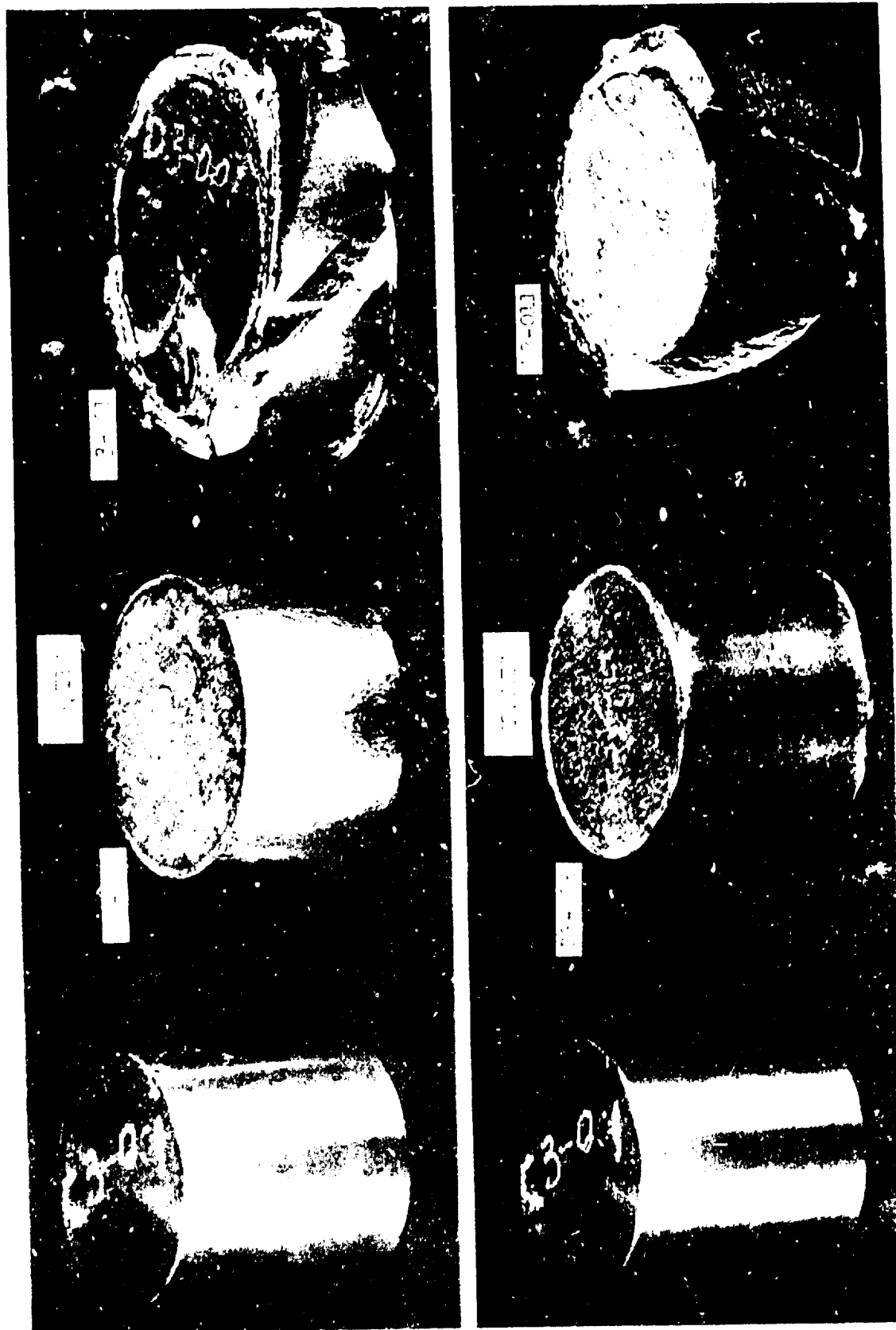
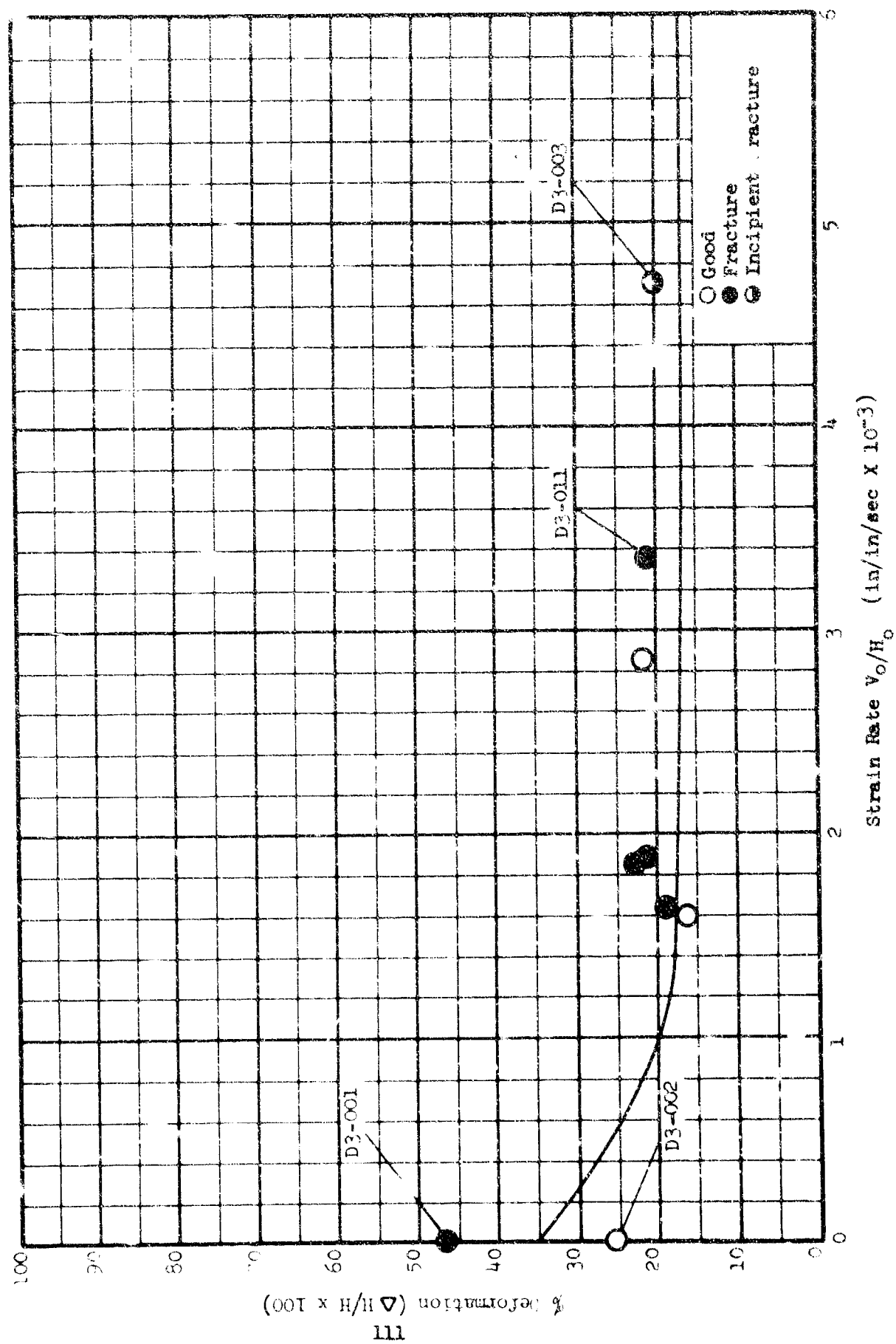


FIGURE 75. Ti-6Al-4V FORGABILITY SPECIMENS AT ROOM TEMPERATURE  
(UTILIZING ENERGY ABSORBING RINGS)



GRAPH 4. FORGEABILITY LIMIT CURVES FOR Ti-6Al-4V AT ROOM TEMPERATURE  
(UTILIZING ENERGY ABSORBING RINGS)



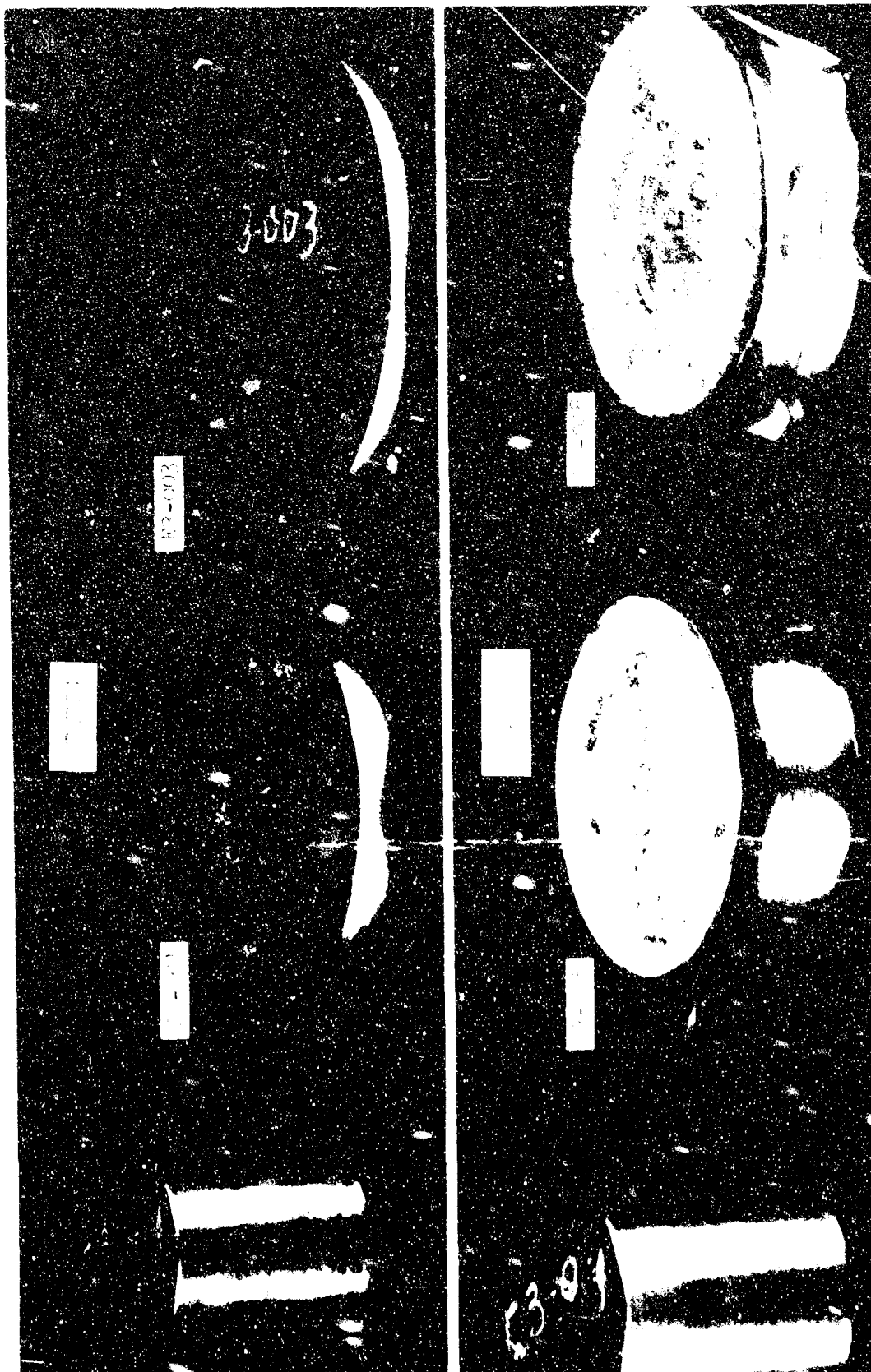
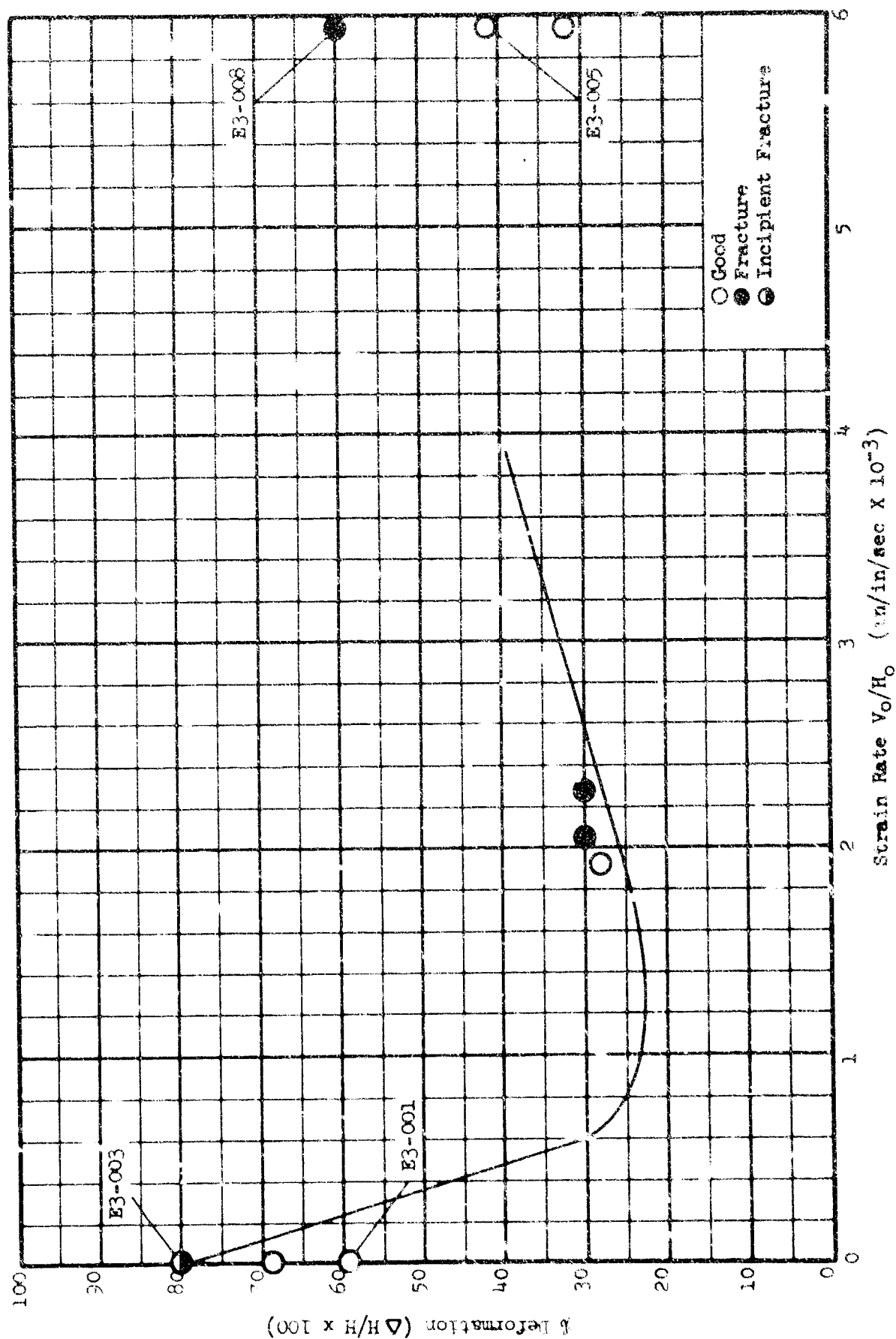


FIGURE 76. 17-4 PH FORGABILITY SPECIMENS AT ROOM TEMPERATURE.  
(UTILIZING ENERGY ABSORBING RINGS)

GRAPH 5. FORGEABILITY LIMIT CURVES FOR 17-4 PH AT ROOM TEMPERATURE  
(UTILIZING ENERGY ABSORBING RINGS)



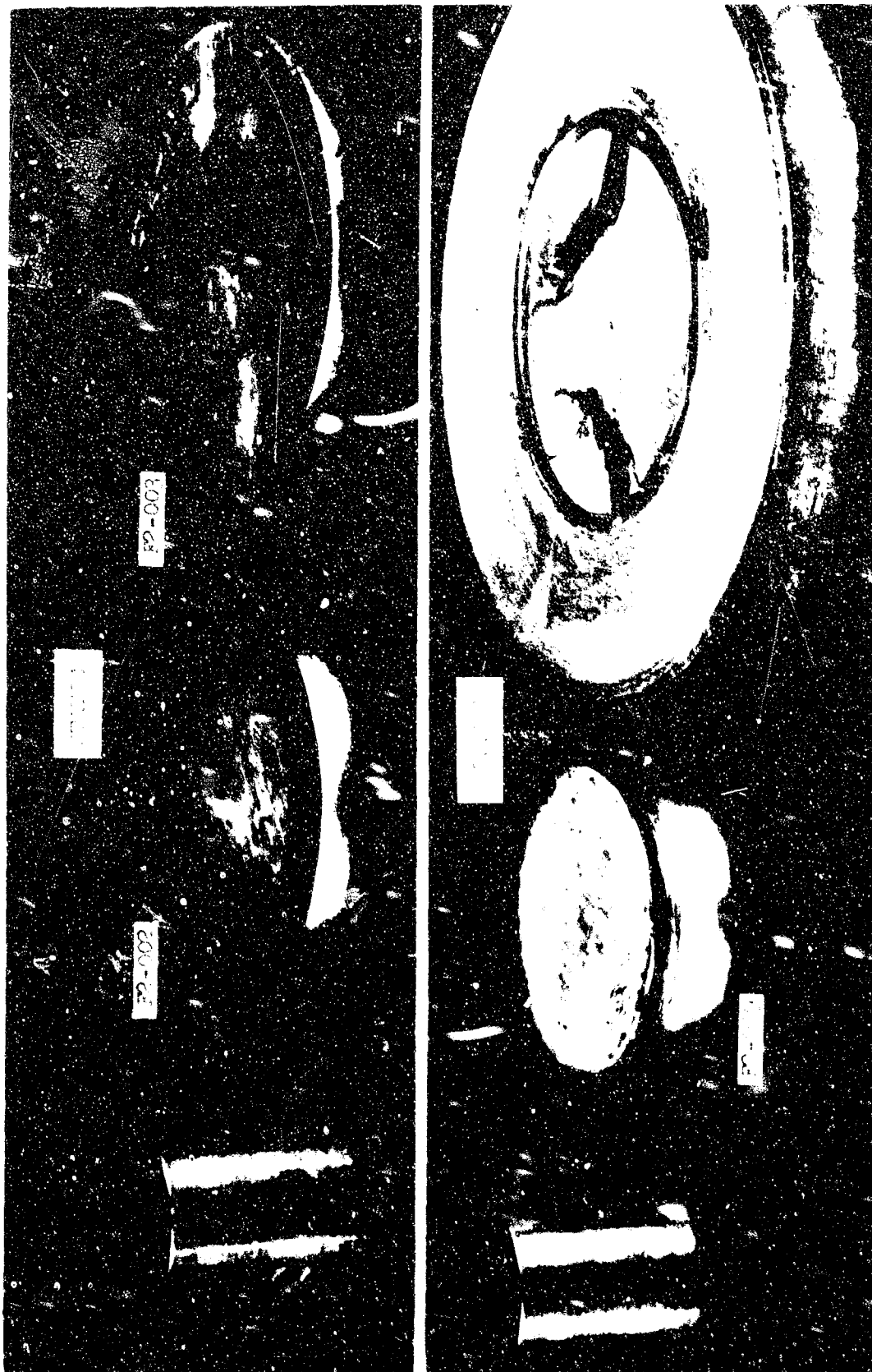
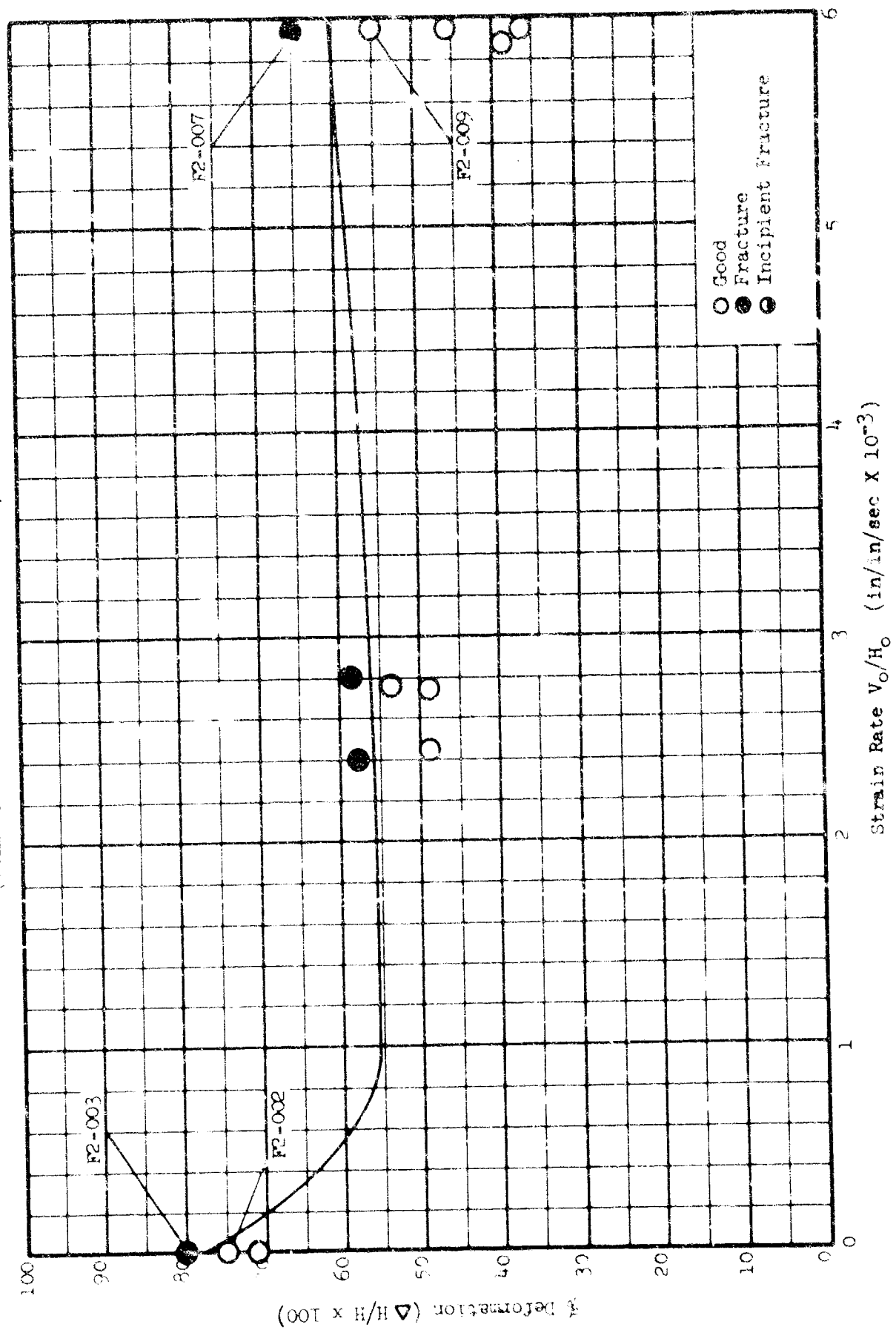


FIGURE 77. A-286 FORGEABILITY SPECIMENS AT ROOM TEMPERATURE  
(UTILIZING ENERGY ABSORBING RINGS)

GRAPH 6. FORMABILITY LIMIT CURVES FOR A-286 AT ROOM TEMPERATURE  
(FURNISHING ENERGY ABSORBING RINGS)



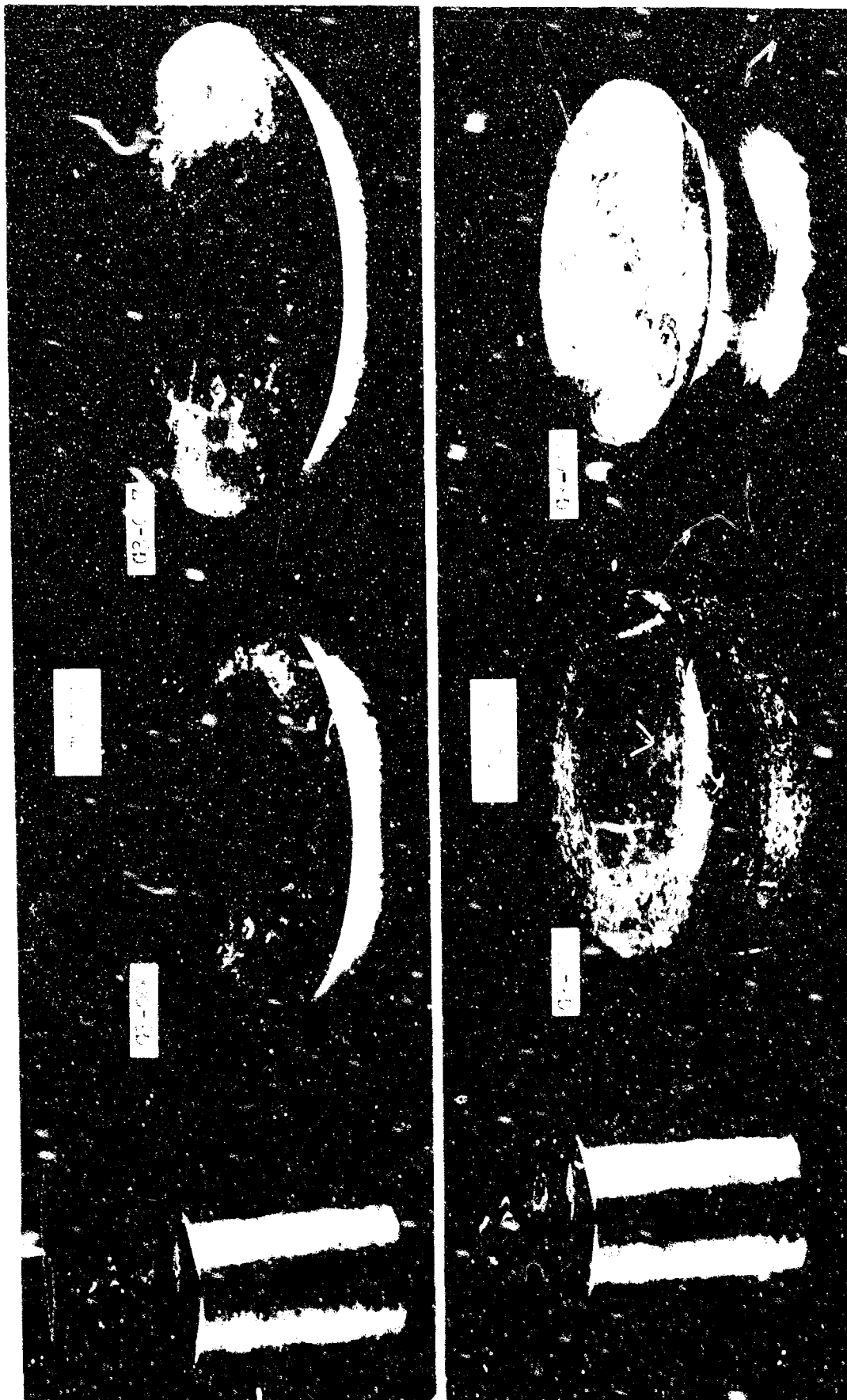
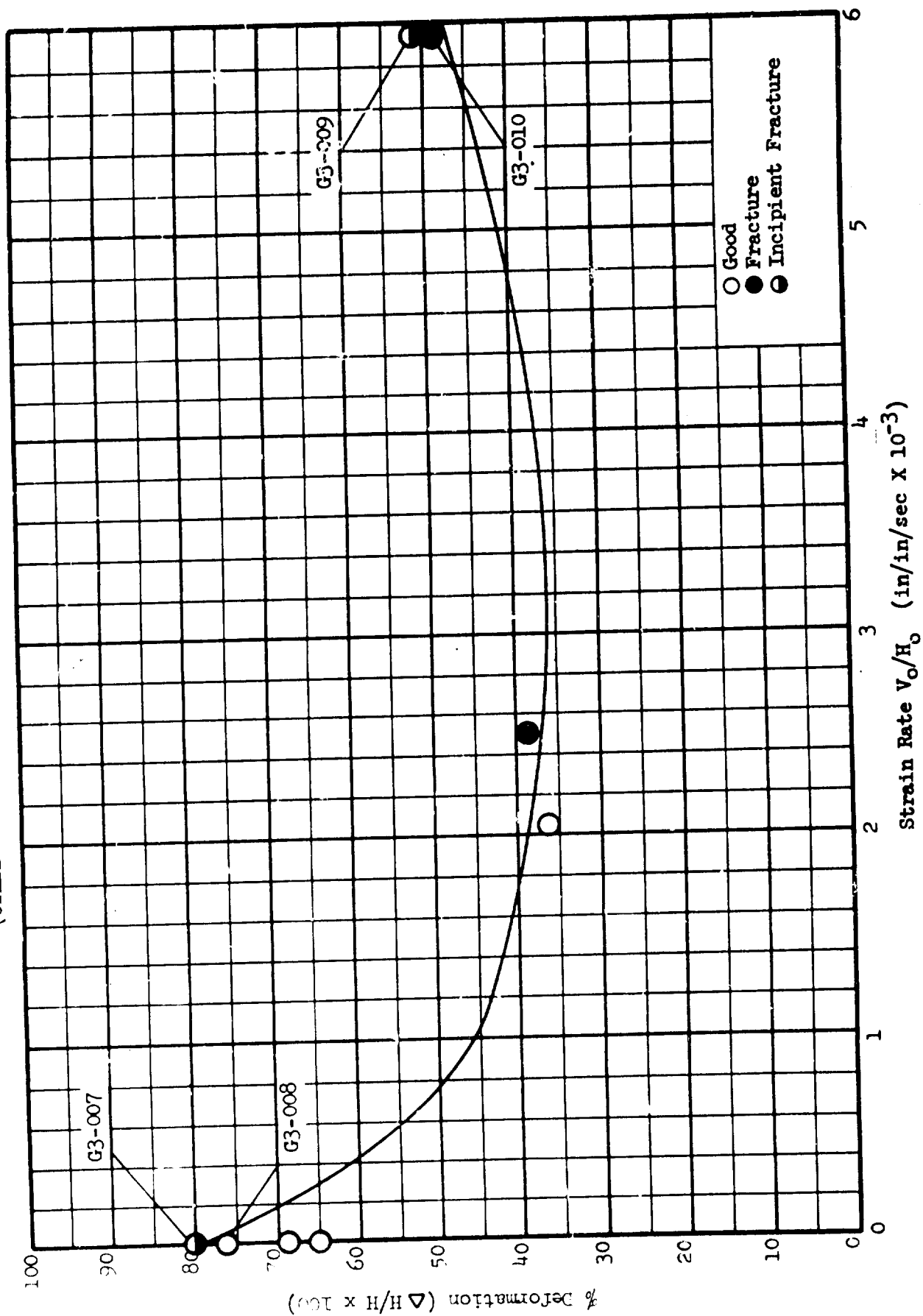
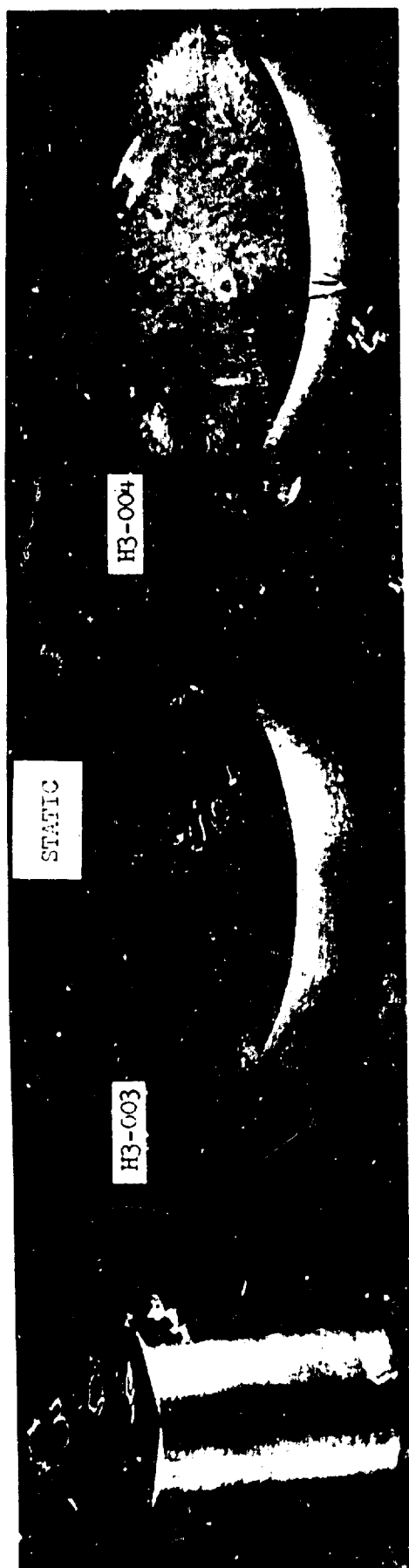


FIGURE 78. VASCOMAX 30 FORGABILITY SPECIMENS AT ROOM TEMPERATURE  
(UTILIZING ENERGY ABSORBING RINGS)

GRAPH 7. FORGEABILITY LIMIT CURVES FOR VASCOMAX 300 AT ROOM TEMPERATURE  
(UTILIZING ENERGY ABSORBING RINGS)





DYNAMIC

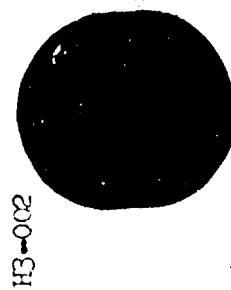
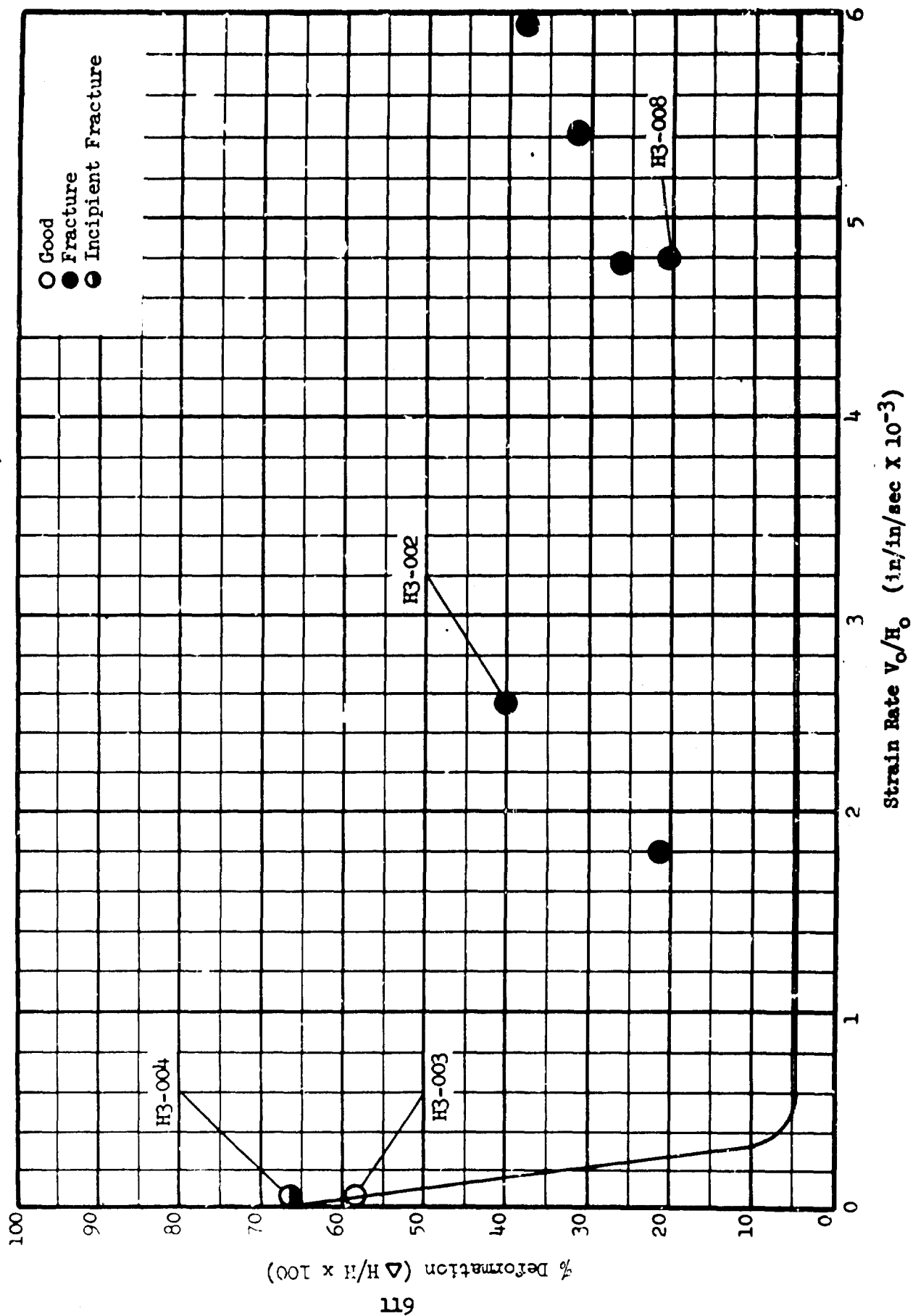


FIGURE 79. TZM FORCEABILITY SPECIMENS AT ROOM TEMPERATURE  
(UTILIZING ENERGY ABSORBING RINGS)



GRAPH 8. FORGEABILITY LIMIT CURVES FOR TZM AT ROOM TEMPERATURE  
(UTILIZING ENERGY ABSORBING RINGS)



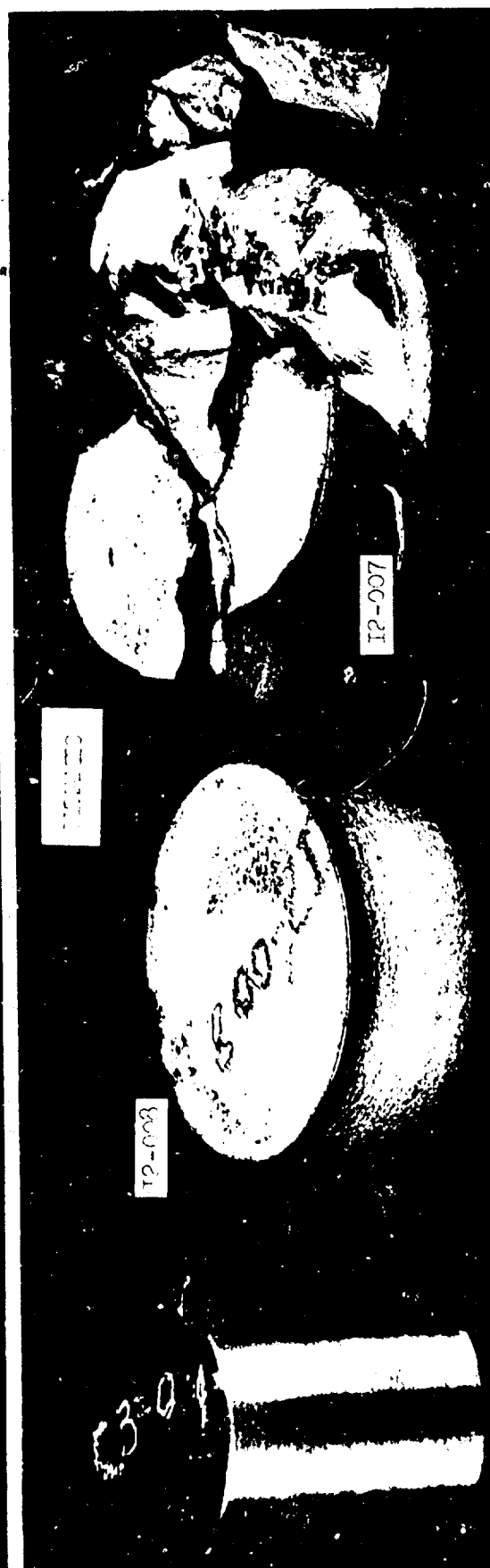
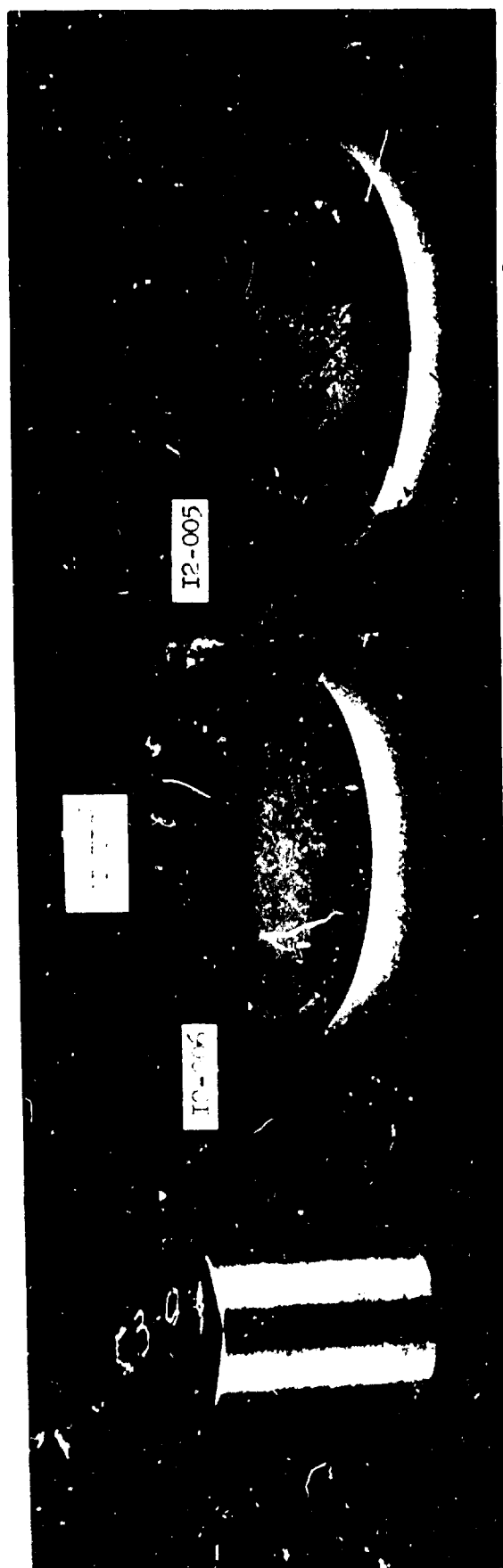
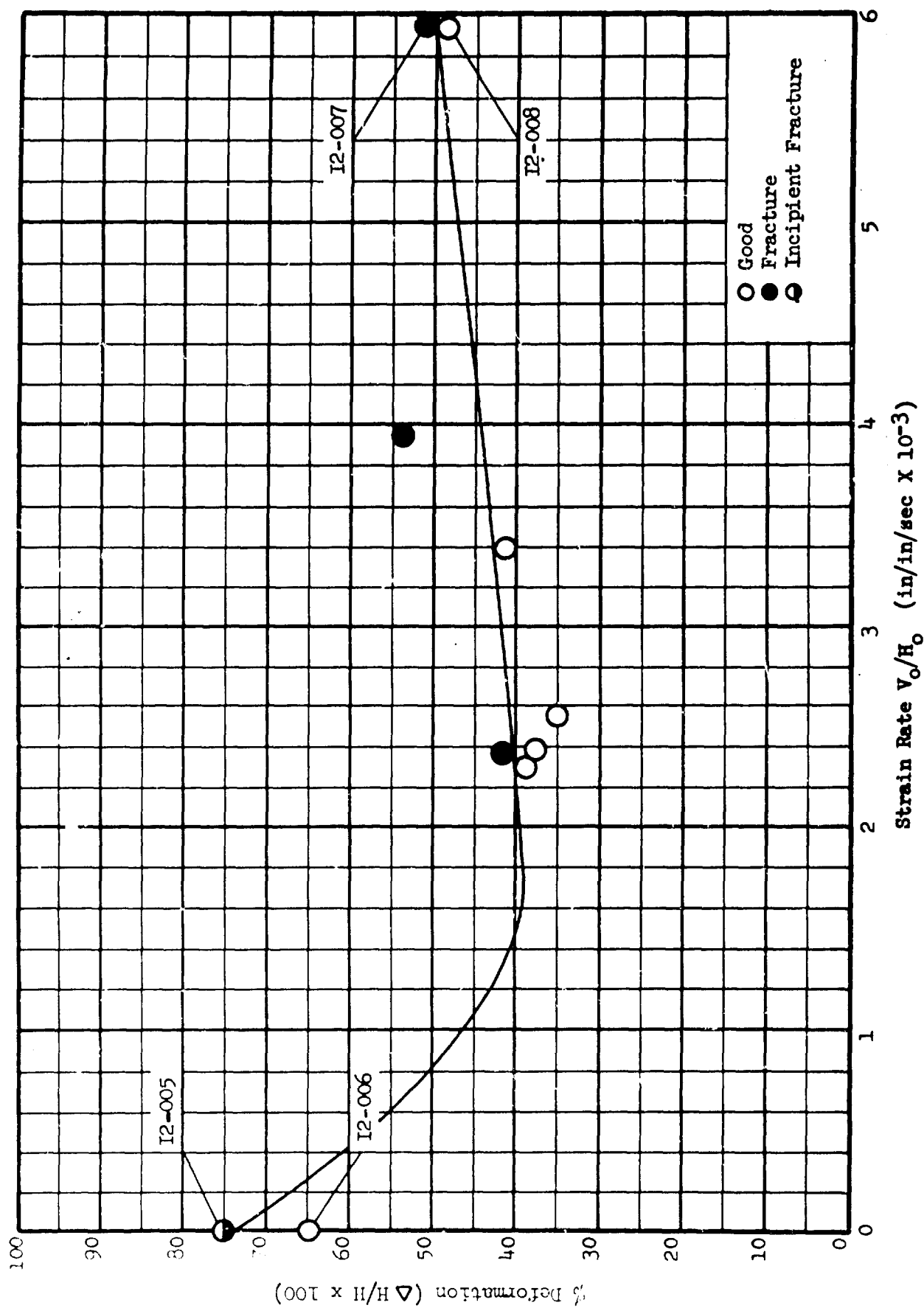


FIGURE 80. RENE' 41 FORGEABILITY SPECIMENS AT ROOM TEMPERATURE  
(UTILIZING ENERGY ABSORBING RINGS)

GRAPH 9. FORGEABILITY LIMIT CURVES FOR PENE' 41 AT ROOM TEMPERATURE  
(UTILIZING ENERGY ABSORBING RINGS)



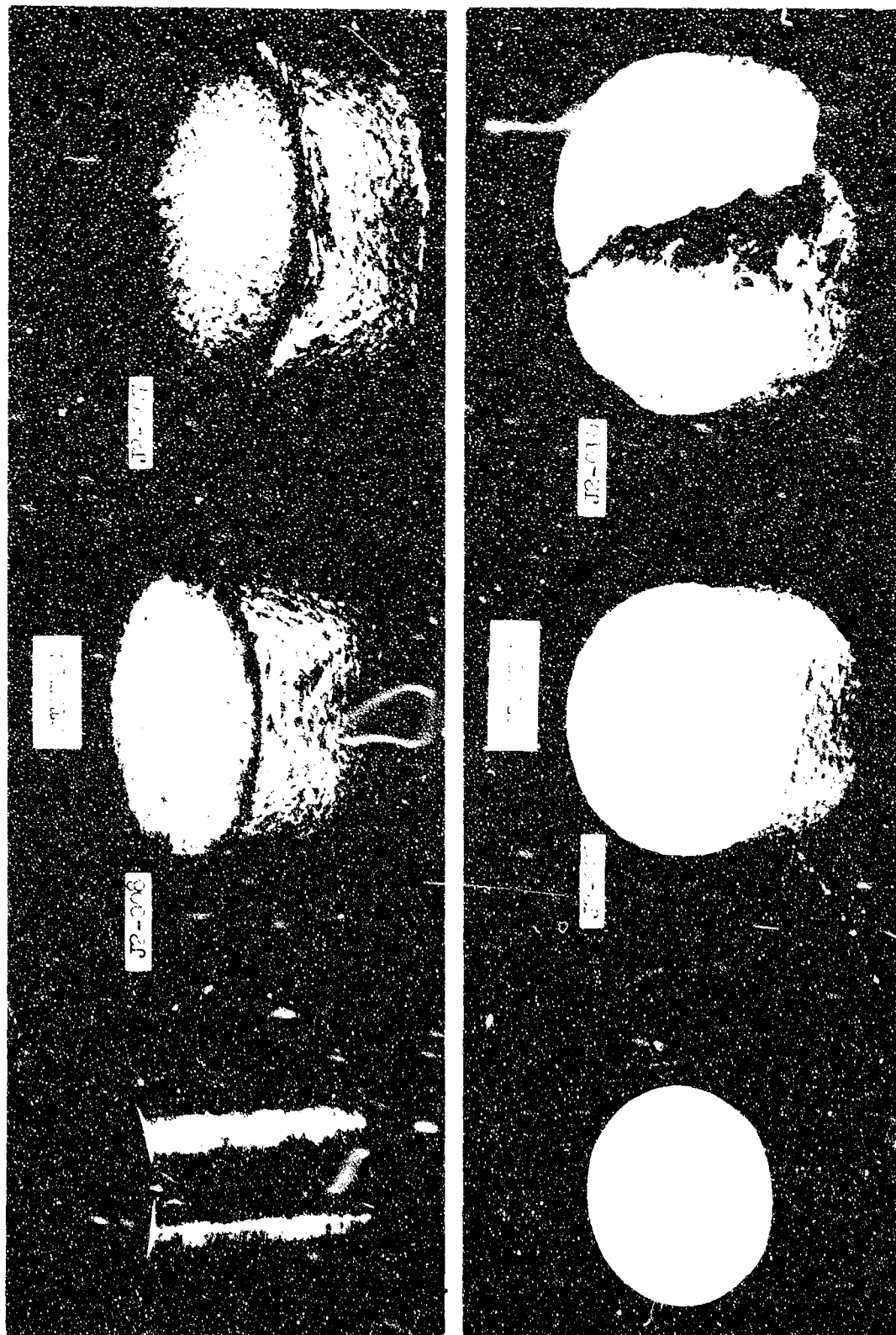
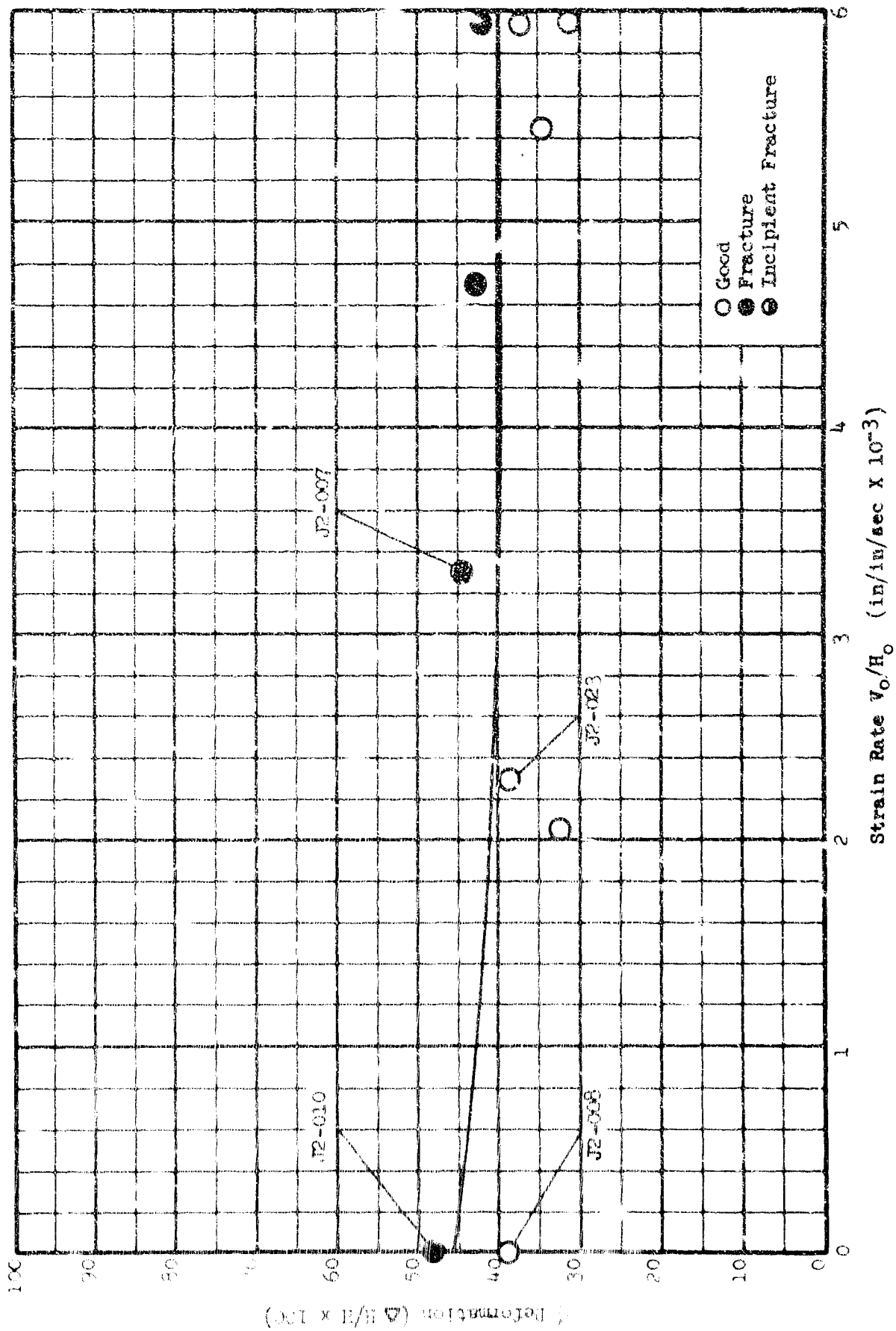


FIGURE 81. L-605 FORGEABILITY SPECIMENS AT ROOM TEMPERATURE  
(UTILIZING ENERGY ABSORBING RINGS)

GRAPH 10. FORGEABILITY LIMIT CURVES FOR 1-605 AT ROOM TEMPERATURE  
(UTILLING ENERGY ABSORBING RINGS)



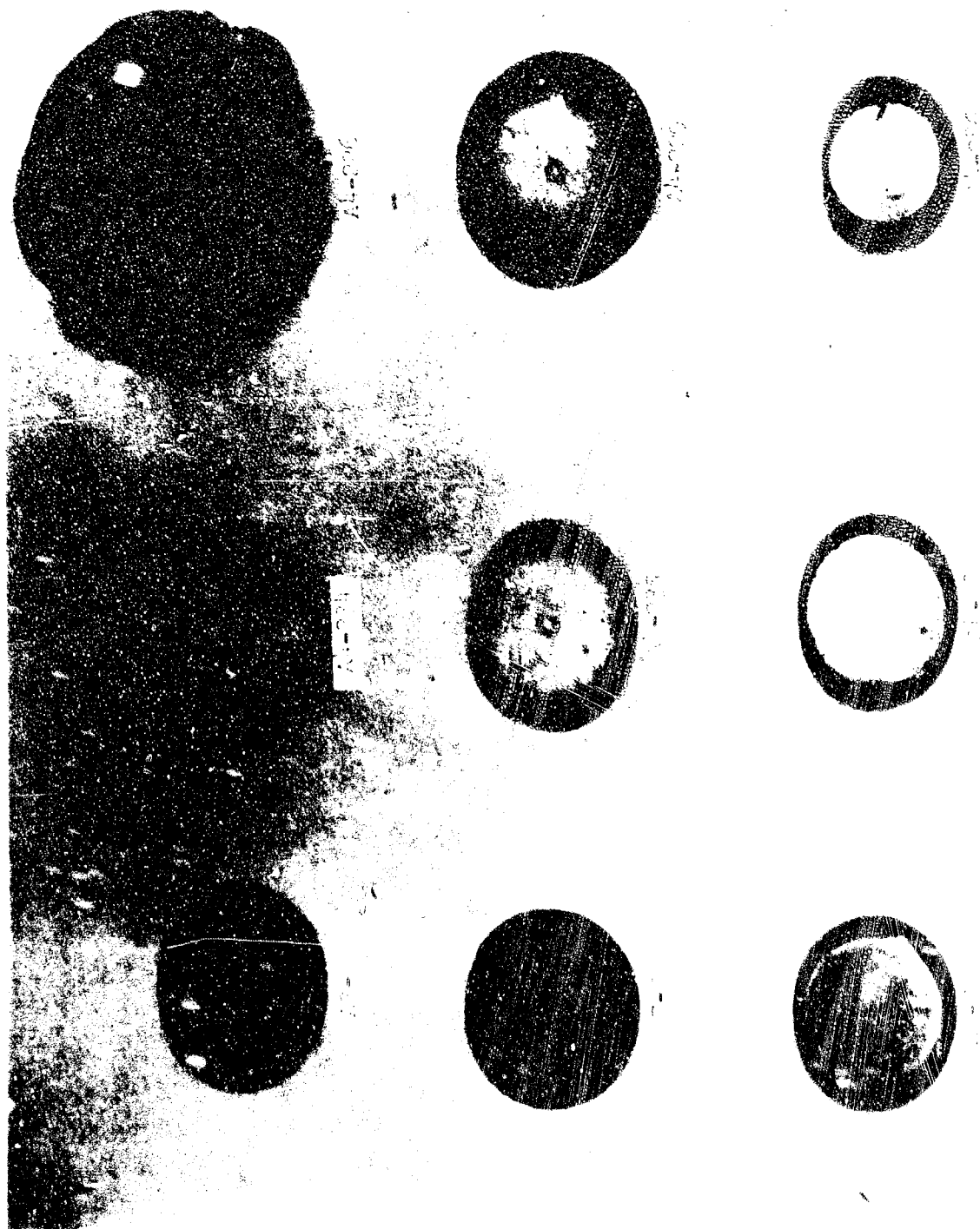
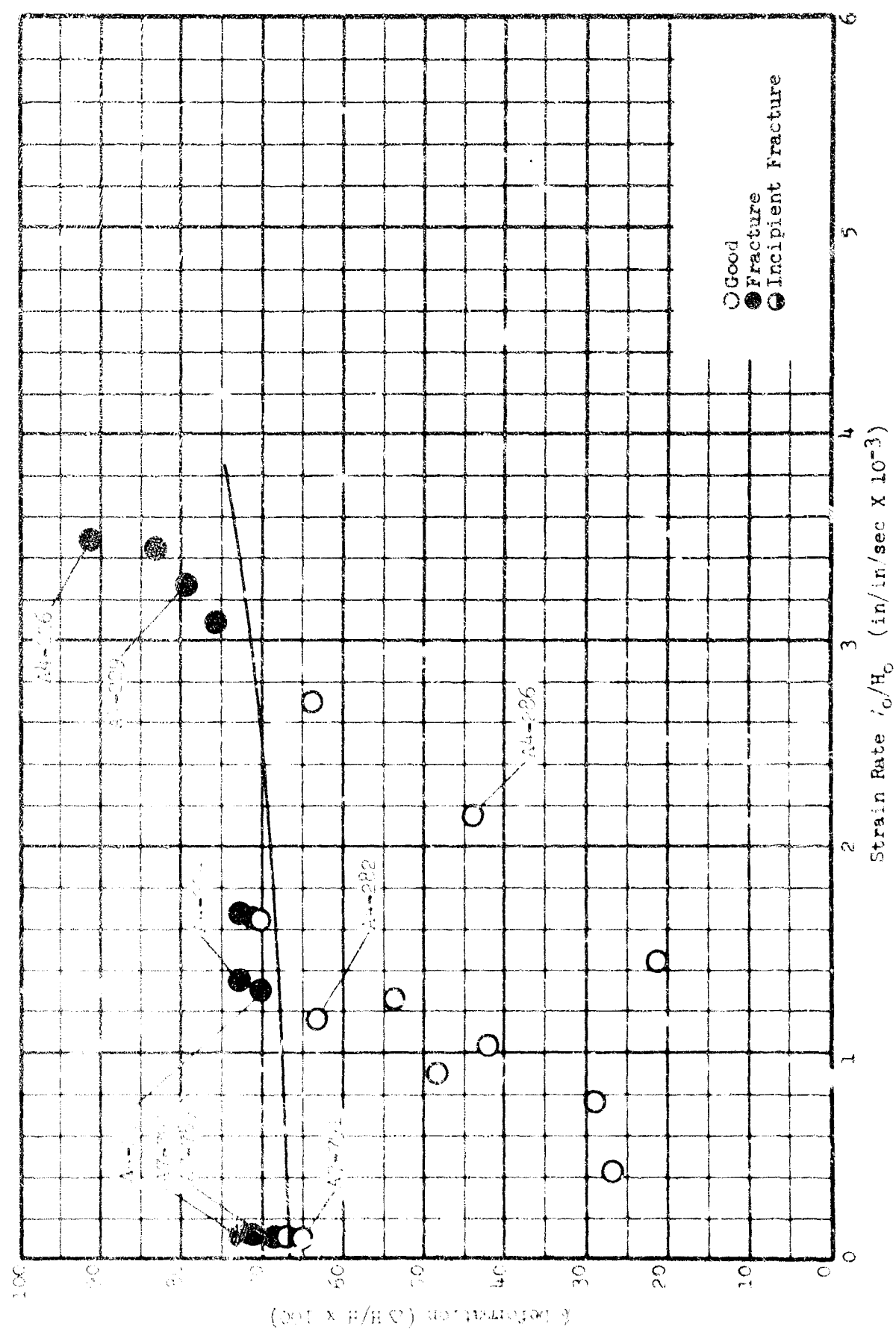


FIGURE 22. 2001-1 AL FORGABILITY LIMIT SPECIMENS AT ROOM TEMPERATURE

GRAPH 11. FORMAL LIT LIMIT CURVES FOR 2024-C AL AT ROOM TEMPERATURE



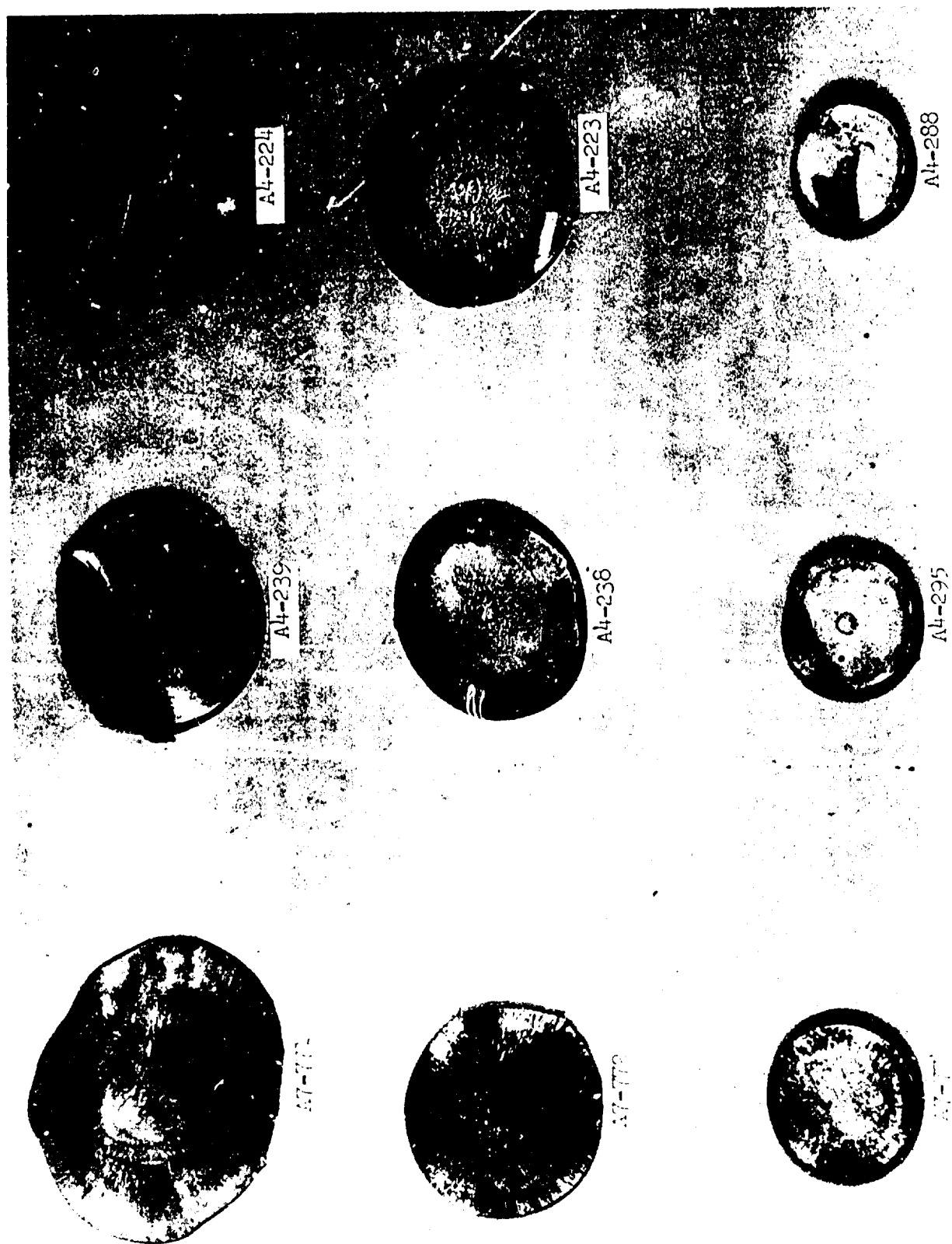
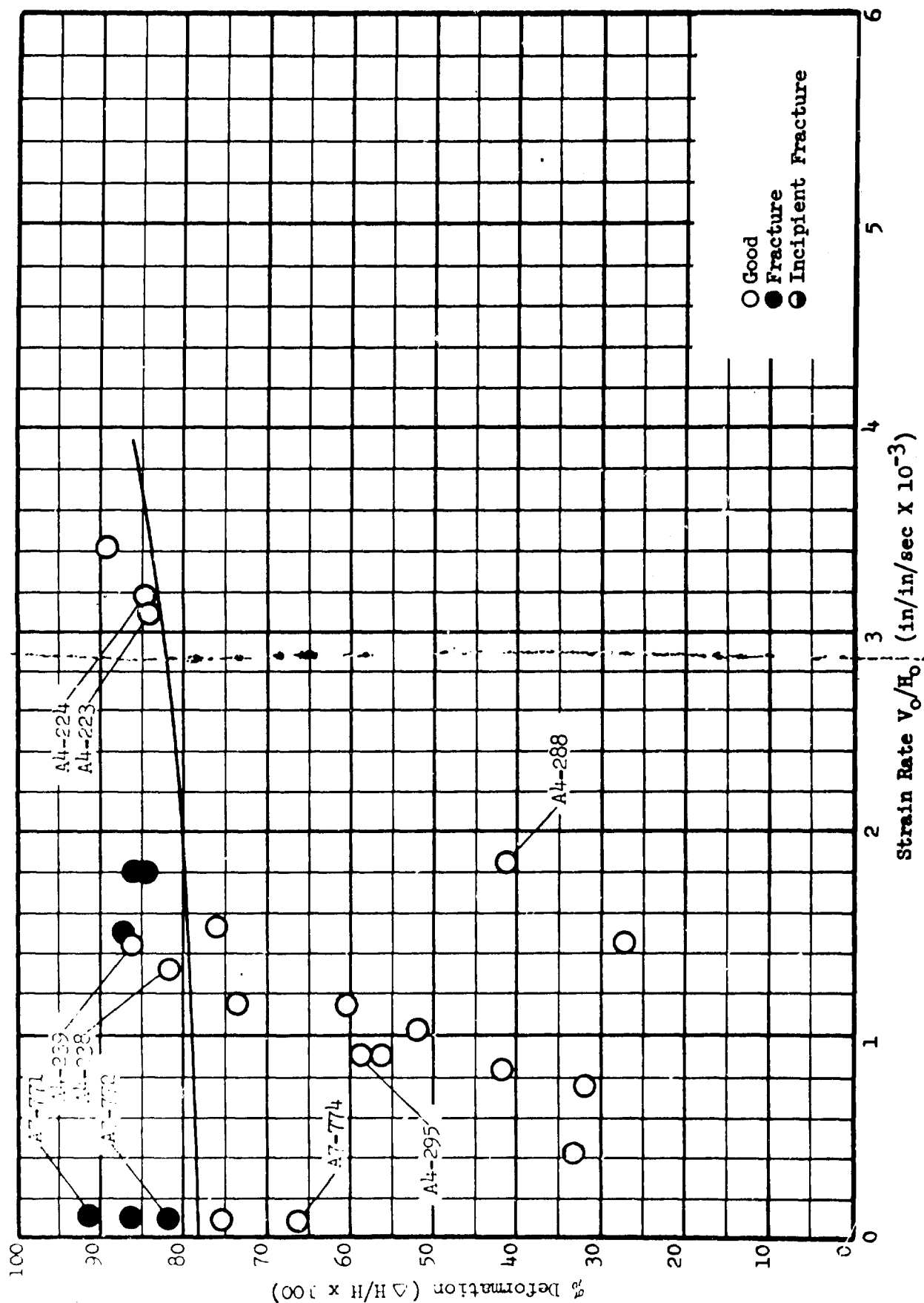
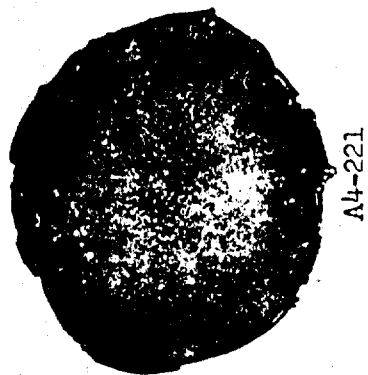


FIGURE 83. 2024-C AL. FORGEABILITY LIMIT SPECIMENS AT 550°F



GRAPH 12. FORGEABILITY LIMIT CURVES FOR 2024-0 AL AT 550°F

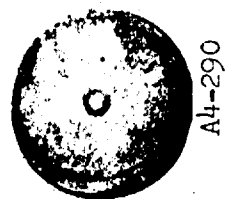




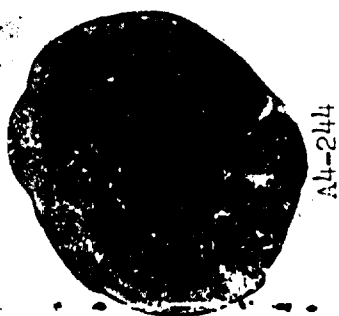
A4-221



A4-220



A4-290



A4-244



A4-243



A4-292



A7-770



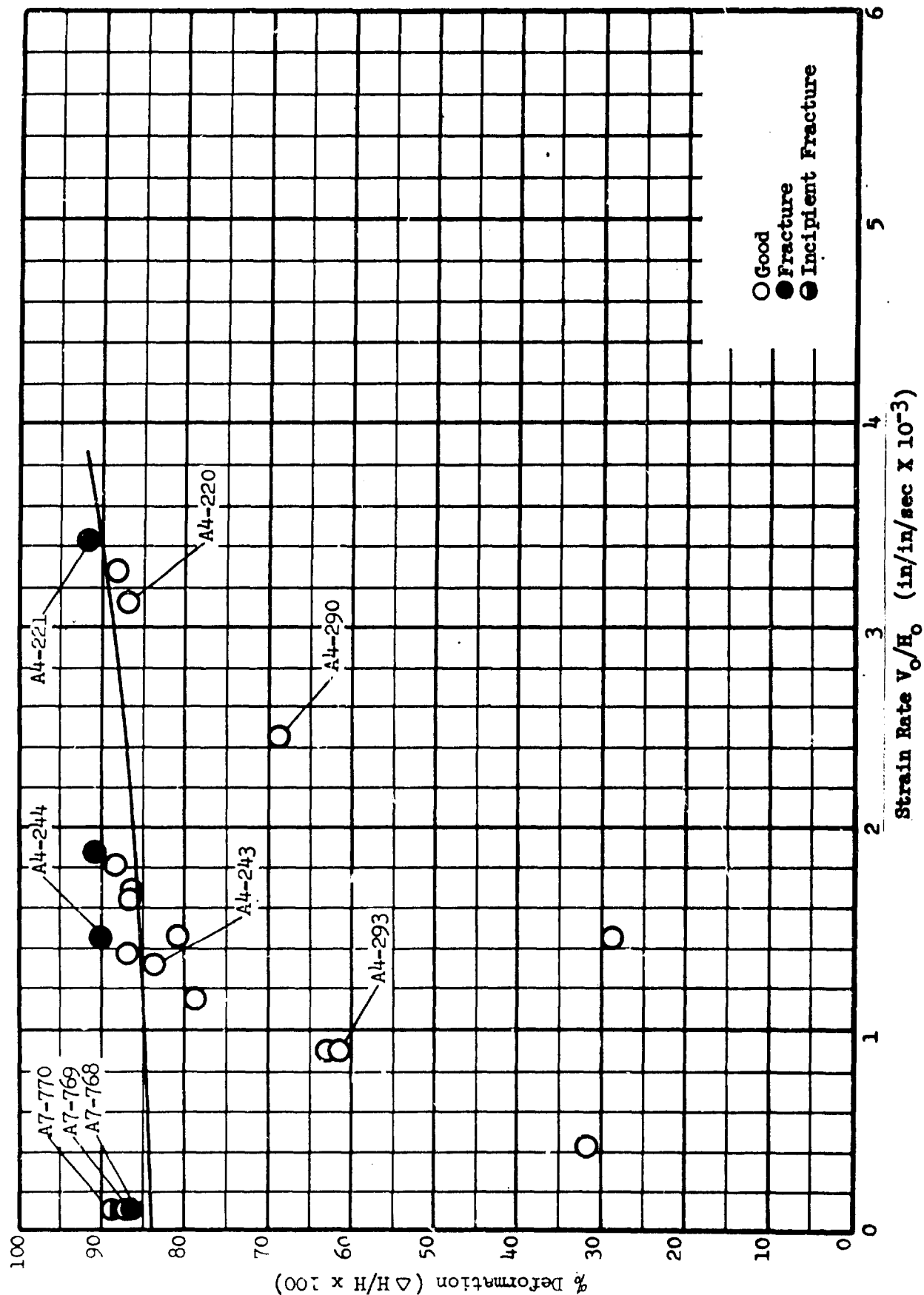
A7-769

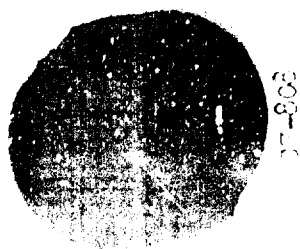


A7-768

FIGURE 84. 2024-O Al FORGEABILITY LIMIT SPECIMENS AT 750°F

GRAPH 13. FORGEABILITY LIMIT CURVES FOR 2024-T3 AL AT 750°F





05-403



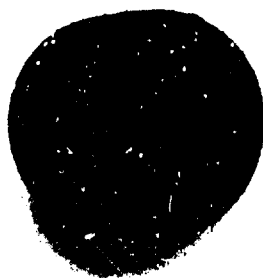
05-410



05-508



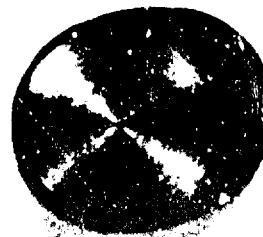
05-509



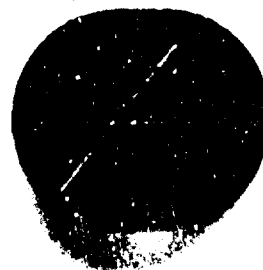
05-411



05-510



05-211



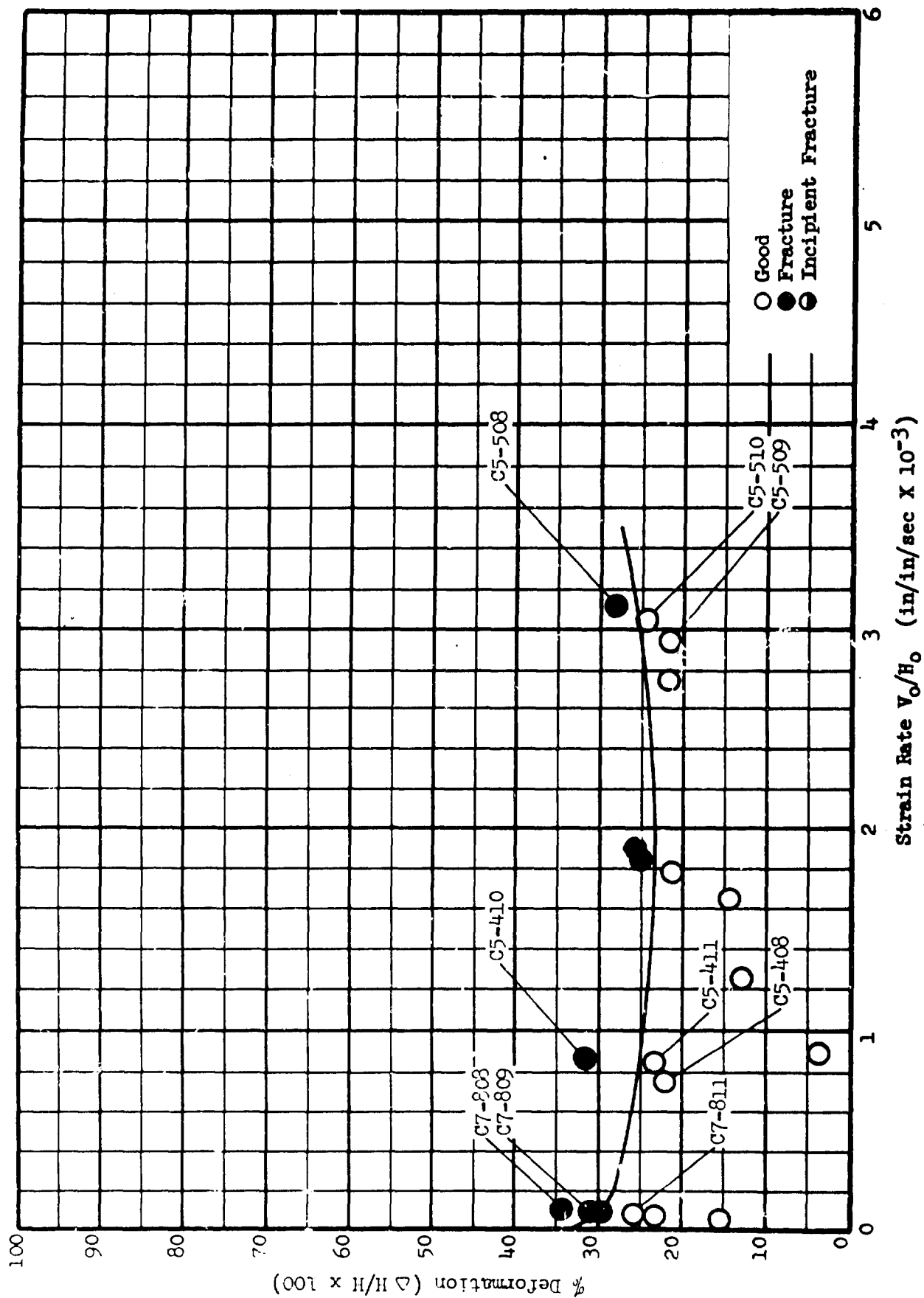
05-402



05-509

FIGURE 85. Ti-5Al-2.5Sn FORGEABILITY LIFT SPECIMENS AT ROOM TEMPERATURE

GRAPH 14. FORGEABILITY LIMIT CURVES FOR Ti-5Al-2.5Sn AT ROOM TEMPERATURE



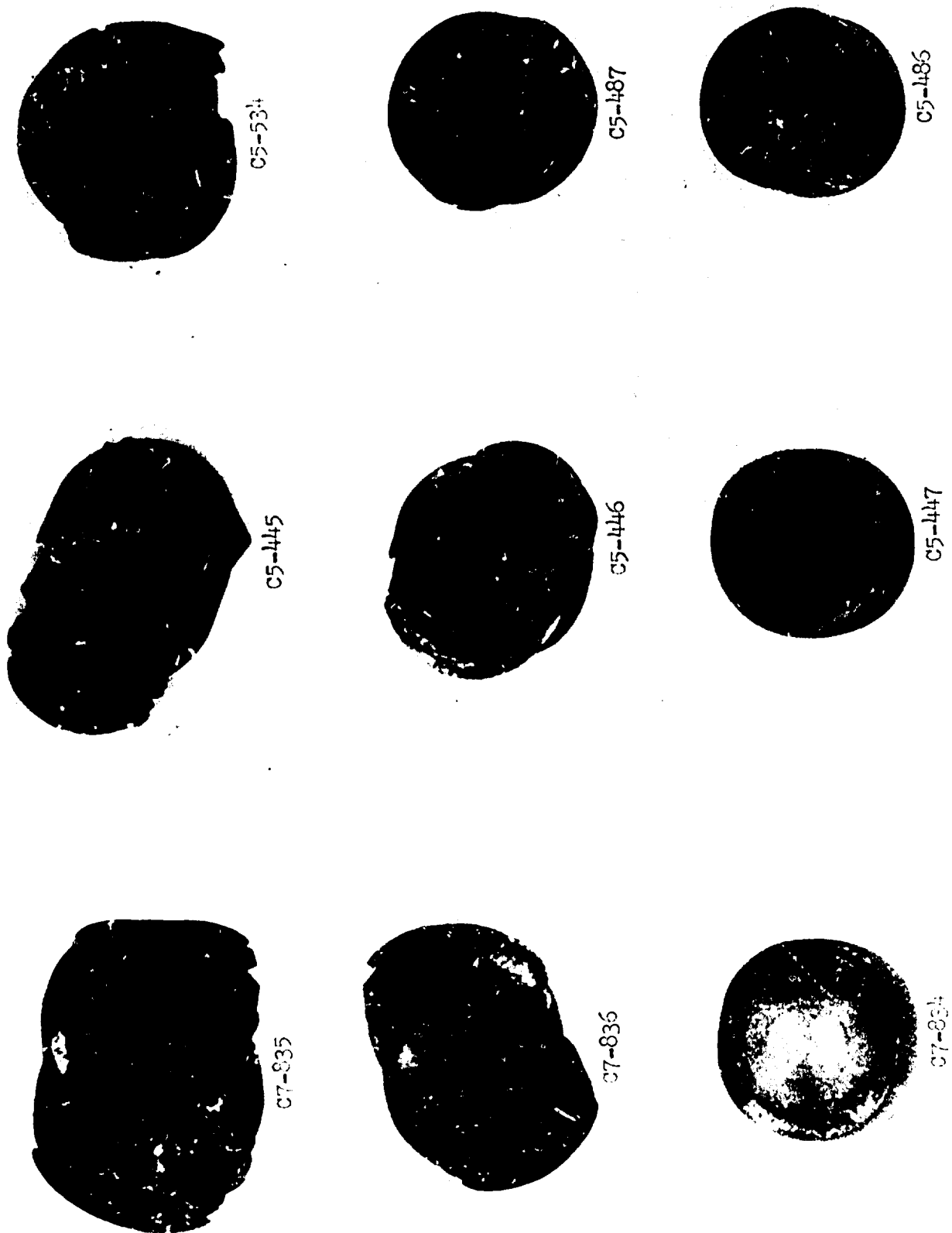
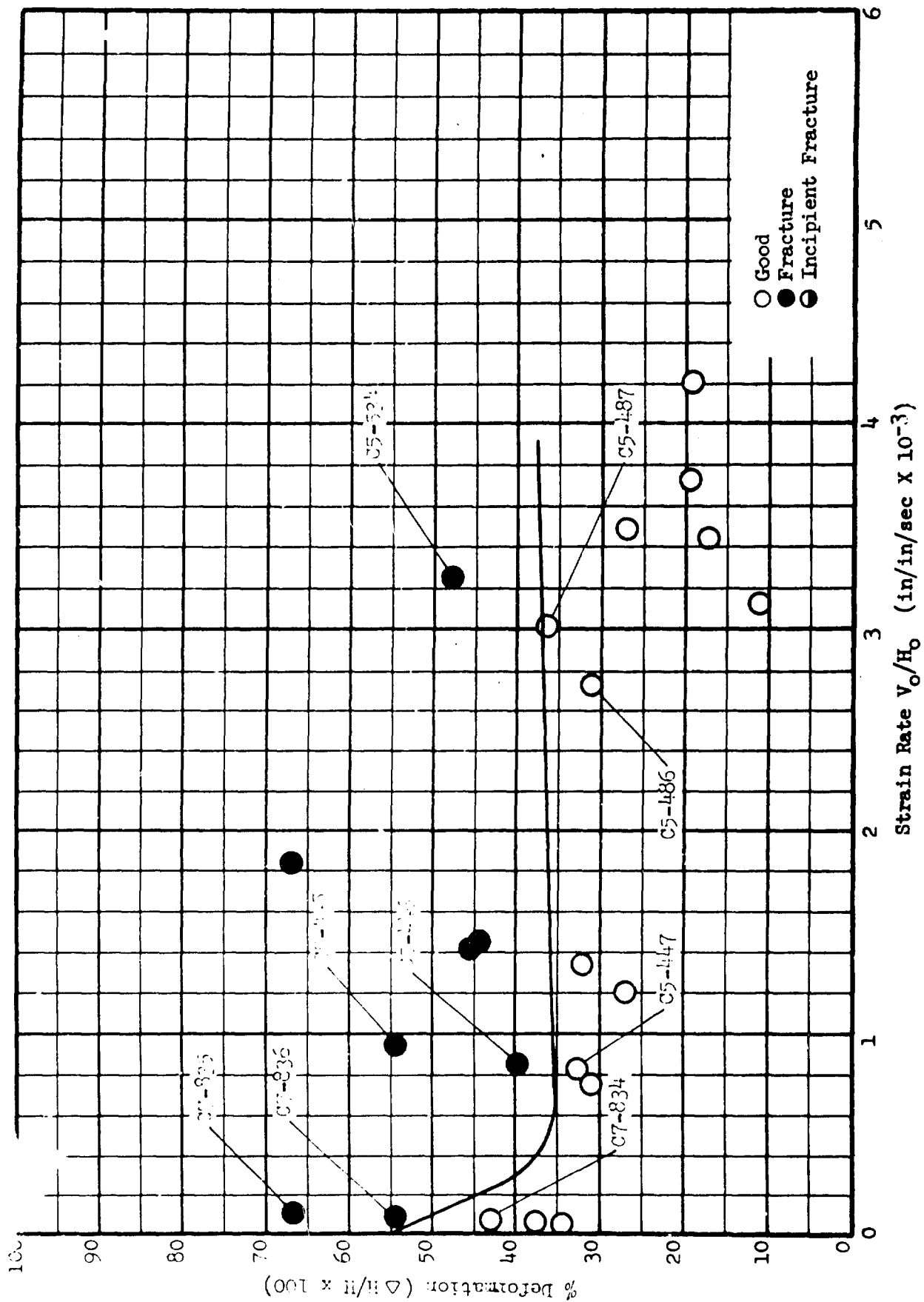


FIGURE 86. Ti-5Al-2.5Sn FORGEABILITY LIMIT SPECIMENS AT 750°F

GRAPH 15. FORMABILITY LIMIT CURVES FOR Ti-5Al-2.5Sn AT 750°F



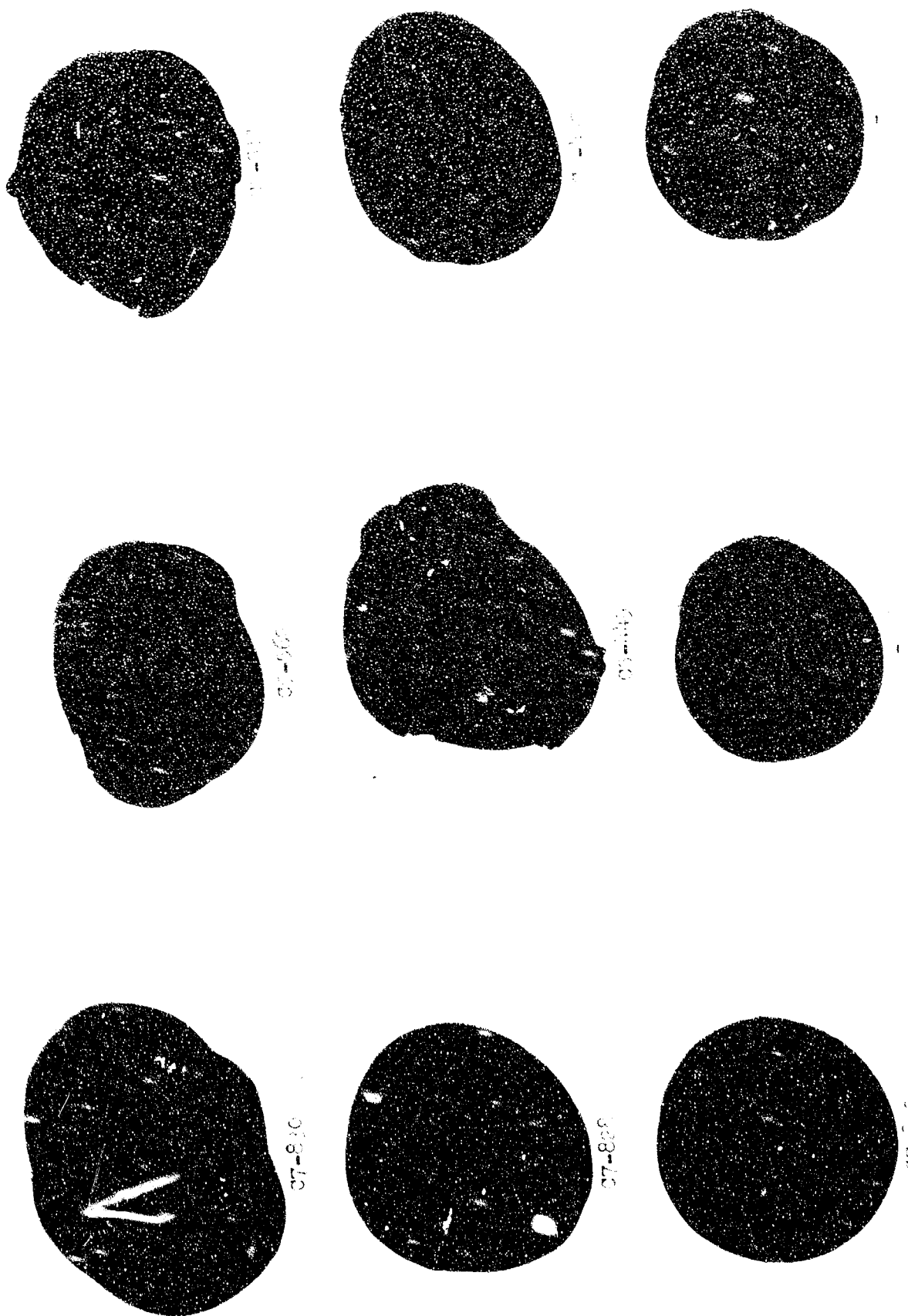
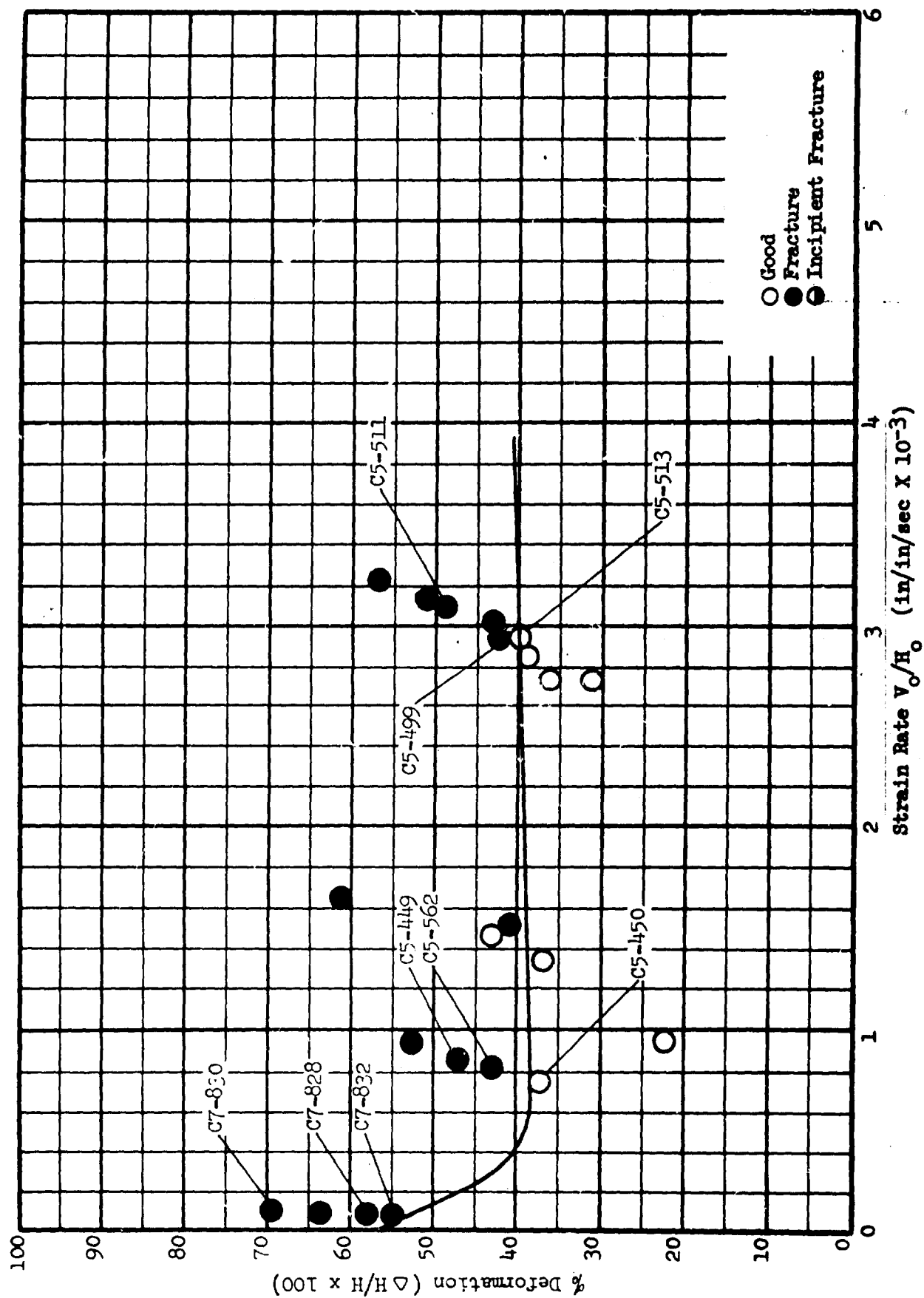
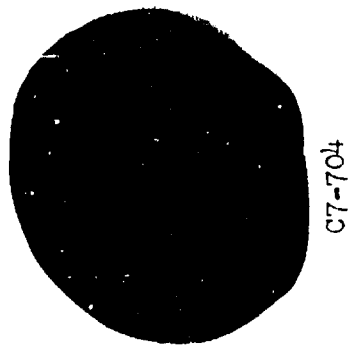


FIGURE 87. Ti-5Al-4.5Sn FORGABILITY LIMIT SPECIMENS AT 10<sup>6</sup> F

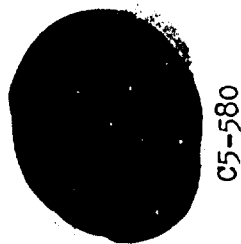


GRAPH 16. FORGEABILITY LIMIT CURVES FOR T1-5AL-2.5Sn AT 1050°F





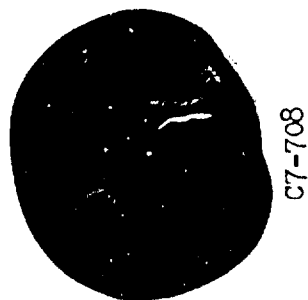
C7-704



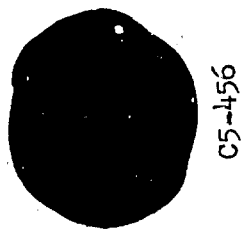
C5-580



C5-530



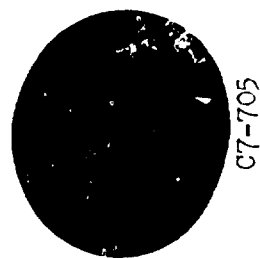
C7-708



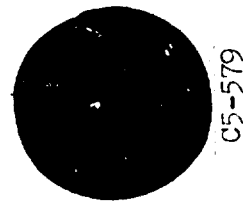
C5-456



C5-532



C7-705



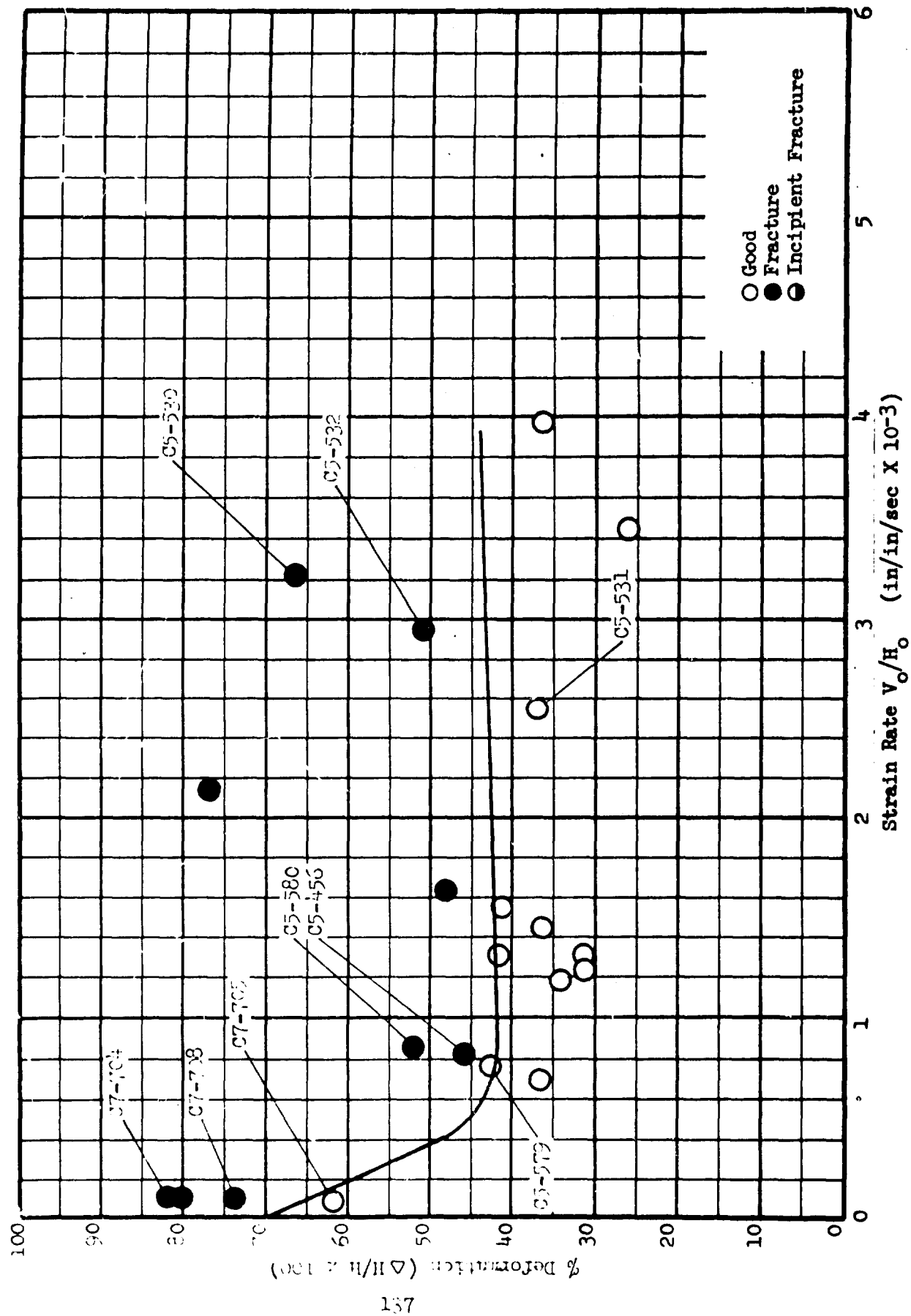
C5-579

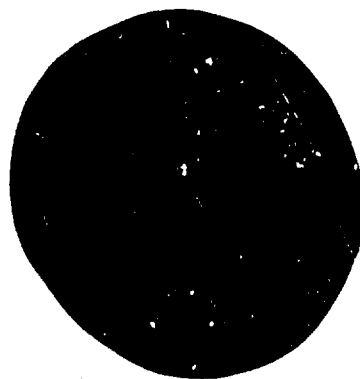


C5-531

FIGURE 88. Ti-5Al-2.5Sn FORGEABILITY LITE SPECIMENS AT 1350°F

GRAPH 17. FORMABILITY LIMIT CURVES FOR Ti-5Al-2.5Sn AT 1350°F





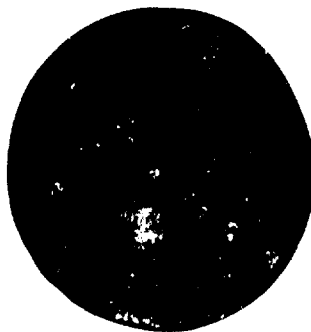
C7-739



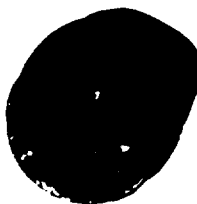
C5-569



C5-515



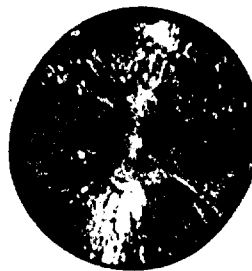
C7-738



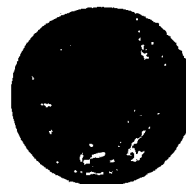
C5-570



C5-516



C7-737



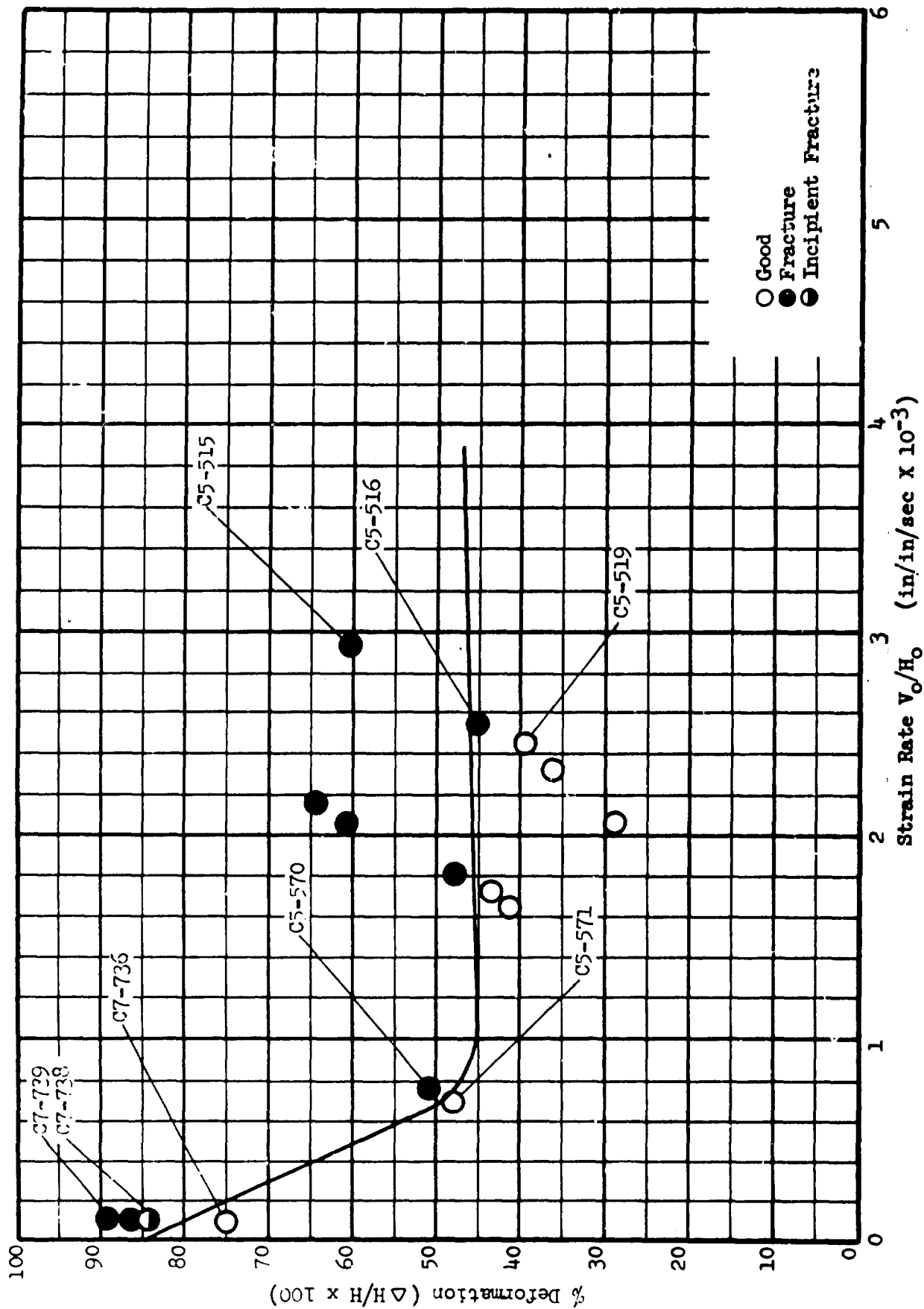
C5-571



C7-529

FIGURE 89. Ti-5Al-2.5Sn FORGEABILITY LIIT SPECIMENS AT 1550°F

GRAPH 18. FORGEABILITY LIMIT CURVES FOR Ti-5Al-2.5Sn AT 1550°F



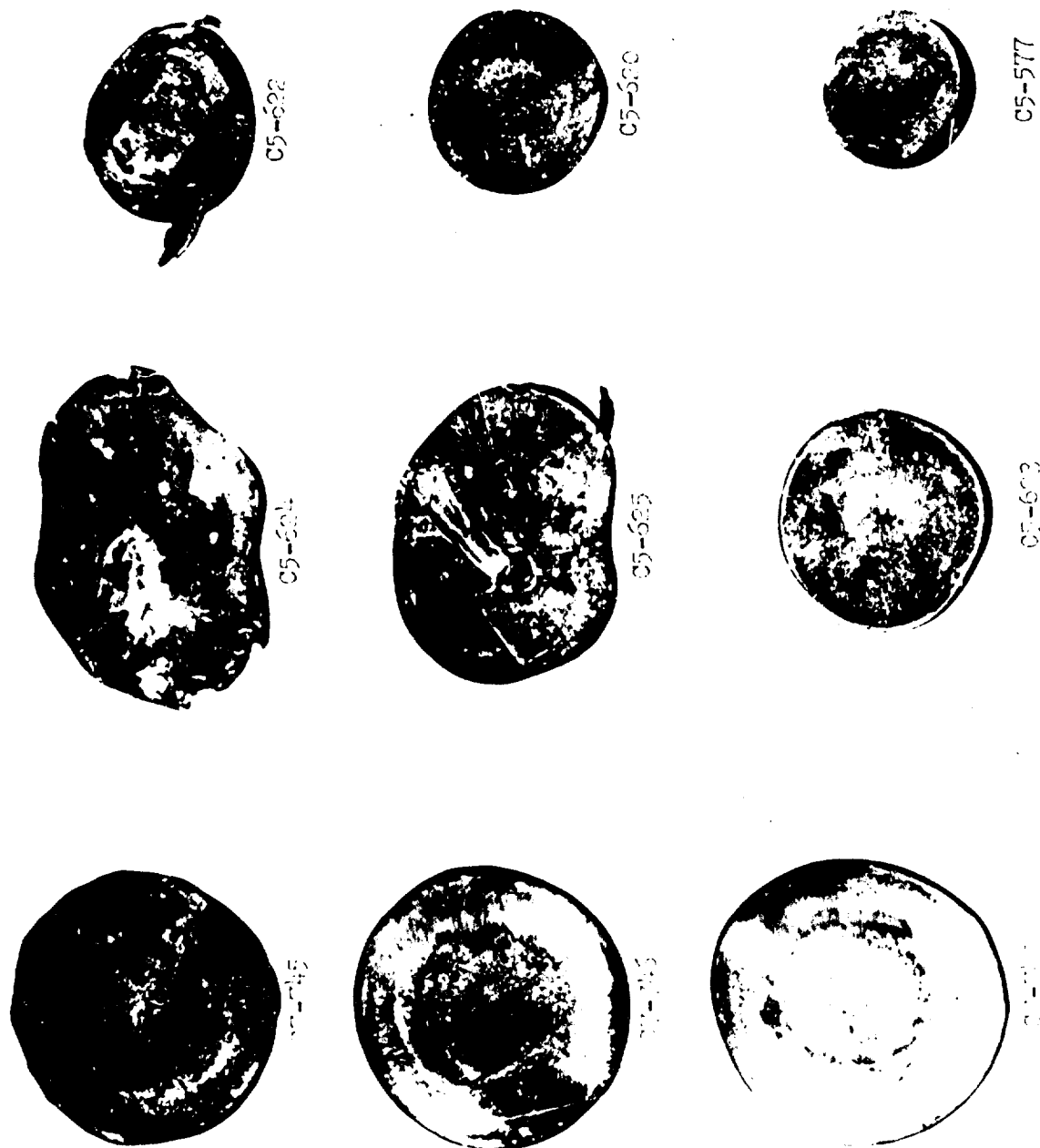
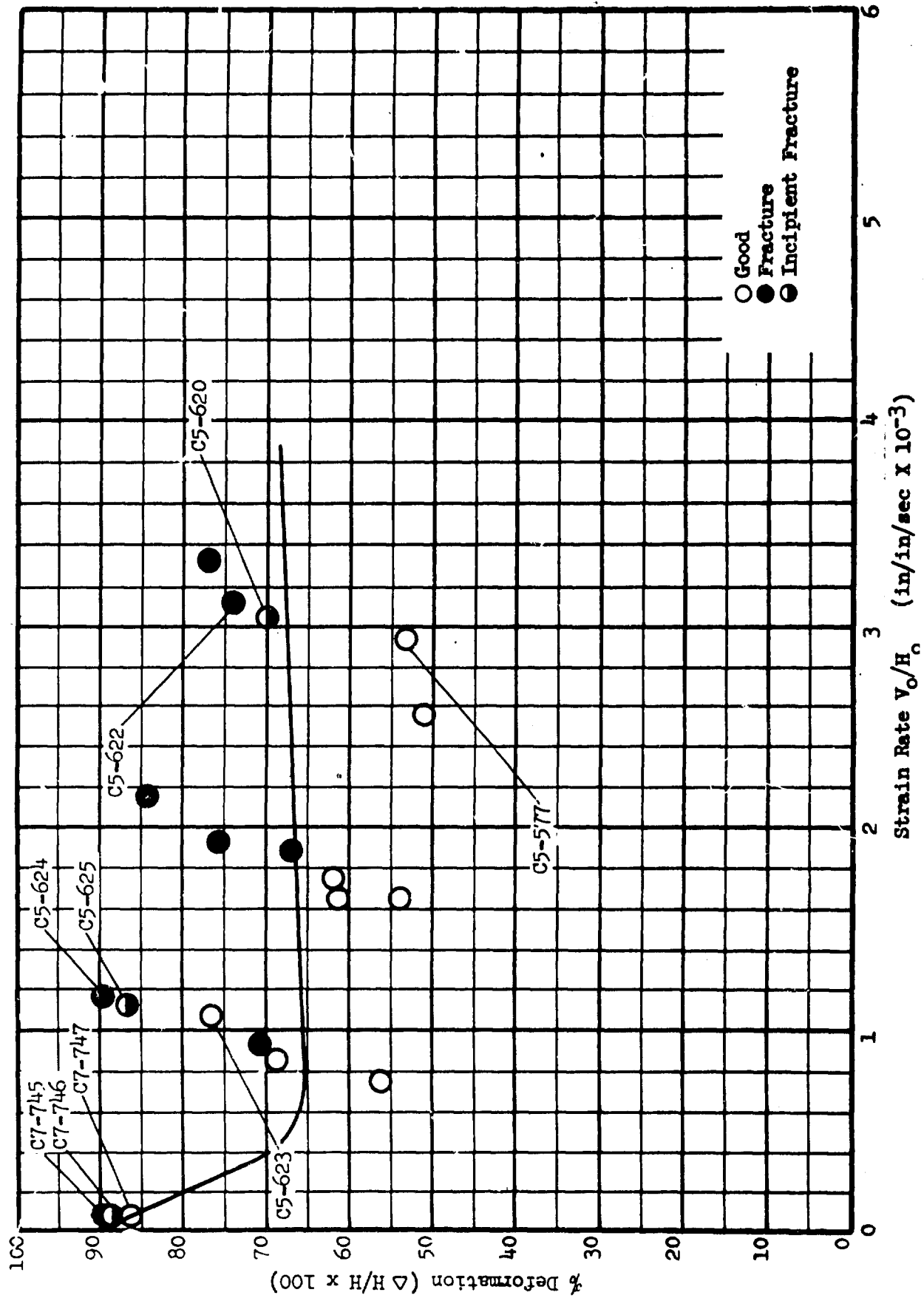


FIGURE 20. Ti-5Al-2.5Sn FORGEABILITY LIMIT SPECIMENS AT 1750°F

GRAPH 19. FORGEABILITY LIMIT CURVES FOR Ti-5Al-2.5Sn AT 1750°F



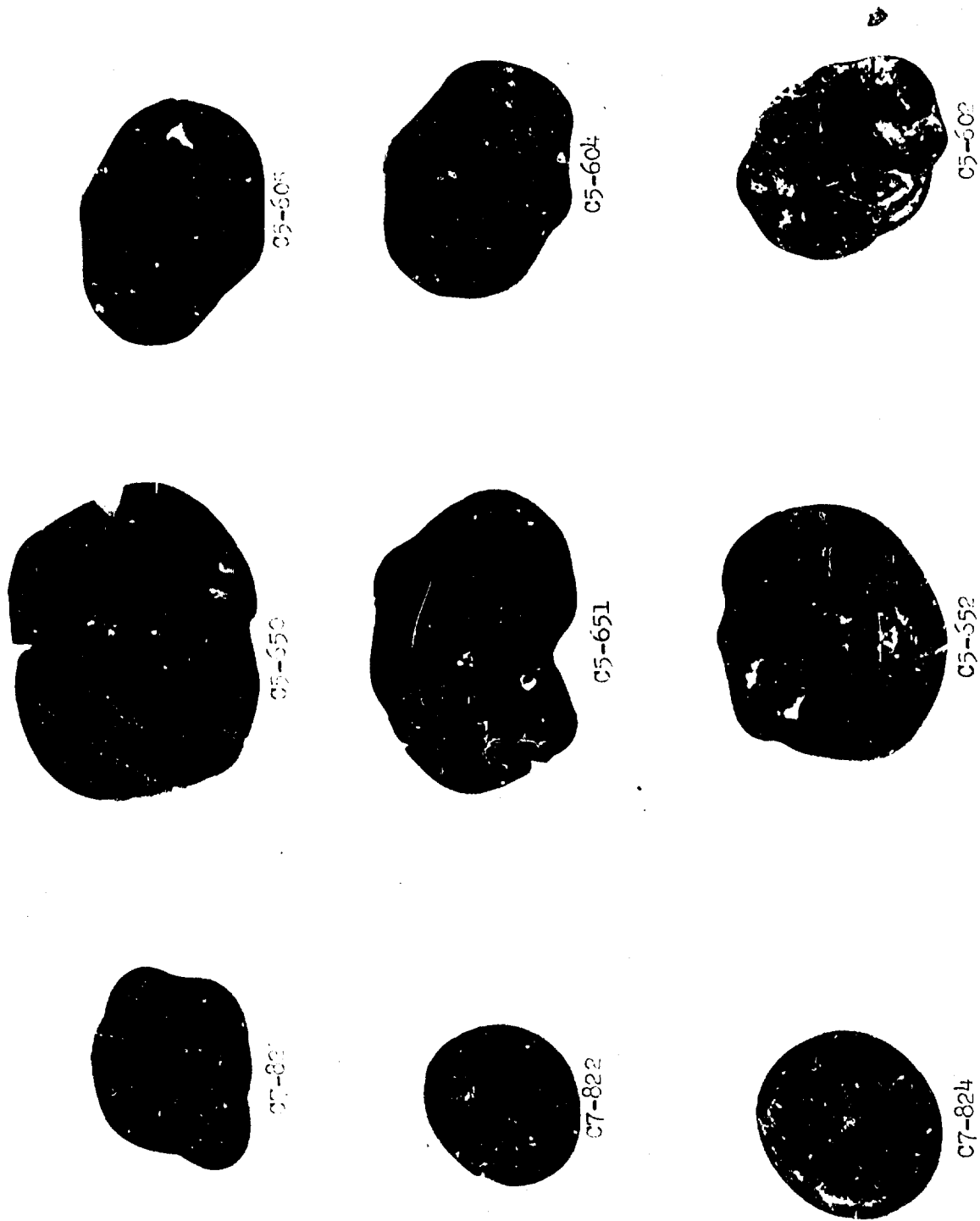
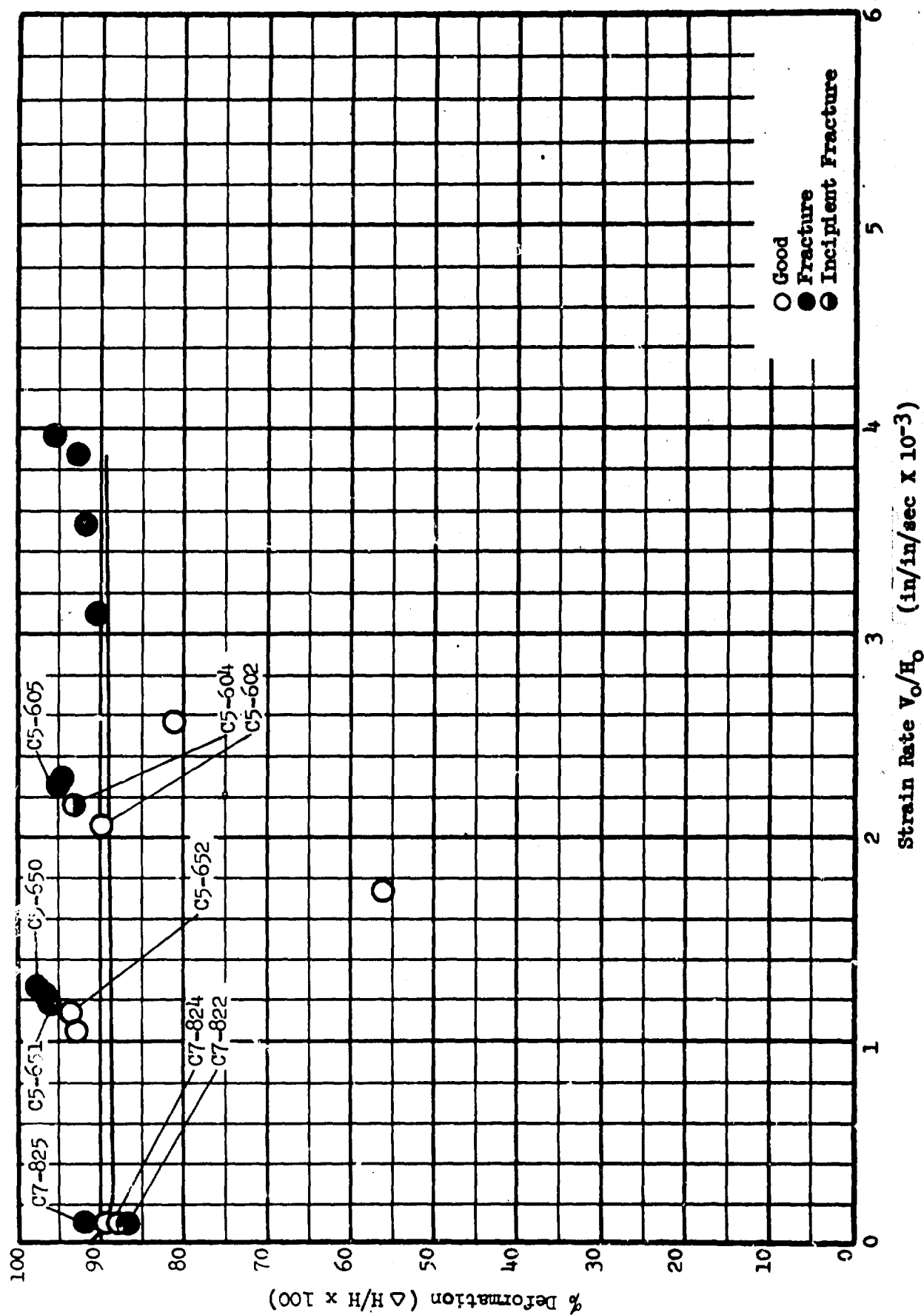


FIGURE 91. Ti-5Al-2.5Sn FORGEABILITY LIMIT SPECIMENS AT 1950°F



GRAPH 20. FORGEABILITY LIMIT CURVES FOR Ti-5Al-2.5Sn AT 1950°F



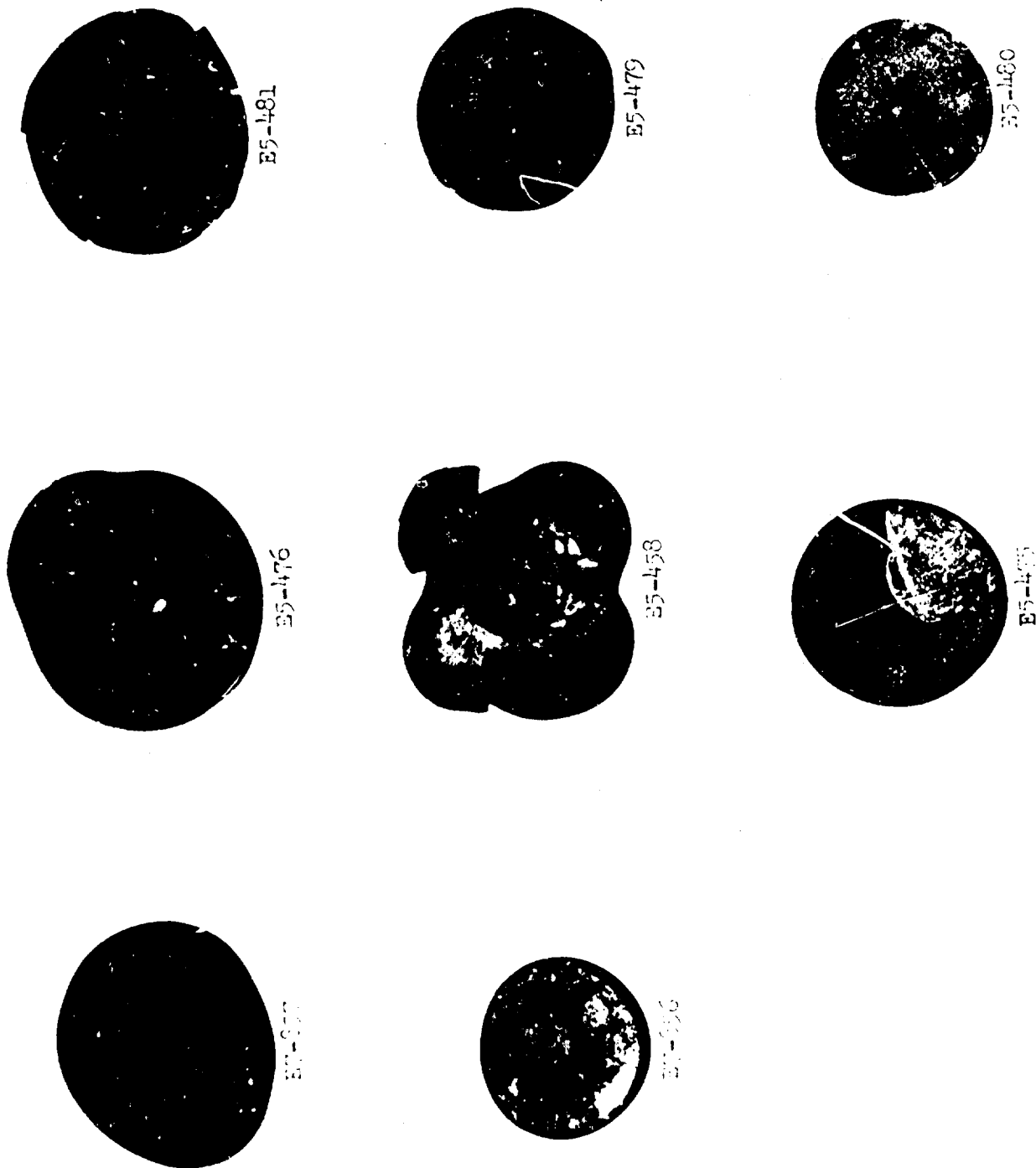
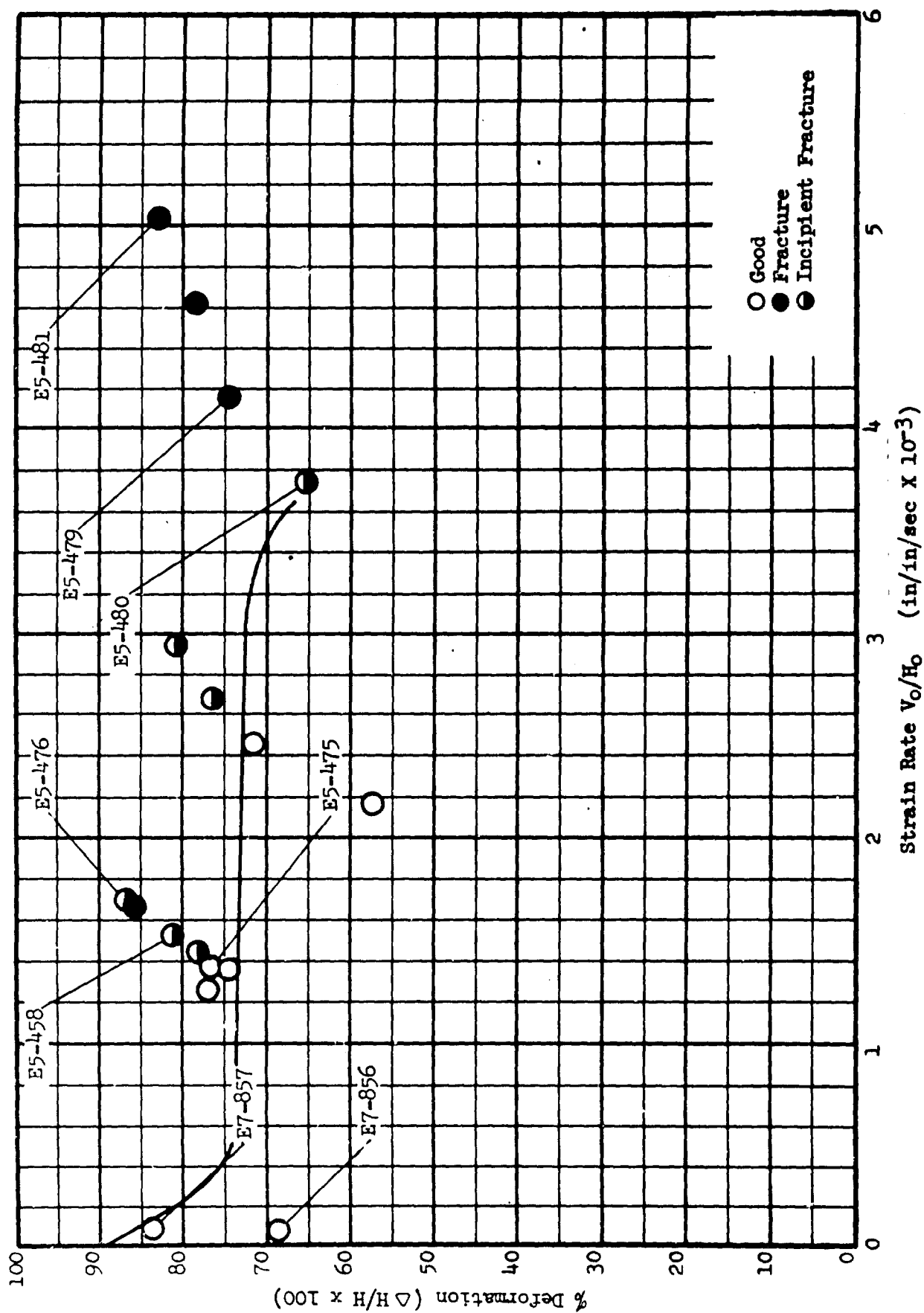


FIGURE 92. 17-4 PH FORGABILITY LIMIT SPECIMENS AT 550°F

GRAPH 21. FORGEABILITY LIMIT CURVES FOR 17-4 PH AT 550°F



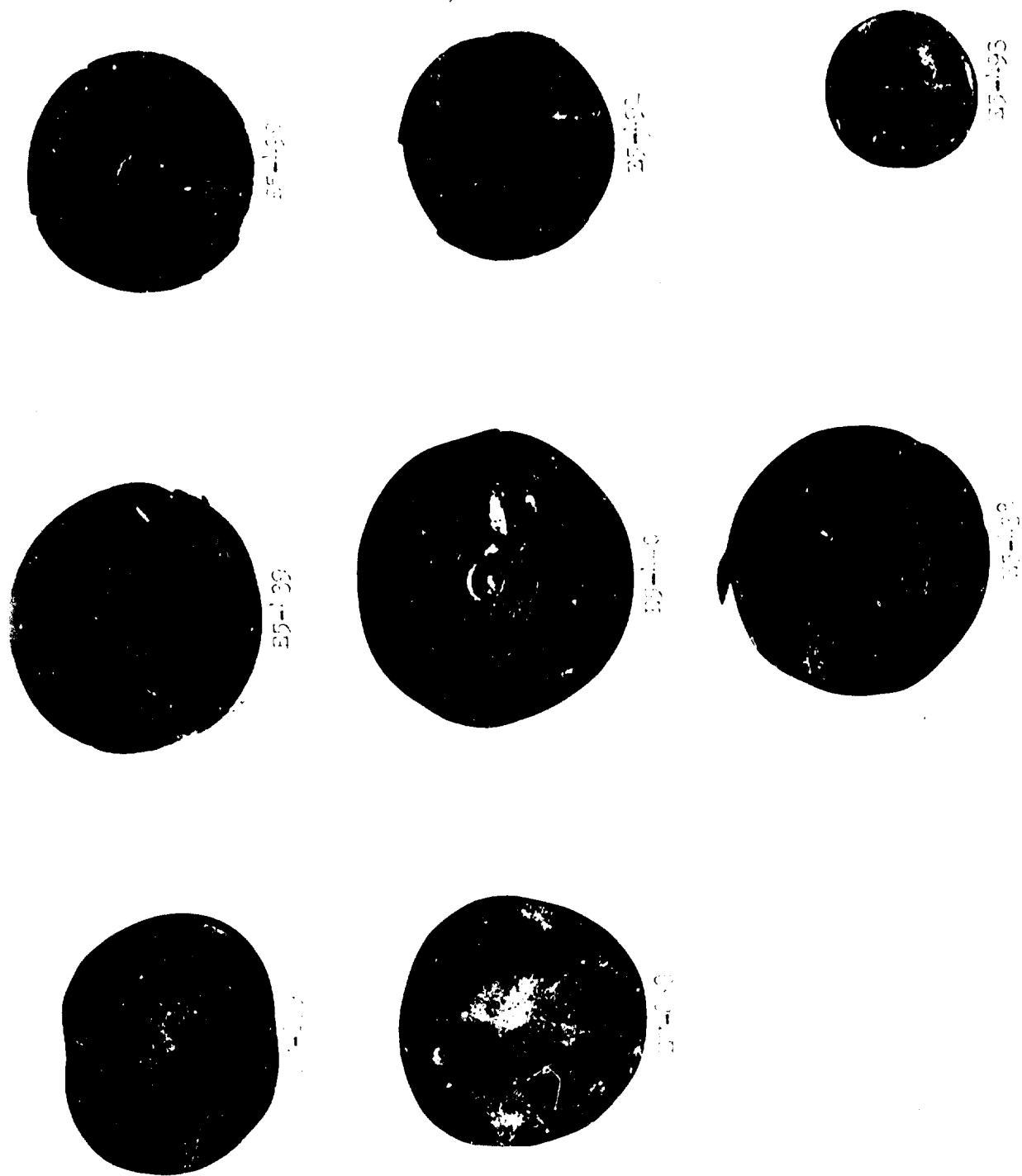
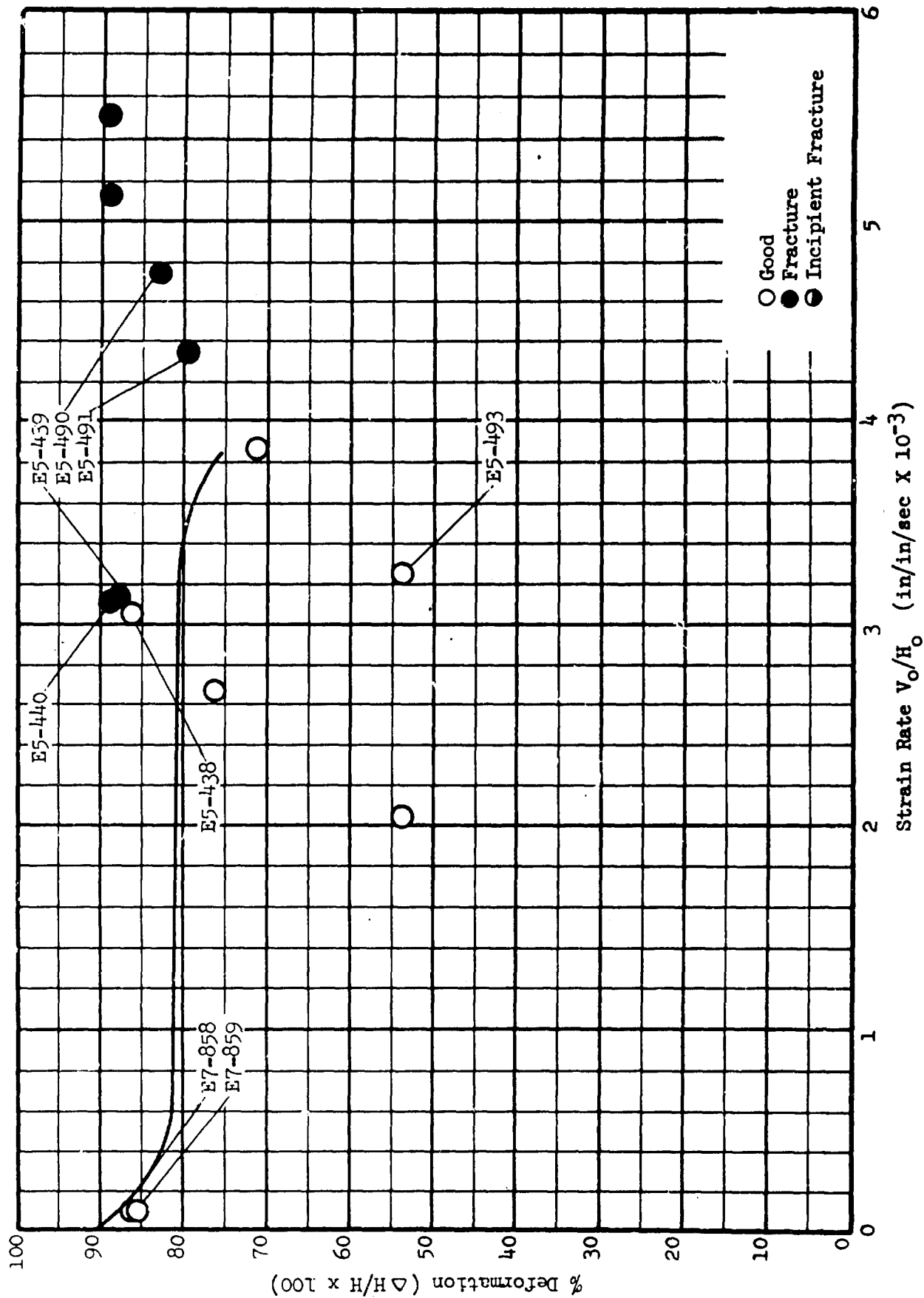


FIGURE 93. 17-4 PH FORCEABILITY LIMIT SPECIMENS AT 950°F

GRAPH 22. FORGEABILITY LIMIT CURVES FOR 17-4 PH AT 950°F





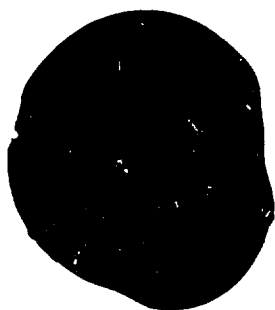
E5-520



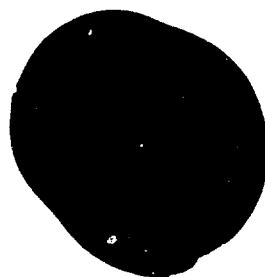
E5-582



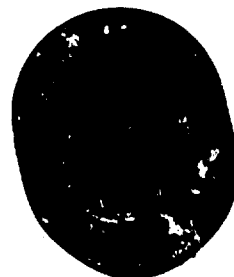
E5-504



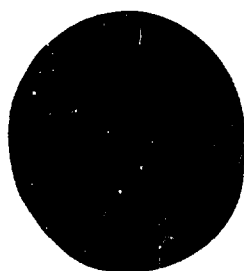
E5-492



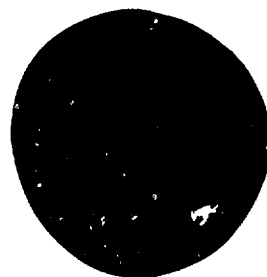
E5-451



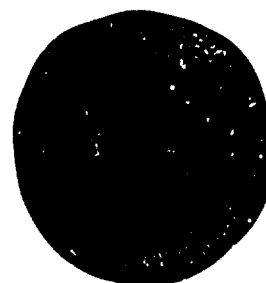
E5-455



E7-710



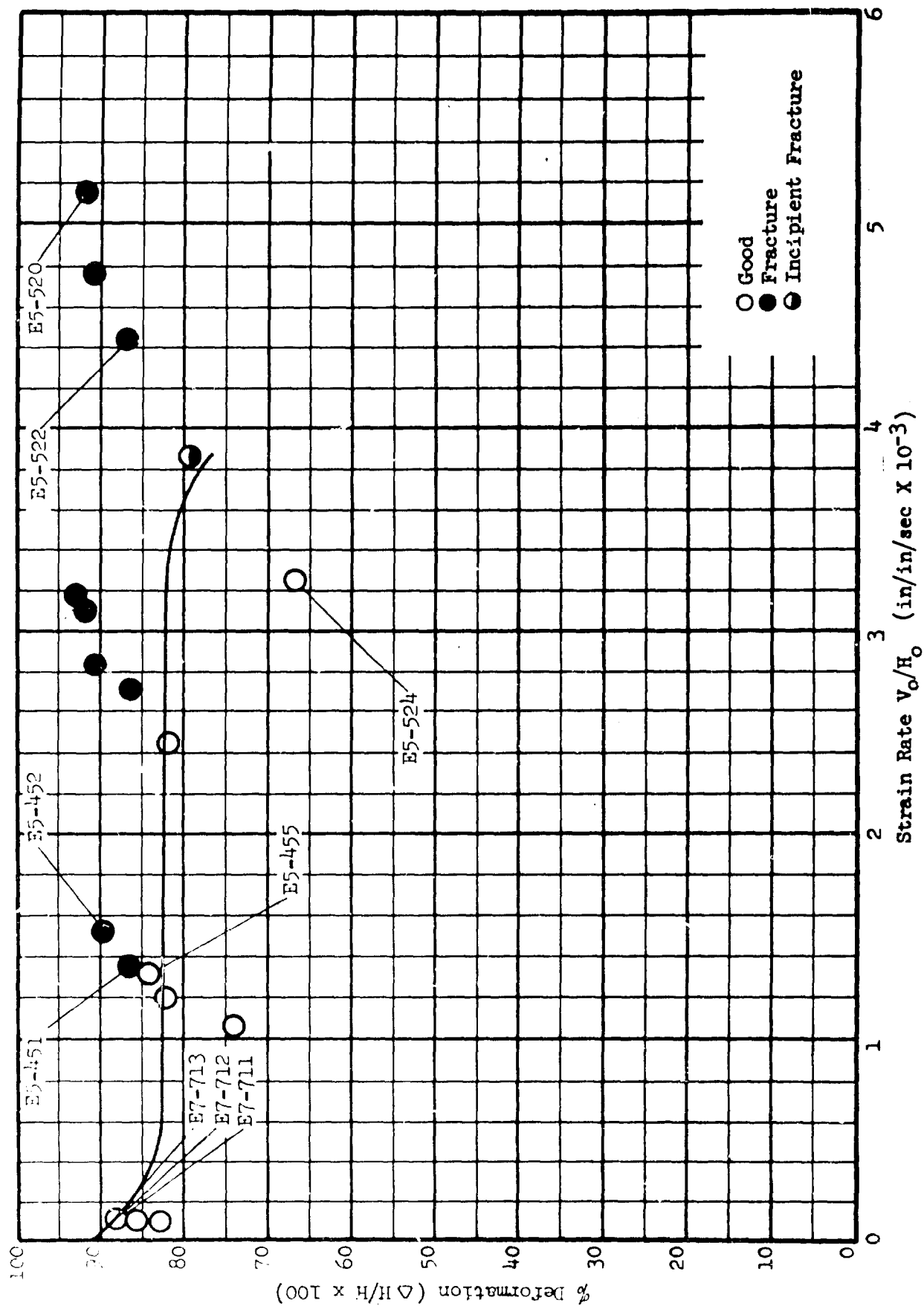
E7-712



E7-711

FIGURE 94. 17-4 PH FORGEABILITY LIMIT SPECIMENS AT 1350°F

GRAPH 23. FORGEABILITY LIMIT CURVES FOR 17-4 PH AT 1350°F



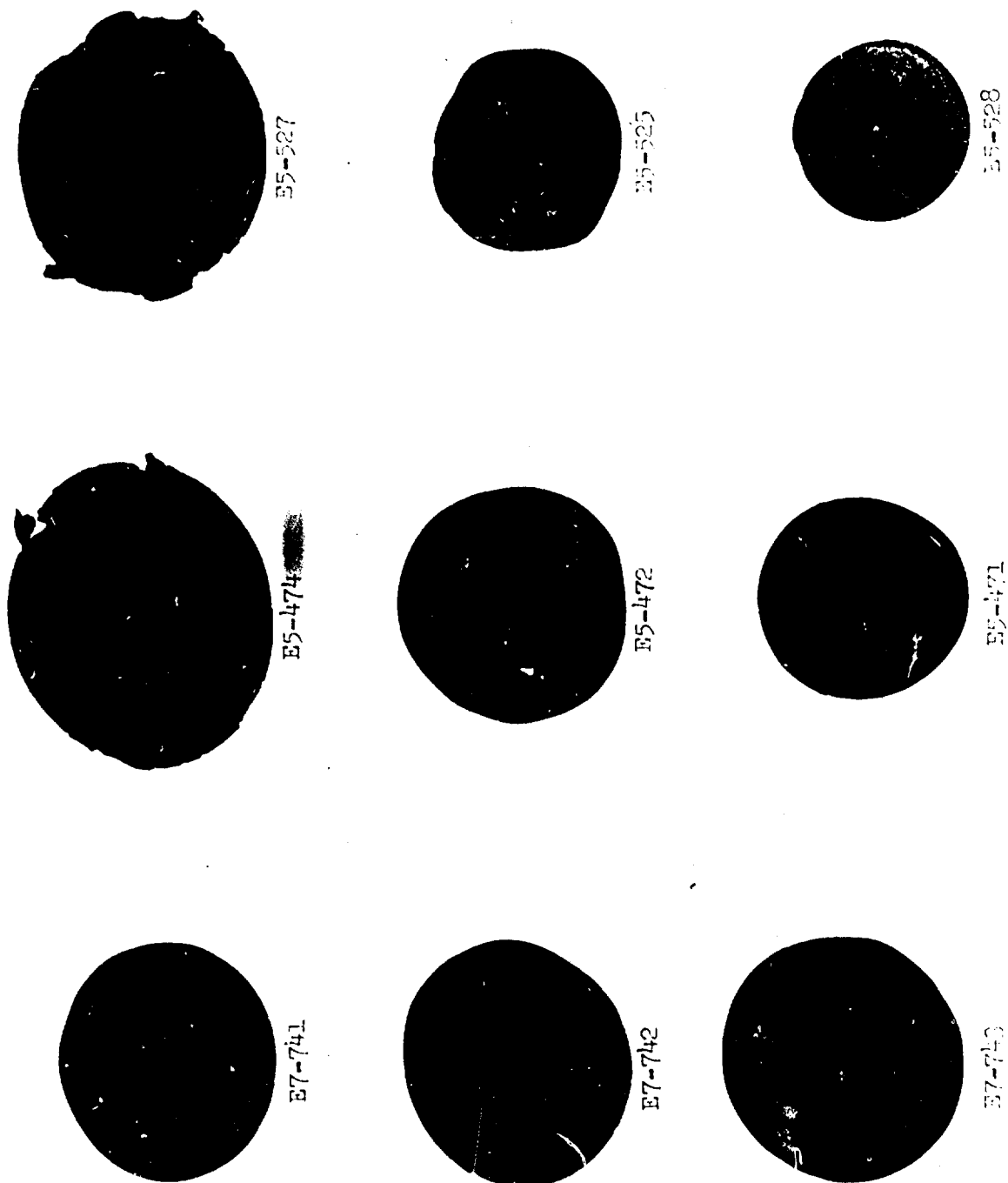
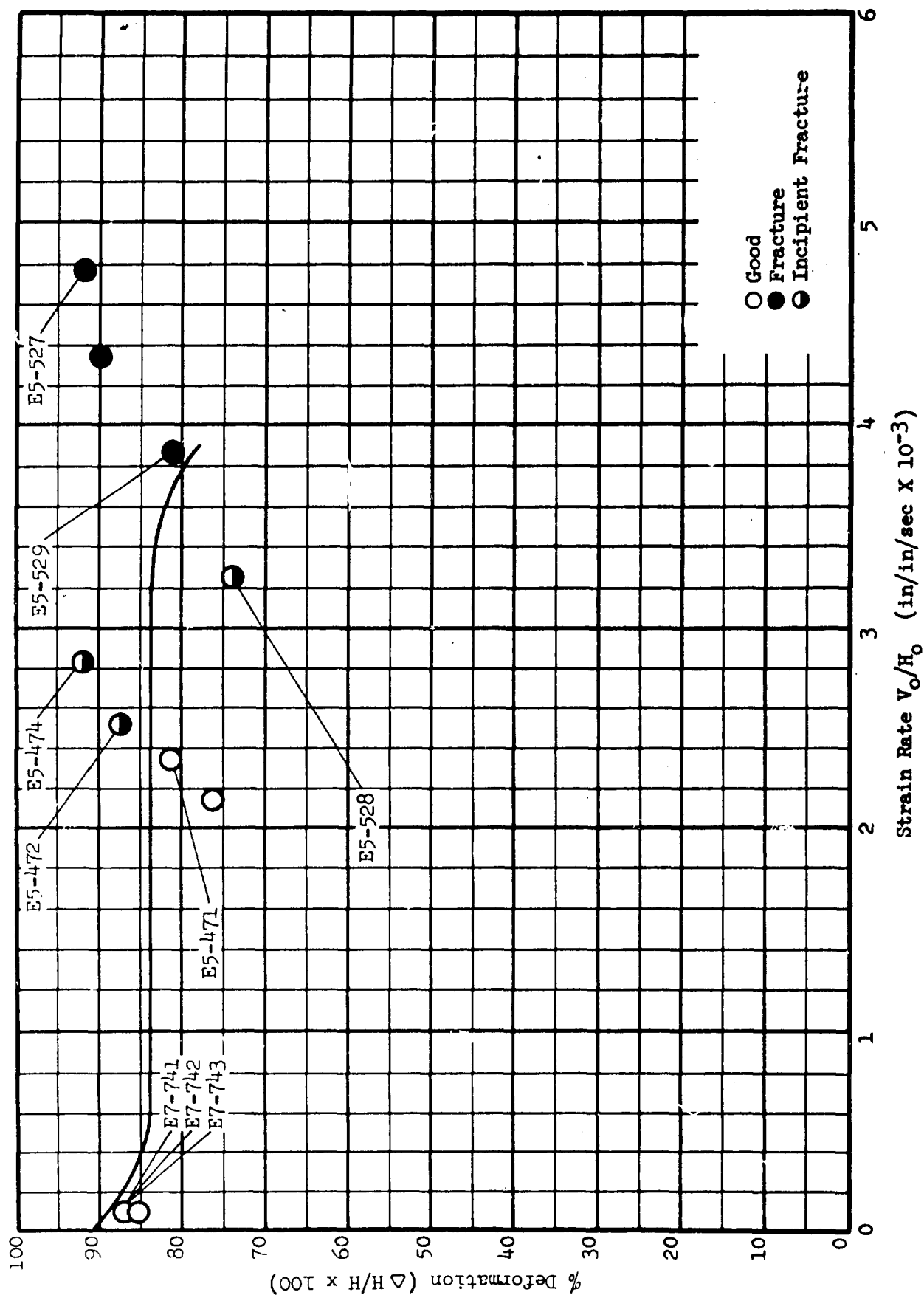
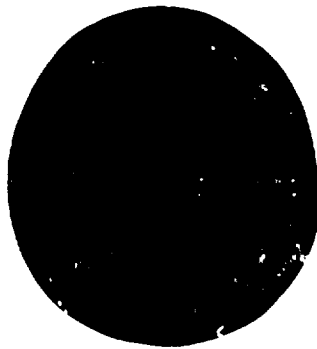


FIGURE 95. 17-4 PH FORGEABILITY LIAT SPECIMENS AT 1550°F



GRAPH 24. FORGEABILITY LIMIT CURVES FOR 17-4 PH AT 1550°F

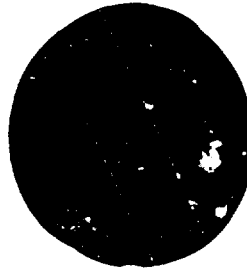




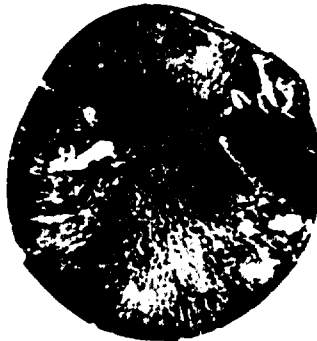
E5-642



E5-643



E5-644



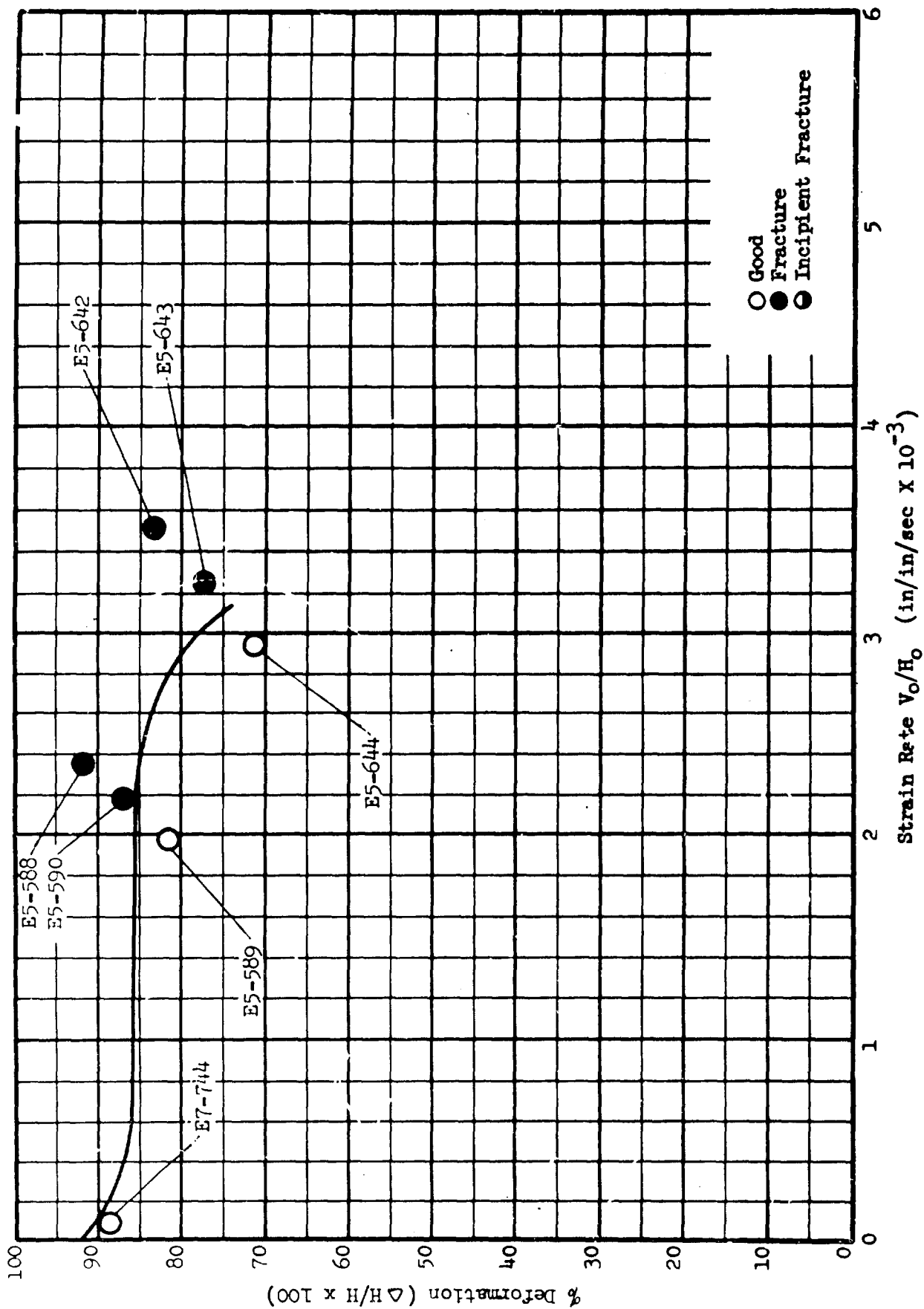
E5-725



E5-726

FIGURE 96 17-4 PH FORGEABILITY LIMIT SPECIMENS AT 1750°F

GRAPH 25. FORGEABILITY LIMIT CURVES FOR 17-4 PH AT 1750°F



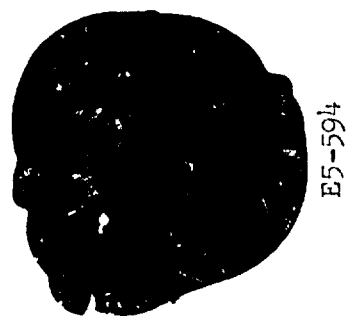
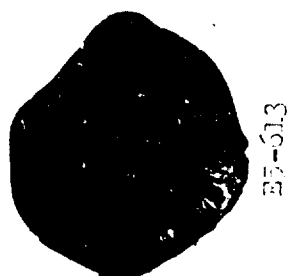
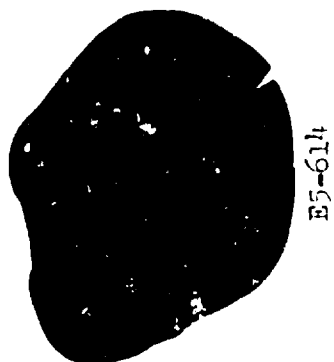
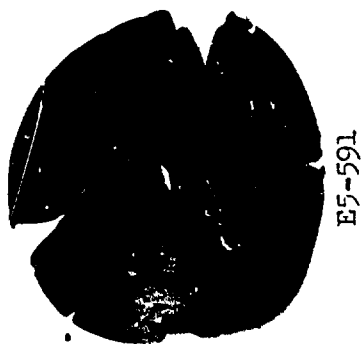
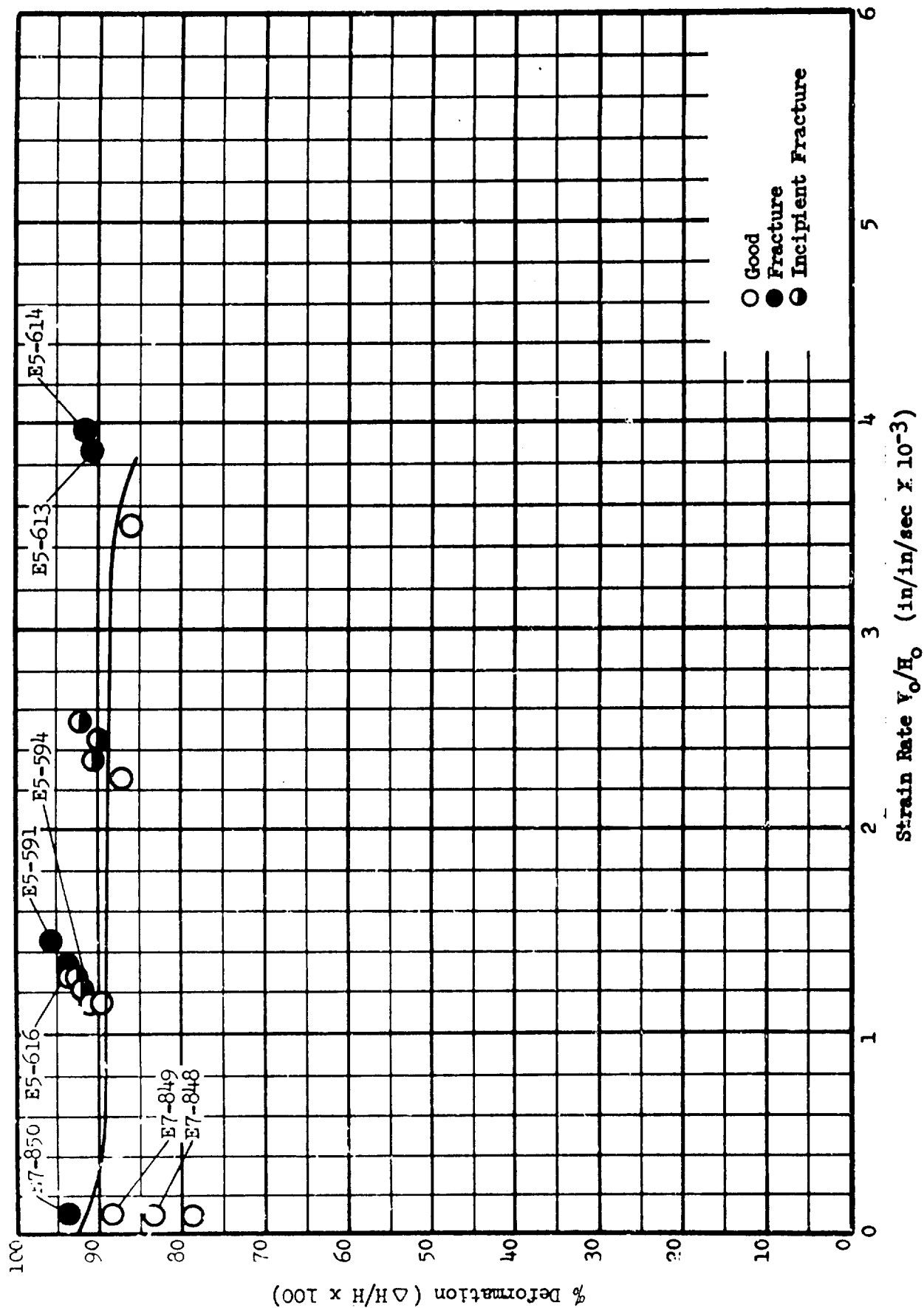
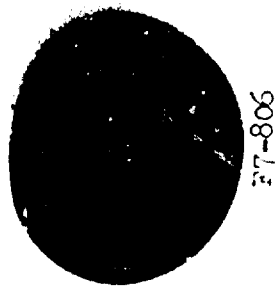


FIGURE 97. 17-4 PH FORGEABILITY LIMIT SPECIMENS AT 1950°F

GRAPH 26. FORGEABILITY LIMIT CURVES FOR 17-4 PH AT 1950° F





F7-806



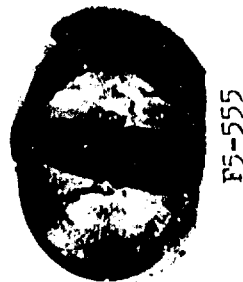
F5-554



F5-503



F7-799



F5-555



F5-505



F7-796



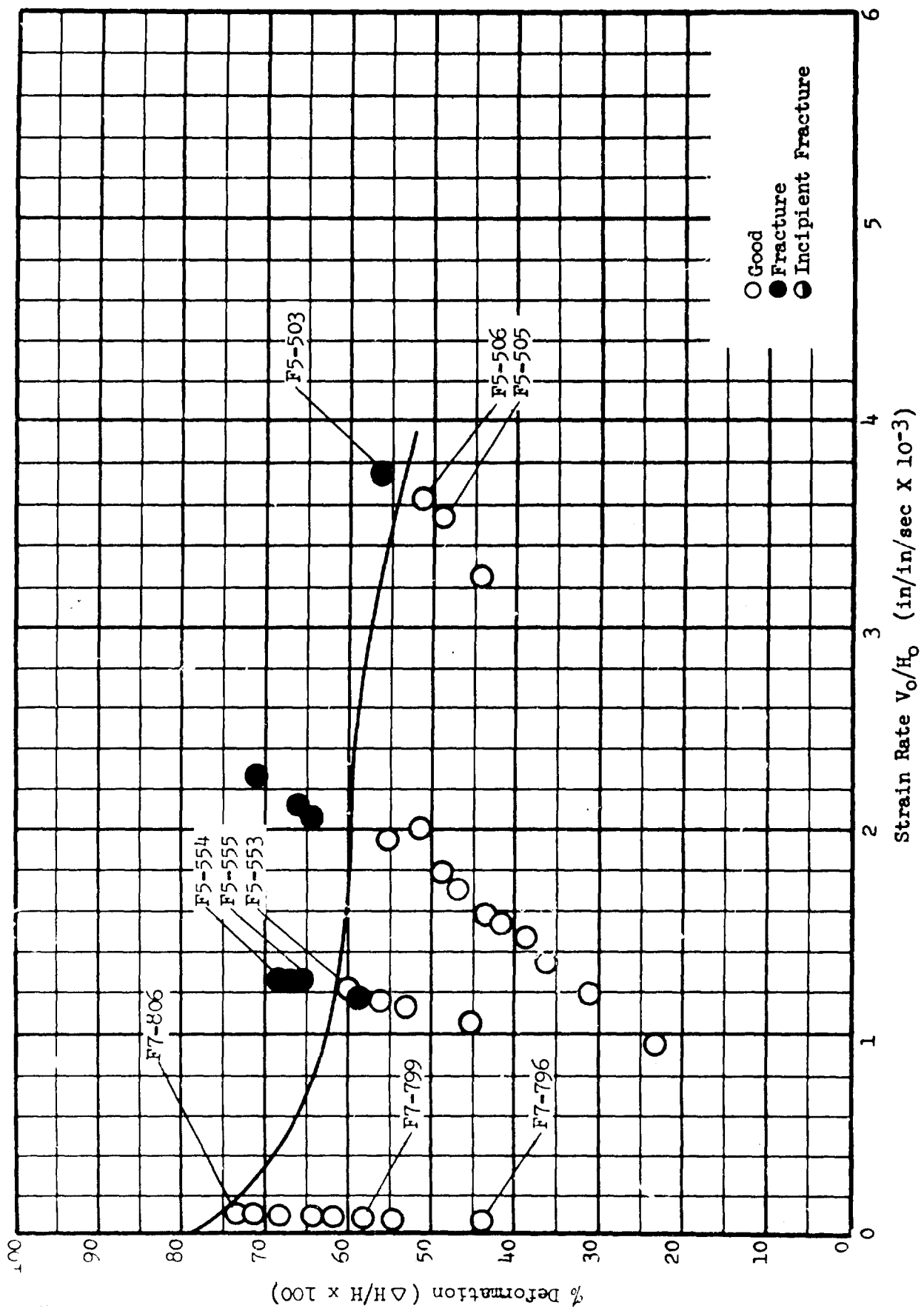
F5-553



F5-505

FIGURE 9. A-286 FORGEABILITY LIMIT SPECIMEN AT ROOM TEMPERATURE

GRAPH 27. FORGEABILITY LIMIT CURVES FOR A-286 AT ROOM TEMPERATURE



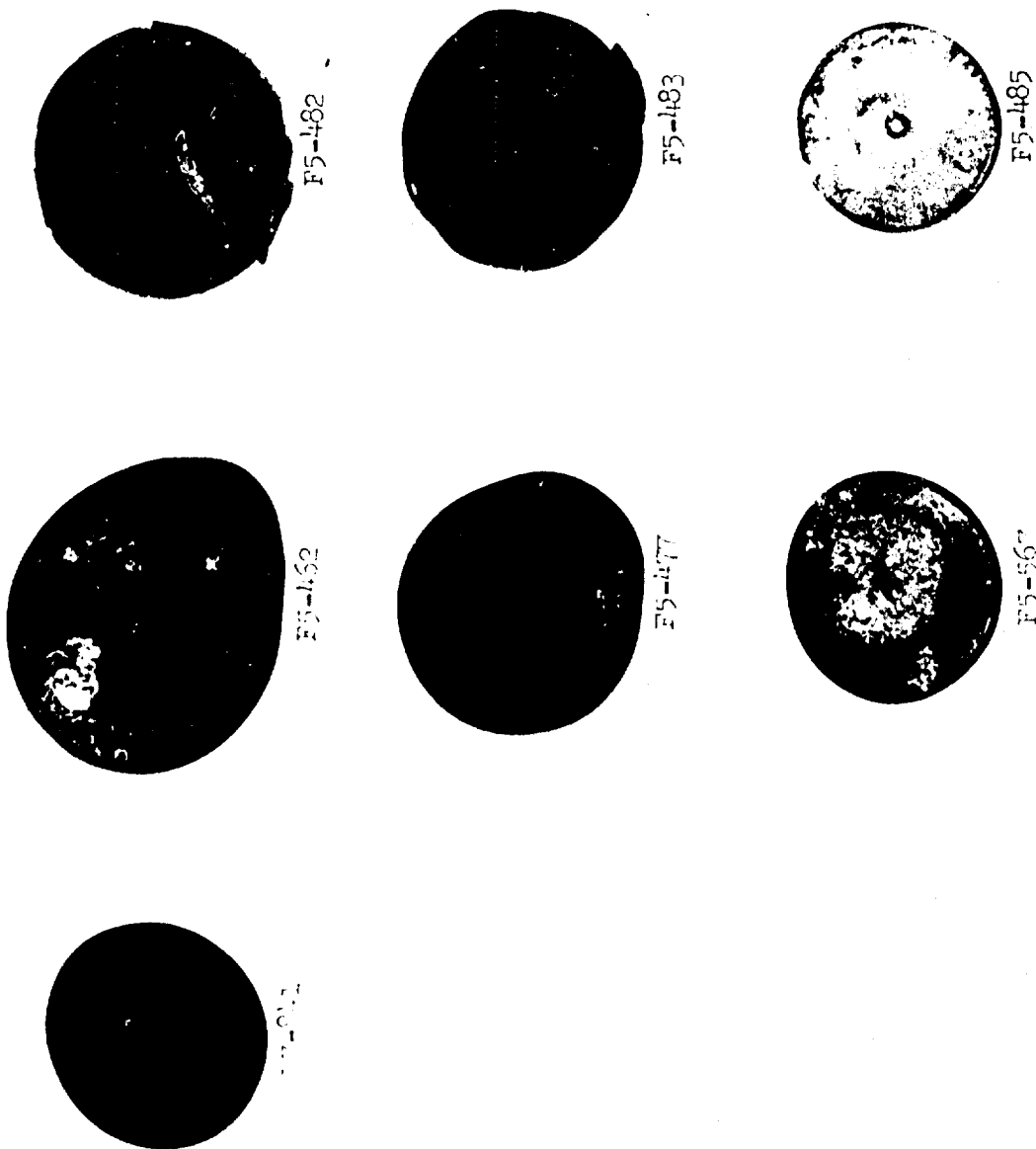
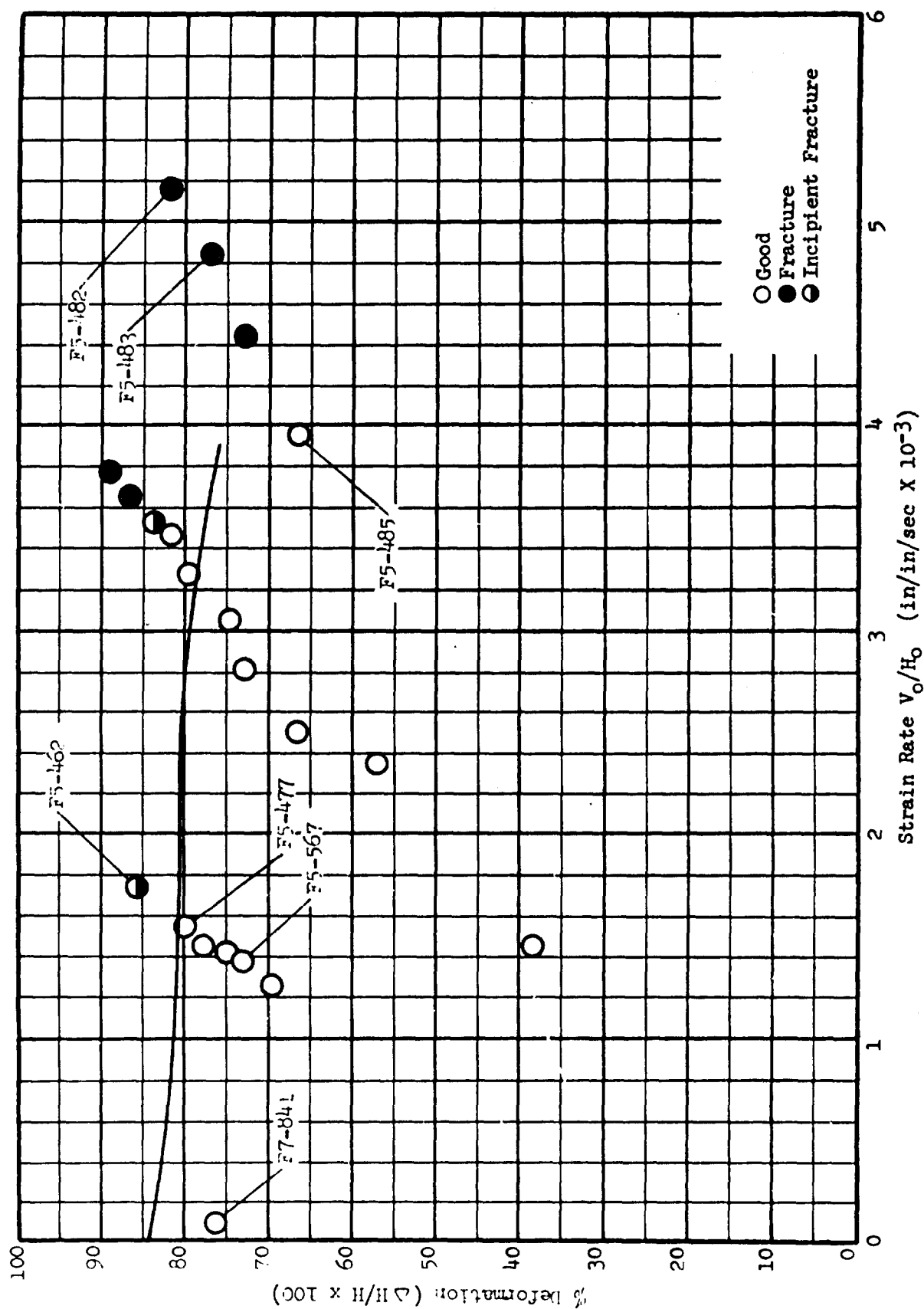


FIGURE 99. A-286 FORGEABILITY LIGHT SPECIMENS AT 550°F



GRAPH 28. FORCEABILITY LIMIT CURVES FOR A-286 AT 550°F



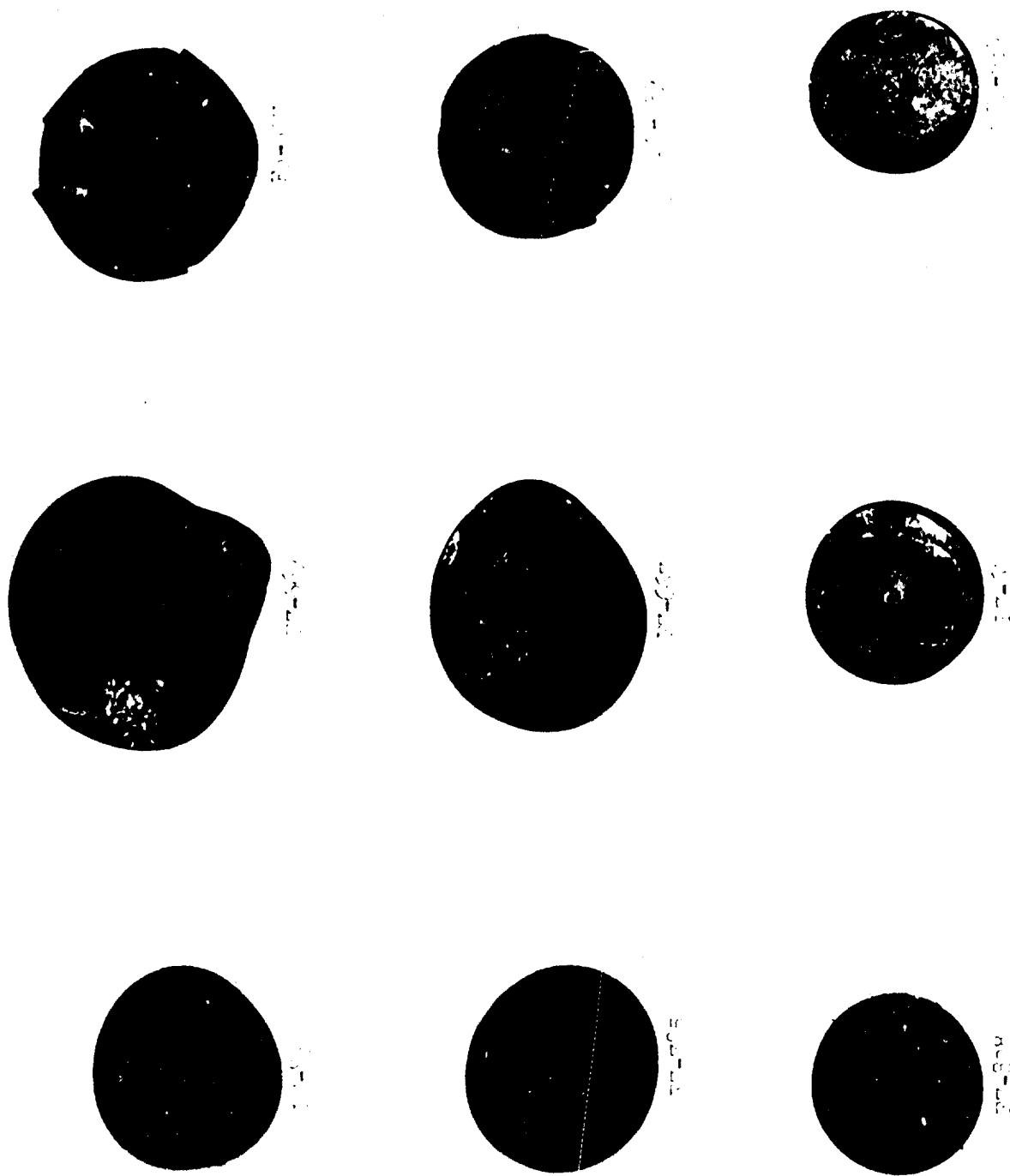


FIGURE 100. A-286 FORGABILITY LIGHT SPECIMENS AT 750°F

A line graph showing the relationship between % Deformation (Y-axis, 0 to 100) and Strain Rate  $V_0/H_0$  (X-axis, 0 to 6, in/in/sec  $\times 10^{-3}$ ). The graph includes data points for various materials, categorized by their condition: Good (open circles), Fracture (filled circles), and Incipient Fracture (half-filled circles). Several materials are labeled with lines pointing to their respective data points: F7-669, F7-667, F7-839, F7-785, F7-838, F7-665, F5-537, F5-539, and F5-535. A legend in the top right corner defines the symbols used.

Material	Strain Rate $V_0/H_0$ (in/in/sec $\times 10^{-3}$ )	% Deformation ( $\Delta H/H \times 100$ )	Condition
F7-839	0.1	68	Good
F7-785	0.2	68	Good
F7-838	0.3	68	Good
F7-669	0.5	88	Good
F7-667	0.6	88	Good
F7-667	0.7	88	Good
F7-667	0.8	88	Good
F7-667	0.9	88	Good
F7-667	1.0	88	Good
F7-667	1.1	88	Good
F7-667	1.2	88	Good
F7-667	1.3	88	Good
F7-667	1.4	88	Good
F7-667	1.5	88	Good
F7-667	1.6	88	Good
F7-667	1.7	88	Good
F7-667	1.8	88	Good
F7-667	1.9	88	Good
F7-667	2.0	88	Good
F7-667	2.1	88	Good
F7-667	2.2	88	Good
F7-667	2.3	88	Good
F7-667	2.4	88	Good
F7-667	2.5	88	Good
F7-667	2.6	88	Good
F7-667	2.7	88	Good
F7-667	2.8	88	Good
F7-667	2.9	88	Good
F7-667	3.0	88	Good
F7-667	3.1	88	Good
F7-667	3.2	88	Good
F7-667	3.3	88	Good
F7-667	3.4	88	Good
F7-667	3.5	88	Good
F7-667	3.6	88	Good
F7-667	3.7	88	Good
F7-667	3.8	88	Good
F7-667	3.9	88	Good
F7-667	4.0	88	Good
F7-667	4.1	88	Good
F7-667	4.2	88	Good
F7-667	4.3	88	Good
F7-667	4.4	88	Good
F7-667	4.5	88	Good
F7-667	4.6	88	Good
F7-667	4.7	88	Good
F7-667	4.8	88	Good
F7-667	4.9	88	Good
F7-667	5.0	88	Good
F7-667	5.1	88	Good
F7-667	5.2	88	Good
F7-667	5.3	88	Good
F7-667	5.4	88	Good
F7-667	5.5	88	Good
F7-667	5.6	88	Good
F7-667	5.7	88	Good
F7-667	5.8	88	Good
F7-667	5.9	88	Good
F7-667	6.0	88	Good
F7-667	6.1	88	Good
F7-667	6.2	88	Good
F7-667	6.3	88	Good
F7-667	6.4	88	Good
F7-667	6.5	88	Good
F7-667	6.6	88	Good
F7-667	6.7	88	Good
F7-667	6.8	88	Good
F7-667	6.9	88	Good
F7-667	7.0	88	Good
F7-667	7.1	88	Good
F7-667	7.2	88	Good
F7-667	7.3	88	Good
F7-667	7.4	88	Good
F7-667	7.5	88	Good
F7-667	7.6	88	Good
F7-667	7.7	88	Good
F7-667	7.8	88	Good
F7-667	7.9	88	Good
F7-667	8.0	88	Good
F7-667	8.1	88	Good
F7-667	8.2	88	Good
F7-667	8.3	88	Good
F7-667	8.4	88	Good
F7-667	8.5	88	Good
F7-667	8.6	88	Good
F7-667	8.7	88	Good
F7-667	8.8	88	Good
F7-667	8.9	88	Good
F7-667	9.0	88	Good
F7-667	9.1	88	Good
F7-66			

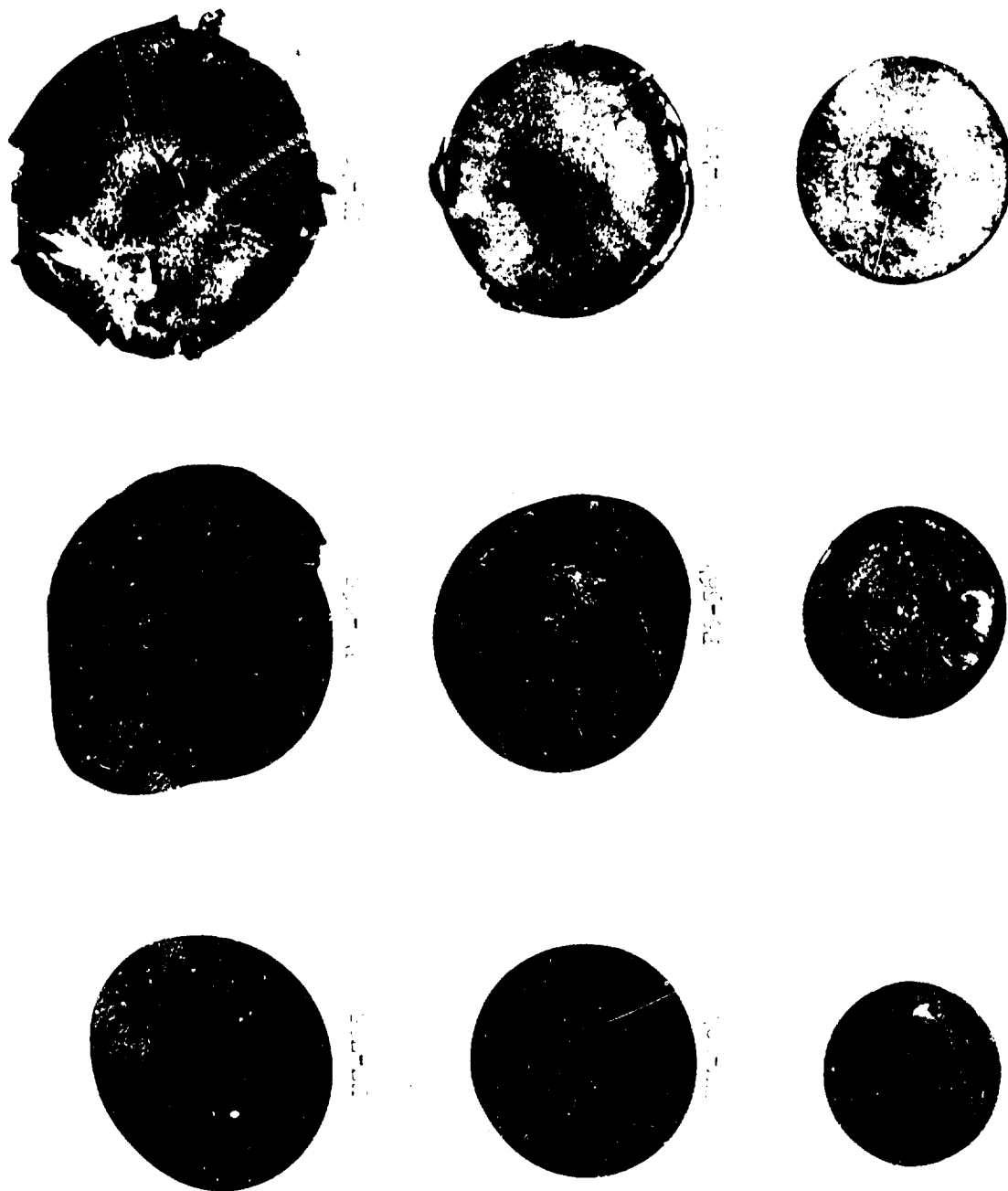
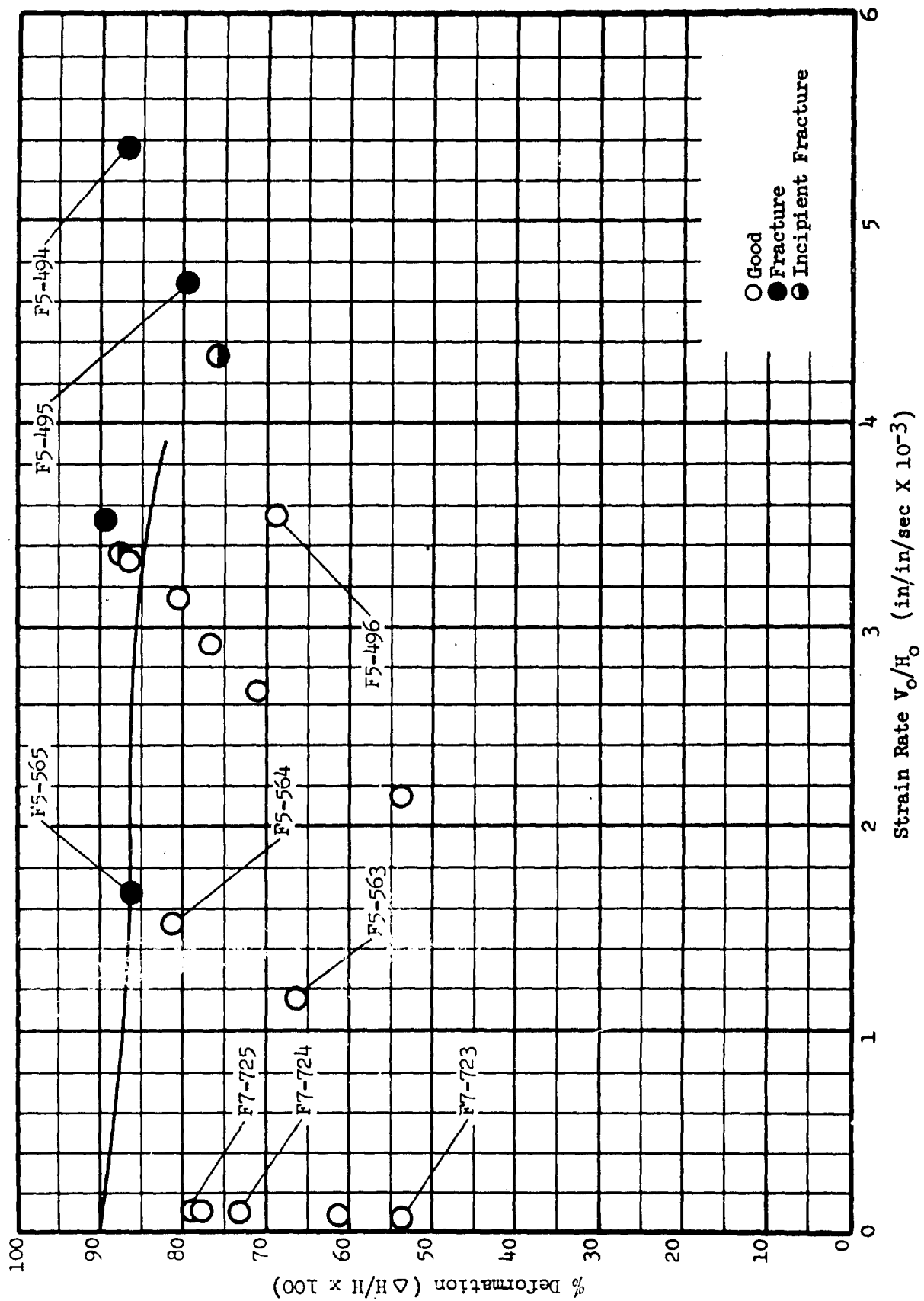


FIGURE 101. A-286 FORGEABILITY LIMIT SPECIMENS AT 950°F

GRAPH 30. FORGEABILITY LIMIT CURVES FOR A-286 AT 950°F



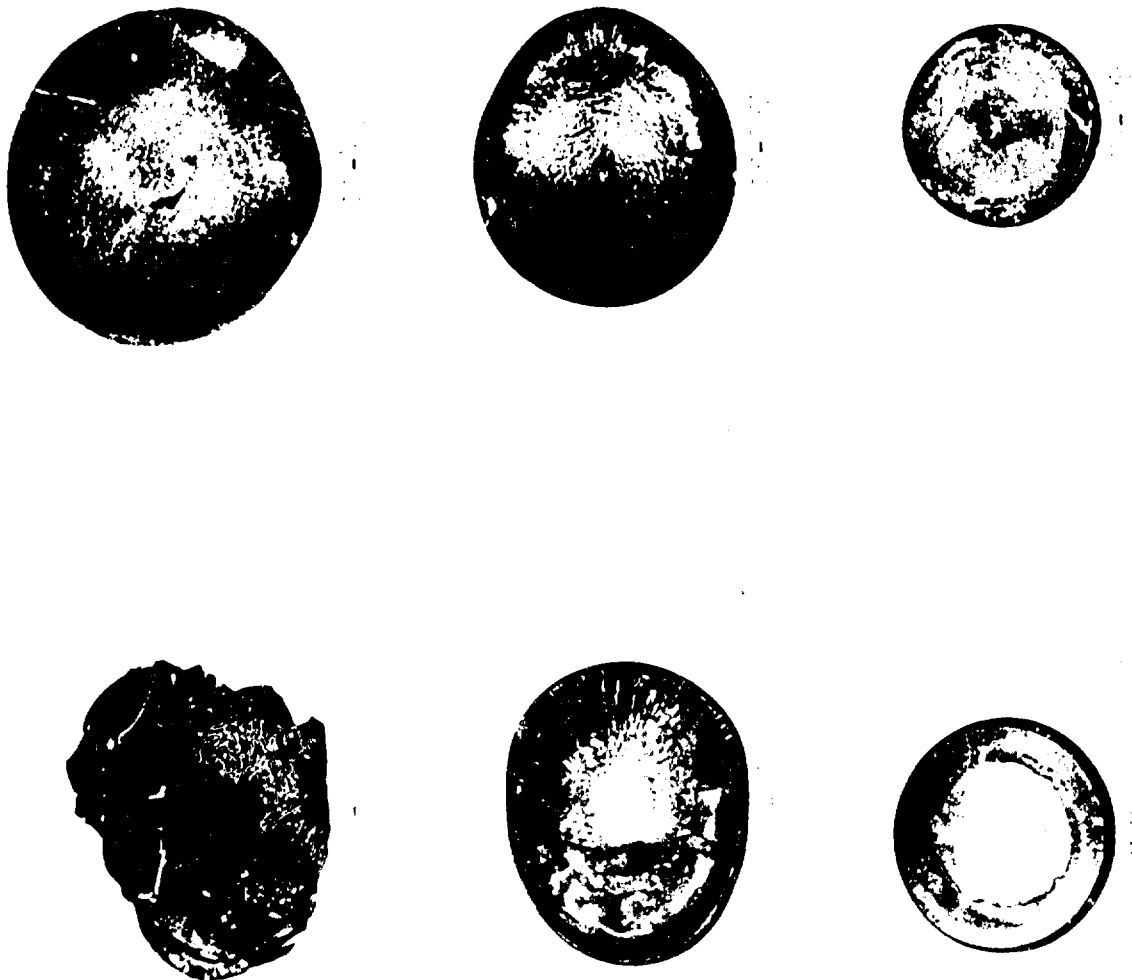
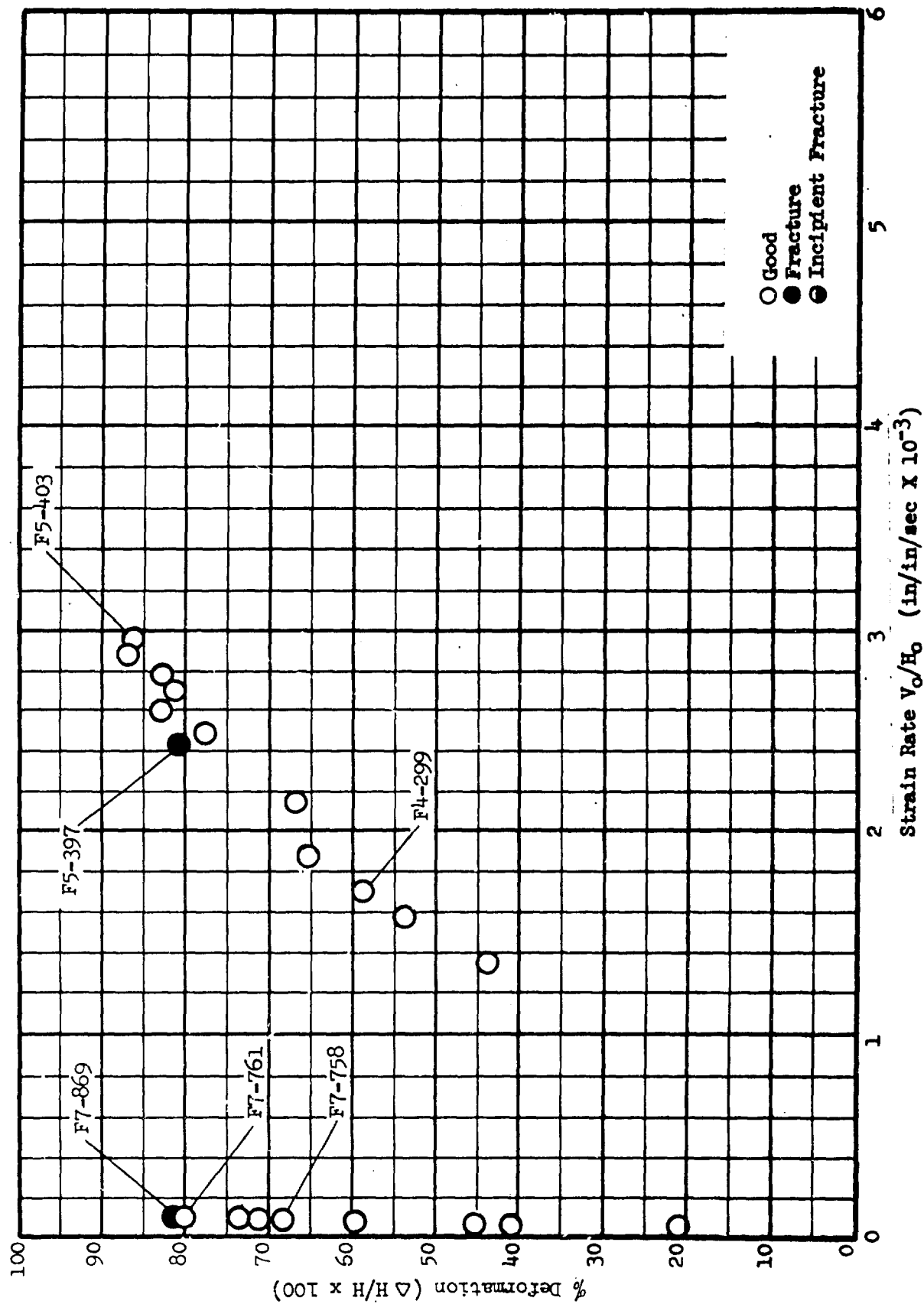


FIGURE 102. A-286 FORGEABILITY LIMIT SPECIMENS AT 1050°F

GRAPH 31. FORGEABILITY LIMIT CURVES FOR A-286 AT 1050°F



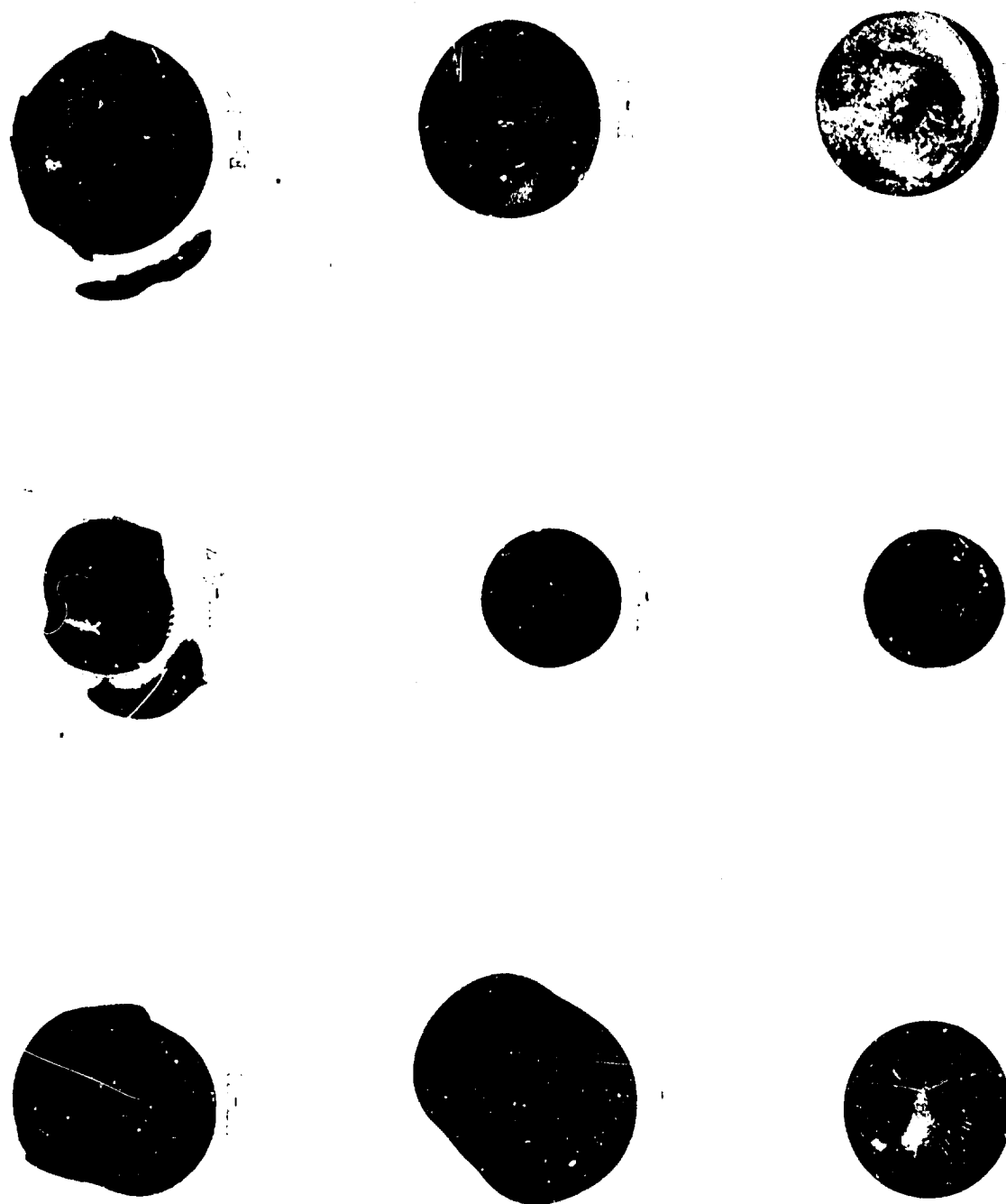
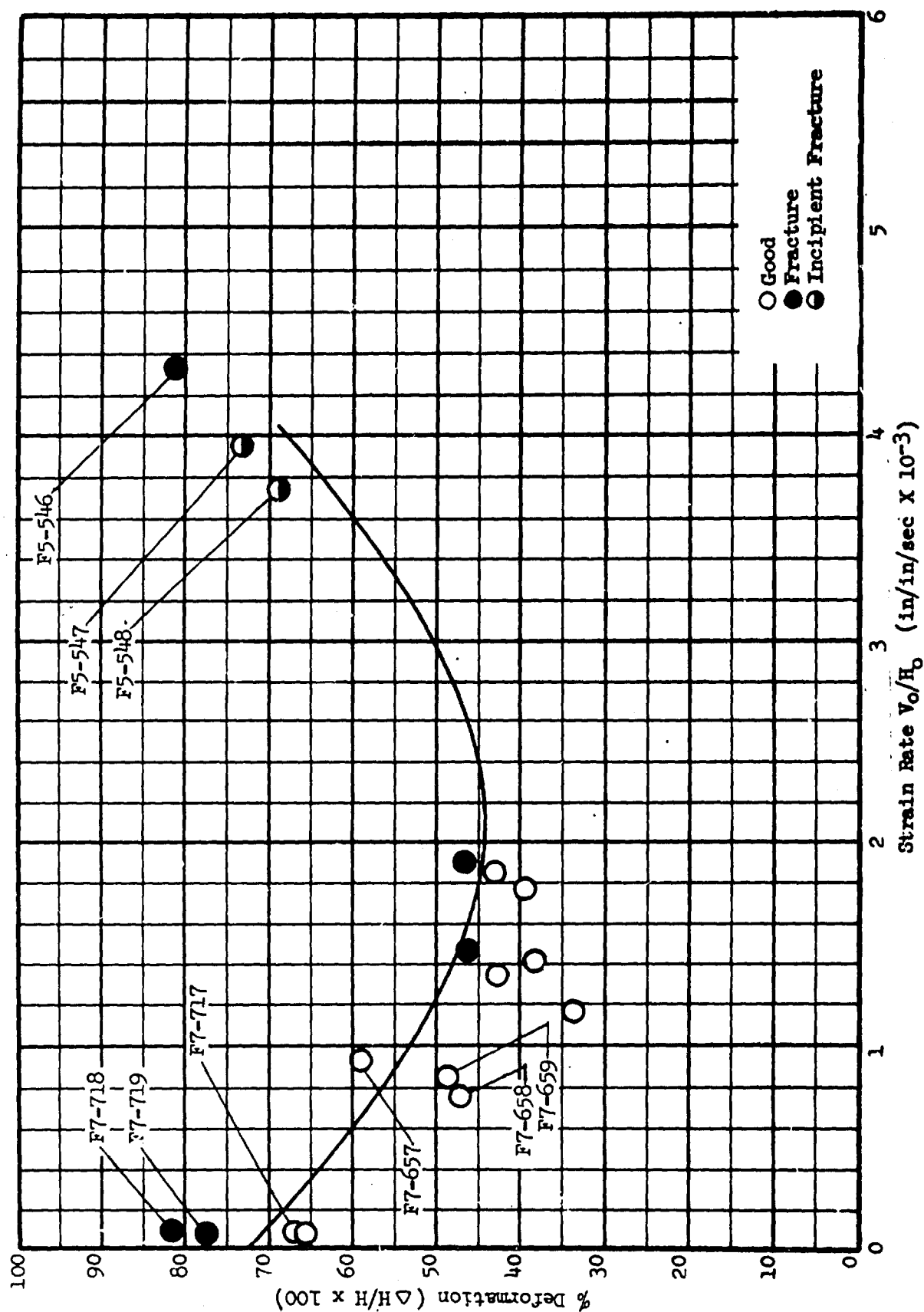


FIGURE 103. A-286 FORGEABILITY LIGHT SPECIMENS AT 1350°F



GRAPH 32. FORGEABILITY LIMIT CURVES FOR A-286 AT 1350°F



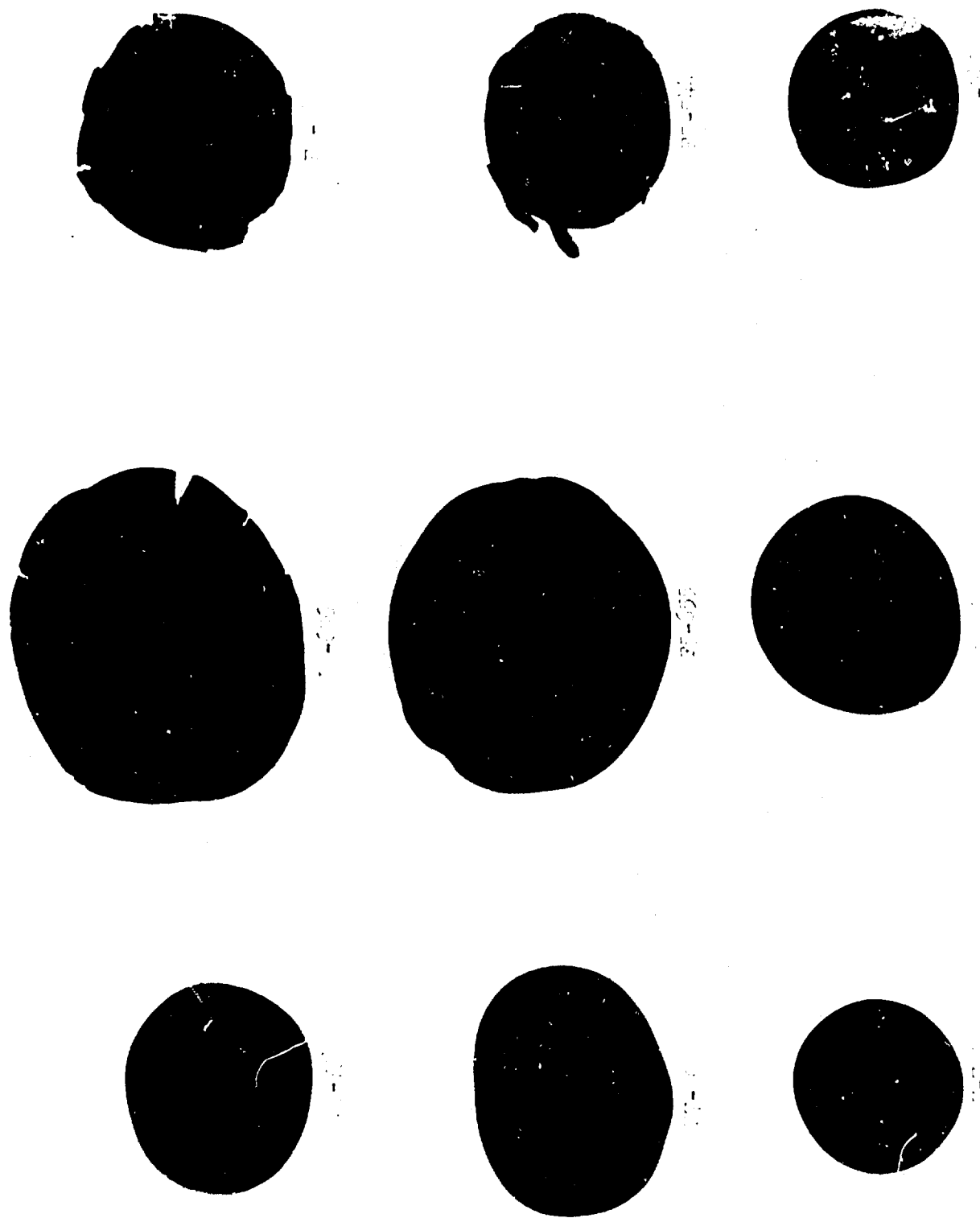
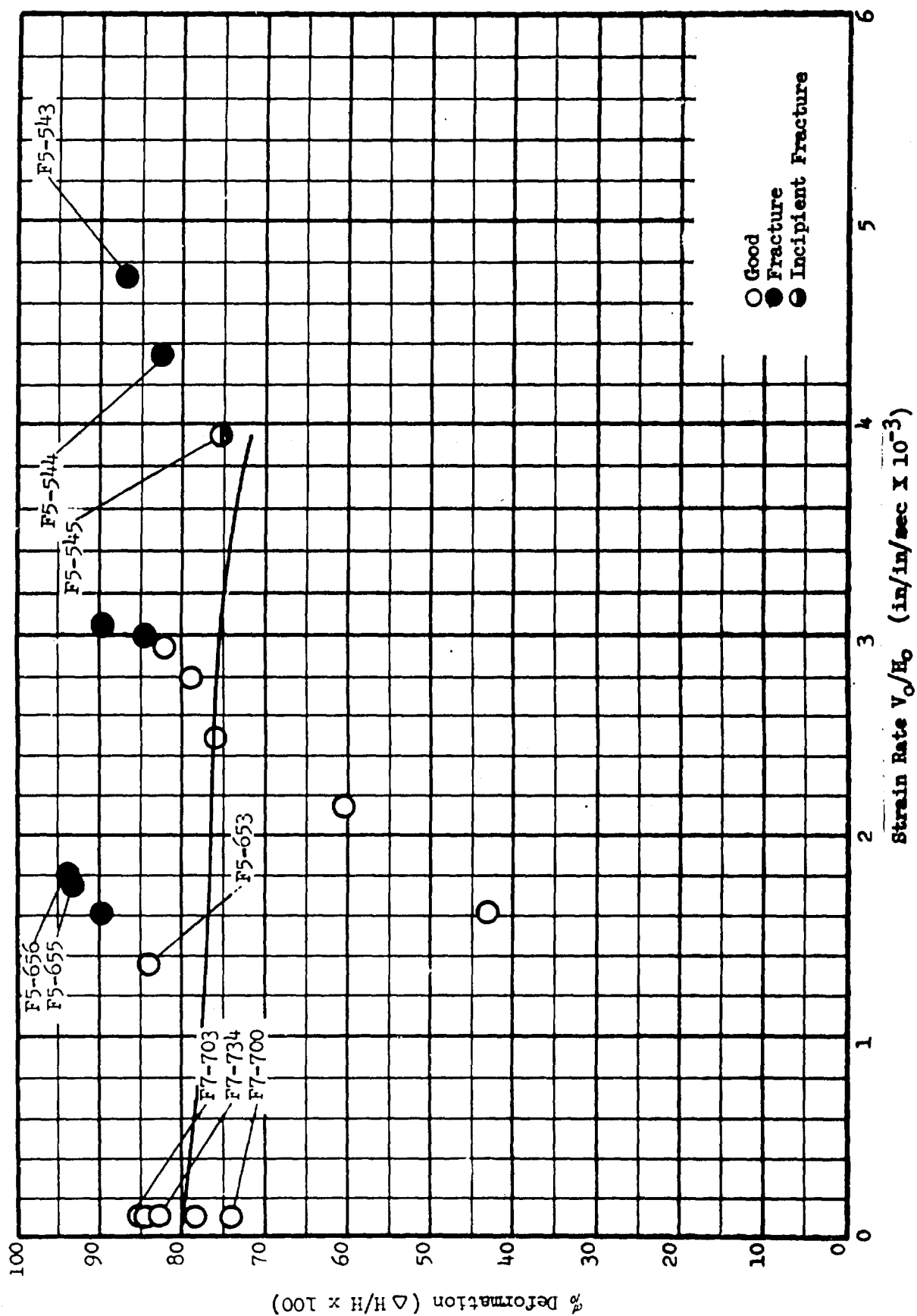


FIGURE 104. A-286 FORGEABILITY LIMIT SPECIMENS AT 1550°F

GRAPH 33. FORGEABILITY LIMIT CURVES FOR A-286 AT 1550°F



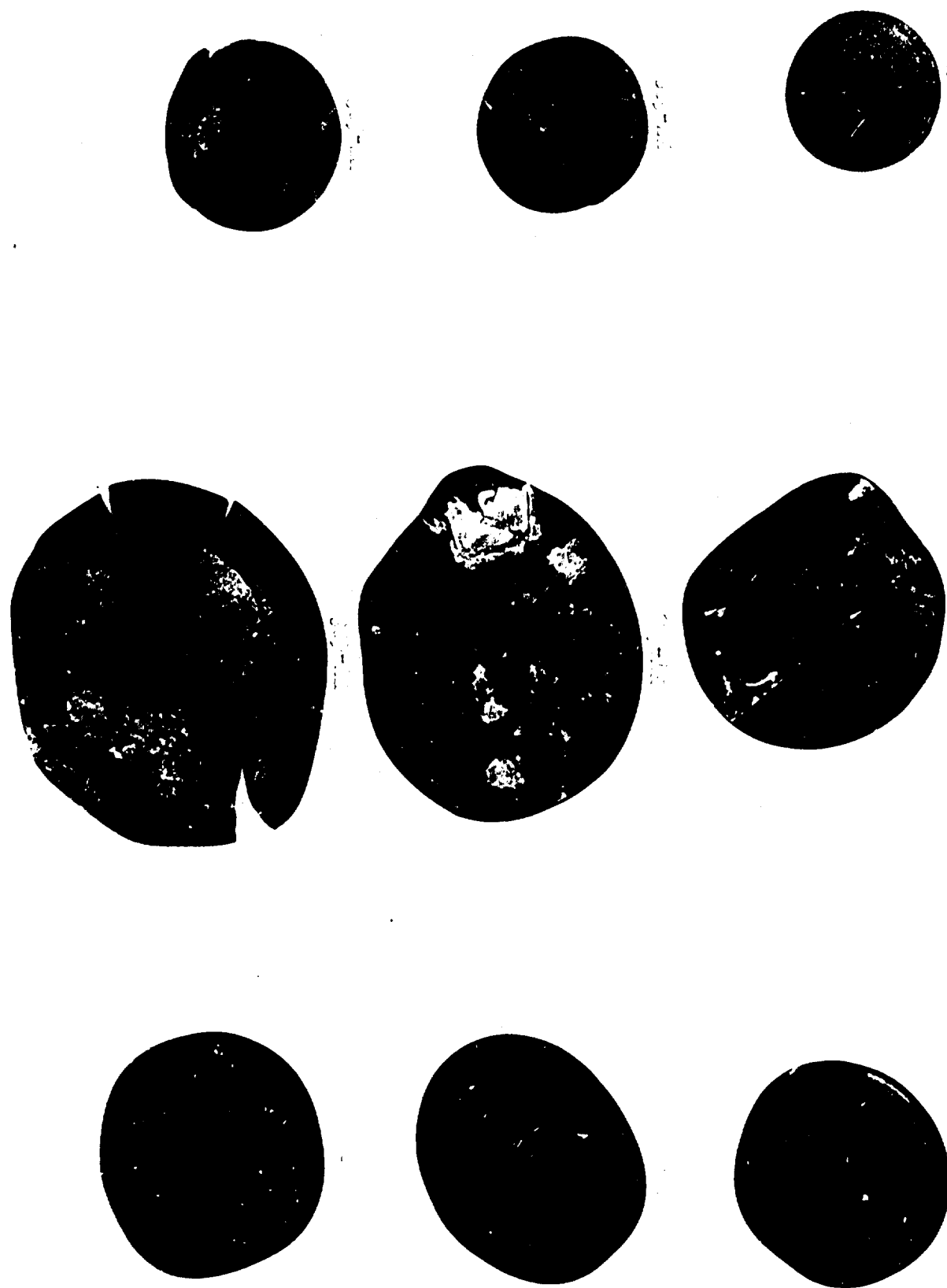


FIGURE 105. A-286 FORGEABILITY LIMIT SPECIMENS AT 1750°F



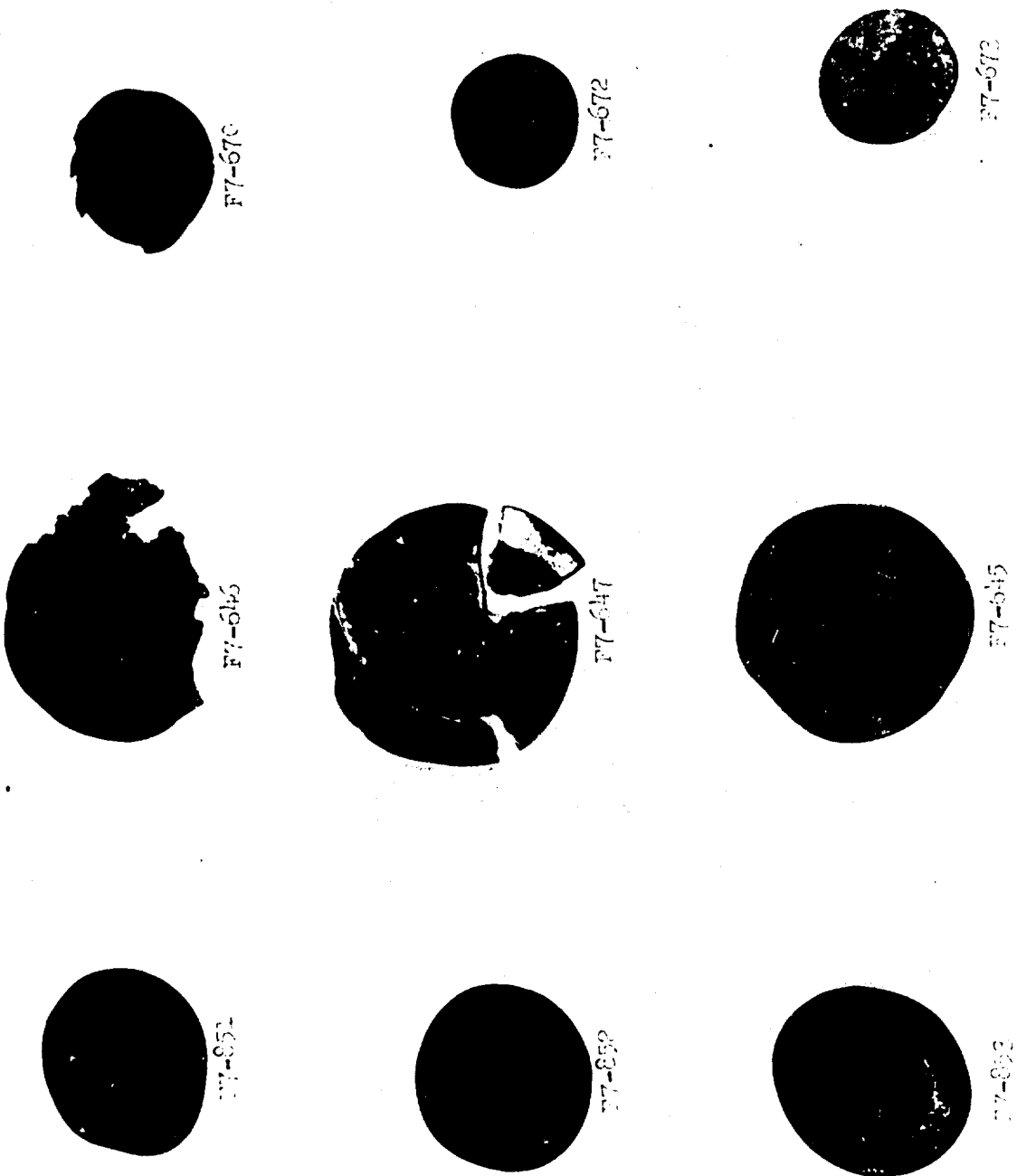
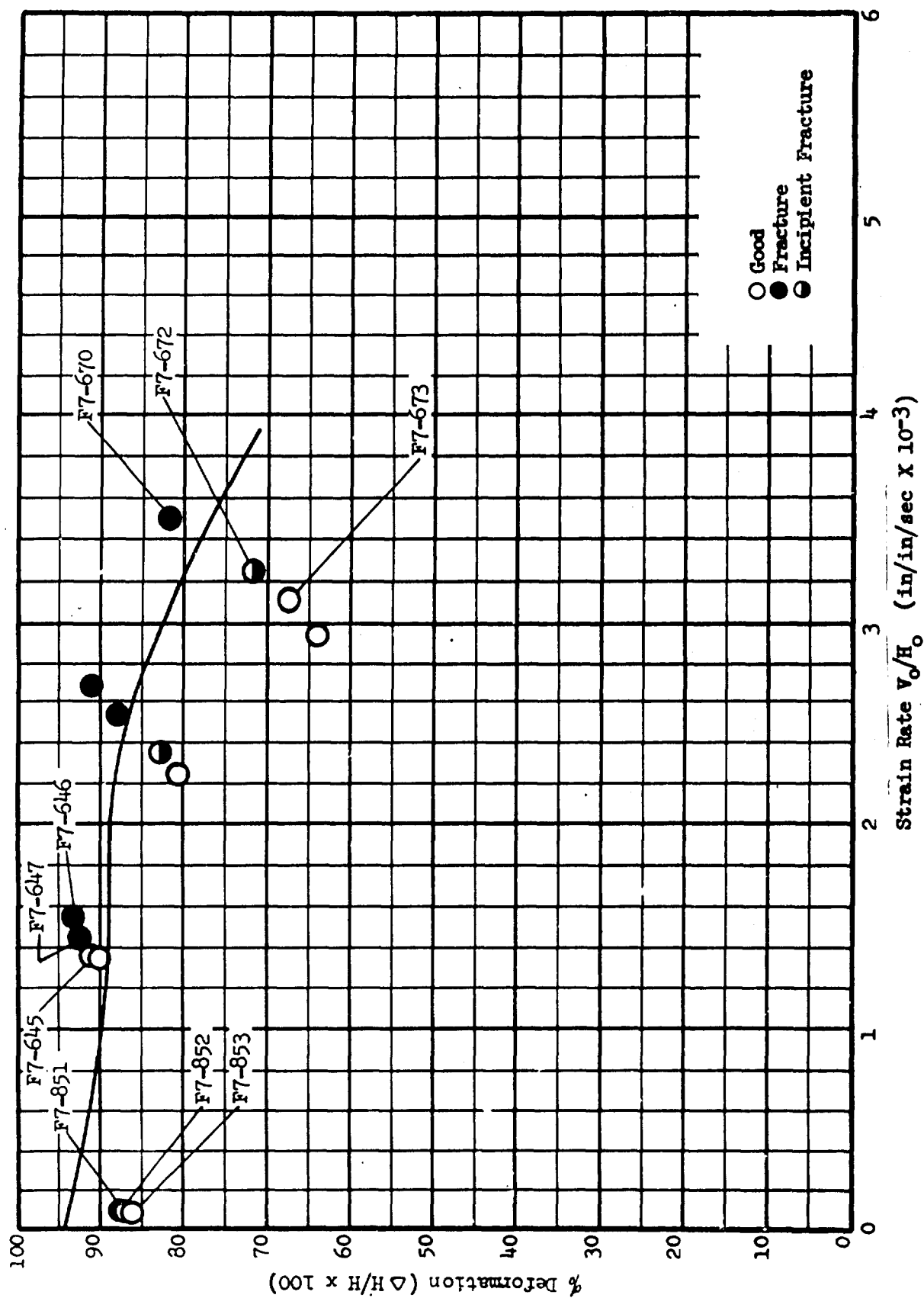
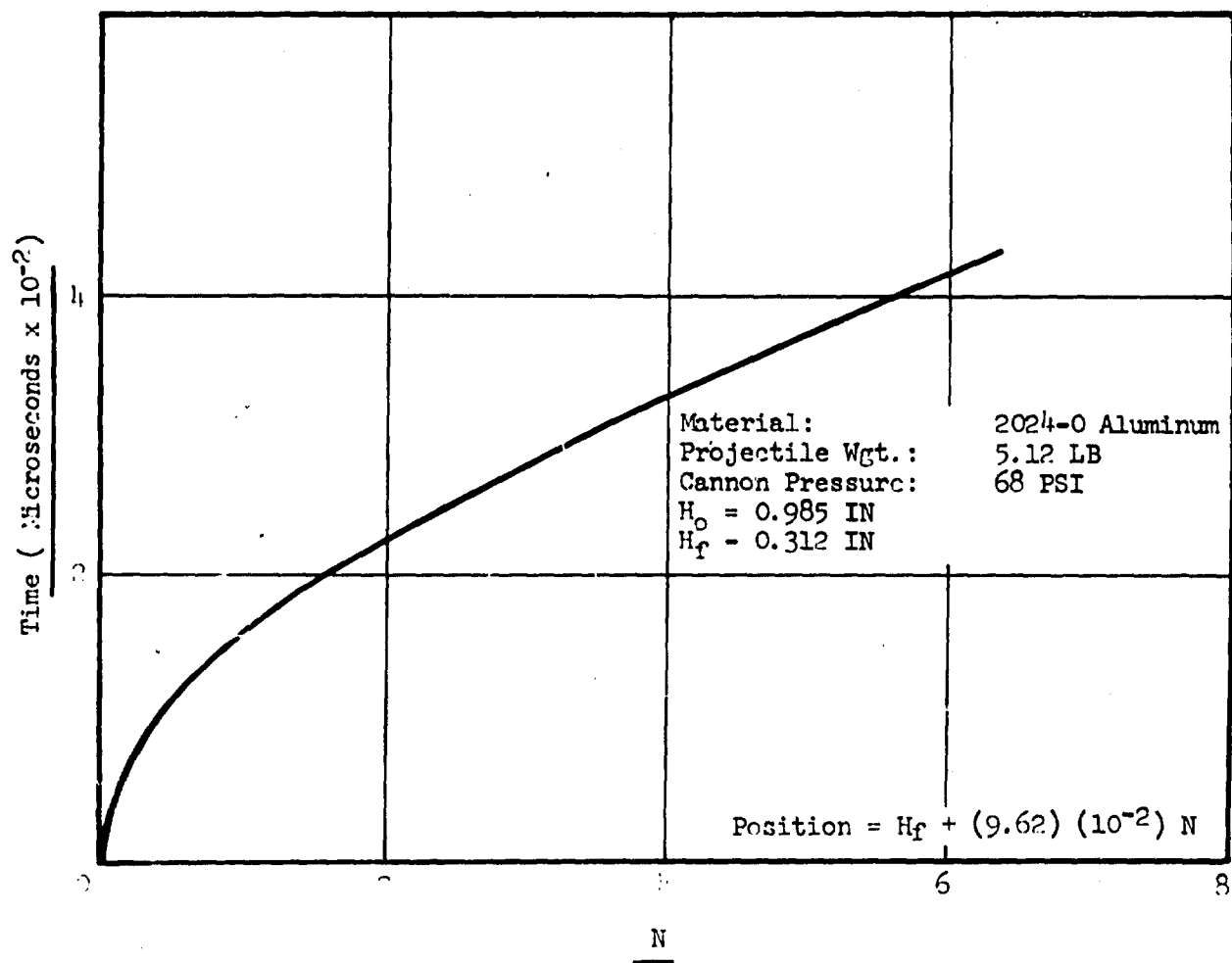


FIGURE 106. A-286 FORGEABILITY LIMIT SPECIMENS AT 1950°F

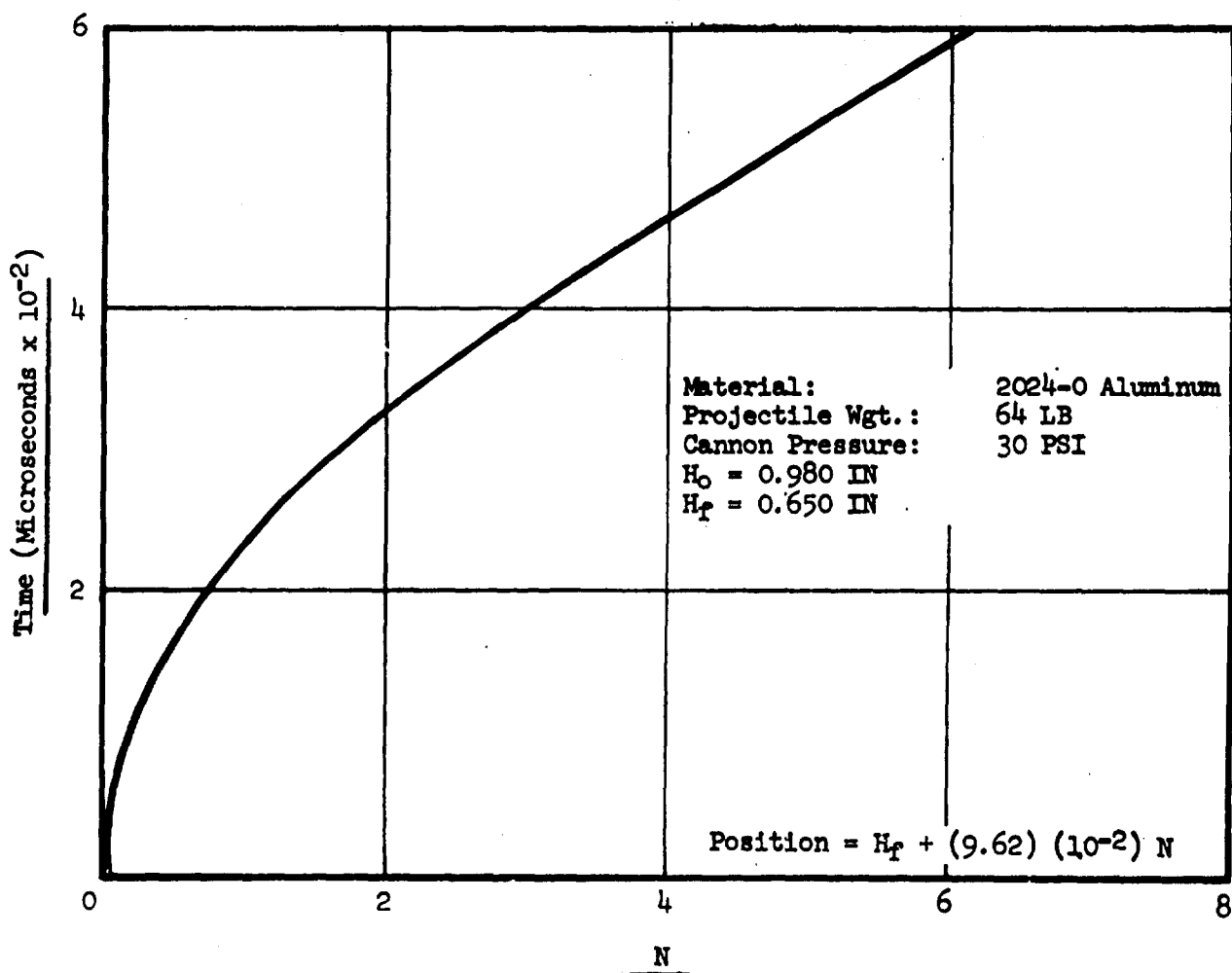
GRAPH 35. FORGEABILITY LIMIT CURVES FOR A-286 AT 1950°F



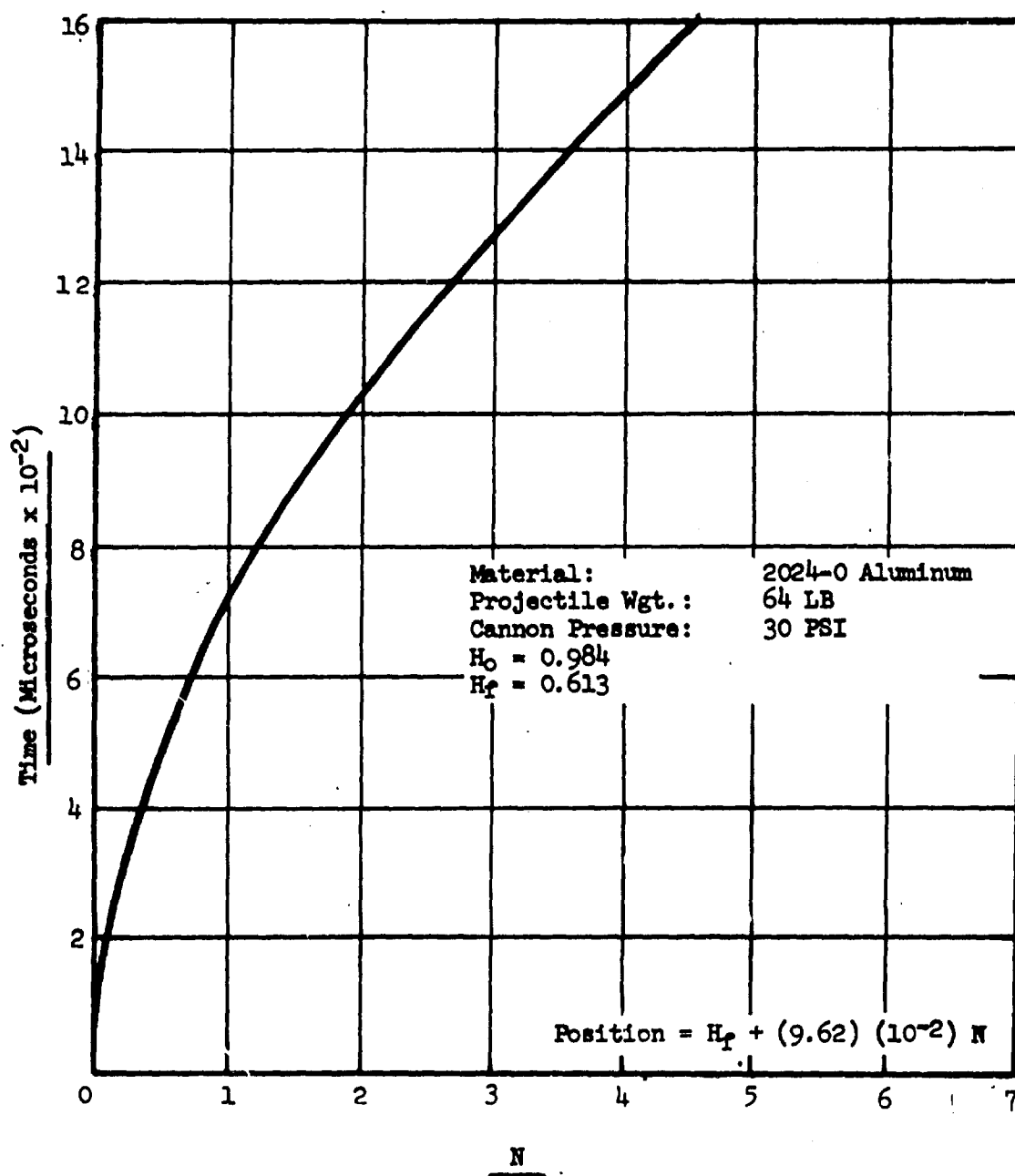


GRAPH 36 POSITION - TIME CURVE FOR SPECIMEN NUMBER A7-943

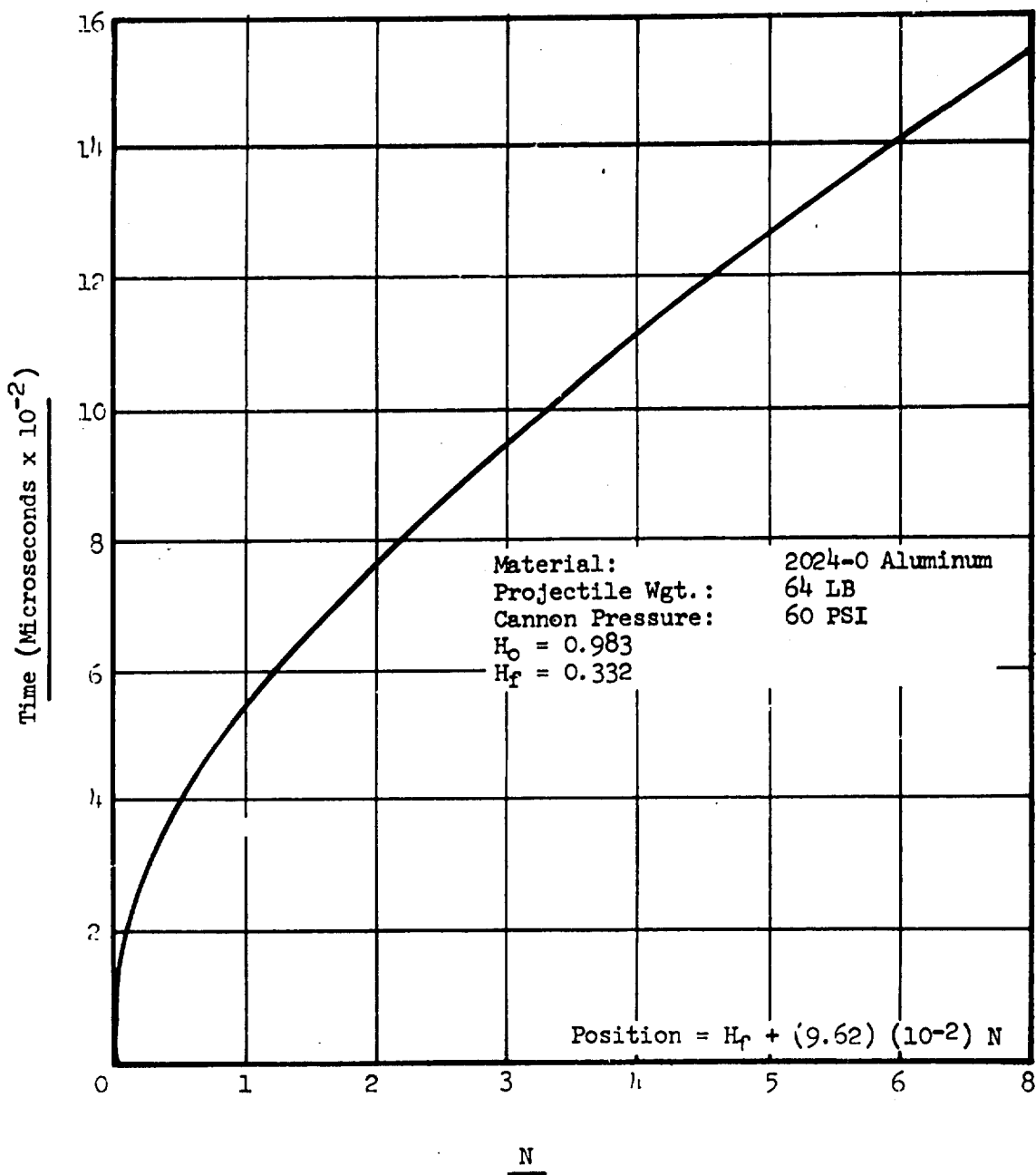




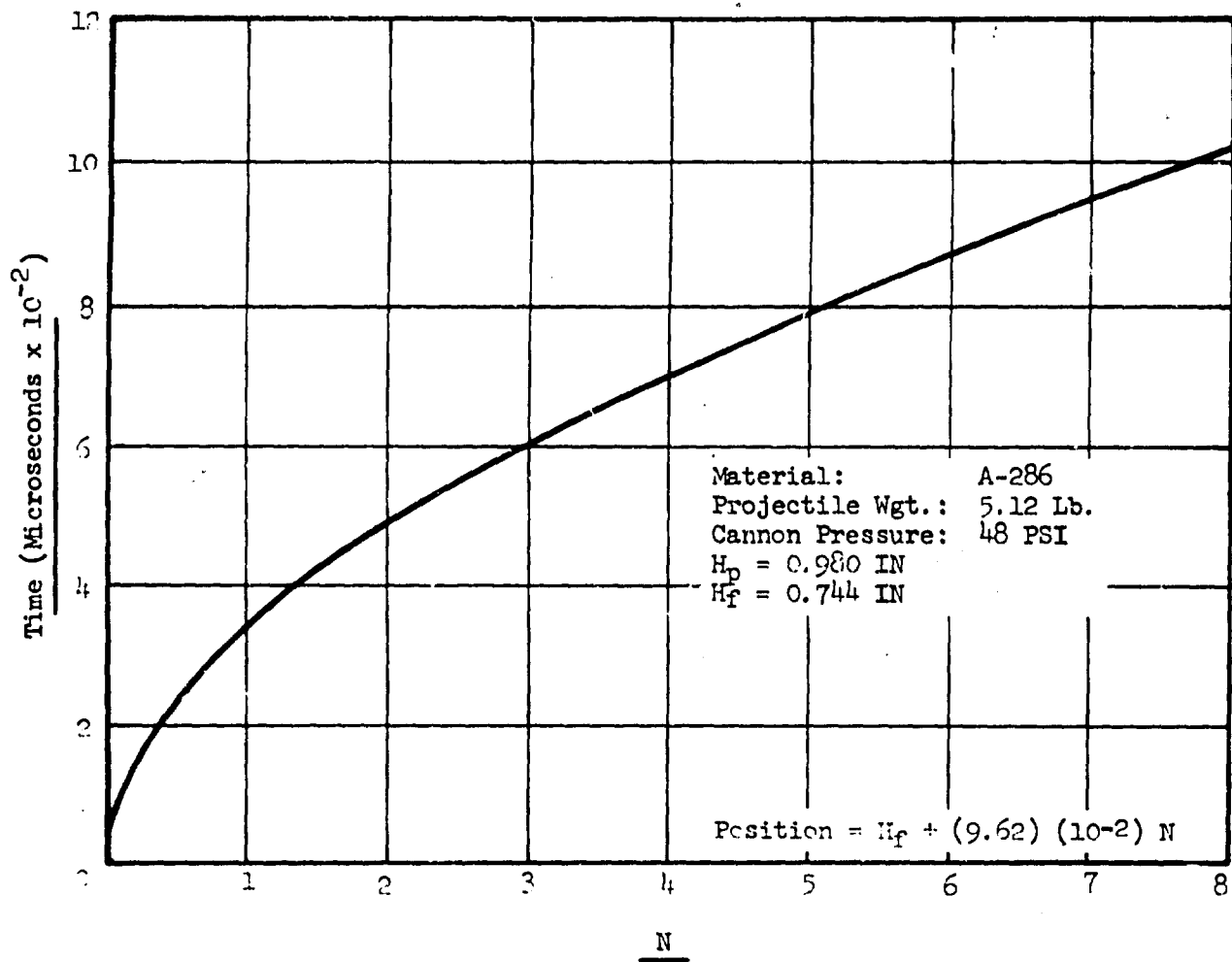
GRAPH 37. POSITION - TIME CURVE FOR SPECIMEN NUMBER A7-940



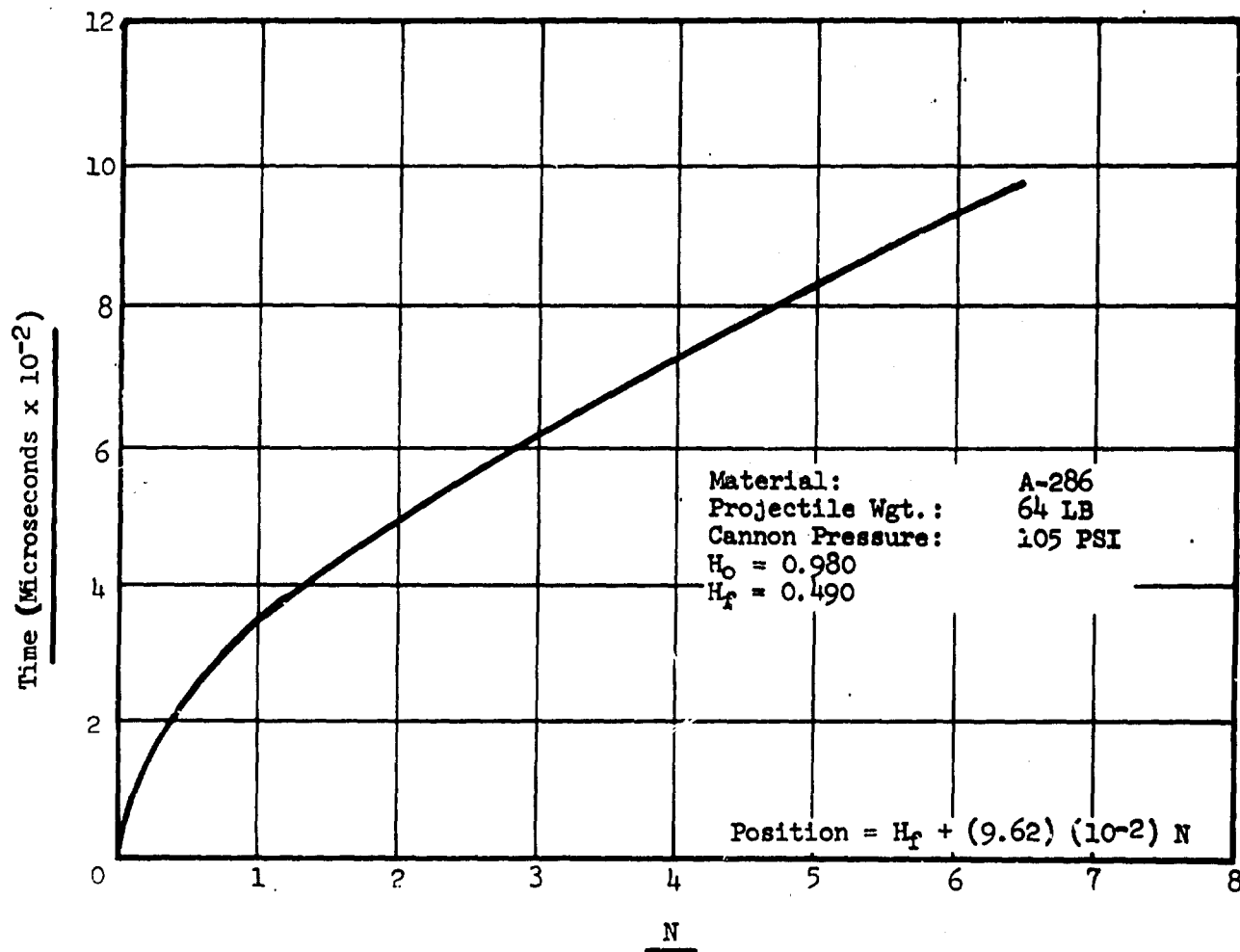
GRAPH 38. POSITION - TIME CURVE FOR SPECIMEN NUMBER A7-927



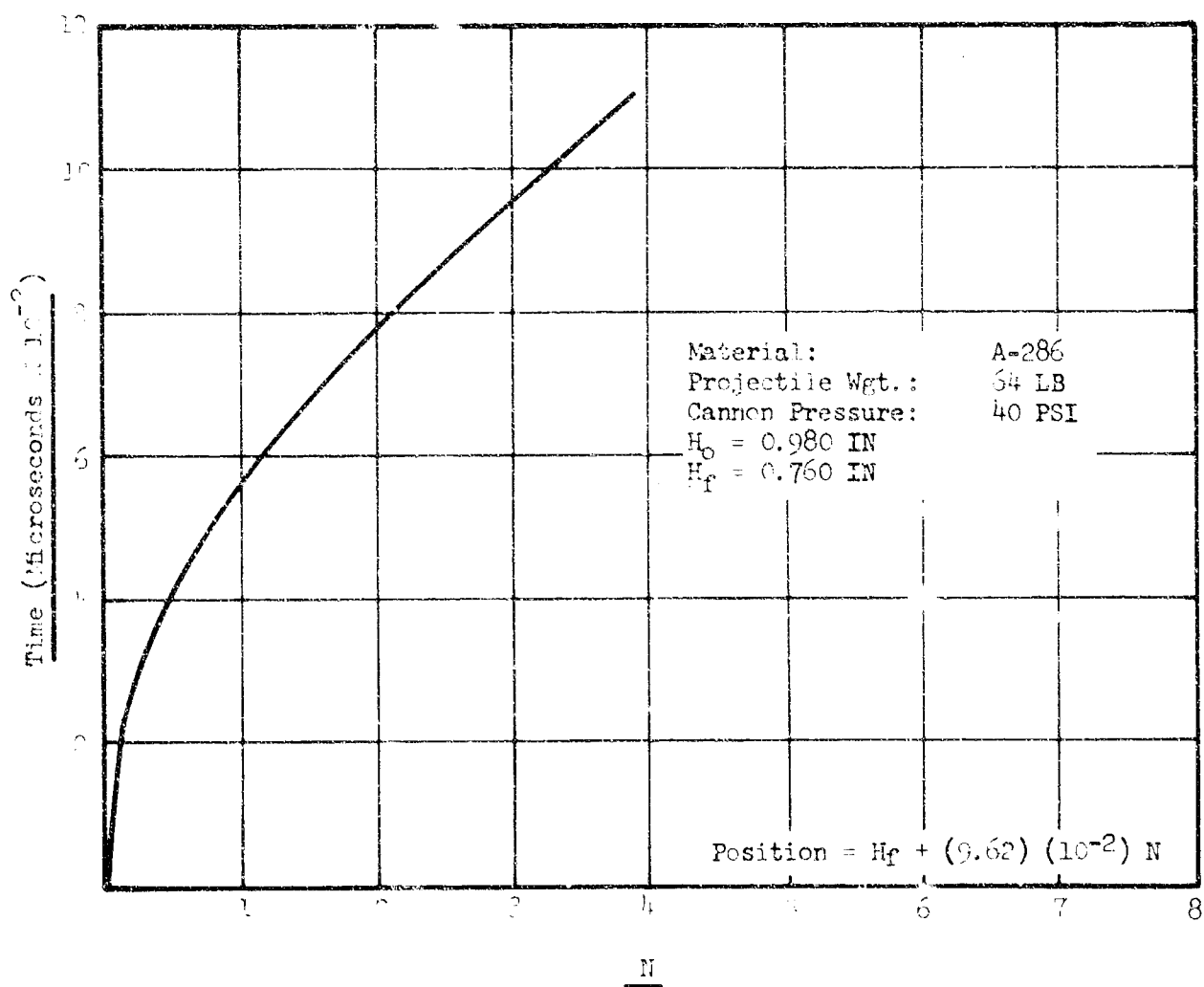
GRAPH 39. POSITION - TIME CURVE FOR SPECIMEN NUMBER A7-925



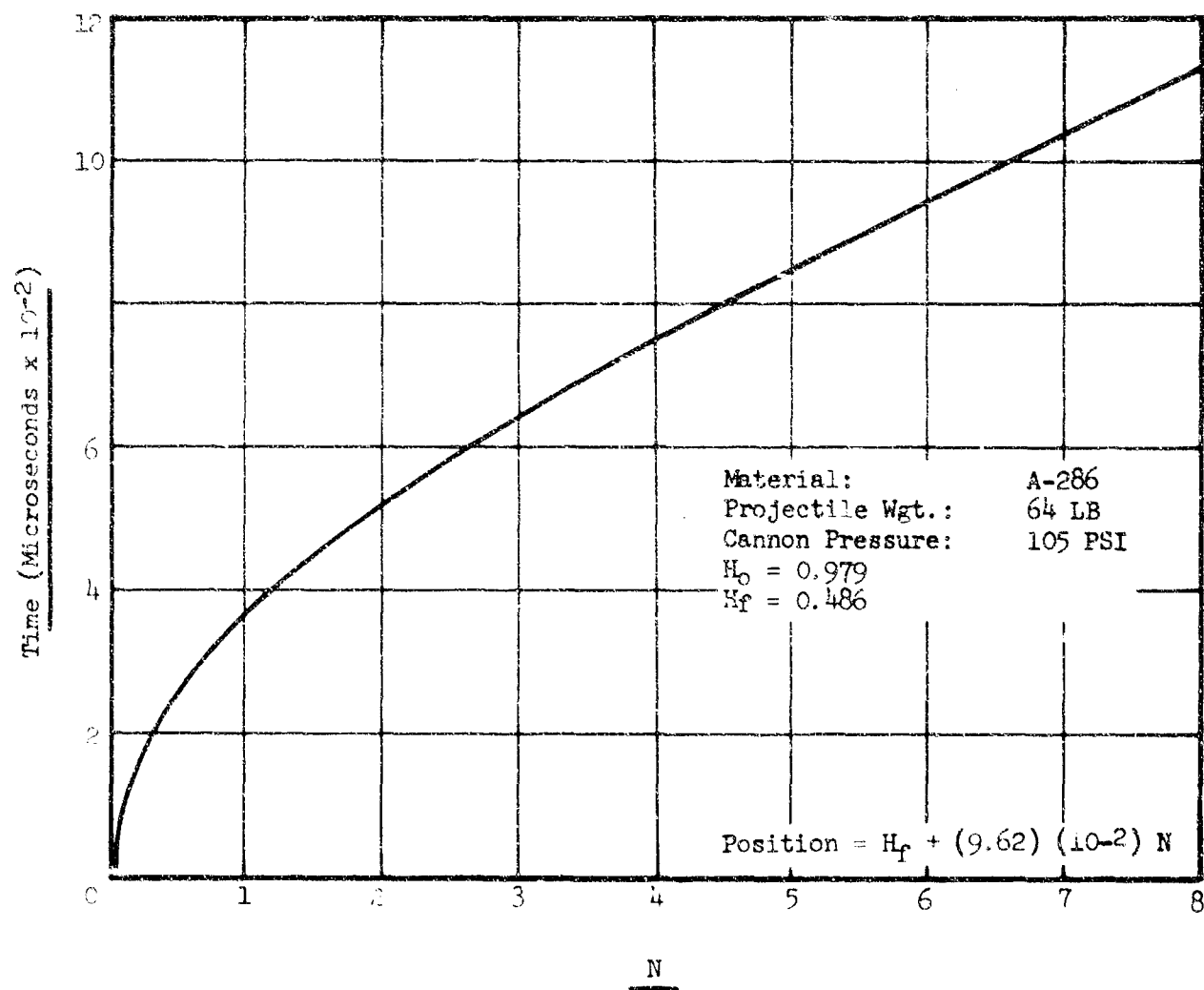
GRAPH 40. POSITION - TIME CURVE FOR SPECIMEN NUMBER F7-944



GRAPH 41. POSITION - TIME CURVE FOR SPECIMEN NUMBER F7-929



GRAPH 42. POSITION - TIME CURVE FOR SPECIMEN NUMBER F7-930



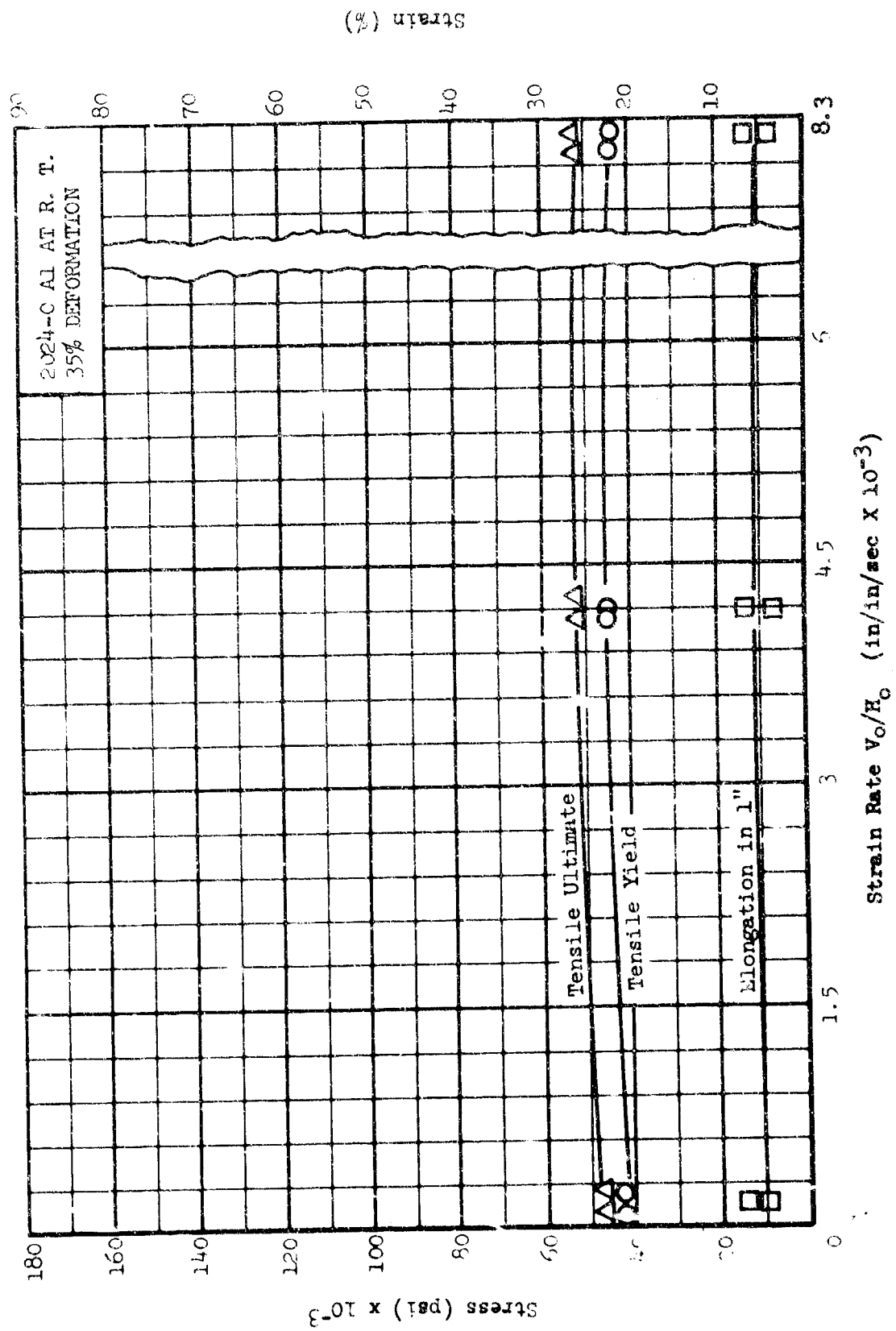
GRAPH 43. POSITION - TIME CURVE FOR SPECIMEN NUMBER F7-931

#### As Forged Material Strength and Ductility

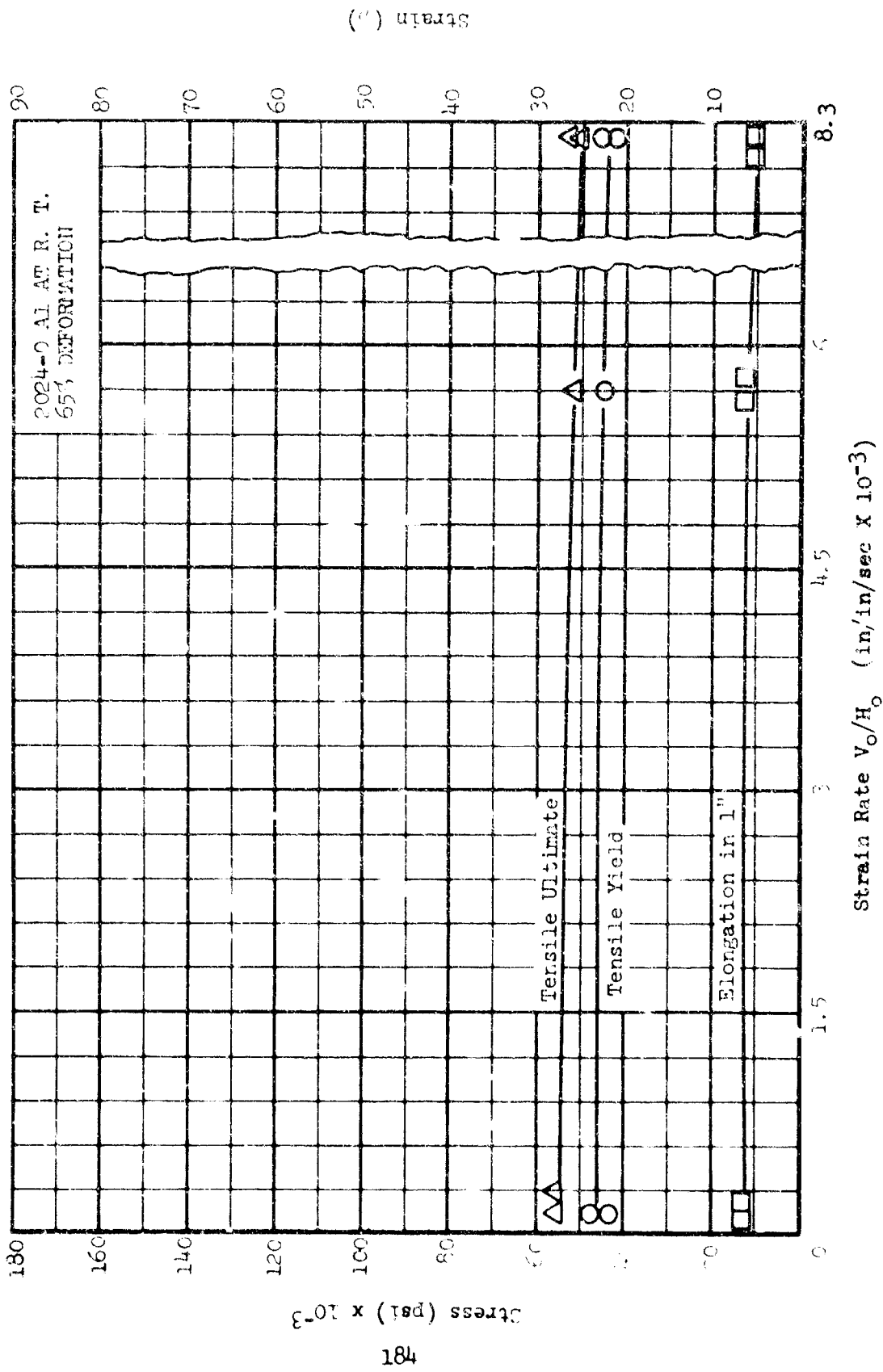
The values for yield strength, ultimate strength and elongation over a one inch gage length are plotted in Graphs 44 and 45. The data was obtained by static testing of standard tensile specimens cut from bars previously upset by a constant amount at various strain rates. These results show the effect of strain rate of forgings on the final strength and ductility for the various materials.



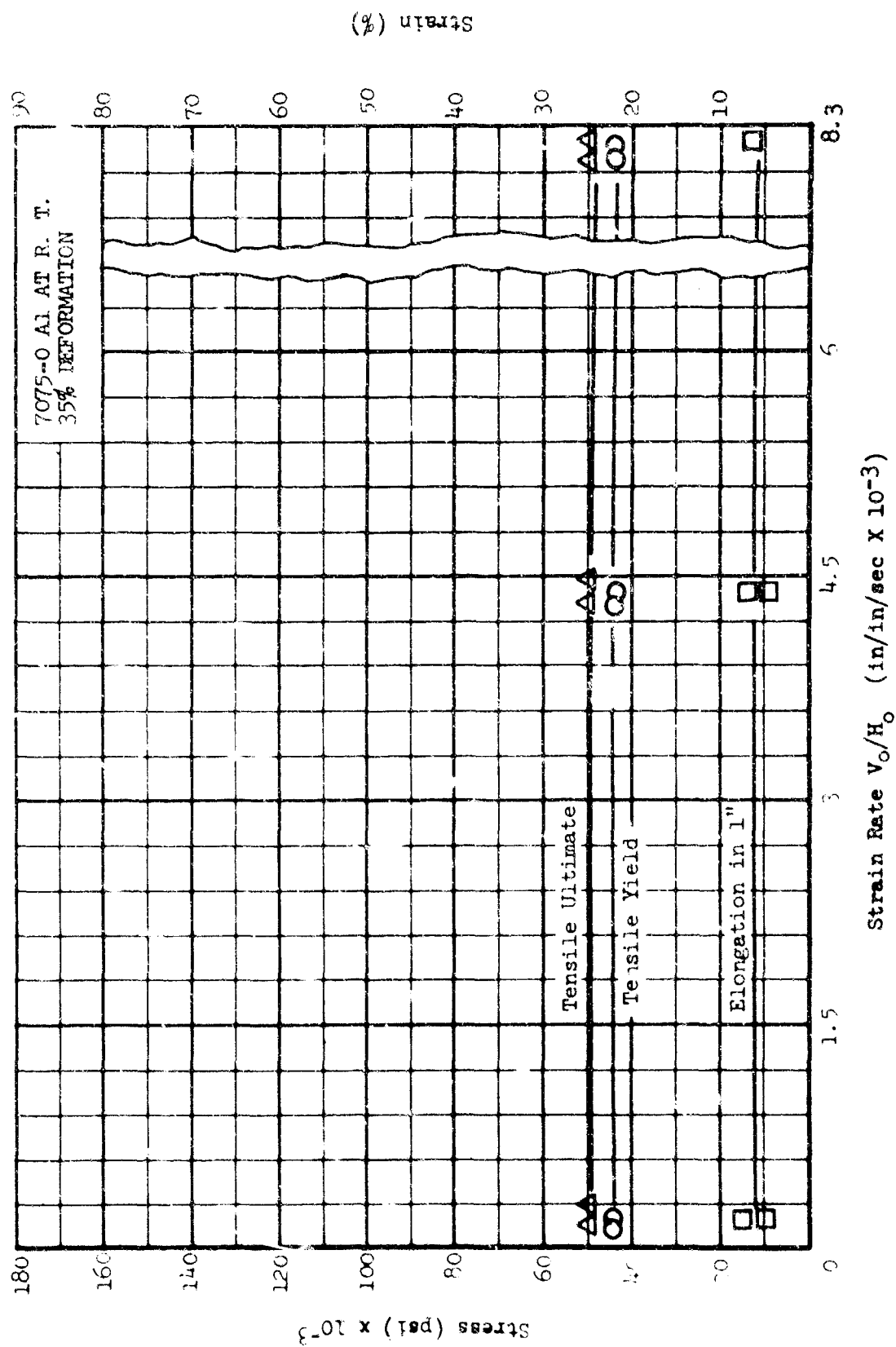
GRAPH 44. MATERIAL STRENGTH AND ELONGATION AS A FUNCTION OF STRAIN RATE



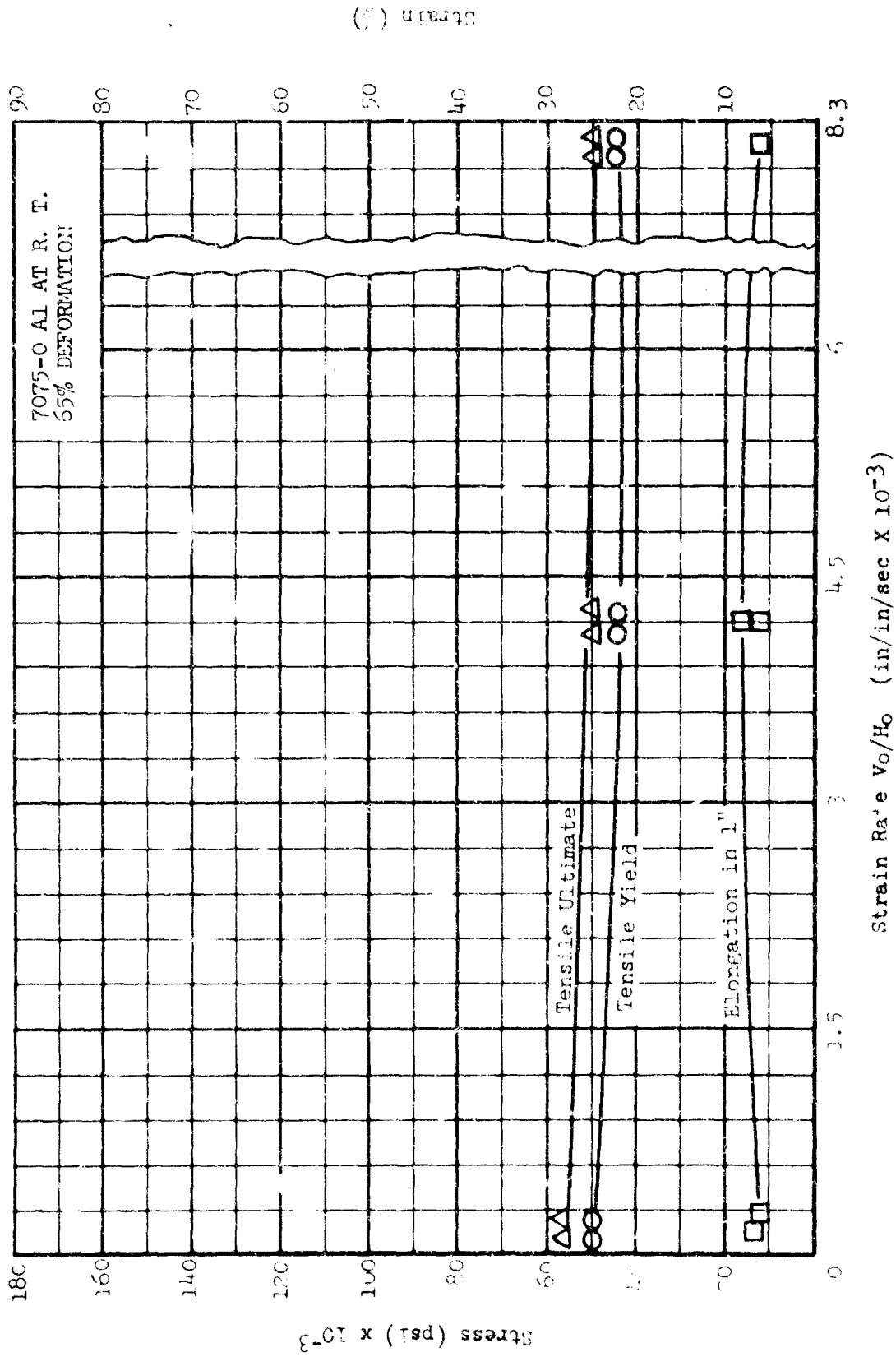
GRAPH 44. MATERIAL STRENGTH AND ELONGATION AS A FUNCTION OF STRAIN RATE (CONT'D)



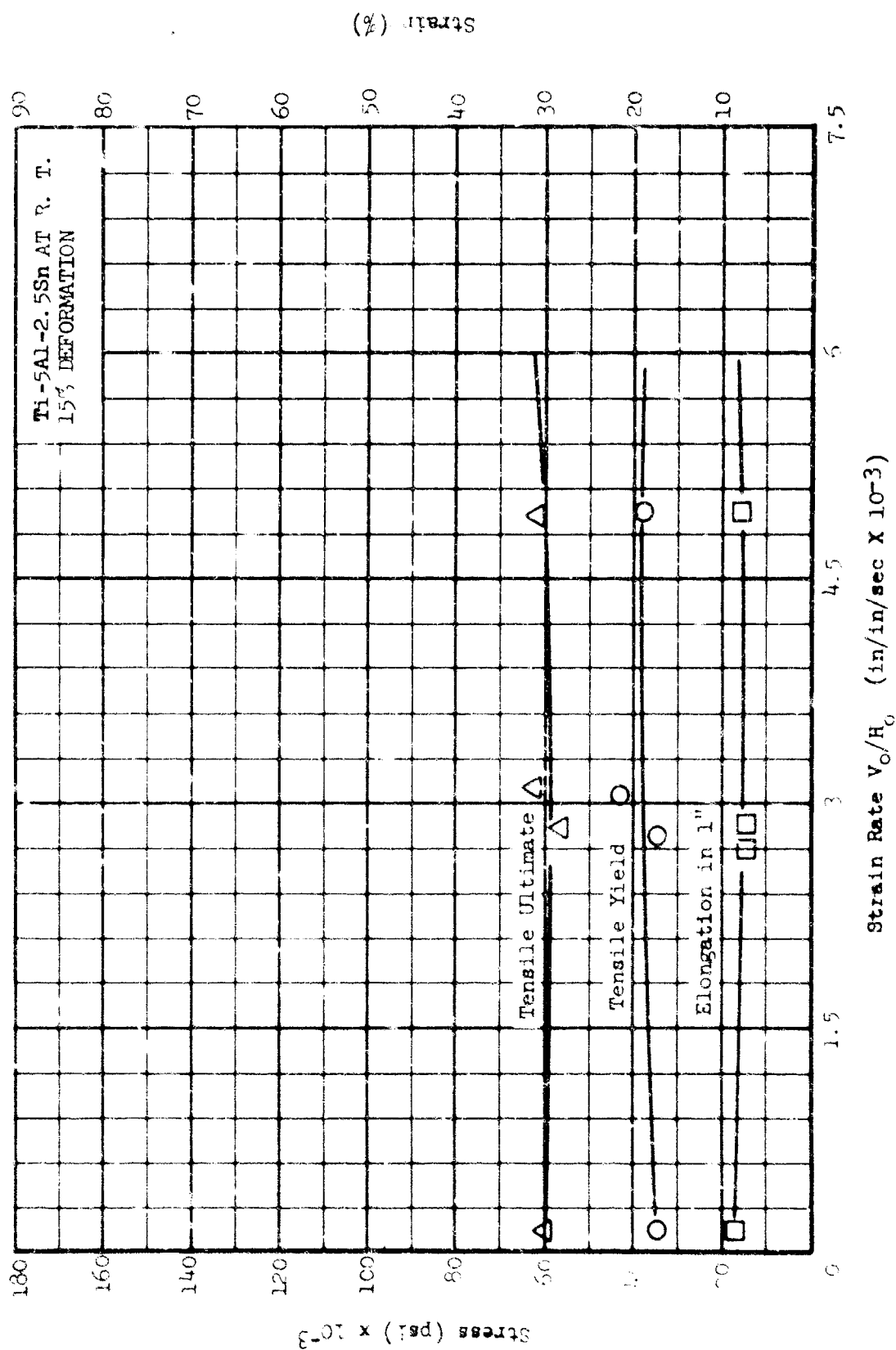
GRAPH 44. MATERIAL STRENGTH AND ELONGATION AS A FUNCTION OF STRAIN RATE (CONT'D)



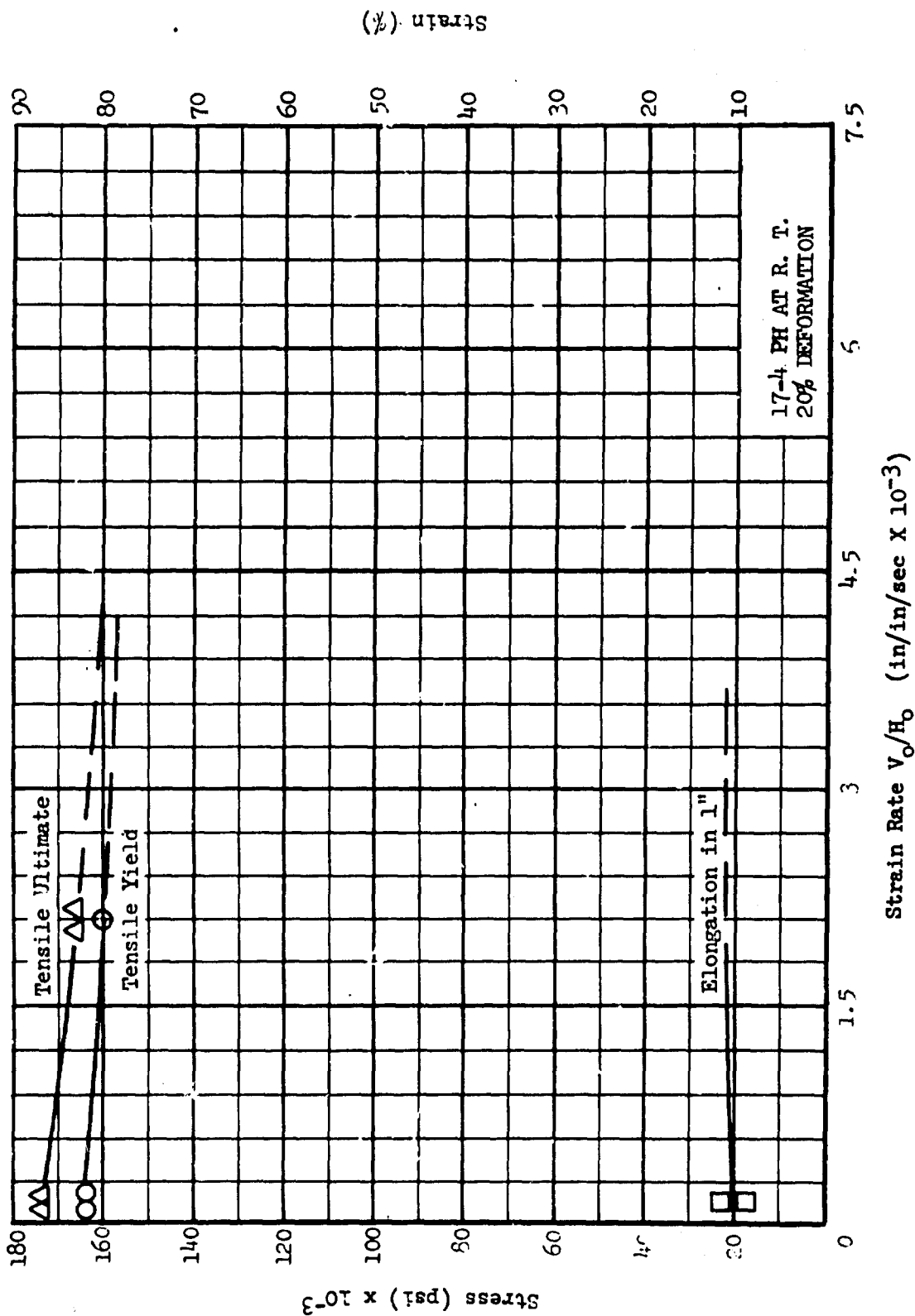
GRAPH 44. MATERIAL STRENGTH AND ELONGATION AS A FUNCTION OF STRAIN RATE (CONT'D)



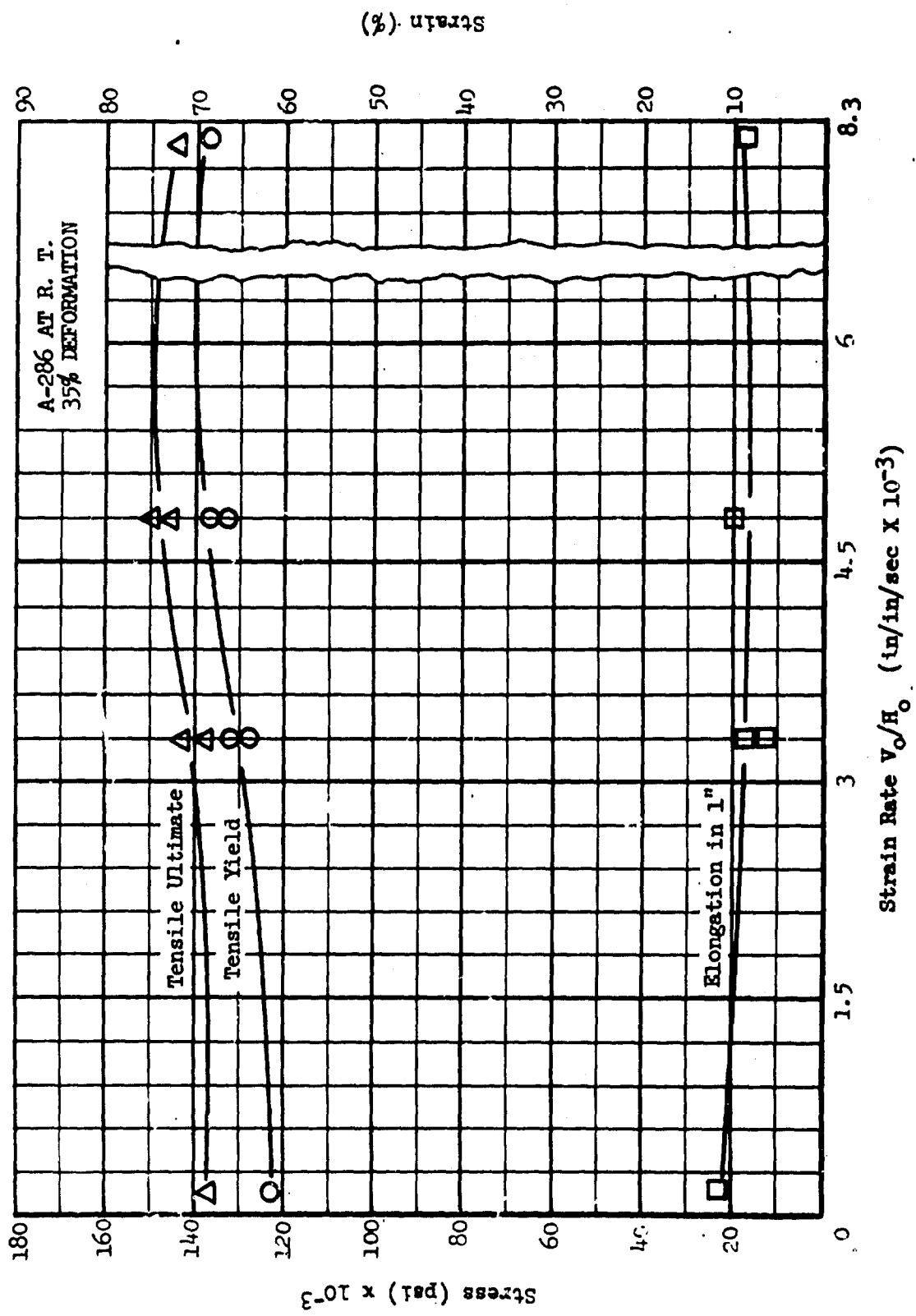
GRAPH 44. MATERIAL STRENGTH AND ELONGATION AS A FUNCTION OF STRAIN RATE (CONT'D)



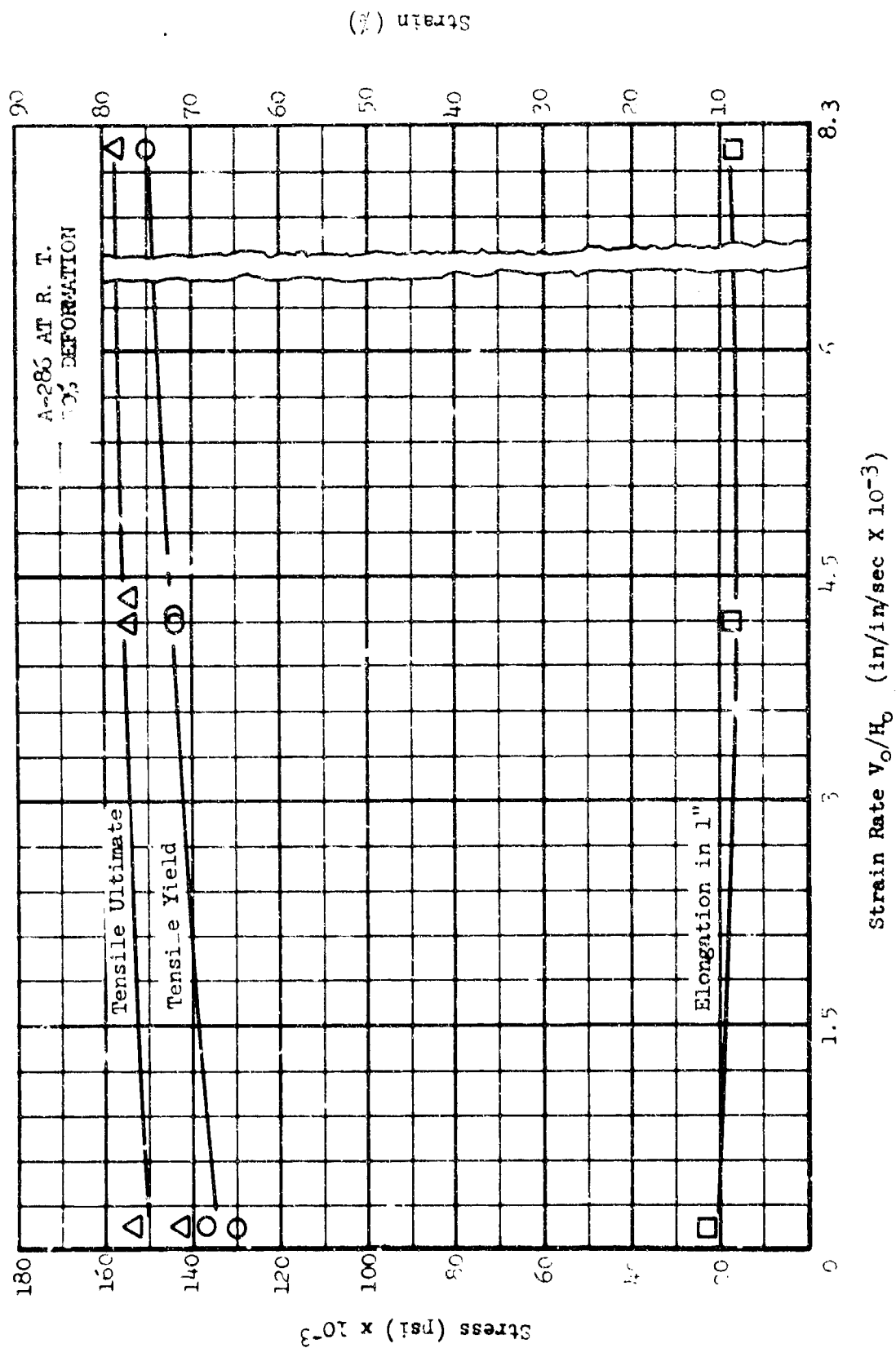
GRAPH 44. MATERIAL STRENGTH AND ELONGATION AS A FUNCTION OF STRAIN RATE (CONT'D)



GRAPH 44. MATERIAL STRENGTH AND ELONGATION AS A FUNCTION OF STRAIN RATE (CONT'D)

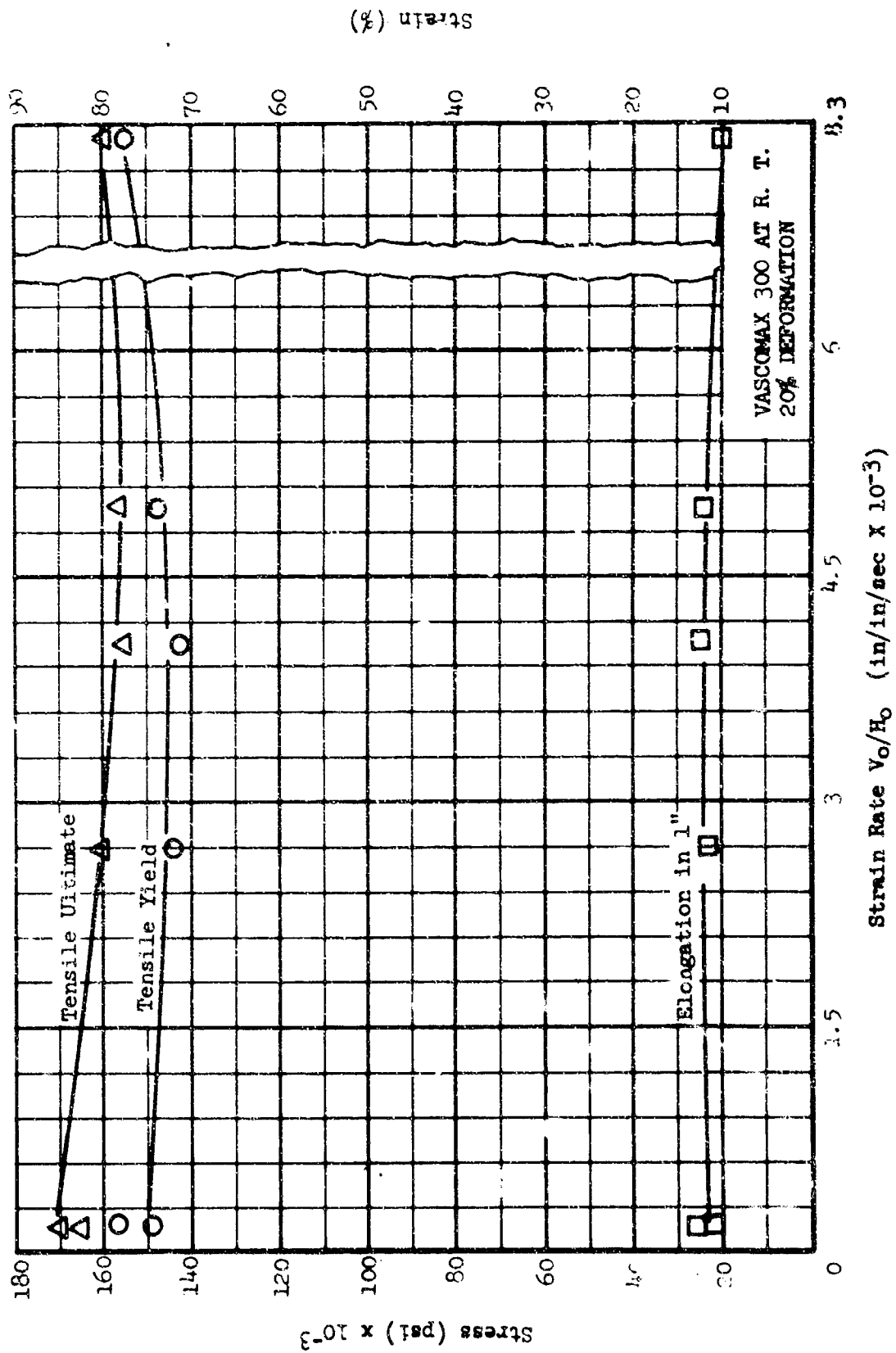


GRAPH 44. MATERIAL STRENGTH AND ELONGATION AS A FUNCTION OF STRAIN RATE (CONT'D)

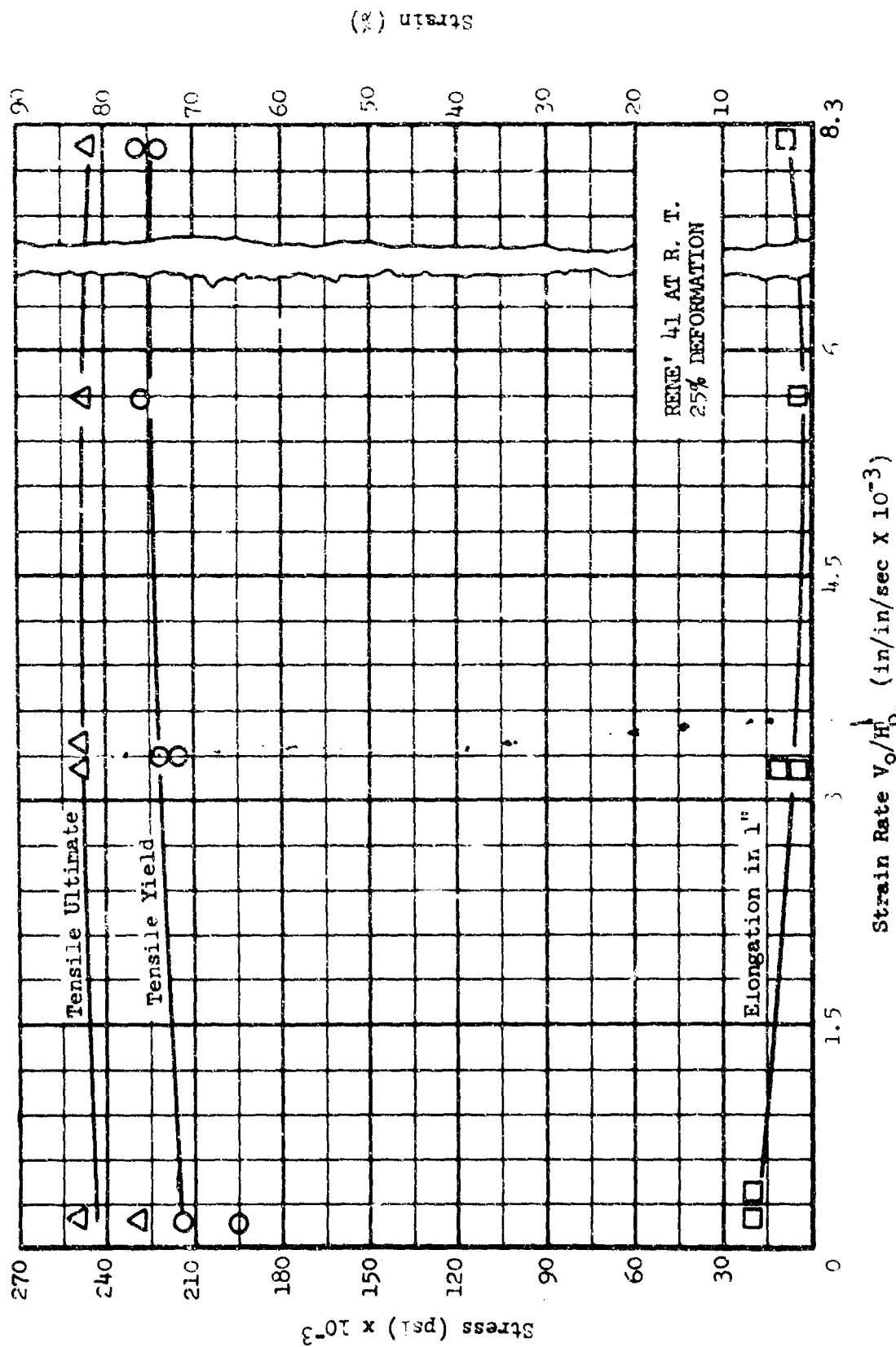




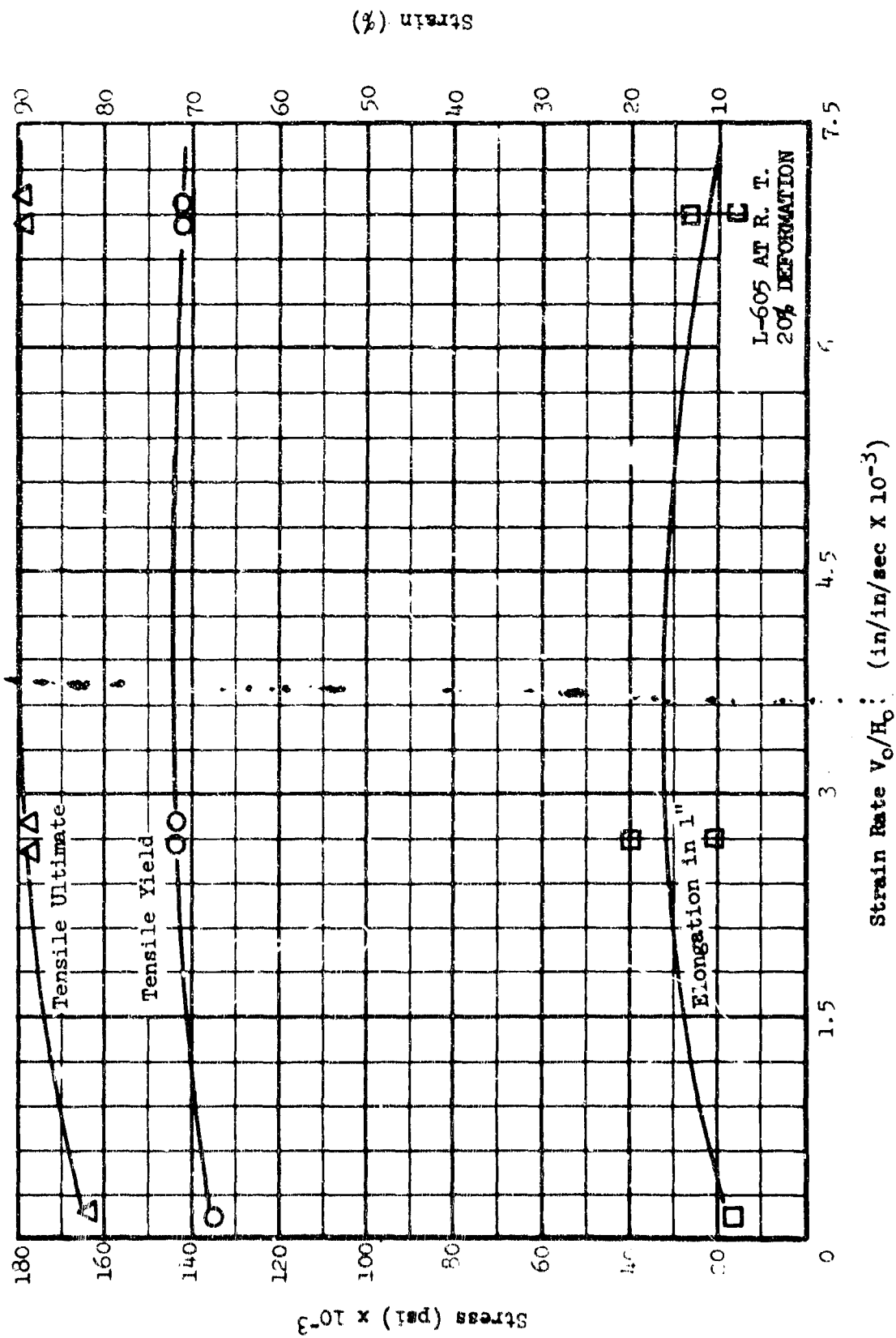
GRAPH 44. MATERIAL STRENGTH AND ELONGATION AS A FUNCTION OF STRAIN RATE (CONT'D)



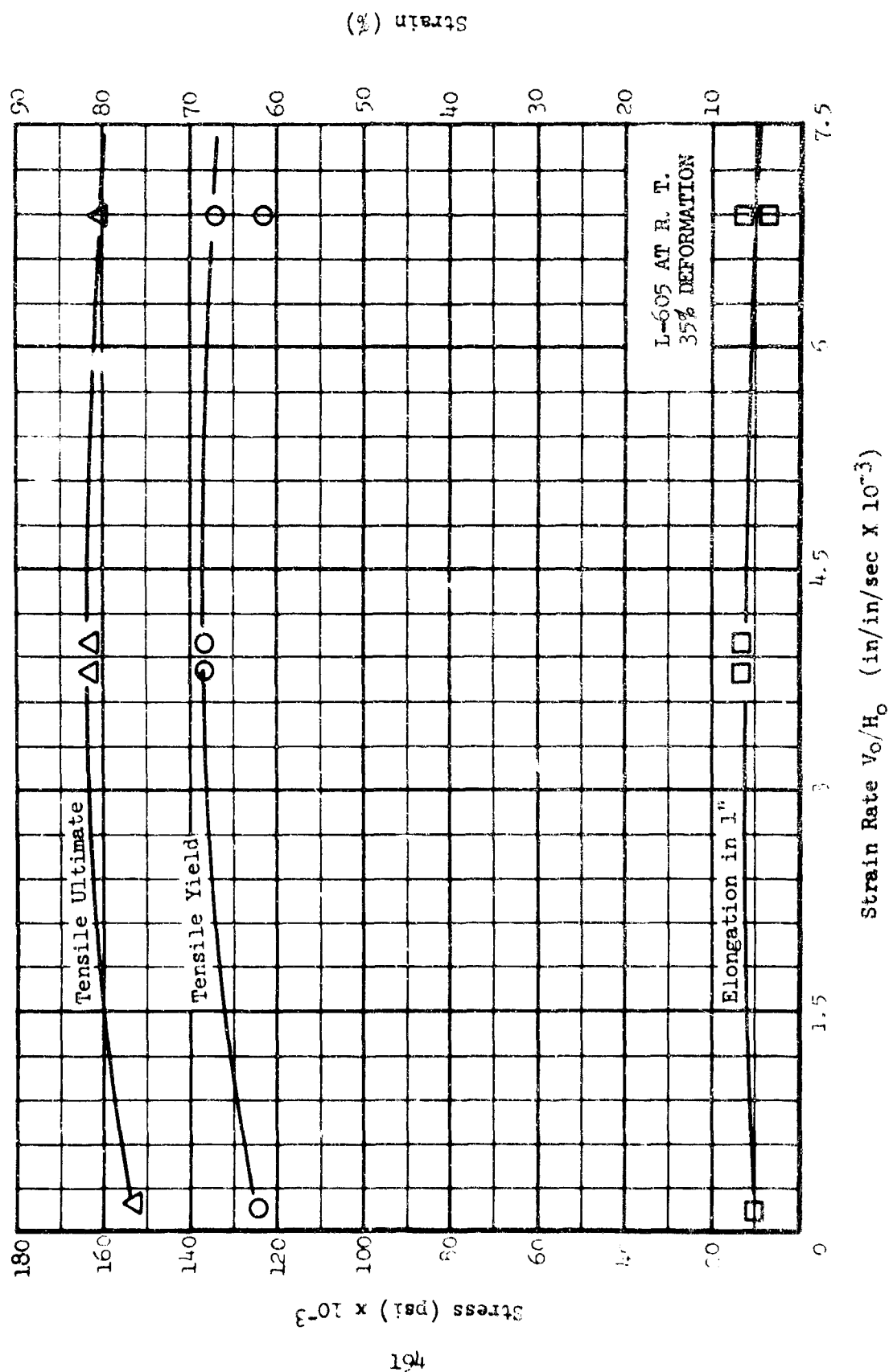
GRAPH 44. MATERIAL STRENGTH AND ELONGATION AS A FUNCTION OF STRAIN RATE (CONT'D)



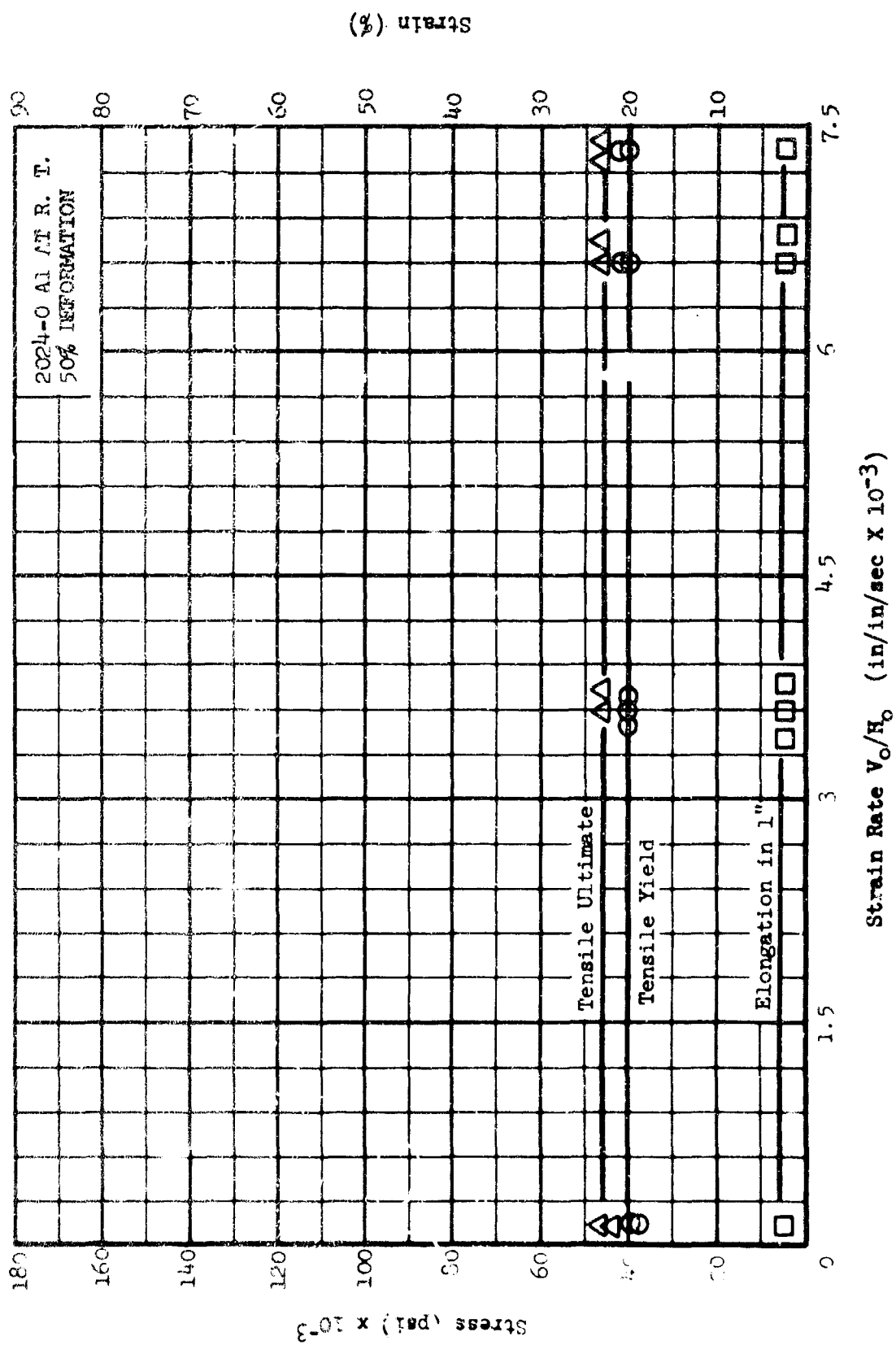
GRAPH 44. MATERIAL STRENGTH AND ELONGATION AS A FUNCTION OF STRAIN RATE (CONT'D)



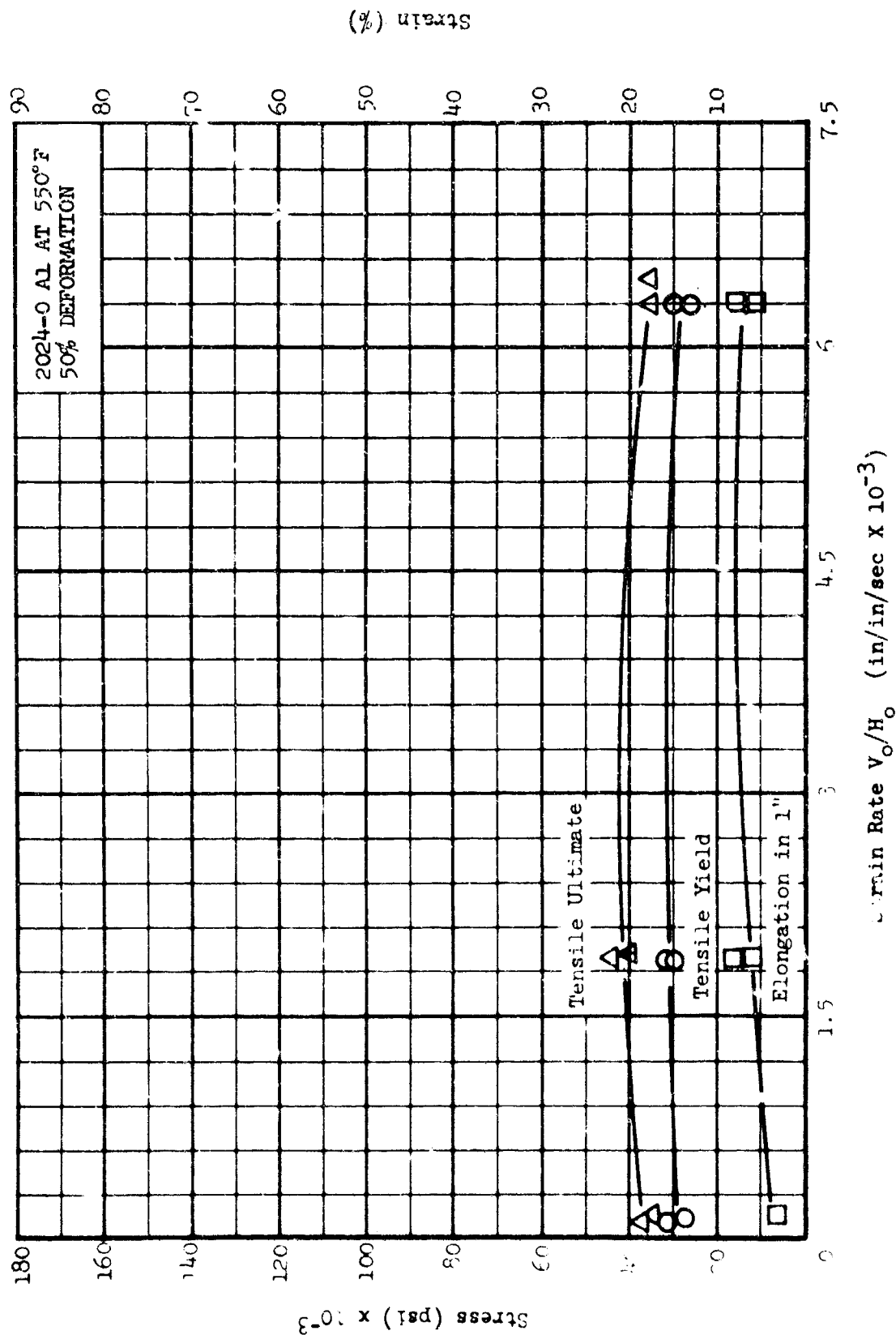
GRAPH 44. MATERIAL STRENGTH AND ELONGATION AS A FUNCTION OF STRAIN RATE (CONT'D)



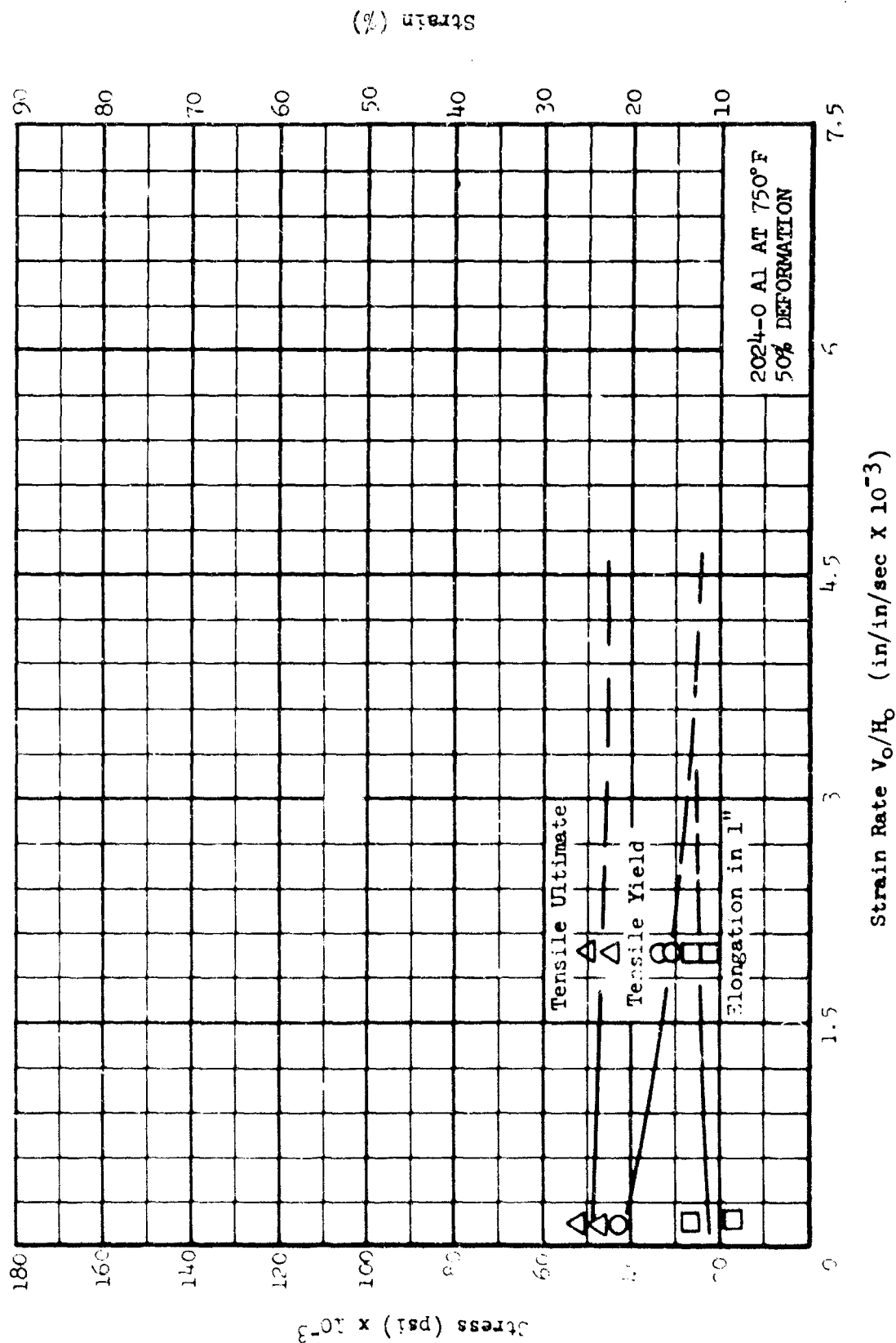
GRAPH 45. MATERIAL STRENGTH AND ELONGATION AS A FUNCTION OF STRAIN RATE



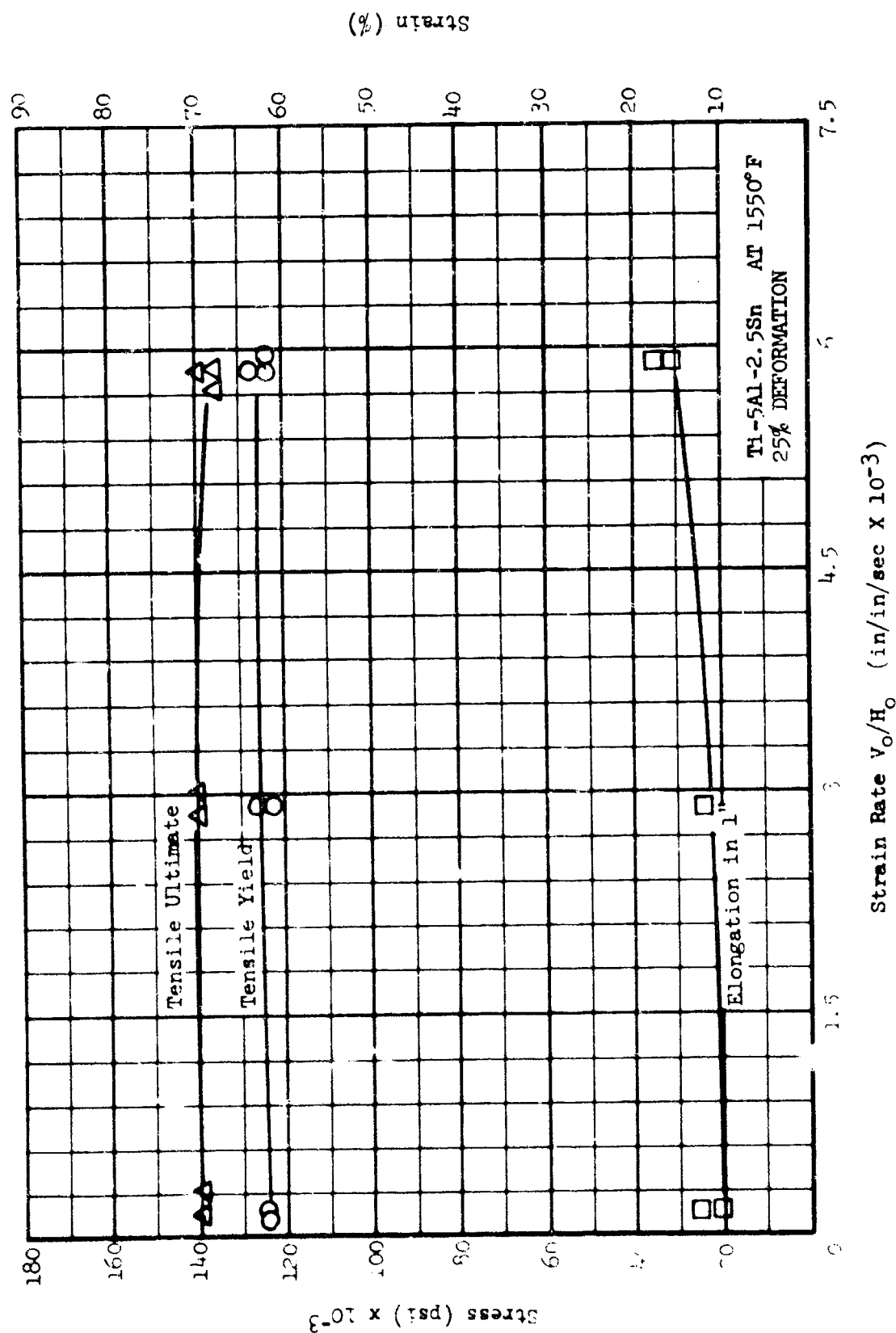
GRAPH 45. MATERIAL STRENGTH AND ELONGATION AS A FUNCTION OF STRAIN RATE (CONT'D)



GRAPH 45. MATERIAL STRENGTH AND ELONGATION AS A FUNCTION OF STRAIN RATE (CONT'D)

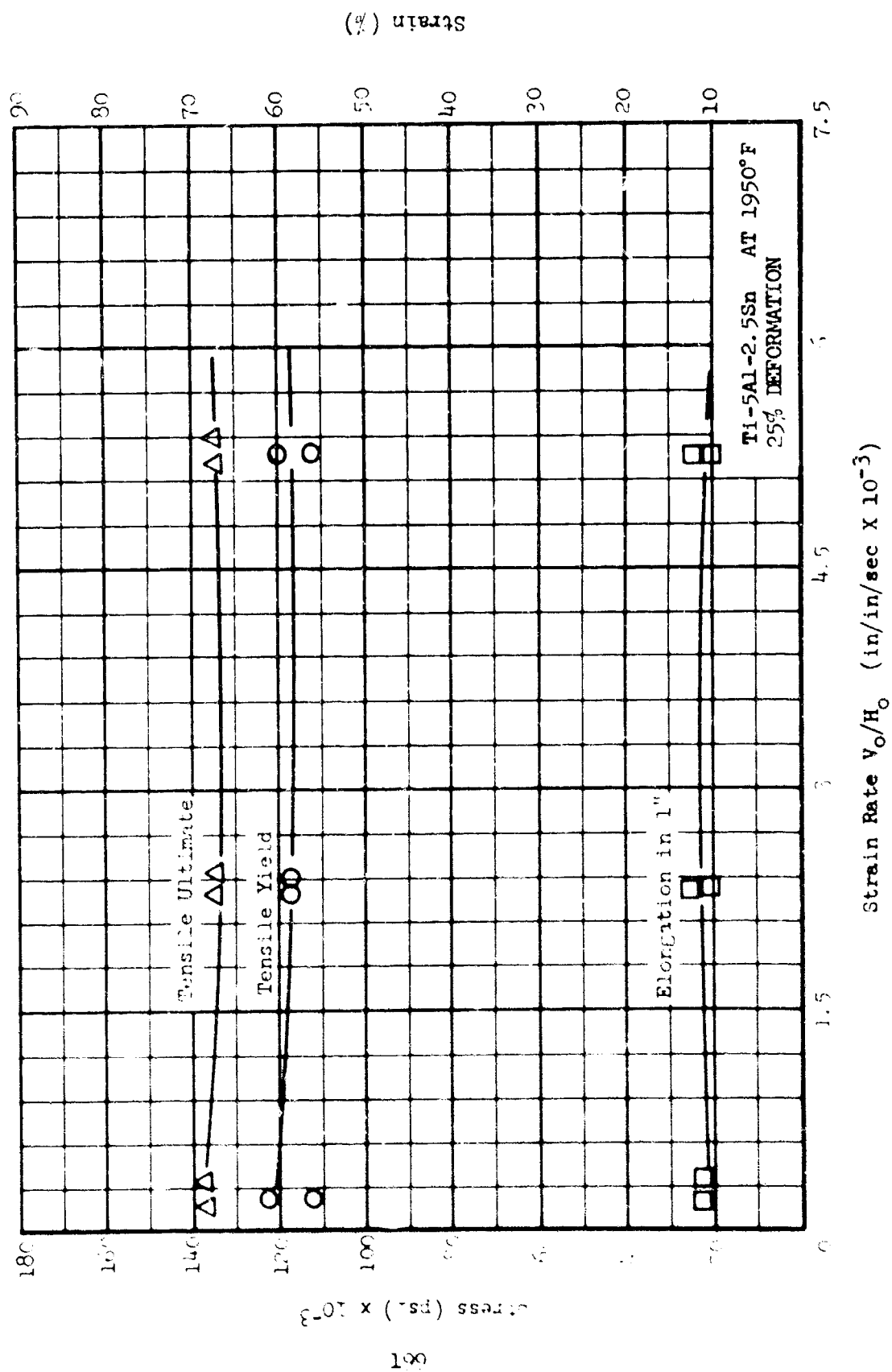


GRAPH 45. MATERIAL STRENGTH AND ELONGATION AS A FUNCTION OF STRAIN RATE (CONT'D)

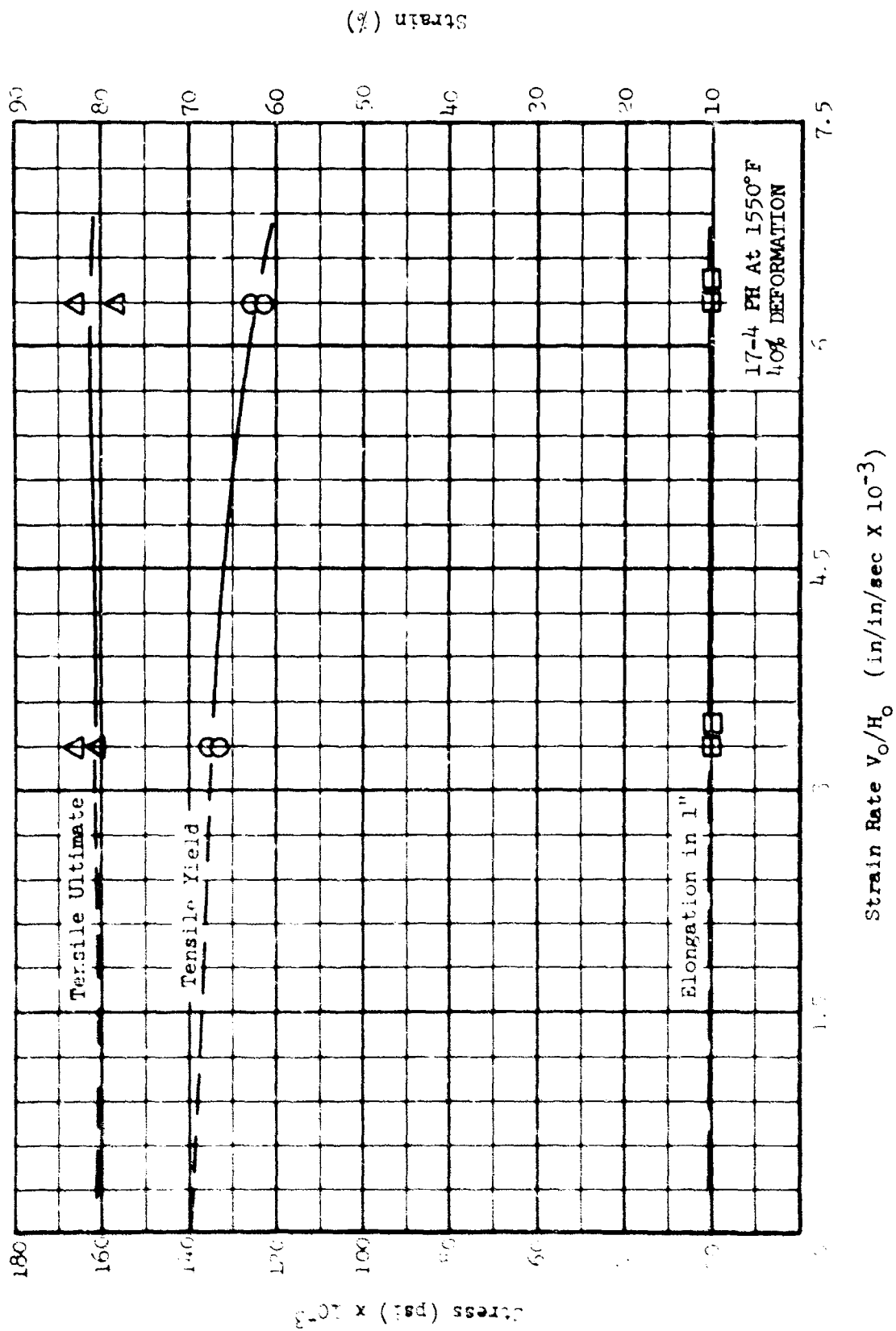




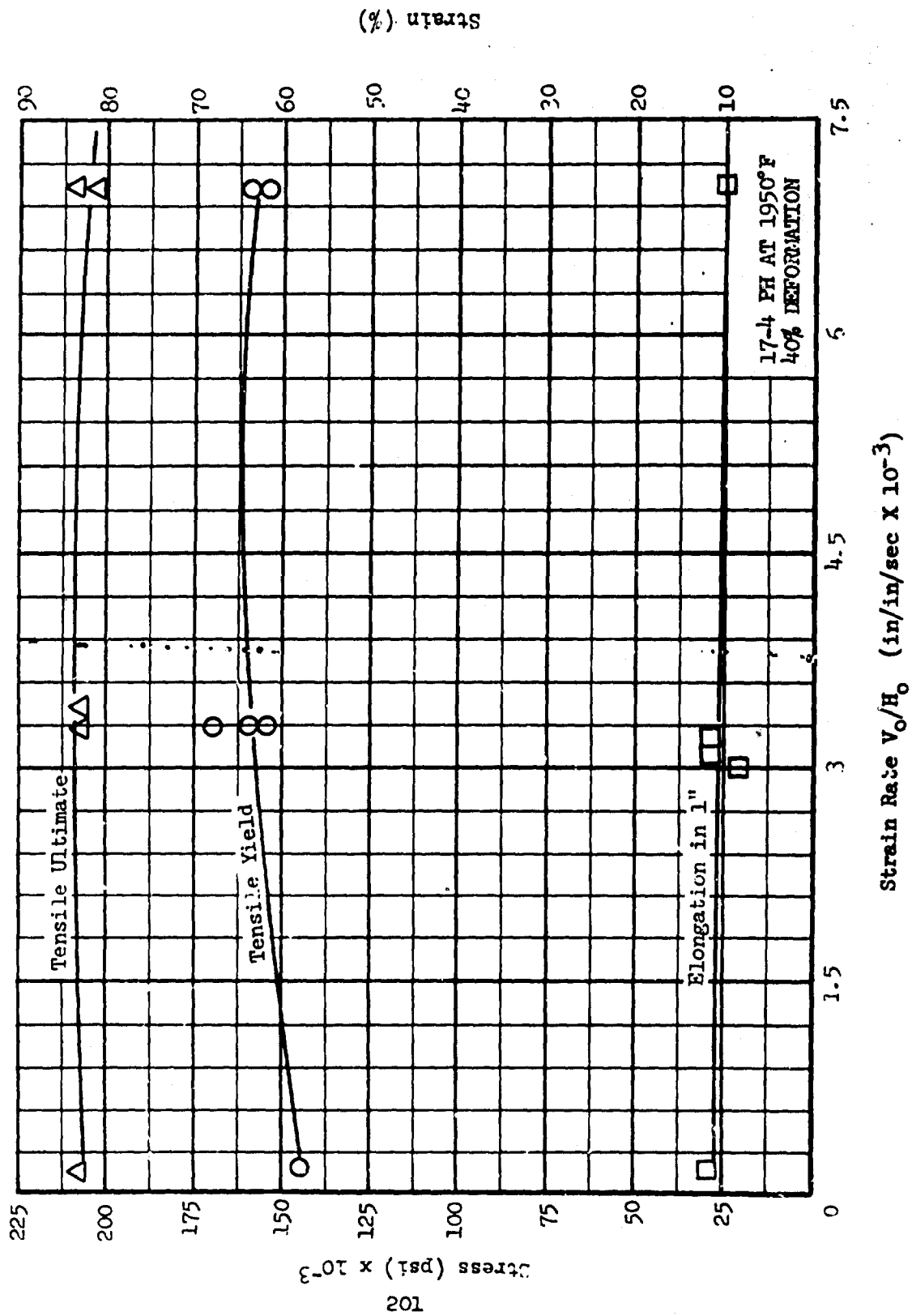
GRAPH 45. MATERIAL STRENGTH AND ELONGATION AS A FUNCTION OF STRAIN RATE (CONT'D)



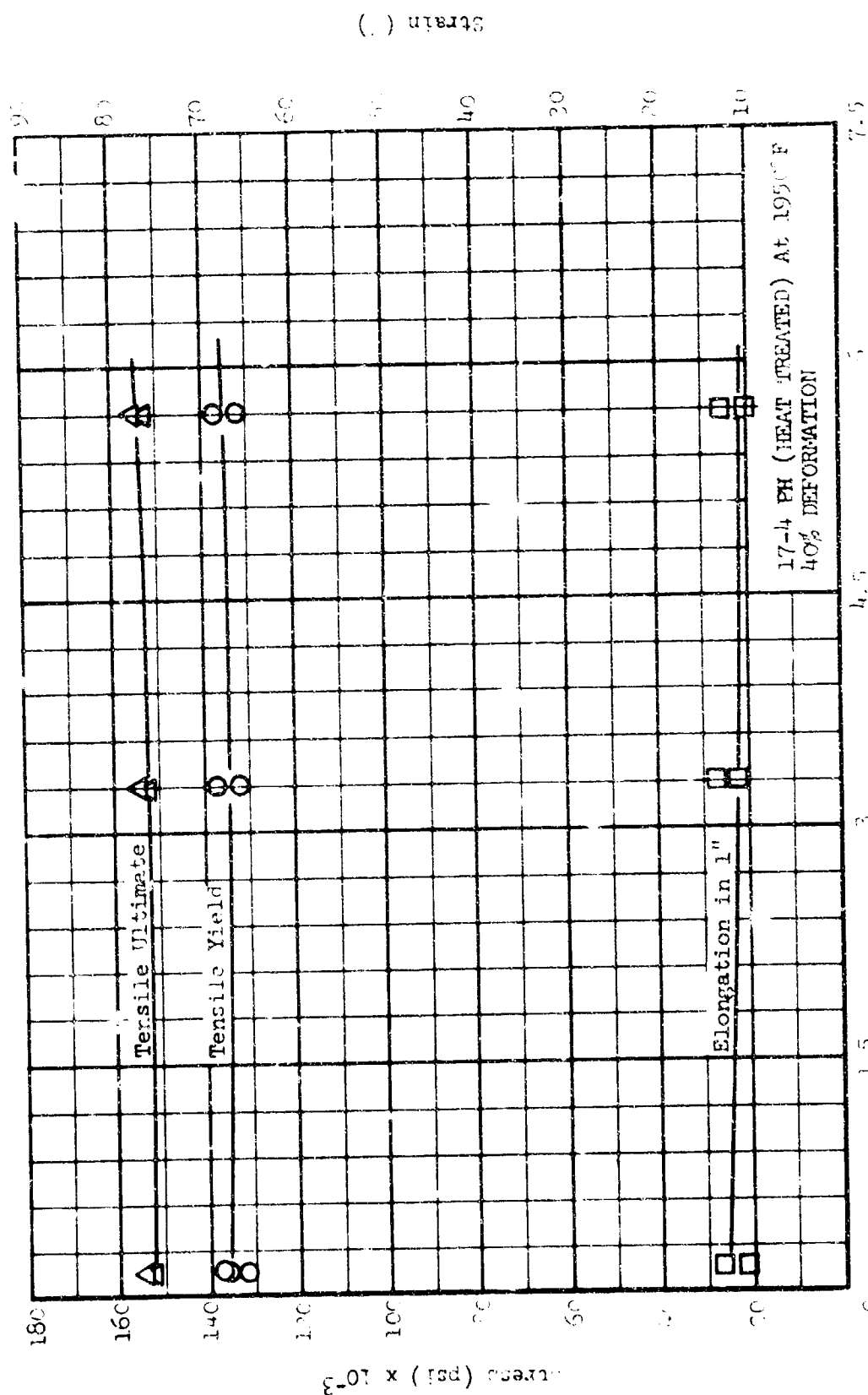
GRAPH 45. MATERIAL STRENGTH AND ELONGATION AS A FUNCTION OF STRAIN RATE (CONT'D)



GRAPH 45. MATERIAL STRENGTH AND ELONGATION AS A FUNCTION OF STRAIN RATE (CONT'D)

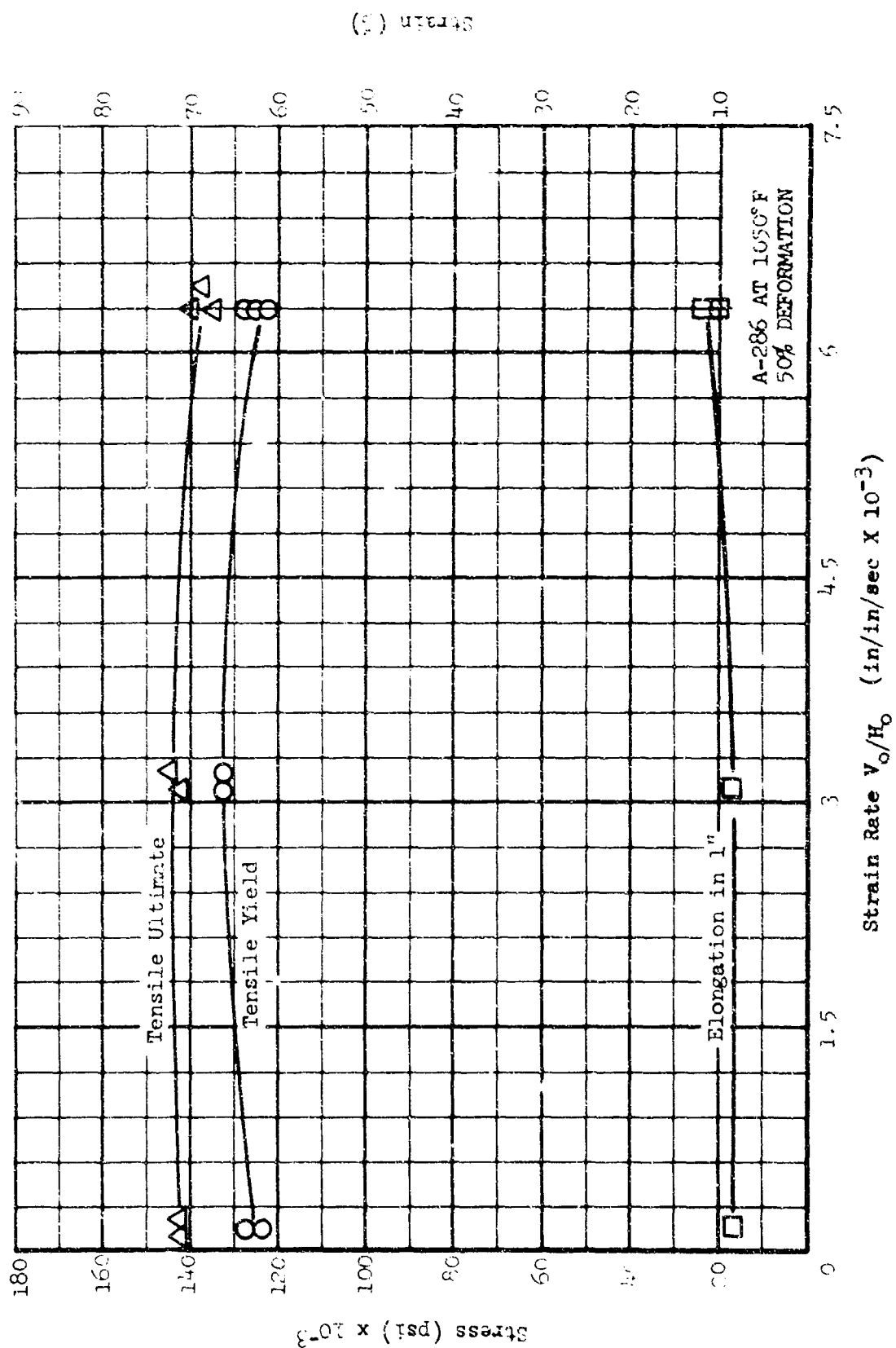


GRAPH 45. MATERIAL STRENGTH AND ELONGATION AS A FUNCTION OF STRAIN RATE (CONT'D)

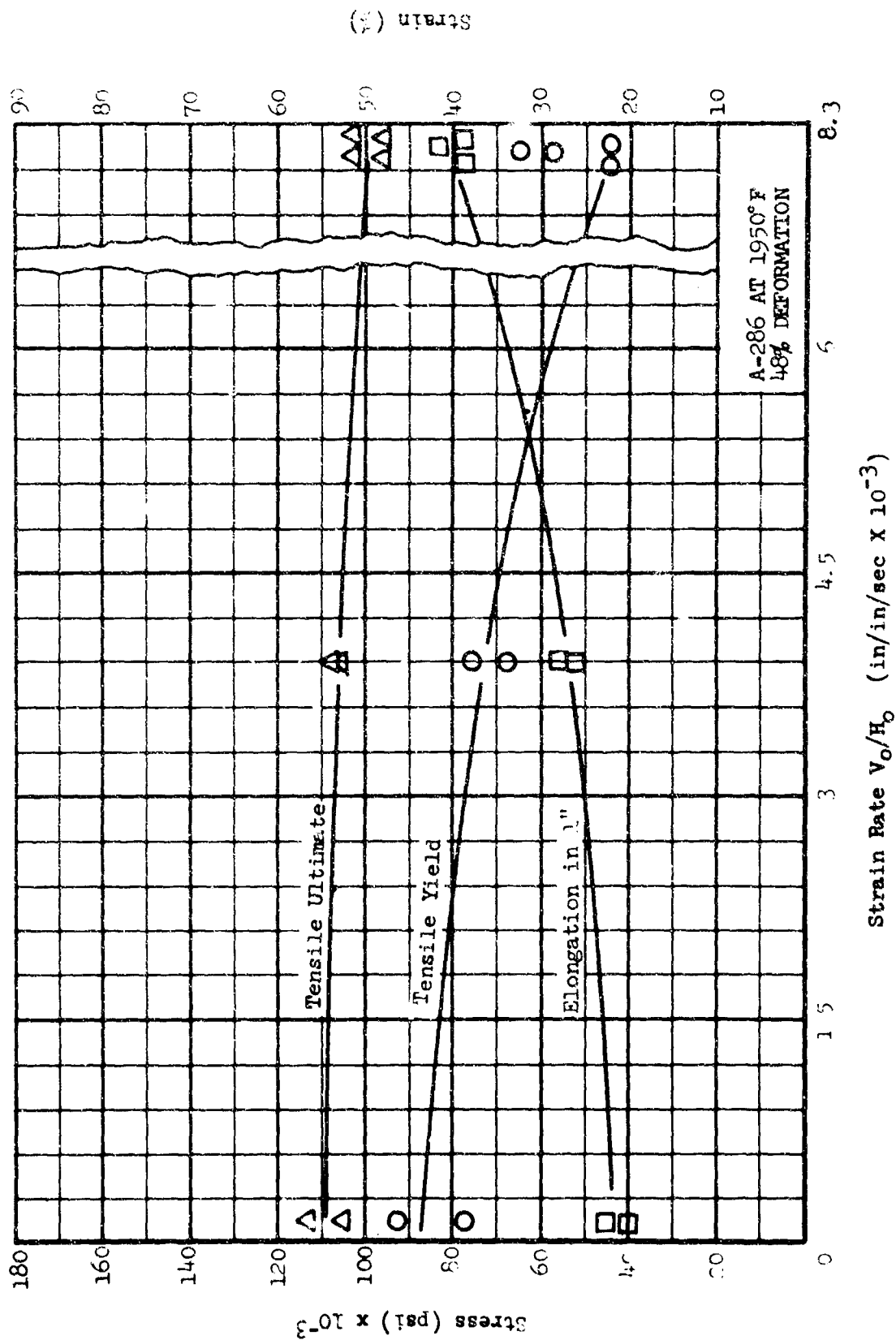


Strain Rate  $V_0/H_0$  ( $\text{in/in/sec} \times 10^{-3}$ )

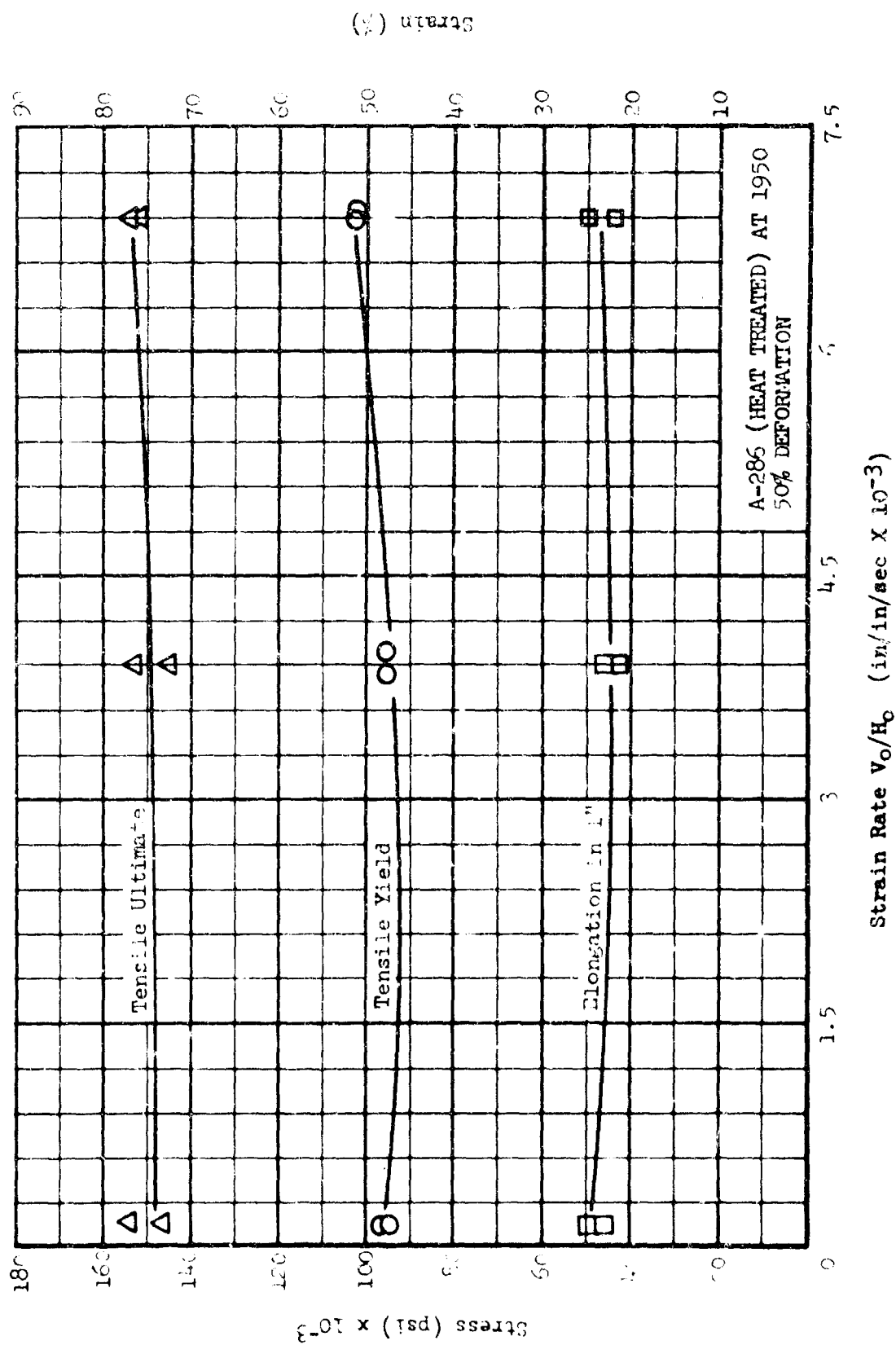
GRAPH 45. MATERIAL STRENGTH AND ELONGATION AS A FUNCTION OF STRAIN RATE (CONT'D)

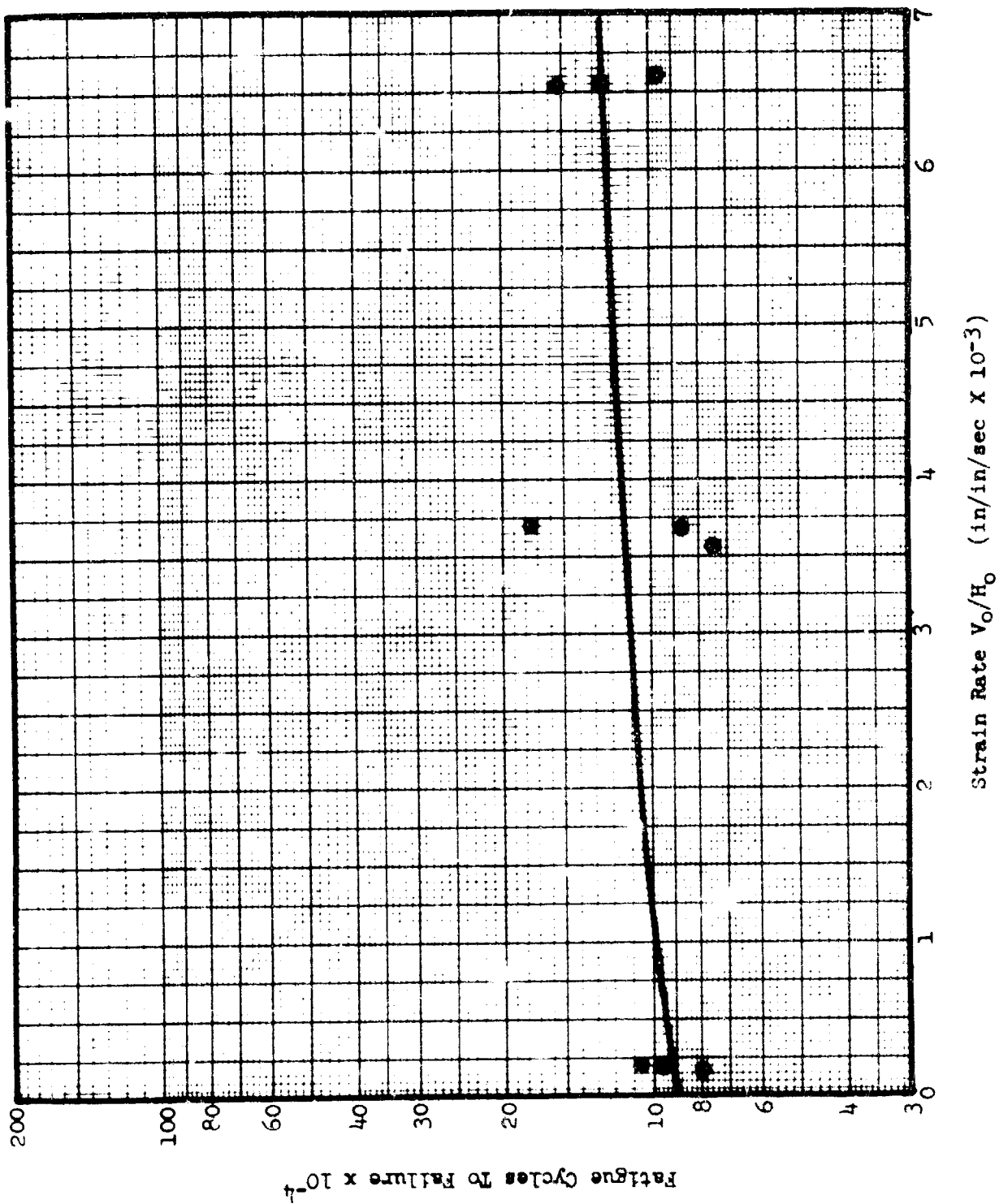


GRAPH 45. MATERIAL STRENGTH AND ELONGATION AS A FUNCTION OF STRAIN RATE (CONT'D)



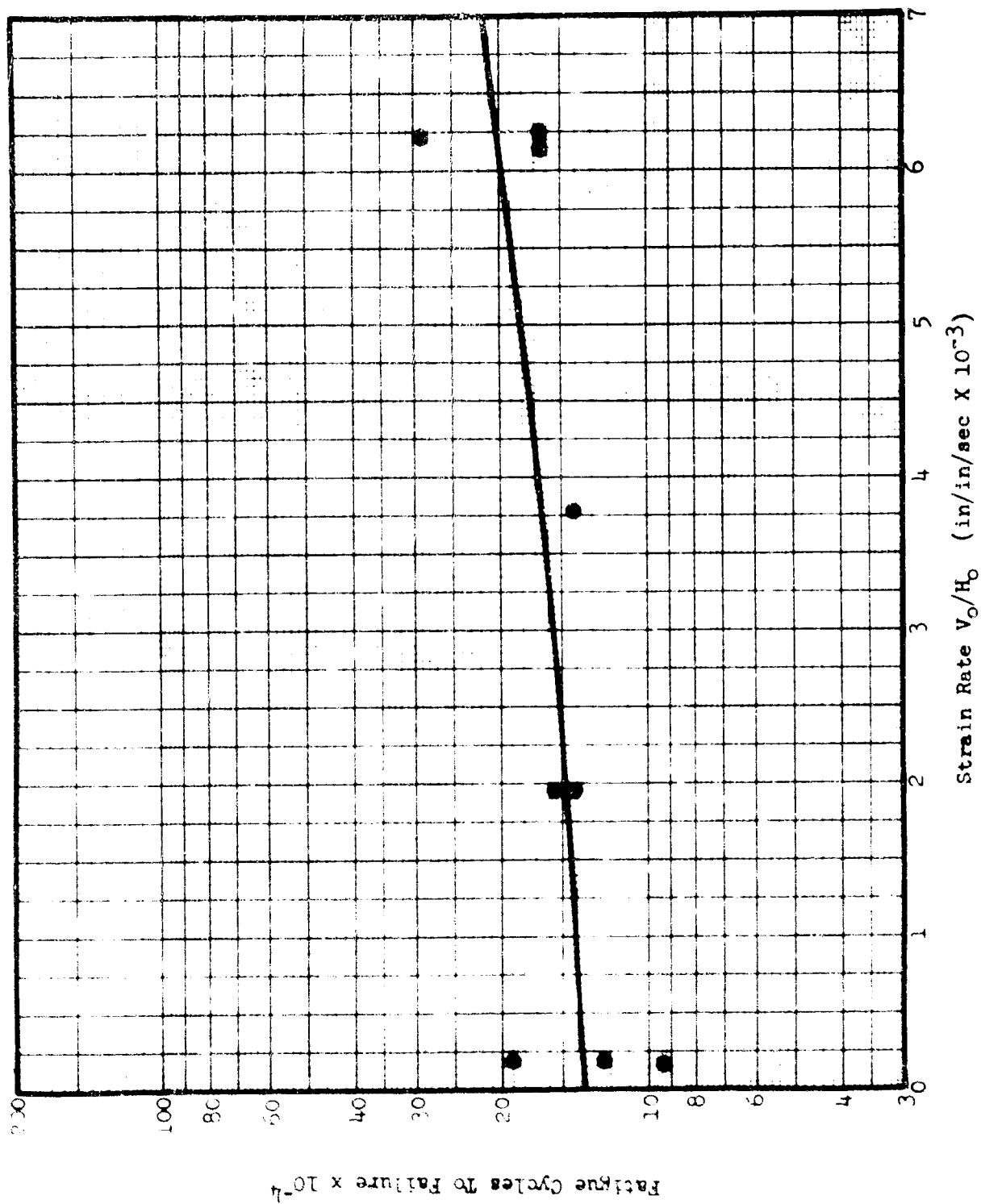
GRAPH 45. MATERIAL STRENGTH AND ELONGATION AS A FUNCTION OF STRAIN RATE (CONT'D)



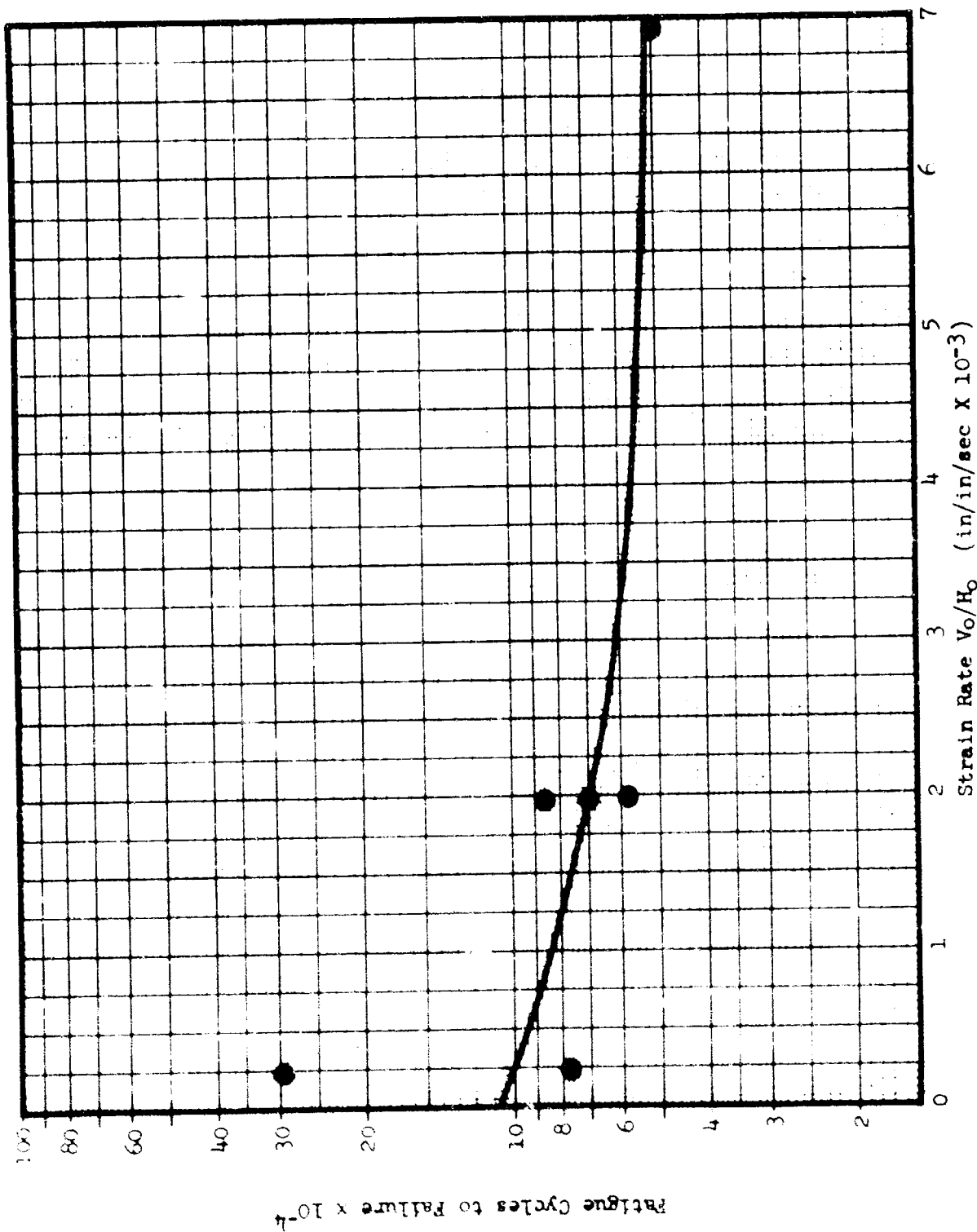


GRAPH 46. EFFECTS OF STRAIN RATE ON FATIGUE FOR 2024-T3 ALUMINUM AT ROOM TEMPERATURE.

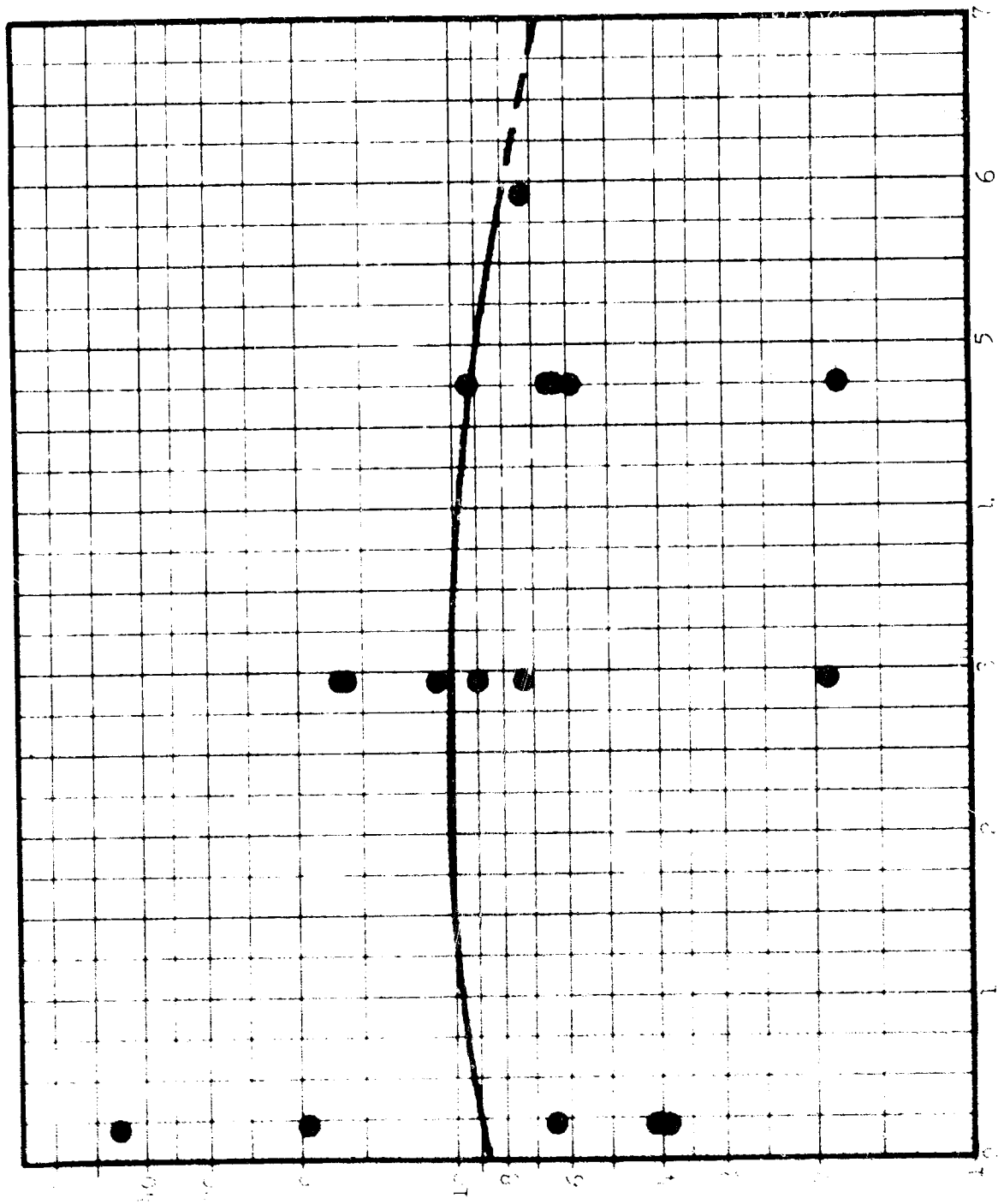




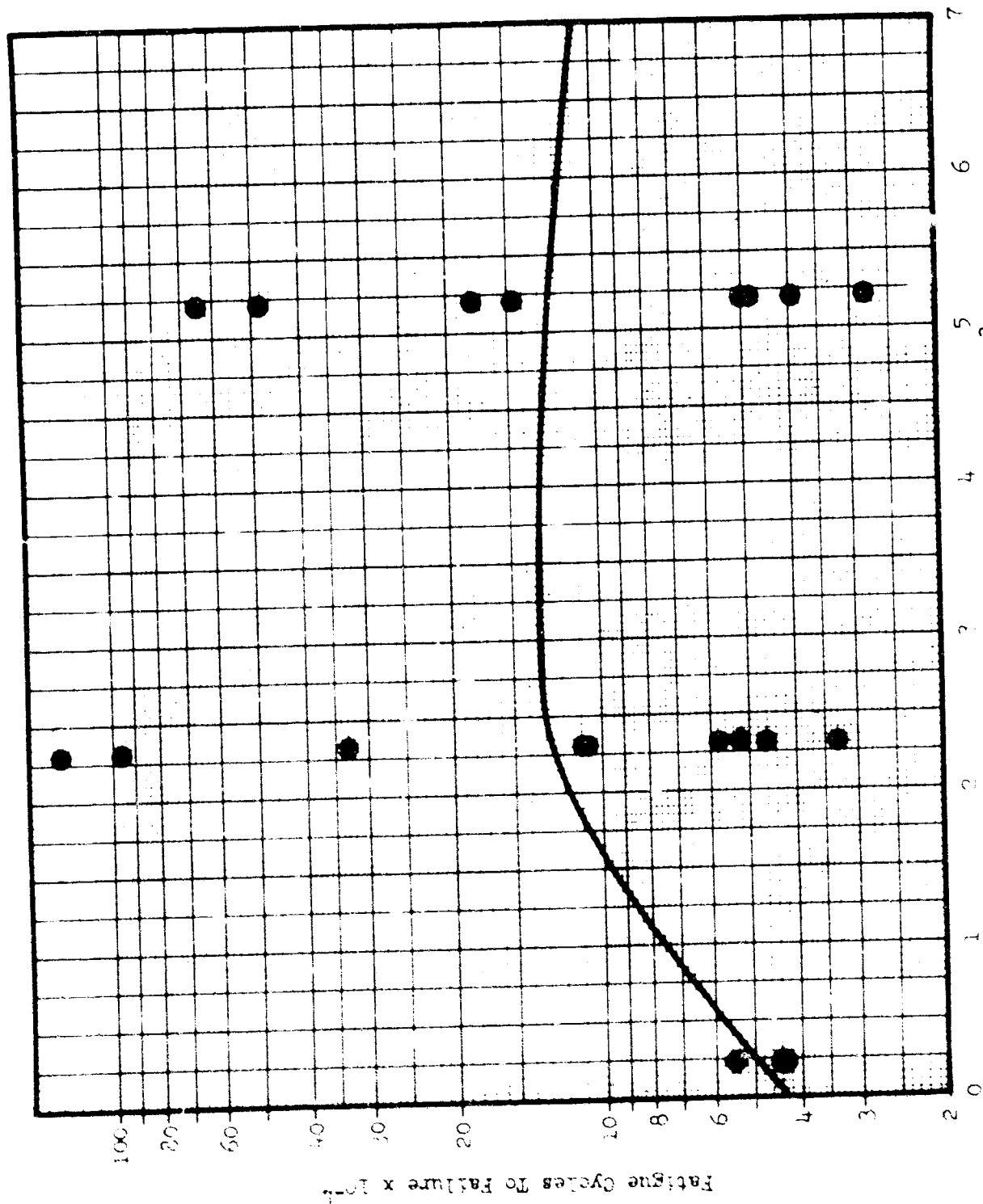
GRAPH 47. EFFECTS OF STRAIN RATE ON FATIGUE FOR 2024-T3 ALUMINUM AT 550°F.



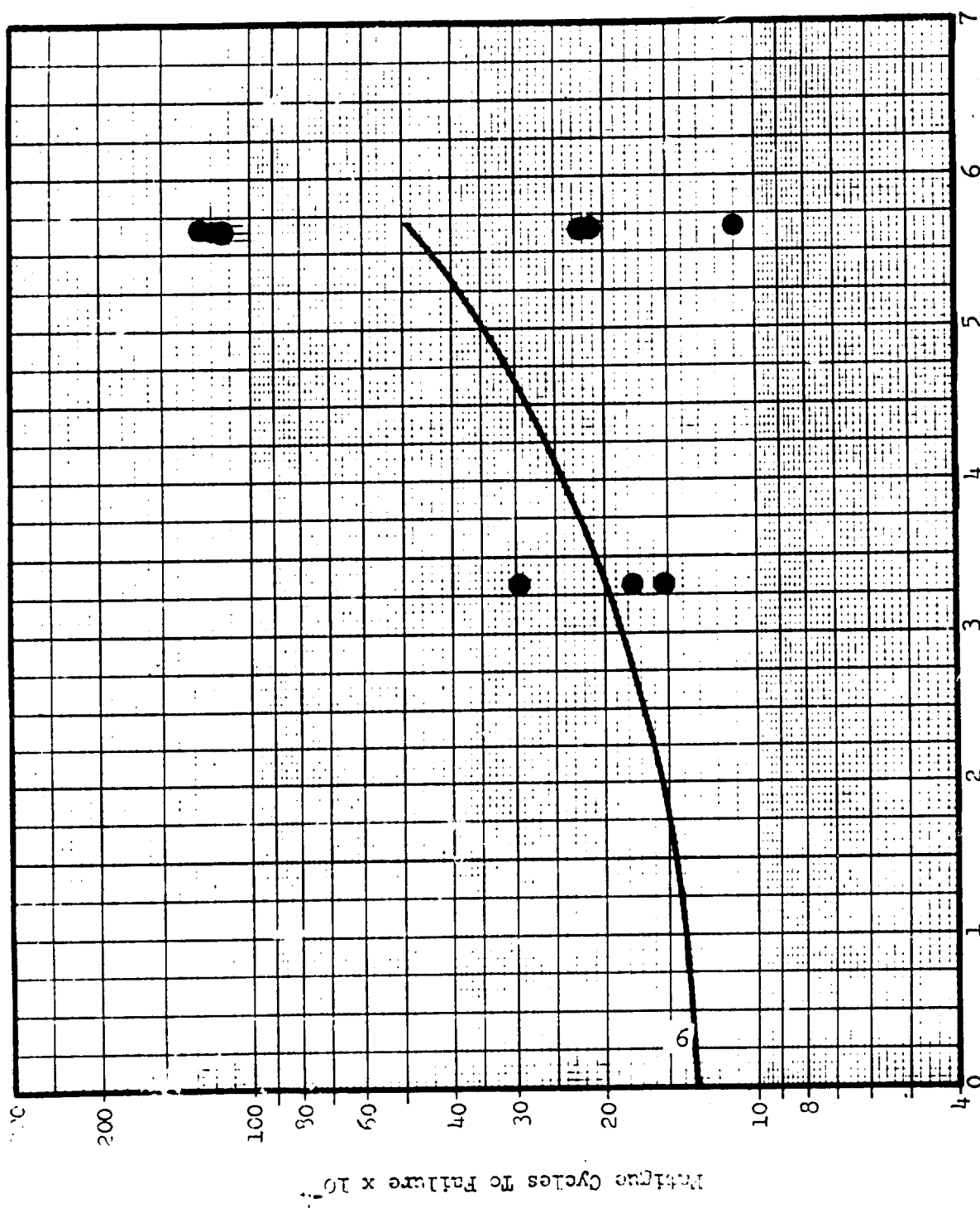
GRAPH 48. EFFECTS OF STRAIN RATE ON FATIGUE FOR 2024-T3 ALUMINUM AT 750°F



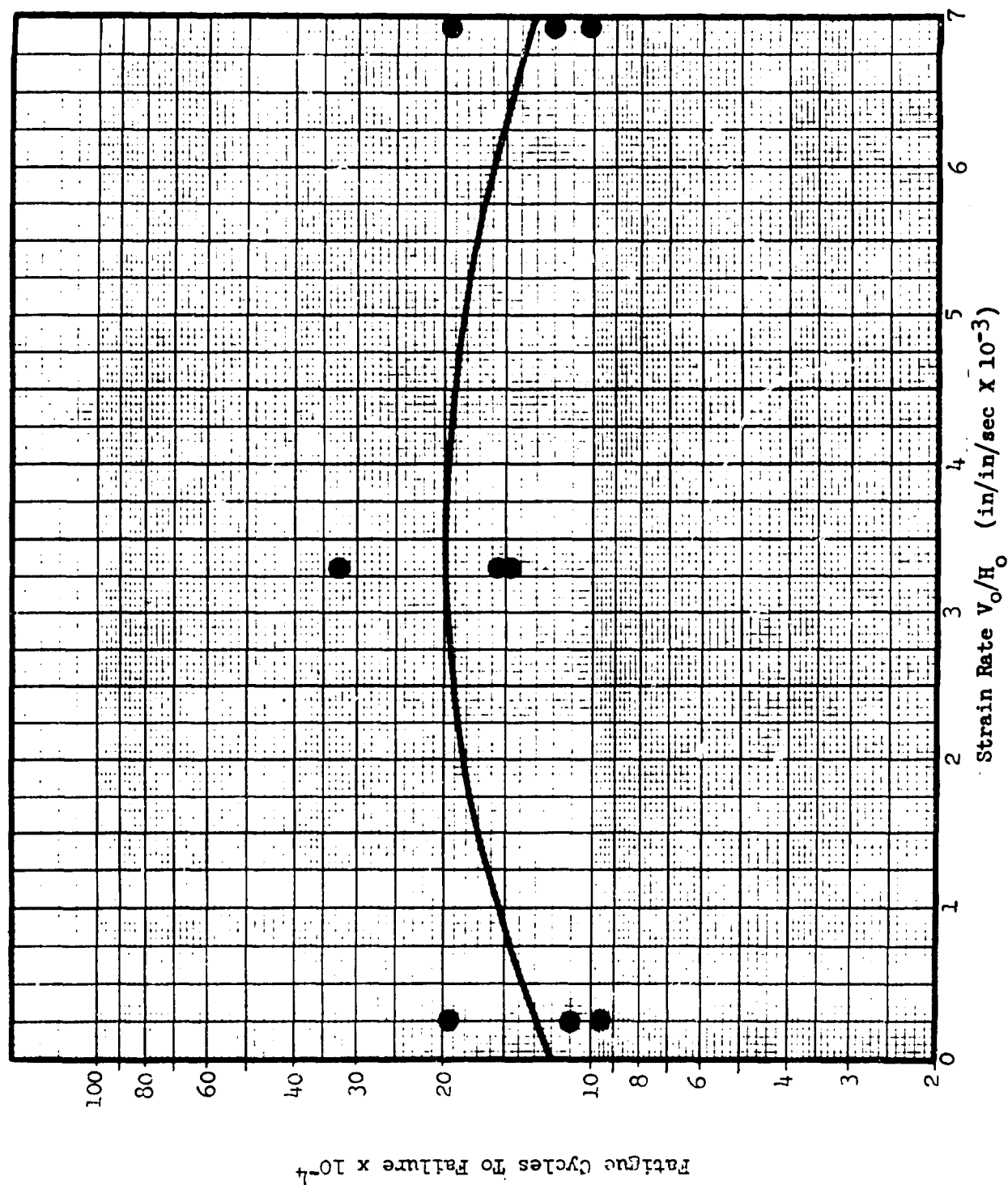
GRAPH 49. EFFECTS OF STRAIN RATE ON FATIGUE FOR 5Al-2.5Sn TITANIUM AT 1550°F



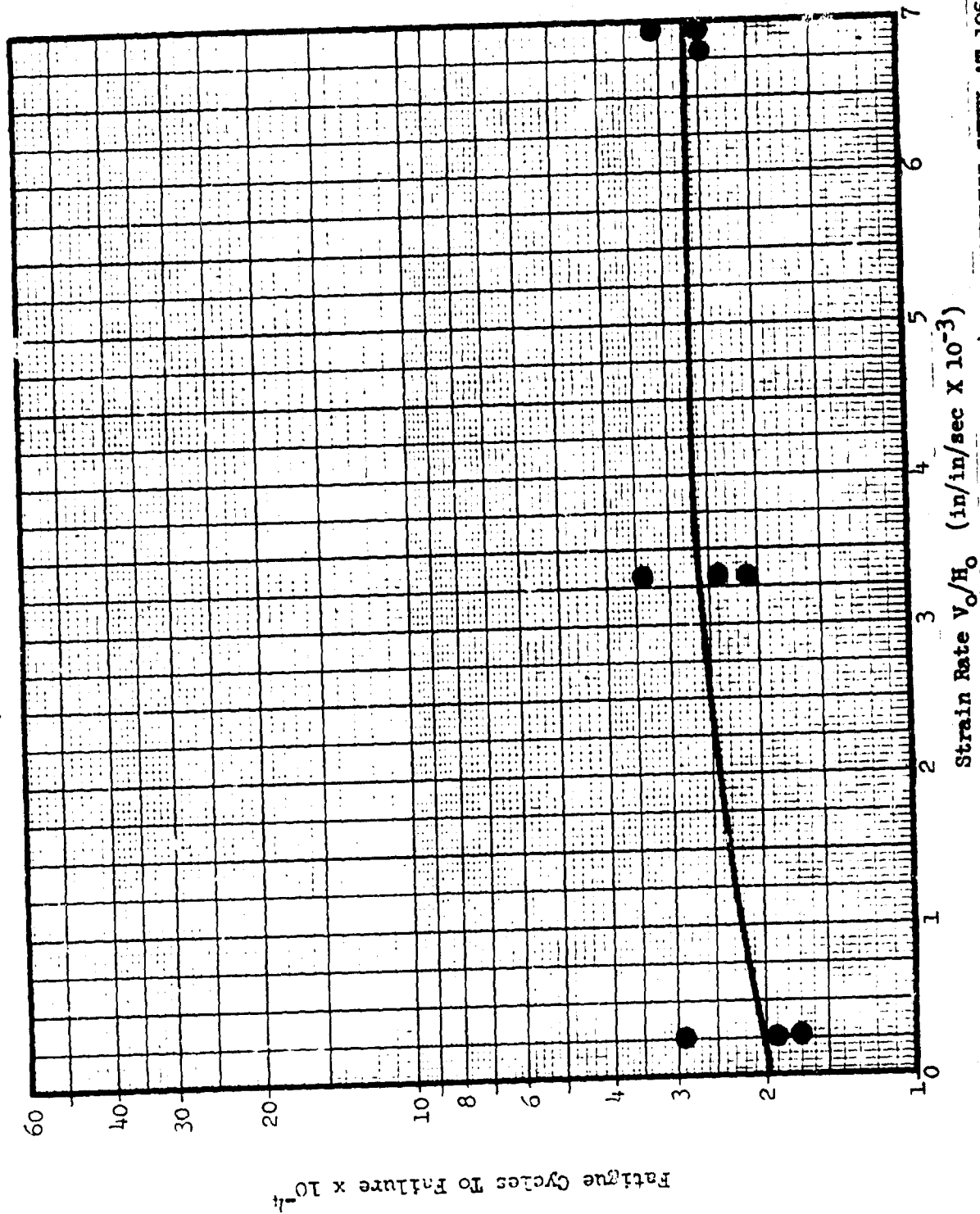
GRAPH 50. EFFECTS OF STRAIN RATE ON FATIGUE FOR 5Al-2.5Sn TITANIUM at 1950°F



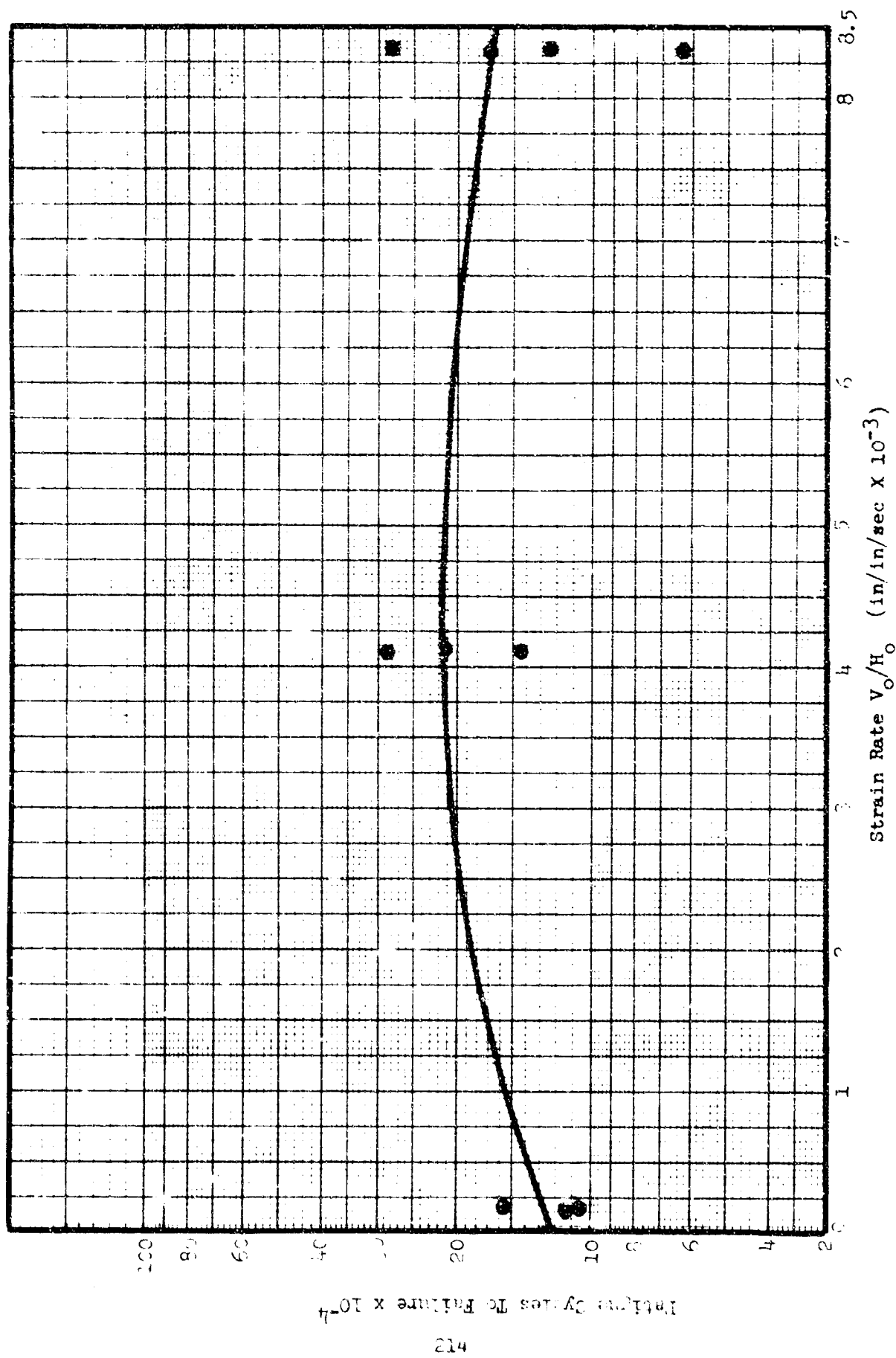
GRAPH 51. EFFECTS OF STRAIN RATE ON FATIGUE FOR 17-4 PH STAINLESS STEEL AT 1550°F



GRAPH 52. EFFECTS OF STRAIN RATE ON FATIGUE FOR 17-4 PH STAINLESS STEEL AT 1950°F

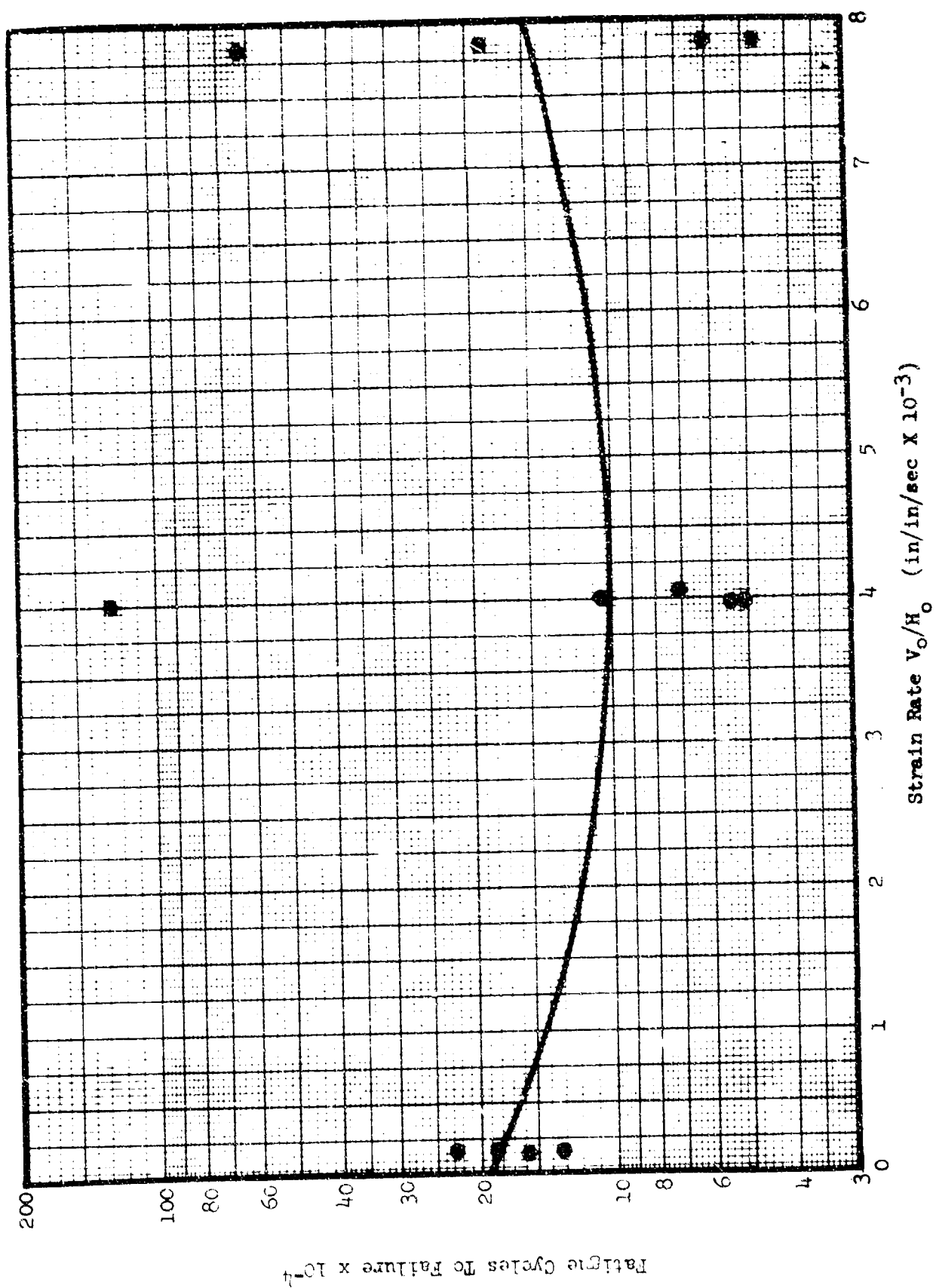


GRAPH 53. EFFECTS OF STRAIN RATE ON FATIGUE FOR HEAT TREATED 17-4 PH STAINLESS STEEL AT 1950°F

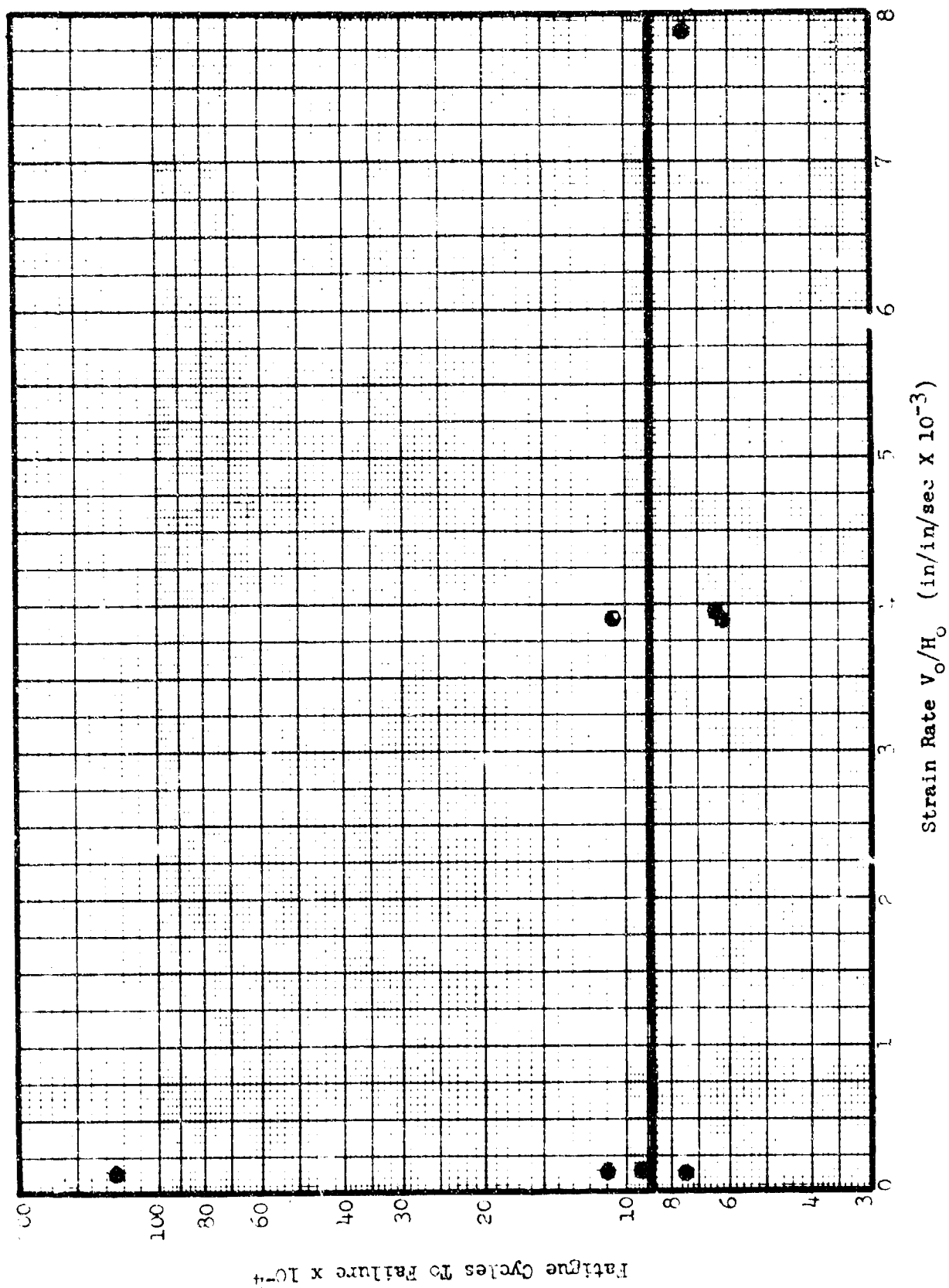


GRAPH 54. EFFECTS OF STRAIN RATE ON FATIGUE FOR A-286 AT 1050°F





GRAPH 55. EFFECTS OF STRAIN RATE ON FATIGUE FOR A-286 AT 1950°F



GRAPH 56. EFFECT OF STRAIN RATE ON FATIGUE FOR HEAT TREATED A-286 AT 1950°F

APPENDIX III

DATA TABLES

### APPENDIX III

#### DATA TABLES

This appendix includes all recorded and calculated data resulting from the experimental evaluation of strain rate and temperature on the ductility and mechanical properties of forged specimens.

TABLE VII. HIGH STRAIN RATE DUCTILITY RESULTS FOR PHASE I SPECIMENS

Material	Temp. ° F	Specimen number	H <sub>0</sub> (In)	H <sub>f</sub> (In)	Proj. Weight (lbs.)	Chamber Pressure (PSI)	Velocity Ft/sec	Strain Rate In/In/Sec	K E Ft - lb	% Red.	Failure Mode
2024-0 Aluminum	Ambient	A3-004	0.998	0.440	---	---	---	Static	---	55.9	G
		A3-002	1.001	0.426	---	---	---	Static	---	57.4	G
		A3-003	0.974	0.387	---	---	---	Static	---	60.3	F
		A3-001	0.995	0.339	---	---	---	Static	---	65.9	F
		A3-005	1.000	0.288	18.6	85	145	1740	6300	71.2	IF
		A3-023	1.500	0.310	7.0	360	400	3200	17,390	79.4	IF
		A3-010	1.000	0.208	5.46	100	270	3240	6300	79.2	G
		A3-006	1.001	0.183	5.46	120	285	3420	7200	81.7	F
		A3-011	1.006	0.331	5.46	335	425	5070	15,320	67.1	G
		A0-001	0.711	0.225	3.71	50	160	2700	1500	68.4	G
		A0-002	0.706	0.170	5.15	60	165	2800	2100	75.9	G
		A0-003	0.703	0.172	3.71	61.5	177	3020	1800	75.5	IF
7075-0	Ambient	A0-004	0.704	0.212	0.875	60	350	5970	1500	69.9	G
		A0-005	0.705	0.150	0.875	79	400	6810	1900	78.7	F
		B2-029	1.000	0.350	---	---	---	Static	---	65.0	G

TABLE VII . HIGH STRAIN RATE DUCTILITY RESULTS FOR PHASE I SPECIMENS (CONTINUED)

Material	Temp. ° F	Specimen number	H <sub>0</sub> (In)	H <sub>f</sub> (In)	Proj. Weight (lbs.)	Chamber Pressure (PSI)	Velocity Ft/sec	Strain Rate In/In/Sec	K E Ft - lb	% Red.	Failure Mode
7075-0 Aluminum	Ambient	B3-003	1.005	0.348	---	---	---	Static	---	65.4	G
		B3-001	0.990	0.311	---	---	---	Static	---	68.6	G
		B2-030	1.000	0.310	---	---	---	Static	---	69.0	IF
		B3-005	1.005	0.147	23.8	100	130	1550	7500	85.4	F
		B2-028	1.500	0.341	7.0	350	410	3280	18,280	77.2	IF
		B2-032	1.500	0.300	7.0	400	420	3360	19,200	80.0	G
		B2-031	1.500	0.215	7.0	475	450	3600	22,000	85.6	F
		B3-010	1.008	0.160	7.5	545	470	5600	25,700	84.1	IF
		C3-002	1.000	0.700	---	---	---	Static	---	30.0	G
		C3-003	1.000	0.650	---	---	---	Static	---	35.0	F
5A1-2.5Sn Titanium	Ambient	C3-006	0.999	0.839	23.8	260	225	2700	19,000	16.0	G
		C3-008	1.001	0.791	23.8	315	245	2940	22,000	21.0	G
		C3-010	1.001	0.740	23.8	425	275	3300	28,000	26.0	F
		C3-004	0.998	0.819	7.0	375	420	5050	19,000	17.9	G
		C3-005	0.997	0.732	7.0	500	450	5420	24,000	26.6	F

TABLE VII. HIGH STRAIN RATE DUCTILITY RESULTS FOR PHASE I SPECIMENS (CONTINUED)

Material	Temp. °F	Specimen number	H <sub>0</sub> (In)	H <sub>f</sub> (In)	Proj. Weight (lbs.)	Chamber Pressure (PSI)	Velocity Ft/sec	Strain Rate In/In/Sec	K E Ft - lb	% Red.	Failure Mode
6Al-4V Titanium	Ambient	D3-002	0.989	0.733	---	---	---	Static	---	25.9	G
		D3-001	1.005	0.683	---	---	---	Static	---	32.0	F
		D3-014	1.002	0.810	67.3	160	130	1560	20,000	19.2	F
		D3-015	0.996	0.835	67.3	243	140	1690	19,000	16.2	G
		D3-012	0.999	0.779	67.3	322	165	1980	25,000	22.0	F
		D3-006	1.008	0.785	23.8	315	245	2920	22,000	22.1	G
		D3-011	1.012	0.800	23.8	450	280	3320	29,000	20.9	F
		D3-004	1.008	0.854	7.0	300	380	4520	15,800	15.3	G
17-4 PH Stainless Steel	Ambient	D3-003	1.010	0.816	7.0	380	410	4870	14,800	20.2	IF
		E3-001	1.000	0.400	---	---	---	Static	---	60.0	G
		E3-002	1.000	0.310	---	---	---	Static	---	69.0	G
		E3-003	1.000	0.206	---	---	---	Static	---	79.4	G
		E3-013	1.002	0.730	67.3	322	165	1980	25,000	27.1	G
		E3-012	1.003	0.710	67.3	410	170	2030	31,000	29.6	F
		E3-011	1.008	0.710	67.3	560	200	2380	40,000	29.6	F

TABLE VII. HIGH STRAIN RATE DUCTILITY RESULTS FOR PHASE I SPECIMENS (CONTINUED)

Material	Temp. °F	Specimen number	H <sub>0</sub> (In)	H <sub>f</sub> (In)	Proj. Weight (lbs.)	Chamber Pressure (PSI)	Velocity Ft/sec	Strain Rate In/In/Sec	K.E. Ft - lb	% Red.	Failure Mode
17-4 PH Stainless Steel	Ambient	E3-010	1.006	0.520	23.8	630	320	3820	33,000	42.3	F
		E3-004	1.005	0.675	18.6	675	350	4290	37,600	32.9	F
		E3-007	1.004	0.679	7.5	670	500	5980	29,200	32.4	G
		E3-005	1.004	0.562	9.0	950	525	6270	40,000	44.0	G
		E3-008	0.997	0.395	9.0	950	525	6320	40,000	60.4	F
A-286 Steel	Ambient	F2-001	1.000	0.280	---	---	---	Static	---	72.0	G
		F2-002	1.000	0.235	---	---	---	Static	---	76.5	G
		F2-003	1.000	0.200	---	---	---	Static	---	80.0	F
		F2-011	1.004	0.427	67.3	560	200	2390	40,000	57.5	F
		F2-012	1.004	0.522	67.3	560	200	2390	40,000	42.0	G
		F2-013	0.993	0.515	67.3	630	210	2540	46,000	48.1	G
		F2-014	1.005	0.476	67.3	700	220	2630	50,000	52.6	G
		F2-015	1.002	0.421	67.3	820	230	2750	56,000	58.0	F
		F2-004	1.006	0.673	9.6	620	450	5370	29,600	33.1	G
		F2-006	1.004	0.670	7.0	620	500	5980	26,600	33.3	G



TABLE VII. HIGH STRAIN RATE DUCTILITY RESULTS FOR PHASE I SPECIMENS (CONTINUED)

Material	Temp. °F	Specimen number	H <sub>0</sub> (in.)	H <sub>f</sub> (in.)	Proj. Weight (lbs.)	Chamber Pressure (PSI)	Velocity Ft/sec	Strain Rate In/In/Sec	K E F - lb	% Red	Failure Mode
A-285 Steel	Ambient	F2-004	1.004	0.314	7.0	620	500	5980	26,600	38.8	G
		F2-006	1.002	0.352	9.0	640	500	5990	37,500	44.3	G
		F2-007	1.005	0.360	9.0	950	525	6270	40,000	64.2	G
		F2-008	1.002	0.370	9.0	950	525	6280	40,000	53.1	F
18% Ni Maraging Steel	Ambient	G3-004	1.000	0.356	---	---	---	Static	---	64.4	IF
		G3-005	1.000	0.318	---	---	---	Static	---	58.2	IF
		G3-006	1.000	0.241	---	---	---	Static	---	75.1	F
		G3-015	1.022	0.665	67.3	410	170	1990	31,200	35.0	G
		G3-001	1.000	0.775	18.0	105	170	2040	7,900	22.5	G
		G3-021	1.000	0.503	13.0	245	195	2340	10,500	39.7	G
		G3-016	1.013	0.640	67.2	570	200	2370	40,000	36.5	F
TZM Moly	Ambient	G3-010	1.007	0.509	9.5	875	510	6080	37,600	49.5	F
		G3-009	1.004	0.480	9.5	950	525	6270	40,000	52.2	IF
		H3-003	1.000	0.420	---	---	---	Static	---	58.0	G
		H3-004	1.000	0.340	---	---	---	Static	---	66.0	IF

TABLE VII. HIGH STRAIN RATE DUCTILITY RESULTS FOR PHASE I SPECIMENS (CONTINUED)

Material	Temp. °F	Specimen number	H <sub>0</sub> (In)	H <sub>f</sub> (In)	Proj. Weight (lbs.)	Chamber Pressure (PSI)	Velocity Ft/sec	Strain Rate In/In/Sec	K E Ft - lb	% Red.	Failure Mode
TZM Moly	Ambient	H3-001	1.002	0.793	12.0	60	150	1800	4200	20.9	F
		H3-002	1.002	0.501	12.0	125	215	2570	8500	40.0	G
		H3-007	1.003	0.740	9.5	450	400	4790	21,900	26.2	F
		H3-008	1.001	0.790	7.0	380	400	4800	19,000	20.1	F
		H3-005	0.998	0.680	9.6	620	450	5410	29,100	31.9	F
		H3-006	1.002	0.620	9.5	850	505	6050	36,800	38.1	F
Rene' 41	Ambient	I2-006	1.00	0.358	---	---	---	Static	---	64.2	G
		I2-005	1.000	0.277	---	---	---	Static	---	72.3	IF
		I2-012	1.007	0.619	67.3	520	185	2200	39,000	38.5	G
		I2-001	1.006	0.580	12.0	105	200	2390	7500	32.4	G
		I2-011	1.006	0.584	67.3	560	200	2300	40,000	41.9	F
		I2-002	1.008	0.645	12.0	130	220	2620	9,000	36.0	G
		I2-003	1.010	0.588	12.0	160	240	2850	15,200	41.8	G
		I3-008	1.006	0.525	9.5	950	525	6260	40,000	47.8	G
L-605	Ambient	J2-008	1.000	0.610	---	---	---	Static	---	39.0	G

TABLE VII. HIGH STRAIN RATE DUCTILITY RESULTS FOR PHASE I SPECIMENS (CONTINUED)

Material	Temp. ° F	Specimen number	H <sub>0</sub> (In)	H <sub>f</sub> (In)	Proj. Weight (lbs.)	Chamber Pressure (PSI)	Velocity Ft/sec	Strain Rate In/In/Sec	K.E. Ft - lb	% Red.	Failure Mode
L-605	Ambient	J2-010	1.000	0.520	---	---	---	Static	---	48.0	F
		J2-021	1.013	0.684	67.3	410	170	2010	31,000	32.5	G
		J2-023	1.013	0.637	67.3	475	180	2130	35,500	37.1	G
		J2-022	1.003	0.574	67.3	560	200	2390	40,000	52.8	F
		J2-007	1.000	0.504	9.5	160	265	3180	10,100	49.6	F
		J2-001	1.000	0.692	9.5	620	450	5400	29,200	30.9	G
		J2-002	1.000	0.679	9.0	620	455	5460	29,200	32.1	G
		J2-011	1.001	0.679	7.0	620	490	5870	27,200	30.4	G
		J2-003	0.999	0.658	7.0	620	490	5880	27,200	34.1	G

TABLE VIII. PHASE I TENSILE PROPERTIES OF FORGED SPECIMENS

Material	Temp. ° F	Specimen Number	% Red.	Tensile Yield (St <sub>y</sub> )	Tensile Ultimate (St <sub>u</sub> )	% Elong. 1" Gage Length	Hardness Ra	Modulus "E" (PSI x 10 <sup>6</sup> )
2024-0 Aluminum	Ambient	A2-004	41.0	45,300	49,200	5.0	45.0	9.7
		A2-008	72.0	47,200	53,100	4.0	42.0	9.2
		A2-010	36.5	45,000	48,900	5.0	39.1	8.3
		A2-011	35.0	44,500	48,300	5.0	33.5	8.9
		A2-012	---	44,600	49,100	6.0	40.0	9.9
		A2-015	36.0	45,100	48,200	5.5	42.0	8.6
		A2-018	72.5	44,100	51,800	6.0	42.5	7.3
		A2-020	---	44,300	49,800	5.0	39.0	9.6
		A2-021	66.0	44,300	54,300	6.0	44.0	9.3
		A2-022	68.5	48,400	54,100	5.0	39.5	9.8
		A2-023	35.0	41,600	47,600	5.5	40.0	8.2
		A2-024	35.0	41,400	46,600	5.0	38.0	8.5
		A2-026	65.5	46,700	52,500	5.0	37.5	8.6
		A2-027	65.5	44,100	50,200	4.0	45.0	8.4
7075-0 Aluminum	Ambient	B2-001	69.5	50,900	54,100	6.0	39.0	10.4
		B2-003	37.5	45,900	48,600	5.0	40.5	10.2
		B2-009	36.8	43,700	46,200	5.5	39.5	9.0

TABLE VIII. PHASE I TENSILE PROPERTIES OF FORGED SPECIMENS (CONT'D)

Material	Temp. ° F	Specimen Number	% Red.	Tensile Yield ( $St_y$ )	Tensile Ultimate ( $St_u$ )	$\frac{1}{2}$ Elong. 1" Gage Length	Hardness	Modulus "E" ( $PSI \times 10^6$ )
7075-0 Aluminum	Ambient	B2-010	56.5	48,200	52,300	6.0	37.0 Ra	7.7
		B2-012	30.0	44,200	47,900	7.0	34.5 Ra	10.4
		B2-013	38.0	46,300	48,300	6.0	37.0 Ra	8.5
		B2-015	69.0	44,000	51,500	8.0	42.5 Ra	8.4
		B2-017	---	46,100	48,300	6.0	42.0 Ra	9.2
		F2-018	66.5	45,800	50,000	6.5	36.0 Ra	9.5
		B2-019	39.0	46,000	48,700	5.0	34.0 Ra	9.8
5Al-2.5Sn Titanium	Ambient	B2-022	68.0	47,700	51,900	6.0	42.5 Ra	8.8
		B2-023	---	51,300	55,600	5.5	42.0 Ra	11.2
		B2-027	69.5	46,400	50,600	6.0	42.5 Ra	8.7
		C1-008	13.0	141,400	162,300	10.0	39.0 Rc	15.5
		C1-011	6.0	133,200	157,900	8.0	39.0 Rc	17.1
Ti-6Al-4V	Ambient	C1-020	11.0	135,200	159,500	9.0	39.0 Rc	15.3
		D2-016	9.2	139,800	163,000	10.0	37.0 Rc	16.1
17-4 PH Stainless Steel	Ambient	E2-014	19.0	166,100	175,300	9.0	36.5 Rc	29.0
		E2-015	18.5	165,100	175,900	10.0	36.0 Rc	28.9
		E2-016	15.0	158,400	163,300	11.0	36.0 Rc	28.6

TABLE VIII. PHASE I TENSILE PROPERTIES OF FORGED SPECIMENS (CONT'D)

Material	Temp. °F	Specimen Number	% Red.	Tensile Yield ( $S_y$ )	Tensile Ultimate ( $S_u$ )	$\frac{1}{2}$ Elong. 1" Gage Length	Hardness Rc	Modulus "E" ( $PSI \times 10^6$ )
A-285 Steel	Ambient	F1-003	35.0	135,700	148,000	10.0	34.0	26.5
		F1-004	48.8	144,400	154,700	8.0	33.6	23.8
		F1-005	36.0	136,900	148,400	10.0	33.0	24.8
		F1-007	40.0	146,400	155,800	9.0	35.0	27.0
		F1-008	46.0	149,400	158,200	9.0	33.6	21.5
		F1-009	48.1	145,900	156,300	9.0	32.6	25.5
		F1-010	---	155,900	168,000	8.0	36.0	25.5
		F1-011	36.0	136,100	144,500	9.0	33.0	24.2
		F1-012	49.5	136,900	154,900	10.0	33.0	24.3
		F1-013	34.0	129,200	138,100	10.0	31.5	23.8
		F1-014	48.5	130,600	147,100	10.0	34.0	27.1
		F1-015	34.5	131,300	141,500	8.0	33.0	25.3
		F1-016	33.0	121,700	138,400	11.0	32.0	27.1
		F1-018	51.0	148,100	160,700	8.0	35.0	23.3
		F2-007	---	157,700	164,400	11.0	37.0	28.1
		F2-016	---	156,300	163,200	10.0	37.0	26.8
Vascomax 300	Ambient	G2-004	19.0	148,600	157,300	12.0	35.0	25.3

TABLE VIII. PHASE I TENSILE PROPERTIES OF FORGED SPECIMENS (CONT'D)

Material	Temp. ° F	Specimen Number	% Red	Tensile Yield ( $S_y$ )	Tensile Ultimate ( $S_u$ )	% Elong. 1" Gage Length	Hardness Rc	Modulus "E" ( $PSI \times 10^6$ )
18% Ni Maraging Steel	Ambient	G2-012	19.5	149,400	164,900	12.0	35.0	24.3
		G2-013	17.2	147,400	157,300	11.0	34.0	21.7
		G2-014	---	152,000	171,100	11.0	37.0	25.9
		G2-015	20.0	158,300	170,600	11.0	36.0	24.1
		G2-017	19.0	156,000	159,600	11.0	35.0	22.8
		G2-018	8.5	143,400	157,100	12.0	36.0	35.4
Rene' 41	Ambient	I1-003	25.8	214,900	246,300	6.0	50.0	26.5
		I1-004	25.2	195,700	230,700	6.0	49.0	26.2
		I1-009	25.4	223,300	248,800	3.0	52.0	27.4
		I1-011	---	227,600	249,800	4.0	51.5	27.8
		I1-013	26.0	227,100	249,300	4.0	52.0	23.9
		I1-015	24.4	230,000	247,200	4.0	51.0	25.3
L-605	Ambient	I1-016	24.2	217,100	246,700	3.0	52.0	28.5
		I1-017	26.0	237,400	252,000	2.0	52.0	28.0
		J1-001	---	220,900	250,100	3.0	53.0	27.6
		J1-002	20.0	152,200	179,700	18.0	46.0	25.9
		J1-003	---	191,200	237,300	4.0	48.0	31.4

TABLE VIII. PHASE I TENSILE PROPERTIES OF FORGED SPECIMENS (CONT'D)

Material	Temp. °F	Specimen Number	% Red.	Tensile Yield ( $S_{ty}$ )	Tensile Ultimate ( $S_{tu}$ )	% Elong. 1" Gage Length	Hardness Rc	Modulus "E" (PSI x $10^6$ )
L-605	Ambient	J1-004	17.8	146,600	178,100	10.0	46.5	24.0
		J1-006	34.5	187,400	230,400	5.0	49.0	24.7
		J1-008	17.5	137,800	167,500	8.0	42.0	25.2
		J1-009	35.0	203,400	242,000	4.0	52.0	34.5
		J1-011	18.0	185,400	224,800	6.0	47.0	26.5
		J1-012	36.0	205,300	244,700	6.0	50.5	31.1
		J1-013	19.4	142,800	174,800	20.0	42.0	26.9
		J1-014	36.0	204,300	244,800	6.0	49.0	33.7
		J1-015	19.0	152,400	178,700	14.0	44.0	29.5
		J1-016	19.6	146,700	179,500	10.0	46.0	25.6
		J1-017	20.2	143,300	173,800	16.0	42.0	28.2
		J1-018	17.0	140,800	184,000	8.0	46.0	23.2



TABLE IX . STATIC FORGEABILITY DATA  
(PERFORMED ON HYDRAULIC PRESS)

Material	Temp. °F	Specimen Number	H <sub>0</sub> (in)	H <sub>f</sub> (in)	Die Temp(°F)	Ram Pressure (Tons)	% Red.	Failure Mode
2024-0 Aluminum	850	A4-100	1.015	0.528	RT	500	48.0	Good
	850	A4-101	1.015	0.334	RT	750	67.1	Good
	RT	A4-102	1.013	---	RT	1500	---	Scrapped
	850	A4-103	1.030	0.185	RT	750	82.0	Fracture
	870	A4-104	1.025	0.222	RT	750	68.3	Fracture
	860	A4-105	1.035	0.219	RT	750	78.8	Fracture
	670	A4-106	1.015	0.274	RT	750	73.0	Good
	650	A4-107	1.030	0.217	RT	750	78.8	Good
	620	A4-108	1.020	0.177	RT	750	82.5	Fracture
	600	A4-109	1.050	0.201	RT	750	80.9	Fracture
	---	A4-110	1.025	---	RT	750	---	Scrapped
	725	A4-111	1.035	0.231	RT	750	77.7	Fracture
	725	A4-112	1.005	0.235	350	750	77.0	Good
	700	A4-113	1.005	0.146	350	750	85.9	Good
	700	A4-114	1.010	0.116	350	750	87.5	Good

TABLE IX . STATIC FORGEABILITY DATA (CONT'D)  
(PERFORMED ON HYDRAULIC PRESS)

Material	Temp. °F	Specimen Number	H <sub>0</sub> (in)	h <sub>f</sub> (in)	Die Temp(°F)	Ram Pressure (Tons)	% Red.	Failure Mode
2024-0 Aluminum	725	A4-115	1.030	0.115	350	750	88.6	Good
	600	A4-116	0.983	0.139	350	500	80.5	Fracture
	600	A4-117	0.979	0.128	500	500	86.9	Good
	600	A4-118	0.975	0.098	500	500	90.0	Good
	600	A4-119	0.975	0.080	500	750	91.7	Good
	600	A4-120	0.981	0.072	500	850	92.7	Good
	600	A4-121	0.982	0.064	500	1000	93.5	Good
	850	A4-122	0.975	0.081	500	800	91.7	Good
	850	A4-123	0.978	0.078	500	800	92.0	Good
	850	A4-124	0.977	0.080	500	850	91.8	Good
	850	A4-125	0.975	0.060	500	900	93.9	Good
	850	A4-126	0.979	0.063	500	1000	93.7	Good; Dies Failed
	1740	C3-301	1.000	0.179	550	750	82.1	Fracture; Dies Failed
	1750	C3-302	1.010	---	550	750	---	Dies Failed
	900	C4-303	0.978	0.135	500	1000	86.2	Fracture
5A1-2.5S1 Titanium								

TABLE IX . STATIC Forgeability Data (CONT'D)  
(PERFORMED ON HYDRAULIC PRESS)

Material	Temp. °F	Specimen Number	H <sub>0</sub> (in)	H <sub>f</sub> (in)	Die Temp(°F)	Ram Pressure (Tons)	% Red.	Failure Mode
5Al-2.5Sn Titanium	900	C4-304	0.977	0.128	500	1000	86.8	Fracture; Dies Failed
	900	C4-305	0.978	0.194	500	900	80.2	Good
	900	C4-306	0.977	0.180	500	950	81.6	Good
	1650	C4-307	0.970	0.195	500	500	80.0	Good
	1650	C4-308	0.962	0.172	500	600	82.2	Fracture
	1650	C4-309	0.975	0.162	500	700	83.4	Good; Die Cupping
	1650	C4-310	0.976	0.146	500	750	85.0	Fracture; Dies Failed
	1200	E3-301	1.010	0.144	550	750	85.7	Good
	1200	E3-302	0.990	0.151	550	700	84.8	Good
	1900	E3-303	1.030	0.120	500	750	87.4	Good
17-4 PH Stainless Steel	1900	E3-304	1.040	0.106	500	800	89.8	Good; Die Cupping
	1200	E3-305	0.982	0.158	500	500	83.8	Good
	1200	E3-306	0.978	0.134	500	600	86.3	Good
	1200	E3-307	0.981	0.124	500	700	87.4	Good; Die Cupping
	1200	E3-308	0.978	0.103	500	800	89.4	Good; Dies Failed

TABLE IX . STATIC FORCEABILITY DATA (CONT'D)  
(PERFORMED ON HYDRAULIC PRESS)

Material	Temp. °F	Specimen Number	H <sub>0</sub> (in)	H <sub>f</sub> (in)	Die Temp(°F)	Ram Pressure (Tons)	% Red.	Failure Mode
17-4 PH Stainless Steel	1900	E3-309	0.969	0.104	500	800	89.3	Good
	1900	E3-310	0.982	0.109	500	800	89.0	Good; Die Cupping
	1900	E3-311	0.981	0.110	500	800	88.9	Good; Dies Failed
A-286 Steel	1250	F2-201	0.995	0.294	500	750	70.5	Good
	1250	F2-202	0.997	0.264	500	750	73.5	Good
	1250	F2-203	0.995	0.415	500	750	57.2	Good
	1400	F2-204	1.000	0.161	500	750	83.9	Good
	1200	F4-205	0.977	0.127	350	750	87.0	Fracture
	1200	F4-206	0.978	0.194	350	600	81.4	Fracture
	1200	F4-207	0.977	0.209	350	500	78.7	Fracture
	1200	F4-208	0.983	0.212	350	500	78.5	Good
	1900	F4-209	0.974	0.173	500	500	82.3	Good
	1900	F4-210	0.975	0.162	500	600	83.5	Good; Die Cupping
	1900	F4-211	0.982	0.127	500	700	87.1	Good; Dies Failed
	1900	F4-212	0.974	0.104	500	800	89.3	Good; Dies Failed

TABLE IX . STATIC Forgeability DATA (CONT'D)  
(PERFORMED ON HYDRAULIC PRESS)

Material	Temp. °F	Specimen Number	H <sub>0</sub> (in)	H <sub>f</sub> (in)	Die Temp(°F)	Ram Pressure (Tons)	% Red.	Failure Mode
A-286	1900	F4-213	0.979	0.105	500	800	89.1	Good; Dies Failed

TABLE X . STATIC DUCTILITY RESULTS

Material	Temp. ° F	Specimen Number	H <sub>o</sub> (In)	H <sub>f</sub> (In)	$\Delta t$ Millisec	Velocity In/Sec	Strain Rate In/In/Sec	$\epsilon_f$ Red.	Failure Mode
2024-0 Aluminum	Ambient	A7-791	0.979	0.342	16.0	62.5	64	65.1	G
		A7-794	0.980	0.320	15.5	64.5	66	67.3	G
		A7-793	0.977	0.307	15.2	65.8	67	68.5	F(1)
		A7-795	0.984	0.308	15.1	66.2	67	68.7	IF(1)
		A7-789	0.978	0.285	14.7	68.0	70	70.9	F(1)
		A7-787	0.976	0.283	14.7	68.0	70	71.0	F(1)
		A7-786	0.961	0.292	14.5	69.0	70	71.3	F(1)
		A7-792	0.980	0.281	14.5	69.0	70	71.3	F(1)
		A7-788	0.979	0.280	14.5	69.0	71	71.4	F(1)
		A7-790	0.976	0.271	13.7	73.0	75	72.2	F(1)
	550	A7-774	0.980	0.334	20.0	50.0	51	65.9	G
		A7-775	0.978	0.243	17.0	58.8	60	75.1	G
		A7-776	0.979	0.241	17.0	58.8	60	75.4	G
		A7-772	0.973	0.177	13.0	76.9	79	81.9	F(1)
		A7-773	0.977	0.138	12.0	83.3	85	85.9	F(1)

TABLE X . STATIC DUCTILITY RESULTS (CONT'D)

Material	Temp. ° F	Specimen Number	H <sub>0</sub> (In)	H <sub>f</sub> (In)	$\Delta t$ Millisec	Velocity In/Sec	Strain Rate In/In/Sec	$\epsilon_f$ Red.	Failure Mode
2024-0 Aluminum	550	A7-771	0.978	0.088	11.0	90.9	93	90.8	F(1)
	750	A7-768	0.978	0.126	12.0	83.3	85	87.1	F(1)
		A7-769	0.981	0.124	11.5	87.0	89	87.4	G
		A7-770	0.981	0.118	11.0	90.9	93	88.0	IF(1)
5A1-2.5Sn Titanium	Ambient	C7-807	0.978	0.830	12.0	83.3	85	15.1	G
		C7-810	0.977	0.752	11.5	87.0	89	23.0	G
		C7-811	0.978	0.731	11.2	89.3	91	25.3	G
		C7-809	0.978	0.679	10.8	92.6	95	30.6	F(1)
		C7-808	0.978	0.644	10.5	95.2	97	34.2	F(1)
		C7-862	0.983	0.689	9.7	103.1	105	29.9	F(1)
	550	C7-845	0.976	0.696	16.5	60.6	62	28.9	G
		C7-846	0.981	0.669	16.0	62.5	64	31.8	G
		C7-842	0.981	0.534	14.0	71.4	73	45.6	IF(1)
		C7-844	0.981	0.471	13.0	76.9	78	52.0	F(1)
		C7-843	0.972	0.437	12.5	80.0	82	55.0	F(1)

TABLE X . STATIC DUCTILITY RESULTS (CONT'D)

Material	Temp. °F	Specimen Number	H <sub>o</sub> (In)	H <sub>f</sub> (In)	$\Delta t$ millisec	Velocity In/Sec	Strain Rate In/In/Sec	$\epsilon_f$ Red.	Failure Mode
5Al-2.5Sn Titanium	750	C7-837	0.979	0.641	14.0	71.1	73	34.5	G
		C7-833	0.973	0.608	13.0	76.9	79	37.5	G
		C7-834	0.974	0.557	12.0	83.2	85	42.8	G
		C7-835	0.989	0.444	11.0	90.9	93	54.7	F(1)
		C7-835	0.973	0.328	10.0	100.0	102	66.5	F(1)
	1050	C7-832	0.977	0.440	13.8	72.5	74	55.0	F(2)
		C7-828	0.978	0.411	13.5	74.1	76	58.0	F(1)(2)
		C7-829	0.975	0.355	12.5	80.0	82	63.6	F(1)(2)
		C7-831	0.975	0.293	12.1	82.6	85	69.9	F(1)(2)
		C7-830	0.980	0.294	12	83.3	85	70.0	F(1)(2)
	1350	C7-705	0.975	0.374	13.0	76.9	79	61.6	G
		C7-708	0.979	0.254	12.0	83.3	85	74.1	F(1)
		C7-706	0.985	0.257	11.5	87.0	88	73.9	F(1)
		C7-704	0.982	0.181	10.5	95.2	97	81.6	F(1)
		C7-704	0.982	0.181	10.5	95.2	97	81.6	F(1)



TABLE X . STATIC DUCTILITY RESULTS (CONT'D)

Material	Temp. °F	Specimen Number	H <sub>o</sub> (In)	H <sub>f</sub> (In)	$\Delta t$ Millisec	Velocity In/Sec	Strain Rate In/In/Sec	$\epsilon_f$ Red.	Failure Mode
5Al-2.5Sn Titanium	1350	C7-707	0.980	0.195	10.0	100.0	102	80.1	F(1)
		C7-736	0.983	0.248	12.5	80.0	81	74.8	G
		C7-737	0.973	0.247	12.0	83.3	86	74.5	G
	1550	C7-738	0.979	0.151	11.0	90.9	93	84.6	IF(1)
		C7-735	0.977	0.135	10.0	100.0	102	86.2	F(1)
		C7-739	0.978	0.107	9.0	111.1	114	89.1	F(1)
		C7-748	0.984	0.141	10.5	05.2	97	85.7	G
	1750	C7-747	0.978	0.116	9.5	105.3	108	88.1	IF(1)
		C7-746	0.983	0.115	9.4	106.4	108	88.3	G
		C7-745	0.985	0.103	9.2	108.7	110	89.5	F(1)
	1950	C7-826	0.979	0.131	18.0	55.6	57	86.6	G
		C7-823	0.974	0.121	11.0	90.9	93	87.6	G
		C7-827	0.979	0.105	10.5	95.2	97	89.3	G
		C7-824	0.980	0.120	10.0	100.0	102	87.8	G
		C7-822	0.980	0.130	9.0	111.1	113	86.7	F(1)

TABLE X . STATIC DUCTILITY RESULTS (CONT'D)

Material	Temp. ° F	Specimen Number	H <sub>o</sub> (In)	H <sub>f</sub> (In)	$\Delta t$ millisec	Velocity In/Sec	Strain Rate In/In/Sec	$\epsilon$ Red.	Failure Mode
17-4 PH Stainless Steel	1950	C7-825	0.975	0.082	8.5	117.6	121	91.6	F(1)
		E7-856	0.980	0.303	10.0	100.0	102	69.1	G
	550	E7-857	0.978	0.159	8.0	125.0	128	83.7	G
		E7-859	0.981	0.142	8.1	123.5	126	85.5	G
	950	E7-858	0.978	0.138	8.0	125.0	128	85.9	G
		E7-709	0.980	0.166	12.0	83.3	85	83.1	G
	1350	E7-710	0.982	0.142	11.0	90.9	93	85.5	G
		E7-711	0.978	0.120	9.5	105.3	108	87.7	G
		E7-712	0.981	0.125	8.2	122.0	124	87.3	G
		E7-713	0.977	0.119	8.0	125.0	128	87.8	G
	1550	E7-740	0.979	0.143	10.0	100.0	102	85.4	G
		E7-743	0.978	0.126	9.0	111.1	114	87.1	G
		E7-742	0.977	0.125	8.8	113.6	116	87.2	G
		E7-741	0.981	0.125	8.7	114.9	117	87.3	G
	1750	E7-744	0.984	0.107	9.0	111.1	113	89.1	G

TABLE X . STATIC DUCTILITY RESULTS (CONT'D)

Material	Temp. °F	Specimen number	H <sub>o</sub> (In)	H <sub>f</sub> (In)	$\Delta t$ milliSec	Velocity In/Sec	Strain Rate In/In/Sec	$\epsilon_f$ Red.	Failure Mode
17-4 PH Stainless Steel	1950	E7-847	0.971	0.202	13.0	76.9	79	79.2	G
		E7-848	0.979	0.158	10.5	95.2	97	83.9	G
		E7-849	0.979	0.112	8.8	113.6	116	88.6	G
		E7-850	0.987	0.057	8.0	125.0	127	94.2	F(2)
A-286 Steel	Ambient	F7-860	0.978	0.742	19.0	52.6	54	24.1	G
		F7-796	0.977	0.544	13.7	73.0	75	44.3	G
		F7-798	0.978	0.441	11.5	87.0	89	54.9	G
		F7-799	0.977	0.413	10.5	95.2	97	57.7	G
		F7-800	0.977	0.373	9.5	105.3	108	61.8	G
		F7-797	0.976	0.447	9.5	105.3	118	71.2	G
		F7-805	0.977	0.281	8.7	114.9	118	71.2	G
		F7-861	0.978	0.280	8.6	116.3	119	71.4	G
		F7-806	0.980	0.262	8.5	117.6	120	73.3	G
		F7-802	0.978	0.305	8.5	117.6	120	68.8	G
		F7-801	0.977	0.348	8.5	117.6	120	64.4	G

TABLE X . STATIC DUCTILITY RESULTS (CONT'D)

Material	Temp. °F	Specimen Number	H <sub>o</sub> (In)	H <sub>f</sub> (In)	$\Delta t$ Millisec	Velocity In/Sec	Strain Rate In./In/Sec	$\epsilon$ Red.	Failure Mode
A-286 Steel	Ambient	F7-804	0.978	0.268	8.2	122.0	125	72.6	G
		F7-803	0.978	0.285	8.0	125.0	128	70.9	G
		F7-841	0.979	0.236	9.0	111.1	114	75.9	G
	550	F7-838	0.980	0.311	12.0	83.3	85	68.3	G
	750	F7-785	0.984	0.233	9.5	110.4	112	76.3	G
		F7-784	0.980	0.222	9.0	111.1	113	77.3	G
		F7-840	0.983	0.224	8.5	117.6	120	77.2	G
		F7-839	0.980	0.222	8.4	119.0	122	77.3	G
		F7-723	0.977	0.453	12.5	80.0	82	53.6	G
	900	F7-722	0.978	0.387	11.5	87.0	89	60.4	G
		F7-724	0.985	0.259	9.5	105.3	107	73.7	G
		F7-726	0.978	0.209	8.5	117.6	120	78.6	G
		F7-725	0.980	0.205	8.3	120.5	123	79.1	G
		F7-754	0.977	0.778	21.0	47.6	49	20.4	G
	1050	F7-755	0.977	0.581	17.5	57.1	58	40.5	G

TABLE X . STATIC DUCTILITY RESULTS (CONT'D)

Material	Temp. ° F	Specimen Number	H <sub>o</sub> (In)	H <sub>f</sub> (In)	$\Delta t$ MilliSec	Velocity In/Sec	Strain Rate In/In/Sec	$\epsilon$ Red.	Failure Mode
A-286 Steel	1050	F7-756	0.980	0.538	15.5	64.5	66	45.1	G
		F7-759	0.983	0.397	13.0	76.9	78	59.6	G
		F7-758	0.979	0.307	10.5	95.2	97	68.6	G
		F7-757	0.981	0.286	10.0	100.0	102	70.8	G
		F7-760	0.979	0.258	9.5	105.3	108	73.6	G
		F7-762	0.979	0.193	9.0	111.1	114	80.3	G
		F7-761	0.979	0.190	8.8	113.6	116	80.6	G
		F7-869	0.978	0.187	8.3	120.5	123	80.9	F(1)
	1350	F7-721	0.979	0.333	12.0	83.3	85	66.0	G
		F7-717	0.979	0.328	11.5	87.0	89	66.5	G
		F7-719	0.980	0.220	10.0	100.0	102	77.6	F(1)
		F7-720	0.981	0.221	9.5	105.3	107	77.5	F(1)
		F7-718	0.981	0.183	8.5	117.6	120	81.3	F(1)
		F7-700	0.994	0.256	12.0	83.3	84	74.2	G
	1550	F7-701	0.962	0.207	10.5	95.2	99	78.5	G

TABLE X . STATIC DUCTILITY RESULTS (CONT'D)

Material	Temp. ° F	Specimen Number	H <sub>o</sub> (In)	H <sub>f</sub> (In)	$\Delta t$ Millisec	Velocity In/Sec	Strain Rate In/In/Sec	$\epsilon_f$ Red.	Failure Mode
A-286 Steel	1550	F7-702	0.977	0.154	9.5	105.3	108	84.2	G
		F7-703	0.980	0.148	8.5	117.6	120	84.9	G
		F7-732	0.978	0.167	8.5	117.6	120	82.9	G
		F7-733	0.980	0.159	8.1	123.5	126	83.8	G
		F7-734	0.981	0.162	8.0	125.0	127	83.5	G
	1750	F7-854	0.980	0.164	9.0	111.1	113	83.3	G
		F7-749	0.983	0.130	8.6	116.3	118	86.8	G
		F7-750	0.981	0.133	8.3	120.5	123	86.4	G
		F7-855	0.980	0.127	8.0	125.0	128	87.0	G
		F7-853	0.979	0.133	9.6	104.2	106	86.4	G
	1950	F7-852	0.979	0.128	9.3	107.5	110	86.9	G
		F7-851	0.979	0.122	9.0	111.1	114	87.5	F(1)

TABLE XI . HIGH STRAIN RATE DUCTILITY RESULTS FOR PHASE II SPECIMENS

Material	Temp. ° F	Specimen number	H <sub>0</sub> (In)	H <sub>f</sub> (In)	Proj. Weight (lbs.)	Chamber Pressure (PSI)	Velocity Ft/sec	Strain Rate In/In/Sec	K E Ft - lb	% Red.	Failure Mode
2024-0 Aluminum	Ambient	A4-287	0.978	0.771	5.44	20	120	1440	1000	21.2	G
		A4-286	0.985	0.551	5.44	40	182	2184	2300	44.1	G
		A4-285	0.980	0.352	5.44	60	225	2700	3530	64.1	G
		A4-227	0.988	0.238	5.44	80	258	3096	4600	75.9	F(1)
		A4-229	0.978	0.199	5.44	90	273	3276	5130	79.7	F(1)
		A4-228	0.980	0.170	5.44	100	285	3420	5660	82.7	F(1)
		A4-226	0.978	0.078	5.44	112	292	3504	6060	92.0	F(1)
		A4-281	0.979	0.709	15.06	20	65	780	1000	28.6	G
		A4-280	0.976	0.564	15.06	30	85	1020	1740	42.2	G
		A4-279	0.980	0.453	15.06	40	105	1260	2620	53.8	G
		A4-230	0.977	0.292	15.06	60	135	1620	4320	70.1	G
		A4-232	0.981	0.280	15.06	62.5	138	1656	4530	71.5	F(1)
		A4-231	0.977	0.261	15.06	65	140	1680	4740	73.3	F(1)
		A4-284	0.978	0.712	23.5	20	35	420	1000	27.2	G
		A4-283	0.981	0.506	23.5	35	75	900	2180	48.4	G

TABLE XI. HIGH STRAIN RATE DUCTILITY RESULTS FOR PHASE II SPECIMENS (CONTINUED)

Material	Temp. ° F.	Specimen number	$\epsilon_0$ (In)	$H_f$ (In)	Weight (lbs.)	Chamber Pressure (PSI)	Velocity Ft/sec	Strain Rate In/In/Sec	K E Ft - lb	% Red.	Failure Mode
2024-O Aluminum	Ambient	A4-202	0.980	0.365	23.5	50	98	1176	3440	62.3	G
		A4-203	0.975	0.291	23.5	52	106	1296	4130	70.2	F(1)
		A4-204	0.973	0.257	23.5	62	113	1356	4500	71.7	F(1)
		A4-205	0.970	0.721	5.44	20	120	1440	1000	27.0	G
	550	A4-206	0.980	0.577	5.44	30	153	1836	1670	41.7	G
		A4-207	0.979	0.154	5.44	30	258	3096	4600	83.8	G
		A4-208	0.973	0.145	5.44	35	265	3180	4659	84.2	G
		A4-209	0.983	0.106	5.44	100	285	3420	5660	89.2	G
		A4-210	0.979	0.664	15.06	20	65	780	1000	32.2	G
		A4-211	0.977	0.568	15.06	22	69	828	1140	42.0	G
		A4-203	0.981	0.473	15.06	30	95	1020	1740	51.8	G
		A4-297	0.980	0.391	15.06	35	95	1140	2170	60.1	G
		A4-204	0.982	0.240	15.06	55	128	1536	3880	75.6	G
		A4-205	0.982	0.154	15.06	70	150	1800	5150	84.3	F(1)
		A4-206	0.979	0.140	15.06	70	150	1800	5150	85.7	F(1)



TABLE III. HIGH STRAIN RATE DUCTILITY RESULTS FOR PHASE II SPECIMENS (CONTINUED)

Material	Temp. ° F.	Specimen number	H <sub>0</sub> (In)	H <sub>f</sub> (In)	Proj. Weight (lbs.)	Chamber Pressure (PSI)	Velocity Ft/sec	Strain Rate In/In/Sec	K E Ft - lb	% Red.	Failure Mode
2024-0 Aluminum	550	A4-295	0.980	0.555	23.5	20	35	420	1000	33.2	G
		A4-235	0.979	0.430	23.5	35	75	900	2180	56.1	G
		A4-295	0.982	0.409	23.5	35	75	900	2180	58.4	G
		A4-237	0.980	0.257	23.5	50	98	1176	3440	73.8	G
		A4-238	0.985	0.184	23.5	60	110	1320	4310	81.3	G
		A4-239	0.983	0.135	23.5	70	120	1440	5140	86.2	G
		A4-240	0.978	0.126	23.5	75	125	1500	5560	87.1	F(1)
		A4-291	0.982	0.695	5.44	20	120	1440	1000	29.2	G
	750	A4-290	0.978	0.301	5.44	50	205	2460	2940	69.2	G
		A4-220	0.980	0.127	5.44	82	260	3112	5050	87.0	G
		A4-222	0.978	0.099	5.44	80	273	3276	5130	87.9	G
		A4-221	0.984	0.077	5.44	100	285	3420	5660	92.2	F(1)
		A4-207	0.983	0.190	15.06	50	120	1440	3480	80.7	G
		A4-208	0.982	0.133	15.06	60	135	1620	4320	86.5	G
		A4-209	0.977	0.135	15.06	65	140	1680	4740	86.2	G

TABLE II. HIGH STRAIN RATE DUCTILITY RESULTS FOR PHASE II SPECIMENS (CONTINUED)

Material	Temp. ° F	Specimen number	H <sub>0</sub> (In)	H <sub>f</sub> (In)	Proj. Weight (lbs.)	Chamber Pressure (PSI)	Velocity Ft/sec	Strain Rate In/In/Sec	K E Ft - lb	% Red.	Failure Mode
2024-0 Aluminum	750	A4-210	0.980	0.115	15.06	70	150	1800	5150	88.3	G
		A4-211	0.980	0.089	15.06	80	155	1860	5950	90.9	F(1)
		A4-294	0.980	0.565	23.5	20	35	420	1000	32.1	G
		A4-293	0.977	0.375	23.5	35	75	900	2180	51.6	G
		A4-241	0.979	0.363	23.5	35	75	900	2180	62.9	G
		A4-242	0.981	0.210	23.5	50	98	1176	3490	78.6	G
		A4-243	0.980	0.159	23.5	60	110	1320	4340	83.8	G
		A4-245	0.981	0.130	23.5	65	115	1380	4720	86.8	G
	950	A4-244	0.983	0.098	23.5	70	120	1440	5150	90.0	F(1)
		A4-292	0.980	0.393	5.44	35	168	2016	2000	59.9	F(1)
		A4-219	0.978	0.232	5.44	50	205	2460	2940	76.3	G
		A4-218	0.977	0.198	5.44	60	225	2700	3530	79.7	F(1)
		A4-214	0.079	0.248	15.06	50	105	1260	2620	74.7	G
		A4-215	0.975	0.245	15.06	45	108	1296	3030	74.9	G
		A4-216	0.981	0.184	15.06	50	120	1440	3450	81.2	F(1)

TABLE XI. HIGH STRAIN RATE DUCTILITY RESULTS FOR PHASE II SPECIMENS (CONTINUED)

Material	Temp. ° F	Specimen number	H <sub>0</sub> (In)	H <sub>f</sub> (In)	Proj. Weight (lbs.)	Chamber Pressure (PSI)	Velocity Ft/sec	Strain Rate In/In/Sec	K E Ft - lb	% Red.	Failure Mode
2024-0 Aluminum	95C	A4-213	0.980	0.159	15.06	50	120	1440	3450	83.8	F(1)
		A4-217	0.977	0.127	15.06	55	128	1536	3880	87.0	F(1)
		A4-212	0.975	0.095	15.06	50	135	1620	4320	90.3	F(1)
		A4-247	0.979	0.629	23.5	20	35	420	1000	35.8	F(1)
		A4-248	0.979	0.57	23.5	25	60	740	1300	48.2	F(1)
		A4-249	0.979	0.409	23.5	30	68	830	1600	58.2	F(1)
		A4-246	0.981	0.255	23.5	35	75	900	2180	74.0	F(1)
		C5-507	0.979	0.762	5.33	70	225	2758	4202	22.2	G
5Al-2.5Sn Titanium	Ambient	C5-509	0.982	0.767	5.33	80	240	2933	4781	21.9	G
		C5-510	0.978	0.736	5.33	85	247	3031	5664	24.7	G
		C5-508	0.985	0.708	5.33	90	255	3107	5397	28.1	F(1)
		C5-364	0.983	0.946	15.06	20	72	879	1213	3.8	G
		C5-365	0.978	0.854	15.06	40	101	1239	2387	12.7	G
		C5-367	0.984	0.841	15.06	60	134	1634	4202	14.5	G
		C5-368	0.982	0.775	15.06	70	146	1784	4988	21.1	G

TABLE XI . HIGH STRAIN RATE DUCTILITY RESULTS FOR PHASE II SPECIMENS (CONTINUED)

Material	Temp. ° F	Specimen number	H <sub>0</sub> (In)	H <sub>f</sub> (In)	Proj. Weight (lbs.)	Chamber Pressure (PSI)	Velocity Ft/sec	Strain Rate In/In/Sec	K E Ft - lb	% Red.	Failure Mode
5Al-2.5Sn Titanium	Ambient	C5-369	0.982	0.735	15.06	75	151	1845	5335	25.2	F(1)
		C5-366	0.980	0.728	15.06	80	155	1898	5622	25.7	F(1)
		C5-408	0.982	0.763	64	60	64	782	4071	22.3	G
		C5-411	0.981	0.749	64	65	67	820	4462	23.7	G
		C5-410	0.979	0.668	64	70	70	858	4871	31.8	F(1)
		C5-409	0.982	---	64	80	76	929	5741	---	F(1)
		C5-486	0.982	0.678	5.33	70	325	2750	4202	31.0	G
	750	C5-487	0.984	0.627	5.33	85	247	3012	5064	36.3	G
		C5-534	0.976	0.506	5.33	100	265	3258	5829	48.2	F(1)
		C5-533	0.980	---	5.33	150	308	3771	7874	---	F(1)
		C4-303	0.975	0.874	5.44	80	255	3139	5462	10.4	G
		C4-304	0.978	0.803	5.44	100	280	3436	6586	17.8	G
		C4-305	0.974	0.784	5.44	120	303	3733	7712	19.5	G
		C4-306	1.108	0.806	5.44	140	323	3498	8764	27.3	G
		C4-307	0.975	0.790	5.44	160	343	4222	9883	19.0	G

TABLE XI . HIGH STRAIN RATE DUCTILITY RESULTS FOR PHASE II SPECIMENS (CONTINUED)

Material	Temp. ° F	Specimen number	H <sub>o</sub> (In)	H <sub>f</sub> (In)	Proj. Weight (lbs.)	Chamber Pressure (PSI)	Velocity Ft/sec	Strain Rate In./In./Sec	K E Ft - lb	% Red.	Failure Mode
5Al-2.5Sn Titanium	750	C4-274	0.975	0.716	23.5	50	98	1206	3505	26.6	G
		C4-275	0.975	0.659	23.5	60	110	1354	4417	32.4	G
		C4-276	0.975	0.530	23.5	65	115	1415	4827	45.6	F(1)
		C4-273	0.973	0.540	23.5	70	120	1480	5256	44.5	F(1)
		C4-272	0.964	0.311	23.5	100	147	1830	7887	67.7	F(1)
		C5-444	0.977	0.677	64	60	64	786	4071	30.7	G
		C5-447	0.981	0.660	64	65	67	819	4462	32.7	G
		C5-446	0.979	0.590	64	70	70	858	4871	39.7	F(1)
	1050	C5-445	0.979	0.450	64	80	76	932	5741	54.0	F(1)
		C5-501	0.980	0.629	5.33	70	225	2755	4202	35.8	G
		C5-512	0.973	0.675	5.33	70	225	2758	4202	31.1	G
		C5-502	0.980	0.603	5.33	75	235	2878	4584	38.3	G
		C5-513	0.986	0.592	5.33	80	241	2933	4821	39.4	G
		C5-499	0.984	0.563	5.33	80	241	2939	4821	42.3	F(1)
		C5-514	0.978	0.553	5.33	85	248	3043	5105	43.5	F(1)

TABLE XI . HIGH STRAIN RATE JCTILITY RESULTS FOR PHASE II SPECIMENS (CONTINUED)

Material	Temp. °F	Specimen number	H <sub>0</sub> (In)	H <sub>f</sub> (In)	Proj. Weight (lbs.)	Chamber Pressure (PSI)	Velocity Ft/sec	Strain Rate In/In/Sec	K E Ft - lb	% Red.	Failure Mode
5Al-2.5Sn Titanium	1050	C5-511	0.986	0.504	5.33	90	255	3103	5397	48.9	F(1)
		C5-500	0.979	0.477	5.33	90	255	3126	5397	51.3	F(1)
		C5-498	0.984	0.415	5.33	100	265	3232	5829	57.8	F(1)
		C4-250	0.977	0.758	23.5	35	78	958	2221	22.4	G
		C4-251	0.973	0.616	23.5	60	110	1357	4417	36.7	G
		C5-390	0.980	0.559	23.5	70	120	1469	5256	43.0	G
		C5-391	0.983	0.586	23.5	75	125	1526	5703	40.4	F(1)
		C4-252	0.956	0.374	23.5	80	130	1632	6168	60.9	F(1)
		C5-450	0.983	0.616	64	60	64	781	4071	37.3	G
		C5-562	0.985	0.563	64	65	67	816	4462	42.8	F(1)
		C5-449	0.981	0.521	64	70	70	856	4871	46.9	F(1)
		C5-448	0.976	0.464	64	80	76	934	5741	52.5	F(1)
	1350	C5-531	0.984	0.625	5.33	60	210	2561	3660	36.5	G
		C5-532	0.979	0.488	5.33	80	241	2954	4821	50.2	F(1)
		C5-530	0.984	0.331	5.33	100	265	3232	5829	66.4	F(1)

TABLE VI. HIGH STRAIN RATE DUCTILITY RESULTS FOR PHASE II SPECIMENS (CONTINUED)

Material	Temp. ° F	Specimen number	H <sub>0</sub> (in)	H <sub>f</sub> (in)	Proj. Weight (lbs.)	Chamber Pressure (PSI)	Velocity Ft/sec	Strain Rate In/In/Sec	K E Ft - lb	% Red.	Failure Mode
5Al-2.5Sn Titanium	1350	C5-529	0.982	---	5.33	200	355	4338	10,460	---	F(1)
		C4-324	0.978	0.730	5.44	100	280	3436	6586	25.4	G
		C4-325	0.977	0.622	5.44	140	223	3967	8764	36.3	G
		C4-322	0.973	0.670	15.06	40	105	1295	2580	31.1	G
		C4-323	0.978	0.622	15.06	50	117	1436	3203	36.4	G
		C5-363	0.983	0.584	15.06	56	128	1563	3834	40.6	G
		C4-321	0.979	0.506	15.06	60	134	1643	4202	48.3	F(1)
		C4-320	0.984	0.225	15.06	100	176	2116	7248	77.1	F(1)
		C4-254	0.970	0.636	23.5	48	96	1188	3364	34.4	G
		C5-389	0.981	0.679	23.5	53	102	1248	3297	30.8	G
		C4-253	0.972	0.571	23.5	58	107	1321	4172	41.3	G
		C5-578	0.980	0.623	64	50	57	698	3230	36.4	G
		C5-579	0.983	0.561	64	60	64	781	4071	42.9	G
		C5-456	0.982	0.537	64	65	67	819	4462	45.2	F(1)
		C5-580	0.983	0.469	64	70	70	855	4871	52.3	F(1)

TABLE XI . HIGH STRAIN RATE DUCTILITY RESULTS FOR PHASE II SPECIMENS (CONTINUED)

Material	Temp. ° F	Specimen number	H <sub>0</sub> (In)	H <sub>f</sub> (In)	Proj. Weight (lbs.)	Chamber Pressure (PSI)	Velocity Ft/sec	Strain Rate In/In/Sec	K E Ft - lb	% Red.	Failure Mode
5Al-2.5Sn Titanium	1550	C5-518	0.933	0.697	5.33	40	170	2075	2399	29.1	G
		C5-517	0.978	0.630	5.33	50	190	2331	2996	35.6	G
		C5-519	0.980	0.595	5.33	55	200	2449	3320	39.3	G
		C5-516	0.981	0.540	5.33	60	210	2569	3660	45.0	F(1)
		C5-515	0.979	0.389	5.33	80	240	2942	4781	60.3	F(1)
		C5-370	0.982	0.582	15.06	60	134	1638	4202	40.7	G
		C5-376	0.984	0.554	15.06	66	142	1732	4718	44.7	G
		C5-375	0.978	0.512	15.06	70	147	1804	5057	47.7	F(1)
		C5-374	0.984	---	15.06	80	159	1939	5916	---	F(1)
		C5-372	0.980	0.385	15.06	90	168	2057	6604	60.7	F(1)(2)
		C5-371	0.980	0.350	15.06	100	177	2167	7331	64.3	F(1)(2)
		C5-571	0.979	0.512	64	50	57	699	3230	47.7	G
		C5-570	0.982	0.487	64	60	64	782	4071	50.4	F(1)(2)
		C5-569	0.982	---	64	100	86	1051	7352	---	F(1)(2)
	1750	C5-575	0.975	0.485	5.33	60	210	2585	3660	50.3	G



TABLE VI . HIGH STRAIN RATE DUCTILITY RESULTS FOR PHASE II SPECIMENS (CONTINUED)

Material	Temp. ° F	Specimen number	H <sub>0</sub> (in)	H <sub>f</sub> (in)	Proj. Weight (lbs.)	Chamber Pressure (PSI)	Velocity Ft/sec	Strain Rate In/In/Sec	K E Ft - lb	% Red.	Failure Mode
5Al-2.5Sn Titanium	1750	C5-577	0.975	0.485	5.33	60	210	2948	3660	50.3	G
		C5-620	0.981	0.309	5.33	85	248	3034	5105	59.4	IF(2,3)
		C5-622	0.980	0.254	5.33	90	254	3110	5355	74.1	F(2)
		C5-576	0.980	0.370	5.33	100	265	3245	5829	62.2	IF(3)
		C5-621	0.979	0.221	5.33	105	272	3334	6141	77.4	F(2)
		C5-619	0.980	0.385	15.06	60	135	1653	4265	60.7	G
		C5-618	0.978	0.241	15.06	80	158	1939	5842	75.4	F(2)
		C5-617	0.980	0.154	15.06	100	177	2167	7331	84.3	F(1)
		C5-584	0.981	0.448	18.0	70	135	1651	5094	54.3	G
		C5-585	0.983	0.375	18.0	80	145	1770	5876	61.9	G
		C5-586	0.984	0.323	18.0	90	155	1890	6715	67.2	F(1)
		C5-583	0.974	0.428	64	60	64	789	4071	56.1	G
		C5-581	0.981	0.306	54	70	70	856	4871	68.8	G
		C5-582	0.980	0.290	64	80	76	931	5741	70.4	F(1)(2)
		C5-623	0.977	0.225	64	100	86	1056	7352	77.0	G

TABLE XI . HIGH STRAIN RATE DUCTILITY RESULTS FOR PHASE II SPECIMENS (CONTINUED)

Material	Temp. °F	Specimen number	H <sub>0</sub> (In)	H <sub>f</sub> (In)	Proj. Weight (lbs.)	Chamber Pressure (PSI)	Velocity Ft/sec	Strain Rate In/In/Sec	K F Ft - lb	% Red	Failure Mode
5Al-2.5Sn Titanium	1750	C5-623	0.979	0.124	64	110	91	1115	8231	87.3	IF(2)
		C5-624	0.981	0.100	64	120	95	1162	8971	89.8	F(2)
		C5-606	0.981	0.436	5.33	30	142	1737	1674	55.6	G
		C5-607	0.978	0.193	5.33	60	210	2577	3660	80.3	G
	1950	C5-608	0.982	0.098	5.33	90	254	3104	5355	90.0	F(1)
		C5-609	0.973	0.075	5.33	120	287	3540	6837	92.2	F(1)
		C5-610	0.976	0.070	5.33	150	315	3873	8236	92.8	F(1)
		C5-611	0.982	0.047	5.33	160	324	3959	8713	95.2	F(1)
		C5-602	0.983	0.100	15.06	90	168	2051	6604	89.8	G
		C5-604	0.980	0.054	15.06	100	177	2167	7331	93.5	IF(2)
		C5-603	0.979	0.053	15.06	110	185	2268	8009	94.6	F(2)
		C5-605	0.984	0.049	15.06	110	185	2256	8009	95.0	F(2)
		C5-601	0.980	---	15.06	120	193	2363	8716	---	F(2)
		C5-649	0.980	0.068	64	100	86	1053	7352	93.1	G
		C5-652	0.980	0.065	64	110	91	1114	8231	93.4	G

TABLE VI. HIGH STRAIN RATE DUCTILITY RESULTS FOR PHASE II SPECIMENS (CONTINUED)

Material	Temp. ° F	Specimen number	H <sub>C</sub> (In)	H <sub>F</sub> (In)	Proj. Weight (lbs.)	Chamber Pressure (PSI)	Velocity Ft/sec	Strain Rate In/In/Sec	K E Ft - lb	% Red.	Failure Mode
5Al-2.5Sn Titanium	1950	C5-651	0.976	0.042	64	120	96	1180	9161	95.7	F(1)
		C5-595	0.981	0.010	64	130	100	1223	9940	95.9	F(1)
		C5-650	0.979	0.024	64	140	103	1263	10,545	97.6	F(1)
17-4 PH Stainless Steel	550	E5-480	0.981	0.342	5.33	140	306	3743	7772	65.2	IF(3)
		E5-479	0.982	0.250	5.33	180	340	4155	9595	74.5	F(3)
		E5-478	0.980	0.219	5.33	230	377	4616	11,797	77.7	F(3)(1)
		E5-481	0.980	0.165	5.33	280	410	5020	13,952	83.1	F(3)(1)
		E5-466	0.973	0.414	15.06	100	177	2183	7300	57.5	G
		E5-467	0.981	0.281	15.06	130	200	2447	9320	71.4	G
		E5-468	0.983	0.231	15.06	160	219	2673	11,175	76.5	IF(2)
		E5-469	0.979	0.101	15.06	200	241	2954	13,533	80.5	IF(2)
		E5-461	0.983	0.225	64	140	103	1257	10,545	77.1	G
		E5-457	0.980	0.247	64	160	112	1371	12,469	74.8	G
17-4		E5-475	0.977	0.227	64	160	112	1376	12,469	76.8	G
		E5-460	0.981	0.213	64	180	118	1443	13,840	78.3	IF(2)

TABLE XI . HIGH STRAIN RATE DUCTILITY RESULTS FOR PHASE II SPECIMENS (CONTINUED)

Material	Temp. ° F	Specimen number	H <sub>0</sub> (In)	H <sub>f</sub> (In)	Proj. Weight (lbs.)	Chamber Pressure (FSI)	Velocity Ft/sec	Strain Rate In/In/Sec	K.E. Ft - lb	% Red.	Failure Mode
17-4 PH Stainless Steel	550	E5-459	0.984	0.192	64	200	125	1524	15,531	80.5	IF(2)
		E5-458	0.986	0.142	64	240	137	1667	18,656	85.6	F(2)
		E5-476	0.979	0.128	64	240	137	1679	18,656	86.9	IF(2)
	950	E5-493	0.985	0.451	5.33	100	265	3228	5829	54.2	G
		E5-492	0.979	0.279	5.33	150	315	3861	8236	71.5	IF(3)
		E5-491	0.979	0.203	5.33	200	355	4351	10,460	79.3	F(3)
		E5-490	0.982	0.165	5.33	250	390	4766	12,624	83.2	F(1)
		E5-489	0.982	0.109	5.33	300	420	5132	14,641	88.9	F(1)
		E5-488	0.983	0.108	5.33	360	450	5493	16,808	89.0	F(1)
		E5-436	0.972	0.445	15.06	84	163	2012	6217	54.2	G
		E5-437	0.981	0.234	15.06	160	218	2668	11,121	76.2	G
		E5-438	0.983	0.137	15.06	220	251	3064	14,742	86.1	G
		E5-440	0.978	0.110	15.06	230	254	3117	15,097	88.8	F(1)(3)
		E5-439	0.983	0.120	15.06	240	256	3125	15,335	87.8	IF(1)
	1350	E5-524	0.979	0.322	5.33	100	265	3248	5829	67.1	G

TABLE VI HIGH STRAIN RATE DUCTILITY RESULTS FOR PHASE II SPECIMENS (CONTINUED)

Material	Temp. ° F	Specimen number	H <sub>0</sub> (in)	H <sub>f</sub> (in)	Proj. Weight (lbs.)	Chamber Pressure (PSI)	Velocity Ft/sec	Strain Rate In/In/Sec	K E Ft - lb	% Red	Failure Mode
17-4 PH Stainless Steel	1350	E5-523	0.978	0.204	5.33	150	315	3865	8236	79.1	IF(3)
		E5-522	0.982	0.125	5.33	210	363	4436	10,937	87.3	F(3)(1)
		E5-521	0.980	0.095	5.33	250	390	4776	12,624	90.2	F(3)(1)
		E5-520	0.979	0.076	5.33	300	420	5148	14,641	92.2	F(3)(1)
		E5-470	0.987	0.179	15.06	130	200	2432	9360	81.9	G
		E5-469	0.978	0.132	15.06	160	220	2699	11,326	86.5	F(1)
		E5-443	0.976	0.094	15.06	180	230	2828	12,379	90.4	F(1)
		E5-442	0.980	0.078	15.06	220	253	3098	14,978	92.0	F(1)
		E5-441	0.981	0.073	15.06	240	260	3180	15,818	92.6	F(1)
		E5-453	0.980	0.251	64	100	86	1053	7352	74.4	G
		E5-454	0.980	0.173	64	130	98	1200	9546	82.4	G
		E5-455	0.979	0.157	64	150	107	1312	11,380	84.6	G
		E5-451	0.986	0.132	64	160	111	1351	12,247	86.6	F(1)
		E5-452	0.979	0.102	64	200	125	1532	15,531	89.6	F(1)(2)
	1550	E5-528	0.980	0.254	5.33	100	265	3245	5829	74.1	IF(3)

TABLE XI . HIGH STRAIN RATE DUCTILITY RESULTS FOR PHASE II SPECIMENS (CONTINUED)

Material	Temp. °F	Specimen number	H <sub>0</sub> (In)	H <sub>f</sub> (In)	Proj. Weight (lbs.)	Chamber Pressure (PSI)	Velocity Ft/sec	Strain Rate In/In/Sec	K E Ft - lb	% Red.	Failure Mode
17-4 PH Stainless Steel	1550	E5-525	0.976	0.186	5.33	150	315	3873	8236	80.9	F(3)
		E5-526	0.978	0.102	5.33	200	355	4356	10,460	89.5	F(3)(1)
		E5-527	0.983	0.081	5.33	250	390	4761	12,624	91.8	F(1)
		E5-473	0.981	0.232	15.06	100	176	2153	7248	76.4	G
		E5-471	0.980	0.188	15.06	120	192	2351	8626	80.8	G
		E5-472	0.982	0.121	15.06	140	206	2517	9930	87.7	IF (1)(2)
		E5-474	0.981	0.077	15.06	180	230	2814	12,379	92.2	IF(1)
		E5-644	0.980	0.282	5.33	80	241	2951	4821	71.2	G
	1750	E5-643	0.979	0.219	5.33	100	265	3248	5829	77.6	IF(3)
		E5-542	0.978	0.161	5.33	120	287	3522	6837	82.5	IF(3)
		E5-589	0.981	0.189	18	100	163	1994	7426	80.7	G
		E5-590	0.980	0.127	18	120	179	2192	8955	87.0	F(1)
		E5-588	0.979	0.096	18	140	193	2366	10,411	92.2	F(1)
		E5-587	0.981	----	18	200	226	2765	14,276	----	F(1)
	1950	E5-612	0.982	0.143	5.33	120	287	3507	6837	85.4	G

TABLE XI . HIGH STRAIN RATE DUCTILITY RESULTS FOR PHASE II SPECIMENS (CONTINUED)

Material	Temp. ° F	Specimen number	H <sub>0</sub> (In)	H <sub>f</sub> (In)	Proj. Weight (lbs.)	Chamber Pressure (PSI)	Velocity Ft/sec	Strain Rate In/In/Sec	K E Ft - lb	% Red.	Failure Mode
17-4 PH Stainless Steel	1950	E5-613	0.983	0.086	5.33	150	315	3845	8236	91.3	F(3)
		E5-614	0.980	0.080	5.33	160	324	3967	8713	91.8	F(1)
		E5-600	0.981	0.123	15.06	110	185	2263	8009	87.5	G
		E5-598	0.982	0.094	15.06	120	193	2358	8716	90.4	IF(2)
		E5-599	0.981	0.098	15.06	130	200	2446	9360	90.0	IF(3)
		E5-597	0.980	0.073	15.06	140	206	2522	9930	92.6	IF(3)
		E5-592	0.979	0.101	64	120	95	1165	8971	89.7	G
		E5-615	0.976	0.093	64	120	95	1168	8971	90.5	G
		E5-596	0.982	0.075	64	130	99	1209	9742	92.4	IF(1)
		E5-594	0.981	0.073	64	140	103	1260	10,545	92.6	IF(1)
		E5-616	0.977	0.067	64	140	103	1265	10,545	93.1	G
		E5-593	0.980	0.063	64	150	108	1322	11,594	93.6	F(1)
A-286 Steel	Ambient	E5-591	0.979	0.045	64	180	118	1446	13,840	95.4	F(1)
		F5-504	0.979	0.542	5.33	100	265	3248	5829	44.6	G
		F5-505	0.976	0.499	5.33	120	287	3528	6837	48.9	G

TABLE XI . HIGH STRAIN RATE DUCTILITY RESULTS FOR PHASE II SPECIMENS (CONTINUED)

Material	Temp. °F	Specimen Number	H <sub>0</sub> (In)	H <sub>f</sub> (In)	Proj. Weight (lbs.)	Chamber Pressure (PSI)	Velocity Ft/sec	Strain Rate In/In/Sec	K E Ft - lb	% Red.	Failure Mode
A-286 Steel	Ambient	F5-505	0.983	0.474	5.33	130	296	3613	7272	51.8	G
		F5-503	0.979	0.423	5.33	140	306	3750	7772	56.8	F(1)
		F4-258	0.983	0.756	23.5	35	78	952	2221	23.1	G
		F4-259	0.981	0.682	23.5	50	98	1199	3505	30.5	G
		F4-260	0.981	0.632	23.5	60	110	1346	4417	35.6	G
		F4-261	0.985	0.504	23.5	70	120	1462	5256	38.7	G
		F4-262	0.976	0.569	23.5	75	125	1537	5703	41.7	G
		F4-263	0.978	0.552	23.5	80	130	1595	6169	43.6	G
		F4-264	0.978	0.518	23.5	90	139	1706	7052	47.0	G
		F4-265	0.982	0.506	23.5	100	147	1796	7887	48.5	G
		F4-266	0.978	0.440	23.5	120	160	1963	9344	55.0	G
		F5-393	0.978	0.478	23.5	125	164	2012	9817	51.1	G
		F5-392	0.977	0.348	23.5	130	168	2064	10,302	64.4	F(1)
		F4-268	0.980	0.337	23.5	140	174	2131	11,051	65.6	F(1)
		F4-267	0.980	0.286	23.5	160	185	2265	12,492	70.8	F(1)



TABLE VI. HIGH STRAIN RATE DUCTILITY RESULTS FOR PHASE II SPECIMENS (CONTINUED)

Material	Temp. ° F	Specimen number	H <sub>0</sub> (in)	H <sub>f</sub> (in)	Proj. Weight (lbs.)	Chamber Pressure (PSI)	Velocity Ft/sec	Strain Rate in/in/Sec	K E Ft - lb	% Red.	Failure Mode
A-286 Steel	Ambient	F5-412	0.978	0.538	64	100	86	1055	7352	45.0	G
		F5-573	0.980	0.461	64	110	91	1114	8231	53.0	G
		F5-552	0.979	0.431	64	120	96	1177	9161	55.9	G
		F5-572	0.977	0.408	64	120	96	1179	9161	58.2	F(1)
		F5-553	0.982	0.396	64	130	99.5	1216	9841	59.7	G
		F5-555	0.977	0.325	64	135	101	1241	10,140	66.7	F(1)
		F5-413	0.981	0.341	64	140	103	1260	10,545	65.2	F(1)
		F5-554	0.981	0.312	64	140	103	1260	10,545	68.2	F(1)(2)
		F5-485	0.982	0.328	5.33	160	324	3959	8713	66.6	G
		F5-484	0.984	0.268	5.33	210	363	4427	10,937	72.8	F(3)
	550	F5-483	0.979	0.225	5.33	260	396	4854	13,046	76.2	F(3)
		F5-482	0.985	0.184	5.33	310	425	5178	14,992	81.3	F(3)(1)
		F5-355	0.975	0.846	15.06	20	72	879	1213	13.2	G
		F5-354	0.981	0.608	15.06	50	119	1451	3314	38.0	G
		F5-345	0.975	0.419	15.06	120	191	2350	8537	57.0	G

TABLE XI . HIGH STRAIN RATE DUCTILITY RESULTS FOR PHASE II SPECIMENS (CONTINUED)

Material	Temp. ° F.	Specimen number	H <sub>0</sub> (In)	H <sub>f</sub> (In)	Proj. Weight (lbs.)	Chamber Pressure (PSI)	Velocity Ft/sec	Strain Rate In/In/Sec	K.E. Ft - lb	% Red.	Failure Mode
A-286 Steel	550	F5-340	0.977	0.327	15.06	150	204	2506	9738	66.5	G
		F5-347	0.977	0.262	15.06	180	229	2813	12,271	73.2	G
		F5-348	0.983	0.249	15.06	220	250	3052	14,625	74.7	G
		F5-349	0.983	0.200	15.06	260	269	3284	16,932	79.7	G
		F5-433	0.973	0.174	15.06	290	281	3466	18,477	82.1	G
		F5-432	0.975	0.148	15.06	300	284	3495	18,874	84.8	IF(3)
		F5-431	0.982	0.163	15.06	310	288	3519	19,409	83.4	IF(3)
		F5-430	0.982	0.158	15.06	320	291	3556	19,815	83.9	IF(3) (3)
		F5-350	0.979	0.141	15.06	320	291	3567	19,815	85.6	IF(1)
		F5-424	0.982	0.150	15.06	330	295	3605	20,364	84.7	F(3)
		F5-351	0.983	0.127	15.06	340	299	3650	20,920	87.1	F(3)(1)
		F5-428	0.980	0.144	15.06	340	299	3661	20,920	85.3	F(1)
		F5-352	0.984	0.108	15.06	380	311	3793	22633	89.0	F(1)
		F5-566	0.981	0.300	64	140	103	1260	10,545	69.4	G
		F5-567	0.981	0.264	64	160	112	1370	12,469	73.1	G

TABLE XI . HIGH STRAIN RATE DUCTILITY RESULTS FOR PHASE II SPECIMENS (CONTINUED)

Material	Temp. °F	Specimen number	H <sub>0</sub> (In)	H <sub>f</sub> (In)	Proj. Weight (lbs.)	Chamber Pressure (PSI)	Velocity Ft/sec	Strain Rate In/In/Sec	K E Ft - lb	% Red.	Failure Mode
A-28, Steel	550	F5-558	0.977	0.245	64	170	115	1413	13,145	74.9	G
		F5-464	0.974	0.213	64	180	118	1454	13,840	77.5	G
		F5-477	0.979	0.197	64	200	125	1532	15,531	79.9	G
		F5-462	0.985	0.141	64	260	142	1730	20,043	85.7	IF(1)
		F5-535	0.971	0.348	5.33	150	315	3893	8236	64.2	G
	750	F5-536	0.981	0.274	5.33	200	355	4343	10,460	72.1	(3) IF(1)
		F5-539	0.980	0.226	5.33	240	382	4678	12,112	76.9	F(3)
		F5-538	0.976	0.195	5.33	270	400	4918	13,280	80.0	F(3)
		F5-537	0.980	0.166	5.33	300	420	5143	14,641	83.1	F(3)(1)
		F5-431	0.980	0.727	15.06	52	125	1531	3656	25.8	G
		F5-435	0.982	0.684	15.06	70	145	1772	4920	30.4	G
		F4-271	0.981	0.475	23.5	80	130	1590	6169	51.6	G
		F4-269	0.977	0.338	23.5	120	160	1965	9344	65.4	G
		F5-394	0.981	0.288	23.5	130	171	2092	10,673	70.6	G
		F4-270	0.981	0.268	23.5	140	174	2128	11,051	72.7	IF(2)

TABLE XI . HIGH STRAIN RATE DUCTILITY RESULTS FOR PHASE II SPECIMENS (CONTINUED)

Material	Temp. ° F	Specimen number	H <sub>0</sub> (In)	H <sub>f</sub> (In)	Proj. Weight (lbs.)	Chamber Pressure (PSI)	Velocity Ft/sec	Strain Rate In/In/Sec	K E. Ft - lb	% Red.	Failure Mode
A-286 Steel	750	F7-665	0.981	0.290	64	140	103	1260	10,545	70.4	G
		F7-666	0.981	0.213	64	180	118	1443	13,840	78.3	G
		F7-667	0.977	0.169	64	220	131	1609	17,058	82.7	IF(1)
		F7-668	0.979	0.132	64	260	142	1741	20,043	86.5	IF(1)
		F7-669	0.982	0.114	64	280	147	1796	21,479	88.4	IF(1)
		F5-496	0.985	0.311	5.33	160	325	3559	8767	68.4	G
	950	F5-497	0.984	0.242	5.33	200	355	4329	10,460	75.4	IF(3)
		F5-498	0.977	0.201	5.33	240	382	4692	12,112	79.4	F(1)(3)
		F5-494	0.980	0.129	5.33	340	440	5388	16,069	86.8	F(1)(3)
		F5-356	0.980	0.450	15.06	100	176	2155	7248	54.1	G
		F5-357	0.978	0.288	15.06	160	219	2687	11,223	70.6	G
		F5-353	0.985	0.232	15.06	200	239	2912	13,366	76.5	G
		F5-358	0.982	0.194	15.06	240	258	3153	15,576	80.2	G
		F5-359	0.985	0.130	15.06	260	273	3326	17,440	86.8	G
		F5-360	0.980	0.122	15.06	270	276	3367	17,825	87.6	IF(1)

TABLE XI . HIGH STRAIN RATE DUCTILITY RESULTS FOR PHASE II SPECIMENS (CONTINUED)

Material	Temp. ° F	Specimen number	H <sub>0</sub> (In)	H <sub>f</sub> (In)	Proj. Weight (lbs.)	Chamber Pressure (PSI)	Velocity Ft/sec	Strain Rate In/In/Sec	K E Ft - lb	% Red.	Failure Mode
A-286 Steel	950	F5-361	0.977	0.102	15.06	280	282	3525	18,609	89.6	F(1)
		F5-363	0.982	0.333	64	120	95	1161	8971	66.1	G
		F5-364	0.975	0.185	64	200	125	1539	15,531	81.0	G
		F5-365	0.981	0.136	64	240	137	1676	18,656	86.1	F(1)
		F4-277	0.978	0.548	23.5	60	110	1350	4417	44.0	G
	1050	F4-278	0.977	0.445	23.5	80	130	1597	6169	54.5	G
		F4-299	0.980	0.408	23.5	90	139	1702	7052	58.4	G
		F5-300	0.972	0.338	23.5	110	152	1877	8433	65.2	G
		F5-396	0.984	0.324	23.5	150	179	2183	11,695	67.1	G
		F5-397	0.982	0.191	23.5	190	199	2432	144,454	89.6	F(1)(2)
		F5-398	0.982	0.221	23.5	200	204	2493	15,190	77.5	G
		F5-399	0.983	0.160	23.5	220	213	2600	15,560	83.7	IF(1)
		F5-400	0.982	0.182	23.5	240	221	2700	17,827	81.5	IF(1)
		F5-401	0.983	0.163	23.5	160	229	2796	19,141	83.4	IF(1)
		F5-402	0.981	0.125	23.5	280	236	2887	20,329	87.3	IF(1)

TABLE VI. HIGH STRAIN RATE UTILITY RESULTS FOR PHASE II SPECIMENS (CONTINUED)

Material	Temp. ° F.	Specimen number	H <sub>0</sub> (in)	H <sub>f</sub> (in)	Proj. Weight (lbs.)	Chamber Pressure (PSI)	Velocity Ft/sec	Strain Rate In/In/Sec	K E Ft - lb	% Red.	Failure Mode
A-286 Steel	1050	F5-403	0.981	0.134	23.5	300	243	2973	21,553	86.3	IF(1)
		F5-542	0.979	0.300	5.33	140	305	3750	7772	69.4	IF(3)
		F5-547	0.976	0.264	5.33	160	324	3984	8713	73.0	IF(1)
		F5-546	0.982	0.192	5.33	200	355	4338	10,460	80.5	F(3)(1)
		F5-414	0.979	0.591	15.06	70	146	179-	4988	39.0	G
		F5-416	0.981	0.561	15.06	75	151	1847	5335	42.8	G
		F5-415	0.981	0.525	15.06	80	155	1896	5622	46.5	F(1)
		F4-255	0.989	0.559	23.5	50	98	1189	3505	33.4	G
		F4-256	0.977	0.562	23.5	60	110	1351	4416	42.5	G
		F5-404	0.975	0.507	23.5	65	115	1414	4827	37.8	G
		F5-257	0.977	0.528	23.5	70	120	1474	5256	46.0	F(1)
		F7-658	0.982	0.524	64	60	64	782	4071	46.6	G
		F7-659	0.985	0.507	64	70	70	852	4871	48.6	G
		F7-657	0.977	0.401	64	80	76	934	5741	59.0	F(1)
	1550	F5-545	0.981	0.243	5.33	160	324	3963	8713	75.2	IF(3)

TABLE XI . HIGH STRAIN RATE DUCTILITY RESULTS FOR PHASE II SPECIMENS (CONTINUED)

Material	Temp. ° F	Specimen number	H <sub>o</sub> (In)	H <sub>f</sub> (In)	Proj. Weight (lbs.)	Chamber Pressure (PSI)	Velocity Ft/sec	Strain Rate In/In/Sec	K E Ft - lb	% Red.	Failure Mode
A-286 Steel	1550	F5-544	0.979	0.157	5.33	200	355	4351	10,460	82.9	F(3)
		F5-543	0.973	0.123	5.33	240	382	4711	12,112	87.4	F(3)(1)
		F5-377	0.981	0.560	15.06	60	134	1631	4202	43.0	G
		F5-378	0.983	0.390	15.06	100	176	2149	7248	60.3	G
		F5-375	0.985	0.238	15.06	140	204	2485	9738	75.8	G
		F5-380	0.981	0.205	15.06	180	229	2801	12,271	79.1	G
		F5-383	0.982	0.173	15.06	200	240	2933	13,478	82.4	G
		F5-382	0.980	0.150	15.06	210	245	3000	14,046	84.7	F(1)
		F5-381	0.986	0.104	15.06	220	250	3043	14,625	89.5	F(1)
		F5-653	0.985	0.156	64	160	111	1325	12,247	84.2	G
		F5-654	0.979	0.099	64	220	131	1606	17,058	89.9	F(1)
		F5-655	0.982	0.070	64	260	142	1735	20,043	92.9	F(1)
		F5-656	0.978	0.065	64	280	147	1804	21,479	93.4	F(1)
		F7-640	0.978	0.356	5.33	80	241	2957	4821	63.6	G
	1750	F7-641	0.983	0.370	5.33	90	254	3100	5355	62.4	G

TABLE II. HIGH STRAIN RATE DUCTILITY RESULTS FOR PHASE II SPECIMENS (CONTINUED)

Material	Temp. °F	Specimen number	H <sub>0</sub> (In)	H <sub>f</sub> (In)	Proj. Weight (lbs.)	Chamber Pressure (PSI)	Velocity Ft/sec	Strain Rate In/In/Sec	K E Ft - lb	% Red.	Failure Mode
A-36 Steel	1750	F7-11	0.074	0.088	5.33	100	265	3248	5829	70.5	IF(3)
		F7-12	0.082	0.092	5.33	120	287	3507	5837	76.4	F(3)
		F7-13	0.081	0.109	15.06	140	206	2520	9930	83.8	G
		F7-14	0.067	0.119	15.06	160	220	2675	11,326	87.9	F(1)
		F7-15	0.060	0.110	15.06	180	231	2829	12,486	88.8	F(1)
		F7-16	0.084	0.089	15.06	200	241	2942	13,591	91.0	F(1)
		F7-17	0.081	0.107	54	160	112	1370	12,469	89.1	G
		F7-18	0.081	0.086	64	200	125	1529	15,531	91.2	G
		F7-19	0.083	0.080	64	220	131	1599	17,058	91.9	IF(1)
		F7-20	0.089	0.099	64	240	137	1672	18,656	94.0	F(1)
	1950	F7-21	0.080	0.347	5.33	80	241	2951	4821	64.6	G
		F7-22	0.099	0.217	5.33	90	255	3125	5397	67.6	G
		F7-23	0.081	0.296	5.33	100	265	3242	5829	72.0	IF(2)
		F7-24	0.080	0.176	5.33	120	287	3514	6837	82.0	F(2)
		F7-25	0.083	0.199	15.06	110	185	2258	8009	80.2	G



TABLE 1. HIGH STRAIN RATE DUCTILITY RESULTS FOR PHASE II SPECIMENS (CONTINUED)

Material	Temp. °F	Specimen number	H <sub>0</sub> (in)	H <sub>f</sub> (in)	Proj. Weight (lbs.)	Chamber Pressure (PSI)	Velocity Ft/sec	Strain Rate In/In/Sec	K.E. Ft - lb	% Red.	Failure Mode
A-286 Steel	1950	F7-636	0.978	0.165	15.06	120	193	2368	8716	83.1	IF(3)
		F7-635	0.981	0.113	15.06	140	206	2520	9930	88.5	F(1)
		F7-634	0.983	0.091	15.06	160	220	2686	11,326	90.7	F(2)
		F7-648	0.985	0.099	64	160	112	1365	12,469	90.0	G
		F7-645	0.980	0.089	64	160	112	1371	12,469	90.9	G
		F7-647	0.978	0.066	64	180	116	1743	13,840	93.3	F(2)
		F7-646	0.973	0.061	64	200	125	1542	15,531	93.7	F(2)

TABLE XII. PHASE II TENSILE PROPERTIES OF FORGED SPECIMENS

Material	Temp. °F	Specimen Number	% Red.	Tensile Yield ( $S_{ty}$ )	Tensile Ultimate ( $S_{tu}$ )	$\frac{1}{2}$ Elong. 1" Gage Length	Hardness Ra	Strain Rate (in/in/sec)
2024-0 Aluminum	Ambient	A6-93	46.0	40,400	43,600	4.0	31	166
		A6-42	43.5	38,000	42,100	4.0	29	185
		A10-29	50.0	40,500	44,300	5.0	31.5	3590
		A10-35	51.6	40,400	44,300	4.0	29.5	3590
		A6-82	49.9	41,700	45,257	4.0	--	3660
		A6-115	49.2	40,200	45,334	5.0	--	3660
		A10-40	48.8	40,200	42,900	5.0	29.5	6650
		A10-50	46.2	41,200	45,400	4.0	27.0	6650
		A6-35	50.2	40,500	45,239	4.0	--	7380
		A6-86	50.3	41,900	46,720	5.0	--	7380
2024-0 Aluminum	550°	A10-6	48.6	32,400	38,400	8.0	30.5	222
		A10-14	50.2	28,300	37,000	8.0	27.0	223
		A6-54	50.6	30,800	41,600	12.0	--	1970
		A6-109	49.0	32,000	42,100	12.0	--	1970
		A6-114	49.5	30,400	40,800	11.0	--	1970
		A10-64	49.4	30,400	36,700	7.0	29.0	6210
		A10-73	48.7	28,200	35,400	9.0	29.0	6210

TABLE XII. PHASE II TENSILE PROPERTIES OF FORGED SPECIMENS (CONT'D.)

Material	Temp. ° F	Specimen Number	% Red.	Tensile Yield ( $St_y$ )	Tensile Ultimate ( $St_u$ )	% Elong. 1" Gage Length	Hardness	Strain Rate (in/in/sec)
2024-0 Aluminum	750°	A10-13	48.9	41,700	51,200	9.0	37.0 Ra	240
		A6-36	47.5	18,000	46,600	15.0	33.0 Ra	230
		A6-23	49.4	31,000	45,950	12.0	--	1970
		A6-116	49.8	33,200	50,440	14.0	--	1970
5Al-2.5Sn Titanium	1550°	C6-95	25.0	126,700	139,900	10.0	--	235
		C6-118	25.4	125,100	140,400	12.0	--	240
		C6-38	25.0	125,000	140,100	12.0	--	2910
		C6-93	26.0	127,800	140,500	12.0	--	2910
		C6-1	23.4	130,000	137,500	17.0	37.0 Rc	5840
		C6-20	23.7	126,800	138,300	15.0	33.0 Rc	5840
5Al-2.5Sn Titanium	1950°	C6-22	23.3	128,900	136,900	17.0	35.5 Rc	5840
		C6-71	26.4	103,600	136,800	13.0	35.5 Rc	6220
		C6-80	27.6	122,700	139,200	12.0	33.0 Rc	236
		C6-117	26.7	117,400	138,700	12.5	33.0 Rc	210
		C6-111	23.7	119,200	135,300	10.0	32.0 Rc	2300
		C6-113	23.7	119,100	136,800	13.0	33.0 Rc	2300
		C6-119	23.5	120,700	136,900	11.0	31.0 Rc	5200

TABLE XII. FIGURE 17 TENSILE PROPERTIES OF FORGED SPECIMENS (CONT'D)

Material	Temp. °F.	Specimen Number	% Red.	Tensile Yield ( $S_{ty}$ )	Tensile Ultimate ( $S_{tu}$ )	% Elong. 1" Gage Length	Hardness Rc	Strain Rate (in/in/sec)
Titanium	1950°	CE-121	24.6	112,400	135,000	10.5	30.5	5200
17-4 PH Stainless Steel	1550°	E6-42	39.6	134,900	165,100	10.0	36.5	3310
		E6-37	40.4	133,600	160,400	10.0	36.0	3310
		E6-55	38.1	125,000	165,500	10.0	36.5	6440
		E6-58	37.5	122,400	158,200	10.0	34.0	6440
		E6-30	39.7	116,700	166,700	12.0	32.5	256
17-4 PH Stainless Steel	1950°	E1-566	39.3	124,300	155,800	9.0	--	3310
		E6-13	42.9	134,800	168,700	11.5	34.5	3460
		E6-121	43.3	127,000	169,900	11.5	37.0	3460
		E1-554	40.3	128,300	165,200	10.0	36.0	7020
		E1-556	39.8	125,300	163,500	10.0	37.0	7020
17-4 PH Stainless Steel (Heat Treated)	1950°	E1-579	38.5	169,000	188,000	11.0	37.0	3320
		E1-583	38.9	164,000	191,000	13.0	42.5	3320
		E1-609	As Received	166,000	189,000	13.0	43.0	--
		E6-1	42.9	172,000	193,000	12.0	43.0	263
		E6-6	41.4	166,000	193,000	12.0	43.5	260
		E6-17	40.9	171,000	194,000	14.0	41.5	260

TABLE XII. FIGURE II TENSILE PROPERTIES OF FORGED SPECIMENS (CONT'D)

Material	Temp. ° F	Specimen Number	% Red. AS Received	Tensile Yield ( $S_{ty}$ )	Tensile Ultimate ( $S_{tu}$ )	% Elong. 1" Gage Length	Hardness Rc	Strain Rate (in./in./sec)
17-4 PH Stainless Steel (Heat Treated)	1950°	E6-19	Received	164,000	193,000	12.0	37.5	--
		E6-48	39.6	165,000	194,000	12.0	42.0	5700
		E6-56	40.3	172,000	193,000	10.0	44.0	5700
A-286 Steel	1950°	F6-18	48.5	126,100	151,000	9.4	--	265
		F6-77	51.6	127,100	141,200	9.0	--	250
		F6-2	49.6	134,500	143,500	9.0	--	4090
		F6-116	48.3	133,100	145,100	9.0	--	4090
		F6-33	49.0	128,400	139,680	11.0	--	8390
		F6-34	48.7	131,000	140,619	12.0	--	8390
		F6-39	48.9	121,600	135,627	10.0	--	8390
		F6-40	49.3	124,300	139,618	11.0	--	8390
A-286 Steel (Heat Treated)	1950°	F9-15	50.9	93,000	153,000	22.0	30.0	3910
		F9-21	48.3	95,000	147,000	25.0	29.0	240
		F9-26	48.8	103,000	152,000	23.0	32.0	6890
		F9-37	48.2	104,000	154,000	25.0	33.0	6880
		F9-40	48.3	97,000	153,000	24.0	31.0	240
		F9-42	48.9	93,000	144,000	23.0	29.0	3910

TABLE XII. TABLE II TENSILE PROPERTIES OF FORGED SPECIMENS (CONT'D)

Material	Temp. °F	Specimen Number	% Red	Tensile Yield (St <sub>y</sub> )	Tensile Ultimate (St <sub>u</sub> )	% Elong. 1" Gage Length	Hardness Rc	Strain Rate (in/in/sec)
A-286 Steel	1050°	P6-20	47.3	77,900	104,300	23.0	21.0	230
		P6-7	47.7	91,600	113,500	20.0	22.0	235
		P6-19	50.2	73,900	107,000	27.0	--	3920
		P6-26	47.7	68,900	108,000	29.0	--	3920
		P6-31	47.2	65,400	103,600	26.0	--	7860
		P6-67	47.3	46,700	95,800	41.0	--	7860
		P6-102	43.1	45,500	95,500	38.0	--	7860
		P6-113	46.6	58,500	101,200	38.0	--	7860

TABLE XIII. FATIGUE DATA FOR STATIC AND DYNAMIC FORCED TEST SPECIMENS

Material	Temp. °F	Specimen Number	Ave St <sub>U</sub>	% Red.	Strain Rate In./In./Sec	Stress Level (% St <sub>U</sub> )	Cycles to Failure (1000's)	Hardness R <sub>C</sub>
2024-0 Aluminum	Ambient	AlO-19	44.7	42.9	206	88	80	---
		AlO-7	44.7	46.5	230	88	107	---
		AlO-11	44.7	46.6	235	88	97	---
		AlO-34	44.7	52.4	3560	88	75	---
		AlO-20	44.7	51.4	3700	88	87	---
		AlO-23	44.7	52.2	3718	88	177	---
		AlO-42	44.7	52.6	6520	88	152	---
		AlO-38	44.7	48.6	6630	88	96	---
		AlO-37	44.7	40.7	6640	88	127	---
		AlO-10	38.4	49.2	222	88	93	---
2024-0 Aluminum	550	AlO-5	38.4	49.3	224	88	125	---
		AlO-18	38.4	50.8	230	88	190	---
		A6-120	38.4	49.8	1990	88	140	---
		A6-11	38.4	49.8	1990	88	155	---
		A6-26	38.4	51.4	3700	88	139	---
		AlO-58	38.4	47.8	6165	88	162	---
		A O-83	38.4	47.8	6225	88	162	---

TABLE XIII. FATIGUE DATA FOR STATIC AND DYNAMIC FORGED TEST SPECIMENS (Cont'd)

Material	Temp. °F	Specimen Number	Ave Stu	$\frac{1}{2}$ Red.	Strain Rate In/In/Sec	Stress Level (% Stu)	Cycles to Failure (1000's)	Hardness R <sub>c</sub>
2024-0 Aluminum	550	A10-75	38.4	50.7	6265	88	290	---
		A6-10	48	47.3	230	88	77	---
		A6-30	48	48.3	235	88	293	---
		A6-5	48	49.4	237	88	103	---
2024-0 Aluminum	750	A6-101	48	50.3	1979	88	86	---
		A6-124	48	50.0	1983	88	70	---
		A6-81	48	49.6	1992	88	58	---
		A6-92	48	50.4	7225	88	50	---
		C6-66	137,500	21.7	202	73	38	37.0
		C6-57	137,500	26.5	223	73	64	37.5
5Al-2.5Sn Titanium	1550	C6-46	137,500	33.4	223	73	41	37.5
		C6-68	137,500	24.2	228	70	449	37.5
		C6-136	137,500	---	---	73	192	36.0
		C6-4	137,500	24.5	2910	73	19	37.5
		C6-87	137,500	24.8	2920	73	109	37.0
		C6-103	137,500	25.4	2920	73	73	37.0
		C6-45	137,500	24.8	2930	73	166	36.5



TABLE XIII. FATIGUE DATA FOR STATIC AND DYNAMIC FORGED TEST SPECIMENS (Cont'd)

Material	Temp. °F	Specimen Number	Ave. St <sub>U</sub>	$\frac{1}{2}$ Red	Strain Rate In/In/Sec	Stress Level (% St <sub>U</sub> )	Cycles to Failure (1000's)	Hardness R <sub>C</sub>
5Al-2.5Sn Titanium	1550	06-39	137,500	23.8	2940	73	161	37.0
		06-86	137,500	23.7	2950	73	90	35.5
		06-7	137,500	24.0	4740	88	18	37.5
		06-6	137,500	23.5	4760	80	59	35.5
		06-32	137,500	25.6	4770	73	64	36.0
		06-14	137,500	21.1	4780	73	66	37.5
		06-8	137,500	24.1	4790	73	93	37.0
		06-30	137,500	23.5	4800	75	93	35.5
		06-23	137,500	23.1	5940	73	---	37.0
		06-115	136,000	20.6	223	73	43	31.5
5Al-2.5Sn Titanium	1550	06-55	136,000	25.2	230	73	44	32.5
		06-52	136,000	25.6	241	73	43	34.0
		06-56	136,000	29.0	265	73	55	31.0
		06-50	136,000	21.6	2310	73	46	34.0
		06-81	136,000	24.6	2310	73	33	35.5
		06-78	136,000	24.8	2310	73	960	33.0
		06-94	136,000	23.1	2320	73	52	35.0

TABLE XIII. FATIGUE DATA FOR STATIC AND DYNAMIC FORGED TEST SPECIMENS (Cont'd)

Material	Temp. ° F	Specimen Number	Ave. St <sub>U</sub>	% Red.	Strain Rate In/In/Sec	Stress Level (% St <sub>U</sub> )	Cycles to Failure (1000's)	Hardness R <sub>C</sub>
5Al-2.5Sn Titanium	950	C6-65	136,000	23.1	2320	73	58	32.0
		C6-75	136,000	23.6	2320	73	306	34.0
		C6-100	136,000	23.6	2320	73	107	32.5
		C6-33	136,000	24.3	2320	73	109	33.0
		C6-53	136,000	24.7	2320	73	1297	34.0
		C6-124	136,000	25.2	5200	73	482	33.0
		C6-89	136,000	21.9	5220	73	39	33.0
		C6-64	136,000	23.4	5220	70	649	33.0
		C6-37	136,000	24.4	5220	73	28	33.5
		C6-106	136,000	24.4	5220	73	148	34.0
		C6-116	136,000	24.4	5220	73	17	36.5
		C6-92	136,000	24.4	5220	73	50	31.5
		C6-94	136,000	23.8	5230	73	48	33.0
17-4 PH Stainless Steel	1550	C6-96	136,000	24.3	5250	70	177	31.0
		E6-40	162	39.7	3316	75	176	35.0
		E6-38	162	38.7	3323	75	206	35.7
		E6-46	162	39.5	3323	75	151	35.5

TABLE XIII. FATIGUE DATA FOR STATIC AND DYNAMIC FORGED TEST SPECIMENS (Cont'd)

Material	Temp. ° F	Specimen Number	Ave. St <sub>U</sub>	% Red	Strain Rate In/In/Sec	Stress Level (% St <sub>U</sub> )	Cycles to Failure (1000's)	Hardness R <sub>C</sub>
17-4 PH Stainless Steel	1550	E6-126	162	36.8	5659	75	213	37.2
		E6-54	162	38.1	5659	75	1262	40.2
		E6-123	162	38.9	5659	75	1122	37.0
		E6-124	162	39.6	5659	75	1203	38.0
		E6-50	162	34.2	5671	75	110	39.5
		E6-131	162	37.8	5683	75	219	37.0
		E6-130	162	38.9	5683	75	325	37.5
		E6-8	162	42.1	253	75	95	36.0
17-4 PH Stainless Steel	1950	E6-18	162	42.7	257	75	110	36.0
		E6-2	162	42.3	262	75	194	37.0
		E1-584	162	39.3	3303	75	147	33.8
		E1-570	162	39.8	3309	75	329	33.0
		E1-591	162	38.9	3323	74	752*	---
		E1-600	162	41.0	3323	75	155	34.2
		E1-573	162	40.0	7124	65	121*	---
		E1-573	162	40.0	7124	75	192*	---
		E1-573	162	40.0	7124	80	15	---

\* No Failure

TABLE XIII. FATIGUE DATA FOR STATIC AND DYNAMIC FORGED TEST SPECIMENS (Cont'd)

Material	Temp. °F	Specimen Number	Ave. St <sub>U</sub>	% Red.	Strain Rate In/In/Sec	Stress Level (% St <sub>U</sub> )	Cycles to Failure (1000's)	Hardness R <sub>C</sub>
17-4 PH Stainless Steel	1950	E1-555	162	40.8	7124	75	195	33.7
		E1-557	162	39.5	7139	75	120	36.0
		E1-568	162	40.6	7185	75	101	33.8
17-4 PH Stainless Steel (Heat Treated)	1950	E6-7	192	41.3	256	75	28	43.0
		E6-11	192	42.0	256	75	17	43.0
		E6-21	192	43.3	256	75	19	42.5
		E1-575	192	38.4	3303	75	24	42.3
		E1-585	192	39.9	3316	75	34	42.5
		E1-602	192	40.2	3323	75	21	44.0
		E1-572	192	39.9	7013	75	31	42.5
		E1-607	192	40.0	7027	75	19	43.1
		E6-14	192	39.7	7038	75	25	43.0
A-286 Steel	1050	E1-567	192	40.5	7038	75	25	42.5
		F6-80	139	48.1	245	85	114	29.5
		F6-64	139	47.2	250	85	109	30.5
		F6-66	139	49.8	257	85	158	31.5
		F6-79	139	49.4	4144	85	219	32.5

TABLE XIII. FATIGUE DATA FOR STATIC AND DYNAMIC FORGED TEST SPECIMENS (Cont'd)

Material	Temp. ° F	Specimen Number	Ave. St <sub>u</sub>	% Red.	Strain Rate In/In/Sec	Stress Level (% St <sub>u</sub> )	Cycles to Failure (1000's)	Hardness R <sub>c</sub>
A-286 Steel	1050	F6-45	139	50.5	4171	85	147	32.0
		F6-88	139	47.1	4188	85	295	30.5
		F6-38	139	48.4	8387	85	279	---
		F6-16	139	49.5	8387	85	170	34.0
		F6-15	139	47.9	8441	85	123	30.0
		F6-35	139	48.5	8441	67	110*	---
		F6-35	139	48.5	8441	75	120*	---
		F6-35	139	48.5	8441	85	61	---
		F9-13	108	47.6	235	85	187	20.5
		F9-32	108	51.4	235	85	154	24.5
A-286 Steel	1950	F9-2	108	52.3	235	85	131	21.0
		F9-3	108	53.1	235	85	225	25.0
		F6-1	108	50.5	3932	65	110*	---
		F6-1	108	50.5	3932	75	120*	---
		F6-1	108	50.5	3932	85	105	---
		F6-110	108	51.1	3941	85	55	110
		F6-78	108	50.3	3949	85	48	---

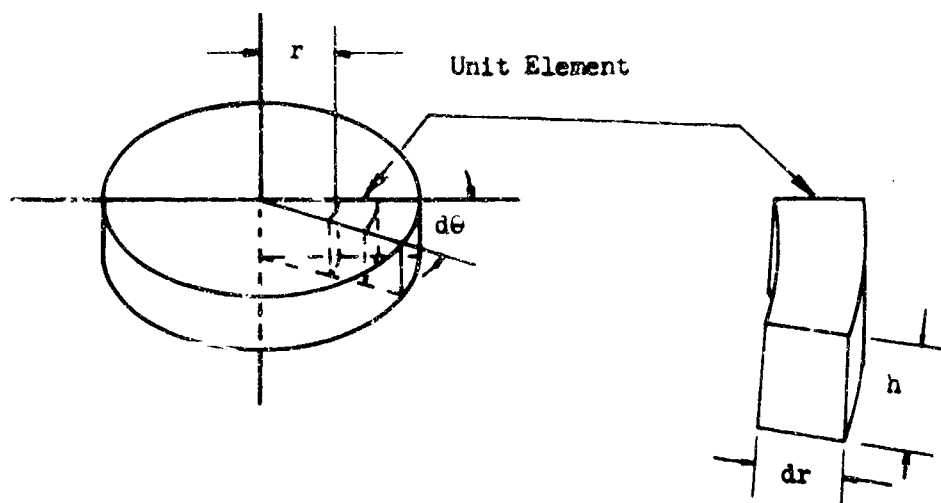
\* No Failure

TABLE XIII FATIGUE DATA FOR STATIC AND DYNAMIC FORCED TEST SPECIMENS (Cont'd)

Material	Temp. ° F.	Specimen Number	Ave. St <sub>u</sub>	$\sigma$ Red	Strain Rate In/In/Sec	Stress Level (% St <sub>u</sub> )	Cycles to Failure (1000's)	Hardness R <sub>c</sub>
A-286 Steel	1950	F6-3	108	48.4	3966	85	1268	26.0
		F6-30	108	49.1	4025	85	66	---
		F6-25	108	46.0	7707	85	620	26.5
		F6-115	100	47.1	7865	85	180	---
		F6-100	108	46.9	7898	85	48	15.2
		F6-59	108	47.0	7915	85	63	13.5
A-286 Steel (Heat Treated)	1950	F9-6	150.5	51.3	234	85	110	32.5
		F9-25	150.5	51.3	235	85	72	37.0
		F9-1	150.5	52.9	235	85	1255	---
		F9-18	150.5	51.9	237	85	93	33.0
		F6-73	150.5	49.9	3924	85	104	32.3
		F6-62	150.5	50.3	3924	85	61	29.0
		F6-83	150.5	51.3	3949	85	62	32.0
		F6-108	150.5	47.8	7898	85	76	36.5

APPENDIX IV  
DEVELOPMENT OF STRESS EQUATIONS

DIFFERENTIAL EQUATION FOR STRESS DISTRIBUTION  
IN A CYLINDRICAL BILLET (STATIC)



1. The forces acting on the unit element are:

		Pressure X area
$F_1$	Axial force	
$F_2$	Radial force on inner area	$\sigma_r \quad rh \quad d\theta$
$F_3$	Radial force on outer area	$(\sigma_r + d\sigma_r)(r + dr)h \quad d\theta$
$F_4$	Frictional force at the billet surface	$2 \mu Pr \quad d\theta \quad dr$
$F_5$	Circumferential compression	$\sigma_c \quad dr \quad h$
$F_6$	Radial component of the circumferential compression	$\sigma_c \quad dr \quad h \quad \frac{d\theta}{2}$

2. Balancing forces in the radial direction

$$F_2 - F_3 - 2 F_4 + 2 F_6 \equiv 0$$

$$[\sigma_r \quad rh \quad d\theta] - [(\sigma_r + d\sigma_r)(r + dr)h \quad d\theta] - [2 \mu Pr \quad d\theta \quad dr] + [2 \sigma_c \quad h \quad dr \quad \frac{d\theta}{2}] = 0$$

3. dividing by  $d\theta$  and expanding:

$$\sigma_r \quad rh - \sigma_r \quad rh - \sigma_r \quad dr \quad h - d\sigma_r \quad rh - d\sigma_r \quad dr \quad h - 2 \mu Pr \quad dr + \sigma_c \quad dr \quad h = 0$$



4. reducing and eliminating second order differentials ( $d\sigma_r dr$ )

$$-\sigma_r dr h - d\sigma_r rh - 2\mu Pr dr + \sigma_c dr h = 0$$

5. dividing by  $hr dr$

$$-\frac{\sigma_r}{r} - \frac{d\sigma_r}{dr} - \frac{2\mu P}{h} + \frac{\sigma_c}{r} = 0$$

$$-\frac{d\sigma_r}{dr} - \left(\frac{\sigma_r - \sigma_c}{r}\right) - \frac{2\mu P}{h} = 0$$

$$\boxed{\frac{d\sigma_r}{dr} + \frac{\sigma_r - \sigma_c}{r} = -\frac{2\mu P}{h}}$$

Eq. 1

Symbols:

$P$  = axial pressure

$r$  = radial distance from center of billet

$\sigma_o$  = tensile yield stress (uniaxial)

$\sigma_r$  = radial stress

$\sigma_c$  = circumferential stress

$h$  = billet height

$\mu$  = coefficient of sliding friction (Coulomb friction)

$R$  = billet radius

### PRESSURE DISTRIBUTION ON A CYLINDRICAL BILLET (STATIC)

1. The three principal stresses acting on a unit element are  $P$ ,  $\sigma_r$  and  $\sigma_c$ . The pressure at any point on the surface sufficient to produce yielding is given by the distortion - energy criterion as:

$$\sigma_o = \frac{1}{\sqrt{2}} \sqrt{(P - \sigma_r)^2 + (\sigma_r - \sigma_c)^2 + (\sigma_c - P)^2}$$

2.  $\sigma_r = \sigma_c$  therefore:

$$\begin{aligned} \sigma_o &= \frac{1}{\sqrt{2}} \sqrt{(P - \sigma_r)^2 + (\sigma_r - P)^2} \\ &= \frac{1}{\sqrt{2}} \sqrt{2P^2 - 4P\sigma_r + 2\sigma_r^2} \\ &= \frac{1}{\sqrt{2}} \sqrt{2(P - \sigma_r)^2} \end{aligned}$$

3. The condition for yielding is satisfied when

$$\sigma_o = P - \sigma_r \quad \text{or}$$

$$P = \sigma_o + \sigma_r$$

$$\boxed{\frac{dP}{dr} = \frac{d\sigma_r}{dr}}$$

EQ. 2

4. combining equations 1 and 2

$$\boxed{\frac{dP}{dr} = - \frac{2}{h} P}$$

EQ. 3

$$\frac{dP}{P} = - \frac{2}{h} dr$$

$$\ln P = - \frac{2}{h} r + \ln c$$

$$P = \ln c \cdot e^{-2r/h}$$

5. when  $r = R$  and  $P = \sigma_o$

$$\ln c = \sigma_o \cdot e^{2R/h}$$

$$P = \sigma_0 e^{2\gamma R/h} \cdot e^{-2\gamma r/h}$$

$$P = \sigma_0 \exp \frac{2\gamma (R - r)}{h}$$

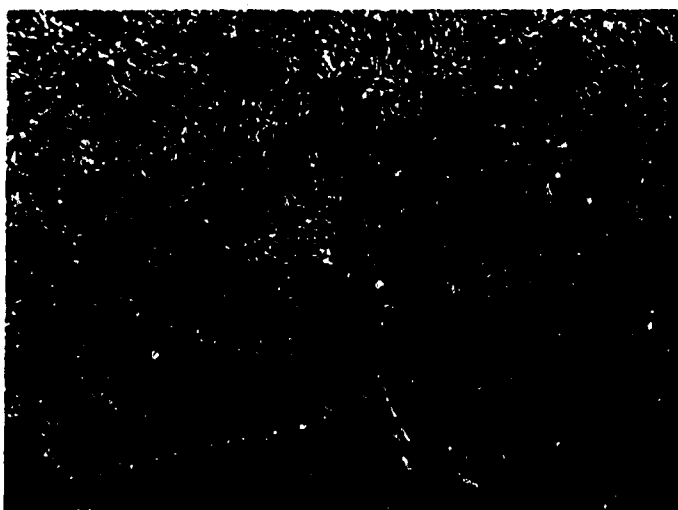
Eq. 4

APPENDIX V  
PHOTOMICROGRAPHS OF STATIC AND  
DYNAMIC FORGED SPECIMENS

Specimen no.: A5-001  
Direction: View no. 3  
Magnification: 100X  
Strain: 79.8%  
Strain rate: Static



Specimen no.: A5-013  
Direction: View no. 3  
Magnification: 100X  
Strain: 78.0%  
Strain rate: 240 (1/sec.)

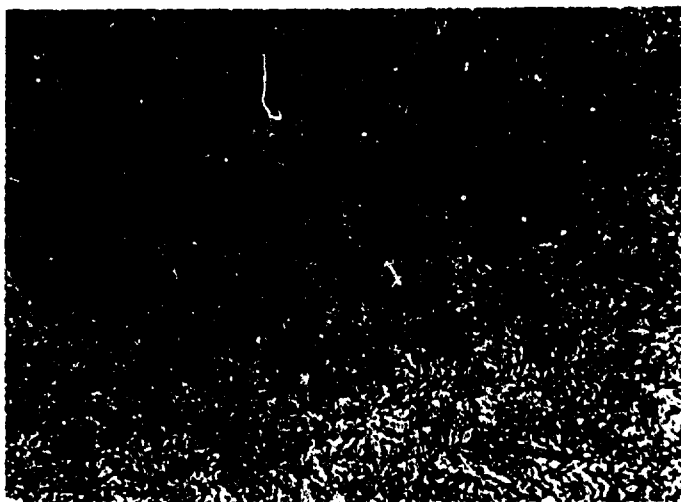


Specimen no.: A5-016  
Direction: View no. 3  
Magnification: 100X  
Strain: 78.5%  
Strain rate: 4400 (1/sec.)

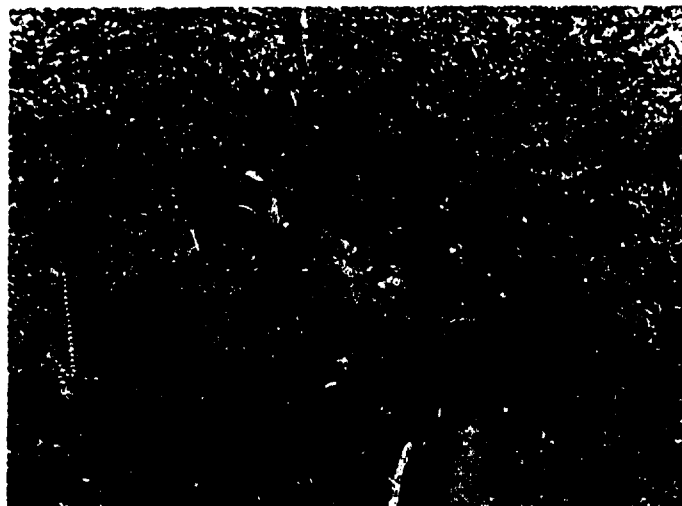


FIGURE 107. AS FORGED MICROSTRUCTURE OF 2024-O ALUMINUM AT THREE (3) DIFFERENT STRAIN RATES (NORMAL VIEW)

Specimen no.: A5-001  
 Direction: View no. 4  
 Magnification: 100X  
 Strain: 79.8%  
 Strain rate: Static



Specimen no.: A5-013  
 Direction: View no. 4  
 Magnification: 100X  
 Strain: 78.0%  
 Strain rate: 240 (1/sec.)



Specimen no.: A5-016  
 Direction: View no. 4  
 Magnification: 100X  
 Strain: 78.5%  
 Strain rate: 4400 (1/sec.)

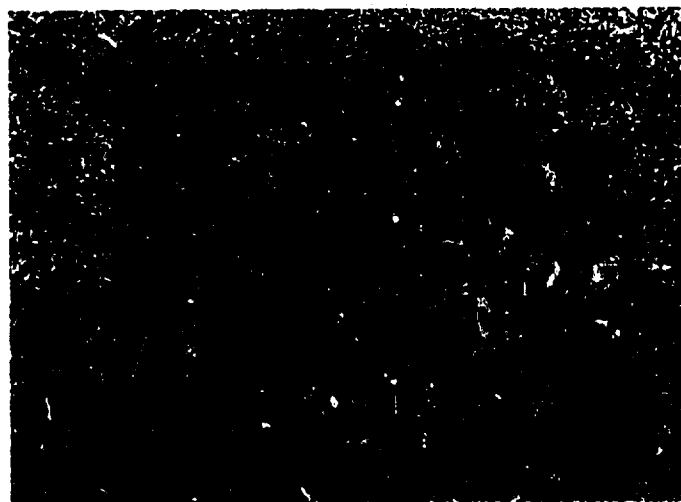
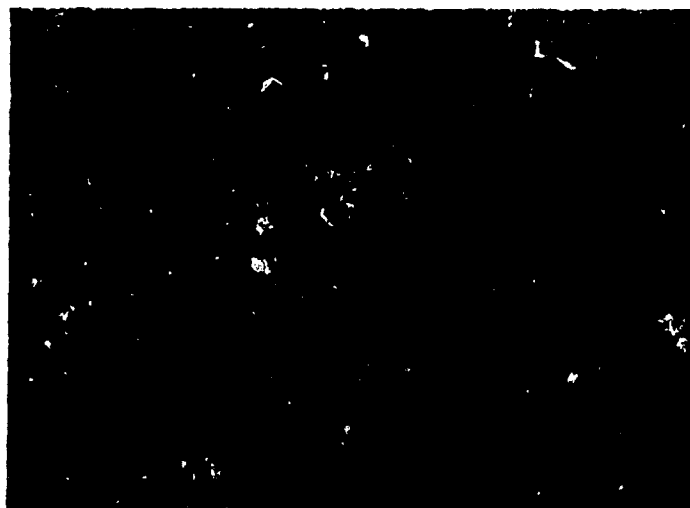


FIGURE 108. AS FORGED MICROSTRUCTURE OF 2024-O ALUMINUM AT THREE (3) DIFFERENT STRAIN RATES (TRANSVERSE VIEW)

Specimen no.: A5-001  
Direction: View no. 5  
Magnification: 100X  
Strain: 79.8%  
Strain rate: Static



Specimen no.: A5-013  
Direction: View no. 5  
Magnification: 100X  
Strain: 78.0%  
Strain rate: 240 (1/sec.)

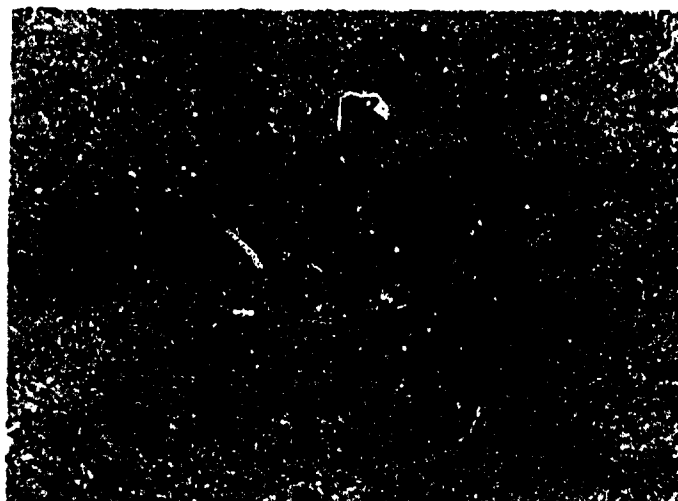


Specimen no.: A5-016  
Direction: View no. 5  
Magnification: 100X  
Strain: 78.5%  
Strain rate: 4400 (1/sec.)



FIGURE 109. AS FORGED MICROSTRUCTURE OF 2024-O ALUMINUM AT THREE (3) DIFFERENT STRAIN RATES (LONGITUDINAL VIEW)

Specimen no.: B3-001  
Direction: View no. 1  
Magnification: 100X  
Strain: 69.0%  
Strain rate: Static



Specimen no.: B3-005  
Direction: View no. 1  
Magnification: 100X  
Strain: 85.3%  
Strain rate: 1700 (1/sec.)



Specimen no.: B3-010  
Direction: View no. 1  
Magnification: 100X  
Strain: 84.1%  
Strain rate: 5600 (1/sec.)



FIGURE 110. AS FORGED MICROSTRUCTURE OF 7075-O ALUMINUM AT THREE (3) DIFFERENT STRAIN RATES (NORMAL VIEW)



Specimen no.: B3-005  
Direction: View no. 2  
Magnification: 100X  
Strain: 85.3%  
Strain rate: 1700 (1/sec.)

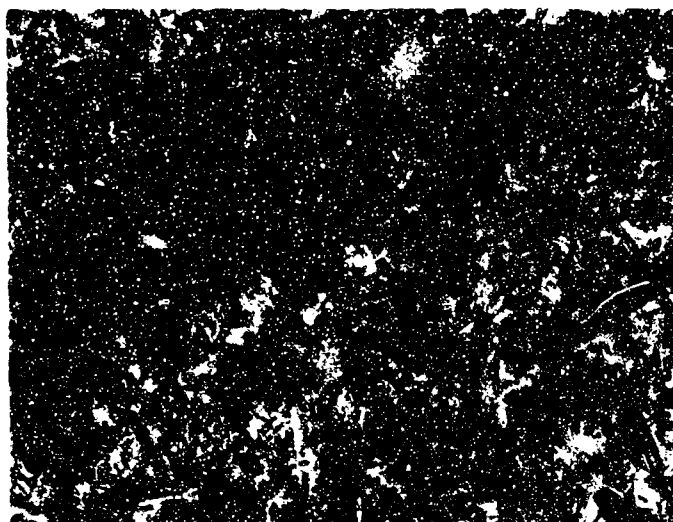


Specimen no.: B3-010  
Direction: View no. 2  
Magnification: 100X  
Strain: 84.1%  
Strain rate: 5600 (1/sec.)



FIGURE 111. AS FORGED MICROSTRUCTURE OF 7075-O ALUMINUM AT TWO (2) DIFFERENT STRAIN RATES (NORMAL VIEW)

Specimen no.: E2-009  
Direction: View no. 3  
Magnification: 100X  
Strain: 34.3%  
Strain rate: 3470 (1/sec.)



Specimen no.: E2-018  
Direction: View no. 3  
Magnification: 100X  
Strain: 20.8%  
Strain rate: 6110 (1/sec.)

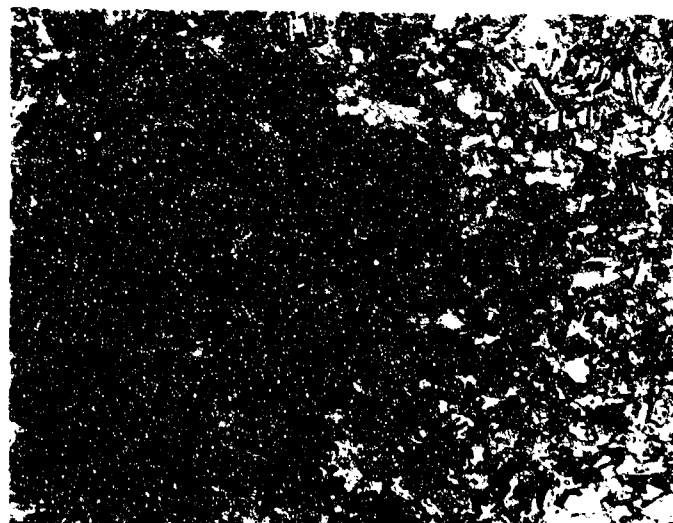
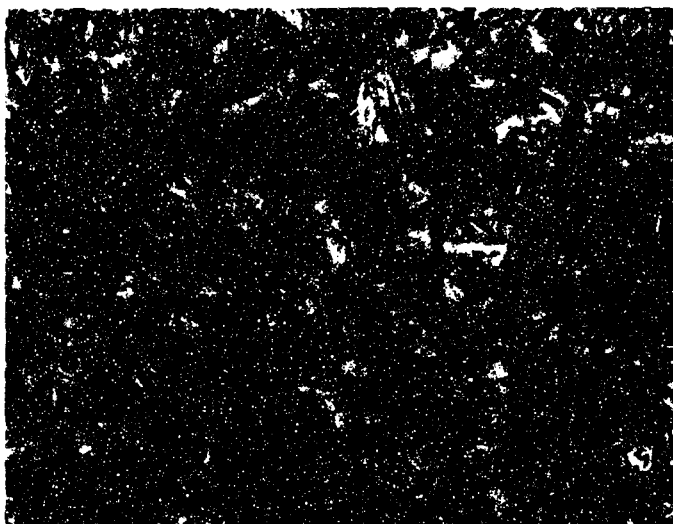


FIGURE 1.1C. AS FORGED MICROSTRUCTURE OF 17-4 PH STAINLESS AT TWO (2) DIFFERENT STRAIN RATES (NORMAL VIEW)

Specimen no.: E2-009  
Direction: View no. 4  
Magnification: 100X  
Strain: 34.3%  
Strain rate: 3470 (1/sec.)



Specimen no.: E2-018  
Direction: View no. 4  
Magnification: 100X  
Strain: 20.8%  
Strain rate: 6110 (1/sec.)



FIGURE 113. AS FORGED MICROSTRUCTURE OF 17-4 PH STAINLESS AT TWO (2)  
DIFFERENT STRAIN RATES (TRANSVERSE VIEW)

Specimen no.: E2-009  
Direction: View no. 5  
Magnification: 100X  
Strain: 34.3%  
Strain rate: 3470 (1/sec.)



Specimen no.: E2-018  
Direction: View no. 5  
Magnification: 100X  
Strain: 20.8%  
Strain rate: 6110 (1/sec.)



FIGURE 114. AS FORGED MICROSTRUCTURE OF 17-4 PH STAINLESS AT TWO (2) DIFFERENT STRAIN RATES (LONGITUDINAL VIEW)

Specimen no.: F1-016  
 Direction: View no. 3  
 Magnification: 250X  
 Strain: 27.1%  
 Strain rate: Static



Specimen no.: F1-003  
 Direction: View no. 3  
 Magnification: 250X  
 Strain: 34.7%  
 Strain rate: 5320 (1/sec.)



Specimen no.: F1-011  
 Direction: View no. 3  
 Magnification: 250X  
 Strain: 34.1%  
 Strain rate: 8130 (1/sec.)

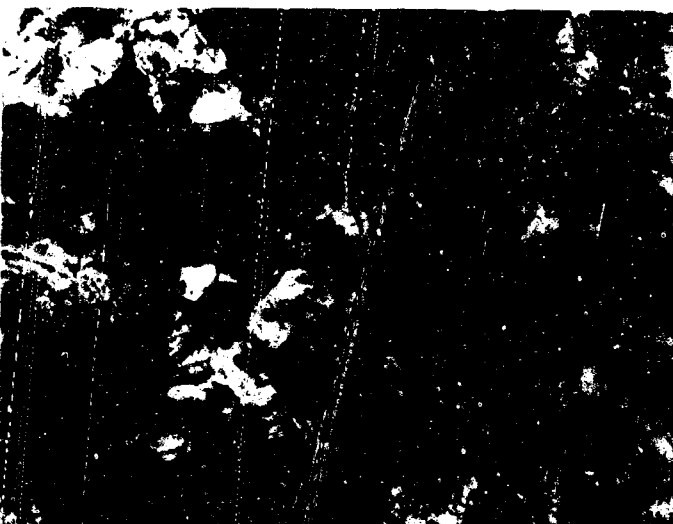
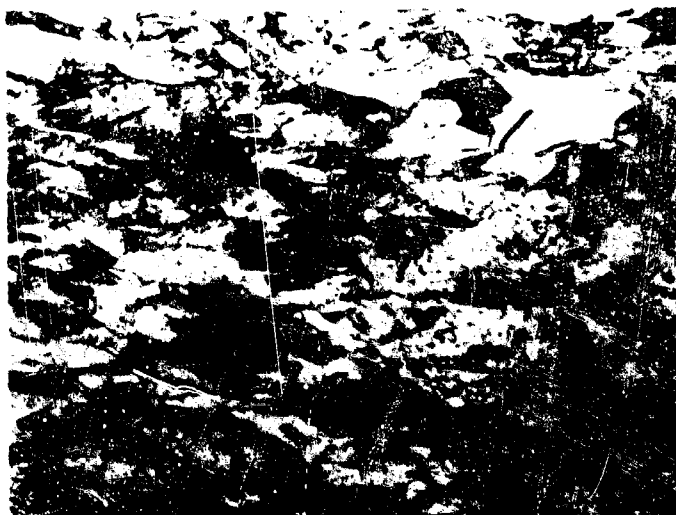
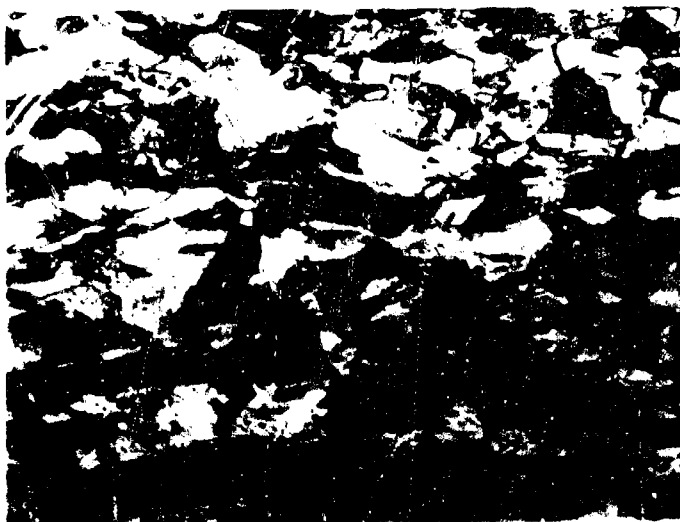


FIGURE 116. AS FORGED MICROSTRUCTURE OF A-36 STEEL AT THREE (3) DIFFERENT STRAIN RATES (NORMAL VIEW)

Specimen no.: Fl-016  
Direction: View no. 4  
Magnification: 250X  
Strain: 27.1%  
Strain rate: Static



Specimen no.: Fl-003  
Direction: View no. 4  
Magnification: 250X  
Strain: 34.7%  
Strain rate: 5320 (1/sec.)



Specimen no.: Fl-011  
Direction: View no. 4  
Magnification: 250X  
Strain: 34.1%  
Strain rate: 8130 (1/sec.)



FIGURE 116. AS FORGED MICROSTRUCTURE OF A-286 STEEL AT THREE (•)  
DIFFERENT STRAIN RATES (TRANSVERSE VIEW)

Specimen no.: F1-016  
Direction: View no. 5  
Magnification: 250X  
Strain: 27.1%  
Strain rate: Static



Specimen no.: F1-003  
Direction: View no. 5  
Magnification: 250X  
Strain: 34.7%  
Strain rate: 5320 (1/sec.)



Specimen no.: F1-011  
Direction: View no. 5  
Magnification: 250X  
Strain: 34.1%  
Strain rate: 8130 (1/sec.)



FIGURE 117. AS FORGED MICROSTRUCTURE OF A-286 STEEL AT THREE (3)  
DIFFERENT STRAIN RATES (LONGITUDINAL VIEW)

Specimen no.: G2-016  
Direction: View no. 3  
Magnification: 250X  
Strain: 20.0%  
Strain rate: Static



Specimen no.: G2-004  
Direction: View no. 3  
Magnification: 250X  
Strain: 17.8%  
Strain rate: 4880 (1/sec.)



Specimen no.: G2-017  
Direction: View no. 3  
Magnification: 250X  
Strain: 19.5%  
Strain rate: 8610 (1/sec.)

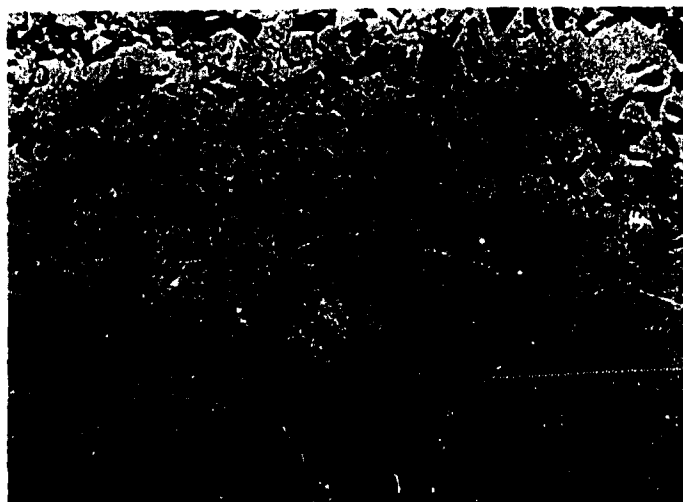


FIGURE 118. AS FORGED MICROSTRUCTURE OF 18% NI MARAGING STEEL AT THREE (3) DIFFERENT STRAIN RATES (NORMAL VIEW)



Specimen no.: G2-016  
 Direction: View no. 4  
 Magnification: 250X  
 Strain: 20.0%  
 Strain rate: Static



Specimen no.: G2-004  
 Direction: View no. 4  
 Magnification: 250X  
 Strain: 17.8%  
 Strain rate: 4880 (1/sec.)



Specimen no.: G2-017  
 Direction: View no. 4  
 Magnification: 250X  
 Strain: 19.5%  
 Strain rate: 8610 (1/sec.)

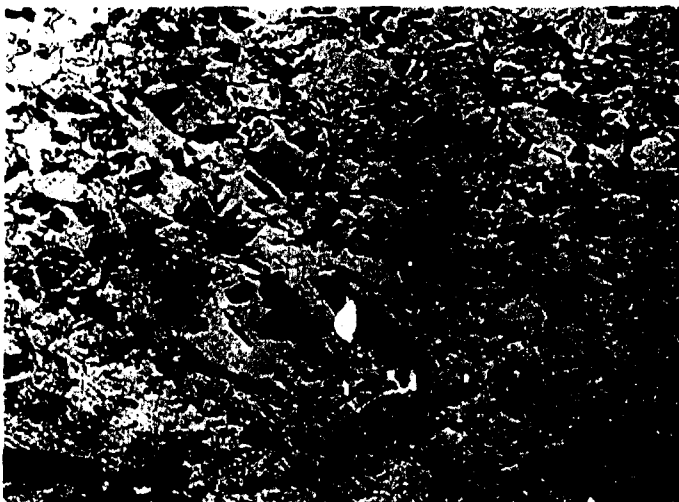
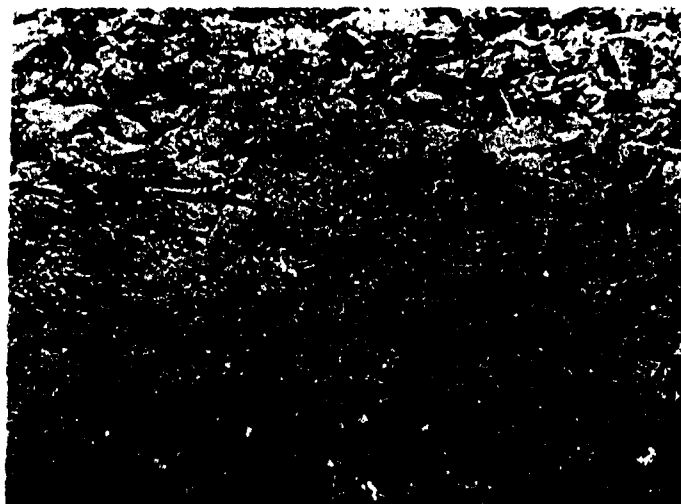


FIGURE 119. AS FORGED MICROSTRUCTURE OF 18% NI MARAGING STEEL AT THREE (3) DIFFERENT STRAIN RATES (TRANSVERSE VIEW)

Specimen no.: G2-016  
Direction: View no. 5  
Magnification: 250X  
Strain: 20.0%  
Strain rate: Static



Specimen no.: G2-004  
Direction: View no. 5  
Magnification: 250X  
Strain: 17.8%  
Strain rate: 4880 (1/sec.)



Specimen no.: G2-017  
Direction: View no. 5  
Magnification: 250X  
Strain: 19.5%  
Strain rate: 8610 (1/sec.)

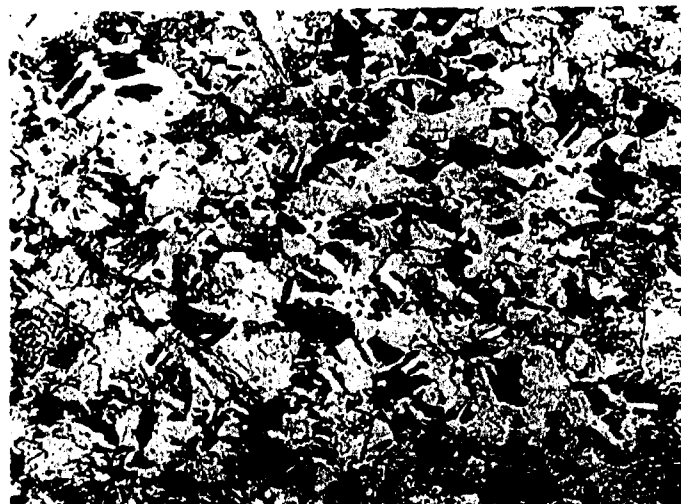


FIGURE 120. AS FORGED MICROSTRUCTURE OF 18% NI MARAGING STEEL AT THREE (3) DIFFERENT STRAIN RATES (LONGITUDINAL VIEW)

Specimen no.: IL-003  
Direction: View no. 3  
Magnification: 100X  
Strain: 26.1%  
Strain rate: Static



Specimen no.: IL-013  
Direction: View no. 3  
Magnification: 100X  
Strain: 26.1%  
Strain rate: 3280 (1/sec.)



Specimen no.: IL-009  
Direction: View no. 3  
Magnification: 100X  
Strain: 25.4%  
Strain rate: 8160 (1/sec.)

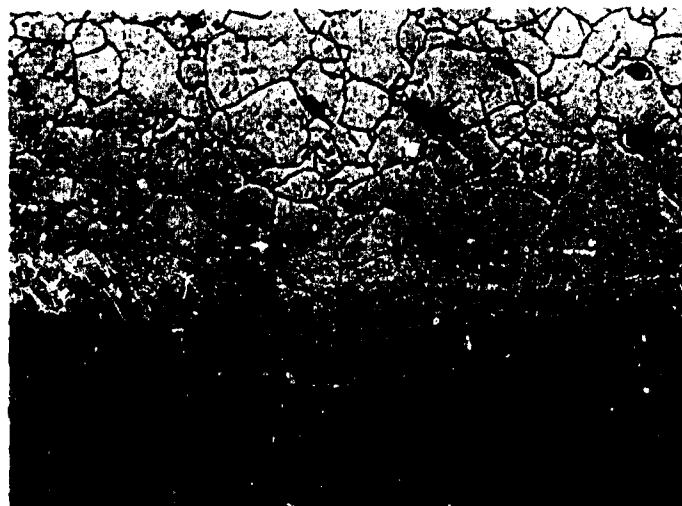
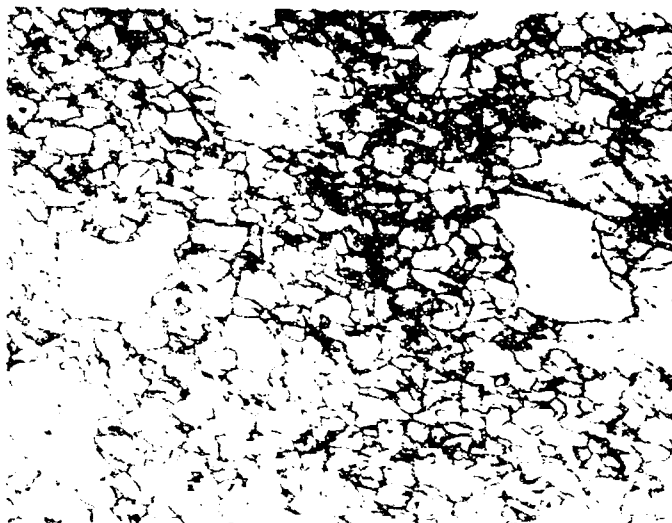
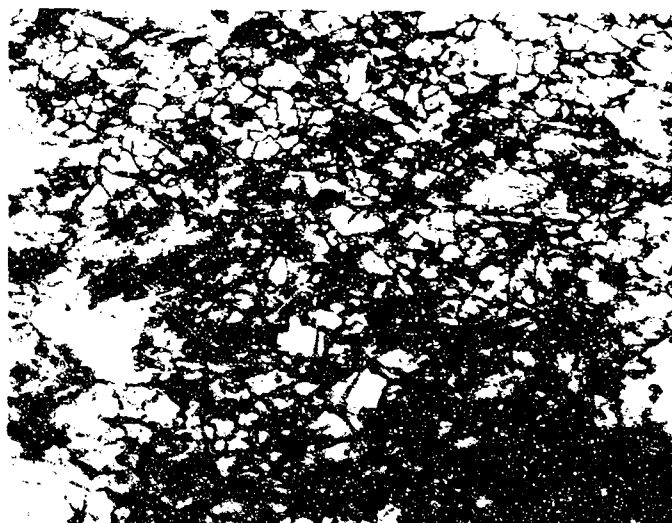


FIGURE 121. AS FORGED MICROSTRUCTURE OF RENE' 41 AT THREE (3) DIFFERENT STRAIN RATES (NORMAL VIEW)

Specimen no.: 11-012  
Direction: View no. 4  
Magnification: 100X  
Strain: 26.1%  
Strain rate: Static



Specimen no.: 11-013  
Direction: View no. 4  
Magnification: 100X  
Strain: 35.4%  
Strain rate: 3280 (1/sec.)



Specimen no.: 11-009  
Direction: View no. 4  
Magnification: 100X  
Strain: 25.4%  
Strain rate: 160 (1/sec.)

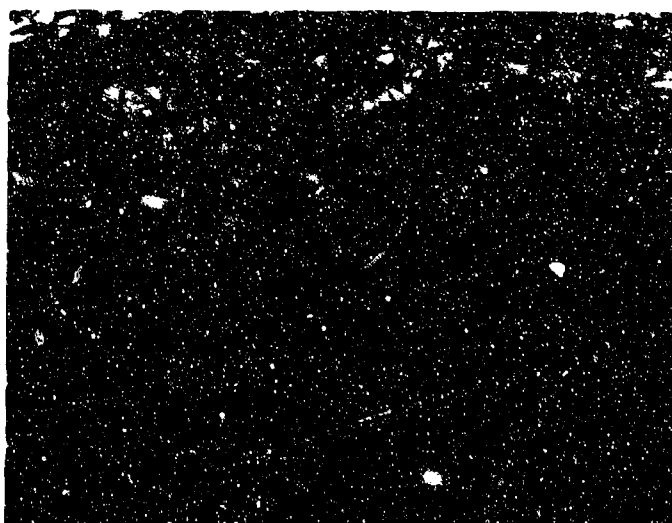
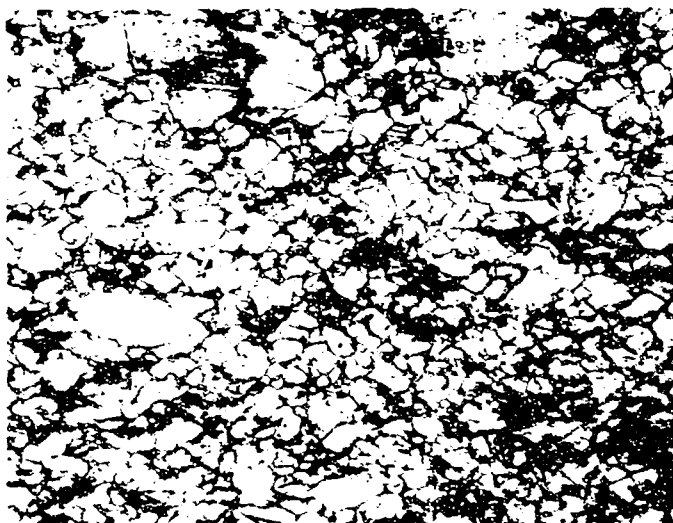
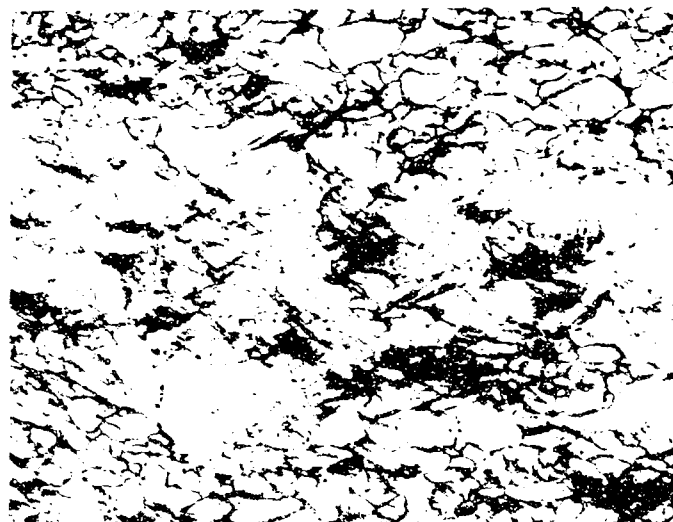


FIGURE 122. AS FORGED MICROSTRUCTURE OF RENE' 41 AT THREE (3)  
DIFFERENT STRAIN RATES (TRANSVERSE VIEW)

Specimen no.: 11-003  
 Direction: View no. 5  
 Magnification: 100X  
 Strain: 26.11  
 Strain rate: Static



Specimen no.: 11-013  
 Direction: View no. 5  
 Magnification: 100X  
 Strain: 35.45  
 Strain rate: 3280 (1/sec.)



Specimen no.: 11-009  
 Direction: View no. 5  
 Magnification: 100X  
 Strain: 25.45  
 Strain rate: 8160 (1/sec.)

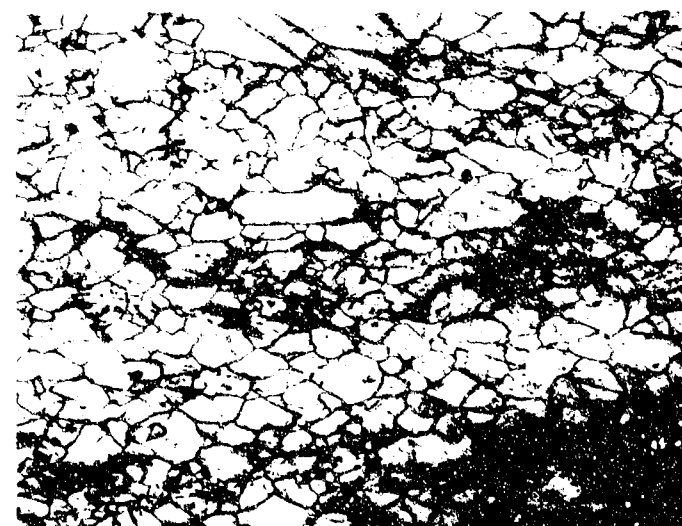
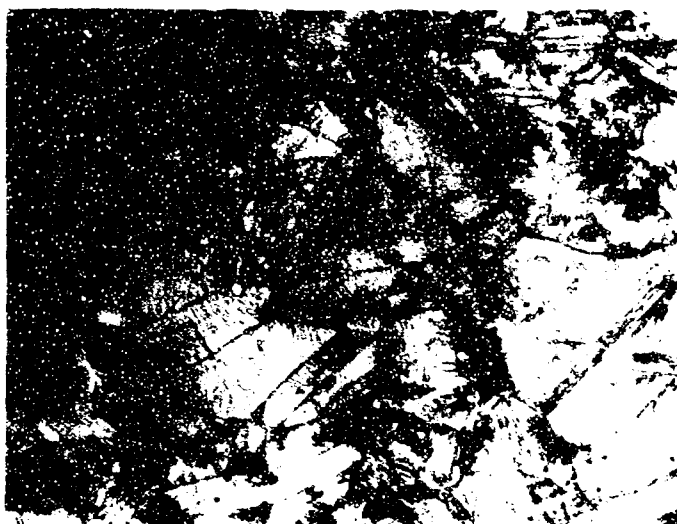


FIGURE 123. AS FORGED MICROSTRUCTURE OF RENE' 41 AT THREE (3) DIFFERENT STRAIN RATES (LONGITUDINAL VIEW)

Specimen no.: J1-006  
 Direction: View no. 3  
 Magnification: 100X  
 Strain: 34.5%  
 Strain rate: Static



Specimen no.: J1-012  
 Direction: View no. 3  
 Magnification: 100X  
 Strain: 35.9%  
 Strain rate: 3710 (1/sec.)



Specimen no.: J1-009  
 Direction: View no. 3  
 Magnification: 100X  
 Strain: 35.0%  
 Strain rate: 7010 (1/sec.)

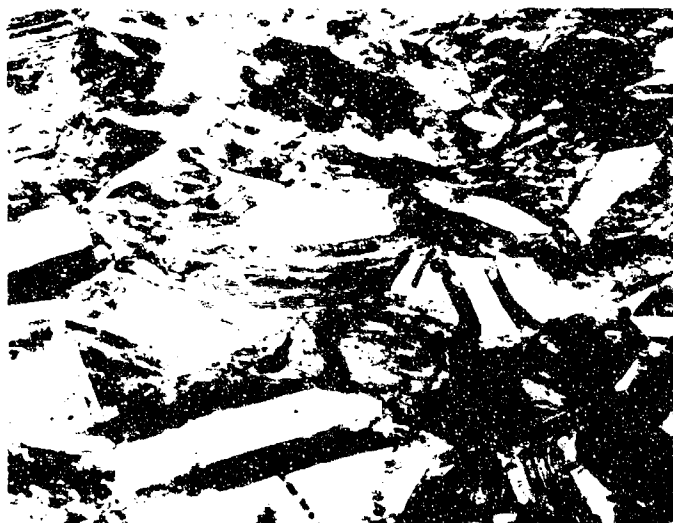


FIGURE 124. AS FORGED MICROSTRUCTURE OF 1605 AT THREE (3) DIFFERENT STRAIN RATES (NORMAL VIEW)

Specimen no.: J1-006  
 Direction: View no. 4  
 Magnification: 100X  
 Strain: 34.5%  
 Strain rate: Static



Specimen no.: J1-012  
 Direction: View no. 4  
 Magnification: 100X  
 Strain: 35.9%  
 Strain rate: 3710 (1/sec.)



Specimen no.: J1-009  
 Direction: View no. 4  
 Magnification: 100X  
 Strain: 35.0%  
 Strain rate: 7010 (1/sec.)



Location of electron  
 photomicrograph .....  
 (Figure 24)

FIGURE 125. AS FORGED MICROSTRUCTURE OF L605 AT THREE (3)  
 DIFFERENT STRAIN RATES (TRANSVERSE VIEW)

Specimen no.: J1-006  
 Direction: View no. 5  
 Magnification: 100X  
 Strain: 34.5%  
 Strain rate: Static



Specimen no.: J1-012  
 Direction: View no. 5  
 Magnification: 100X  
 Strain: 35.9%  
 Strain rate: 3710 (1/sec.)



Specimen no.: J1-019  
 Direction: View no. 5  
 Magnification: 100X  
 Strain: 35.0%  
 Strain rate: 7010 (1/sec.)

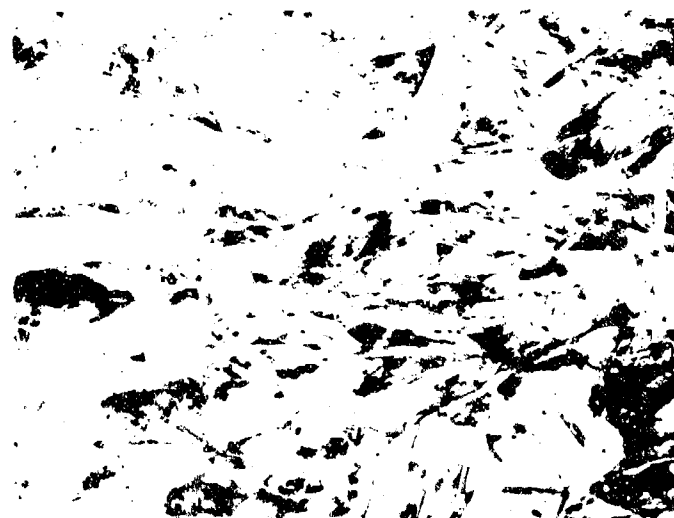


FIGURE 126. AS FORGED MICROSTRUCTURE OF L605 AT THREE (3) DIFFERENT STRAIN RATES (LONGITUDINAL VIEW)



APPENDIX VI  
DETAILED DESCRIPTION OF EQUIPMENT

## APPENDIX VI

### DETAILED DESCRIPTION OF EQUIPMENT

#### Static Upset

##### Introduction

Static upset tests in this program were performed using conventional hydraulic presses with a special purpose tool to act as a load spreader. Although all of the Phase I static tests were conducted using this equipment, serious difficulties were encountered in attempting elevated temperature upset tests at these low ram speeds. Severe die quenching occurred using room temperature dies particularly at the larger deformations. Heated dies proved unsatisfactory primarily because of die failure at temperatures high enough to maintain a reasonably constant billet temperature during upset. Because of this tooling problem it was necessary to utilize drop hammer equipment for the low velocity, elevated temperature tests of Phase II.

##### Equipment for Static Upset

All Phase I static testing was completed using presses with 600, 1000 and 2500 ton capacities. The 2500 ton Lake Erie hydraulic press is shown in Figure 127 with the static upset tooling.

This tooling was designed to fulfill three functions. The first function being to distribute the forces over the press platens. This was accomplished using load spreaders, illustrated in Figure 128. The second function was to hold hardened anvils or die inserts that could be easily removed for regrinding in the event of surface damage. These inserts, illustrated in Figure 129, were fabricated from 4340 tool steel hardened to Rockwell 48-52 and ground flat to a surface finish on the order of RMS-20. The third function was to help the press operator maintain a constant strain rate during upset. To accomplish this a special deflection gage, Figure 130, was constructed. This gage was also useful in obtaining the required amount of upset in the static forging of bar specimens used in the elevation of mechanical properties.

#### Drop Hammer Upset Forging

##### Introduction

The use of the drop hammer for low velocity, elevated temperature testing was dictated because of severe die quenching problems encountered using a hydraulic press. This equipment was required to establish low velocity forgeability limits using cylindrical billets and to upset bar shape specimens for tensile and fatigue testing in the 4 to 10 ft. per second range at temperatures from ambient to 2000°F.

##### Forging Equipment

The test set-up illustrated in Figure 131 consisted of a special forging tool used

in a single action Chambersburg air hammer. The upper and lower insert anvils are held in a hardened 4340 adapter ring by set screws. Both upper and lower rings are bolted to mild steel plates that act as load spreaders. The upper plate was designed with the maximum allowable overhang mass in order to obtain a maximum energy at the lowest possible ram velocity. Four mild steel stop blocks, adjustable by shims, were used to limit the travel of the moving ram. These stop blocks were used only for the bar shape specimens where a precise amount of deformation was required.

#### Ram Velocity Measurement

The velocity of the moving ram was measured over the last inch of travel before impact by causing an electrical circuit to be completed through spaced contracts. The time interval for the ram to travel one inch was recorded photographically from an oscilloscope trace as shown schematically in Figure 132.

### High Velocity Forging Equipment

#### Introduction

The room temperature tests of Phase I were comparatively simple to perform from a mechanical standpoint since the billets could be located in position on the anvil by hand well in advance of the forging operation. For elevated temperature upsetting, the procedures are complicated by two conditions. First the hot billet must be held in such a way that the holding mechanism does not impose restraints that might change the data and second the billet must be transferred from the furnace and forged in a short period of time in order to minimize the effects of surface cooling. The high velocity forging equipment consists of a high pressure gas operated projectile accelerator with special billet heating and handling equipment, operated through a pre-programmed remote control system.

#### High Velocity Projectile Gun

The basic test machine consists of a pressure chamber, quick opening valve, barrel, and a fixed anvil assembly as shown schematically in Figure 133. Solenoid valves, actuated remotely, provide automatic sequencing of the projectile return vacuum system, as well as the pressure chamber loading, and firing functions. This portion of the system is shown in Figures 133 and 134. The system also provides monitoring for unsafe conditions in the high pressure range. Logic circuits in the control system automatically stops the system in the event of operator error or mechanical mal-function and indicate, by lights on the control panel, the source of the mal-function.

#### Heating Equipment For Cylindrical Forgeability Specimens

Two furnaces are required to perform forgeability tests on the cylindrical and bar shaped billets. A small commercial muffle furnace, Thermolyne Type 1500, is used for preheating billets to be forged at the higher temperatures in order to shorten the waiting time. The specimen temperature is raised to final value in a special furnace designed and fabricated as a part of the billet handling mechanism as shown in Figures 135 and 136. A complete electrical schematic

of the furnace installation is shown in Figure 138.

#### Billet Handling Mechanism

The test billet was moved from the final heating furnace into position on the anvil in two operations. During the final heating stage, the specimen was held under a light spring compression between two rods as shown in Figure 139.

As soon as the required forging temperature was reached, the billet was moved out of the furnace and transferred from the holding rods to light disposable spring clips attached to a carriage moving normal to the furnace center line which moves the billet into forging position. The complete handling mechanism is shown schematically in Figure 135. Photographs of the installation and details of the spring clips are shown in Figure 137.

#### Billet Heating and Handling Mechanism for Bar Specimens

The bar specimens were heated in a separate furnace located directly above the forging anvil and dropped into position from the furnace several seconds prior to impact. The equipment for performing this operation is shown in Figure 140.

#### Central Control System

The central control system shown in Figures 141 and 142 is a versatile design capable of patch cord programming to supply 110 VAC power to 15 actuation channels in any sequence desired. Automatic process operation is obtained by a relay logic controlled stepping relay. The system is programmed to step through a sequence of actuations conditionally, comparing the actual state of the system at each step with the program required. Lamps on the lower edge of the front panel indicate which actuators are operable as well as the condition of the limit switches associated with each actuator. The vertical row of switches and lamps provide control over the mode of operation desired.

Flexibility of programming is achieved by supplying power to the stepping relay logic circuits through a diode matrix, hence any one of the 26 positions on the stepping relay may be used to control any combination of actuators. Provision is made for holding a given actuator in either of its two positions through a sequence of steps during which time other actuators are operated.

If desired, a mixed automatic and manual program may be patched to provide automatic operation of a given sequence of actuators after which the system holds pending a manual restart by the operator. This is particularly useful when a visual observation is required in the process.

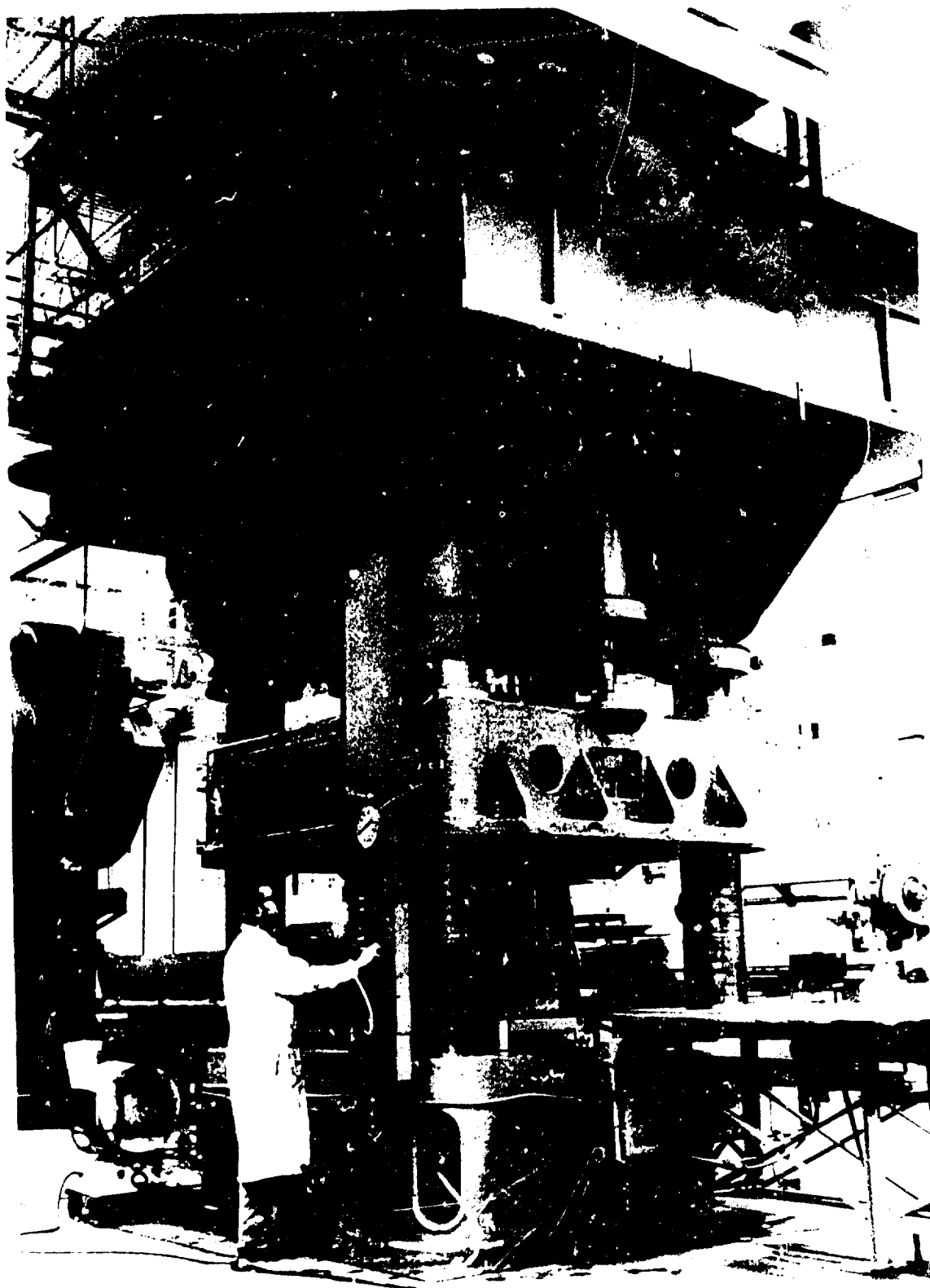


FIGURE 127. 2500 TON LAKE ERIE HYDRAULIC PRESS

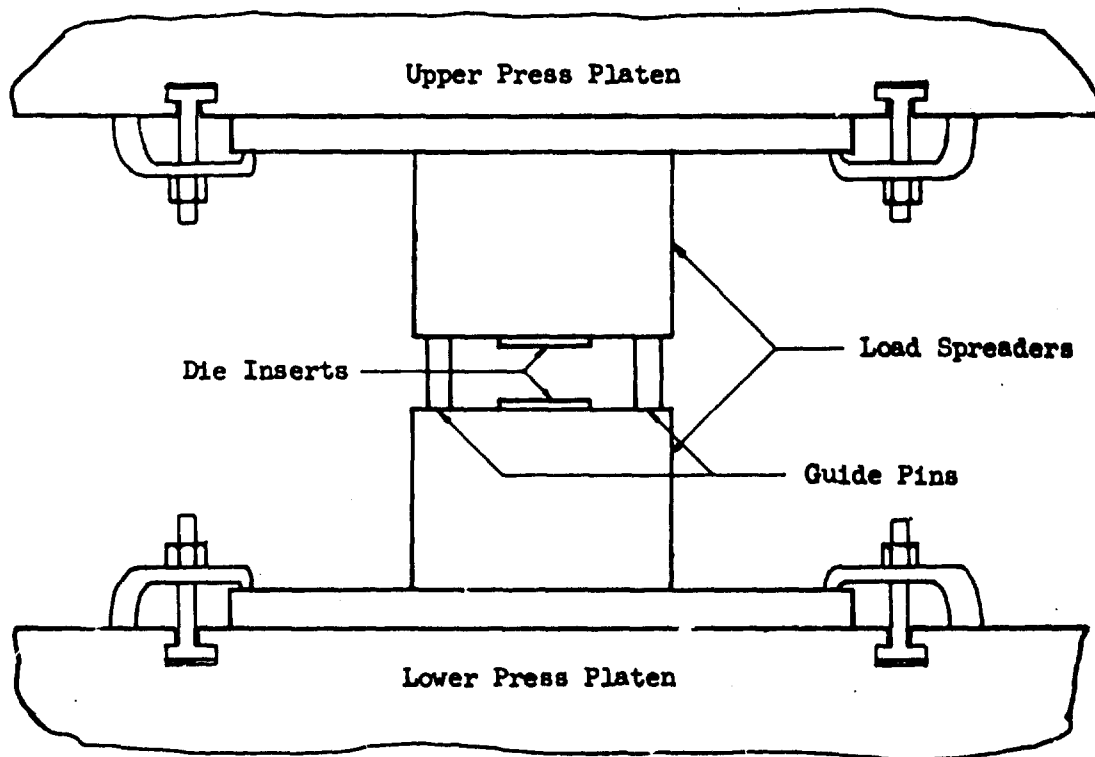


FIGURE 128. STATIC UPSET TOOLING

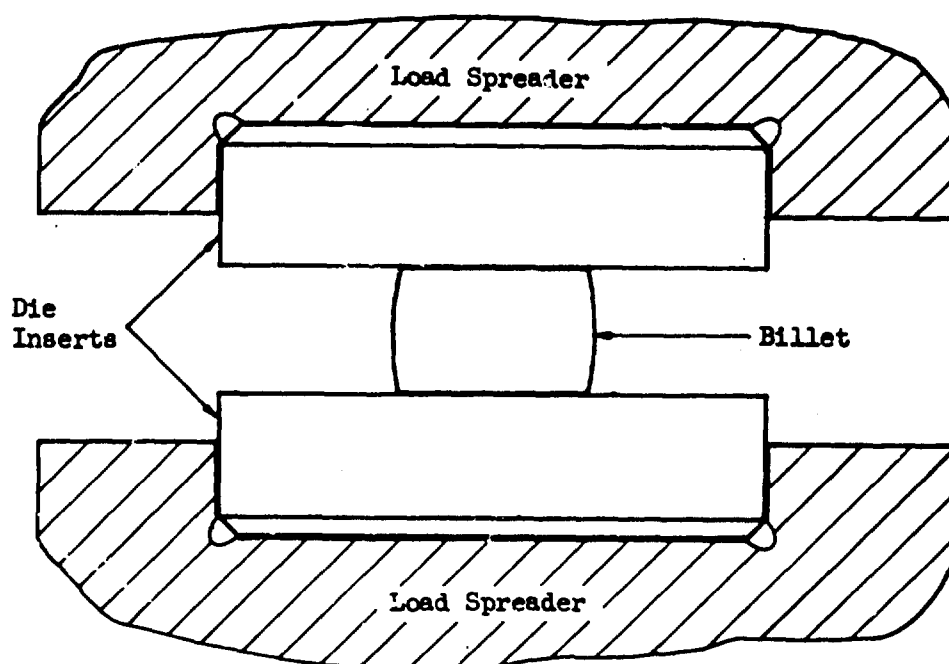


FIGURE 129. TYPICAL HARDENED STEEL DIE INSERTS FOR STATIC UPSET TESTS

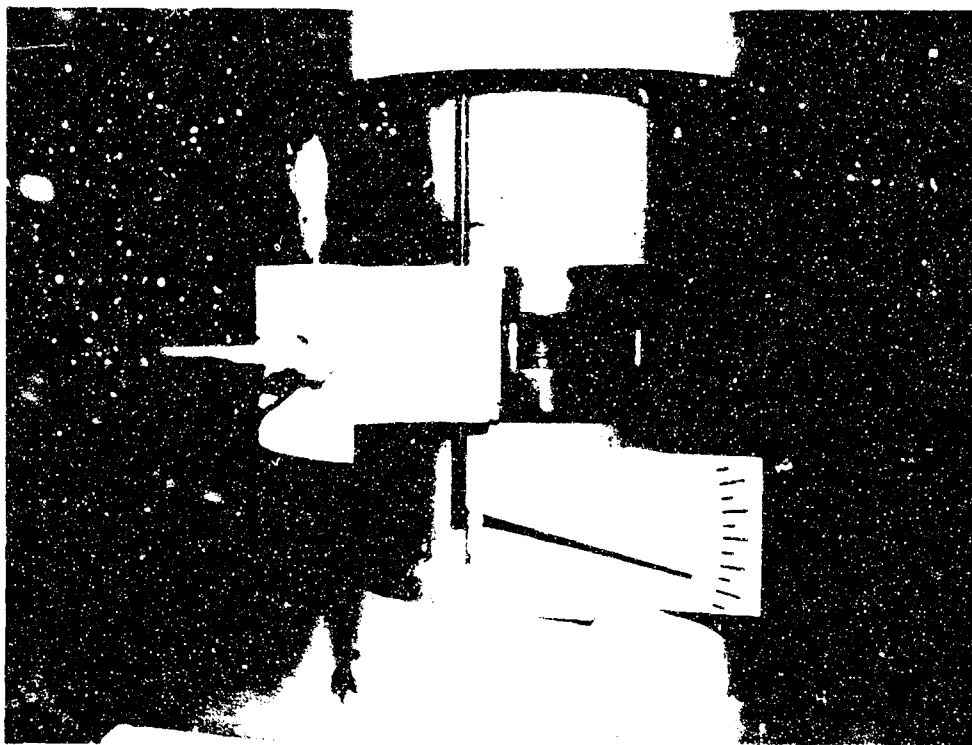


FIGURE 130. SPECIAL DEFLECTION GAGE FOR  
STATIC UPSET TESTS

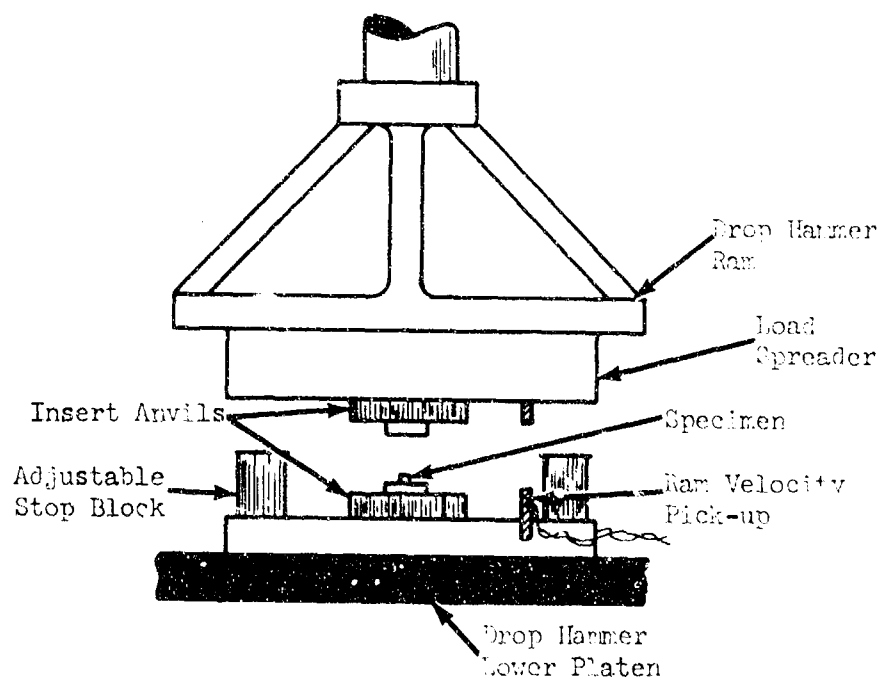


FIGURE 131. LOW VELOCITY, ELEVATED TEMPERATURE UPSET  
TEST EQUIPMENT

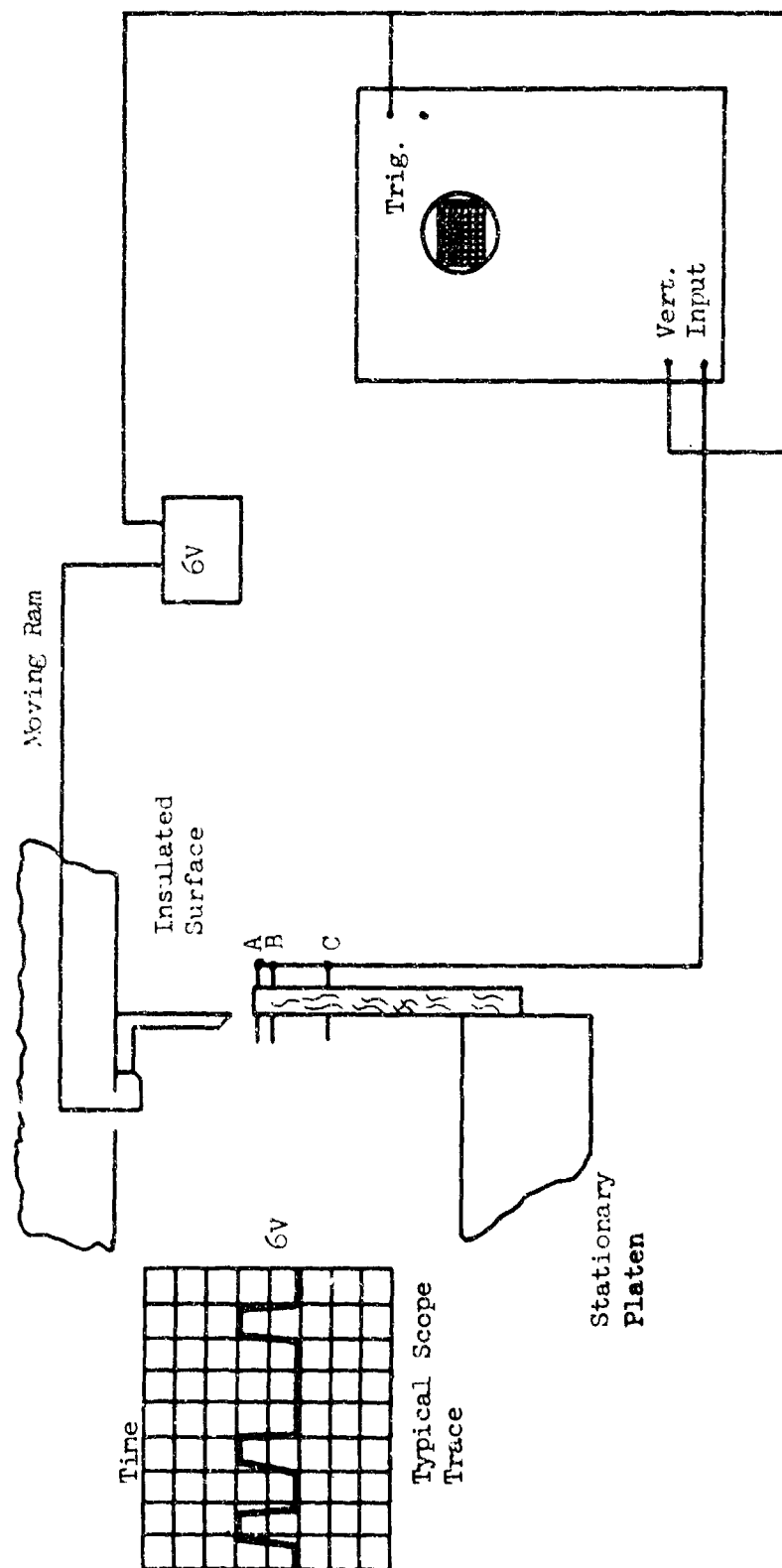


FIGURE 132. VELOCITY MEASUREMENT FOR DROP HAMMER FORGEABILITY TESTS.



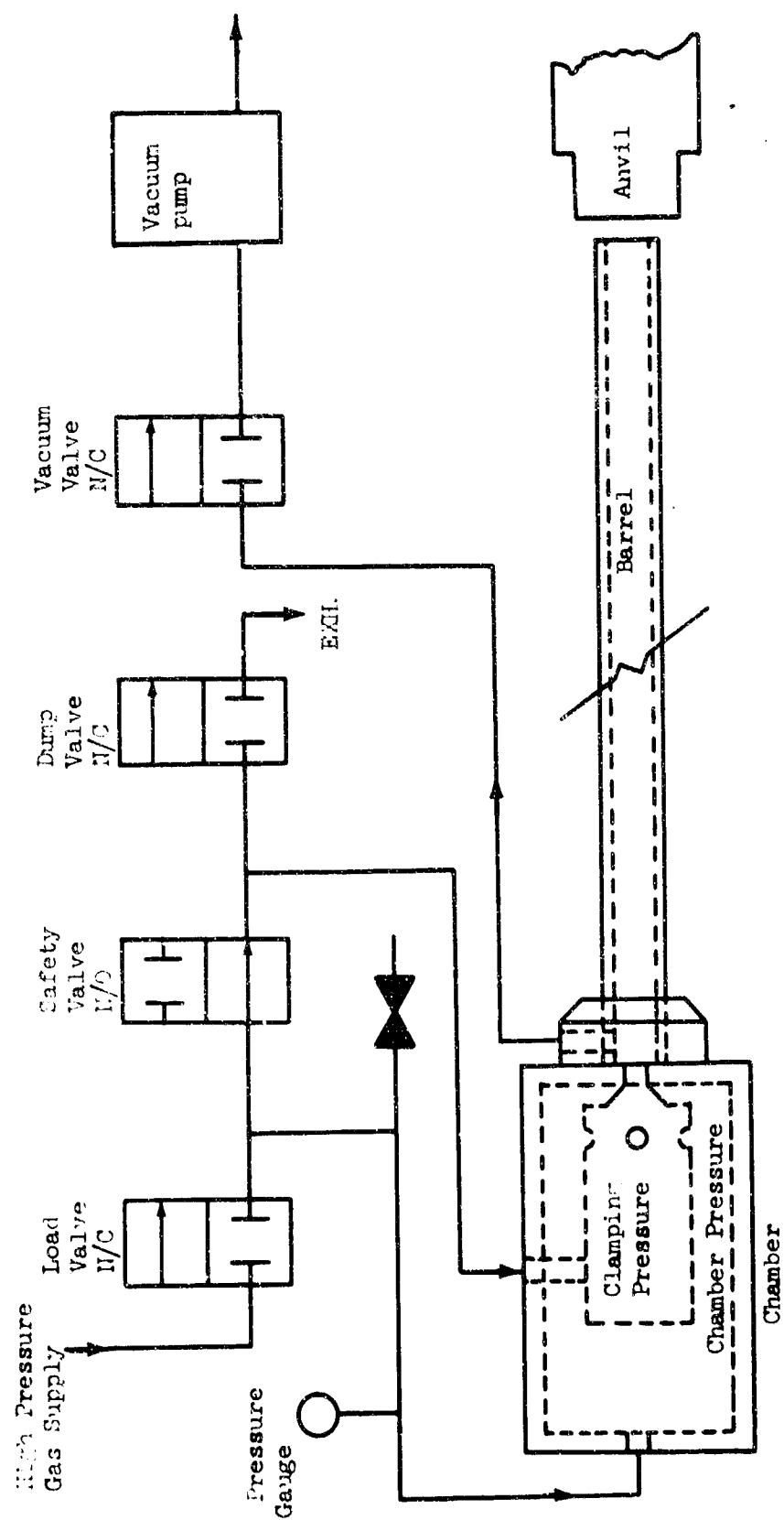


FIGURE 133. PRESSURE CHAMBER VALVING DIAGRAM

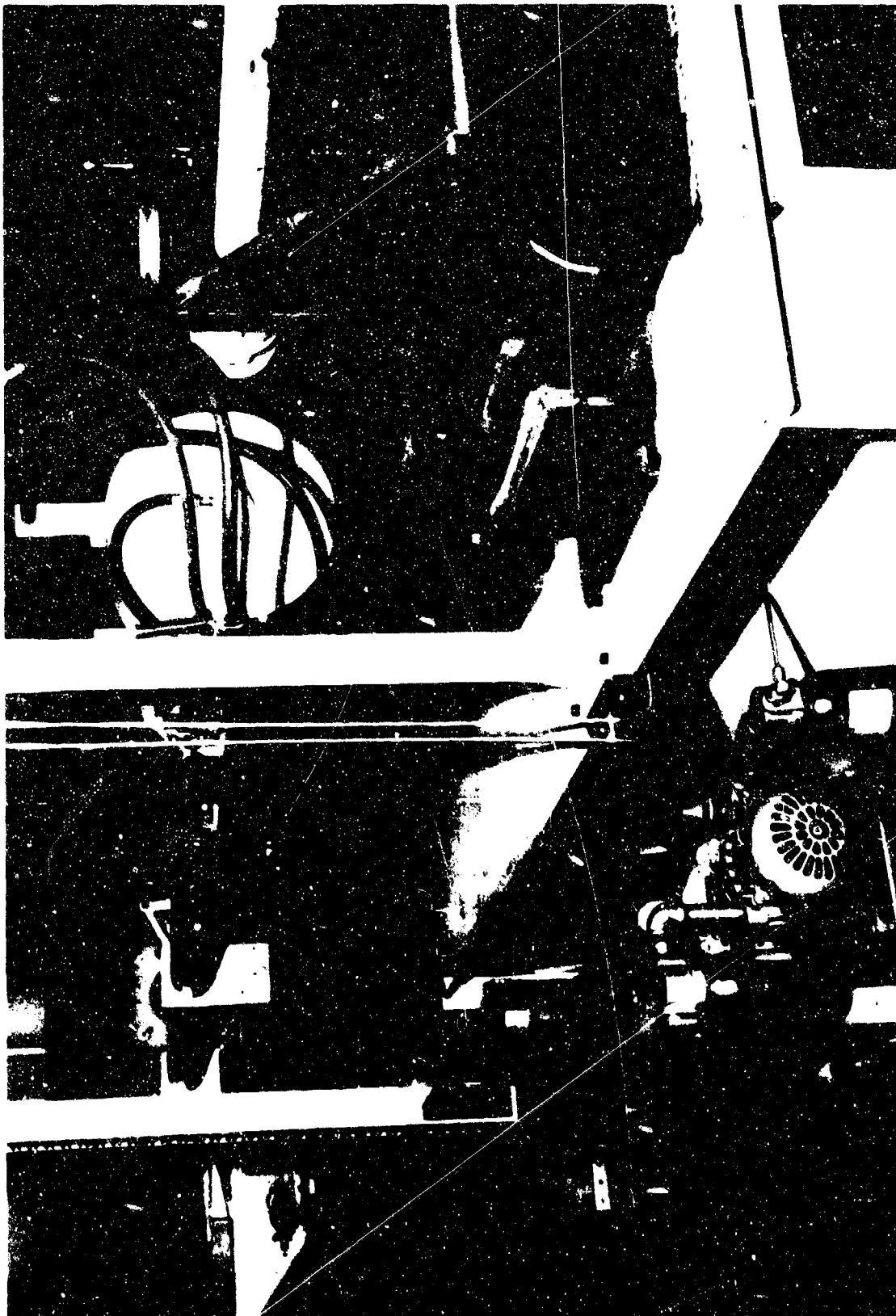


FIGURE 134. HIGH PRESSURE VALVING AND VACUUM SYSTEM

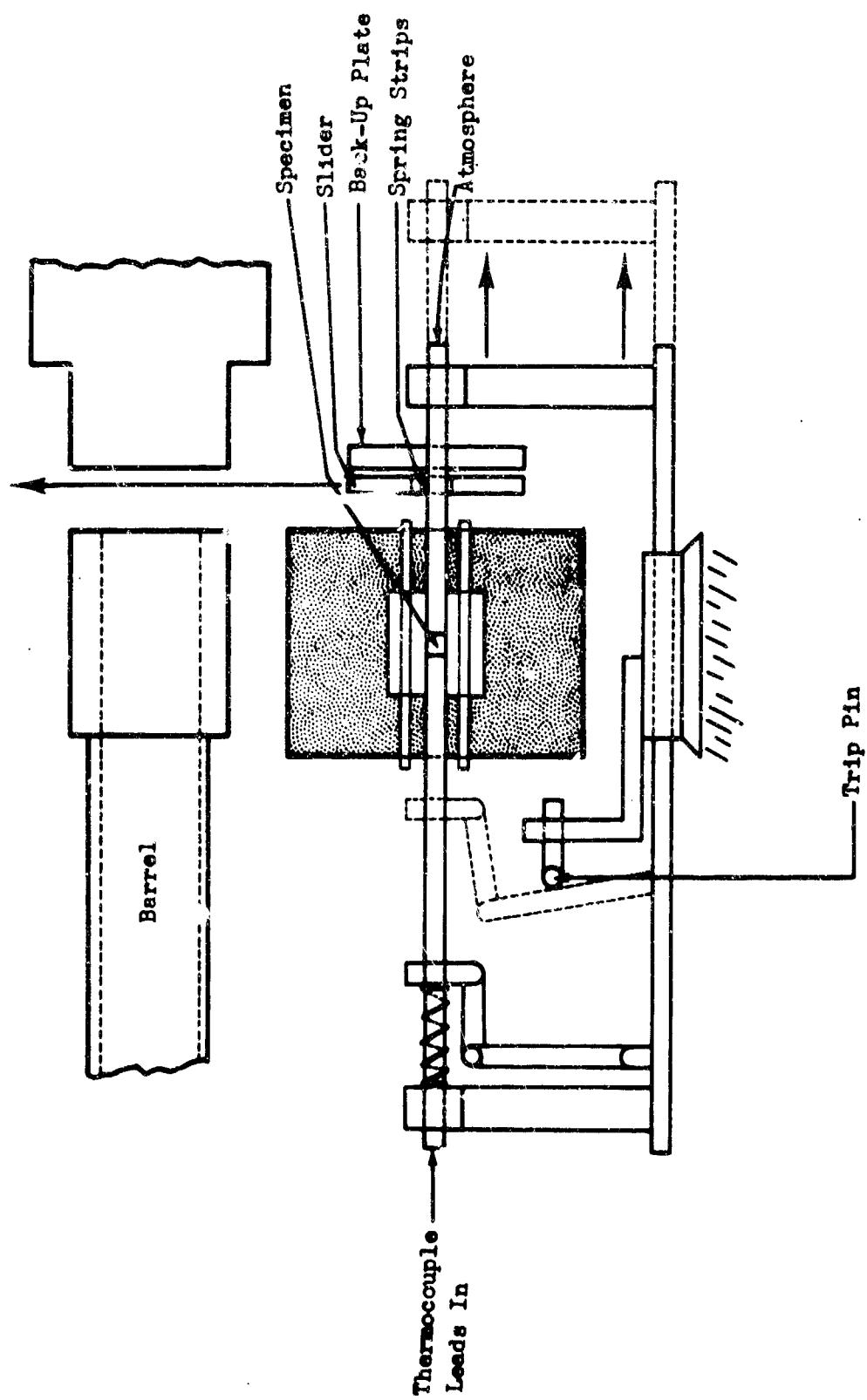


FIGURE 135. SCHEMATIC OF AUTOMATIC BILLET LOADING MECHANISM FOR FURNACE HEATED SPECIMENS

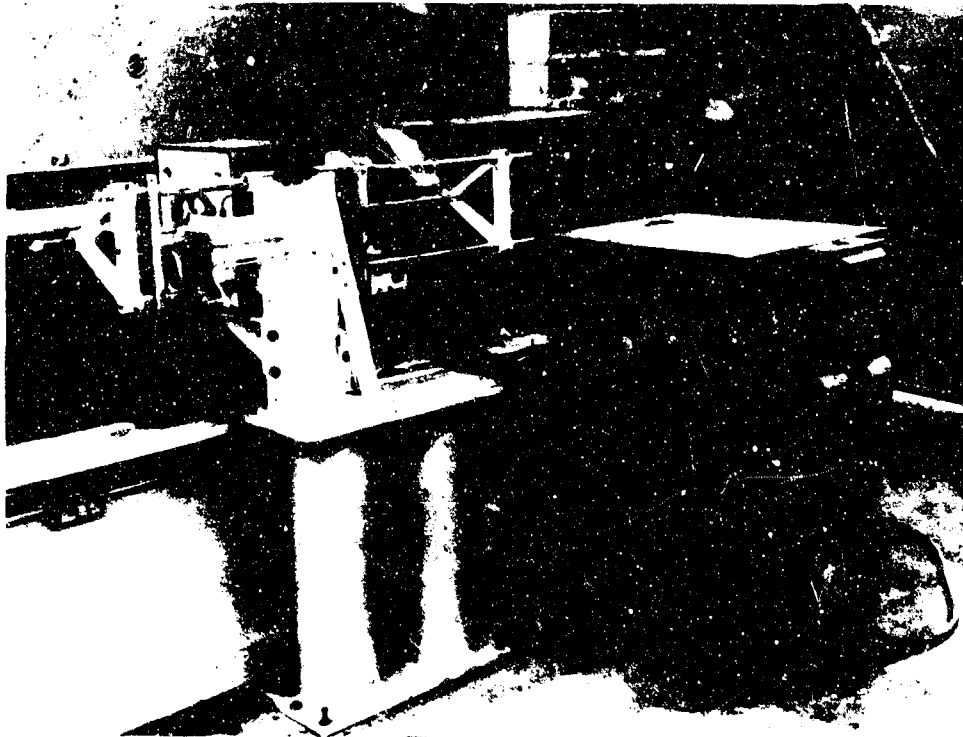


FIGURE 136. SPECIMEN HOLDING FIXTURE FOR ELEVATED TEMPERATURE TESTING.

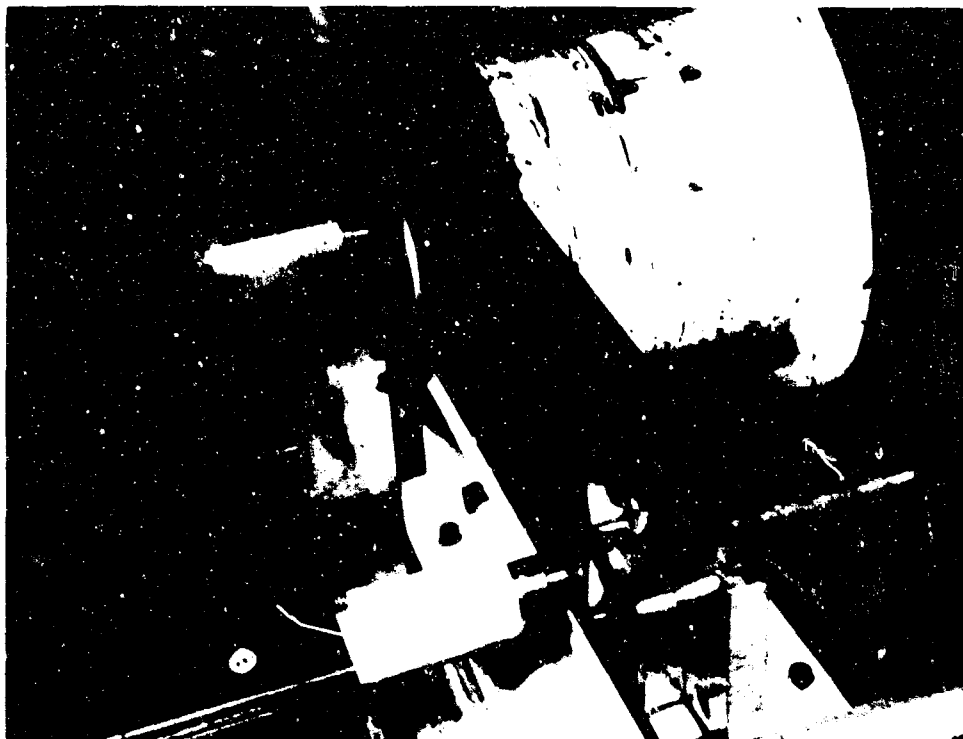


FIGURE 137. AUTOMATIC LOADING MECHANISM FOR ELEVATED TEMPERATURE TESTING.

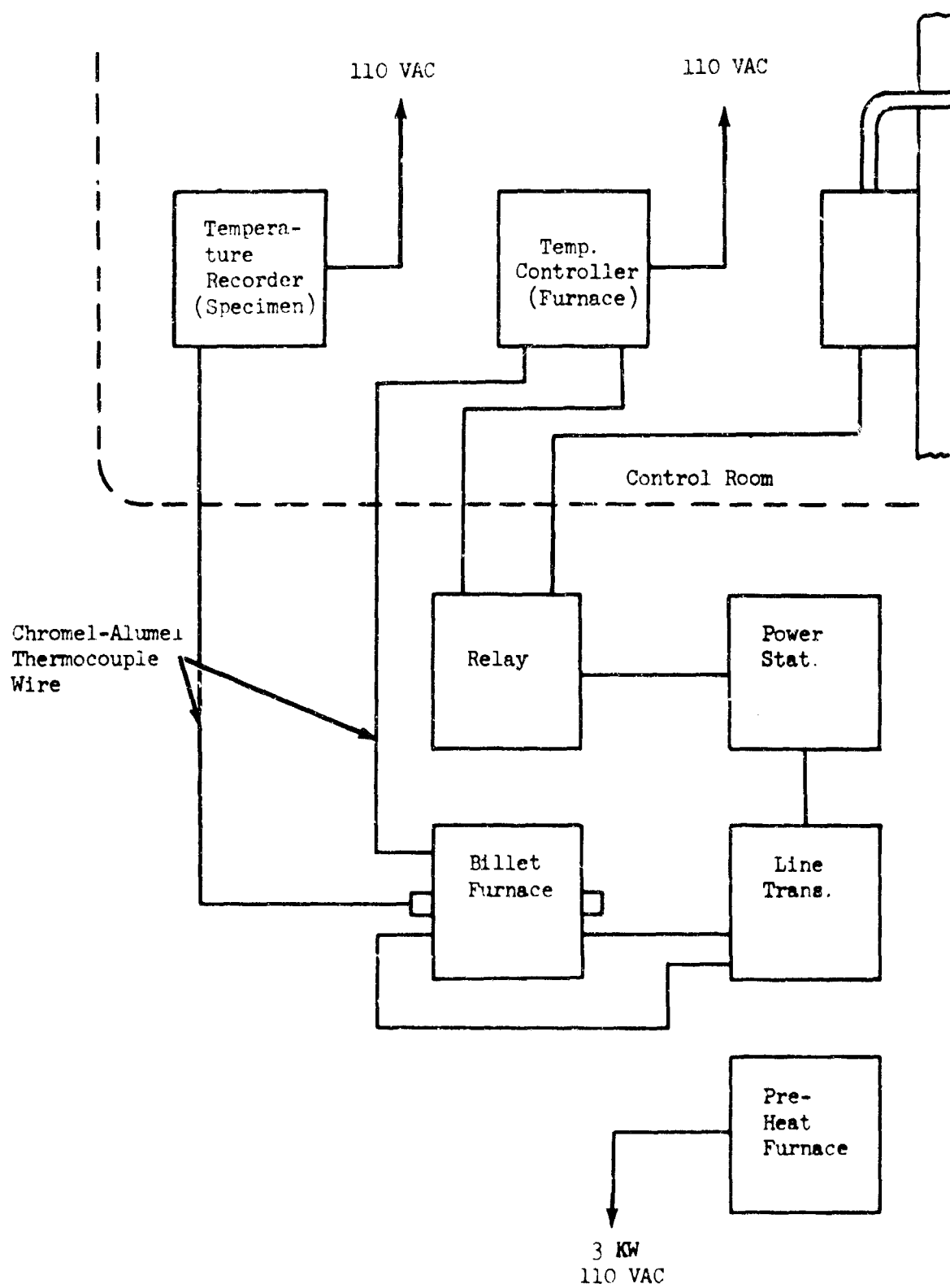


FIGURE 138. SCHEMATIC OF BILLET HEATING SYSTEM

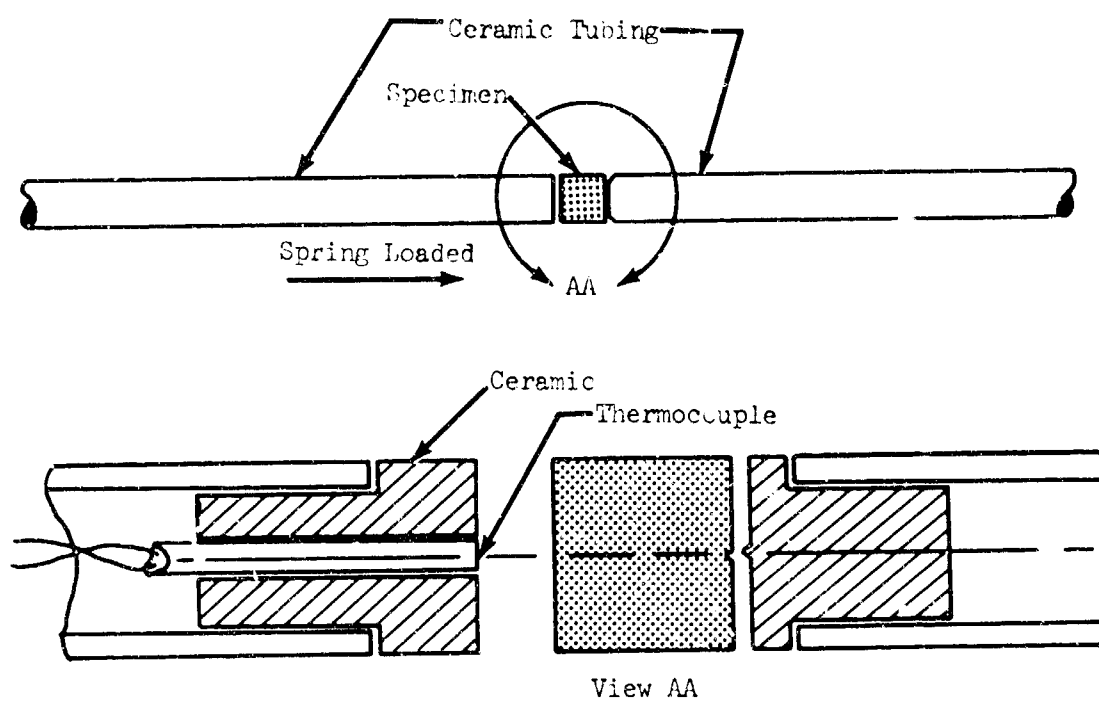


FIGURE 139. BILLET IN HEATING POSITION

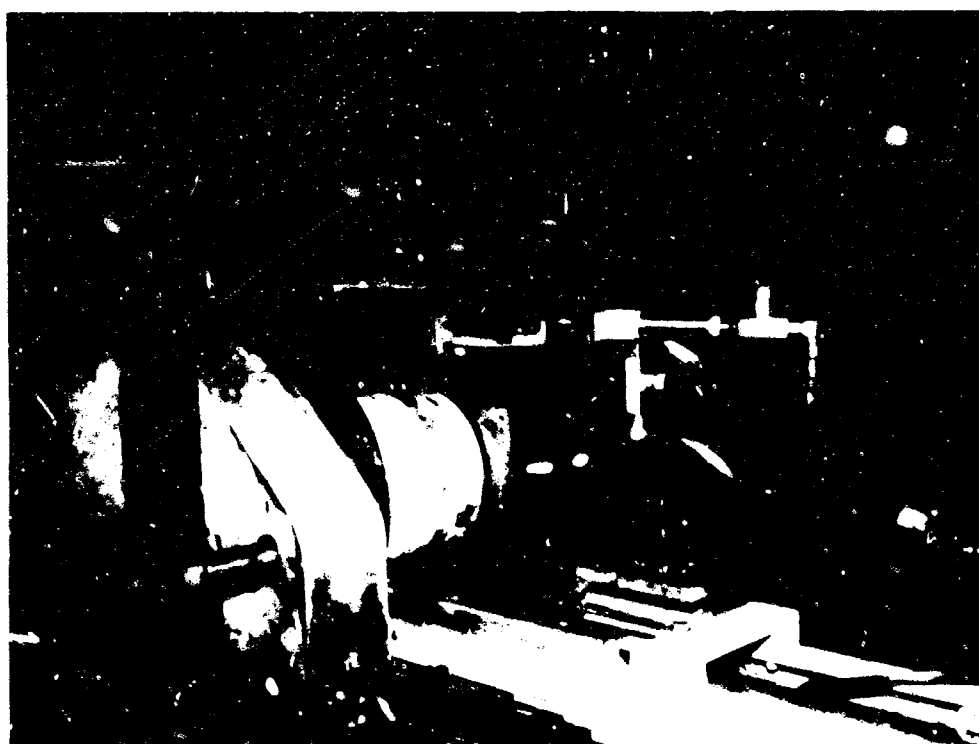


FIGURE 140. BAR UPSET LOADING MECHANISM

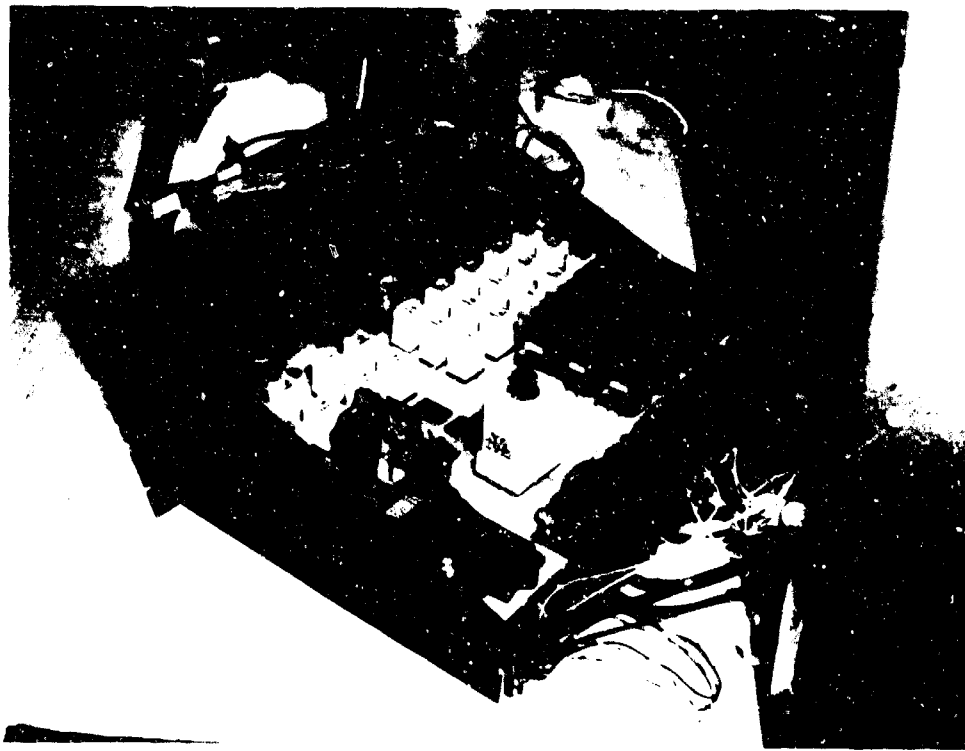


FIGURE 141. REAR VIEW OF CONTROL SYSTEM

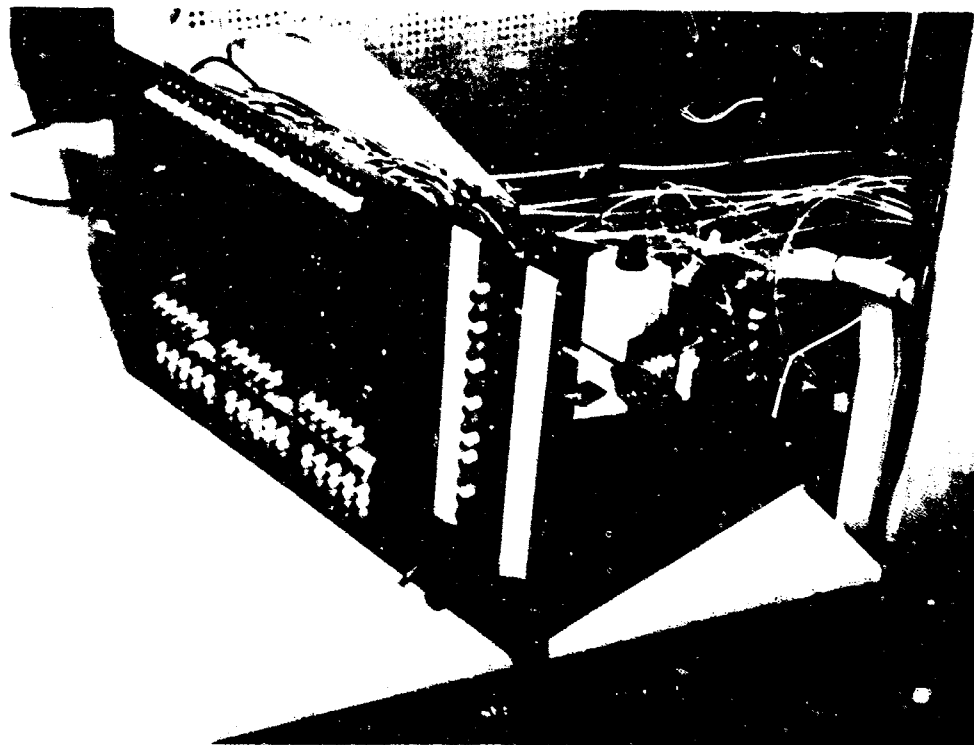


FIGURE 142. FRONT PANEL VIEW OF CONTROL SYSTEM

APPENDIX VII

MEASUREMENT AND CALIBRATION OF  
VELOCITY OF THE COMPRESSED GAS GUN



# APPENDIX V.1

## MEASUREMENT AND CALIBRATION OF MUZZLE VELOCITY OF THE COMPRESSED GAS GUN

The projectile impact velocity was measured using a Tektronic type 535 oscilloscope and C-12 camera. The velocity was calculated from variations in the scope trace produced by a voltage generated in two magnetic pickups mounted in the barrel as shown in Figure 143.

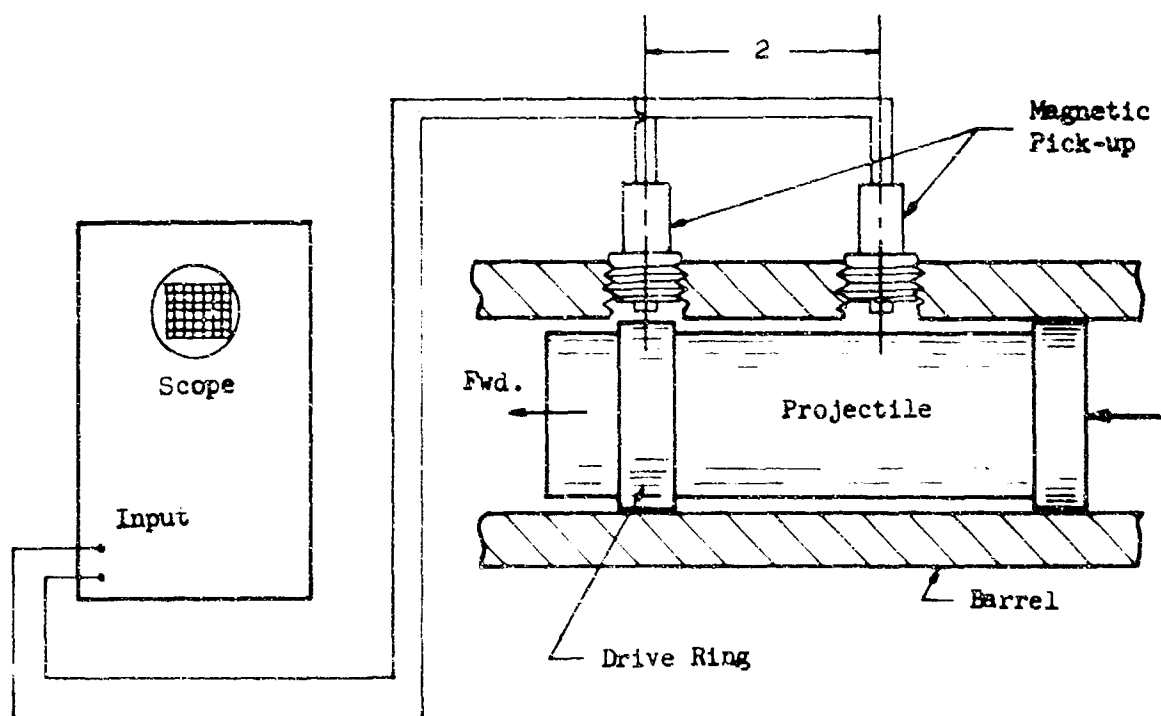
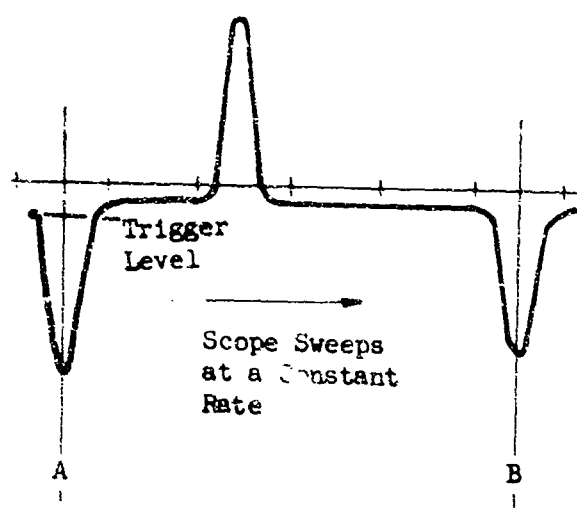
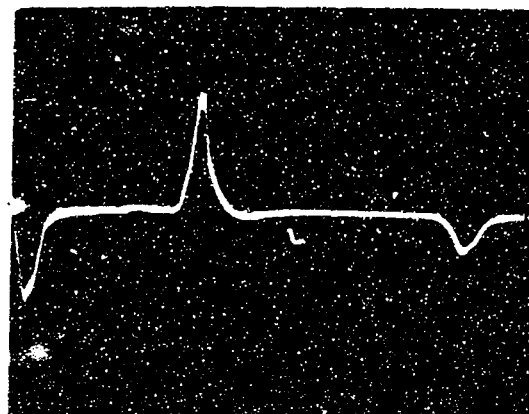


FIGURE 143. INSTRUMENTATION FOR PROJECTILE VELOCITY MEASUREMENT

The scope, set for single sweep internally triggered operation, is triggered by the voltage generated as the leading edge of the forward bearing ring approaches the aft pick-up. A voltage peak of reverse polarity occurs as the aft edge of the forward bearing ring leaves the pick-up. The pattern is repeated as the bearing ring passes the forward pick-up. Idealized and actual scope traces are shown in Figure 144. The projectile velocity is then calculated from the known time interval (scope sweep rate) for a point on the projectile to travel a measured distance between the magnetic pick-ups.



(a) Idealized



(b) Actual

Note: Points A & B occur when the aft edge of the drive band is at the approximate center of the magnetic pick-up.

FIGURE 144. TYPICAL OSCILLOSCOPE CURVE FOR MEASURING PROJECTILE VELOCITIES

In order to accelerate the testing, projectile velocities for most of the tests in this program were based on gas chamber pressure, projectile mass, and the equations of motion for the gas gun parameters. This method was carefully checked over a wide range of parameters and found to be well within the accuracy limits required. Figure 145 exhibits the close agreement between calculated and experimental velocities. Figure 146 shows the muzzle velocity and muzzle energy as functions of gas chamber pressure and projectile mass.

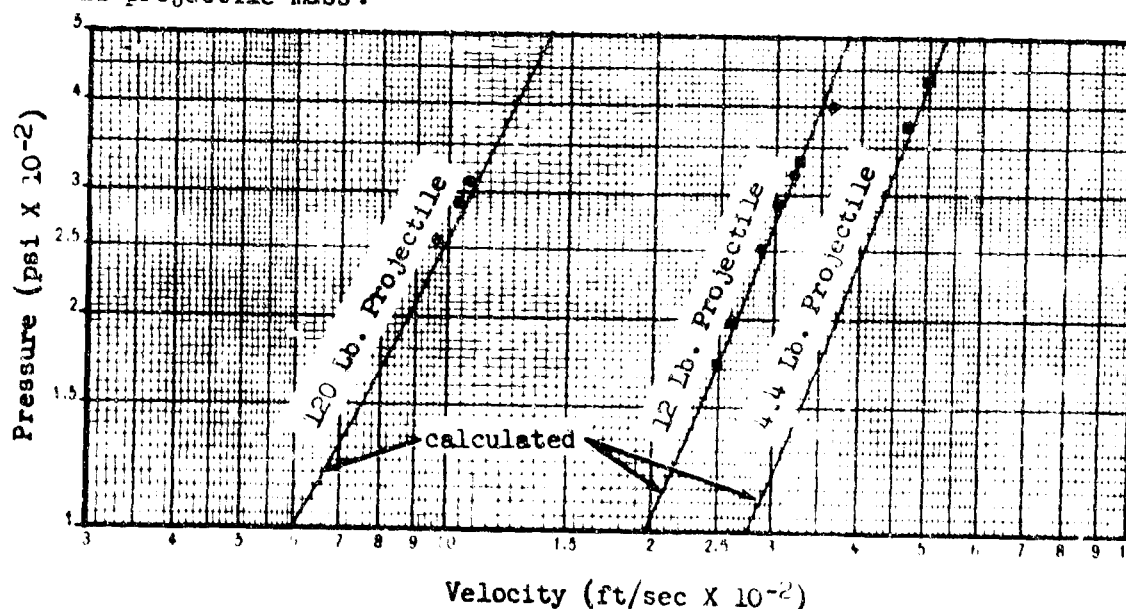


FIGURE 145. EXPERIMENTAL VERIFICATION OF ANALYTICALLY PREDICTED PROJECTILE VELOCITIES

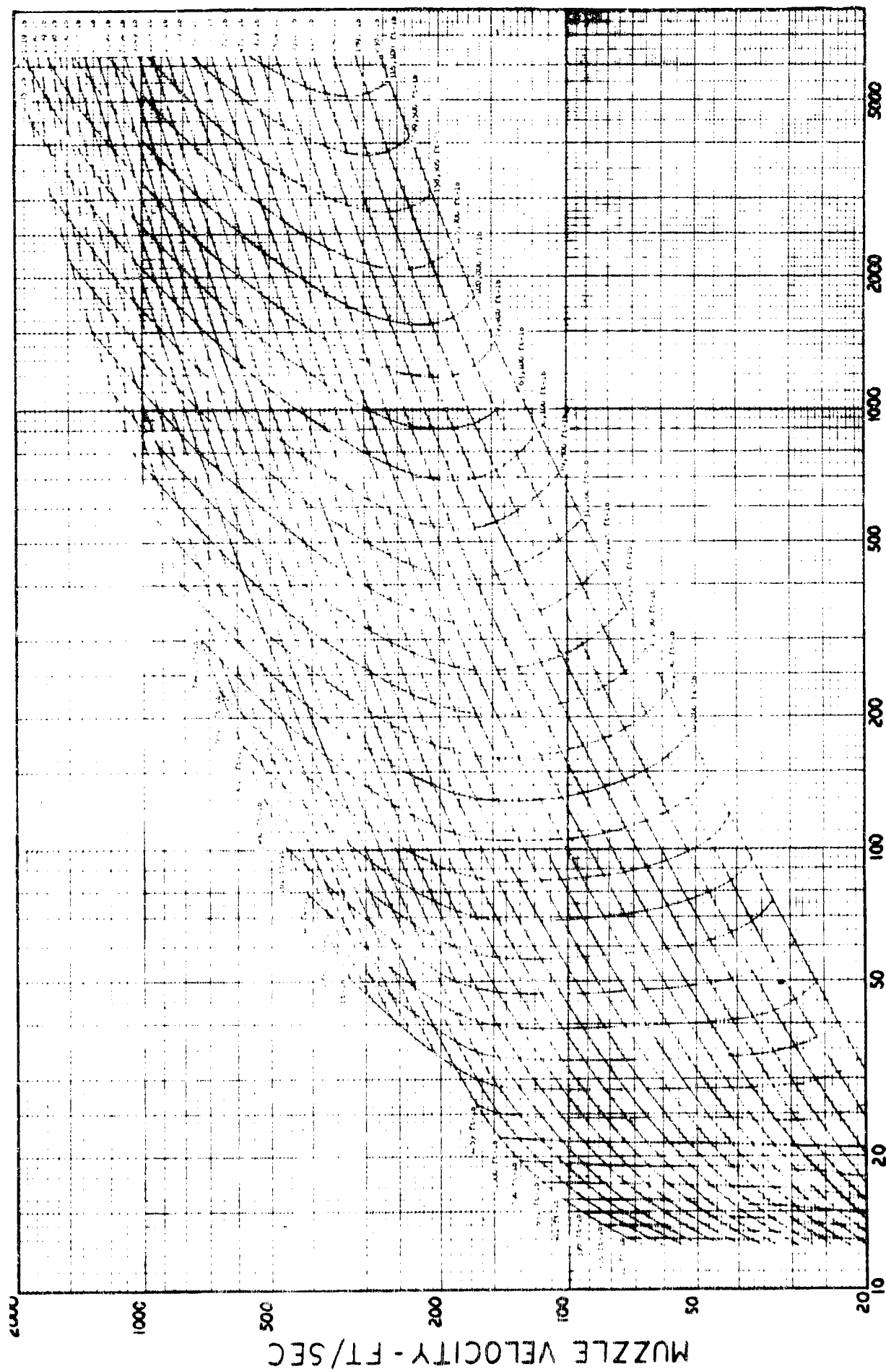


FIGURE 1-46. MUZZLE VELOCITY AND ENERGY VS CHAMBER PRESSURE AND PROJECTILE MASS

#### REFERENCES

- (1) "Press-Forging Thin Sections" by William Schraeder and D. A. Webster, Journal of Applied Mechanics, September 1949.
- (2) "Estimation of Dynamic Forces in Very High Speed Impact Forging" by M. J. Hillier, Trans. ASME Dec. 1965, Paper No. 65-WA/PROD-1.
- (3) Advanced Theoretical Formability - Manufacturing Technology by W. W. Wood et al, AFML-TR-64-411, January 1965.
- (4) The Investigation of High Dynamic Pressures upon the Metallurgical Properties of Iron and Titanium Based Alloys by A. W. Hall et al, ASD TTR-62-535, February 1963.
- (5) A Method for the Determination of the Coefficient of Friction of Metals under Conditions of Bulk Plastic Deformation by A. T. Male and M. G. Cockcroft, Journal of Institute of Metals, Vol. 93, 1964 and 1965.
- (6) A Study of Forging Variables, by H. J. Henning et al, Report No. ML-TDR-64-95, Contract Nr. AF 33(600)-42963, Battelle Memorial Institute, March 1964.

Unclassified

Security Classification

## DOCUMENT CONTROL DATA - R &amp; D

Security Classification of title, body of abstract and indexing annotation must be entered when the overall report is classified.

1. CONTRACTING ORIGINATOR'S NAME (Corporate name)		2a. REPORT SECURITY CLASSIFICATION	
Vought Aeronautics Division LTV Aerospace Corporation Dallas, Texas 75222		Unclassified	
3. REPORT TITLE		2b. GROUP	
Final Report on High Velocity Forging Technology		N/A	
4. DESCRIPTIVE NOTES (Type of report and inclusive dates)			
Final Report 1 December 1966 to 30 November 1968			
5. AUTHOR(S) (First name, middle initial, last name)			
D. W. Truelock J. R. Russell C. M. Phelan			
6. REPORT DATE	7b. TOTAL NO. OF PAGES	7c. NO. OF REFS	
November 1968	358	6	
8a. CONTRACT OR GRANT NO.	9a. ORIGINATOR'S REPORT NUMBER(S)		
F 33615-67-C-1179	N/A		
8b. PROJECT NO.	9b. OTHER REPORT NO(S) (Any other numbers that may be assigned this report)		
9-133	None		
10. DISTRIBUTION STATEMENT This document is subject to special export controls and each transmittal to foreign governments or foreign nationals may be made only with prior approval of the Manufacturing Technology Division, Air Force Materials Laboratory, Wright-Patterson Air Force Base, Ohio 45433			
11. SUPPLEMENTARY NOTES		12. SPONSORING MILITARY ACTIVITY	
None		Advanced Fabrication Techniques Branch Air Force Materials Laboratory Wright-Patterson Air Force Base, Ohio 45433	
13. ABSTRACT			
<p>This is a manufacturing methods program to investigate the dynamic response of selected aerospace alloys deformed by upset forging from room temperature to 1950°F at impact strain rates from quasi-static (100 in/in/sec.) to 8000 in/in/sec. This was accomplished in two phases. Phase I included the selection and the ambient temperature forging of ten representative aerospace materials to evaluate the effects of strain rate on material forgeability and to select four of the most responsive materials for extensive testing at elevated temperatures. In Phase II, the four selected materials were forged at varying combinations of strain rate and temperature to determine the conditions for optimum forgeability and mechanical properties including tensile yield, tensile ultimate, elongation, hardness and fatigue. This report covers a period of eighteen months and is divided into five sections: Introduction, Technical Background, Test Materials, Phase I Room Temperature Screening, and Phase II Elevated Temperature Testing.</p> <p>This document is subject to special export controls and each transmittal to foreign nationals may be made only with prior approval of the Advanced Fabrication Techniques Branch, Manufacturing Technology Division, Air Force Materials Laboratory, Wright-Patterson Air Force Base, Ohio.</p>			

DD FORM 1473

FORM 1473

Unclassified

Security Classification

Unclassified

Security Classification

14 KEY WORDS	LINK A		LINK B		LINK C	
	ROLE	WT	ROLE	WT	ROLE	WT
High Velocity Forging Strain rate effects on forgeability and final mechanical properties for selected alloys at different forging temperatures Forging energy requirement Grain flow						

Unclassified

Security Classification